The Ischemic Penumbra

Edited by
Geoffrey A. Donnan
Jean-Claude Baron
Stephen M. Davis
Frank R. Sharp

informa
healthcare

The Ischemic Penumbra

NEUROLOGICAL DISEASE AND THERAPY

1. Handbook of Parkinson's Disease, *edited by William C. Koller*
2. Medical Therapy of Acute Stroke, *edited by Mark Fisher*
3. Familial Alzheimer's Disease: Molecular Genetics and Clinical Perspectives, *edited by Gary D. Miner, Ralph W. Richter, John P. Blass, Jimmie L. Valentine, and Linda A. Winters-Miner*
4. Alzheimer's Disease: Treatment and Long-Term Management, *edited by Jeffrey L. Cummings and Bruce L. Miller*
5. Therapy of Parkinson's Disease, *edited by William C. Koller and George Paulson*
6. Handbook of Sleep Disorders, *edited by Michael J. Thorpy*
7. Epilepsy and Sudden Death, *edited by Claire M. Lathers and Paul L. Schraeder*
8. Handbook of Multiple Sclerosis, *edited by Stuart D. Cook*
9. Memory Disorders: Research and Clinical Practice, *edited byTakehiko Yanagihara and Ronald C. Petersen*
10. The Medical Treatment of Epilepsy, *edited by Stanley R. Resor, Jr., and Henn Kutt*
11. Cognitive Disorders: Pathophysiology and Treatment, *edited by Leon J. Thal, Walter H. Moos, and Elkan R. Gamzu*
12. Handbook of Amyotrophic Lateral Sclerosis, *edited by Richard Alan Smith*
13. Handbook of Parkinson's Disease: Second Edition, Revised and Expanded, *edited by William C. Koller*
14. Handbook of Pediatric Epilepsy, *edited by Jerome V. Murphy and Fereydoun Dehkharghani*
15. Handbook of Tourette's Syndrome and Related Tic and Behavioral Disorders, *edited by Roger Kurlan*
16. Handbook of Cerebellar Diseases, *edited by Richard Lechtenberg*
17. Handbook of Cerebrovascular Diseases, *edited by Harold P. Adams, Jr.*
18. Parkinsonian Syndromes, *edited by Matthew B. Stern and William C. Koller*
19. Handbook of Head and Spine Trauma, *edited by Jonathan Greenberg*
20. Brain Tumors: A Comprehensive Text, *edited by Robert A. Morantz and John W. Walsh*
21. Monoamine Oxidase Inhibitors in Neurological Diseases, *edited by Abraham Lieberman, C. Warren Olanow, Moussa B. H. Youdim, and Keith Tipton*
22. Handbook of Dementing Illnesses, *edited by John C. Morris*
23. Handbook of Myasthenia Gravis and Myasthenic Syndromes, *edited by Robert P. Lisak*
24. Handbook of Neurorehabilitation, *edited by David C. Good and James R. Couch, Jr.*
25. Therapy with Botulinum Toxin, *edited by Joseph Jankovic and Mark Hallett*
26. Principles of Neurotoxicology, *edited by Louis W. Chang*
27. Handbook of Neurovirology, *edited by Robert R. McKendall and William G. Stroop*
28. Handbook of Neuro-Urology, *edited by David N. Rushton*
29. Handbook of Neuroepidemiology, *edited by Philip B. Gorelick and Milton Alter*
30. Handbook of Tremor Disorders, *edited by Leslie J. Findley and William C. Koller*
31. Neuro-Ophthalmological Disorders: Diagnostic Work-Up and Management, *edited by Ronald J. Tusa and Steven A. Newman*
32. Handbook of Olfaction and Gustation, *edited by Richard L. Doty*
33. Handbook of Neurological Speech and Language Disorders, *edited by Howard S. Kirshner*
34. Therapy of Parkinson's Disease: Second Edition, Revised and Expanded, *edited by William C. Koller and George Paulson*
35. Evaluation and Management of Gait Disorders, *edited by Barney S. Spivack*
36. Handbook of Neurotoxicology, *edited by Louis W. Chang and Robert S. Dyer*

37. Neurological Complications of Cancer, *edited by Ronald G. Wiley*
38. Handbook of Autonomic Nervous System Dysfunction, *edited by Amos D. Korczyn*
39. Handbook of Dystonia, *edited by Joseph King Ching Tsui and Donald B. Calne*
40. Etiology of Parkinson's Disease, *edited by Jonas H. Ellenberg, William C. Koller and J. William Langston*
41. Practical Neurology of the Elderly, *edited by Jacob I. Sage and Margery H. Mark*
42. Handbook of Muscle Disease, *edited by Russell J. M. Lane*
43. Handbook of Multiple Sclerosis: Second Edition, Revised and Expanded, *edited by Stuart D. Cook*
44. Central Nervous System Infectious Diseases and Therapy, *edited by Karen L. Roos*
45. Subarachnoid Hemorrhage: Clinical Management, *edited by Takehiko Yanagihara, David G. Piepgras, and John L. D. Atkinson*
46. Neurology Practice Guidelines, *edited by Richard Lechtenberg and Henry S. Schutta*
47. Spinal Cord Diseases: Diagnosis and Treatment, *edited by Gordon L. Engler, Jonathan Cole, and W. Louis Merton*
48. Management of Acute Stroke, *edited by Ashfaq Shuaib and Larry B. Goldstein*
49. Sleep Disorders and Neurological Disease, *edited by Antonio Culebras*
50. Handbook of Ataxia Disorders, *edited by Thomas Klockgether*
51. The Autonomic Nervous System in Health and Disease, *David S. Goldstein*
52. Axonal Regeneration in the Central Nervous System, *edited by Nicholas A. Ingoglia and Marion Murray*
53. Handbook of Multiple Sclerosis: Third Edition, *edited by Stuart D. Cook*
54. Long-Term Effects of Stroke, *edited by Julien Bogousslavsky*
55. Handbook of the Autonomic Nervous System in Health and Disease, *edited by C. Liana Bolis, Julio Licinio, and Stefano Govoni*
56. Dopamine Receptors and Transporters: Function, Imaging, and Clinical Implication, Second Edition, *edited by Anita Sidhu, Marc Laruelle, and Philippe Vernier*
57. Handbook of Olfaction and Gustation: Second Edition, Revised and Expanded, *edited by Richard L. Doty*
58. Handbook of Stereotactic and Functional Neurosurgery, *edited by Michael Schulder*
59. Handbook of Parkinson's Disease: Third Edition, *edited by Rajesh Pahwa, Kelly E. Lyons, and William C. Koller*
60. Clinical Neurovirology, *edited by Avindra Nath and Joseph R. Berger*
61. Neuromuscular Junction Disorders: Diagnosis and Treatment, *Matthew N. Meriggioli, James F. Howard, Jr., and C. Michel Harper*
62. Drug-Induced Movement Disorders, *edited by Kapil D. Sethi*
63. Therapy of Parkinson's Disease: Third Edition, Revised and Expanded, *edited by Rajesh Pahwa, Kelly E. Lyons, and William C. Koller*
64. Epilepsy: Scientific Foundations of Clinical Practice, *edited by Jong M. Rho, Raman Sankar, and José E. Cavazos*
65. Handbook of Tourette's Syndrome and Related Tic and Behavioral Disorders: Second Edition, *edited by Roger Kurlan*
66. Handbook of Cerebrovascular Diseases: Second Edition, Revised and Expanded, *edited by Harold P. Adams, Jr.*
67. Emerging Neurological Infections, *edited by Christopher Power and Richard T. Johnson*

68. Treatment of Pediatric Neurologic Disorders, *edited by Harvey S. Singer, Eric H. Kossoff, Adam L. Hartman, and Thomas O. Crawford*
69. Synaptic Plasticity: Basic Mechanisms to Clinical Applications, *edited by Michel Baudry, Xiaoning Bi, and Steven S. Schreiber*
70. Handbook of Essential Tremor and Other Tremor Disorders, *edited by Kelly E. Lyons and Rajesh Pahwa*
71. Handbook of Peripheral Neuropathy, *edited by Mark B. Bromberg and A. Gordon Smith*
72. Carotid Artery Stenosis: Current and Emerging Treatments, *edited by Seemant Chaturvedi and Peter M. Rothwell*
73. Gait Disorders: Evaluation and Management, *edited by Jeffrey M. Hausdorff and Neil B. Alexander*
74. Surgical Management of Movement Disorders (HBK), *edited by Gordon H. Baltuch and Matthew B. Stern*
75. Neurogenetics: Scientific and Clinical Advances, *edited by David R. Lynch*
76. Epilepsy Surgery: Principles and Controversies, *edited by John W. Miller and Daniel L. Silbergeld*
77. Clinician's Guide To Sleep Disorders, *edited by Nathaniel F. Watson and Bradley Vaughn*
78. Amyotrophic Lateral Sclerosis, *edited by Hiroshi Mitsumoto, Serge Przedborski and Paul H. Gordon*
79. Duchenne Muscular Dystrophy: Advances in Therapeutics, *edited by Jeffrey S. Chamberlain and Thomas A. Rando*
80. Handbook of Multiple Sclerosis, Fourth Edition, *edited by Stuart D. Cook*
81. Brain Embolism, *edited by Louis R. Caplan and Warren J. Manning*
82. Handbook of Secondary Dementias, *edited by Roger Kurlan*
83. Parkinson's Disease: Genetics and Pathogenesis, *edited by Ted M. Dawson*
84. Migraine, *Russell Lane and Paul Davies*
85. Migraine and Other Headache Disorders, *edited by Richard B. Lipton and Marcelo Bigal*
86. Restless Legs Syndrome: Diagnosis and Treatment, *edited by William G. Ondo*
87. Handbook of Dementing Illnesses, Second Edition, *edited by John C. Morris, James E. Galvin, and David M. Holtzman*
88. Acute Stroke: Bench to Bedside, *edited by Anish Bhardwaj, Nabil J. Alkayed, Jeffrey R. Kirsch, and Richard J. Traystman*
89. Brain Tumors: Practical Guide to Diagnosis and Treatment, *edited by Joachim M. Baehring and Joseph M. Piepmeier*
90. Handbook of Dystonia, *edited by Mark A. Stacy*
91. Deep Brain Stimulation for Parkinson's Disease, *edited by Gordon H. Baltuch and Matthew B. Stern*
92. Handbook of Parkinson's Disease, Fourth Edition, *edited by Rajesh Pahwa and Kelly E. Lyons*
93. The Ischemic Penumbra, *edited by Geoffrey A. Donnan, Jean-Claude Baron, Stephen M. Davis, and Frank R. Sharp*

The Ischemic Penumbra

Pathophysiology, Imaging and Therapy

Edited By

Geoffrey A. Donnan
National Stroke Research Institute, Austin Health
University of Melbourne, Victoria, Australia

Jean-Claude Baron
Addenbrooke's Hospital and University of Cambridge, UK

Stephen M. Davis
Royal Melbourne Hospital and University of Melbourne, Victoria, Australia

Frank R. Sharp
University of California, Davis, USA

informa
healthcare

New York London

Informa Healthcare USA, Inc.
270 Madison Avenue
New York, NY 10016

Printed in the United States of America on acid-free paper
10 9 8 7 6 5 4 3 2 1

International Standard Book Number-10: 0-8493-3990-1 (Hardcover)
International Standard Book Number-13: 978-0-8493-3990-5 (Hardcover)

Library of Congress Cataloging-in-Publication Data

The ischemic penumbra / [edited by] Geoffrey A. Donnan ... [et al.].
p. ; cm. -- (Neurological disease and therapy ; v. 93)
Includes bibliographical references and index.
ISBN-13: 978-0-8493-3990-5 (hb : alk. paper)
ISBN-10: 0-8493-3990-1 (hb : alk. paper)
1. Cerebral ischemia--Pathophysiology. 2. Cerebrovascular disease. I. Donnan, G. A. (Geoffrey A.) II. Series.
[DNLM: 1. Cerebrovascular Accident--diagnosis. 2. Cerebrovascular Accident--therapy. 3. Diagnostic Imaging--methods. W1 NE33LD v.93 2007 / WL 355 I7675 2007]

RC388.5.I825 2007
616.8'106--dc22 2007000619

Visit the Informa Web site at
www.informa.com

and the Informa Healthcare Web site at
www.informahealthcare.com

This book is dedicated to our parents,
who made it all possible.

Foreword

Time is brain–penumbra is brain–brain is life.

The ischemic penumbra is an enigma and is the key to stroke pathophysiology and treatment. The term is used exhaustively and has become the major rationale for the early delivery of stroke care. Knowledge about the penumbra, its variability, and its ever-changing extension and individuality has dramatically changed stroke treatment. Paradoxically, it is still poorly understood. Animal experiments contributed to the early concepts and allowed investigators to establish blood flow thresholds. Information gained from these studies and those with multitracer positron emission tomography defining the penumbra in humans for the first time have been in existence for more than 20 years; it was the translation into the management of stroke and the design of clinical trials that took longer than expected. The ultra-early treatment concept of the early intravenous tissue plasminogen activator studies, specifically the National Institute of Neurological Disorders and Stroke trial, opened the eyes of most stroke physicians. Finally, it became clear that time was the most important variable in stroke treatment and that this translated into the presence of penumbral tissue. Hence, the "time is brain" concept arose.

The next logical step was to look for mechanisms and tools that would allow the replacement of a time-based therapy by a pathophysiologically based treatment window. It led to the introduction of perfusion–diffusion mismatch magnetic resonance imaging and computerized tomography angiography–computed tomography perfusion. These techniques offered information about pathophysiological variables that would correspond to penumbral tissue, never forgetting that it always would be just a snapshot of something penumbra-like at the time of assessment.

This volume, edited by eminent scientists and clinicians who are experts in the field of stroke pathophysiology and treatment, together with contributions by a prestigious list of scientists involved in penumbral research, provides the first comprehensive book on one of the most important concepts in acute stroke research and management. There is a comprehensive review of the history, background, pathophysiology, and application of the penumbra, from concept to stroke management. There is no doubt that the reader of this volume will gain a deeper understanding of the penumbra, given that there is a consolidation of about half a century of research that finally led to the first approved treatment of acute ischemic stroke. The book will be judged a success if, as it will undoubtedly do, it stimulates readers to explore the penumbra further and advance knowledge in the area. The most important outcome is recanalization and reperfusion or, better, saving penumbral tissues and saving brain.

Werner Hacke, MD, PhD
Department of Neurology
University of Heidelberg
Heidelberg, Germany

Preface

In the world of acute ischemic stroke, nothing is more important than an understanding of the ischemic penumbra. The whole concept of the existence of salvageable tissue, that is, the penumbra, is based on the daily clinical observation of almost immediate and early recovery from an episode of hemiparesis or other clinical expression of occlusion of a blood vessel within any of the arterial territories of the brain. Indeed, even before there was an appreciation of the complexities of the ischemic cascade, many clinicians dealing with stroke understood that something akin to the ischemic penumbra was likely to exist. These ideas, which fueled pivotal experimental studies to document the penumbra, clashed with the then prevailing dogma that the ischemic brain was doomed to die within minutes of onset of the clinical event. It is because of this central positioning of the penumbra in stroke outcome and therapy that we felt that a volume dedicated to its existence was timely.

The editors are all clinical scientists working in the field of stroke, but coming from different perspectives. In particular, we have backgrounds in imaging and therapies for stroke, as well as its pathophysiology and neurochemistry. Hence, we have tried to draw together an overview of the ischemic penumbra viewed predominantly from the clinical perspective, but providing the reader with a solid component of the more basic experimental and neurochemical aspects. Also, we are of an opinion that this should also be put in historical context. Here we have been particularly fortunate in having an enthusiastic contribution from Professor Lindsay Symon, who had such a pivotal role in defining the ischemic penumbra during the 1970s by means of a series of rigorous animal experiments. We have also included chapters that summarize aspects of the penumbra in a way that has not been done before, such as providing an overall view of species differences in thresholds for the penumbra and its duration. The duration of the penumbra is particularly relevant if we are to extend the time window for treatment so more patients can benefit from modern therapies.

In bringing together ideas about the definition, criteria, and the various penumbral imaging modalities now available, one message becomes quite clear. Although already clearly useful in the clinical setting, the concept of the ischemic penumbra is still evolving as there is still no entirely satisfactory definition, and the operational criteria for its existence need refining. Perhaps even more obviously, there is no ideal imaging technique to confirm its presence. Each of the penumbral imaging techniques described in this volume have their advantages and disadvantages, and none really directly and precisely images the penumbra as originally defined. One conclusion that can be drawn from this is that the penumbra is still a fertile area of research with many new discoveries of importance still to be made.

Hence, we hope that this volume is a useful resource for clinicians, researchers, and students alike who have an interest in the ischemic penumbra. While we have attempted to include a broad range of elements of the penumbra together, there are, of course, always areas that could have been strengthened and others that may have been overemphasized. As the first major attempt to paint a scientific picture of the penumbra on one canvas, we hope that this has been a reasonable start. If the benefit achieved is to enhance penumbral research even to a small extent, we will have realized our aim of helping those who, unfortunately, have been the victims of stroke.

Geoffrey A. Donnan
Jean-Claude Baron
Stephen M. Davis
Frank R. Sharp

Contents

Contributors

Hongyu An Department of Radiology, University of North Carolina at Chapel Hill, Chapel Hill, North Carolina U.S.A.

Jean-Claude Baron Department of Clinical Neurosciences and Stroke Unit, Addenbrooke's Hospital, University of Cambridge, Cambridge, U.K.

Bernd Bauer Max Planck Institute for Neurological Research, Cologne, Germany

Julien Bogousslavsky Clinique Valmont–Genolier, Montreux, Switzerland

Ken Butcher Division of Neurology, University of Alberta, Edmonton, Alberta, Canada

Numthip Chitravas National Stroke Research Institute, Austin Health, Victoria, Australia

Antoni Davalos Department of Neurosciences, Hospital Germans Trias i Pujol, Universitat Autonoma de Barcelona, Badalona, Spain

Stephen M. Davis Department of Neurology, Royal Melbourne Hospital and University of Melbourne, Melbourne, Victoria, Australia

John A. Detre Departments of Neurology and Radiology, University of Pennsylvania, Philadelphia, Pennsylvania, U.S.A.

Ulrich Dirnagl Department of Experimental Neurology Charité, Humboldt University, Berlin, Germany

Christian Dohmen Department of Neurology, University of Cologne, Cologne, Germany

Geoffrey A. Donnan National Stroke Research Institute, Austin Health, University of Melbourne, Melbourne, Victoria, Australia

Jens Peter Dreier Department of Experimental Neurology Charité, Humboldt University, Berlin, Germany

Timothy Q. Duong Yerkes Imaging Center, Division of Neuroscience and Department of Neurology, Emory University, Atlanta, Georgia, U.S.A.

Marc Fisher University of Massachusetts/Memorial Healthcare, Worcester, Massachusetts, U.S.A.

Rudolf Graf Max Planck Institute for Neurological Research, Cologne, Germany

Rishi Gupta Department of Neurology, Michigan State University, Lansing, Michigan, U.S.A.

Jun Hatazawa Department of Nuclear Medicine and Tracer Kinetics, Osaka University Graduate School of Medicine, Suita, Osaka, Japan

Wolf-Dieter Heiss Max Planck Institute for Neurological Research, Cologne, Germany

Konstantin-A. Hossmann Max Planck Institute of Neurological Research, Cologne, Germany

David W. Howells Department of Medicine, University of Melbourne, National Stroke Research Institute, Austin Health, Melbourne, Victoria, Australia

Chung Y. Hsu Department of Neurology, Washington University School of Medicine, St. Louis, Missouri, U.S.A., and Dr. Chi-Chin Huang Stroke Research Center, Taipei Medical University, Taipei, Taiwan

Tudor G. Jovin Department of Neurology, Stroke Institute, University of Pittsburgh Medical Center, VA Pittsburgh Health Care System, Pittsburgh, Pennsylvania, U.S.A.

Chelsea S. Kidwell Department of Neurology, Georgetown University and Washington Hospital Center, Washington, D.C., U.S.A.

Juliane Klehmet Department of Experimental Neurology Charité, Humboldt University, Berlin, Germany

Jin-Moo Lee Department of Neurology, Washington University School of Medicine, St. Louis, Missouri, U.S.A.

Weili Lin Department of Radiology, University of North Carolina at Chapel Hill, Chapel Hill, North Carolina, U.S.A.

Xinshe Liu Department of Neurology and M.I.N.D. Institute, University of California at Davis, Sacramento, California, U.S.A.

Romesh Markus Department of Neurology, St. Vincent's Hospital, and Department of Medicine, University of New South Wales, Sydney, Australia

Andreas Meisel Department of Experimental Neurology Charité, Humboldt University, Berlin, Germany

Patrik Michel Neurology Service, Centre Hospitalier Universitaire Vaudois, Lausanne, Switzerland

Günter Mies Max Planck Institute of Neurological Research, Cologne, Germany

Ramez R. Moustafa Department of Clinical Neurosciences and Stroke Unit, Addenbrooke's Hospital, University of Cambridge, Cambridge, U.K.

Adrian Parry-Jones Faculty of Life Sciences, University of Manchester, Manchester, U.K.

Anna M. Planas Institute for Biomedical Research of Barcelona (IIBB)–Spanish Research Council (CSIC), Institut d'Investigacions Biomèdiques August Pi I Sunyer (IDIBAPS), Barcelona, Spain

Jane F. Prosser Department of Neurology, Royal Melbourne Hospital, Melbourne, Victoria, Australia

Ruiqiong Ran Department of Neurology and M.I.N.D. Institute, University of California at Davis, Sacramento, California, U.S.A.

David Reutens Department of Medicine, Monash Medical Center, Melbourne, Victoria, Australia

Joachim Röther Department of Neurology, Klinikum Minden, Hannover Medical School, Minden, Germany

Nancy J. Rothwell Faculty of Life Sciences, University of Manchester, Manchester, U.K.

Johann R. Selvarajah Faculty of Medical and Human Sciences, University of Manchester, Manchester, and Salford Royal Hospitals NHS Foundation Trust, Salford, U.K.

Frank R. Sharp Department of Neurology and M.I.N.D. Institute, University of California at Davis, Sacramento, California, U.S.A.

Eku Shimosegawa Department of Radiology and Nuclear Medicine, Akita Research Institute of Brain and Blood Vessels, Akita, Japan

Jan Sobesky Department of Neurology, University of Cologne, Cologne, Germany

Neil J. Spratt Department of Medicine, University of Melbourne, National Stroke Research Institute and Austin Health, Melbourne, Victoria, Australia

Anthony J. Strong Department of Clinical Neuroscience, King's College London, London, U.K.

Lindsay Symon Institute of Neurology and the National Hospital, London University, London, U.K.

Alexander Thiel Department of Neurology, University of Cologne, Cologne, Germany

Omar Touzani University of Caen, Cyceron, Caen, France

Pippa J. Tyrrell Faculty of Medical and Human Sciences, University of Manchester, Manchester, and Salford Royal Hospitals NHS Foundation Trust, Salford, U.K.

Toshihiro Ueda Department of Neuroendovascular Therapy, Stroke Center, Tokyo Saiseikai Central Hospital, Tokyo, Japan

Katie Vo Mallinckrodt Institute of Radiology, Washington University School of Medicine, St. Louis, Missouri, U.S.A.

Steven Warach Section of Stroke Diagnostics and Therapeutics, National Institutes of Neurological Disorders and Stroke, National Institutes of Health, Bethesda, Maryland, U.S.A.

Lawrence R. Wechsler Department of Neurology, Stroke Institute, University of Pittsburgh Medical Center, Pittsburgh, Pennsylvania, U.S.A.

Karl Wienhard Max Planck Institute for Neurological Research, Cologne, Germany

Max Wintermark Department of Radiology, Neuroradiology Section, University of California at San Francisco, San Francisco, California, U.S.A.

Yang Wu Department of Biomedical Engineering, University of North Carolina at Chapel Hill, Chapel Hill, North Carolina, U.S.A.

Huichun Xu Department of Neurology and M.I.N.D. Institute, University of California at Davis, Sacramento, California, U.S.A.

Howard Yonas Department of Neurosurgery, University of New Mexico Health Sciences Center, Albuquerque, New Mexico, U.S.A.

Quan Zhu Department of Electrical and Computer Engineering, Duke University, Durham, North Carolina, U.S.A.

SECTION I: THE ISCHEMIC PENUMBRA: AN OVERVIEW

1 The Ischemic Penumbra—The Beginning

Lindsay Symon
Institute of Neurology and the National Hospital, London University, London, U.K.

INTRODUCTION

Like all cerebral vascular concepts, the ischemic penumbra did not arise from nowhere, and a little background information may be of interest. The concept emanated from The Neurosurgical Experimental Laboratory at The Institute of Neurology in Queen Square, which I formed when I came back from my Rockefeller year in the United States in 1964. I had been stimulated toward research by a number of people, including my old Professor of General Surgery in Aberdeen (Bill Wilson) and my mentor and friend in the National Institute for Medical Research (NIMR) (Wilhelm Feldberg). Though he had no direct interest in the cerebral circulation himself, he gave me facilities in his laboratory during an appointment as a Research Fellow of the Medical Research Council, and a great deal of encouragement. This enabled me to set up a program of experiments on collateral circulation (1–3). My surgical chief (Valentine Logue), although no research worker himself, saw a need for the development of basic scientific research in British neurosurgery and enthusiastically supported the formation of an experimental laboratory.

Since the days of Cohnheim, in the nineteenth century, the paucity of collateral circulation to the deep nuclei of the cerebral hemispheres had been recognized. By the middle of the twentieth century, however, there was persuasive experimental and clinical evidence that the situation in the cortical circulation was quite different and that functional anastomoses existed between the major vessels in the leptomeninges. The fluctuating nature of weakness following aneurysmal surgery and the curious phenomenon of the transient ischemic attack made it clear that some critical level of perfusion must exist in the brain. It was with these thoughts that I began the programs first in NIMR and then in Queen Square. Early work in the National Institute on the dog and cat had convinced me that the cerebral circulation of these animals, particularly the arrangements of the afferent and basal vessels, differed significantly from primates, and the subsequent work, both in NIMR and later, was carried out exclusively on large primates. The complexity of the preparations was such that I preferred to carry out all surgery myself. The basic technique was borrowed from electrophysiology, with a thermostatically warmed paraffin pool to protect the exposed cortex, and vascular occlusion carried out by the transorbital route (Fig. 1). Fortunately, my appointment to the staff of the National Hospital was combined with an appointment to the external staff of the Medical Research Council, and for many years, one day per week could be devoted to experimental surgery, each experiment occupying many hours, and data analysis then extending over most of the next week.

With the support of the Medical Research Council, therefore, experimental primate research was undertaken at first with a single technician and a variety of Fellows, and then with the invaluable help of Neil Branston, a young physiologist who came back to Britain from John Meyer's laboratory in the United States (Fig. 2).

At that time regional cerebral blood flow (RCBF) was a topic of great interest. Lassen and Ingvar had pioneered the xenon clearance technique in man and had begun the Association, which subsequently became the International Society for Cerebral Blood Flow and Metabolism. At the National Hospital there was a group of interested clinicians: John Marshall, the Chairman of the group; and Ralph Ross-Russell, both physicians; George Du Boulay, a radiologist; and myself, a surgeon and experimentalist. Through these and the International Society we had a great deal of communication across Europe and with one another. The xenon clearance technique was suitable for man but not very suitable for the analysis of animal RCBF—the probes were simply too large. We were fortunate, therefore, in being joined for a year by Emil Pasztor,

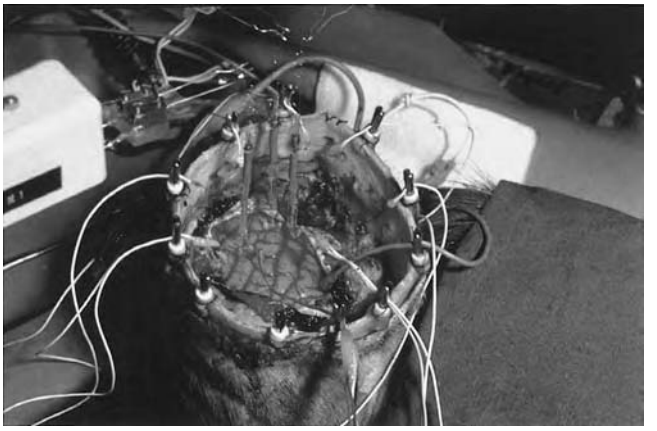

FIGURE 1 (*See color insert.*) The preparation showing multiple electrodes inserted into the cerebral cortex in a paraffin pool.

subsequently the director of the Institute of Neurosurgery in Budapest, who had spent some time in Norway learning the technique of hydrogen clearance. The electronics of the system were far from adequate, however, and it was Neil Branston and Nick Dorsch, research fellow from Australia, subsequently our first assistant in the clinic and now neurosurgeon in Westmead Hospital in Sydney, who put together an adequate electronic package to enable us to make multipoint RCBF studies using the technique of hydrogen clearance. By this method we were able to map the autoregulatory capacities of the cerebral circulation and to document the effects of middle cerebral occlusion in the primate, studying autoregulation and negative reactivity, which had already become known as intracerebral steal (4–7). In parallel with this, the recovery experiments conducted by myself and Kemp Clark from Dallas, Texas, U.S.A. who was on a sabbatical, demonstrated the close similarity between the experimental stroke in the primate and stroke in man (7).

The next step came with the use of evoked responses to determine the degree of reduction in cerebral blood flow (CBF) necessary to abolish electrical activity, and from this emerged the concept of thresholds of ischemia, evoked response failing pretty swiftly below levels of 20 mL/100 gU of RCBF and completely silent by about 12 mL/100 g per minute. We found that this threshold of failure could be re-crossed by the simple elevation of blood pressure, since autoregulation had failed in the ischemic area and pathology could, therefore, be fought by physiological means (8). We took this into the clinic in the technique of induced hypertension to combat ischemic events following aneurysm surgery, and in this we closely paralleled work done by Bill Hunt and his associates in Cleveland, Ohio, U.S.A.

FIGURE 2 (*See color insert.*) Lindsay Symon (*left*) and Neil Branston (*right*) working on the penumbral model.

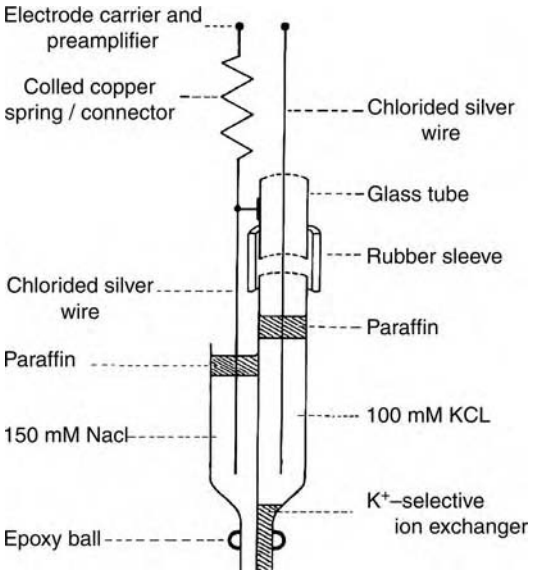

FIGURE 3 A diagram of a double-barreled microelectrode. The twin barrels are fused together and then drawn out to a twin point—a few microns in diameter. The electrode assembly is supported on its electrical connections formed as a spring. The collar allows it to sit gently on the pia, and assures that it does not penetrate beyond the cortex. A third barrel for simultaneous measurement of calcium and potassium could be added. Details of the construction of these electrodes may be found in the Ph.D. theses of Robert Pullen and Robert Harris in the library of the Institute of Neurology, University of London, United Kingdom.

In the course of discussion at the International CBF meeting in Aviemore in Scotland, Branston and I discussed with the Scandinavians the possible explanation for electrical failure. Hodgkin's work on electrical transmission in nerves was well known and it seemed to me that some disturbance of potassium metabolism might well hold the key. Dieter Heuser in Eberhard Betz's laboratory in Tubingen had developed an electrode using ion sensitive resin, which, in combination with a reference electrode, enabled measurement of potassium ions in brain tissue during changes in circulation or other circumstances. Jens Astrup from Lassen's laboratory in Copenhagen, Denmark, had gone to Tubingen to study these electrodes, and had already successfully used them. We invited him across to London to combine potassium and electrophysiological measurements with determinations of RCBF. The original electrodes, large and with separate active and reference barrels, were, however, unsuitable for multiple measurements. In the laboratory at that time we had some very deft young technicians, Robert Pullen and Robert Harris, who miniaturized these electrode systems by combining the reference and ion selective barrels together in a tiny electrode which, properly balanced, could sit upon the pia just penetrating the cortex. Thus refined, potassium electrodes could be used in multiple sites and, indeed, eventually a triple-barreled ion-sensitive microelectrode (ISM) was used to monitor both potassium and calcium (Fig. 3). These ISMs enabled us to measure focal potassium concentration in multiple areas of reduced blood flow or in the region of an evoked response.

What then emerged was that at a critical level of reduction of CBF, potassium, normally at a very low concentration in the extracellular space, suddenly increased; clearly membrane failure had occurred and potassium was leaking from the cells into the extracellular space (Fig. 4). In subsequent experiments, a similar level was detected for calcium, which went in the reverse way, having been plentiful in the extracellular space it suddenly declined, indicating that it had passed from the extracellular space into cells. The level of this membrane failure was very sharp—around 10 mL per 100 g per minute—and very clearly distinct both in terms of RCBF and in terms of area from the failure of the evoked response. Once again, both thresholds could be re-crossed by prompt elevation of the systemic arterial blood pressure (9,10). We then had experimental evidence of failure of evoked response without failure of membrane function in an area surrounding a more dense area of ischemia, where membrane function also failed (Fig. 5). Examining the autopsy data from two-year infarcts in the recovery primates, which clearly documented the extent of infarction, it was clear that this was vastly smaller than the area of brain involved in electrical silence in the acute experiments.

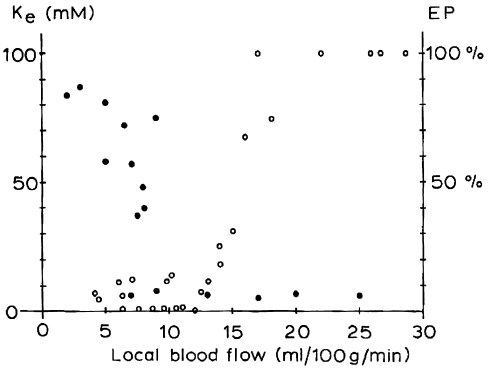

FIGURE 4 The two thresholds recorded in a group of experiments from somatosensory evoked responses and adjacent potassium sensitive micro-electrodes. Potassium concentration on left vertical axis and evoked potential amplitude on the right. *Abbreviations*: EP, evoked potential amplitude; K_e, potassium (symbol).

We, therefore, had evidence that an infarct, at any rate in the acute stages, was surrounded by an area of brain from which evoked responses could not be obtained, and yet in which the lethal phenomena of membrane failure had not occurred. It was also clear that in the acute circumstances the area of electrical silence could be reduced by elevation of the blood pressure and also the threshold for membrane failure re-crossed if the efforts to reperfuse were made in time. Interestingly, we also observed spontaneous transient increases in extracellular potassium from time to time in this area. Though we could not at that time demonstrate propagation of these transients, it seemed possible that they might be involved in recruitment of the ischemic area, with enlargement of the area of the ischemic core.

We took this material into the clinic, reinforcing our view that the correct way to treat postoperative ischemia due to vasospasm or other reasons, following aneurysm surgery, was elevation of the systemic blood pressure with metaraminol and this, together with hypervolemia, became a fairly standard neurosurgical maneuver (11). I well remember a postoperative aneurysm patient who developed arm weakness the day following surgery. As John Marshall, my physician colleague, watched we resolved the hemiparesis by infusing metaraminol intravenously. Over the next few hours, if the systemic blood pressure was allowed to fall, the hemiparesis would recur, to resolve again as the blood pressure was raised. Such a phenomenon commonly would last for a day or two, and as the presumed vasospasm receded, the blood pressure could be returned to normal levels. John was convinced!

At that time Anthony Strong, who writes elsewhere in this volume, was one of our research fellows and I recall going across Guildford Street from the lab to the dining room discussing this curious zone, which we had documented. It seemed to me that it was rather like the area around the center of a candle flame, where there is a small bright zone known as the penumbra. We considered that the correct name for this area was the ischemic penumbra and so it proved. Astrup and Lassen pointed out that in a complete eclipse of the sun there was a

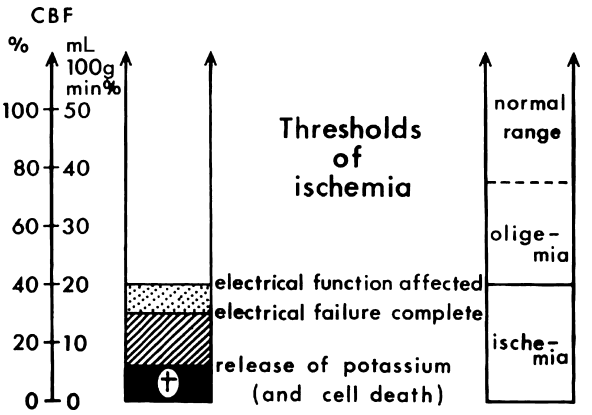

FIGURE 5 A figurative diagram of thresholds of ischemia from the results of our experiments. *Abbreviation*: CBF, cerebral blood flow.

FIGURE 6 (*See color insert.*) Lindsay Symon surrounded by some of his team in his laboratory. (*Left to right*) Neil Branston; Terry Hope, Research Fellow; Robert Harris, Technician; Lindsay Symon; Anthony Strong, MRC Fellow; Jens Astrup, Visiting Fellow.

bright zone around which was also known as the penumbra. Whichever one likes to take as the scientific basis of the sobriquet is a matter of choice.

As with all concepts, the application of an acceptable name popularized the concept, and the term penumbral ischemia was born. Subsequently, in our own lab, Obrenovitch devoted a great deal of time by careful micro-profusion systems, analyzing the movement of amines in relation to penumbral ischemia (11–13). In particular, he demonstrated that the predominant interest in glutamate as a source of cellular damage in ischemia was unjustified. Indeed, glutamate simply happened to be there in great concentration, as the others amines emerged in membrane failure at the same time as glutamate, but, being in much smaller concentration, were much more difficult to measure. It can be seen that all these experiments were exacting and required a team effort (Fig. 6). The concept of penumbral ischemia, therefore, has undoubtedly stimulated a great deal of experimental and clinical research, as the remainder of this volume will attest.

But that's how it was in the beginning.

REFERENCES

1. Symon L. Observations on the leptomeningeal collateral circulation in dogs. J Physiol 1960; 154:1–14.
2. Symon L. Studies of leptomeningeal collateral circulation in Macacus rhesus. J Physiol 1961; 159:68–86.
3. Symon L. A comparative study of middle cerebral pressure in dogs and macaques. J Physiol 1967; 191(3):448–465.
4. Pasztor E, Symon L, Dorsch NW, Branston NM. The hydrogen clearance method in assessment of blood flow in cortex, white matter, and deep nuclei of baboons. Stroke 1973; 4(4):556–567.
5. Symon L, Pasztor E, Dorsch NW, Branston NM. Physiological responses of local areas of the cerebral circulation in experimental primates determined by the method of hydrogen clearance. Stroke 1973; 4(4):632–642.
6. Symon L, Pasztor E, Branston NM. The distribution and density of reduced cerebral blood flow following acute middle cerebral artery occlusion: an experimental study by the technique of hydrogen clearance in baboons. Stroke 1974; 5(3):355–364.
7. Symon L, Dorsch NW, Crockard HA. The production and clinical features of a chronic stroke model in experimental primates. Stroke 1975; 6(5):476–481.
8. Branston NM, Symon L, Crockard HA, Pasztor E. Relationship between the cortical evoked potential and local cortical blood flow following acute middle cerebral artery occlusion in the baboon. Exp Neurol 1974; 45(2):195–208.
9. Branston NM, Strong AJ, Symon L. Extracellular potassium activity, evoked potential and tissue blood flow. Relationships during progressive ischemia in baboon cerebral cortex. J Neurol Sci 1977; 32(3):305–321.
10. Astrup J, Symon L, Branston NM, Lassen NA. Cortical evoked potential and extracellular K+ and H+ at critical levels of brain ischemia. Stroke 1977; 8(1):51–57.
11. Symon L. Disordered cerebro-vascular physiology in aneurysmal subarachnoid hemorrhage. Acta Neurochir (Wien) 1978; 41(1–3):7–22.

12. Obrenovitch TP, Urenjak J, Richards DA, Ueda Y, Curzon G, Symon L. Extracellular neuroactive amino acids in the rat striatum during ischemia: comparison between penumbral conditions and ischemia with sustained anoxic depolarisation. J Neurochem 1993; 61(1):178–186.
13. Obrenovitch TP, Zilkha E. High extracellular potassium, and not extracellular glutamate, is required for the propagation of spreading depression. J Neurophysiol 1995; 73(5):2107–2114.

2 The Ischemic Penumbra: Overview, Definition, and Criteria

Geoffrey A. Donnan
National Stroke Research Institute, Austin Health, University of Melbourne, Melbourne, Victoria, Australia

Jean-Claude Baron
Department of Clinical Neurosciences and Stroke Unit, Addenbrooke's Hospital, University of Cambridge, Cambridge, U.K.

Stephen M. Davis
Department of Neurology, Royal Melbourne Hospital and University of Melbourne, Melbourne, Victoria, Australia

Frank R. Sharp
Department of Neurology and M.I.N.D. Institute, University of California at Davis, Sacramento, California, U.S.A.

INTRODUCTION

Prior to the 1970s, ischemic tissue death was generally believed to be relatively sudden and irreversible. When compared to other areas of basic research, the number of investigators involved in experimental cerebral ischemia was relatively few, so progress was slow. Although clinicians were aware of the clinical paradigm in which transient cerebral ischemic attacks occurred with a full recovery within 24 hours without any evidence of cerebral infarction, explanations such as "hypertensive crisis" or "arterial spasm" were proposed to account for these episodes. In the mid-1950s, however, the embolic theory for transient ischemic attacks (TIAs) became widely accepted, which stimulated a number of investigators to consider the possibility that the ischemic process itself was potentially reversible and its progression to infarction was not inevitable. Interestingly, it was later shown using modern imaging techniques such as computed tomography (CT) and magnetic resonance imaging (MRI) that small cerebral infarcts do occur in a proportion of patients who present with transient ischemic attacks (1), although these infarcts were usually quite small. In the pre-imaging era it was not possible to make these in vivo observations. Nevertheless, clinician researchers began to investigate the mechanisms for the potential reversibility of the ischemic process.

Indeed, as outlined in the preceding chapter, in the early 1970s Lindsay Symon and his group at Queen Square started to think about the issue of the relationship between tissue function, ischemia, and infarction in some detail (2–8). They used a baboon model of cerebral ischemia induced by clipping of the middle cerebral artery to demonstrate for the first time that there was a mismatch between cerebral function as documented by somato-sensory evoked potentials and cerebral blood flow (CBF) at various threshold levels (2). They were also able to show that the region of cerebral dysfunction, as recorded by somato-sensory potentials, could be restored to its previously normal state with improvement of CBF. They later coined the term "ischemic penumbra" for this region, which was functionally impaired but structurally intact (8). The term was particularly appropriate in that it captured the ephemeral character of the tissue it described and its physical location around the infarct core. In astronomy, the penumbra refers to "the partly shaded outer region of the shadow cast by an opaque object, especially that of the shadow cast by the earth or moon over an area experiencing a partial eclipse" (from the Latin paene "almost" and umbra "shadow") (9).

Three separate brain compartments were identified by Symon et al. in their baboon model of focal cerebral ischemia as CBF was progressively lowered. That is, oligemic tissue where

cerebral function was normal in spite of the reduction in blood flow, the penumbra where cerebral function (somato-sensory evoked potentials) became impaired at about 20 mL/100 g cerebral tissue/min and the ischemic core with thresholds in the baboon model established at about 6 to 10 mL/100 g tissue/min (8). The original diagram illustrating these thresholds is shown in Figure 5 of Chapter 1. Interestingly, during carotid endarterectomy in humans it was shown that electrical activity was ablated at about the same level of CBF reduction of 20 mL /100 g/ min (10,11).

At about the time that the concepts of the ischemic penumbra were being developed, remarkable advances were also being made in understanding the mechanisms of cerebral ischemia and the complexity of the ischemic cascade. The excito-toxicity model of cellular damage was proposed by Olney in 1969 (12) and later (1984) it was shown that components of the cascade could be attenuated and some neuroprotection afforded by the glutamate antagonist MK801 (13). Since it seemed likely that much of the ischemic cascade that occurs in the core of the infarct was taking place within the ischemic penumbra, this cemented its importance and placed it at the forefront of clinical and basic cerebral ischemia research.

While the time dependent nature of the development of infarction was appreciated by earlier investigators, it was brought into sharp relief by Jones et al. who meticulously established thresholds for focal cerebral ischemia in awake monkeys with reference to time of vessel occlusion (Fig. 1) (14). This was also confirmed by Garcia et al. (15). By the early 1980s, claims were being made that the ischemic penumbra may exist in humans using xenon CBF methodology, a technique which had been used in patients with stroke since the 1960s (16). However, the first demonstration of the existence of the ischemic penumbra in humans was accomplished using positron emission tomography (PET) in 1980 and 1981 (17,18). Here, the concept of a mismatch between reduced CBF in the presence of a relatively preserved, or even normal, cerebral metabolic rate of oxygen consumption ($CMRO_2$) was introduced. As a result of this mismatch an increased oxygen extraction fraction (OEF) occurred, usually above the 30% to 40% seen in normals up to a theoretical maximum of 100%. Other investigators also used this approach and, in particular, showed that the penumbra was more often distributed in the cerebral cortex in humans with quite marked increases in OEF and less so in the basal ganglia region (19–26). These early studies using PET techniques, made no attempt to determine if the penumbra was in white as well as grey matter because of the low resolution of the images. Reassuringly, the topographical distribution of the penumbra was similar to that demonstrated in monkeys and other subhuman primates and was documented to persist for as long as 48 hours after stroke onset (24).

Also during the 1980s MRI made its first appearance. After the initial excitement of the realization that probable areas of infarction could be seen early after the onset of symptoms, perhaps even minutes using diffusion weighted imaging (DWI) (27), the technique of perfusion weighted imaging (PWI) was developed and soon superimposed on the DWI image. Indeed, it was Warach and Edelman who inferred that a DWI/PWI mismatch might represent the

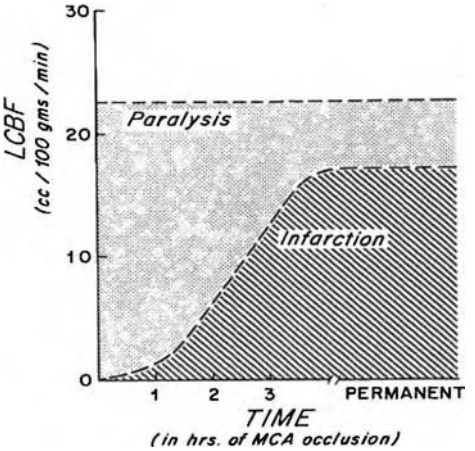

FIGURE 1 Ischemia thresholds. When local cerebral blood flow (LCBF) falls below about 23 cc/100 gm/min, reversible paralysis occurs. Even profound ischemia is reversible for a brief time. When 1CBF falls below 10 cc/100 gm/min for two hours, or below 18 cc/100 gm/min during permanent occlusion, irreversible infarction occurs. *Abbreviations*: MCA, middle cerebral artery; LCBF, local cerebral blood flow. *Source*: From Ref. 14.

penumbra and provide a practical, in vivo method for assessing individual patients with potentially reversible penumbral tissue (28). However, it was Baron's group who first proved the presence of the ischemic penumbra in humans using multitracer PET technology in a series of studies during the mid-90s (29–33). To achieve this, they combined in the same frame of reference the acute stage PET and late stage structural imaging (defining the final infarct), and proposed an operational model of the penumbra as contrasted with the other three tissue categories (i.e., core, oligemia, and normal). To validate the presence of penumbra, they compared these topographical compartments with acute stage and outcome neurological scores, and were able to verify their hypotheses that the volume of (core + penumbra) was significantly correlated with acute stage neurological scores, and that the volume of the eventually noninfarcted penumbra was positively correlated with neurological recovery (i.e., the change in scores from the acute stage to the outcome endpoint). Using this model, they also showed that, whereas in some patients no penumbra was present as early as a few hours after stroke onset, in others as much of 52% of the final infarct was still in a penumbral state as late as 16 hours after onset. Although factors influencing this duration in individuals remained uncertain, they emphasized the idea of extending the time window in individual patients using technologies to image the ischemic penumbra (34).

Two other PET radio ligands were introduced at about this time, which further advanced our understanding of the penumbra. C11-flumazenil PET pioneered by Heiss et al. (35,36) exploited the knowledge that flumazenil bound to central diazepam receptors which were located on neurons and that C11-flumazenil PET was able to document pan and selective neuronal loss (37). Selective neuronal loss in focal ischemia had been first suggested in humans by Lassen during the early 1980s (38,39). Although only assessable in the cortex, the mismatch between CBF and loss of C11-flumazenil binding proved to be a useful penumbral marker. The loss of C11-flumazenil binding was predictive of infarction and hence was a useful means of identifying the infarct core. For example, this technique was used to show that as much as 70% of tissue may be already infarcted in the cortex as early as three hours poststroke in selected patients, emphasising the need for very early reperfusion strategies to be implemented if significant volumes of tissue were to be salvaged and, correspondingly, better clinical outcomes be achieved (35). It was pointed out, however, that in other patients of this series, large fractions (up to 85%) of the final infarct were still viable even as late as 12 hours after onset (40). In parallel with these findings, the Melbourne group developed 18F-fluoromisonidazole (18FMISO) as a penumbral marker and validated this in humans (38,39,41–45). They were able to confirm in a systematic way that penumbral duration extended well out to 48 hours in selected patients and, even more importantly, the proportion of penumbra salvaged was independent of time and that spontaneous tissue salvage beyond 12 hours continued to be associated with clinical improvement and better clinical outcomes (43).

Based on the previously mentioned outcomes, at the systems level, the penumbra emerges as a tissue that is neurophysiologically impaired; hypoperfused and hypoxic (as evidenced by high OEF or 18F-MISO uptake) but metabolically preserved (as evidenced by $CMRO_2$ and C11-flumazenil binding above certain thresholds); at risk of infarction but that can be rescued with early therapy; and whose rescue would result in better functional recovery, in proportion with the amount of tissue saved.

In parallel with the earlier studies, however, significant advances had been made by the new millennium in the basic science of cerebral ischemia: there was a better understanding of the ischemic cascade in both grey and white matter, it was shown that blockade of numerous points within the cascade could be exploited as neuroprotective mechanisms and the genomics revolution had opened new possibilities in understanding the penumbra and ischemic process (46). The concept of the "molecular penumbra" was introduced in which the genomic response to cerebral ischemia was found to be topographically distributed around the infarct core (47). These advances in the basic science of cerebral ischemia resulted in the penumbra being variously defined at the cellular as well as molecular levels, occasionally to embrace any phenomenon that surrounds the core, regardless of the perfusion level or time since occlusion—even defining events that followed reperfusion. At the same time, in the clinical sphere, CT perfusion was found to be a useful alternative to MR in providing in vivo images of the ischemic penumbra in humans (48,49). The technique of CT perfusion had been in existence for some time but

was rendered more practical by the development of spiral CT that enabled multislice images to be generated within a very short timeframe. Using an injected bolus of gadolinium, the infarct core was defined by a collapse of cerebral blood volume (CBV) of <40%, while the penumbra was identified as a mismatch between the area of hypoperfusion and the CBV identified infarct core (48,49). It is hoped that newer MR techniques such as BOLD imaging, in which areas of increased OEF may be identified (50), and the use of arterial spin labeling in which quantitative CBF information may be generated may further advance our understanding of the in vivo imaging of the ischemic penumbra (51,52).

However, as can be seen from the preceding discussion, there is a real need to have a reasonable definition of the penumbra, which encompasses the concept of the dynamic changes involved and to develop criteria by which many of the penumbral markers can be judged.

THE DEFINITION OF THE ISCHEMIC PENUMBRA

There have been a number of definitions used over the years, the majority of which are listed in Table 1 (8,53–57). The following modification of a previous definition (57) embodies most of the concepts discussed earlier:

> The ischemic penumbra is ischemic tissue which is functionally impaired and is at risk of infarction but has the potential to be salvaged by reperfusion and/or other strategies. If not salvaged this tissue is progressively recruited into the infarct core, which will expand with time into the maximal volume originally at risk.

CRITERIA FOR THE ISCHEMIC PENUMBRA

When developing criteria for the existence of the ischemic penumbra using specific markers, one needs to incorporate the concepts of the identification of a tissue under ischemic stress, which has the capability of being salvaged and when this does occur it translates into improved clinical outcomes. For clinical purposes, any penumbral measure or marker which does not fulfil these criteria (when tested) would be difficult to endorse as a true representation of the ischemic penumbra as it is currently understood. The criteria presented in Table 2 are a refinement of earlier thoughts on this subject (45,57,58).

TABLE 1 Definitions of the Ischemic Penumbra

Definition	Authors
The condition of the ischemic brain with flow between two thresholds—the upper threshold of electrical failure and the lower threshold of energy failure and ion pump failure. This tissue may recover without irreversible damage if residual blood flow is maintained on the safe side of the threshold for energy and ion pump failure.	Astrup J et al. (8)
Penumbral tissue is an equivalent to "viable tissue," the fate of which is undetermined because it might turn into necrosis but it still has the potential of preserving morphological integrity and of functional recovery.	Heiss WD and Graf R (53)
An area that can be rescued by pharmacological agents.	Kinouchi H, Sharp FR, Koistinaho J, et al. (54)
A region of constrained blood supply in which energy metabolism is preserved.	Hossmann KA et al. (55)
Fundamentally reversible tissue.	Hakim AM (56)
Severely ischemic, functionally impaired tissue at risk of infarction that will be saved if reperfused before it is irreversibly damaged, but that otherwise will be progressively recruited into the core until maximum infarct extension is reached.	Baron JC (57)
Ischemic tissue, which is functionally impaired and is at risk of infarction but has the potential to be salvaged by reperfusion and/or other strategies. If not salvaged this tissue is progressively recruited into the infarct core, which will expand with time into the maximal volume originally at risk.	Donnan GA et al. (as above in this chapter)

TABLE 2 Criteria for the Ischemic Penumbra

1. An area of hypoperfused, abnormal tissue with physiological and /or biochemical characteristics consistent with cellular dysfunction but not death.
2. The tissue is within the same ischemic territory as the infarct core.
3. Demonstration that the tissue can survive or progress to pan-necrosis.
4. Salvage of this tissue is related to better clinical outcome.

IDENTIFYING THE ISCHEMIC PENUMBRA: ESTABLISHED MARKERS

Numerous markers have been used to identify the ischemic penumbra since its first description in the 1970s. Interestingly, not all have been validated conclusively (as yet) according to our criteria outlined in Table 2. These markers are mainly used in animal models where it is more difficult, or not even within the scope of the investigators, to establish a relationship between tissue salvage and improved clinical outcome. Typically, animals are sacrificed to obtain an immediate in vitro quantification of the distribution of the marker. For example, FMISO as an hypoxic marker in animal models has not, as yet, fulfilled this criterion (59–61). One may ask as to why there are so many penumbral markers spanning the animal experimental and clinical spheres. The main reason is that no marker is perfect and each was developed with a different purpose in mind. This is particularly so in experimental studies in which animal models, tissues or cellular preparation are used. Here there are many instances where a "penumbral" model has been developed more to study biochemical processes than study the characteristics of the penumbra per se. For example, the mismatch between protein synthesis and energy depletion in the rat model of cerebral ischemia was first proposed to study the differential expression of the HSP72 gene in regions of ischemic stress (62). Conversely, the MR DWI/PWI mismatch concept was very much driven by the need to have a simpler and more generalizable technique than PET to identify potentially salvageable tissue (28). This was in an era when potential therapies were looming but none at that time were proven to be effective. An important consideration is that while each of these markers is identifying tissue which fulfils the criteria for the ischemic penumbra, there is no doubt that each identifies somewhat different but overlapping volumes. For example, protein synthesis is quite sensitive to CBF reductions and probably becomes impaired at around 30 mL/100 g/min, whereas, electrical impairment begins at around 20 mL/100 g/min (55). These differences do not diminish the usefulness of each of them as markers, which the reader must take into account. The common feature to all techniques is that they can be used to identify variable volumes of ischemic brain tissue that is potentially salvageable. In other words, tissue that is a target for therapy is demarcated. One must bear in mind the caveats associated with each technique when viewing a summary of these with the number of criteria fulfilled in Table 3.

Mismatch Between Electrical Function and Cerebral Blood Flow

As mentioned earlier, this is the original technique around which the whole concept of the ischemic penumbra was built (2–8). Hence, it has the huge advantage of precedent and was used to establish the threshold for oligemic, penumbral, and ischemic core interfaces, which have been confirmed in numerous models. However, it is now rarely used because it is a very complicated measurement (see Chapter 1) and there are better measures of tissue dysfunction giving improved spatial resolution. Similarly, the measures of CBF have improved from the days of the use of hydrogen electrodes, which only gave a very focal picture of blood flow in the immediate vicinity of the electrode tip. The original baboon model of focal cerebral ischemia with clipping of the middle cerebral artery is also used less commonly because of the expense and ethical difficulties with its use. The technique was first validated according to our criteria in that an area of hypoperfused abnormal tissue with physiological characteristics having cellular dysfunction but not death was identified by somato-sensory evoked potentials, topographically this area surrounded the final infarct core and it was shown that this tissue was salvaged or died depending on the state of reperfusion (6,62–64). Further, salvage of the tissue as evidenced by return of somato sensory evoked potentials (SSEP) amplitudes were associated with better clinical outcome (6,62–64).

TABLE 3 Established Markers of the Ischemic Penumbra

Marker	Technique	Criteria fulfilled (by number from Table 2)	Key references
1. Mismatch between electrical function and CBF	SEP and H2 electrodes in Baboon stroke model	1, 2, 3	Branston et al. (3) Astrup et al. (7) Jones et al. (14)
2. Increased oxygen extraction fraction	Multitracer PET animal models and humans	1, 2, 3, 4	Baron et al. (85)
3. Mismatch of neuronal integrity and CBF	Flumazenil PET and CBF measure in animal models and humans	1, 2	Heiss et al. (36)
4. Mismatch PWI and DWI	MR in animal models and humans	1, 2, 3, 4	Baird and Warach (86)
5. Hypoxic marker	[18F]FMISO PET in animal models and humans	1, 2, 3, 4	Read et al. (87) Markus et al. (43)
6. Mismatch of cerebral protein synthesis and energy depletion	CPS and ATP levels measured in animal models	1, 2	Hata et al. (88)
7. Mismatch between molecular expression of proteins and CBF	In situ hybridization techniques in animal models	1, 2	Sharp et al. (47)
8. Mismatch between CBV (infarct core) and perfusion impairment (penumbra)	CT perfusion in humans	1, 2, 3, 4	Wintermark et al. (48,49)

Abbreviations: CBF, cerebral blood flow; CBV, cerebral blood volume; CPS, cerebral protein synthesis; DWI, diffusion weighted imaging; MR, magnetic resonance; PET, positron emission tomography; PWI, perfusion weighted imaging; SEP, sensory evoked potentials.

Mismatch of Cerebral Blood Flow and Cerebral Metabolic Rate of Oxygen with Increased Oxygen Extraction Fraction Using Multi-tracer Positron Emission Tomography

As the modality in which the ischemic penumbra was first demonstrated in humans, this technique is regarded as the penumbral gold standard (17,18). Its significant advantage is not only its early precedence in the field but the biological plausibility of the use of CBF and $CMRO_2$ parameters, given that ischemia is driven by reduction in CBF and the wellbeing of cells is evidenced by their oxygen consumption. The generation of the additional marker of oxygen extraction fraction (OEF) is also useful since it emphasizes the presence of cells under stress with increased oxygen extraction as CBF reduces to a trickle (57). The significant disadvantage of multi-tracer PET is its high cost, limited availability, the need for arterial sampling for quantitation, and the cumbersome, time consuming nature of the procedure. While the measurement of CBF has been shortened by the use of the bolus injection technique (64) rather than steady state (it should be noted that while the CBF bolus technique is quicker, it is also more complicated because of the need for a dynamic arterial input function and much less accurate in situations of low blood flow), oxygen consumption still requires inhalation of $^{15}O_2$ with a mask which can be difficult in some patients. Nevertheless, from this technique was generated all the original human data on the ischemic penumbra and it still acts as an important comparator for the more recently developed clinical techniques.

Mismatch Between Cerebral Blood Flow and Neuronal Integrity

While not able to live in isolation without their glial support structures, neurons are certainly the most important cells in the central nervous system. Hence, to have a measure of neuronal integrity imaged in vivo is a considerable advance. As mentioned earlier, the work of Lassen et al. (38) had suggested that neuronal integrity was not an all or none phenomenon and may

be an important consideration in the penumbral story. Fortuitously, central benzodiazepine receptors are located on neurons only and may be labeled by flumazenil and conveniently imaged by PET using the C11 radioligand (36). The mismatch between CBF and neuronal integrity as a marker of potentially salvageable tissue is clinically useful and represents a significant advance (35). The main disadvantage is that the ligand can currently be imaged only by PET with all the aforementioned cost and availability limitations. Of interest, a single photo emission computed tomography (SPECT) analogue of flumazenil, iomazenil has been used clinically (65). Another limitation is the obvious restriction to imaging in grey matter in which neurons lie so that the 50% of human brain, which represents the white matter compartment is unable to be imaged (36,45,66,67).

Validation against our suggested criteria are, as yet, incomplete but the mismatched tissue certainly fulfil criteria 1 and 2. There has also been some validation against triple tracer PET showing that increased areas of OEF correlate approximately with the CBF/neuronal integrity mismatch regions. Areas with 11C-flumazenil (FMZ) binding decreased below this threshold corresponded to regions with markedly decreased $CMRO_2$ (<60 micromol/100 g/min) (68).

Magnetic Resonance Diffusion Weighted Imaging/Perfusion Weighted Imaging Mismatch

It is reasonable to say that MR has "popularized" the concept of the ischemic penumbra since the technique has become commonly used by clinicians, even those not actively involved in research. Its huge advantage is its noninvasive quality with no radiation involved such that repeated studies can be performed. It is more generally available than PET, although is still moderately expensive and not as universally available as CT perfusion.

Its disadvantages relate to those experienced for MR generally, that is; inability to image those with claustrophobia, unable to lie still during the imaging procedure, or the presence of pacemakers or metallic objects in situ. The problem of patient movement is an issue because of the duration of most studies, although this is being reduced down to 15 to 20 minutes, and even shorter with recent MR designs (69). All of these issues can be a problem in elderly stroke patients such that not all patients are eligible for study. There are also some uncertainties about the meaning of the mismatch in that the interface between oligemia, penumbra, and infarct core remains uncertain (70). The initial belief that DWI represented infarct core has proven to be more complex than originally proposed and is the subject of ongoing research. Again, the measure is semiquantitative, which is a further limitation, although apparent diffusion coefficient (ADC) is an absolute measurement on the DWI. However, there is no doubt that this technique represents one of the most significant advances in penumbral imaging and has been validated according to our four criteria.

Hypoxic Marker with ^{18}F-Fluoromisonidazole Positron Emission Tomography

This marker was developed because of the need to have a more simple and direct image of the ischemic penumbra using PET technology given the complexities of the approaches mentioned earlier (41–44). Hence, its advantage is the directness of its measure (no mismatch required) and lessening of coregistration errors and the simplicity of the technique (only one image required over a 20-minute period). However, like its other PET counterparts, it suffers from the other PET limitations of cost and access problems. A further limitation is that imaging has to be delayed two hours after administration of the tracer to allow for equilibrium, which hinders its clinical use, and is more a research than clinical tool. It has been validated by all four criteria for the ischemic penumbra in that, uptake of the hypoxic marker suggests that cells are biologically active although under hypoxic stress, the marker has been shown to be associated with the infarct core, in the same vascular territory, the tissue has been shown to either survive or become infarcted and the proportion of salvaged tissue directly correlates with better clinical outcomes (43).

Mismatch of Cerebral Protein Synthesis and Energy Depletion

Various animal models and experimental approaches have been used to provide a basic understanding of the sequence of events that occur in the ischemic penumbra in the brain.

One of the earliest descriptions of a biochemical penumbra, beginning in the 1970s by Hossmann et al., was the local decrease of cerebral protein synthesis that occurs following focal ischemia. Protein synthesis falls once CBF decreases below 50% of normal (50 mL/100 g/min in rodent models; 25 mL/100 g/min in primate and man). Protein synthesis remains low in areas that go on to infarct, and recovers in the areas of the penumbra that survive the focal ischemia (55). Importantly, this group further characterized these changes of protein synthesis and correlated them with ATP in the same regions. Indeed, they were able to compartmentalize tissue in a region of focal ischemia as normal [ATP and cerebral protein synthesis (CPS), preserved]; penumbral tissue (ATP preserved, but CPS decreased); and infarct core (ATP and CPS decreased) (62). The penumbra, as described by preserved ATP but decreased CPS, is an area that can be salvaged pharmacologically and improve neurological outcome, thus fulfilling the tenets for a marker of the penumbra. In addition, this ATP/CPS definition of the penumbra correlates with molecular markers, including Hsp70 as noted in the following sections.

Other Biochemical Markers of the "Penumbra"

Many changes of the biochemistry of the brain occur following a focal decrease of blood flow. Hossman provided an excellent review of some of these changes (55). Though decreased protein synthesis is one of the first events to occur during focal ischemia in brain, there are subsequently hundreds, if not thousands of changes in the tissue related to decreased oxygen and glucose delivery to the tissue. One of these is the change of gene expression as noted in the next section. In addition, there are immediate changes of oxygen extraction, glucose transport, and as oxygen becomes limiting, increases of lactate and decreases of pH take place. This is followed by changes of transport of glucose, glutamate, and many other molecules. As energy reserves fail with falling ATP and phosphocreatine, the ionic gradients fail and tissue infarction occurs. This is outlined in Figure 2, Chapter 3 of this book, as derived from Hossmann (55). Some of these processes occur only in the core where infarction occurs. Some of the changes occur in the region immediately adjacent to the core, in an area smaller than the clinically defined penumbra. Other changes occur in the tissue described as "penumbra" throughout this book. Finally, other changes occur in a region probably much wider than the penumbra—potentially in all of the tissue where blood flow decreased below normal and potentially in tissues even connected to the ischemic tissue but which were never actually ischemic. These changes are all relevant in terms of understanding the processes that result in infarction or survival of cells in the penumbra, but most of them do not correlate with the region that can be described as a salvageable penumbra with improved function.

Molecular Markers of the Penumbra

Concurrent with better understanding of the biochemical events occurring in the penumbra, a better understanding of the genes expressed following focal ischemia has developed. Sharp et al. first proposed that regions where Hsp70 protein and mRNA were expressed represented the region defined as the clinical penumbra (54,71). Indeed, Hata et al. went on to show that the penumbra described by Normal ATP but decreased CPS (see previous section) colocalized with the region of Hsp70 mRNA expression virtually precisely (62). This area of decreased CPS, normal ATP, and Hsp70 expression has been shown to be quite large shortly after focal ischemia, and then decrease over time as the perfusion deficit persists. In addition, this region is pharmacologically salvageable as shown by multiple parallel studies using the suture model in rats.

It is notable that the expression of many other molecules has not correlated with the penumbra as it is being described in this book. For example, c-fos is expressed throughout the entire hemisphere of animals and in subcortical structures that are not ischemic, following middle cerebral artery strokes (72). These changes of c-fos expression have been postulated to be due to spreading depression and synaptic changes between infracted cortex and interconnected structures. In addition, many apoptotic genes are expressed only in the core of an infarct or, at most, at the margins of an infarct and are not expressed throughout the penumbra. In addition, even a hypoxia response factor like hypoxia-inducible factor-1 (HIF-1) appears to be expressed not only in the entire territory where CBF decreases—more than the "penumbra"—but in some cases in areas outside of decreased flow regions. Hence, gene expression changes

have been shown to demonstrate "multiple molecular penumbras," a concept which simply reinforces the idea that many changes occur in, around, and even at some distance from areas of focal infarction (72). Only some of these molecular changes, for example, Hsp70-, probably coregister with the penumbra, as described by perfusion diffusion mismatch and other parameters currently being developed in humans.

Mismatch Between Cerebral Blood Volume and Perfusion Impairment (Penumbra Using Computerized Tomography Perfusion)

Given that CT is so universally available in most developed countries and becoming so in developing countries, any penumbral measure using this technology represents a significant opportunity to generalize access to penumbral imaging to the general clinical community. Hence, when Wintermark et al. from the Lausanne group in Switzerland took advantage of the newer spiral CT technology to apply the already existing knowledge about the potential to measure perfusion with injected iodinated contrast agent to devise a penumbral measure this was a considerable advance (48,49). Based on the knowledge that reduced CBV was associated with infarct core from experimental and early clinical studies, they were able to validate topographically using this technique and that the mismatch between this region and the perfusion defect most likely represented potentially salvageable penumbral tissue. In a relatively short space of time they have fulfilled all four criteria for a penumbral marker in that the mismatch area represents compromised tissue, is present in the same arterial territory as the infarct core, either goes on to survive or become infarcted, and the proportion of salvageable tissue is related to better clinical outcomes. The disadvantages of the technique lie with the radiation exposure associated with CT, the need for injection of iodine contrast agent, and the limitation currently to two to four major slices. In spite of this, because of its accessibility and ease of use it may become the "workhorse" for penumbral identification in future clinical trials and, indeed, identification of patients for emerging therapies.

ADDITIONAL PENUMBRAL MARKERS

There have been a number of other concepts that have been considered to be consistent with the penumbra and may be penumbral markers. However, for a variety of reasons, these have not come into universal use or, in the view of the authors, do not adequately fullfil the criteria for penumbra. These are as follows:

Penumbral Measures Based on Cerebral Blood Flow Indices Alone

A variety of semiquantitative and quantitative measures of CBF in both animal models and humans have been used to establish absolute and relative values for the thresholds of the oligemic/penumbral limit and the penumbral/infarct core limit. It could be argued, therefore, that these more unidimensional approaches are able to define the presence of the ischemic penumbra. Indeed, in 1983 Lassen et al. used intra-arterial xenon 133 (133Xe) in ischemic stroke patients to infer the presence of ischemic penumbra for the first time using this technique, although this was well after the pattern of CBF and OEF thought to represent the penumbra had already been described using PET technology (16). The intravenous xenon 133 methodology (73) lacked adequate spatial resolution (two-dimensional) to validate the thresholds according to current criteria. The intra-arterial 133Xe method, which had higher spatial resolution but was also a two-dimensional method, was also used at about this time (74). Further, the concepts of tissue outcome and clinical correlations were not considered by investigators of this era. A major shortfall of the Xenon CBF technique generally was that, as with any CBF measurement, there was no certainty that ischemic core was being imaged given that it could already be partially reperfused. The same argument applies to isolated CBF measures in animal models such as iodoantipyrine autoradiography.

Diffusion Weighted Image/T2 Magnetic Resonance Signatures

Welch et al. used information they had gained in their focal rat model of cerebral ischemia to develop a signature pattern utilizing DWI and T2 parameters to predict tissue recovery or

necrosis. They then used these signatures in humans to develop five MR signatures, two of which predicted either cell recovery or progression to necrosis, which would be consistent with the ischemic penumbra (75–78). This signature relationship with respect to time between DWI and T2 is certainly useful, and at the time of publication in 1995 contributed significantly to knowledge in the area. However, with the technological advances made with DWI imaging in the interim, the PWI/DWI mismatch concept has probably superseded this approach. However, it is interesting to note that the reversibility of DWI has subsequently been demonstrated both in animal models and humans and, indeed, portions of the DWI lesion are penumbral (70,79). Furthermore, it has been demonstrated that after initial regression of the DWI lesion (presumably penumbra) a re-expansion may occur which may reflect reperfusion injury (80). Hence, as our knowledge of the changes in DWI with time increased together with corresponding ADC changes, a more sophisticated approach to the DWI/PWI mismatch concept may develop which incorporates components of the DWI lesion.

Absolute Apparent Diffusion Coefficient Thresholds

Hoehn-Berlage et al. at the Max Planck Institute also used a focal rat model of cerebral ischemia to correlate MR signatures with an index of penumbral and core tissue (81). They defined infarct core as a total breakdown of energy metabolism using autoradiographic imaging techniques while the penumbral region was defined as the region surrounding this with normal energy balance but severe acidosis. They found that the corresponding ADC values were thresholded at 90% of control values for the severe acidosis threshold and 77% of controls for infarct core. In reality, the definition here is a combination of acidosis/energy mismatch and ADC thresholds. When these were correlated with CBF thresholds, absolute values were approximately 20 mL/100 g/min for infarct core threshold and 30 mL/100 g/min for acidosis threshold. In essence, therefore, these investigators have used a mismatch between energy levels and acidosis as a penumbral marker. In other words, potentially salvageable tissue was identified, which had a normal energy balance but severe acidosis, whereas the infarct core was defined a total breakdown of energy metabolism. This was then correlated with absolute ADC values to obtain thresholds of 90% and 77%, respectively. While the energy/acidosis mismatch concept seems quite reasonable, the ADC threshold issue can be grouped with the DWI comments as in section diffusion weighted image/T2 magnetic resonance signatures, in which it can be stated that more work needs to be done before a sophisticated penumbral definition is reached in combination with PWI indices, if ever achievable. There is a need to demonstrate that severely acidotic tissue with normal energy balance is salvageable as per criteria 3, and that this salvageable tissue correlates with better clinical outcomes.

A Possible Expansion of the Concept of Penumbra—Mildly Hypoperfused but at Risk Tissue

The standard three compartments consist of oligemic, penumbra, and necrotic tissue, and it is classically considered that only the penumbra is at risk of infarction. However, the possibility that oligemic or even sufficiently perfused tissue at the time of imaging after acute ischemic stroke can be at risk of infarction has been discussed (35,40). This tissue would not contribute to acute stage clinical deficit but could still become infarcted, perhaps only under unusual circumstances. This volume is of variable extent and the reasons for its eventual necrosis are unclear. However, one could postulate that processes may have commenced, such as apoptosis or inflammatory changes, which were not attenuated and infarction has occurred. Other possibilities include loss of autoregulation due to low perfusion pressure; placing the tissue at risk of becoming penumbral and even infarcted if systemic blood pressure drops or severe vasogenic edema develops; and detrimental changes in tissue oxygen supply, metabolic needs, or pH due to hypoxia, hyperthemia, or hypergylycemia, respectively, despite stable CBF (35,40). A final possibility is that further subclinical events such as further thrombo-embolism have been responsible for its demise. Hence, even though not penumbral stricto sensu, this compartment may represent a further legitimate target for therapy, particularly neuroprotective agents or interventions likely to minimize the occurrence of secondary events.

Other Biochemical Markers of Tissue Dysfunction at Various Thresholds

In animal models, it has been demonstrated that a clear sequence of biochemical events occurs as CBF is gradually reduced. Although there are difficulties in correlating these because of differences in animal species and the use of differing anesthetic agents (many of which may be neuroprotective), an approximate representation of the absolute CBF values in mL per 100 mg per minute at which these changes occur is shown in Figure 2, Chapter 3. Initially, protein synthesis is inhibited at a threshold of about 0.5 mL per gram per minute, then anerobic glycolysis is stimulated at around 0.35 mL per gram per minute and, lastly, a loss of energy status occurs at about 0.20 mL per gram per minute. Hossmann et al. were able to exploit this knowledge using 14C-iodoantipyrine autoradiography with ATP induced bioluminescence to quantitate blood flow reductions with energy failure (55). They were also able to image pH using autoradiography and used the mismatch between the region of energy failure and acidosis as a penumbral marker. This approach also probably exaggerates the penumbral region compared to the classical definition since evoked potentials disappear between 0.15 mL and 0.25 mL per gram per minute. Whether all tissue defined by this marker has the potential to survive or go on to become infarcted is unclear.

CONCLUSIONS

In this chapter we have reviewed most of the described penumbral markers and tried to put them in the context of their origins and usefulness, mainly from the clinical and therapeutic perspective. As can be seen, the more established markers have proven to be more useful to investigators, or perhaps captured their imagination. The field is constantly evolving and, as mentioned earlier, the number of markers used for potentially salvageable tissue suggests that no single marker is perfect and each may be employed usefully for specific purposes. The established markers discussed are all consistent with our definition of the penumbra, and fulfil, most criteria. Others require more work or have not yet proven to be useful or practical in the experimental or clinical setting. Regardless, the penumbral concept is robust and clinically useful. Given the rapid developments in therapies for acute ischemic stroke and the need to identify meaningful targets, penumbral imaging is already coming into regular clinical usage (82–84); although, whether it is truly beneficial for functional outcome remains to be formally documented. This constitutes a remarkable—and perhaps unique—example of incorporation of a complex pathophysiological concept into daily clinical routine.

REFERENCES

1. Albers GW, Caplan LR, Easton JD, et al. Transient ischemic attack—proposal for a new definition. N Engl J Med 2002; 347:1713–1716.
2. Symon L, Pasztor E, Branston NM. The distribution and density of reduced cerebral blood flow following acute middle cerebral artery occlusion: An experimental study by the technique of hydrogen clearance in baboons. Stroke 1974; 5:355–364.
3. Branston NM, Symon L, Crockard HA, Pasztor E. Relationship between the cortical evoked potential and local cortical blood flow following acute middle cerebral artery occlusion in the baboon. Exp Neurol 1974; 45:195–208.
4. Branston NM, Symon L. Proceedings: Depression of the cortical evoked potential with reduction of local blood flow in baboons. J Physiol 1974; 241:98P–99P.
5. Astrup J, Symon L, Branton N, Lassen N. Thresholds of cerebral ischemia. In: Schmiedek P, ed. Microsurgery for Stroke. Berlin: Springer, 1976:16–21.
6. Branston NM, Strong AJ, Symon L. Extracellular potassium activity, evoked potential and tissue blood flow. Relationships during progressive ischaemia in baboon cerebral cortex. J Neurol Sci 1977; 32: 305–321.
7. Astrup J, Symon L, Branston NM, Lassen NA. Cortical evoked potential and extracellular k+ and h+ at critical levels of brain ischemia. Stroke 1977; 8:51–57.
8. Astrup J, Siesjo BK, Symon L. Thresholds in cerebral ischemia—the ischemic penumbra. Stroke 1981; 12:723–725.
9. The Concise Oxford Dictionary (p 1012). Oxford University Press, 1995.
10. Boysen G, Engell HC, Henriksen H. The effect of induced hypertension on internal carotid artery pressure and regional cerebral blood flow during temporary carotid clamping for endarterectomy. Neurology 1972; 22:1133–1144.

11. Sharbrough FW, Messick JM Jr, Sundt TM Jr. Correlation of continuous electroencephalograms with cerebral blood flow measurements during carotid endarterectomy. Stroke 1973; 4:674–683.
12. Olney JW. Brain lesions, obesity, and other disturbances in mice treated with monosodium glutamate. Science 1969; 164:719–721.
13. Simon RP, Swan JH, Griffiths T, Meldrum BS. Blockade of *N*-methyl-D-aspartate receptors may protect against ischemic damage in the brain. Science 1984; 226:850–852.
14. Jones TH, Morawetz RB, Crowell RM, et al. Thresholds of focal cerebral ischemia in awake monkeys. J Neurosurg 1981; 54:773–782.
15. Garcia JH, Mitchem HL, Briggs L, et al. Transient focal ischemia in subhuman primates. Neuronal injury as a function of local cerebral blood flow. J Neuropathol Exp Neurol 1983; 42:44–60.
16. Olsen TS, Larsen B, Herning M, Skriver EB, Lassen NA. Blood flow and vascular reactivity in collaterally perfused brain tissue. Evidence of an ischemic penumbra in patients with acute stroke. Stroke 1983; 14:332–341.
17. Baron JC, Bousser M-G, Comar D, Kellershon C. Human hemispheric infarction studied by positron emission tomography and the ^{15}O inhalation technique. In: Caillé JM, Salamon G, eds. Computerized Tomography. Berlin: Springer-Verlag, 1980:231–237.
18. Baron JC, Bousser MG, Rey A, Guillard A, Comar D, Castaigne P. Reversal of focal "misery-perfusion syndrome" by extra-intracranial arterial bypass in hemodynamic cerebral ischemia. A case study with ^{15}O Positron Emission Tomography. Stroke 1981; 12:454–459.
19. Baron JC, Bousser MG, Comar D, Soussaline F, Castaigne P. Noninvasive tomographic study of cerebral blood flow and oxygen metabolism in vivo. Potentials, limitations, and clinical applications in cerebral ischemic disorders. Eur Neurol 1981; 20:273–284.
20. Lenzi GL, Frackowiak RS, Jones T. Cerebral oxygen metabolism and blood flow in human cerebral ischemic infarction. J Cereb Blood Flow Metab 1982; 2:321–335.
21. Wise RJ, Bernardi S, Frackowiak RS, Legg NJ, Jones T. Serial observations on the pathophysiology of acute stroke. The transition from ischaemia to infarction as reflected in regional oxygen extraction. Brain 1983; 106(Pt 1):197–222.
22. Powers WJ, Grubb RL Jr, Darriet D, Raichle ME. Cerebral blood flow and cerebral metabolic rate of oxygen requirements for cerebral function and viability in humans. J Cereb Blood Flow Metab 1985; 5:600–608.
23. Hakim AM, Pokrupa RP, Villanueva J, et al. The effect of spontaneous reperfusion on metabolic function in early human cerebral infarcts. Ann Neurol 1987; 21:279–289.
24. Heiss WD, Huber M, Fink GR, et al. Progressive derangement of periinfarct viable tissue in ischemic stroke. J Cereb Blood Flow Metab 1992; 12:193–203.
25. Ackerman R, Lev M, Mackay B, et al. PET studies in acute stroke: Findings and relevance to therapy. J Cereb Blood Flow Metab 1989; 9:S359.
26. Baron JC, Rougemont D, Bousser M, Lebrun-Grandie P, Iba-Zizen M, Chiras J. The characteristics of the misery-perfusion syndrome in the cute phase of cerebral infarction. In: Lassen N, Symon L, Baron J, eds. Penombre et Ischemie Cerebrale. Paris: Libbey, 1986:25–30.
27. Moseley ME, Kucharczyk J, Mintorovitch J, et al. Diffusion-weighted MR imaging of acute stroke: correlation with T2-weighted and magnetic susceptibility-enhanced MR imaging in cats. AJNR Am J Neuroradiol 1990; 11(13):423–429.
28. Warach S, Gaa J, Siewert B, Wielopolski P, Edelman R. Acute human stroke studied by whole brain echo planar diffusion-weighted magnetic resonance imaging. Ann Neurol 1995; 37:231–241.
29. Marchal G, Serrati C, Rioux P, et al. PET imaging of cerebral perfusion and oxygen consumption in acute ischaemic stroke: Relation to outcome. Lancet 1993; 341:925–927.
30. Marchal G, Rioux P, Serrati C, et al. Value of acute-stage positron emission tomography in predicting neurological outcome after ischemic stroke: Further assessment. Stroke 1995; 26:524–525.
31. Marchal G, Furlan M, Beaudouin V, et al. Early spontaneous hyperperfusion after stroke. A marker of favourable tissue outcome? Brain 1996; 119(Pt 2):409–419.
32. Marchal G, Furlan M, Beaudouin V, et al. Early spontaneous hyperperfusion after stroke: A marker of favourable tissue outcome? Brain 1996; 119:409–419.
33. Furlan M, Marchal G, Viader F, Derlon JM, Baron JC. Spontaneous neurological recovery after stroke and the fate of the ischemic penumbra. Ann Neurol 1996; 40:216–226.
34. Baron JC, von Kummer R, del Zoppo GJ. Treatment of acute ischemic stroke. Challenging the concept of a rigid and universal time window. Stroke 1995; 26:2219–2221.
35. Heiss WD, Kracht LW, Thiel A, Grond M, Pawlik G. Penumbral probability thresholds of cortical flumazenil binding and blood flow predicting tissue outcome in patients with cerebral ischaemia. Brain 2001; 124:20–29.
36. Heiss WD, Graf R, Fujita T, et al. Early detection of irreversibly damaged ischemic tissue by flumazenil positron emission tomography in cats. Stroke 1997; 28:2045–2051; discussion 2051–2042.
37. Sette G, Baron JC, Young AR, et al. In vivo mapping of brain benzodiazepine receptor changes by positron emission tomography after focal ischemia in the anesthetized baboon. Stroke 1993; 24:2046–2057; discussion 2057–2048.

38. Lassen NA, Vorstrup S. Ischemic penumbra results in incomplete infarction: Is the sleeping beauty dead? [letter]. Stroke 1984; 15:755–758.
39. Lassen N, Olsen T, Hojgaard K, Skriver E. Incomplete infarction: a CT-negative irreversible ischaemic brain lesion. J Cereb Blood Flow Metab 1983; 3:602–603.
40. Baron JC. Mapping the ischaemic penumbra with PET: a new approach. Brain 2001; 124:2–4.
41. Markus R, Donnan GA, Kazui S, et al. Statistical parametric mapping of hypoxic tissue identified by ^{18}F-fluoromisonidazole and positron emission tomography following acute ischemic stroke. Neuroimage 2002; 16:425–433.
42. Markus R, Reutens DC, Kazui S, et al. Topography and temporal evolution of hypoxic viable tissue identified by ^{18}F-fluoromisonidazole positron emission tomography in humans after ischemic stroke. Stroke 2003; 34:2646–2652.
43. Markus R, Reutens DC, Kazui S, et al. Hypoxic tissue in ischaemic stroke: Persistence and clinical consequences of spontaneous survival. Brain 2004; 127:1427–1436.
44. Markus R, Donnan G, Kazui S, Read S, Reutens D. Penumbral topography in human stroke: Methodology and validation of the 'penumbragram'. Neuroimage 2004; 21:1252–1259.
45. Donnan GA, Davis SM. Neuroimaging, the ischaemic penumbra, and selection of patients for acute stroke therapy. Lancet Neurol 2002; 1:417–425.
46. Dirnagl U, Iadecola C, Moskowitz MA. Pathobiology of ischaemic stroke: an integrated view. Trends Neurosci 1999; 22:391–397.
47. Sharp FR, Lu A, Tang Y, Millhorn DE. Multiple molecular penumbras after focal cerebral ischemia. J Cereb Blood Flow Metab 2000; 20:1011–1032.
48. Wintermark M, Reichhart M, Cuisenaire O, et al. Comparison of admission perfusion computed tomography and qualitative diffusion- and perfusion-weighted magnetic resonance imaging in acute stroke patients. Stroke 2002; 33:2025–2031.
49. Wintermark M, Reichhart M, Thiran JP, et al. Prognostic accuracy of cerebral blood flow measurement by perfusion computed tomography, at the time of emergency room admission, in acute stroke patients. Ann Neurol 2002; 51:417–432.
50. van Zijl PC, Eleff SM, Ulatowski JA, et al. Quantitative assessment of blood flow, blood volume and blood oxygenation effects in functional magnetic resonance imaging. Nat Med 1998; 4:159–167.
51. Edelman RR, Siewert B, Darby DG, et al. Qualitative mapping of cerebral blood flow and functional localization with echo-planar mr imaging and signal targeting with alternating radio frequency. Radiology 1994; 192:513–520.
52. Williams DS, Detre JA, Leigh JS, Koretsky AP. Magnetic resonance imaging of perfusion using spin inversion of arterial water. Proc Natl Acad Sci U.S.A. 1992; 89:212–216.
53. Heiss WD, Graf R. The ischemic penumbra. Curr Opin Neurol 1994; 7:11–19.
54. Kinouchi H, Sharp FR, Koistinaho J, Hicks K, Kamii H, Chan PH. Induction of heat shock hsp70 mrna and hsp70 kda protein in neurons in the 'penumbra' following focal cerebral ischemia in the rat. Brain Res 1993; 619:334–338.
55. Hossmann KA. Viability thresholds and the penumbra of focal ischemia. Ann Neurol 1994; 36:557–565.
56. Hakim AM. The cerebral ischemic penumbra. Can J Neurol Sci 1987; 14:557–559.
57. Baron JC. Mapping the ischaemic penumbra with PET: Implications for acute stroke treatment. Cerebrovasc Dis 1999; 9:193–201.
58. Donnan G, Davis S. Errata - "definition of ischaemic penumbra" panel missing from original publication (lancet neurology 1:417–425, 2002.). Lancet Neurol 2003; 2:594.
59. Lythgoe MF, Williams SR, Busza AL, et al. The relationship between magnetic resonance diffusion imaging and autoradiographic markers of cerebral blood flow and hypoxia in an animal stroke model. Magn Reson Med 1999; 41:706–714.
60. Lythgoe MF, Williams SR, Wiebe LI, McEwan AJ, Gordon I. Autoradiographic imaging of cerebral ischaemia using a combination of blood flow and hypoxic markers in an animal model. Eur J Nucl Med 1997; 24:16–20.
61. Saita K, Chen M, Spratt NJ, et al. Imaging the ischemic penumbra with 18f-fluoromisonidazole in a rat model of ischemic stroke. Stroke 2004; 35:975–980.
62. Hata R, Maeda K, Hermann D, Mies G, Hossmann KA. Evolution of brain infarction after transient focal cerebral ischemia in mice. J Cereb Blood Flow Metab 2000; 20:937–946.
63. Hata R, Maeda K, Hermann D, Mies G, Hossmann KA. Dynamics of regional brain metabolism and gene expression after middle cerebral artery occlusion in mice. J Cereb Blood Flow Metab 2000; 20:306–315.
64. Lammertsma A, Hoffman J, Frackowiak R, Huang S, Weinberg I, Phelps M. A new dynamic technique to measure regional cerebral blood flow. J Cereb Blood Flow Metab 1987; 7:S577.
65. Dey HM, Seibyl JP, Stubbs JB, et al. Human biodistribution and dosimetry of the spect benzodiazepine receptor radioligand iodine-123-iomazenil. J Nucl Med 1994; 35:399–404.
66. Donnan G, Wright P, Markus R, Phan TG, Reutens D. The ischaemic penumbra: The evolution of a concept. In: Davis S, Fisher M, Warach S, eds. Magnetic resonance imaging in stroke. Cambridge: Cambridge University Press, 2003:191–206.

67. Ho PW, Reutens DC, Phan TG, et al. Is white matter involved in patients entered into typical trials of neuroprotection? Stroke 2005; 36(12):2742–2744.
68. Heiss WD, Grond M, Thiel A, et al. Permanent cortical damage detected by flumazenil positron emission tomography in acute stroke. Stroke 1998; 29:454–461.
69. JM UK-I, Trivedi RA, Graves MJ, et al. Utility of an ultrafast magnetic resonance imaging protocol in recent and semi-recent strokes. J Neurol Neurosurg Psychiatry 2005; 76:1002–1005.
70. Kidwell CS, Saver JL, Mattiello J, et al. Thrombolytic reversal of acute human cerebral ischemic injury shown by diffusion/perfusion magnetic resonance imaging. Ann Neurol 2000; 47:462–469.
71. Kinouchi H, Sharp FR, Hill MP, Koistinaho J, Sagar SM, Chan PH. Induction of 70-KDA heat shock protein and hsp70 mrna following transient focal cerebral ischemia in the rat. J Cereb Blood Flow Metab 1993; 13:105–115.
72. Sharp JW, Sagar SM, Hisanaga K, Jasper P, Sharp FR. The nmda receptor mediates cortical induction of fos and fos-related antigens following cortical injury. Exp Neurol 1990; 109:323–332.
73. Lassen NA, Henriksen L, Paulson O. Regional cerebral blood flow in stroke by 133xenon inhalation and emission tomography. Stroke 1981; 12:284–288.
74. Olesen J, Friberg L, Olsen TS, et al. Timing and topography of cerebral blood flow, aura, and headache during migraine attacks. Ann Neurol 1990; 28:791–798.
75. Welch KM, Windham J, Knight RA, et al. A model to predict the histopathology of human stroke using diffusion and T2-weighted magnetic resonance imaging. Stroke 1995; 26:1983–1989.
76. Knight RA, Dereski MO, Helpern JA, Ordidge RJ, Chopp M. Magnetic resonance imaging assessment of evolving focal cerebral ischemia. Comparison with histopathology in rats. Stroke 1994; 25:1252–1261; discussion 1261–1252.
77. Helpern JA, Dereski MO, Knight RA, Ordidge RJ, Chopp M, Qing ZX. Histopathological correlations of nuclear magnetic resonance imaging parameters in experimental cerebral ischemia. Magn Reson Imaging 1993; 11:241–246.
78. Dereski MO, Chopp M, Knight RA, Rodolosi LC, Garcia JH. The heterogeneous temporal evolution of focal ischemic neuronal damage in the rat. Acta Neuropathol (Berl) 1993; 85:327–333.
79. Guadagno JV, Warburton EA, Aigbirhio FI, et al. Does the acute diffusion-weighted imaging lesion represent penumbra as well as core? A combined quantitative PET/MRI voxel-based study. J Cereb Blood Flow Metab 2004; 24:1249–1254.
80. Kidwell CS, Saver JL, Starkman S, et al. Late secondary ischemic injury in patients receiving intraarterial thrombolysis. Ann Neurol 2002; 52:698–703.
81. Hoehn-Berlage M, Norris DG, Kohno K, Mies G, Leibfritz D, Hossmann KA. Evolution of regional changes in apparent diffusion coefficient during focal ischemia of rat brain: The relationship of quantitative diffusion NMR imaging to reduction in cerebral blood flow and metabolic disturbances. J Cereb Blood Flow Metab 1995; 15:1002–1011.
82. Schellinger PD, Fiebach JB, Jansen O, et al. Stroke magnetic resonance imaging within 6 hours after onset of hyperacute cerebral ischemia. Ann Neurol 2001; 49:460–469.
83. Rother J, Schellinger PD, Gass A, et al. Effect of intravenous thrombolysis on MRI parameters and functional outcome in acute stroke <6 hours. Stroke 2002; 33:2438–2445.
84. Ribo M, Molina CA, Rovira A, et al. Safety and efficacy of intravenous tissue plasminogen activator stroke treatment in the 3- to 6-hour window using multimodal transcranial doppler/MRI selection protocol. Stroke 2005; 36:602–606.
85. Baron JC, Rougemont D, Soussaline F, et al. Local interrelationships of cerebral oxygen consumption and glucose utilization in normal subjects and in ischemic stroke patients: A positron tomography study. J Cereb Blood Flow Metab 1984; 4:140–149.
86. Baird AE, Warach S. Magnetic resonance imaging of acute stroke. J Cereb Blood Flow Metab 1998; 18:583–609.
87. Read SJ, Hirano T, Abbott DF, et al. Identifying hypoxic tissue after acute ischemic stroke using PET and 18f-fluoromisonidazole. Neurology 1998; 51:1617–1621.
88. Hata R, Mies G, Wiessner C, et al. A reproducible model of middle cerebral artery occlusion in mice: Hemodynamic, biochemical, and magnetic resonance imaging. J Cereb Blood Flow Metab 1998; 18:367–375.

3 Perfusion Thresholds in Cerebral Ischemia

Ramez R. Moustafa and Jean-Claude Baron
Department of Clinical Neurosciences and Stroke Unit, Addenbrooke's Hospital, University of Cambridge, Cambridge, U.K.

INTRODUCTION

The brain generates almost all its energy by oxidation of glucose and is, therefore, vitally dependent on a continuous and stable blood supply. It follows that in focal cerebral ischemia, energy-dependent cellular processes will fail in parallel to the restriction of blood flow, both spatially and over time. During the past few decades, extensive research has been undertaken to quantify the thresholds of cerebral blood flow (CBF) associated with failure of cellular function and integrity (1,2). This was greatly aided by the availability of techniques to measure CBF in various experimental stroke models as well as man, and the realization that focal ischemia results in incomplete and heterogeneous reduction of blood flow (3) (Fig. 1). The two principal CBF thresholds, which constitute the basis of the operational definition of the ischemic penumbra, are discussed in detail in Chapter 4. These are namely, the "infarction threshold," below which tissue will inevitably proceed to infarction, and the "penumbral threshold," below which tissue is functionally impaired but still viable (4). In addition to these major events, several other cellular processes will fail in ischemia according to a fairly constant hierarchy determined by energy needs and biologic significance (Fig. 2, Table 1). This chapter will review the flow thresholds for failure of those functional and metabolic processes and shed light on their relationships and determinants.

It is, however, essential to briefly clarify the relationship of the penumbra and infarction thresholds to another two important perfusion thresholds: that of "electrical failure" at which the electrical activity of the brain ceases; and that of "membrane failure" at which ion gradients across the cell membrane cannot be maintained. From the time of the early studies defining the concept of the penumbra (3), it has been known that those respective thresholds closely coincide. Nonetheless, it is also known that tissue fate is not determined by electrical failure or membrane failure per se, as they are both immediate responses to ischemia and can be recovered completely (3). Hence, the correspondence of these events with tissue viability only indicates that they parallel key steps in the cascade leading to cell death.

About Cerebral Blood Flow Thresholds

It is, first of all, important to address the merits and limitations of the flow threshold approach to cerebral ischemia. The main benefit has been, and continues to be, the insights gained into the pathophysiology of ischemic brain injury and the implications this has on the clinical care of stroke patients. Nonetheless, emphasizing thresholds in ischemia may imply that absolute CBF is the sole determinant of tissue injury, whereas in fact this is not true. Some biological processes, such as protein synthesis (vide infra) are perturbed during ischemia at CBF levels that are very close to normal. Such levels are not known to disturb the energy state of brain tissue and are commonly encountered outside the context of acute stroke, apparently exerting no effect.

Furthermore, several factors may alter flow thresholds. Oxygen availability is a critical parameter for cellular functioning and thus flow thresholds would be expected to rise under hypoxic conditions (3). A similar effect could also be expected in anemia. Conversely, ischemic preconditioning and neuro-protectants may lower the thresholds for ischemic injury and afford more tolerance to lesser CBF levels (1). Some of the known flow thresholds vary with time, such that they rise as time elapses after the onset of ischemia (Table 1). The most familiar example of this phenomenon is that of the infarction threshold, which gradually approaches the

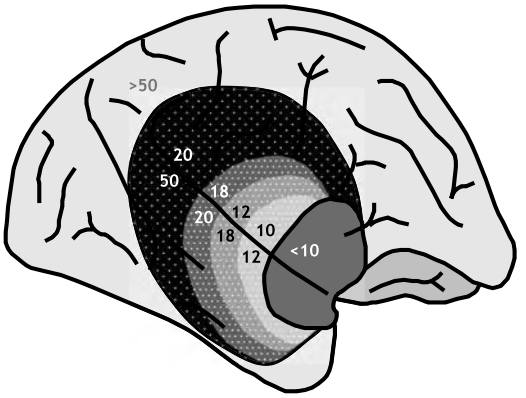

FIGURE 1 (*See color insert.*) The spatial pattern of cerebral blood flow (CBF) reduction following middle cerebral artory (MCA) occlusion in the baboon. Values indicate CBF in mL/100 g/min.

penumbral threshold within a few hours of stroke (4) (see Chapter 4). However, for several other thresholds, time dependence has not been fully addressed. It is thus critical to recognize these temporal and physiologic dependencies and interpret flow thresholds in context with other variables within the ischemic tissue and the organism as a whole.

Another limitation of perfusion thresholds is that they, by definition, dichotomously separate a state of normality from a state of abnormality. Yet, it should be remembered that the thresholds discussed here are rather oversimplified and indicate the point at which substantial perturbation of the biological process in question occurs rather than imply such a sudden transition from presence to absence or vice versa.

Finally, since the resting (or baseline) CBF varies from one animal species to another, flow thresholds will also vary proportionally. In what follows, we will therefore present the relative threshold in addition to the absolute threshold whenever possible, but it is left to the reader to appreciate the correspondence across the various experimental models and species.

Cerebral Blood Flow Thresholds and the Partial Pressure of Oxygen

From a metabolic perspective, it is the hypoxia rather than the reduction of blood flow itself that adversely affects tissue function. Nonetheless, direct quantification of the partial pressure of oxygen in tissue (PtO_2) has several technical limitations, and noninvasive techniques are not yet fully developed (5,6). Blood flow may thus, at least for the time being, be used to reflect tissue oxygenation status provided that this relationship is well characterized. Unfortunately, the data available in this regard remain scarce.

Farrar (7) concurrently measured CBF and PtO_2 using paired platinum electrodes in cats ventilated with 100% oxygen during occlusion of the middle cerebral artery (MCA). He found

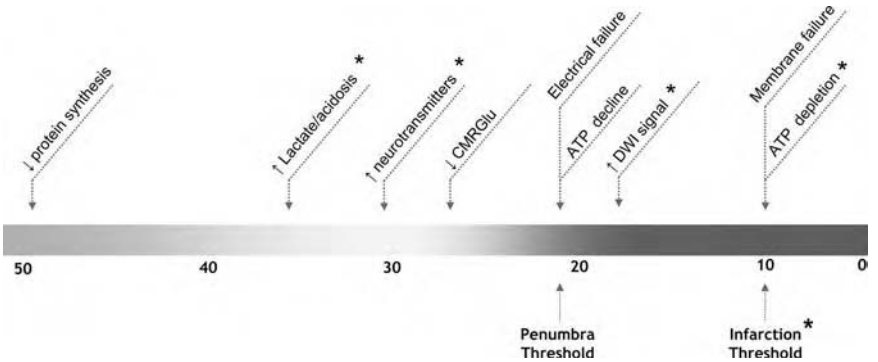

FIGURE 2 (*See color insert.*) Perfusion thresholds for perturbations in cellular function and metabolism during focal ischemia. Scale represents cerebral blood flow in mL/100 g/min; (*) indicates that threshold varies over time. *Source*: Modified from Ref. 1.

TABLE 1 Perfusion Thresholds for Functional and Metabolic Changes in Focal Cerebral Ischemia

	Threshold				
Parameter	**Gerbils**	**Rats**	**Cats**	**Primates**	**Humans**
Electrophysiology					
EEG/ECoG	18–23 (isoelectric)		20 (abnormal)	16–20 (abnormal) 15 (isoelectric)	20–23 (abnormal) 16 (isoelectric)
EP			20 (low amplitude)	20 (low amplltude) 15 (abolished—cortical) 10 (abolished—subcortical)	
Spontaneous unit activity			18 (range 6–22)		
Metabolism					
Ions					
K	23	15	10–15	6–11	
Na			10–15	6–11	
Ca		15	10–15	10	
Water					
Edema			10	20 (begins) 5 (maximal)	
Impedance			30		
DWI signal	15–20 (begins to rise) 4–7 (maximal)	30 → 41			15 → 24
Energy					
ATP	12–20 (decline) 10 (depleted)	13 → 19		20	
PCr	18–23 (decline) 10 (depleted)	20		20	
Glucose utilization	35 (transient rise) 25 (decline)				
Acidosis/lactate	20–27	35–40 → 47		20–30	
Neurotransmitters					
Glutamate			20 → 30		
GABA		48% (release begins) 20% (massive release)	20 → 30		
Adenosine			25		
Glycine		48% (release begins) 20% (massive release)	10 → 30		
Protein	100 (decline) 40 (arrest)	55 [50–80%] (decline) 35 [40%] (complete)			$CMRO_2$ 20–49%

All thresholds are CBF in mL/100g/min except where otherwise indicated. Percentages are of normal baseline → indicates a rise of threshold over time.
Abbreviations: ATP, adenosine triphosphate; $CMRO_2$, cerebral metabolic rate of oxygen; DWI, diffusion-weighted imaging; ECoG, electrocorticography; EEG, electroencephalography; EP, evoked potentials; GABA, γ-amino-butyric acid; PCr, phosphocreatine.

that CBF and PtO_2 had a fairly linear relationship up to six hours after occlusion. Administration of Fluosol-DA (an oxygen carrying fluorocarbon) resulted in a greater PtO_2 for a given CBF level, yet expectedly did not alter the linearity of the relationship. Moreover, the PtO_2 threshold for infarction, remained constant at around 7 to 8 mmHg, whereas the CBF threshold for infarction was dependent on the time of intervention with Fluosol-DA ranging from 10 mL/100 g/min at 15 minutes to 18 mL/100 g/min at two hours postocclusion.

Harris et al. (8) also measured CBF and PtO_2 concurrently in a baboon MCA occlusion model under 100% oxygen (Fig. 3). They found that PtO_2 progressively decreases with the decline of CBF, reaching 30% of normal levels at around 30 mL/100 g/min. Below this level of blood flow, PtO_2 continued to decrease but at a somewhat slower rate, likely because of a decrease in the rate of oxygen utilization in tissue.

Finally, in patients suffering head injury, Doppenberg et al. (9) reported a close linear correlation between decline of tissue PtO_2 measured using Clark electrodes and the decrease of CBF measured by Xenon computed tomography ($r = 0.74$). Closer inspection of their data, however, suggests that the relationship may be more complex. In any case, the validity of extrapolating these results to ischemic stroke is uncertain owing to the differences in the pathophysiologic mechanisms involved.

Overall, the relationship between PtO_2 and CBF may be assumed, for practical purposes, to be linear but its slope is altered by the prevalent cerebral metabolic rate of oxygen ($CMRO_2$).

FLOW THRESHOLDS FOR ELECTROPHYSIOLOGIC CHANGES

Electrical activity is the most energy-consuming process in nervous tissue and its impairment is a hallmark of ischemic injury. Shutdown of electrical function can be understood as a homeostatic mechanism aimed at protecting neurons from the effects of a reduced blood supply (10). Indeed, events that increase the metabolic demand of brain tissue, such as peri-infarct depolarization waves, are known to precipitate the penumbra into inevitable damage by disrupting this homoeostatic mechanism.

Degrees of flow limitation that impact electrical function have been investigated at three levels of organization: electroencephalography (EEG) and electrocorticography (ECoG) have been used to reflect global electrical activity in the cerebral cortex, evoked potentials (EPs) to reflect the electrical activity along specific somato–sensory and auditory pathways, and measurements from single neurons to reflect spontaneous unit activity (Table 1).

Electroencephalography/Electrocorticography

In gerbils subjected to graded hypotension, the ECoG becomes isoelectric when CBF falls to 18 to 23 mL/100 g/min (about 40% of the normal CBF of 51 ± 7 mL/100 g/min) (11). Notably, this threshold is higher than that for adenosine tri-phosphate (ATP) depletion, which was seen to start in that experiment at 12 to 14 mL/100 g/min.

In baboons, with a normal CBF around 50 mL/100 g/min, EEG abnormalities occur when CBF falls to 16 to 17 mL/100 g/min (3). Similarly, in Macaque monkeys and even in cats,

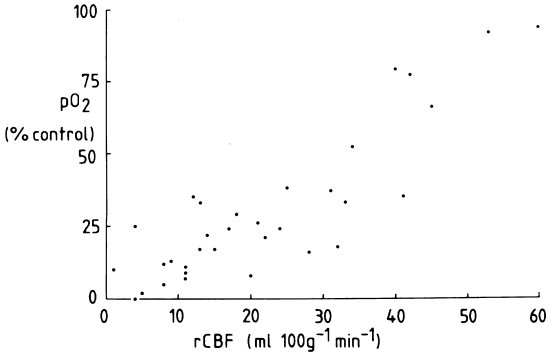

FIGURE 3 The effect of progressive reduction of cerebral blood flow on cortical PO_2 in baboons. *Source*: From Ref. 8, Figure 1.

it was shown that the ECoG becomes abnormal below 20 mL/100/min and isoelectric below 15 mL/100 g/min (12,13).

In humans, clamping of the carotid artery during carotid endarterectomy (CEA) has allowed the investigation of the electrophysiological response to hypoperfusion produced in the corresponding hemisphere (14–16). It was shown that the EEG decreases in amplitude when regional cerebral blood flow drops below 20 to 23 mL/100 g/min and becomes isoelectric at around 16 mL/100 g/min. The close correspondence of these thresholds to those found in other species is noteworthy. Nonetheless, the effects of anesthesia may alter these thresholds significantly owing to the changes in the metabolic demands of the brain and in the flow–metabolism relationship. For instance, Messick et al. (17) reported that whereas during halothane anesthesia the threshold for EEG changes is around 20 mL/100 g/min, it is closer to 10 mL/100 g/min during isoflurane anesthesia. The EEG reflects brain metabolism and its frequency indices correlate well with the $CMRO_2$ (18). A corresponding correlation also exists for CBF provided the normal coupling of flow and metabolism prevails in the brain. The effects of anesthesia on the threshold for EEG changes can thus be understood on the basis of its effects on baseline CBF and $CMRO_2$.

Evoked Potentials

EPs are the electrical signals generated by the nervous system in response to sensory stimuli and consist of a series of waves that reflect sequential activation of neural structures along the sensory pathways. They therefore represent cortical, subcortical, as well as peripheral components of these pathways. As would be expected, the cortical component is affected by ischemia at flow levels that are comparable to those affecting the EEG. Shimada et al. (13) have shown that in cat, the amplitude of auditory EP diminishes below 20 mL/100 g/min. Similarly, in baboons and Macaque monkeys, the amplitude of EPs was shown to decrease when CBF falls below 20 mL/100 g/min and abolished below 15 mL/100 g/min (3,12,19).

The subcortical components of EPs, however, appear to have higher tolerance to ischemia and can be detected at significantly lower CBF levels. Branston et al. (20) compared the effects of hypoperfusion on each component of the sensory EP and showed that, whereas the cortical response was abolished in the range of 15 to 20 mL/100 g/min the subcortical responses, recorded from the thalamus and medial lemniscus, tolerated ischemia as low as 10 mL/100 g/min. In dogs, Okada et al. (21) similarly demonstrated that EPs were abolished at around 20 mL/100 g/min in the cortex, but remained detectable at flows around 10 mL/100 g/min in the basal ganglia. These results emphasize the differential tolerance of brain tissue compartments to ischemia, and may account for the longer tolerance to ischemia in basilar occlusion compared to MCA occlusion (MCAO).

Spontaneous Unit Activity

In contrast to the integrated network activity reflected by EEG and EPs, investigating the electrical activity of individual neuronal units has revealed an intriguing differential tolerance to ischemia among neural populations. Heiss et al. studied the action potentials recorded from individual cortical neurones following MCAO in cats (22). They found that spontaneous neuronal spike activity rapidly ceases as local blood flow falls below 18 mL/100 g/min. However, in a later experiment they showed that although the activity of most neuronal populations conformed to this threshold, it varied from 22 mL/100 g/min down to 6.4 mL/100 g/min in some resistant neurons (23). This emphasizes the principle of selective neuronal vulnerability and argues against an absolute flow threshold below which spontaneous activity of cortical neurones homogeneously disappears or becomes irrecoverable. Moreover, they showed that individual neuronal vulnerability, duration of ischemia, and residual blood flow interact to influence the postischemic recovery of spontaneous activity. Some neurons resumed function after severe ischemia with flow values below 9 mL/100 g/min for more than 20 minutes and represented the resistant subpopulation. Neurones exposed to moderate ischemia for 20 minutes uniformly showed rapid recovery within 18 minutes, whereas neurons exposed to severe ischemia of short duration or to moderate ischemia (between 9 and 22 mL/100 g/min)

for longer periods, required between 19 and 50 minutes to recover. Notably, in recovering neurons, electrical discharge patterns were abnormal during early recovery, showing grouped spikes or periodic discharges but not seizure activity, before slowly normalizing as flow returned to baseline values.

FLOW THRESHOLDS FOR METABOLIC CHANGES

The metabolic disturbances occurring within ischemic brain tissue will be addressed here separately. Nonetheless, one needs to bear in mind that most of them are spatially and temporally interdependent (Figs. 2 and 4). Some of these dependencies are fairly well defined, but many remain speculative and require further confirmation, particularly as regards their evolution over time.

Ion Homeostasis

At the level of flow that is insufficient to sustain any energy production, the cell membrane fails to maintain the physiologic gradients across it and dramatic disruption of ion and water homeostasis ensues. The main disturbances that occur comprise massive efflux of K^+ to the extracellular space; reciprocal influx of Na^+, Cl^- and water into the cells; and consequent anoxic membrane depolarization (1). Influx of Ca^{++} also occurs in parallel and is believed to contribute to cellular toxicity (24). The CBF threshold for these changes is known as the threshold of "ion pump failure" or "membrane failure." As noted before, this often coincides with the infarction threshold of irreversible tissue damage, but they are not synonymous. Energy metabolism and ionic gradients may indeed initiate or contribute to neuronal damage but are themselves essentially reversible even after prolonged ischemia (3).

In nonhuman primates, the threshold of the sharp rise of extracellular potassium and increase in intracellular Na–K ratio has been determined in several studies to be between 6 and 11 mL/100 g/min (12,25–27) (refer to Table1). The differences in the exact CBF values probably represent methodological differences, but importantly, in each of these experiments, K^+ efflux occurred at a lower threshold than electrical failure and coincided with the threshold for energy

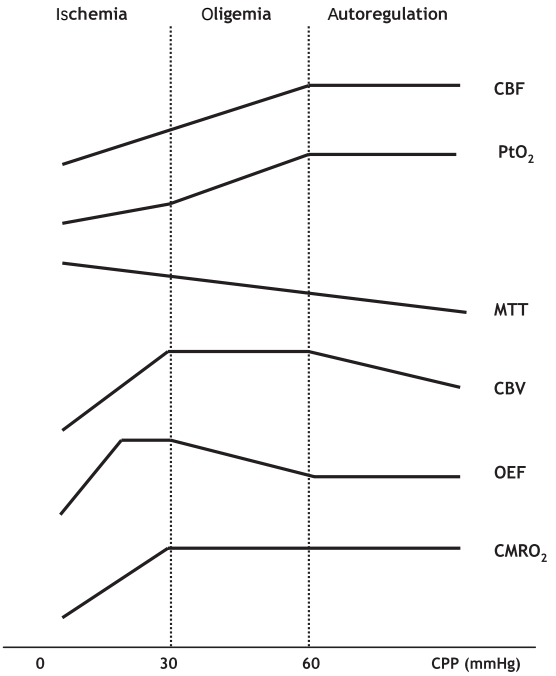

FIGURE 4 Illustrative representation of the relative changes in hemodynamic and metabolic parameters during progressive reduction of cerebral perfusion pressure.

depletion. The changes in Ca^{++} have also been reported to occur at the same threshold in primates (25). Notably, tissue infarction does not necessarily coincide with these ionic gradient changes since the infarction threshold varies with time, such that even severe ischemia with CBF below 5 mL/100 g/min does not induce histological damage if sustained only for a short duration (less than 45 minutes) (28). Conversely, reduction of CBF just below the penumbra threshold (i.e., ~20 mL/100 g/min) will result in tissue infarction if prolonged for several hours (see Chapter 4).

In cats, the intracellular sodium/potassium ratio of brain tissue increases and the extracellular Ca^{++} decreases at flow values below 10 to 15 mL/100 g/min (29). Similarly, in rats, the flow threshold for such changes has been determined as 15 mL/100 g/min (30). Mies et al. (31) found a higher threshold for K^+ efflux in gerbils (23 mL/100 g/min), and this was rightly attributed to methodological and species differences of the resting CBF.

Energy Metabolism

The critical dependence of the brain on the supply of oxygen and glucose is for the production of energy-rich phosphorus compounds, mainly phosphocreatine (PCr) and ATP. To sustain this supply, CBF is closely maintained under normal conditions within a narrow range through an autoregulatory mechanism that continuously modulates vascular resistance to counteract variations in cerebral perfusion pressure (CPP). In conditions of hemodynamic failure, the substantial reduction of CPP further induces a series of vascular and metabolic compensatory mechanisms that struggle to maintain the substrate supply and a constant rate of glucose and oxygen utilization in the tissues (Fig. 4) (32). When these mechanisms are exhausted, energy production then fails and its consequences become manifest.

Before any reduction of CBF becomes evident, the first set of compensatory mechanisms comprises arteriolar dilatation, slowing of the local circulation, and an increase in regional cerebral blood volume (CBV). This can be demonstrated in primates as a linear increase in CBV with gradually induced reduction of arterial blood pressure (33) and in humans as a negative linear correlation between CPP and CBV (34). If, however, this vascular autoregulatory capacity is exceeded, blood flow starts to fall whereas oxygen consumption still remains unchanged. This results in an increase in extraction of oxygen from the blood from the normal 40% up to a theoretical 100% and continues until CBF has reached values close to the penumbra threshold. Temma et al. (35) have demonstrated this phenomenon in rats where a decrease of CBF from 67 ± 22 mL/100 g/min to 44 ± 17 mL/100 g/min for one hour was accompanied by an increase in the oxygen extraction fraction (OEF) from $42 \pm 13\%$ to $50 \pm 19\%$. The increase in OEF during hypoperfusion was also demonstrated in humans using the ratio of CBF to CBV as an index of CPP. It was shown that OEF remains unchanged until this ratio reaches 5.5 to 6 min^{-1} and then starts to rise steeply (34,36), whereas tissue oxygen utilization is relatively unchanged. The ratio of CBF to CBV is sensitive to variations in CPP and correlates with it over a wide range (37). It is, mathematically, the reciprocal of the mean transit time (MTT) in tissue, which itself can be seen to rise linearly with progressive reduction of CPP (Fig. 4).

With further decline of blood flow, and the CBF/CBV ratio, the limitation of substrate delivery results in an "energy crisis," manifesting a measurable decrease of the $CMRO_2$, and to a lesser extent the metabolic rate of glucose (CMRGlu) in the tissues (34). Under normal circumstances in humans, a close correlation exists in brain tissue between CBF, $CMRO_2$, and CMRGlu. The ratio between these metabolic rates is normally around 6 moles of oxygen per mole of glucose. In regions of recent, or even chronic hemispheric stroke, the linear correlation is preserved but the metabolic ratio is altered to around 2 moles of oxygen per mole of glucose (38,39) indicating that anerobic glycolysis is utilized preferentially in these tissues. Anerobic glycolysis is sometimes also seen in areas with low OEF, where $CMRO_2$ is not limited by substrate delivery, and it has been suggested that the response of nonneuronal cells to ischemia might be at least partly responsible for this (39). Of note, the progressive decrease of CMRGlu and the switch to anerobic glycolysis seem to be preceded by a transient rise in the metabolic rate of glucose that is still not fully explained (40).

The stimulation of anerobic glycolysis is reflected by a rise in tissue lactate production and a decline of tissue pH. Kohno et al. (41) observed that after 30 minutes of MCAO in the rat, the threshold for tissue acidosis was 40 mL/100 g/min and at two hours it rose to

47 mL/100 g/min. Harris and Symon, similarly, demonstrated a linear decrease in rat cortical tissue pH at flow levels below 35 mL/100 g/min (30). In baboons, Obrenovitch et al. (42) correspondingly found an increase in tissue lactate between 20 and 30 mL/100 g/min. Clearly, these flow levels are well above the penumbra threshold. Curiously however, in the gerbil, Crockard et al. (43) found that tissue pH remained almost unchanged until flow fell below 20 mL/100 g/min, and then abruptly declined. This result is somewhat unusual since gerbils have a generally higher baseline CBF than other species and thus a higher absolute threshold would be expected. Indeed, in later experiments on gerbils, the decline of tissue glucose content and acidosis were observed at higher CBF values (35 mL/100 g/min and 21–27 mL/100 g/min, respectively) (11,40).

The final stage of disturbance of energy metabolism is reached when CBF continues to fall beyond the levels described so far. At this stage, PCr and ATP are gradually depleted and all energy-dependent cellular mechanisms progressively fail. The thresholds for this stage of energy failure have been determined in several species, and although they differ, they follow a consistent sequence of progression. In gerbils, PCr and ATP begin to decline slowly at around 20 mL/100 g/min and become undetectable below 10 mL/100 g/min (11,40,43). Allen et al. (44) reported a higher threshold at which phosphorus energy compounds begin to fall (30 mL/100 g/min), but confirmed the sharp decline at CBF values below 20 mL/100 g/min, supporting earlier results. In baboons, a similar rapid decline below 20 mL/100 g/min has also been reported (42). Naritomi et al. (11) have further suggested that the beginning of decrease in PCr occurs at a higher threshold than for ATP (18–23 vs. 12–14 mL/100 g/min, respectively), which might account for some of the variability between studies. In any case, the close correspondence of these thresholds for energy decline to that of electrical failure and to the penumbra threshold is worth noting, as it provides a plausible pathophysiologic association between the various disturbances seen in this stage of ischemic injury (Fig. 2).

Likewise, the threshold for complete depletion of ATP roughly coincides with the threshold for membrane failure and with the infarction threshold, and even parallels the rise of the infarction threshold with elapsed time after experimental ischemia (Fig. 2). This has been confirmed in two separate studies on rats, where the threshold for ATP depletion was found to rise from 13 mL/100 g/min after 30 minutes to 19 mL/100 g/min at two hours (41) and from 18 ± 9 mL/100 g/min at one hour to 31 ± 9 mL/100 g/min at 12 hours (45).

Neurotransmitters

Substantial changes in the concentrations of various neurotransmitters and neuro-active substances occurs during ischemia and are believed to have a significant impact on the ischemic penumbra (2). This is particularly relevant in the case of glutamate where a considerable body of evidence has accumulated regarding its excito-toxicity to neurones in acute stroke (46). Adenosine, which is mainly generated by ATP catabolism, is also of particular significance as it has protective properties against ischemic injury (47), possibly through the modulation of glutamate neurotoxicity (48). Furthermore, accumulation of amino acids may also contribute to tissue acidosis (8), and thus compound the metabolic derangement in the already fragile ischemic environment.

Blood flow thresholds have been observed mainly for changes in neurotransmitter amino acids and, to a lesser extent, for modulator amino acids (2,13). In cats, it was shown that the CBF threshold of glutamate and γ-amino-butyric acid (GABA) release is around 20 mL/100 g/min during the first hour after focal ischemia and that it rises to 30 mL/100 g/min after 6 to 15 hours (13,49,50). There was also a similar time-dependent rise in the threshold for release of glycine (from 10 to 30 mL/100 g/min). The release of those amino acids had a lower threshold and was more delayed than that of purine catabolites and adenosine, which reached a peak level 30 minutes after ischemia but returned to normal within two hours. The transient release of adenosine has also been observed in other studies using the same model and was shown to occur at a higher threshold (25 mL/100 g/min) than that of glutamate release (49,51).

In rats, a similar sequence has been observed by Takagi et al. (52) where moderate release of glutamate, GABA, and glycine occurred when CBF fell below 48% of control values and massive release was seen below 20% of control levels.

Water Homeostasis

The brain tissue water content rises in ischemia as a consequence of various metabolic disturbances and massive shifts of water between the extra and intracellular tissue compartments (1). The decrease in extracellular water can be detected by measuring the electrical impedance directly in brain tissue. In experiments on cats, increase in cortical water content and cortical impedance were both seen when flow fell below 10 to 15 mL/100 g/min but not when it was maintained above that level even in the presence of disturbed energy metabolism (53). In later experiments on cats subjected to two hours MCA occlusion (54), the changes in water content and extracellular volume were further clarified. Cortical impedance was found to rise sharply after one minute of occlusion and stabilized after 30 to 60 minutes. Correspondingly, the calculated extracellular volume correlated to blood flow early after occlusion, and at two hours a threshold separating normal from reduced extracellular space could be identified around 25 to 32 mL/100 g/min. Brain water content, on the other hand, correlated with these changes in extracellular volume only in the early stages of ischemia but not at two hours, indicating the existence of other processes such as vasogenic edema.

In baboons subjected to unilateral ischemia, brain edema measured by microgravimetry begins in the cortex at CBF values around 20 mL/100 g/min and becomes maximal when it falls to 5 mL/100 g/min (55–57). Bell et al. (55) further noted that the occurrence of edema parallels tissue infarction and respects its dependence on time as well as blood flow. Accordingly, animals subjected to short periods of MCA occlusion followed by reperfusion do not show significant edema formation, whereas those subjected to longer periods of hypoperfusion below 35% to 40% of normal CBF do. These observations corroborate the results found in an earlier study by Garcia et al. (58) where they also showed that the degree of edema (indicated by neuronal vacuolation) induced by transient ischemia depended on the product of percent reduction of CBF and duration of occlusion. Little or no edema was seen when that product value remained below 100, whereas almost all local neurones showed evidence of vacuolation at values around 150 (i.e., 75% CBF reduction for two hours).

Diffusion Imaging

During the past decade or so, diffusion-weighted magnetic resonance imaging has increasingly been used to depict changes in tissue water during ischemia. The diffusion-weighted imaging (DWI) signal intensity increases in acute ischemia as a result of an apparent lowering of the diffusion coefficient (ADC) of water, yet the mechanisms of this restricted diffusion in ischemic tissue (and indeed in any biological tissue) are still not fully understood (59). At present, there is satisfactory evidence attributing it largely to the occurrence of cytotoxic edema with intracellular limitation of net molecular displacement and shrinkage of the extracellular space (60).

The CBF thresholds for DWI signal increase (or the underlying ADC decrease) are outlined in Table 1, yet two issues arise when considering them. First, these thresholds appear to change over time after the onset of stroke or experimental ischemia, such that a given CBF corresponds to a different DWI signal intensity at different time points. In gerbils, for example, the DWI signal intensity starts to rise as early as 2.5 minutes following complete bilateral carotid artery occlusion and continues to rise further for up to 60 minutes (61). On reperfusion, the intensity then gradually declines over 20 minutes to almost preocclusion levels. Thus inevitably, the time of observation will affect the determined CBF threshold for DWI signal increase, which in turn makes it difficult to compare studies that do not use similar observation times.

The other issue that needs to be considered is whether the determined CBF threshold corresponds to simply any increase in DWI signal intensity or only to a significant increase beyond a certain cutoff value. This is particularly relevant when trying to relate the changes in DWI to other metabolic processes, such as ATP depletion, based on the coincidence of their CBF thresholds. For example, following MCA occlusion in rats, the threshold for increase in DWI signal intensity was generally found to be around 40 mL/100 g/min (41,62–67), ranging from 34 mL/100 g/min at 30 minutes and 41 mL/100 g/min at two hours (41). However, when a significantly reduced ADC was arbitrarily defined by Mancuso et al. (68) as a reduction of >15% of contralateral value, this spatially corresponded to regions with CBF below 25 mL/100 g/min at 30 minutes and below 35 mL/100 g/min at 90 minutes.

These differences in the temporal and spatial definitions of the DWI lesion account for many of the inconsistencies in defining a CBF threshold for its appearance and in relating it to a single state of tissue damage. This has been emphasized in recent studies in humans (69–71) that argue against it being the representative of tissue that has become homogeneously and irreversibly damaged. Other studies on humans have also elucidated many aspects of the relationship between ADC and CBF. Lin et al. (72) reported that following an initial gradual decline, an abrupt and significant reduction of ADC occurred at CBF values around 15 mL/100 g/min (Fig. 5). Consistent with the experiments on other species, the threshold was time dependent, rising to 24 mL/100 g/min at later time points between 4.5 and 6.5 hours. Beyond method-related errors, this time dependence may explain why some studies in humans have reported ADC changes at CBF as high as 50 mL/100 g/min and explains the difficulty of identifying an absolute ADC threshold for irreversible damage (73). In a recent study by Guadagno et al. (74), the relationships of ADC to CBF and oxygen metabolism were investigated using magnetic resonance imaging (MRI) and PET, respectively. The ADC remained essentially unchanged until CBF reached values around 20 mL/100 g/min. Below this threshold the ADC declined linearly in relation to CBF, and the relationship varied with elapsed time from the onset. In contrast, the relationship of ADC to $CMRO_2$ was only seen when the latter was severely reduced and was more reliable at >6 hours from stroke onset.

PROTEIN METABOLISM

Gene expression (and hence protein synthesis) appears to be the most sensitive metabolic process to the effects of ischemia and begins to be disturbed when blood flow falls only slightly below normal (1). It was initially suggested that regions of suppressed protein synthesis could represent the maximum spatial extent of the tissue at risk of infarction (45,75). However, it subsequently became clear that the inhibition of protein synthesis is almost complete above the CBF threshold of the penumbra, and hence does not determine the risk of infarction—at least under usual circumstances (1,2).

It is not yet clear if the inhibition of protein synthesis is a direct consequence of the alteration of blood flow and/or oxygen availability or rather that it occurs in peri-ischemic areas as a remote effect that is electrically or chemically mediated. Intuitively, the suppression of protein synthesis may serve to reduce the metabolic requirements of neurones and thus evade an energy crisis. However, it is now recognized that, at least initially, the suppression of protein synthesis is not arbitrary, but rather very specific to a complex array of protein populations and thus may serve a biological purpose beyond simply conserving energy (45,76). Furthermore, some protein populations are selectively overexpressed during ischemia, and these mostly represent activation of a cellular stress response in which heat-shock proteins, unfolded proteins, endoplasmic reticulum kinases, caspases, and many others come to action (76–78). Current evidence suggests that protein synthesis inhibition (PSI) comprises an acute reversible phase mediated through phosphorylation of translational initiation factors by the PKR-like-eIF2α-kinase

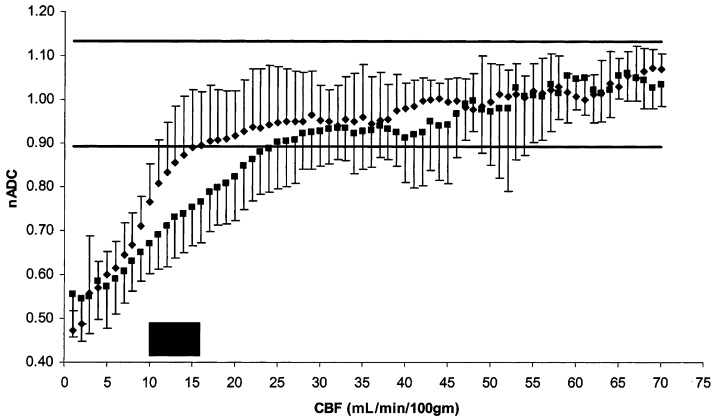

FIGURE 5 Relationship between cerebral blood flow (CBF) and normalized apparent diffusion coefficient (ADC) in acute stroke patients imaged within four hours (♦) and beyond four hours (■) of symptom onset. Solid box indicates the range of CBF at which the nADC is significantly different between the two groups. *Source*: From Ref. 72.

(PERK), and a persistent phase related to cell survival that may represent a lack of recovery of acute PSI or a parallel process mediated by other factors (77). This has two major implications: (*i*) that selective gene expression and the translational changes that ensue may explain the phenomenon of ischemic preconditioning and tolerance induced by transient or sublethal ischemia (79); and (*ii*) that the persistence of cellular stress responses initiates apoptotic programmed cell death and hence may explain the selective loss of neurones in areas remote from the penumbra and core of cerebral ischemia (76,80).

In gerbils, Xie et al. (75) demonstrated that protein synthesis begins to decline below 100 mL/100 g/min and is arrested at 40 mL/100 g/min (cf. CBF in control gerbils 180–220 mL/100 g/min). In the rat MCAO model, Mies et al. (45) showed that inhibition begins at CBF values around 55 mL/100 g/min and becomes complete at 35 mL/100 g/min. These thresholds were stable up to 12 hours following occlusion, in contrast to the rising threshold of concurrently measured ATP depletion. The same group later showed (81) that the threshold for suppression of protein synthesis can be significantly lowered (to 19 ± 4 mL/100 g min) by the glutamate antagonist MK-801 and suggested that this effect may be mediated by suppression of peri-infarct depolarizations.

Also in rats, Jacewicz et al. (82) found that CBF reduction to 50 to 80 mL/100 g/min inhibited the synthesis of many proteins and that on further reduction to 40 mL/100 g/min, synthesis was limited to only a small group of protein and polypeptides. Importantly, they also demonstrated that some selected proteins involved in the cellular stress response became overexpressed in this flow range and dominated protein synthesis below 25 mL/100 g/min. This selective expression has been demonstrated in other experimental studies such as that of Goda et al. (83) showing that heat-shock proteins are induced when CBF is transiently lowered to 20% of the resting normal level.

No data is available on the CBF threshold for PSI in primates or humans. However, the relationship of gene expression to $CMRO_2$ has been studied in a baboon model of focal ischemia. Ali et al. (84) determined that a selective increase in the expression of transforming growth factor-beta 1 (TGF-β1) messenger ribonucleic acid (mRNA) up to 25-fold can be observed in regions where $CMRO_2$ ranged from 20% to 49% of normal values following permanent MCA occlusion. Similarly, in a cluster analysis of the expression of 74 genes following permanent focal ischemia in the same model (85), differential expression of gene groups was observed in regions of $CMRO_2$ reductions between 48% and 66% of normal.

THRESHOLDS OF NEUROLOGIC FUNCTIONING

The end result of all disturbances that occur in response to ischemic restriction of perfusion is the manifested clinical effect on neurologic function. It is reasonable to think that this failure of integrated functioning of the brain coincides with the failure of electrical function and impending energy crisis, though an exact threshold may be more difficult to pinpoint, especially for complex functions such as cognition that may be disturbed by minor or transient alterations of flow selectively targeting particular neuronal populations (86).

To correlate neurologic function to changes in flow, Jones et al. (28) used the hydrogen clearance technique to serially measure CBF in awake Macaque monkeys subjected to varying degrees and durations of MCA occlusion. A neurologic deficit appeared in all the animals within seconds of MCAO and became maximal between 10 and 30 minutes. The severity of the deficit was inversely related to the decline in CBF, and they were able to define a "paralysis threshold" for reversible loss of motoric function (independent of time) at around 23 mL/100 g/min. With further decline of CBF below that threshold, the severity linearly increased until the deficit was complete at around 8 to 9 mL/100 g/min. On reperfusion, they observed that the extent of neurologic recovery was a function of the duration of ischemia. This latter observation was pivotal in the formulation of the concept of time dependence of irreversible damage.

In humans, it has been reported as early as 1954 (87) that neurologic signs appear with hypotension when CBF falls below 29 mL/100 g/min. Two further studies on patients undergoing CEA (88,89) also showed that impaired neurologic function is seen postoperatively if CBF falls below 30% of baseline CBF (~45 mL/100 g/min) and 30 mL/100 g/min, respectively. However, the limited resolution of the techniques used in these early studies overestimates the regional CBF as these average values may have included some areas with normal flow.

CONCLUSION

The availability of techniques to quantify cerebral perfusion has permitted the definition of CBF thresholds for cerebral tissue viability and the various other perturbations occurring in brain tissue during acute ischemia. The insights gained from this line of investigation have expanded our appreciation of the cerebral response to ischemic injury and encouraged the exploration of novel means of modifying it by therapeutic intervention. Moreover, the concurrence of thresholds for certain processes has prompted the investigation of their possible inter-relationships and has had a significant impact on characterizing the penumbra. The variation of flow thresholds over time has attested to the dynamic and evolving nature of ischemia and provided hope in salvaging the ischemic brain even beyond restoring cerebral perfusion. In the future, thresholds for ischemic injury may become defined by means other than CBF, perhaps tissue oxygen tension or another immediately effective equivalent of perfusion. This might allow an even more accurate understanding of the penumbra and, by consequence, the enigma of ischemic stroke.

REFERENCES

1. Hossmann KA. Viability thresholds and the penumbra of focal ischemia. Ann Neurol 1994; 36(4): 557–565.
2. Heiss WD. Experimental evidence of ischemic thresholds and functional recovery. Stroke 1992; 23(11):1668–1672.
3. Astrup J, Siesjo BK, Symon L. Thresholds in cerebral ischemia—the ischemic penumbra. Stroke 1981; 12(6):723–725.
4. Baron JC. Perfusion thresholds in human cerebral ischemia: historical perspective and therapeutic implications. Cerebrovasc Dis 2001; 11(suppl 1): 2–8.
5. Hoffman WE, Charbel FT, Gonzalez-Portillo G, Ausman JI. Measurement of ischemia by changes in tissue oxygen, carbon dioxide, and pH. Surg Neurol 1999; 51(6):654–658.
6. Hou H, Grinberg OY, Grinberg SA, Demidenko E, Swartz HM. Cerebral tissue oxygenation in reversible focal ischemia in rats: multi-site EPR oximetry measurements. Physiol Meas 2005; 26(1): 131–141.
7. Farrar JK. Tissue pO2 threshold of ischemic cell damage following MCA occlusion in cats. J Cereb Blood Flow Metab 1991; 11(suppl 2):S553.
8. Harris RJ, Richards PG, Symon L, Habib AH, Rosenstein J. pH, K+, and PO2 of the extracellular space during ischaemia of primate cerebral cortex. J Cereb Blood Flow Metab 1987; 7(5):599–604.
9. Doppenberg EM, Zauner A, Bullock R, et al. Correlations between brain tissue oxygen tension, carbon dioxide tension, pH, and cerebral blood flow—a better way of monitoring the severely injured brain? Surg Neurol 1998; 49(6): 650–654.
10. Astrup J. Energy-requiring cell functions in the ischemic brain. Their critical supply and possible inhibition in protective therapy. J Neurosurg 1982; 56(4): 482–497.
11. Naritomi H, Sasaki M, Kanashiro M, Kitani M, Sawada T. Flow thresholds for cerebral energy disturbance and Na+ pump failure as studied by in vivo 31P and 23Na nuclear magnetic resonance spectroscopy. J Cereb Blood Flow Metab 1988; 8(1):16–23.
12. Morawetz RB, Crowell RH, DeGirolami U, et al. Regional cerebral blood flow thresholds during cerebral ischemia. Fed Proc 1979; 38(11):2493–2494.
13. Shimada N, Graf R, Rosner G, Heiss WD. Differences in ischemia-induced accumulation of amino acids in the cat cortex. Stroke 1990; 21(10):1445–1451.
14. Sharbrough FW, Messick JM Jr, Sundt TM Jr. Correlation of continuous electroencephalograms with cerebral blood flow measurements during carotid endarterectomy. Stroke 1973; 4(4):674–683.
15. Trojaborg W, Boysen G. Relation between EEG, regional cerebral blood flow and internal carotid artery pressure during carotid endarterectomy. Electroencephalogr Clin Neurophysiol 1973; 34(1):61–69.
16. Sundt TM Jr, Sharbrough FW, Anderson RE, Michenfelder JD. Cerebral blood flow measurements and electroencephalograms during carotid endarterectomy. J Neurosurg 1974; 41(3):310–320.
17. Messick JM Jr, Casement B, Sharbrough FW, et al. Correlation of regional cerebral blood flow (rCBF) with EEG changes during isoflurane anesthesia for carotid endarterectomy: critical rCBF. Anesthesiology 1987; 66(3):344–349.
18. Ingvar DH, Sjolund B, Ardo A. Correlation between dominant EEG frequency, cerebral oxygen uptake and blood flow. Electroencephalogr Clin Neurophysiol 1976; 41(3):268–276.
19. Branston NM, Symon L, Crockard HA, Pasztor E. Relationship between the cortical evoked potential and local cortical blood flow following acute middle cerebral artery occlusion in the baboon. Exp Neurol 1974; 45(2):195–208.
20. Branston NM, Ladds A, Symon L, Wang AD. Comparison of the effects of ischaemia on early components of the somatosensory evoked potential in brainstem, thalamus, and cerebral cortex. J Cereb Blood Flow Metab 1984; 4(1):68–81.

21. Okada Y, Shima T, Yamamoto M, Uozumi T. Regional cerebral blood flow, ensory evoked potentials, and intracranial pressure in dogs with MCA occlusion by embolization or trapping. J Neurosurg 1983; 58(4):500–507.
22. Heiss WD, Hayakawa T, Waltz AG. Cortical neuronal function during ischemia. Effects of occlusion of one middle cerebral artery on single-unit activity in cats. Arch Neurol 1976; 33(12):813–820.
23. Heiss WD, Rosner G. Functional recovery of cortical neurons as related to degree and duration of ischemia. Ann Neurol 1983; 14(3): 294–301.
24. Xiong ZG, Zhu XM, Chu XP, et al. Neuroprotection in ischemia: blocking calcium-permeable acid-sensing ion channels. Cell 2004; 118(6):687–698.
25. Harris RJ, Symon L, Branston NM, Bayhan M, Changes in extracellular calcium activity in cerebral ischaemia. J Cereb Blood Flow Metab 1981; 1(2): 203–209.
26. Astrup J, Symon L, Branston NM, Lassen NA. Cortical evoked potential and extracellular K+ and H+ at critical levels of brain ischemia. Stroke 1977; 8(1): 51–57.
27. Branston NM, Strong AJ, Symon L. Extracellular potassium activity, evoked potential and tissue blood flow. Relationships during progressive ischaemia in baboon cerebral cortex. J Neurol Sci 1977; 32(3):305–321.
28. Jones TH, Morawetz RB, Crowell RM, et al. Thresholds of focal cerebral ischemia in awake monkeys. J Neurosurg 1981; 54(6):773–782.
29. Hossmann KA, Schuier FJ. Experimental brain infarcts in cats. I. Pathophysiological observations. Stroke 1980; 11(6):583–592.
30. Harris RJ, Symon L. Extracellular pH, potassium, and calcium activities in progressive ischaemia of rat cortex. J Cereb Blood Flow Metab 1984; 4(2):178–186.
31. Mies G, Kloiber O, Drewes LR, Hossmann KA. Cerebral blood flow and regional potassium distribution during focal ischemia of gerbil brain. Ann Neurol 1984; 16(2):232–237.
32. Nemoto EM, Yonas H, Chang Y. Stages and thresholds of hemodynamic failure. Stroke 2003; 34(1):2–3.
33. Grubb RL Jr, Phelps ME, Raichle ME, Ter-Pogossian MM. The effects of arterial blood pressure on the regional cerebral blood volume by X-ray fluorescence. Stroke 1973; 4(3):390–399.
34. Sette G, Baron JC, Mazoyer B, et al. Local brain haemodynamics and oxygen metabolism in cerebrovascular disease. Positron emission tomography. Brain 1989; 112(Pt 4):931–951.
35. Temma T, Magata Y, Kuge Y, et al. Estimation of oxygen metabolism in a rat model of permanent ischemia using positron emission tomography with injectable15O-O2. J Cereb Blood Flow Metab 2006; 26(12):1577–1583.
36. Gibbs JM, Wise RJ, Leenders KL, Jones T. Evaluation of cerebral perfusion reserve in patients with carotid-artery occlusion. Lancet 1984; 1(8372):310–314.
37. Schumann P, Touzani O, Young AR, et al. Evaluation of the ratio of cerebral blood flow to cerebral blood volume as an index of local cerebral perfusion pressure. Brain 1998; 121(Pt 7):1369–1379.
38. Baron JC, Rougemont D, Soussaline F, et al. Local interrelationships of cerebral oxygen consumption and glucose utilization in normal subjects and in ischemic stroke patients: a positron tomography study. J Cereb Blood Flow Metab 1984; 4(2):140–149.
39. Wise RJ, Rhodes CG, Gibbs JM, et al. Disturbance of oxidative metabolism of glucose in recent human cerebral infarcts. Ann Neurol 1983; 14(6):627–637.
40. Paschen W, Mies G, Hossmann KA. Threshold relationship between cerebral blood flow, glucose utilization, and energy metabolites during development of stroke in gerbils. Exp Neurol 1992; 117(3):325–333.
41. Kohno K, Hoehn-Berlage M, Mies G, Back T, Hossmann KA. Relationship between diffusion-weighted MR images, cerebral blood flow, and energy state in experimental brain infarction. Magn Reson Imaging 1995; 13(1):73–80.
42. Obrenovitch TP, Garofalo O, Harris RJ, et al. Brain tissue concentrations of ATP, phosphocreatine, lactate, and tissue pH in relation to reduced cerebral blood flow following experimental acute middle cerebral artery occlusion. J Cereb Blood Flow Metab 1988; 8(6):866–874.
43. Crockard HA, Gadian DG, Frackowiak RS, et al. Acute cerebral ischaemia: concurrent changes in cerebral blood flow, energy metabolites, pH, and lactate measured with hydrogen clearance and 31P and 1H nuclear magnetic resonance spectroscopy. II. Changes during ischaemia. J Cereb Blood Flow Metab 1987; 7(4):394–402.
44. Allen KL, Busza AL, Proctor E, et al. Controllable graded cerebral ischaemia in the gerbil: studies of cerebral blood flow and energy metabolism by hydrogen clearance and 31P NMR spectroscopy. NMR Biomed 1993; 6(3):181–186.
45. Mies G, Ishimaru S, Xie Y, Seo K, Hossmann KA. Ischemic thresholds of cerebral protein synthesis and energy state following middle cerebral artery occlusion in rat. J Cereb Blood Flow Metab 1991; 11(5):753–761.
46. Rothman SM, Olney JW. Glutamate and the pathophysiology of hypoxic—ischemic brain damage. Ann Neurol 1986; 19(2):105–111.
47. von Lubitz DK, Dambrosia JM, Kempski O, Redmond DJ. Cyclohexyl adenosine protects against neuronal death following ischemia in the CA1 region of gerbil hippocampus. Stroke 1988; 19(9): 1133–1139.

48. Corradetti R, Lo Conte G, Moroni F, Passani MB, Pepeu G. Adenosine decreases aspartate and glutamate release from rat hippocampal slices. Eur J Pharmacol 1984; 104(1–2):19–26.
49. Matsumoto K, Graf R, Rosner G, Shimada N, Heiss WD. Flow thresholds for extracellular purine catabolite elevation in cat focal ischemia. Brain Res 1992; 579(2):309–314.
50. Matsumoto K, Graf R, Rosner G, Taguchi J, Heiss WD. Elevation of neuroactive substances in the cortex of cats during prolonged focal ischemia. J Cereb Blood Flow Metab 1993; 13(4):586–594.
51. Shimada N, Graf R, Rosner G, et al. Ischemic flow threshold for extracellular glutamate increase in cat cortex. J Cereb Blood Flow Metab 1989; 9(5):603–606.
52. Takagi K, Ginsberg MD, Globus MY, et al. Changes in amino acid neurotransmitters and cerebral blood flow in the ischemic penumbral region following middle cerebral artery occlusion in the rat: correlation with histopathology. J Cereb Blood Flow Metab 1993; 13(4):575–585.
53. Schuier FJ, Hossmann KA. Experimental brain infarcts in cats. II. Ischemic brain edema. Stroke 1980; 11(6):593–601.
54. Matsuoka Y, Hossmann KA. Cortical impedance and extracellular volume changes following middle cerebral artery occlusion in cats. J Cereb Blood Flow Metab 1982; 2(4):466–474.
55. Bell BA, Symon L, Branston NM. CBF and time thresholds for the formation of ischemic cerebral edema, and effect of reperfusion in baboons. J Neurosurg 1985; 62(1):31–41.
56. Symon L, Branston NM, Chikovani O. Ischemic brain edema following middle cerebral artery occlusion in baboons: relationship between regional cerebral water content and blood flow at 1 to 2 hours. Stroke 1979; 10(2):184–191.
57. Branston NM, Bell BA, Hunstock A, Symon L. Time and flow as factors in the formation of post-ischemic edema in primate cortex. Adv Neurol 1980; 28: 291–298.
58. Garcia JH, Mitchem HL, Briggs L, et al. Transient focal ischemia in subhuman primates. Neuronal injury as a function of local cerebral blood flow. J Neuropathol Exp Neurol 1983; 42(1):44–60.
59. Norris DG, Niendorf T, Leibfritz D. Health and infarcted brain tissues studied at short diffusion times: the origins of apparent restriction and the reduction in apparent diffusion coefficient. NMR Biomed 1994; 7(7):304–310.
60. Schaefer PW, Grant PE, Gonzalez RG. Diffusion-weighted MR imaging of the brain. Radiology 2000; 217(2):331–345.
61. Busza AL, Allen KL, King MD, et al. Diffusion-weighted imaging studies of cerebral ischemia in gerbils. Potential relevance to energy failure. Stroke 1992; 23(11):1602–1612.
62. Hoehn-Berlage M, Norris DG, Kohno K, et al. Evolution of regional changes in apparent diffusion coefficient during focal ischemia of rat brain: the relationship of quantitative diffusion NMR imaging to reduction in cerebral blood flow and metabolic disturbances. J Cereb Blood Flow Metab 1995; 15(6):1002–1011.
63. Perez-Trepichio AD, Xue M, Ng TC, et al. Sensitivity of magnetic resonance diffusion-weighted imaging and regional relationship between the apparent diffusion coefficient and cerebral blood flow in rat focal cerebral ischemia. Stroke 1995; 26(4):667–674; discussion 674–675.
64. Wang Y, Hu W, Perez-Trepichio AD, et al. Brain tissue sodium is a ticking clock telling time after arterial occlusion in rat focal cerebral ischemia. Stroke 2000; 31(6):1386–1391; discussion 1392.
65. Henninger N, Sicard KM, Schmidt KF, Bardutzky J, Fisher M. Comparison of ischemic lesion evolution in embolic versus mechanical middle cerebral artery occlusion in Sprague Dawley rats using diffusion and perfusion imaging. Stroke 2006; 37(5):1283–1287.
66. Shen Q, Meng X, Fisher M, Sotak CH, Duong TQ. Pixel-by-pixel spatiotemporal progression of focal ischemia derived using quantitative perfusion and diffusion imaging. J Cereb Blood Flow Metab 2003; 23(12):1479–1488.
67. Calamante F, Lythgoe MF, Pell GS, et al. Early changes in water diffusion, perfusion, T1, and T2 during focal cerebral ischemia in the rat studied at 8.5 T. Magn Reson Med 1999; 41(3):479–485.
68. Mancuso A, Karibe H, Rooney WD, et al. Correlation of early reduction in the apparent diffusion coefficient of water with blood flow reduction during middle cerebral artery occlusion in rats. Magn Reson Med 1995; 34(3):368–377.
69. Kidwell CS, Saver JL, Mattiello J, et al. Thrombolytic reversal of acute human cerebral ischemic injury shown by diffusion/perfusion magnetic resonance imaging. Ann Neurol 2000; 47(4):462–469.
70. Fiehler J, Knudsen K, Kucinski T, et al.Predictors of apparent diffusion coefficient normalization in stroke patients. Stroke 2004; 35(2):514–519.
71. Guadagno JV, Warburton EA, Jones PS, et al. The diffusion-weighted lesion in acute stroke: heterogeneous patterns of flow/metabolism uncoupling as assessed by quantitative positron emission tomography. Cerebrovasc Dis 2005; 19(4):239–246.
72. Lin W, Lee JM, Lee YZ, et al. Temporal relationship between apparent diffusion coefficient and absolute measurements of cerebral blood flow in acute stroke patients. Stroke 2003; 34(1):64–70.
73. Hamon M, Marie RM, Clochon P, et al. [Quantitative relationships between ADC and perfusion changes in acute ischemic stroke using combined diffusion-weighted imaging and perfusion MR (DWI/PMR)]. J Neuroradiol 2005; 32(2):118–124.

74. Guadagno JV, Jones PS, Fryer TD, et al. Local relationships between restricted water diffusion and oxygen consumption in the ischemic human brain. Stroke 2006; 37(7):1741–1748.
75. Xie Y, Mies G, Hossmann KA. Ischemic threshold of brain protein synthesis after unilateral carotid artery occlusion in gerbils. Stroke 1989; 20(5):620–626.
76. DeGracia DJ, Montie HL. Cerebral ischemia and the unfolded protein response. J Neurochem 2004; 91(1):1–8.
77. DeGracia DJ, Acute and persistent protein synthesis inhibition following cerebral reperfusion. J Neurosci Res 2004; 77(6):771–776.
78. Mengesdorf T, Proud CG, Mies G, Paschen W. Mechanisms underlying suppression of protein synthesis induced by transient focal cerebral ischemia in mouse brain. Exp Neurol 2002; 177(2): 538–546.
79. Burda J, Hrehorovska M, Bonilla LG, et al. Role of protein synthesis in the ischemic tolerance acquisition induced by transient forebrain ischemia in the rat. Neurochem Res 2003; 28(8):1213–1219.
80. Paschen W, Mengesdorf T. Endoplasmic reticulum stress response and neurodegeneration. Cell Calcium 2005; 38(3–4):409–415.
81. Mies G, Kohno K, Hossmann KA. MK-801, a glutamate antagonist, lowers flow threshold for inhibition of protein synthesis after middle cerebral artery occlusion of rat. Neurosci Lett 1993; 155(1): 65–68.
82. Jacewicz M, Kiessling M, Pulsinelli WA. Selective gene expression in focal cerebral ischemia. J Cereb Blood Flow Metab 1986; 6(3):263–272.
83. Goda H, Yao H, Nakane H, et al. Cerebral blood flow threshold and regional heterogeneity of heat shock protein 72 induction following transient forebrain ischemia in rats. Neurochem Res 1999; 24(5):679–683.
84. Ali C, Docagne F, Nicole O, et al. Increased expression of transforming growth factor-beta after cerebral ischemia in the baboon: an endogenous marker of neuronal stress? J Cereb Blood Flow Metab 2001; 21(7):820–827.
85. Chuquet J, Benchenane K, Liot G, et al. Matching gene expression with hypometabolism after cerebral ischemia in the nonhuman primate. J Cereb Blood Flow Metab 2002; 22(10):1165–1169.
86. Baron JC. How healthy is the acutely reperfused ischemic penumbra? Cerebrovasc Dis 2005; 20(suppl 2):25–31.
87. Finnerty FA Jr, Witkin L, Fazekas JF. Cerebral hemodynamics during cerebral ischemia induced by acute hypotension. J Clin Invest 1954; 33(9):1227–1232.
88. Jennett WB, Harper AM, Gillespie FC. Measurement of regional cerebral blood-flow during carotid ligation. Lancet 1966; 2(7474):1162–1163.
89. Boysen G, Ladegaard-Pedersen HJ, Valentin N, Engell HC. Cerebral blood flow and internal carotid artery flow during carotid surgery. Stroke 1970; 1(4):253–260.

4 Duration and Thresholds of the Ischemic Penumbra in Different Species

Omar Touzani
University of Caen, Cyceron, Caen, France

Jean-Claude Baron
Department of Clinical Neurosciences and Stroke Unit, Addenbrooke's Hospital, University of Cambridge, Cambridge, U.K.

INTRODUCTION

The concept of the ischemic penumbra was originally introduced on the basis of studies in a model of focal cerebral ischemia in the baboon. The initial description of the penumbra linked changes in electrical activity and membrane function in the brain to threshold levels of cerebral blood flow (CBF). The penumbra was described as a moderately hypoperfused cerebral region in which electrical failure had occurred but oxygen supply level was sufficient to maintain membrane homeostasis and, thus, cellular viability. The description of CBF thresholds has, indeed, been remarkably helpful in the analysis of the penumbra. In this chapter, flow thresholds in different species are addressed.

Evidence exists in the literature to show that the ischemic penumbra is a dynamic and its evolution toward irreversible damage is a gradual process. This is important because it implies that timely therapeutic intervention should be possible. The volume of the ischemic penumbra gradually decreases with time elapsed following the arterial occlusion. Nonetheless, the dynamics of this process will depend on species, strain, and stroke model used; the initial severity of ischemia; and the existence of concomitant pathology (e.g., chronic hypertension, diabetes). The temporal evolution of the ischemic penumbra can be documented by two approaches: (*i*) analyzing the delay between the onset of ischemia and a successful therapeutic intervention, and (*ii*) imaging the temporal evolution of functional parameters that would predict final tissue outcome. Data obtained with these two approaches are discussed in different animal species as well as in the human.

DURATION OF THE PENUMBRA

Abundant data suggest that brain injury secondary to an arterial occlusion is a dynamic process and is slower than previously believed. Although irreversible damage occurs rapidly in the most severely affected brain region, damage in peripheral regions of less severe ischemia or "penumbra" may develop over many hours and possibly even days. Characterizing the kinetics of the ischemic penumbra is crucial since the time frame in which the ischemic penumbra is present will inform the window of therapeutic opportunity.

Much of the evidence for the progression of ischemic brain damage derives from animal studies. Nonetheless, comparing the available data is difficult because different models of cerebral ischemia, with different severities of the insult, have been employed in different species and strains. Although animal models allow measurements of a given parameter at multiple time points throughout the acute, subacute, and chronic stages of ischemia, associated variables such as the occurrence of reperfusion; the type of anesthesia; premorbid chronic arterial hypertension or diabetes; age; gender; and arterial blood pressure, glucose level, and brain temperature during the experiment, might all modify the hemodynamics and the biochemical status of cerebral tissue, and thus affect the dynamics of the ischemic penumbra. In the present chapter, we will discuss the duration of the ischemic penumbra in the most widely used animal species, namely the rodent, cat, and nonhuman primate, as well as in the human.

Duration of the Penumbra in Rodents

Middle cerebral artery occlusion (MCAO) models are the most widely used for the study of focal cerebral ischemia in rodents. The pertinence of these models has been discussed in detail elsewhere (1,2). Among rodents, the rat is the most used species for the investigation of the pathophysiology of stroke. In this species, it is easier to occlude the MCA under the control of physiological parameters and to undertake behavioral and neuroimaging examinations. Nonetheless, the recent development of gene-manipulated mice has encouraged the use of models of cerebral ischemia in mice (3).

Interventional Studies

Informative data regarding the evolution of ischemic injury in rodents can be drawn from interventional studies. As by definition the duration of the penumbra describes the therapeutic window, an effect of a beneficial therapeutic intervention can only be expected as long as penumbral tissue is present. A wide range of therapeutic strategies have been explored in rodents subjected to ischemia with the aim of protecting the penumbra from evolving toward infarction and improving the outcome after stroke. Description of these strategies is beyond the scope of the present review; the reader can refer to published reviews (4,5). Here we will illustrate the concept through some examples.

Studies that used quantitative neuropathology in the chronic stage to examine the effects of restoration of CBF at different time points following the occlusion have provided evidence that infarction volume progressively increases over the first two to four hours. In rats, Nagasawa and Kogure (6) showed that one-hour intraluminal MCAO induced only mild, scattered ischemic damage. However, both three- and six-hours occlusive periods resulted in severe cell changes in the ipsilateral cortex. Zea Longa et al. (7) demonstrated that the neuropathological changes (assessed 72 hours after MCAO) were more extensive in rats that underwent permanent occlusion than those subjected to temporary occlusion (of two to four hours). In a similar study, Memezawa et al. (8) reported that 15 minutes of MCAO leads to selective neuronal necrosis, while 60 minutes induced frank infarction in both caudoputamen and cortex. Moreover, the infarct size increased progressively with increasing occlusion time up to 120 to 180 minutes. Using a model of temporary focal neocortical infarction in spontaneously hypertensive rats (SHR), both Kaplan et al. (9) and Buchan et al. (10) found that the cortical infarction is a function of time and reaches its maximum in three to four hours, following the occlusion. Several studies (11–13) have shown that neuropathological changes evolve more rapidly in the caudoputamen than in the cortex. This different rate of infarct progression is attributed to the more severe initial ischemia in the striatum compared to the cortex, where collateral circulation can maintain a higher perfusion.

Relatively to the rat, few data regarding the histological evolution of ischemic brain lesion in mice are available. In the studies of Hata et al. (3,14), the penumbra, defined as the tissue volume with preserved adenosine tri-phosphate (ATP) and reduced protein synthesis, was present at three hours following the MCA occlusion and its volume was approximately 50% of the core volume at this time point. Subsequent deterioration of the so-defined penumbra has been observed up to six hours of permanent MCAO. Reperfusion, with rt-PA after one hour of MCAO, resulted in reversal of metabolic deterioration (15).

In addition to restoration of CBF following temporary arterial occlusion, several pharmacological treatments have been shown to reduce brain damage when administered after the induction of ischemia (Table 1). Administration of carbamylated erythropoietin (CEPO), a modified form of erythropoietin that is not erythropoitic, conferred a significant neuroprotection even when the treatment was initiated four hours after permanent MCAO (27). Albumin can reduce infarct volume by 60% to 65% and markedly reduces the extent of brain swelling, with a therapeutic window extending to four hours (29). A few agents might even be active with an extraordinary therapeutic window up to 8 to 12 hours (24,34). These studies and others are summarized in Table 1.

Although these pharmacological findings document on the duration of the salvageable penumbra, the efficacy of a given treatment will also depend on the importance of the targeted events in the development of the lesion and on the dosing regimen (bolus, infusion or repeated doses).

TABLE 1 Pharmacological Neuroprotection in Animal Models

Mechanism of action	Drug (route)	Model/species	Initiation of treatment	Time of analysis	Neuroprotective effect (%)	References
Inflammation	SCR1sLe^x (iv)	tMCAO/mice	45 min post-MCAO	1 day	85	(16)
Inflammation	Minocycline (iv)	tMCAO/rats	4 h post-MCAO	3 days	63	(17)
Inflammation	PS519 (iv)	tMCAO/rats	2 h post-MCAO	3 days	40	(18)
Inflammation, apoptosis, free radical generation	Carvedilol (sc)	tMCAO/rats	2 days pre-MCAO	2 days	40	(19)
Inflammation, apoptosis	Ac-YVAD.cmk (icv)	pMCAO/rats	10 min post-MCAO	6 days	25	(20)
Apoptosis	z-VAD (icv)	tMCAO/rats	30 min pre-MCAO	2 days	29	(21)
Apoptosis, proteinase inhibition	Neuroserpin (icv)	tMCAO/rats	Immediately after MCAO	3 days	64	(22)
Enhancement of inhibitory activity of GABA	Tiagabine (ip)	tMCAO/rats	4 h post-MCAO	3 day	67	(23)
NMDA receptor antagonism	Gonatokin-G (iv)	tMCAO/rats	8 h post-MCAO	1 day	47	(24)
NMDA receptor antagonism	AR-R15896AR (iv)	tMCAO/cats	30 min post-MCAO	8 h	67	(25)
AMPA receptor antagonism	YM872 (iv)	tMCAO/rats	2 h post-MCAO	7 days	–35	(26)
Multiple mechanisms	CEPO (iv)	tMCAO/rats	4 h post-MCAO	24 h	30	(27)
Glutamate increase	2-PMPA (iv)	tMCAO/rats	90 min post-MCAO	2 days	30	(28)
Hemodilution	Albumin	tMCAO/rats	4 h post-MCAO	3 days	61	(29)
Free radical generation, neuronal NOS inhibition	BN 80933 (iv)	tMCAO/rats	4 h post-MCAO	7 days	69	(30)
Free radical generation	NXY-059 (iv)	tMCAO/rats	5 h post-MCAO	2 days	65	(31)
Free radical generation	S-PBN (ip)	pMCAO/rats	2 h post-MCAO	3 days	35	(32)
Sodium channel blockade	BIII 890CL (sc)	pMCAO/ rats	5 min post-MCAO	2 days	40	(33)
Multiple mechanisms	Ethyl pyruvate	tMCAO/rats	12 h post-MCAO	2 days	56	(34)

Abbreviations: icv, intracerebroventricular; ip, intraperitoneal; iv, intravenous; pMCAO, permanent middle cerebral artery occlusion; sc, subcutaneous; tMCAO, temporary middle cerebral artery occlusion.

Neuroimaging Studies

Thanks to the development of magnetic resonance imaging (MRI), many studies have addressed the temporo-spatial evolution of brain damage in rodents subjected to focal stroke. The advantage of this approach is the possibility to study the lesion in the most acute stage with subsequent and valuable temporal information in the same animal (35–38).

Early ischemic lesions seen on diffusion-weighted imaging (DWI) expand progressively over time and reach maximal volumes approximately three hours after permanent MCAO in the rat. At this time, the DWI lesion volume becomes equivalent in size to the final infarction measured histologically (39–41). Although it has well-described limitations (42–44), the use of the mismatch between perfusion-weighted magnetic resonance imaging (PWI) and DWI to delineate the putative penumbra also argues for a progressive shrinkage of the at-risk tissue following permanent focal ischemia in the rat. This profile of evolution is exemplified by the study of Shen et al. (45) in which the volume of apparent diffusion coefficient (ADC)-defined lesion increased gradually until it converged with the hypoperfused tissue volume at three hours (Fig. 1). Interestingly, these authors have recently shown the existence of substantial differences in the temporal evolution of the diffusion/perfusion mismatch in two rat strains subjected to the same MCAO protocol (46), with the evolution of DWI-defined damage being slower in Wistar–Kyoto rats than in Sprague–Dawley rats. These data provide an example to argue that the spatio-temporal evolution of the penumbra is complex and can be influenced by factors as apparently mundane as the strain used.

In models of transient ischemia in rats, the pattern of evolution of MRI abnormalities is more complex and depends on the duration of ischemia. The initial DWI hyperintensity can partially or completely vanish following reperfusion after brief MCAO (less than one hour). However, this recovery may not invariably identify tissue rescue, since a secondary DWI lesion may reappear and expand at late time points (12–48 hours) (47–50). Areas showing secondary reappearance of the DWI lesion are prone to exhibit selective neuronal loss at postmortem (51). Studies are needed to analyze whether the brain tissue that undergoes delayed secondary ischemic damage has penumbral properties and can be entirely salvaged by a therapeutic intervention.

Positron emission tomography (PET) has provided valuable informative data on the presence of the penumbra and its temporal evolution in larger animal species as well as in man (*vide infra*). Similar data are not available as yet in rodents in part due to the limited spatial resolution of current PET machines. Nonetheless, Saita et al. (52) recently reported the use of ^{18}F-fluoromisonidazole (^{18}F-FMISO), a PET tracer of hypoxic cells that has shown promise as a marker to image the penumbra in humans [see subsequently in this volume and Markus et al. (53)], in an ex vivo autoradiographic paradigm, reported increased tracer uptake in the affected area. Consistent with Saita et al. a recent in vivo study by Takasawa et al. (54), suggests ^{18}F-FMISO can demonstrate the penumbra using dedicated high resolution PET in the rat subjected to MCAO.

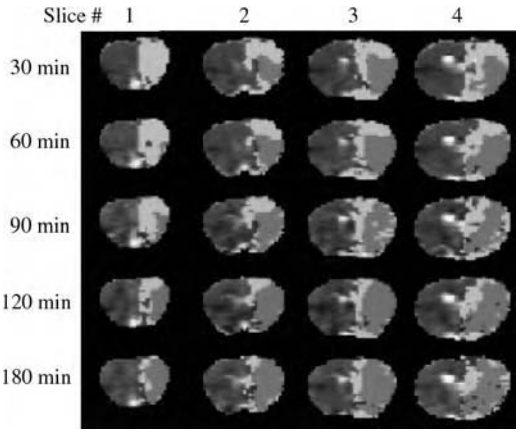

FIGURE 1 (*See color insert.*) The spatiotemporal evolution of CBF and ADC, measured with MRI, at different times following MCAO in the rat. The core region with marked reduced CBF and ADC is shown in orange. The "mismatch" zone with reduced CBF but slightly reduced ADC is shown in yellow. The nonaffected area with normal CBF and ADC is in grey. Between 30 minutes and 180 minutes of ischemia, the area of "mismatch" decreased progressively, SP indicating a progressive recruitment of the penumbra in infarction. *Abbreviations*: CBF, cerebral blood flow; ADC, apparent diffusion coefficient; MRI, magnetic resonance imaging; MCAO, middle cerebral artery occlusion. *Source*: From Ref. 45.

As a summary of the studies in rodents discussed earlier, one might deduce that ischemic brain damage in this species generally evolves during a two- to four-hour period following the induction of ischemia.

Duration of the Penumbra in Cats

Although cats present the advantage of being a gyrencephalic species, they have been much less used to model acute stroke compared to rodents, especially during the last decade. The data regarding the duration of the penumbra in this species are somewhat sparse.

Interventional Studies

The available neuropathological data obtained at different time points after the induction of ischemia indicate that the evolution toward brain infarction is less rapid in cats than in rodents. In awake cats subjected to MCAO, Weinstein et al. (55) found no infarct with ischemic periods lasting less than four hours; ischemia lasting five to eight hours produced infarcts significantly smaller than those seen after permanent occlusion. These findings are in accordance with those reported by Sundt et al. (56) in anesthetized cats. More recently, Taguchi et al. (57) also have shown that four hours occlusion in this species led to a larger infarction than that induced by one or two hours ischemia. In this study, however, periods of ischemia longer than four hours were not examined.

A variety of pharmacological agents have been tested in stroke models in the cat. Nonetheless, the great majority of these have been administered before or immediately after the onset of ischemia (58–61). Therefore no information about the therapeutic window or the temporal progression of brain damage can be drawn from these studies. *N*-methyl–D-aspartate (NMDA) receptor antagonists have been shown to reduce infarction volume by about 50% when administered two hours postocclusion (62,63). Baskin et al. (64) have demonstrated that treatment with selective kappa-opioid agonists, initiated six hours following the induction of permanent MCAO and continued through seven days, resulted in significant reduction of brain infarction.

Neuroimaging Studies

The evolution of the ischemic penumbra in cats has been documented by studies using repeated measurements of hemodynamic and metabolic parameters with PET. Heiss et al. (65) showed that animals subjected to MCAO displayed a region with reduced CBF, relatively preserved cerebral metabolic rate of oxygen ($CMRO_2$) and increased oxygen extraction fraction (OEF). This pattern indicative of the ischemic penumbra (66) shrunk concentrically from the center of the ischemic zone to the periphery of the middle cerebral artery (MCA) territory over a period extending to at least four hours. Conversely, the center of the ischemic region gradually developed the pattern consistent with irreversible damage (i.e., very low CBF and $CMRO_2$, normal or low OEF). Further reversible ischemia studies from the same authors showed that in the animals surviving 24 hours of reperfusion, the OEF remained elevated throughout the ischemic episode; however, the initial OEF increase disappeared within 60 minutes of onset of ischemia in those cats that died during the reperfusion period (67). In cats dying during the observation period, extended postischemic hyperperfusion accompanied marked decrease of $CMRO_2$ and cerebral metabolic rate of glucose (CMRGlu). In these cats, large infarcts developed and intracranial pressure increased fatally. Such results further illustrate the importance of the severity of ischemia in relation to its duration for the progression and irreversibility of ischemic brain damage.

As a general conclusion, the progression of the ischemic brain lesion is slower in the cat than that observed, in general, in rodents.

Duration of the Penumbra in Nonhuman Primates

Nonhuman primates are the species of choice to study the pathophysiology and the treatment of cerebral ischemia, because of the close similarities with the human cerebrovascular system, brain metabolism, gyrencephaly, and grey to white matter ratio (68). Although landmark studies regarding the ischemic penumbra have been carried out in nonhuman primates, these species have been relatively less used during the last two decades.

Interventional Studies

Few studies have quantitatively assessed infarct volume in the chronic stage in nonhuman primates. In a qualitative study in awake macaques subjected to MCAO, DeGirolami et al. (69) noted that short occlusion periods (15–60 minutes) were associated with preferential neuronal loss in poorly circumscribed cortical regions—a situation termed "selective necrosis"—whereas a consolidated necrosis was not observed until eight hours of MCAO. This evolution of damage has been reported to be much slower in the study of Meier-Ruge et al. (70). Using a histochemical, rather than histopathological technique, these authors demonstrated a progression of infarct volume during the 48 hours following permanent occlusion of the MCA in the anesthetized macaque. Recent quantitative histopathological experiments performed in the anesthetized baboon have shown that infarction volume, quantified at the chronic stage, was significantly smaller when reperfusion was initiated six hours after MCAO than following 20 hours MCAO or permanent MCAO (71,72). These findings suggest that in this model, the infarct still grows between 6 and 20 hours of occlusion time and the window of therapeutic opportunity remains open beyond six hours of ischemia. These data may appear to be in disagreement with the much cited study by Jones et al. (73) implying that infarction reaches its maximal size at three hours of MCAO. However, this latter investigation, which was performed in the awake macaque, focused on the probability of individual tissue compartment to evolve toward necrosis relative to local residual CBF, and not on the spatio-temporal expansion of an infarction volume in the ischemic brain (see later). Close examination of their data however, entirely supports the idea that at three hours, infarct volume has not reached its maximum (Fig. 2).

As in cats, neuroprotection studies in the nonhuman primate are rare despite the recent recommendation to use larger gyrencephalic species to test the efficacy of a therapeutic intervention (74). In the macaque, Tacrolimus (FK506), an immunosuppressive drug, conferred significant neuroprotection with a window of three hours following MCAO (75,76). In these studies, however, longer delays have not been examined. In a permanent ischemia in the marmoset, a new world monkey, Marshall et al. (77) reported that NXY-059, a nitrone-based free-radical-trapping agent, improves the neurological outcome and reduces the infarct size even when administration was delayed for up to four hours after stroke onset. Interestingly,

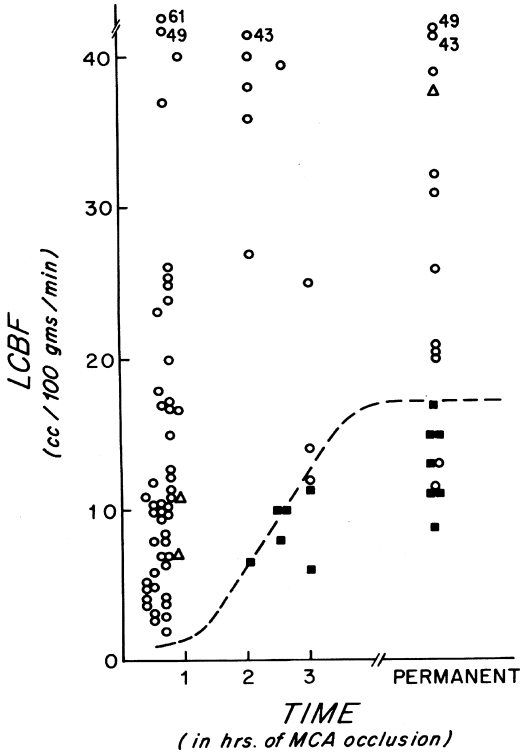

FIGURE 2 Relationships between local cerebral blood flow (LCBF), as measured by hydrogen clearance technique, and ultimate infarction as a function of the duration of middle cerebral artery occlusion (MCAO). Open circles represent normal tissue, triangles represent the periphery of the infarct, filled boxes represent infarcted tissue. Dashed line approximates infarction threshold: when LCBF falls below this critical value, infarction occurs. *Source*: From Ref. 73.

a recent randomized controlled trial suggests that this agent may have clinical benefit when administered within six hours of onset of stroke (78).

Neuroimaging Studies

As discussed earlier, ^{15}O–based PET studies have used combinations of low CBF, relatively preserved or normal $CMRO_2$, and a high OEF to distinguish tissue at risk of infarction, but potentially recoverable from irreversibly damaged tissue, characterized by severely reduced CBF and $CMRO_2$ with variable OEF (66). In the baboon subjected to permanent MCAO, Pappata et al. (79) observed progressive derangement of oxygen metabolism over four hours—the latest time point examined in this study. Further sequential investigations made both in the acute, subacute, and chronic stages of ischemia, showed that the severely hypometabolic tissue volume, taken as an index of irreversible damage, progressively increased over at least 24 hours following permanent MCAO in the baboon (80). This expansion of damage was reversed by restoration of CBF after six hours of ischemia (81,82). Although in this model of stroke cortical ischemia is relatively moderate since infarction affects mainly the deep structures of the MCA territory and the insular cortex, the findings from these experiments support the concept of a dynamic penumbra that progresses relatively slowly toward irreversible damage, unless a therapeutic intervention is instituted. Interestingly, these studies in baboons documented that not only the insular cortex regions but also the striato-capsular area could be salvaged from infarction by reperfusion at six hours (72). Recently, serial CBF measurements in the macaque subjected to thrombotic occlusion of the MCA showed also a progressive enlargement of the hypoperfused region over at least 24 hours after the insult (83).

Based on the few available quantitative animal studies discussed earlier, one might deduce that the delay before the establishment of the maximal ischemic brain lesion is proportional to the size of the species (or, at least, its brain). Nonetheless, as we have discussed before, the progression of ischemic brain damage is known to be influenced by a variety of factors including the severity of the primary insult, age, pre-existence of concomitant pathologies such as arterial hypertension and diabetes, physiological variables like brain temperature and blood glucose level, and also, of course, the anesthetic regimen.

Duration of the Penumbra in Man

Evidence for the existence and the evolution of the penumbra in humans mainly derives from functional neuroimaging techniques (51). Nonetheless, reflecting the well-known heterogeneity of stroke disease in man, the extent and the progression of ischemic brain damage is highly variable among patients (84).

Although repeated PET examinations in both the acute and chronic stages of ischemia are difficult to perform in human stroke due to logistical and ethical reasons, the use of this technique has revealed, in some patients, the presence of areas of low blood flow, preserved $CMRO_2$, and markedly increased OEF as late as 16 hours after the clinical onset, and even beyond in a few patients (85,85a). These penumbral areas may, or may not, eventually evolve to infarction, as documented by computed tomography (CT) scans performed in the chronic stage of stroke (86). Demise of the penumbra is signaled by dramatic decreases in the OEF indicating the precipitous fall in tissue's oxygen consumption when penumbra is recruited into the core (87,88). As theoretically expected, the volume of the penumbra that escapes infarction is highly correlated with neurological recovery (89). Read et al. (90,91), have employed PET with ^{18}F-FMISO, a marker of hypoxic tissue, to distinguish between irreversibly damaged and potentially viable penumbral tissue in acute-stroke patients. They reported the presence of a significant volume of peri-infarct hypoxic tissue as late as 42 hours after stroke. The volume of this hypoxic tissue declined with time after stroke, which they interpreted as the expansion of the infarct core occurring at the expense of penumbral tissue (53). Furthermore, the fate of the hypoxic tissue identified using this technique correlated to clinical recovery up to 48 hours from stroke onset (92). In accordance with these PET observations, MRI investigations have also demonstrated a relatively slow progression of ischemic brain damage in some patients. The expansion of ischemic lesions defined by DWI has been found to occur over the first 24 hours of ischemic stroke (93–95). Similarly, the use of the mismatch between DWI and PWI to map the penumbra

has shown that so-defined regions are present up to six hours after the insult in around 75% of MCA territory stroke patients (96), and may persist for up to 24 hours (96,97). As with PET, the volume of mismatch tissue salvaged correlates with neurological recovery (98). Recently, however, the definition of the penumbra, based on this mismatch, has been criticized by several authors (42,43).

The progressive evolution of abnormalities seen with PET and MRI supports the dynamic nature of the penumbra and suggests that in a fraction of patients there may be salvageable tissue at extended time points after the clinical onset. Nonetheless, significant penumbra can be absent in other patients even very early after stroke onset, due to extensive core or early extensive/complete reperfusion (see later). Within the hypoperfused but viable tissue that evolves to infarction, Heiss et al. (99) distinguished a genuinely penumbral area with CBF below a critical threshold of 12 mL/100 g/min, and more extensive areas of less severely hypoperfused tissue that may survive for extended time intervals; only the former would be amenable to hyperacute reperfusion therapy. However, numerous studies have shown the penumbra threshold to be closer to 20 mL/100 g/min in human (Table 3) (85,89,100). More recent studies documenting benefit of reperfusion as late as nine hours after stroke onset also support this view (see later). Using Xenon CT, Kaufmann et al. (101) failed to document significant penumbra within six hours of stroke onset, but this study was criticized on methodological grounds (102).

As in laboratory animals, the duration of the penumbra in man can also be inferred from interventional studies. Reperfusion induced by thrombolysis has been shown to be an effective therapeutic strategy in acute ischemic stroke when initiated within three hours of onset of symptoms (103). However, the use of multimodal brain imaging in acute stroke should help to identify those patients at risk of an enlarging infarct and may expand the therapeutic window beyond three hours in these selected patients (104). Accordingly, the Pro-Act II randomized trial of intra-arterial thrombolyis up to six hours in patients selected on the presence of proximal MCAO on cerebral angiography showed significant benefit of treatment versus placebo (105). Furthermore, among others, Ribo et al. (106) have shown successful use of stroke MRI in selecting patients for intravenous tissue plasminogen activator (t-PA) in the three- to six-hour window. Similarly, the novel thrombolytic, desmoteplase, has been shown to be associated with a higher rate of reperfusion and better clinical outcome compared with placebo when administered intravenously between three to nine hours after acute ischemic stroke in patients selected on the presence of perfusion/diffusion mismatch (107,108). These clinical observations further attest to a prolonged therapeutic window in some patients and stress the importance of the use of neuroimaging techniques to map the potentially viable tissue in individual patients (109). Formal demonstration of the benefit (or not) of MR imaging to select candidates for thrombolysis despite added time awaits completion of current trials such as EPITHET.

Although penumbral tissue may persist in some patients up to 16 to 24 hours after clinical stroke onset, in others it may disappear very early, which demonstrates considerable pathophysiological heterogeneity underlying acute MCA stroke, and has very important clinical implications with respect to therapeutic thrombolysis. For instance, the prospective ^{15}O PET study of Marchal et al. (84,110) showed that in some patients the core is seen to widely extend into cortical areas as early as four hours after onset, probably from inadequate pial collaterals, while in other patients hyperperfusion with preserved $CMRO_2$ involves the entire MCA territory in the same timescale, indicative of early spontaneous recanalization. Notably, in contrast with the presence of penumbra where outcome is unpredictable, the former PET pattern invariably predicts poor outcome and malignant infarction, while the latter invariably predicts excellent outcome, independent of admission clinical scores. Clearly, thrombolysis would not appear logical in the latter patients, and potentially harmful in the former. These three pathophysiological PET patterns are illustrated in Figure 3. Importantly, the same three main pathophysiological patterns have been documented with MR-based DWI/PWI (97,111,112).

THRESHOLDS OF THE PENUMBRA

Thanks to the pioneering works of Symon et al. (113), two ischemic flow thresholds have been introduced: the electrical (or penumbra) threshold, corresponding to the CBF level below which spontaneous or evoked brain electrical activity fails, and the viability (or infarction) threshold,

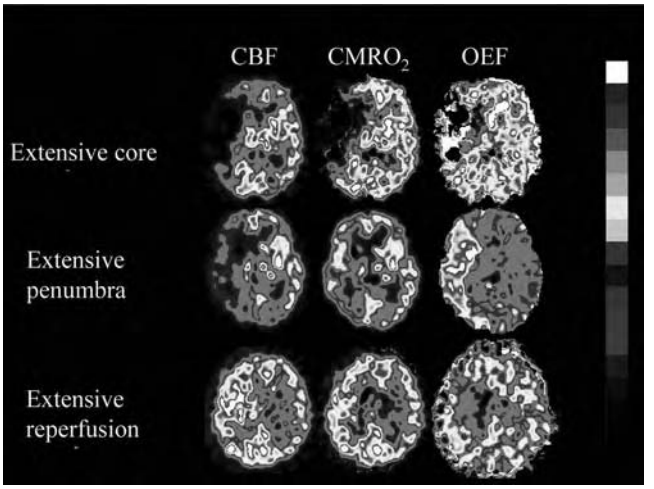

FIGURE 3 (*See color insert.*) The three main pathophysiological positron emission tomography patterns observed in the acute stage of anterior circulation stroke. The pseudo color scale on the right goes from lowest pixel values (black) to maximum pixel values (white), adjusted for each image.

that is, the flow level below which irreversible neuronal damage occurs. These two thresholds therefore define the upper and lower flow limits of the penumbra (85,114). In these initial studies, loss of membrane homeostasis with efflux of potassium was used as a marker of irreversible structural injury. In subsequent investigations, viability thresholds have been operationally defined based on different techniques such as neuropathology, metabolic autoradiography, and physiological and morphological neuroimaging (85,115).

Reference to CBF thresholds is of crucial importance to analyze the penumbra. However, it should be emphasized that the absolute values of these thresholds are not universally constant, but will depend on different important factors like the animal species studied, the nature of the anesthetic agents employed (if any), the physiological conditions (e.g., systemic blood pressure, body temperature, plasma glucose), the technique used for perfusion measurements, and the presence or not of a given therapeutic manipulation (116). In addition, although the penumbra threshold is time-independent, the infarction threshold increases with time elapsed since MCAO (73), eventually reaching the penumbra threshold, when all the penumbra has been recruited into the core. In other words, the more hypoperfused tissue will tend to progress to infarction the earliest. Only the studies that aimed to determine, as opposed to studies that simply applied, the penumbra and infarction thresholds for CBF and $CMRO_2$ will be discussed here. The reader is referred to method-specific chapters in this volume regarding thresholds derived with other variables such as ^{11}C-Flumazenil, the MTT/TTP, the cerebral blood volume (CBV), and the ADC.

Thresholds in Rodents

The baseline CBF values in rodents are around twice those measured in nonhuman primates (117). Neuronal density and brain metabolism in these animals are also greater, relative to those of primates (118,119). Therefore, one assumes that, at any particular time period following an arterial occlusion, the absolute thresholds of the penumbra in rodents would be higher than in larger species.

Harris and Symon (120), using similar procedures as in their initial baboon studies (see subsequently), reported that in the rat subjected to cerebral ischemia, the extracellular K^+ increases at CBF levels around 15 mL/100 g/min. This threshold, indicative of irreversible damage, was higher than that observed in the baboon brain (121). Following permanent MCAO in the rat, Bolander et al. (122) have reported that when CBF was below 24 mL/100 g/min (15% of preocclusion values), brain tissue undergoes infarction; whereas regions with CBF above 20% of control, do not show any histological alterations. These threshold values are consistent with those reported in other rat studies in which postmortem histology was employed to identify irreversible brain damage (Table 2) (45,46,123–125). In spontaneously hypertensive rats subjected to periods of ischemia longer than three hours, the CBF threshold for infarction was

TABLE 2 Thresholds in Different Animal Models of Cerebral Ischemia

Species	Anesthesia	Methods of ischemia	Time following ischemia	Threshold for infarction	Technique of CBF measurement	Outcome	References
Rat	Halothane	Bilateral CCA+ hypotension	Immediately after MCAO	15	Hydrogen clearance	K^+ efflux	(120)
Rat	Halothane	tMCAO	2 h	30	IAP	Histopathology	(124)
Rat	Pentobarbital	pMCAO	Up to 6 h	24	IAP	Histopathology	(122)
Rat	Halothane	pMCAO	5 min	10 %	IAP	Histopathology	(126)
Rat	Halothane	pMCAO	4 h	25	IAP	Histopathology	(125)
Rat	Halothane	pMCAO	30 min	24	IAP	Histopathology	(123)
SHR	Halothane	pMCAO	3 h	50	IAP	Histopathology	(127)
Rat	Isoflurane	pMCAO	3 h	30	MRI	TTC	(45,46)
Rat	Halothane	pMCAO	30 min	34	IAP	DWI	(130)
Rat	Halothane	pMCAO	2 h	41	IAP	DWI	(130)
Rat	Halothane	pMCAO	30 and 120 min	13 to 19	IAP	ATP	(130)
Rat	Halothane	pMCAO		19 to 32	IAP	ATP	(131)
Rat	Halothane	pMCAO	2 h	18	IAP	ATP	(129)
Cat	Ketamine	t MCAO	0–140 min	9 to 22	Hydrogen clearance	SNA	(132)
Cat	Halothane	t MCAO	30 and 60 min	15 and 40	Microspheres	TTC and MRI	(140)
Cat	Halothane	t MCAO	2 h	12–15	Hydrogen clearance	Histopathology	(138)
Baboon	a-chloralose	pMCAO	Immediately after MCAO	10	Hydrogen clearance	K^+	(121)
Macaque	Awake	tMCAO	2–3 h	12	Hydrogen clearance	Histopathology	(143)
Macaque	Awake	tMCAO	1.5–2 h	5	Hydrogen clearance	Histopathology	(73)
Macaque	Awake	tMCAO	3 h	12	Hydrogen clearance	Histopathology	(73)
Macaque	Awake	pMCAO	Permanent	18	Hydrogen clearance	Histopathology	(73)

Abbreivations: IAP, iodoantipyrine autoradiography; SHR, spontaneously hypertensive rat; SNA, spontaneous neuronal activity; TTC, triphenyl tetrazolium chloride; pMCAO, permanant middle cerebral artery occlusion; tMCAO, temporary middle cerebral artery occlusion.

50 mL/100 g/min (127). This critical CBF value is approximately two-fold higher than that observed in normotensive rats. This might explain the difference in vulnerability between hypertensive and normotensive rats (128). It is also interesting to note that the absolute values of CBF thresholds for infarction reported in the normotensive rats are higher than those observed in nonhuman primates (see later). This implies that any extrapolation of these values between the rats and primates would be meaningless.

Critical CBF thresholds have also been examined by correlation with DWI, ATP metabolism, and other measurements (115). Hoehn-Berlage et al. (129) reported an infarction threshold of approximately 18 mL/100 g/min at two hours after MCAO, by correlating CBF autoradiography with ATP depletion. This threshold is time dependent since it was around 13 mL/100 g/min at 30 minutes, following the occlusion (130). A similar pattern of time dependency was observed when CBF values were correlated with the increase of signal intensity in DWI (Table 2) (130).

Thresholds in Cats

Using electrophysiological techniques, Heiss and Rosner (132) have shown in cats that recovery of neuronal activity is a function of both the severity and the duration of blood flow impairment. Spontaneous neuronal activity recovered rapidly when blood flow was maintained between 9 to 22 mL/100 g/min for up to 20 minutes; however, most of neurons required longer periods to recover their activity when CBF was below 9 mL/100 g/min for less than 20 minutes or between 9 and 22 mL/100 g/min for up to two hours. Histological analyses revealed no abnormality or slight ischemic changes in cases with electrical recovery, while regions with irreversible neuronal failure displayed selective necrosis of individual cells or total infarction (132). This study is of importance in that neuronal reaction to decreased CBF was highly heterogeneous among neurons examined. This indicates different vulnerability of neurons to ischemia and in turn may explain the selective neuronal loss observed in laboratory animals, and occasionally also in humans (47,133–137).

In a neuropathological study of cats subjected to two hours MCAO followed by recirculation for two hours, Tamura et al. (138) observed histological signs of cell damage in all regions with flows below 12 mL/100 g/min and in some regions with flows between 12 and 15 mL/100 g/min (Table 2). These perfusion thresholds were similar to those reported in the monkey following two to three hours of ischemia (73,139). More recently, Miyabe et al. (140) showed, through the use of sequential DWI, that irreversible damage was delineated by blood flow of <15 mL /100 g/min at 30 minutes of ischemia and <40 mL/100 g/min at 60 minutes of ischemia. Again, this study in the cat illustrates the dependency of flow thresholds for ischemic injury with time.

Thresholds in Nonhuman Primates

As mentioned earlier, the concept of critical flow thresholds that define the penumbra has mainly emerged from experimental investigations in nonhuman primates. In the baboon subjected to MCAO, reduction of CBF beyond an ischemic threshold of approximately 15 mL/100 g/min (approximately 35% of control values) led to complete failure of the somatosensory evoked potential, which could be reversed if CBF was promptly increased above this threshold (141,142). The same group, using the same stroke model, also showed that massive release of intracellular K^+ occurred only when CBF reached a level of 6 mL/100 g/min (121). These two flow thresholds identify an ischemic condition in which brain tissue has lost its function but still maintains its membrane integrity, and thus viability. Subsequent investigations in the awake macaque have confirmed these findings (143) and extended them to integrate the time component. Indeed, in the studies of Jones et al. (73), a reduction in blood flow led to the development of a neurologic deficit. When average local CBF was greater than 21 to 23 mL/100 g/min, little or no deficit could be detected, however, when CBF dropped below a "paralysis threshold," mild deficits were noted that progressed to complete hemiplegia when CBF was less than 8 to 9 mL/100 g/min. In these investigations, the infarction threshold clearly depended on the duration of ischemia (Fig. 2). Based on the several published reports from this series of investigations (73,139,144), an infarction threshold was not observed until occlusion times of 1.5 to 2 hours, where it was approximately 5 mL/100 g/min, and then increased to ~12 mL/100 g/min

for three hours ischemia and ~18 mL/100 g/min with permanent occlusion, that is, close to the clinically eloquent threshold of ~22 mL/100 g/min. The dependency of infarction on both flow impairment and duration clearly illustrates the concept of the dynamic penumbra. Importantly, selective neuronal necrosis was observed in the striatum for occlusion times one to two hours and CBF in the range of 5 to 18 mL/100 g/min (139), suggesting that early reperfusion of the penumbra can arrest its progression to pan-necrosis but cannot save all the neurons, with some vulnerable neurons dying out in the peri-infarct area. Also, Marcoux et al. (139) suggested lower infarction thresholds for the white than for the grey matter.

In more recent nonhuman primate studies, perfusion thresholds of infarction were examined through the use of functional imaging. Yonas et al. (145,146), studying anesthetized baboons with selective occlusion of the lateral striate arteries by electrocoagulation, demonstrated with a Xe-CT method that CBF less than 8 to 10 mL/100 g/min for six hours or shorter results in infarction in the involved regions. Kuge et al. (147) observed that ischemic regions with CBF below 40% of contralateral hemisphere (10–16 mL/100 g/min) were associated with consolidated infarction one hour following clots injection. Although these infarction thresholds are comparable to those reported by Jones et al. (73), differences between these values could be attributed to the method used to induce ischemia, duration of ischemia, anesthesia regimen, and techniques used for CBF measurements.

Perfusion and Metabolic Thresholds in Man

As stated above, it is crucial for optimal acute-stroke management to be able to discriminate between irreversibly damaged brain tissues (i.e., core), mildly hypoperfused tissue that recovers spontaneously (i.e., oligemia), and more seriously hypoperfused but viable tissue that may progress to infarction if left untreated (i.e., the penumbra). In this section we review the reported CBF and $CMRO_2$ thresholds for penumbra and infarction in humans. By definition, a threshold determines the boundary between two tissue categories, so only the studies that have formally determined (either visually or statistically) the value best separating ROIs or voxels with different outcomes are reported here (i.e., infarction or no infarction, either spontaneously or after thrombolysis); in other words, studies that report only mean values for tissue compartments are not considered. Also, only those studies that have analyzed patients with persistent arterial occlusion and/or high OEF to determine the penumbra threshold are considered; in other words, studies that did not exclude already reperfused patients have been excluded from this review. Finally, the thresholds derived from acute-stroke studies using tomographic imaging techniques are only discussed here; an account of classic studies of hemispheric CBF, electroencephalography (EEG), and clinical status during carotid clamping are described elsewhere (85).

Positron Emission Tomography

PET has been leading the way in the analysis of these different regions in man (85,148): Multitracer ^{15}O studies defined the penumbra as tissue with reduced CBF but relatively preserved $CMRO_2$ and raised OEF. Although this definition appropriately excludes situations of low perfusion with normal or reduced OEF—reflecting diaschisis and partially reperfused tissue, respectively—it still encompasses both benign oligemia and genuine penumbra (100). There is, therefore, a need to augment this definition by both perfusion thresholds separating these two high OEF compartments, and clinical/functional correlates, specifically: (*i*) the volume of the penumbra must contribute to acute-stage neurological deficit, and (*ii*) the volume of penumbra that eventually escapes infarction must predict neurological recovery, that is, the difference between admission and outcome scores (89). Through the use of PET combined with late structural MRI or CT scan to map the eventually infarcted tissue, several investigations have determined the CBF or $CMRO_2$ thresholds for the penumbra and irreversible damage (Table 3).

Regarding CBF, initial studies using ROIs and/or subacute stage scanning found that a flow less than ~12 mL/100 g/min indicated the core of ischemia which evolved inevitably toward necrosis (149–152). However, subsequent studies performed within the 5 to 18 hours time window and assessing the tissue fate at the voxel level, reported probabilistic infarction thresholds of ~7 to 8 mL/100 g/min (89,153). In the Furlan et al. 1996 study (89),

TABLE 3 Flow (Top) and $CMRO_2$ (Bottom) Thresholds in Man

Threshold for irreversible damage	Threshold for the penumbra	Time following ischemia	Technique of CBF measurement	Technique of imaging infarction	Reference
12	ND	2 to 38 d	PET	CT	(149)
15	19	8 d to 3 yr	PET	CT	(151)
12	18	10–38 h	PET	CT	(152)[d]
ND	22	7–18 h	PET	CT	(86)[d]
7	17	5–16 h	PET	CT	(85)[d]
8.4	ND	5–18 h	PET	CT	(153)[d]
4.8	14.1	2–12 h	PET	MRI	(99)
35%	ND	≤6 h	PET	MRI	(154)
35%[a]	70%	≤6 h	SPECT	CT	(168)
40%	60%	2.5–6 h	SPECT	CT	(172)
25	35	≤6 h	SPECT	CT	(159)
25–55%[b]	55%	2-12 h	SPECT	CT	(158)
20 (GM), 12 (WM)	ND	≤6 h	MRI	MRI	(162)[a]
ND	59% (21[c])	≤6 h	MRI	MRI	(170)
36%	79%	1–12 h	MRI	MRI	(171)
ND	48% (24[c])	3.5–22 h	MRI	MRI	(169)
6	20	1–6 h	Xe-CT	CT	(101)
$CMRO_2$ thresholds					
1.7	N/A	2–38 d	PET	CT	(149)
1.5	N/A	2–24 h	PET	CT	(167)
1.3	N/A	8 d–3 yr	PET	CT	(151)
~1.3	N/A	3.5–16 h	PET	MR	(156)
0.87	N/A	7–18 h	PET	CT	(153)[a]
45%	N/A	≤6 h	PET	MRI	(154)

The values for CBF and $CMRO_2$ are in mL/100g.min and when indicated in percentage of contralateral hemisphere.
[a]Threshold for hemorrhagic transformation after thrombolysis.
[b]Time-dependent increase in infarction threshold.
[c]Value calculated assuming normal global CBF in man is 50 mL/100 g.min.
[d]Voxel-based studies (remaining studies were all ROI_based).
Abbreviations: GM, gray matter; N/A, not applicable; ND, not determined; WM, white matter.

acute-stage multitracer PET was combined with serial clinical scoring from admission and outcome CT. Using a spatial-temporal-clinical model, they found that flow values between 7 and 22 mL/100 g/min probabilistically defined the penumbra with an uncertain fate, while flow above 22 mL/100 g/min indicated hypoperfused areas with high chance for spontaneous recovery—predicted clinical correlations were found for both compartments. Although the infarction threshold has not been systematically assessed at different time points, it would be

expected, based on monkey studies (73) to be lower with more acute studies. Accordingly, studying patients in the 2 to 12 hours time window, Heiss et al. (99) reported a probabilistic grey matter infarction thresholds of 4.8 mL/100 g/min; however, in this same study the penumbra threshold was reported as being 14.1 mL/100 g/min, which is on the low side perhaps due to the use of a bolus CBF method and ROIs (85). Interestingly, both Furlan et al. (89) and Shimosegawa et al. (154) found that the portion of the penumbra that ultimately progressed to frank infarction had lower CBF and $CMRO_2$ values, on average, than the portion that eventually escaped infarction, in agreement with the experimental concept that the process of recruitment of the penumbra into the core targets, in the first instance, the most hypoperfused penumbral tissue.

Regarding the $CMRO_2$ infarction threshold, PET studies using the ROI approach reported critical values ranging 1.3 to 1.7 mL/100 g/min below which irreversible damage invariably occurred (149,151,155). However, studies performed at the voxel level reported a probabilistic infarction threshold of 0.87 mL/100 g/min for mixed grey and white matter voxels, unrelated to time elapsed since stroke onset within the 7 to 18 hours window (153), and of 1.3 mL/100 g/min for grey matter ROIs, using a different PET technique, in the 3.5 to 16 hours window (156)—consistent with these critical values. Overall, and in contrast with the CBF, the $CMRO_2$ infarction threshold does not appear to depend on time since stroke onset, although no study has yet formally addressed this issue. Interestingly, in the Marchal et al. (153) study, applying the CBF and $CMRO_2$ probabilistic infarction thresholds to the same data set yielded largely overlapping voxel populations, yet allowed to significantly increase the total voxel number, probably because of their probabilistic nature. Note that reduced OEF alone is not a reliable predictor of infarction (153). Interestingly in the Marchal et al. study (153) a probabilistic CBV infarction threshold of 1.64 mL/100 g was found, which, however, fell just short of statistical significance.

Other Imaging Modalities

As PET technology is restricted to a few centers worldwide and requires complex logistics for investigations of acute-stroke patients, other techniques have been employed in order to analyze perfusion thresholds that distinguish the penumbra and the core (Table 3). However, it must be noted that, apart from the still unreplicated Lee et al. (157) MR study, these techniques provide only perfusion, not $CMRO_2$ or OEF, which constrains their predictive power. In addition, because of technical issues discussed elsewhere in this volume, they rarely allow truly absolute CBF values to be derived, or if so, with such degree of uncertainty that only perfusion values relative to the contralateral mirror ROI (or voxel population) are generally considered.

In SPECT perfusion studies using mainly ^{99m}Tc-HMPAO, CBF penumbra thresholds ranging from 25% to 55% of the contralateral hemisphere have been reported (Table 3), with suggestion of increase with time (158). Some of this variability may be due to the fact that it is impossible with SPECT to differentiate ischemic from partially reperfused tissue (159). Rather consistent penumbra threshold around 55% to 70% of the contralateral values were found in these studies (Table 3), somewhat on the high side probably because of the method used.

Recently, many investigations have been performed to assess the potential of MR-based PWI in determining perfusion levels for infarction/DWI lesion growth or recovery. As shown in Table 3, however, few studies only have determined actual thresholds, but when reported, the values appear overall consistent with other studies (Table 3). Note that in all these studies the model used to determine the thresholds implied that the acute DWI represents irreversibly damaged tissue, an assumption now known to be inaccurate (see earlier), while the penumbra threshold defined the hypoperfused tissue that progressed to infarction, that is, the severely affected penumbra.

CT perfusion has been used recently in clinical studies to map the core and penumbra, using thresholds derived from CBV and CBF, namely CBF reduction >34% (relative to opposite hemisphere) and CBV <2.5mL/100mL for the core, and CBF reduction >34% but CBV >2.5 mL/100mL for the penumbra. Although these thresholds have been validated against DWI/PWI and have shown the expected correlations with clinical recovery (160,161), they have not been formally validated as yet (see Chapter 10, this volume, for further details).

General Comments

The modality-related differences and some of the variability in the thresholds reported among the studies and summarized in Table 3 can be attributed to a host of additional factors. The use of ROI- or voxel-based analysis is particularly important. Voxel-based thresholds are necessary for clinical applications, in order to map the penumbra and the core. However, they are more difficult to perform, and the mix of gray and white matter may be an issue. Both the penumbra and the infarction thresholds are likely to differ between grey and white matter. For instance, the recent DWI/PWI study of Bristow et al. (162) reports significantly higher grey matter than white matter CBF infarction threshold. These findings, which concur with earlier data from monkey studies (73), suggest that a single common threshold applied to both tissues will overestimate extent of tissue at risk in white matter and underestimate it in grey matter. Solutions to this problem applicable in the acute stage of stroke for decision-making purposes are not readily available but may use, for instance, spatially-normalized segmentation templates. On the other hand, ROIs, by providing averaged values, will tend to overestimate the true infarction threshold and underestimate the true penumbra threshold. The variable size of the ischemic areas results in partial volume effects, particularly in early PET studies and with SPECT. As stated, the delay between the stroke and scanning affects the measured infarction threshold. As well demonstrated in animal studies, the infarction threshold is time dependent and is likely to increase even within short time intervals (see earlier) (Fig. 2). This is exemplified by the MR study of Lin et al. (163) in which patients examined two to four hours after the stroke had a CBF threshold for ADC decrease of 15 mL/100 g/min, whereas in patients examined between 4.5 and 6.5 hours this threshold was on an average 24 mL/100 g/min) (see Chapter 3). Finally, although MR does not easily access OEF/$CMRO_2$, it allows access to the ADC, which is related to the severity of the ischemic injury. Variable combinations of several perfusion variables (e.g., MTT and CBV in addition to CBF) together with the ADC value and/or the volume of affected tissue appear to provide more reliable prediction of final infarction than the CBF alone and are being extended at present (164–166).

CONCLUSION

The studies discussed in the present chapter show clearly that the ischemic penumbra is a dynamic process and its kinetics of evolution toward irreversible necrosis is species dependent, and is likely slower in human than small laboratory animals. However, within each species, multiple factors are capable of influencing the duration of the penumbra, above all, the time elapsed since stroke onset. The better characterization of critical flow thresholds for the penumbra, and their temporal evolution will help to identify this region as well as its duration, and thus to optimize the management of acute stroke.

REFERENCES

1. Macrae IM. New models of focal cerebral ischaemia. Br J Clin Pharmacol 1992; 34(4):302–308.
2. Hossmann KA. Animal models of cerebral ischemia. 1. Review of literature. Cerebrovasc Dis 1991; 1:2–15.
3. Hata R, Mies G, Wiessner C, et al. A reproducible model of middle cerebral artery occlusion in mice: hemodynamic, biochemical, and magnetic resonance imaging. J Cereb Blood Flow Metab 1998; 18(4):367–375.
4. Dirnagl U, Iadecola C, Moskowitz MA. Pathobiology of ischaemic stroke: an integrated view. Trends Neurosci 1999; 22:391–397.
5. Lee JM, Zipfel GJ, Choi DW. The changing landscape of ischaemic brain injury mechanisms. Nature 1999; 399(6738 suppl):A7–A14.
6. Nagasawa H, Kogure K. Correlation between cerebral blood flow and histologic changes in a new model of middle cerebral artery occlusion. Stroke 1989; 20:1037–1043.
7. Zea Longa E, Weinstein PR, Carlson S, et al. Reversible middle cerebral artery occlusion without craniectomy in rats. Stroke 1989; 20:84–91.
8. Memezawa H, Smith ML, Siesjö BK. Penumbral tissues salvaged by reperfusion following middle cerebral artery occlusion in rats. Stroke 1992; 23:552–559.
9. Kaplan B, Brint S, Tanabe J, et al. Temporal thresholds for neocortical infarction in rats subjected to reversible focal cerebral ischemia. Stroke 1991; 22:1032–1039.
10. Buchan AM, Xue D, Slivka A. A new model of temporary focal neocortical ischemia in the rat. Stroke 1992; 23:273–279.

11. Garcia JH, Liu KF, Ho KL. Neuronal necrosis after middle cerebral artery occlusion in wistar rats progresses at different time intervals in the caudoputamen and cortex. Stroke 1995; 26:636–643.
12. Li Y, Chopp M, Garcia JH, et al. Distribution of the 72-kd heat shock protein as a function of transient focal cerebral ischemia in rats. Stroke 1992; 23:1292–1298.
13. Zhang RL, Chopp M, Garcia JH, et al. Temporal profile of ischemic tissue damage, neurotrophil response, and vaccular plugging following permanent and transient (2 h) middle cerebral artery occlusion in the rat. J Neurol Sci 1994; 125:3–10.
14. Hata R, Maeda K, Hermann D, et al. Dynamics of regional brain metabolism and gene expression after middle cerebral artery occlusion in mice. J Cereb Blood Flow Metab 2000; 20:306–315.
15. Hara T, Mies G, Hossmann KA. Effect of thrombolysis on the dynamics of infarct evolution after clot embolism of middle cerebral artery in mice. J Cereb Blood Flow Metab 2000; 20(10):1483–1491.
16. Huang J, Kim LJ, Mealey R, Marsh et al. Neuronal protection in stroke by an sLex-glycosylated complement inhibitory protein. Science 1999; 285:595–599.
17. Yrjanheikki J, Tikka T, Keinanen R, et al. A tetracycline derivative, minocycline, reduces inflammation and protects against focal cerebral ischemia with a wide therapeutic window. Proc Natl Acad Sci USA 1999; 96:13496–13500.
18. Phillips JB, Williams AJ, Adams J, et al. Proteasome inhibitor PS519 reduces infarction and attenuates leukocyte infiltration in a rat model of focal cerebral ischemia. Stroke 2000; 31:1686–1693.
19. Savitz SI, Erhardt JA, Anthony JV, et al. The novel beta-blocker, carvedilol, provides neuroprotection in transient focal stroke. J Cereb Blood Flow Metab 2000; 20:1197–1204.
20. Rabuffetti M, Sciorati C, Tarozzo G, et al. Inhibition of caspase-1-like activity by Ac-Tyr-Val-Ala-Asp-chloromethyl ketone induces long-lasting neuroprotection in cerebral ischemia through apoptosis reduction and decrease of proinflammatory cytokines. J Neurosci 2000; 20:4398–4404.
21. Li H, Colbourne F, Sun P, et al. Caspase inhibitors reduce neuronal injury after focal but not global cerebral ischemia in rats. Stroke 2000; 31:176–182.
22. Yepes M, Sandkvist M, Wong MK, et al. Neuroserpin reduces cerebral infarct volume and protects neurons from ischemia-induced apoptosis. Blood 2000; 96:569–576.
23. Yang Y, Li Q, Wang CX, et al. Dose-dependent neuroprotection with tiagabine in a focal cerebral ischemia model in rat. Neuroreport 2000; 11:2307–2311.
24. Williams AJ, Dave JR, Phillips JB, et al. Neuroprotective efficacy and therapeutic window of the high-affinity N-methyl-D-aspartate antagonist conantokin-G: in vitro (primary cerebellar neurons) and in vivo (rat model of transient focal brain ischemia) studies. J Pharmacol Exp Ther 2000; 294:378–386.
25. Sutherland GR, Perron JT, Kozlowski P, et al. AR-R15896AR reduces cerebral infarction volumes after focal ischemia in cats. Neurosurgery 2000; 46:710–719.
26. Kawasaki-Yatsugi S, Ichiki C, Yatsugi S, et al. Neuroprotective effects of an AMPA receptor antagonist YM872 in a rat transient middle cerebral artery occlusion model. Neuropharmacology 2000; 39:211–217.
27. Leist M, Ghezzi P, Grasso G, et al. Derivatives of erythropoietin that are tissue protective but not erythropoietic. Science 2004; 305(5681):239–242.
28. Slusher BS, Vornov JJ, Thomas AG, et al. Selective inhibition of NAALADase, which converts NAAG to glutamate, reduces ischemic brain injury. Nat Med 1999; 5:1396–1402.
29. Belayev L, Liu Y, Zhao W, et al. Human albumin therapy of acute ischemic stroke: marked neuroprotective efficacy at moderate doses and with a broad therapeutic window. Stroke 2001; 32:553–560.
30. Chabrier PE, Auguet M, Spinnewyn B, et al. BN 80933, a dual inhibitor of neuronal nitric oxide synthase and lipid peroxidation: a promising neuroprotective strategy. Proc Natl Acad Sci USA 1999; 96:10824–10829.
31. Kuroda S, Tsuchidate R, Smith ML, et al. Neuroprotective effects of a novel nitrone, NXY-059, after transient focal cerebral ischemia in the rat. J Cereb Blood Flow Metab 1999; 19:778–787.
32. Yang Y, Li Q, Shuaib A. Neuroprotection by 2-h postischemia administration of two free radical scavengers, alpha-phenyl-n-tert-butyl-nitrone (PBN) and N-tert-butyl-(2-sulfophenyl)-nitrone (S-PBN), in rats subjected to focal embolic cerebral ischemia. Exp Neurol 2000; 163:39–45.
33. Carter AJ, Grauert M, Pschorn U, et al. Potent blockade of sodium channels and protection of brain tissue from ischemia by BIII 890 CL. Proc Natl Acad Sci USA 2000; 97:4944–4949.
34. Yu YM, Kim JB, Lee KW, et al. Inhibition of the cerebral ischemic injury by ethyl pyruvate with a widetherapeutic window. Stroke 2005; 36(10):2238–2243.
35. Dijkhuizen RM, Nicolay K. Magnetic resonance imaging in experimental models of brain disorders. J Cereb Blood Flow Metab 2003; 23(12):1383–1402.
36. Gill R, Sibson NR, Hatfield RH, et al. A comparison of the early development of ischaemic damage following permanent middle cerebral artery occlusion in rats as assessed using magnetic resonance imaging and histology. J Cereb Blood Flow Metab 1995; 15:1–11.
37. Jiang Q, Zhang RL, Zhang ZG, et al. Diffusion-, T2-, and perfusion-weighted nuclear magnetic resonance imaging of middle cerebral artery embolic stroke and recombinant tissue plasminogen activator intervention in the rat. J Cereb Blood Flow Metab 1998; 18:758–767.
38. Knight RA, Ordidge RJ, Helpern JA, et al. Temporal evolution of ischemic damage in rat brain measured by proton nuclear magnetic resonance imaging. Stroke 1991; 22:802–808.

39. Dardzinski BJ, Sotak CH, Fisher M, et al. Apparent diffusion coefficient mapping of experimental focal cerebral ischemia using diffusion-weighted echo-planar imaging. Magn Reson Med 1993; 30:318–325.
40. Roussel SA, van Bruggen N, King MD, et al. Monitoring the initial expansion of focal ischaemic changes by diffusion-weighted MRI using a remote controlled method of occlusion. NMR. Bio Med 1994; 7:21–28.
41. Minematsu K, Li L, Fisher M, et al. Diffusion-weighted magnetic resonance imaging: rapid and quantitative deatection of focal bein ischemia. Neurology 1992; 42:235–240.
42. Sobesky J, Zaro Weber O, Lehnhardt FG, et al. Does the mismatch match the penumbra? Magnetic resonance imaging and positron emission tomography in early ischemic stroke. Stroke. 2005; 36(5):980–985.
43. Kidwell CS, Alger JR, Saver JL. Beyond mismatch: evolving paradigms in imaging the ischemic penumbra with multimodal magnetic resonance imaging. Stroke 2003; 34(11):2729–2735.
44. Guadagno JV, Donnan GA, Markus R, et al. Imaging the ischaemic penumbra. Curr Opin Neurol 2004; 17(1):61–67.
45. Shen Q, Meng X, Fisher M, et al. Pixel-by-pixel spatiotemporal progression of focal ischemia derived using quantitative perfusion and diffusion imaging. J Cereb Blood Flow Metab 2003; 23:1479–1488.
46. Bardutzky J, Shen Q, Henninger N, et al. Differences in ischemic lesion evolution in different rat strains using diffusion and perfusion imaging. Stroke 2005; 36(9):2000–2005.
47. Li F, Han SS, Tatlisumak T, et al. Reversal of acute apparent diffusion coefficient abnormalities and delayed neuronal death following transient focal cerebral ischemia in rats. Ann Neurol 1999; 46:333–342.
48. Li F, Liu KF, Silva MD, et al. Transient and permanent resolution of ischemic lesions on diffusion-weighted imaging after brief periods of focal ischemia in rats: correlation with histopathology. Stroke 2000; 31:946–954.
49. Zarow GJ, Graham SH, Mintorovitch J, et al. Diffusion-weighted magnetic resonance imaging during brief focal cerebral ischemia and early reperfusion: evolution of delayed infarction in rats. Neurol Res 1995; 17:449–454.
50. Neumann-Haefelin T, Kastrup A, de Crespigny A, et al. Serial MRI after transient focal cerebral ischemia in rats: dynamics of tissue injury, blood-brain barrier damage, and edema formation. Stroke 2000; 31(8):1965–1972.
51. Guadagno JV, Warburton EA, Aigbirhio FI, et al. Does the acute DWI lesion represent penumbra as well as core? A combined quantitative PET-MR voxel-based study. J Cerebr Blood Flow Metabol 2004; 24:1249–1254.
52. Saita K, Chen M, Spratt NJ, et al. Imaging the ischemic penumbra with ^{18}F-fluoromisonidazole in a rat model of ischemic stroke. Stroke 2004; 35(4):975–980.
53. Markus R, Reutens DC, Kazui S, et al. Topography and temporal evolution of hypoxic viable tissue identified by 18F-fluoromisonidazole positron emission tomography in humans after ischemic stroke. Stroke 2003; 34(11):2646–2652.
54. Takasawa M, Beech JS, Fryer TD, et al. Imaging of brain hypoxia in permanent and temporary middle cerebral artery occlusion in the rat using (18) F-fluoromisonidazole and positron emission tomography: a pilot study. J Cerel Blood Flow Metab 2006, Oct 11 [Epub ahead of Print].
55. Weinstein PR, Anderson GG, Telles DA. Neurological deficit and cerebral infarction after temporary middle cerebral artery occlusion in unanesthetized cats. Stroke 1986; 7:318–324.
56. Sundt TM, Grant WC, Garcia JH. Restoration of middle cerebral artery flow in experimental infarction. J Neurosurg 1969; 31:311–322.
57. Taguchi J, Graf R, Rosner G, et al. Prolonged transient ischemia results in impaired CBF recovery and secondary glutamate accumulation in cats. J Cereb Blood Flow Metab 1996; 16(2):271–279.
58. Baskaya MK, Rao AM, Donaldson D, et al. Protective effects of ifenprodil on ischemic injury size, blood-brain barrier breakdown, and edema formation in focal cerebral ischemia. Neurosurgery 1997; 40(2):364–370.
59. Watson JC, Doppenberg EM, Bullock MR, et al. Effects of the allosteric modification of hemoglobin on brain oxygen and infarct size in a feline model of stroke. Stroke 1997; 28(8):1624–1630.
60. Yatsugi S, Takahashi M, Kawasaki-Yatsugi S, et al. Neuroprotective effect of YM90K, a novel AMPA/kainate receptor antagonist, in focal cerebral ischemia in cats. J Cereb Blood Flow Metab 1996; 16(5):959–966.
61. Akiho H, Iwai A, Tsukamoto S, et al. Neuroprotective effect of YM-39558 in focal cerebral ischemia in cats. Neuropharmacology 1998; 37(2):159–168.
62. Park CK, Nehls DG, Graham DI, et al. Focal cerebral ischaemia in the cat: treatment with the glutamate antagonist MK-801 after induction of ischaemia. J Cereb Blood Flow Metab 1988; 8(5):757–762.
63. Gotti B, Duverger D, Bertin J, et al. Ifenprodil and SL 82. 0715 as cerebral anti-ischemic agents. I. Evidence for efficacy in models of focal cerebral ischemia. J Pharmacol Exp Ther 1988; 247: 1211–1221.
64. Baskin DS, Widmayer MA, Browning JL, et al. Evaluation of delayed treatment of focal cerebral ischemia with three selective kappa-opioid agonists in cats. Stroke 1994; 25(10):2047–2053.

65. Heiss WD, Graf R, Wienhard K, et al. Dynamic penumbra demonstrated by sequential multitracer PET after middle cerebral artery occlusion in cats. *J Cereb Blood Flow Metab* 1994; 14:892–902.
66. Baron JC. Mapping the ischaemic penumbra with PET: implications for acute stroke treatment. *Cerebrovasc Dis* 1999; 9:193–201.
67. Heiss WD, Graf R, Lottgen J, et al. Repeat positron emission tomographic studies in transient middle cerebral artery occlusion in cats: residual perfusion and efficacy of postischemic reperfusion. J Cereb Blood Flow Metab 1997; 17:388–400.
68. Fukuda S, del Zoppo GJ. Models of focal cerebral ischemia in the nonhuman primate. Ilar J 2003; 44:96–104.
69. DeGirolami U, Crowell RM, Marcoux FW. Selective necrosis and total necrosis in focal cerebral ischemia. Neuropathologic observations on experimental middle cerebral artery occlusion in the macaque monkey. J Neuropath Exp Neurol 1984; 43:57–71.
70. Meier-Ruge W, Bruder A, Theodore D. Histochemical and morphometric investigation of the pathogenesis of acute brain infarction in primates. Acta Histochemica 1992; 42:S59–S70.
71. Giffard C, Young AR, Mézenge F, et al. Histopathological effects of delayed reperfusion after middle cerebral artery occlusion in the anesthetized baboon. Brain Res Bull 2005; 30(4):335–340.
72. Young AR, Touzani O, Derlon JM, et al. Early reperfusion in the anesthetized baboon reduces brain damage following middle cerebral artery occlusion: a quantitative analysis of infarction volume. *Stroke* 1997; 28:632–737.
73. Jones TH, Morawetz RB, Crowell RM, et al. Thresholds of focal cerebral ischemia in awake monkeys. J Neurosurg 1981; 54:773–782.
74. STAIR: Stroke Therapy Academic Industry Roundtable. Recommendations for standards regarding preclinical neuroprotective and restorative drug development. Stroke 1999; 30:2752–2758.
75. Takamatsu H, Tsukada H, Noda A, et al. FK506 attenuates early ischemic neuronal death in a monkey model of stroke. J Nucl Med 2001; 42(12):1833–1840.
76. Furuichi Y, Maeda M, Moriguchi A, et al. Tacrolimus, a potential neuroprotective agent, ameliorates ischemic brain damage and neurologic deficits after focal cerebral ischemia in nonhuman primates. J Cereb Blood Flow Metab 2003; 23(10):1183–1194.
77. Marshall JW, Cummings RM, Bowes LJ, et al. Functional and histological evidence for the protective effect of NXY-059 in a primate model of stroke when given 4 hours after occlusion. Stroke 2003; 34(9):2228–2233.
78. Lees KR, Zivin JA, Ashwood T, et al. NXY-059 for acute ischemic stroke. N Engl J Med 2006; 354(6):588–600.
79. Pappata S, Fiorelli M, Rommel T, et al. PET study of changes in local brain hemodynamics and oxygen metabolism after unilateral middle cerebral artery occlusion in baboons. J Cereb Blood Flow Metab 1993; 13:416–424.
80. Touzani O, Young AR, Derlon JM, et al. Sequential studies of severely hypometabolic tissue volumes after permanent middle cerebral artery occlusion. A positron emission tomographic investigation in anesthetized baboons. *Stroke* 1995; 26:2112–2119.
81. Touzani O, Young AR, Derlon JM, et al. Progressive impairment of brain oxidative metabolism reversed by reperfusion following middle cerebral artery occlusion in anaesthetized baboons. *Brain Res* 1997; 767:17–25.
82. Young AR, Sette G, Touzani O, et al. Relationships between high oxygen extraction fraction in the acute stage and final infarction in reversible middle cerebral artery occlusion. An investigation in anaesthetized baboons with positron emission tomography. J Cereb Blood Flow Metab 1996; 16:1176–1188.
83. Maeda M, Takamatsu H, Furuichi Y, et al. Characterization of a novel thrombotic middle cerebral artery occlusion model in monkeys that exhibits progressive hypoperfusion and robust cortical infarction. J Neurosci Methods 2005; 146:106–115.
84. Marchal G, Serrati C, Rioux P, et al. PET imaging of cerebral perfusion and oxygen consumption in acute ischaemic stroke : relation to outcome. Lancet 1993; 341:2–4.
85. Baron JC. Perfusion thresholds in human cerebral ischemia: historical perspective and therapeutic implications. Cerebrovasc Dis 2001; 11(suppl 1):2–8.
85a. Baron JC. Mapping the ischaemic penumbra with PET: a new approach. Brain 2001; 124:2–4 (Editorial).
86. Marchal G, Beaudouin V, Rioux P, et al. Prolonged persistence of substantial volumes of potentially viable brain tissue after stroke: a correlative PET-CT study with voxel-based data analysis. *Stroke* 1996; 27:599–606.
87. Baron JC, Bousser MG, Comar D, et al. Non invasive tomographic study of cerebral blood flow and oxygen metabolism in vivo: potentials, limitations and clinical applications in cerebral ischemic disorders. Eur Neurol 1981; 20:273–284.
88. Wise RJS, Bernardi S, Frackowiak RSJ, et al. Serial observations on the pathophysiology of acute stroke. The transition from ischaemia to infarction as reflected in regional oxygen extraction. Brain 1983; 106:197–222.

89. Furlan M, Marchal G, Viader F, et al. Spontaneous neurological recovery after stroke and the fate of the ischemic penumbra. *Ann Neurol* 1996; 40:216–226.
90. Read SJ, Hirano T, Abbott DF, et al. Identifying hypoxic tissue after acute ischemic stroke using PET and 18F-fluoromisonidazole. *Neurology* 1998; 51:1617–1621.
91. Read SJ, Hirano T, Abbott DF, et al. The fate of hypoxic tissue on ^{18}F-fluoromisonidazole positron emission tomography after ischemic stroke. *Ann Neurol* 2000; 48:228–235.
92. Markus R, Reutens DC, Kazui S, et al: Hypoxic tissue in ischaemic stroke: persistence and clinical consequences of spontaneous survival. Brain 2004; 127:1427–1436.
93. Baird AE, Benfield A, Schlaug G, et al. Enlargement of human cerebral ischemic lesion volumes measured by diffusion-weighted magnetic resonance imaging. Ann Neurol 1997; 41(5):581–589.
94. Beaulieu C, de Crespigny A, Tong DC, et al. Longitudinal magnetic resonance imaging study of perfusion and diffusion in stroke: evolution of lesion volume and correlation with clinical outcome. *Ann Neurol* 1999; 46:568–578.
95. Schwamm LH, Koroshetz WJ, Sorensen AG, et al. Time course of lesion development in patients with acute stroke: serial diffusion- and hemodynamic-weighted magnetic resonance imaging. *Stroke* 1998; 29:2268–2276.
96. Darby DG, Barber PA, Gerraty RP, et al. Pathophysiological topography of acute ischemia by combined diffusion-weighted and perfusion MRI. Stroke 1999; 30:2043–2052.
97. Barber PA, Darby DG, Desmond PM, et al. Prediction of stroke outcome with echoplanar perfusion- and diffusion-weighted MRI. *Neurology* 1998; 51:418–426.
98. Baird AE, Lovblad KO, Dashe JF, et al. Clinical correlations of diffusion and perfusion lesion volumes in acute ischemic stroke. Cerebrovasc Dis 2000; 10(6):441–448.
99. Heiss WD, Kracht LW, Thiel A, et al. Penumbral probability thresholds of cortical flumazenil binding and blood flow predicting tissue outcome in patients with cerebral ischaemia. Brain 2001; 124:20–29.
100. Lassen NA. Pathophysiology of brain ischemia as it relates to the therapy of acute ischemic stroke. Clin Neuropharmacol 1990; 13(suppl 3):S1–S8.
101. Kaufmann AM, Firlik AD, Fukui MB, et al. Ischemic core and penumbra in human stroke. *Stroke* 1999; 30:93–99.
102. Baron JC, Marchal G. Ischemic core and penumbra in human stroke. Stroke 1999; 30:1150–1153. (letter)
103. The National Institute of Neurological Disorders and Stroke rt-PA Stroke Study Group. Tissue plasminogen activator for acute ischemic stroke. *N Engl J Med* 1995; 333:1581–1587.
104. Baron JC, von Kummer R, del Zoppo GJ. Treatment of acute ischemic stroke. Challenging the concept of a rigid and universal time window. Stroke 1995; 26:2219–2221.
105. Furlan A, Higashida R, Weschsler L, et al. Intra-arterial prourokinase for acute ischemic stroke. The PROACT II study: a randomized controlled trial. Prolyse in Acute Cerebral Thromboembolism. JAMA 1999; 282(21):2003–2011.
106. Ribo M, Molina CA, Rovira A, et al. Safety and efficacy of intravenous tissue plasminogen activator stroke treatment in the 3–6-h window using multimodal transcranial Doppler/MRI selection protocol. Stroke 2005; 36:602–606.
107. Hacke W, Albers G, Al-Raw Y, et al. DIAS Study Group. The Desmoteplase in Acute Ischemic Stroke Trial (DIAS): a phase II MRI-based 9-hour window acute stroke thrombolysis trial with intravenous desmoteplase. Stroke 2005; 36(1):66–73.
108. Furlan AJ, Eyding D, Albers GW, et al. Dose Escalation of Desmoteplase for Acute Ischemic Stroke (DEDAS): evidence of safety and efficacy 3 to 9 hours after stroke onset. Stroke 2006; 37(5): 1227–1231.
109. Molina CA, Saver JL. Extending reperfusion therapy for acute ischemic stroke. Emerging pharmacological, mechanical, and imaging strategies. Stroke 2005; 36:2311–2320.
110. Marchal G, Rioux P, Serrati C, et al. Value of acute-stage positron emission tomography in predicting neurological outcome after ischemic stroke: further assessment. Stroke 1995; 26(3):524–525.
111. Kidwell CS, Saver JL, Mattiello J, et al. Diffusion-perfusion MRI characterization of post-recanalization hyperperfusion in humans. Neurology 2001; 57(11):2015–2021.
112. Thomalla GJ, Kucinski T, Schoder V, et al. Prediction of malignant middle cerebral artery infarction by early perfusion- and diffusion-weighted magnetic resonance imaging. Stroke 2003; 34(8): 1892–1899.
113. Symon L, Branston NM, Strong AJ Extracellular potassium activity, evoked potential and rCBF during experimental cerebral ischaemia in the baboon. Acta Neurol Scand Suppl. 1977; 64:110–111.
114. Astrup J, Siesjo BK, Symon L. Thresholds in cerebral ischemia—the ischemic penumbra. *Stroke* 1981; 12:723–725.
115. Hossmann KA. Viability thresholds and the penumbra of focal ischemia. *Ann Neurol* 1994; 36:557–565.
116. Touzani O, Roussel S, MacKenzie ET. The ischaemic penumbra. Curr Opin Neurol 2001; 14(1):83–88.
117. Clarke DD, Sokoloff L. Circulation and energy metabolism of the brain. In: Siegl GJ et al. eds. Basic Neurochemistry: Molecular, Cellular and Medical Aspects. 6th ed. Philadelphia: Lippincott-Raven Publishers, 1999:637–670.

118. Tower DB, Young OM. The activities of butyrylcholinesterase and carbonic anhydrase, the rate of anaerobic glycolysis, and the question of a constant density of glial cells in cerebral cortices of various mammalian species from mouse to whale. J Neurochem 1973; 20(2):269–278.
119. Kennedy C, Sakurada O, Shinohara M, et al. Local cerebral glucose utilization in the normal conscious macaque monkey. Ann Neurol 1978; 4(4):293–301.
120. Harris RJ, Symon L. Extracellular pH, potassium, and calcium activities in progressive ischaemia of rat cortex. J Cereb Blood Flow Metab 1984; 4(2):178–186.
121. Astrup J, Symon L, Branston NM, et al. Cortical evoked potential and extracellular K^+ and H^+ at critical levels of brain ischemia. Stroke 1977; 8:51–57.
122. Bolander HG, Persson L, Hillered L, et al. Regional cerebral blood flow and histopathological changes after middle cerebral artery occlusion in rats. Stroke 1989; 20:930–937.
123. Tamura A, Graham DI, McCulloch J, et al. Focal cerebral ischaemia in the rat: Regional cerebral blood flow determined by [14C]iodoantipyrine autoradiography following middle cerebral artery occlusion. J Cereb Blood Flow Metab 1981; 1(1):61–69.
124. Zhao W, Belayev L, Ginsberg MD. Transient Middle Cerebral Artery Occlusion by Intraluminal Suture: II. Neurological Deficits, and Pixel-Based Correlation of Histopathology with Local Blood Flow and Glucose Utilization. J Cereb Blood Flow Metab 1997; 17, 1281–1290.
125. Tyson GW, Teasdale GM, Graham DI, et al. Focal cerebral ischemia in the rat : topography of hemodynamic and histopathologic changes. Ann Neurol 1984; 15:559–567.
126. Hakim AM, Hogan MJ, Carpenter S. Time course of cerebral blood flow and histological outcome after focal cerebral ischemia in rats. Stroke 1992; 23(8):1138–1143.
127. Jacewicz M, Tanabe J, Pulsinelli W.A. The CBF threshold and dynamics for focal cerebral infarction in spontaneously hypertensive rats. J Cereb Blood Flow Metab 1992; 12:359–370.
128. Duverger D, MacKenzie ET. The quantification of cerebral infarction following focal ischemia in the rat: influence of strain, arterial pressure, blood glucose concentration, and age. J Cereb Blood Flow Metab 1988; 8(4):449–461.
129. Hoehn-Berlage M, Norris DG, Kohno K, et al. Evolution of regional changes in apparent diffusion coefficient during focal ischemia of rat brain: the relationship of quantitative diffusion NMR imaging to reduction in cerebral blood flow and metabolic disturbances. *J Cereb Blood Flow Metab* 1995; 15:1002–1011.
130. Kohno K, Hoehn-Berlage M, Mies G, et al. Relationship between diffusion-weighted MR images, cerebral blood flow, and energy state in experimental brain infarction. *Magn Reson Imaging* 1995; 13:73–80.
131. Mies G, Xie, Y, Seo, K, et al. Ischemic thresholods of cerebral protein synthesis and energy state following middle cerebral artery occlusion in rat. J Cereb Blood Flow Metab 1991; 11:753–761.
132. Heiss WD, Rosner G. Functional recovery of cortical neurons as related to degree and duration of ischemia. Ann Neurol 1983; 14 :294–301.
133. Pulsinelli WA, Brierley JB, Plum F. Temporal profile of neuronal damage in a model of transient forebrain ischemia. Ann Neurol 1982; 11(5):491–498.
134. Mies, G, Auer, L.M, Ebhardt, G, et al. Flow and neuronal density in tissue surrounding chronic infarction. Stroke 1983; 14:22–27.
135. Garcia JH, Liu KF, Ye ZR, Gutierre JA. Incomplete infarct and delayed neuronal death after transient middle cerebral artery oclusion in rats. Stroke 1997:28(11):2303–2309.
136. Torvik A, Svindland A. Is there a transitional zone between brain infarcts and the surrounding brain? A histological study. Acta Neurol Scand 1986; 74:365–370.
137. Baron JC. How healthy is the acutely reperfused ischemic penumbra? Cerebrovasc Dis 2005; 20(suppl 2):25–31.
138. Tamura A, Asano T, Sano K. Correlation between rCBF and histological changes following temporary middle cerebral artery occlusion. Stroke 1980; 11:487–493.
139. Marcoux FW, Morawetz RB, Crowell RM, et al. Differential regional vulnerability in transient focal cerebral ischemia. Stroke 1982; 13:339–346.
140. Miyabe M, Mori S, van Zijl PCM, et al. Correlation of the average water diffusion constant with cerebral blood flow and ischemic damage after transient middle cerebral artery occlusion in cats. J Cereb Blood Flow Metab 1996; 16:881–891.
141. Branston NM, Symon L, Crockard HA, et al. Relationship between the cortical evoked potential and local cortical blood flow following acute middle cerebral artery occlusion in the baboon. Exp Neurol 1974; 45(2):195–208.
142. Branston NM, Symon L, Crockard HA. Recovery of the cortical evoked response following temporary middle cerebral artery occlusion in baboons: relation to local blood flow and PO2. Stroke 1976; 7(2):151–157.
143. Morawetz RB, Crowell RH, DeGirolami U, et al. Regional cerebral blood flow thresholds during cerebral ischemia. Fed Proc 1979; 38(11):2493–24934.
144. Morawetz RB, De Girolami U, Ojemann RG, et al. Cerebral blood flow determined by hydrogen clearance during middle cerebral artery occlusion in unanesthetized monkeys. Stroke 1978; 9:143–149.

145. Yonas H, Gur D, Classen D et al. Stable xenon enhanced computed tomography in the study of clinical and pathologic correlates of focal ischemia in baboons. Stroke 1988 19(2):228–238.
146. Yonas H, Gur D, Classen D et al. Stable exnon-enhanced CT measurement of cerebral blood flow in reversible focal ischemia in baboons. J Neurosurg 1990:73(2):266–273.
147. Kuge Y, Yokota C, Tagaya M, et al. Serial changes in cerebral blood flow and flow-metabolism uncoupling in primates with acute thromboembolic. J Cereb Blood Flow Metab 2001; 21(3): 202–210.
148. Heiss WD. Ischemic penumbra: evidence from functional imaging in man. J Cereb Blood Flow Metab 2000; 20(9):1276–1293.
149. Baron JC, Rougemont D, Bousser M-G, et al. Local CBF, oxygen extraction fraction (OEF), and CMRO2: Prognostic value in recent supratentorial infarction in humans. J Cereb Blood Flow Metab 1983; 3(suppl 1):S1–S2.
150. Baron JC, Rougernont D, Soussaline F et al. Local interrelationships of cerebral oxygen consumption and glucose utilization in normal subjects and in ischemic stroke patients; a positron tomography study J Cereb Blood Flow Metab 1984;4(2):140–149.
151. Powers W, Grubb R, Darriet D, et al. Cerebral blood flow and cerebral metabolic rate of oxygen requirements for cerebral function and viability in humans. J Cereb Blood Flow Metab 1985; 5:600–608
152. Hakim AM, Evans AC, Berger L, et al. The effect of nimodipine on the evolution of human cerebral infarction studied by PET. J Cereb Blood Flow Metab 1989; 9(4):523–534.
153. Marchal G, Benali K, Iglesias S, et al. Voxel-based mapping of irreversible ischemic damage with PET in acute stroke. Brain 1999; 122:2387–2400.
154. Shimosegawa E, Hatazawa J, Ibaraki M, Toyoshima H, Suzuki A. Metabolic penumbra of acute brain infarction: A correlation with infarct growth. Ann Neurol 2005;57:495–500
155. Heiss WD, Huber M, Fink GR et al. Progressive derangement of perinfarct viable tissue in ischemic stroke J Cereb Blood Flow Metab 1992;12(2):193–203.
156. Heiss WD, Grond M, et al. Permanent Cortical Damage Detected by Flumazenil Positron Emission Tomography in Acute Stroke. Stroke. 1998; 29:454–461.
157. Lee JM, Vo KD, An H, et al. Magnetic resonance cerebral metabolic rate of oxygen utilization in hyperacute stroke patients. Ann Neurol 2003; 53(2):227–232.
158 Ueda T, Sakaki S, Yuh WT, et al.Outcome in acute stroke with successful intra-arterial thrombolysis and predictive value of initial single-photon emission-computed tomography. J Cereb Blood Flow Metab 1999; 19(1):99–108.
159. Umemura A, Suzuka T, Yamada K. Quantitative measurement of cerebral blood flow by (99m)Tc-HMPAO SPECT in acute ischaemic stroke: usefulness in determining therapeutic options. J Neurol Neurosurg Psychiatry 2000; 69(4):472–478.
160. Wintermark M, Reichhart M, Cuisenaire O, et al. Comparison of admission perfusion computed tomography and qualitative diffusion- and perfusion-weighted magnetic resonance imaging in acute stroke patients. Stroke 2002a; 33:2025–31.
161. Wintermark M, Reichhart M, Thiran JP, et al. Prognostic accuracy of cerebral blood flow measurement by perfusion computed tomography, at the time of emergency room admission, in acute stroke patients. Ann Neurol 2002b; 51:417–32.
162. Bristow MS, Simon JE, Brown RA, et al. perfusion and diffusion in acute ischemic stroke: human gray and white matter have different thresholds for infarction. J Cereb Blood Flow Metab 2005; 25(10):1280–1287.
163. Lin W, Lee JM, Lee YZ, et al. Temporal relationship between apparent diffusion coefficient and absolute measurements of cerebral blood flow in acute stroke patients. Stroke 2003; 34:64–70.
164. Fiehler J, von Bezold M, Kucinski T, et al. Cerebral blood flow predicts lesion growth in acute stroke patients. Stroke. 2002; Oct;33(10):2421–2425.
165. Wu O, Koroshetz WJ, Østergaard L, et al. Predicting tissue outcome in acute human cerebral ischemia using combined diffusion- and perfusionweighted MR imaging. Stroke 2001; 32:933–942.
166. Shen Q, Ren H, Fisher M, Duong TQ. Statistical prediction of tissue fate in acute ischemic brain injury. J Cereb Blood Flow Metab 2005; 25:1336–1345
167. Ackerman RH, Lev MH, Mackay BC, et al. PET studies in acute stroke: Findings and relevance to therapy. J Cereb Blood Flow Metab 1989; 9(suppl 1):S359
168. Ezura M, Takahashi A, Yoshimoto T. Evaluation of regional cerebral blood flow using single photon emission tomography for the selection of patients for local fibrinolytic therapy of acute cerebral embolism. Neurosurg Rev 1996; 19(4):231–236.
169. Liu Y, Karonen JO, Vanninen RL, et al. Cerebral hemodynamics in human acute ischemic stroke: a study with diffusion-and perfusion-weighted magnetic resonance imaging and SPECT. J Cereb Blood Flow Metab 2000; 20(6):910–920.
170. Rohl L, Ostergaard L, Simonsen CZ, et al. Viability thresholds of ischemic penumbra of hyperacute stroke defined by perfusion-weighted MRI and apparent diffusion coefficient. Stroke 2001 32(5):1140–1146.

5 The Ischemic Cascade: Events Within the Penumbra

Juliane Klehmet, Ulrich Dirnagl, Jens Peter Dreier, and Andreas Meisel
Department of Experimental Neurology Charité, Humboldt University, Berlin, Germany

INTRODUCTION

Although the sequence of molecular and cellular events following cerebral ischemia is highly complex, research over the last decades has revealed that ischemia induced pathophysiology appears to follow a stereotypic, spatio-temporal pattern. In this chapter we will review those events, with particular emphasis on the ischemic penumbra. Conceptually, we will treat ischemia-induced pathobiology as a cascade of interlinked mechanisms, which ultimately lead to either cell death or survival.

Due to the high demand of brain tissue for oxygen and glucose, a disruption of blood supply within minutes leads to substrate depletion in the affected brain region. In addition, toxic metabolites accumulate. The cellular energy deficit leads to a collapse of ion gradients and membrane potentials—neurons and glial cells depolarize. Depending on the extent and duration of energy deficiency, the cells will suffer not only a functional, but also a structural breakdown. Key to our understanding of mechanisms of survival and cell death after cerebral ischemia is the concept of the ischemic penumbra and infarct core, as discussed in earlier chapters. The latter is a spatially and temporally dynamic brain region. While the infarct core within hours becomes necrotic, the penumbra over hours or even days can either undergo cell death via necrosis or apoptosis, or survive via spontaneous or therapeutic reperfusion, endogenous protective mechanisms, or neuroprotective intervention. The penumbra is, therefore, considered as "tissue at risk," and the mechanisms that lead to delayed cell death or survival within the penumbra are subject of intense research, as they provide targets for a specific neuroprotective therapy (1,2).

In the following sections, we have stratified the complex events occuring after cerebral ischemia into pathophysiological entities. We are aware of the fact that these processes do overlap in space and time, that this represents an oversimplification, and that some of the mechanisms could have been categorized differently. However, we feel that portraying these events as "cascade" greatly simplifies the task of reviewing the current literature, as well as the generation of testable hypotheses.

We will begin by reviewing the early elements of the ischemic cascade, which are excitotoxicity, the formation of reactive oxygen free radicals, tissue acidosis, and the occurrence of peri-infarct-depolarizations. We will then look at the more delayed events of inflammation, programmed cell death, DNA damage, and repair. Although excitotoxicity and peri-infarct-depolarizations start within minutes or hours after the onset of ischemia they may go on for days within penumbral tissue. They trigger both inflammation and programmed cell death. The complex changes in gene expression programs not only lead to the expression of destructive proteins involved in inflammation and apoptosis, but also to a host of protective proteins that contribute to the amelioration of ischemic damage. At the end of this review we will, therefore, briefly summarize what is known about such endogenous protective mechanisms, which have the potential to provide us with novel therapeutic options.

EXCITOTOXICITY

Among the first cellular consequences of cerebral ischemia is a slow rise of extracellular potassium accompanied by extracellular acidification. Whereas the acidification may be due to lactate accumulation, the slow rise of extracellular potassium is probably due to decreased sodium pump activity and activation of Ca^{2+} or ATP-gated K^+ channels (3). In this phase,

neurons hyperpolarize, which possibly helps them to conserve energy. With continued shortage of oxygen and glucose, after one or two minutes hyperpolarization is followed by neuronal depolarization caused by a failure of the outwardly transporting, ATP-dependent pumps, in particular the sodium pump, to balance the Gibbs-Donnan forces, which result from the high intracellular concentration of impermeant anions attracting diffusible cations, from the extracellular space. The depolarization of neurons causes the activation of voltage-gated calcium channels and the release of excitatory amino acids into the extracellular space (ECS). Glutamate accumulates in the ECS since the re-uptake by astrocytes and neurons is impeded. In the further course of ischemia, glutamate transport reverses, such that glutamate is not only released synaptically, but also actively transported from the intra- to the extracellular space. The activation of glutamate receptors [*N*-methyl–D-aspartate (NMDA) and alpha-amino-3-hydroxy-5-methyl-4-isoxazoleproplonic acid (AMPA)] leads directly or indirectly to a further augmentation of the intracellular calcium concentration. In addition, the activation of metabotropic glutamate receptors results in the mobilization of intracellular calcium stores via activation of phospholipase C (PLC) and production of inositol-triphosphate (IP_3). Altogether, the result is a massive disturbance of ion homeostasis, and so called "anoxic depolarization". Anoxic depolarization represents the largest network event in the central nervous system (CNS). For comparison, the changes of extracellular potassium are about six-fold greater than those during a tonic–clonic epileptic seizure. During anoxic depolarization, water passively follows Na^+ and Cl^- ions into the intracellular space so that the cells swell and the extracellular volume shrinks by about 70%. If energy is not restored in time, these changes cause rapid cellular lysis. This lytic type of cell death, also referred to as necrosis, is primarily observed in the core of the infarction. If the cells escape this form of disintegration, as in the penumbra, excitotoxicity may initiate molecular events that lead to apoptosis and inflammation (2,4). One of the major controversies regarding anoxic depolarization concerns the question whether glutamate receptor antagonists are sufficient to block anoxic depolarization or not (5–8). Glutamate receptor antagonists may only be effective in high doses and in very young animals (8).

PERI-INFARCT DEPOLARIZATIONS

In brain slices, anoxic depolarization starts at multiple sites "propagating outwards like the ripples from several stones thrown in a pond" (7). A thorough analysis of the spread of anoxic depolarization after middle cerebral artery occlusion in rats in vivo was provided by Nallet et al. (9). Their finding of a relatively short time lag between the onsets of anoxic depolarization at different recording sites in the neocortex supported the assumption of a spread from multiple elicitation sites. In addition to the anoxic depolarization in the ischemic core, shorter-lasting large slow voltage shifts, so-called peri-infarct depolarizations, start at the borderzone of the ischemic core region and propagate as peri-infarct depolarizations through the penumbra into healthy tissue, where they adopt typical features of spreading depression.

Spreading depression represents an electrochemical wave that propagates through grey matter at a rate of 2–5 mm/min. Whereas the magnitude of the intra-/extracellular ion and volume changes are similar between spreading depression and anoxic depolarization, spreading depression is not preceded by cessation of unit firing, but unit firing stops simultaneously with the large slow voltage shift. Furthermore, there is no gradual rise of extracellular potassium or extracellular acidification preceding the large slow voltage shift. In contrast to anoxic depolarization, spreading depression is easily blocked by NMDA receptor antagonists. After spreading depression cells repolarize within one or two minutes after the event. However, spreading depression causes some metabolic imbalance (10,11) due to excessive ion changes. The redistribution of sodium and potassium requires activation of the energy-driven sodium pump. This additional energy burden is matched by an increase in cerebral blood flow (CBF) under normal conditions (12).

Leão discovered spreading depression as well as anoxic depolarization and he already noted the similarity between both network events (13). Branston et al. (1977) were the first to describe the incidence of spreading depression in the context of ischemic stroke (14). Peri-infarct depolarizations represent the spectrum of large slow voltage shifts between anoxic depolarization and spreading depression. They propagate similarly as spreading depression (15,16), but activated neuronal metabolism is not sufficiently matched by an increase in CBF, as evidenced

by a delay in energy-dependent repolarization (17). CBF may even decrease in response to peri-infarct depolarizations, as shown in mice. This vasoconstriction further aggravates the mismatch between energy demand and supply (18). Such an inverse hemodynamic response to spreading depression resulting in a spreading ischemia was earlier described for a condition with reduced nitric oxide (NO) concentration and increased baseline extracellular potassium in rats (19,20,21). Decreased NO concentration in focal ischemia may result from lack of molecular oxygen or a disturbance of endothelial NO synthase. A rise of baseline potassium in the penumbra is well known (22) (see also under "Excitotoxicity" of this chapter).

In models of experimental focal ischemia the incidence of peri-infarct depolarizations correlates with infarct size (23). This may be a causal relationship, because elicitation of spreading depression remote from the infarct region increased infarct volumes when the depolarization waves propagated into the penumbra (24–26). Conversely, drugs that decreased the frequency of peri-infarct depolarizations were neuroprotective (27–30). Interestingly, in rats two different periods with peri-infarct depolarizations were observed after middle cerebral artery occlusion, which were separated by a quiescent period of ~8 hours (30). Infarct maturation, that is progression of the ischemic core into the penumbra, was associated with peri-infarct depolarizations over 24 hours. Peri-infarct depolarizations in patients with head trauma even recurred within a period of several days after the initial trauma (31).

OXYGEN FREE RADICALS

As a consequence of ischemia and particularly of reperfusion, reactive oxygen free radicals such as superoxide, hydrogen peroxide, and hydroxyl radical are generated. Nitric oxide is produced via the activation of calcium-calmodulin-dependent nitric oxide synthase (NOS). NO reacts with superoxide radicals and forms the highly reactive peroxy-nitrite radical. Further sources for oxygen free radicals in damaged brain tissue are the breakdown products of adenosine phosphates, which contribute to radical production via xanthine oxidase and the iron catalyzed Haber-Weiss reaction. The many different radical species that are formed after ischemia and reperfusion can react with virtually any cellular component (carbohydrates, amino acids, DNA, phospholipids) and damage them. The peroxidation of membrane lipids releases further radicals—and further glutamate. Oxygen free radicals gain even more significance when new oxygen reaches the damaged tissue by virtue of reperfusion, or in the penumbra where oxygen supply has not ceased entirely (2,4).

Hypoxia itself as well as the elevated intracellular concentration of calcium ions and free radicals disrupt the function of neuronal mitochondria. Consequently, a so-called mitochondrial permeability transition pore (MTP) in the mitochondrial membrane may form. Besides impeding ATP production through loss of mitochondrial potential, the MTP leads to mitochondrial swelling, a burst of free oxygen radicals, and the release of pro-apoptotic molecules. Thus, a vicious cycle of further disintegration is fuelled [see subsequently) (2,32)]. This vicious cycle is counterbalanced in part by anti-oxidative enzymes like manganese-superoxide dismutase (Mn-SOD) and the cytosolic forms of copper-zinc superoxide dismutase (CuZn-SOD). These may prevent the breakdown of the mitochondrial membrane and thus induce the release of cytochrome C, which otherwise might trigger apoptosis (33).

TISSUE ACIDOSIS

Proton balance is intimately linked with glucose metabolism. With reduced oxygen availability, anaerobic glycolysis as the only remaining source of ATP production leads to tissue acidosis. It has long been assumed that this acidosis is one of the main deleterious mechanisms in ischemic stroke. This so-called "lactate-acidosis-hypothesis" is often quoted as explanation for the "glucose parado" of cerebral ischemia. This paradox refers to the observation that excessive supply of glucose, the most important source of energy of the brain, during focal cerebral paradox does not reduce tissue damage as expected, but instead worsens it (34). However, the mechanism by which this happens and whether levels of acidosis reached in brain ischemia can generate brain tissue damage at all are still far from being clear. The pH dependent transition of Fe(III) to Fe(II) and the release of iron from molecular storages might facilitate the Haber-Weiss reaction that forms toxic oxygen free radical species (see preceding). Besides the

production of different species of oxygen free radicals, acidosis also interferes with intracellular protein synthesis. However, the lactate-acidosis-hypothesis has been challenged. Particularly, the fact that acidosis blocks the NMDA-receptor and thus has an anti-excitotoxic effect indicates the complexities of the role of acidosis in cerebral ischemia (2).

Similarly debated are the findings on hyperglycemia during stroke. Experimental data from animal models show a detrimental effect of hyperglycemia during focal cerebral ischemia (35–37). Clinical data demonstrate that hyperglycemia during the acute phase of stroke worsens prognosis (38–40). Persisting hyperglycemia beyond the acute phase is also an independent prognostic factor for larger infarct volume and poorer functional outcome in stroke patients (41). It is a matter of debate as to whether these observations are due to a causal relationship or whether hyperglycemia is an epiphenomenon, possibly due to a stress reaction (i.e., an effect of concomitant catecholamine and glucocorticoid release proportional to initial tissue damage) (42,43). The controversial role of stroke associated lactate-acidosis has already been discussed. An alternative concept is the glucocorticoid hypothesis (44). This concept suggests that hyperglycemia enhances the release of glucocorticoids, which are also released during ischemia as part of the stress reaction. Glucocorticoids have been shown to be directly cytotoxic (45), and the blockade of glucocorticoid receptors reduces the damaging effect of hyperglycemia (44). On the other hand, hyperglycemia and acidosis are protective in vitro (46,47), and some experimental studies demonstrate that hyperglycemia can also have a beneficial effect under special circumstances (48,49).

In this controversy, a recent human study reveals the following: it demonstrated with perfusion- and diffusion-MR imaging and spectroscopy that stroke patients with hyperglycemia accumulate lactate in the penumbra. While the perfusion-diffusion-mismatch (as a measure of the size relation of penumbra and core) was similar in the normoglycemic and hyperglycemic groups, the eventual infarct size and disability scores were significantly greater in the hyperglycemic group (50). While it could still be argued that initially hyperglycemic patients were likely to be longstanding or latent diabetics with an overall worse microvascular state, we take this study, in combination with much of the experimental animal data, as strong indicator for the vulnerability of the penumbra to hyperglycemia. Indirectly, this study also corroborates the lacatacidosis theory, which, however, still lacks direct proof.

INFLAMMATION

Postischemic inflammation is an essential component in the pathogenesis of ischemic stroke. The inflammatory response is a double-edged sword contributing to ischemic brain injury but also initiating tissue regeneration. It is characterized by an influx of leukocytes and increase in vascular permeability. This process involves the upregulation of endothelial and leukocytic adhesion receptors and the release of chemoattractants. Inflammation might be a promising therapeutic target, because of a much longer therapeutic time window compared to the early processes discussed previously.

Leukocyte-Endothelium Interaction

The early stage of inflammation, which starts a few hours after the onset of ischemia, is characterized by the expression of adhesion molecules in the vascular endothelium as well as on circulating leukocytes (51).

Thus, leukocytes adhere to the endothelium and transmigrate from the blood into the brain parenchyma, which is of decisive importance for stroke induced brain inflammation (52–54). Neutrophils, which are important components of the innate immune response, are capable to produce a number of potentially harmful substances. These include toxic oxygen metabolites, destructive enzymes, and proinflammatory cytokines. Polymorphonuclear leukocytes are early participants of the microvascular response, followed by mononuclear cells entering the ischemic territory and, in particular, the penumbra. The invasion of nonresident inflammatory cells requires the rapid appearance of adhesion receptors.

Upregulated endothelial adhesion molecules like ICAM-1, VCAM-1, P-Selectin, and E-Selectin facilitate the interaction between endothelium and leucocytes as first steps of

transmigration of white blood cells from blood into the tissue. Important players in this process are the β_2-integrins CD11b/CD18 (Mac-1) and CD11a/CD18 (LFA-1) (55,56). P-Selectin and E-Selectin are essential in the stage of rolling during leukocyte/endothelial interaction. P-Selectin has been shown to be upregulated as early as 15 minutes following induction of ischemia, whereas E-Selectin is induced within two hours of ischemia (57). ICAM-1, which is most crucial for the integrin-mediated leukocyte adhesion to activated endothelium, is upregulated very early in cerebral injury (58).

ICAM-1 mRNA and the ICAM-1 surface protein have been detected within one to two hours after ischemia onset (59). Elevated ICAM-1 levels in the ischemic hemisphere have also been demonstrated in brains of acute stroke patients (60).

Neutrophil activation has been demonstrated to play a critical role in neuronal injury following cerebral ischemia, particularly during reperfusion (61–63).

Accumulation of neutrophils together with red blood cells, fibrin, and platelets leads to capillary plugging and reduction of blood flow on the microvascular level. This enhances stasis of the already impaired microcirculation (64). These results provide the basis for the therapeutic blockade of molecules crucial for the adhesion of neutrophils to the microvascular endothelium. Thus, blockade of these molecules intends to inhibit the influx of neutrophils into the ischemic territory and thereby to improve the local CBF.

An important focus has been on blocking the neutrophil integrins LFA-1 (CD11a/CD18) and Mac-1 (CD11b/CD18), as well as on the endothelial molecules ICAM-1, P-Selectin, and E-Selectin (65–67). The role of these molecules mediating interaction between neutrophils and endothelial receptors during cerebral ischemia was studied by using knockout mice. For example, Mac-1 knockout mice have 26% smaller infarct volumes in comparison to wild type mice (68). CD-18 knockout mice demonstrated a 57% decrease in infarct size following transient focal cerebral ischemia. Interestingly, this neuroprotective effect was not observed in models of a permanent ischemia (69). Likewise, ICAM-1 knockouts demonstrate not only a significant reduction of neutrophil adhesion to the endothelium four hours following reperfusion, but also an increased CBF, smaller infarcts, and lower mortality compared to wild type mice (70). These results were corroborated by experiments using monoclonal antibodies blocking the corresponding endothelial and leukocytic receptors.

Antibodies blocking E and P-Selectins, ICAM-1, CD18, or CD11, not only reduce the number of infiltrating leucocytes, but also the infarct volumes (71). Blocking the α4-component of VLA-4 ($\alpha 4\ \beta 1$), another integrin more specific for lymphocytes also reduces the volume of infarction (72). A novel, nonantibody based approach using recombinant neutrophil inhibitory factor (RNIF) exerts neuroprotection in a reperfusion model of ischemic stroke, but not in a model of permanent ischemia (73).

RNIF is a 41 kD recombinant hookworm protein blocking neutrophil adhesion. This substance is also promising in combination therapy with rt-PA in order to extend the therapeutic window of thrombolysis. In a model of embolic stroke, when co-administered with rt-PA RNIF, it decreases neutrophil influx into the ischemic area, improves outcome, and reduces the infarct size, even when treatment started four hours after ischemia onset.

Based on the preclinical evidence of leukocyte and endothelial interaction a number of therapeutic agents have been designed to be applied in human studies. Enlimomab, a monoclonal murine anti-ICAM-1 antibody was administered to patients with acute stroke within six hours after the onset of clinical symptoms. Unfortunately, the outcome was more than disappointing, patients who received enlimomab had a worse clinical outcome and a 43% increase in mortality over the first 90 days. Moreover, a significantly higher rate of adverse events were documented in the enlimomab group. This failure is mainly explained by the fact that enlimomab is a murine antibody, which possibly affects the complement system (74).

The failure of enlimomab shifted the interest to using nonantibody molecule inhibitors of neutrophil adhesion. As mentioned earlier, preclinical success in using RNIF to extend the time window of t-PA lead to the initiation of a phase IIb trial—the Acute Stroke Therapy by Inhibition of Neutrophils (ASTIN) trial. RNIF was administered in different doses to stroke patients within six hours after the onset of clinical symptoms. This innovative trial, which used a Bayesian dose finding protocol, had to be terminated after an interim analysis of 966 patients who demonstrated futility. Likewise, a phase III trial (HALT-Stroke), which investigated the influence of

Leukarrest™, a humanized, anti-MAC-1 (CD11b/18) antibody, failed in an interim analysis for improvement in functional outcomes (75).

Microglia and Monocytes: Residents and Travelers

A major part in inflammation is ascribed to the population of microglial cells. These cells are the primary immunoeffectors of the CNS and make up about 20% of the entire glial mass, which means that they are as numerous in the brain as neurons. Activation of microglia is a striking feature in the penumbra. The cells change their shape from a highly ramified cell to an amoeboid form, and they proliferate. They also express a number of characteristic surface molecules (for instance MHCI and MHCII), and are capable of antigen presentation (76–79). Similar to leukocytes, activated microglia is able to produce a variety of pro-inflammatory cytokines [also cytotoxic metabolites (especially oxygen free radicals such as peroxy-nitrite and superoxide) and enzymes (for instance cathepsins)]. In addition, microglia is phagocytically active. The inhibition of microglial activation turned out to be protective in experimental stroke models (80). On the other hand, activated microglia has also been shown to release anti-inflammatory cytokines (such as transforming growth factor-beta 1) and growth factors (81). Because of the Janus-faced nature of microglial products (destructive, e.g., free radicals, vs. protective, e.g., growth factors) the overall role of microglia in cerebral ischemia is not clear at present. It is very likely that microglia at different time points plays different roles, with protective or regenerative activities occurring days or even weeks after the onset of ischemia.

Besides the activated resident microglia, monocytes from the blood also migrate into the affected brain tissue. This transmigration is mediated by a chemokine, monocyte attractant protein 1 (MCP-1), which is induced one or two days after ischemia (82). Moreover, within 14 days poststroke about one third of these transmigrated cells differentiate into microglial cells, which are indistinguishable from resident microglia (83). A trans-differentiation into astrocytes has also been observed by some groups (84, 85), but was disputed by others (86). Nevertheless, an important role of astrocytes during inflammation has been recognized; they join the ranks of liberators of both pro-inflammatory as well as neuroprotective factors such as erythropoietin (EPO), TGF-β_1, or metallothionein 2 (87–89).

Cytokines: Controller and Mediators of Inflammation

Activated leukocytes (granulocytes, monocyte/macrophages, lymphocytes) as well as neurons and glial cells (astrocytes, microglia) produce cytokines and chemokines (90,91). In particular, pro-inflammatory cytokines like TNFα, IL-1 and IL-6 play a major role as mediators of this inflammatory response. They link the early, excitotoxic phase with the phase of inflammation (52–54,92). The regulation of these cytokines depends on transcription factors like NFκB, which, in turn, are activated by oxygen free radicals (93, 94). Cytokine-mRNA and also the proteins of TNFα and IL-1 can be, previously, found a few hours after induction of experimental focal cerebral ischemia (92). Expression of IL-6 follows after about 24 hours (95). These cytokines are mainly liberated from microglial cells and macrophages (90–91). In stroke patients it was demonstrated that the intrathecal concentration of IL-1 and IL-6 correlated with infarct size (96). Cytokine receptor antagonists reduce the infarct volume in animal models. For example, blockade of TNFα by TNF-binding proteins reduces brain injury after focal cerebral ischemia (97). The role of TNFα is not entirely clear, however, since mice without TNFα-receptor (TNFR2) have larger infarcts (98). In part, these conflicting results may reflect different signal transduction cascades activated by the two TNFα–receptors TNFR1 and TNFR2 (99). Arguable is also the role of increased IL-6 induction, since IL-6 knockouts do not have smaller infarcts than their littermates (100). Further to the induction of adhesion molecules, the earlier-mentioned cytokines also render the blood brain barrier (BBB) more permeable, and induce pro-thrombotic functions of the endothelium (101).

Besides the expression of pro-inflammatory cytokines, there is also an induction of anti-inflammatory cytokines like TGF-1β or IL-10. These cytokines downregulate inflammation and thus exert a protective effect in the context of cerebral ischemia (102–105). The neuroprotective action of TGF-β1 is well known (87). Interestingly, this cytokine seems to be of particular

importance for the phenomenon of immunological tolerance. Similar to ischemic tolerance (see later), it is possible to induce an immunologically tolerant state toward ischemia. This protection is induced by immunogenetic proteins (for instance myelin basic protein, MBP) and mediated by a certain lymphocyte population expressing TGF-β1 (106–108). In contrast to ischemic tolerance, immunological tolerance is longer lasting. Whereas in ischemic tolerance the protection does not last longer than seven days, protection extends over months in the case of immunological tolerance.

Next to the cytokines, two other proteins stand in the limelight of the inflammatory phase: inducible nitric oxide synthase (INOS) and cyclo-oxygenase 2 (COX2).

Nitric Oxide and Inducible Nitric Oxide Synthase

Nitric oxide, a gaseous, reactive, and diffusible radical, plays an important role in the regulation of a wide range of physiological processes, including cellular immunity, angiogenesis, and neurotransmission. NO is synthesized from L-arginine by the action of nitric oxide synthases (NOS). NO can diffuse across the cell membrane and react with a variety of targets. Nitric oxide (NO) is involved in normal cellular function as well as pathologic processes. NOS is known to exist in at least three isoforms. Under physiological conditions NO is generated mainly by an endothelial (eNOS) and a neuronal isoform (NNOS). Both isoforms are constitutively expressed. In contrast, the third isoform is inducible (iNOS) and mainly active in inflammatory processes (109). Whereas the constitutive isoforms are mainly regulated by a Ca^{2+}-dependent binding of calmodulin to the enzyme, INOS is regulated by its rate of expression. Nitric oxide (NO) may react with superoxide to the highly cytotoxic peroxynitrite (110). NO can trigger apoptosis by several pathways, for example by damaging DNA and p53 induction (111). During inflammation, INOS can generate cytotoxic levels of NO. The induction of INOS has been demonstrated in experimental stroke models both on mRNA and on protein level (112). Maximal protein expression occurs after about 24 hours. INOS is induced in neutrophils infiltrating the ischemic area and in cerebral blood vessels in the ischemic territory (113). INOS has also been detected in human brains after ischemic stroke using immunohistochemistry. Moreover, intrathecal levels of nitrate were shown to be elevated in stroke patients as long as three months after stroke, correlating with stroke size and severity of the neurological deficits. Inhibition of INOS by aminoguanidin and 1400W reduced the size of experimental infarcts by about 30%, even if the treatment is delayed 24 hours after onset ischemia (114–116). Furthermore, INOS knockout mice had smaller infarct volumes and less neurological deficits compared to wild type mice (117). These studies suggest that NO synthesized by INOS functions as an important factor in the delayed progression of ischemic damage.

Cyclo-oxygenase-2

COX is a rate-limiting enzyme in the synthesis of prostaglandins and thromboxans. Two isoforms have been described: COX 1 and COX 2. COX1 is known to be expressed constitutively in many cells, where it produces prostanoids for the normal cellular function. COX2 is expressed under normal conditions at low levels in some cells, such as neurons, and can be upregulated in response to mitogens, inflammatory mediators, and hormones (118).

In animal stroke models COX2 is mainly expressed in neurons, neutrophils, and vascular cells of the penumbra (119). Recently, COX2 has also been found in human brains after ischemic stroke. The enzyme has a destructive effect on the penumbral tissue mainly via the production of oxygen free radicals and toxic prostanoids (52,54), since both, genetic and pharmacological inhibition of COX2 have a protective effect (120,121). The expression kinetics of COX2 are similar to that of INOS. In addition, cells producing COX2 are in close proximity to cells expressing INOS, suggesting that NO produced by INOS activates COX2. Therefore, some deleterious effects of INOS might be mediated through COX2 reaction products. This hypothesis is supported by the observation that the COX2 inhibitor NS-398 attenuates ischemic brain damage in wild-type mice but not in INOS deficient mice (122).

COX2 as well as INOS are promising targets for the treatment of stroke patients because blocking them is still effective even 6 to 24 hours after ischemia (115,121).

Vascular Integrity and Damage of the Blood–Brain Barrier

The function of the blood–brain barrier (BBB) depends on integrity of its cellular matrix consisting of endothelial cells, basal lamina, and astrocytes. Cerebral ischemia causes damage to this matrix and disturbs its intercellular signalling. Once the BBB is disrupted, inflammatory cells can move easily into damaged areas and can itself release inflammatory molecules, such as bradykinin, histamine, cytokines, platelet-activating factors. Central to these damaging processes are proteases like cathepsins, plasminogen activators (PA), and the matrix metalloproteinases (MMP). The action of the MMPs, a group of more than 20 zinc-endopeptidases, has been extensively studied. Proteolytic destruction of the basal membrane by MMPs permits the immigration of leukocytes and promotes vasogenic edema. MMP-2 and MMP-9 are expressed within one to three hours after cerebral ischemia (123). Microvascular endothelial cells, neutrophils, monocytes/microglia and natural killer cells express large amounts of MMPs when activated (124). The degree of their expression correlates with the degree of BBB-breakdown; MMP-9 expression correlates with the opening of the BBB and the risk of hemorrhagic transformation (125). MMP-2 expression correlates with the degree of neuronal injury (123,126,127). Pharmacological inhibition of MMPs prevents this breakdown and reduces stroke volumes. Mice with targeted disruption of MMP-9 are partly protected from cerebral ischemia (128,129).

In the brain, tPA is expressed mainly in neurons, astrocytes, and microglia. Several studies have shown that tPA may be neurotoxic (130), but experiments with tPA-knockout mice have produced conflicting data (131,132). Since recombinant tPA is the sole licensed drug for thrombolytic therapy, these findings may be highly relevant to current therapeutic practice. tPA has, furthermore, been shown to induce MMP-9 and might, thus, be capable of—at least indirect—BBB damage (133). The same probably holds for recombinant tPA, which may explain the occurence of secondary hemorrhages after thrombolytic stroke therapy (129,134,135). Animal experiments have demonstrated that delayed rtPA treatment (as in patients) leads to a significantly higher degree of BBB damage as well as mortality. The pharmacological inhibition of MMPs is capable of reversing this effect of rtPA (136). In addition, tPA enhances NMDA-mediated calcium signaling and subsequent excitotoxic neuronal injury (137). It is a matter of controversy whether this detrimental effect is due to a cleavage of the NR1 subunit of the NMDA receptor by tPA or not (138).

The example of rtPA demonstrates once again that a thorough understanding of the complex pathophysiological mechanisms of ischemia is conditional to the further refinement of our therapeutic arsenal. The development of effective and low-risk thrombolytic therapies remains among the main targets of pharmacological research in the field of stroke treatment (134). One promising approach is the development of novel plasminogen activators, such as recombinant desmodus rotundus salivary plasminogen activator (DSPA-α1; desmoteplase). Experimental evidence indicates that desmoteplase has pharmacological and toxicological properties, which are superior to rtPA (139,140). Results from a recently published phase II trial are also encouraging (141).

PROGRAMMED CELL DEATH AND APOPTOSIS

Ischemia induced apoptosis has a similar time frame as inflammation. A number of reviews have dealt extensively with the significance of apoptosis in the pathophysiology of ischemia (2,4,142–145). In focal cerebral ischemia, apoptosis of neurons occurs after short periods of vascular occlusion (146), which are too short to induce pannecrosis (i.e., infarction), or in the regions bordering the infarct (i.e., the penumbra). Apoptosis after stroke was also described in regions remote from the infarct, for example the ipsilateral thalamus, a phenomenon ascribed to synaptic disconnection (147).

Apoptosis can be triggered in two ways, by intrinsic (i.e., basically mitochondrial) or by extrinsic activation. Ligation of the Fas-receptor, for example by TNF-α, triggers the extrinsic pathway. Intrinsic triggers of apoptosis in the context of ischemia are elevated concentrations of intracellular calcium, reactive oxygen species, or glutamate, as well as increased DNA damage. By damaging the mitochondrial membranes, both pathways directly or indirectly lead to the activation of caspases.

Caspases are a hierarchical group of at least 14 cysteine dependent and aspartate specific proteases. They exist in every cell in the form of their inactive precursor proteins, which are

activated by cleavage. Apoptosis is essentially an active and energy dependent cellular deconstruction process. In cerebral ischemia, caspases 1, 3, 8, and 9 are involved, of which caspases 8 and 9 are the initiators of a signaling cascade that activates the so-called "execution" caspase 3. Caspase 1 is predominantly engaged in cytokine activation (142,144). Caspase 3 is of importance in the context of cerebral ischemia (143), and also, its genetic or pharmacological inhibition is neuroprotective in a number of neurodegenerative conditions (148,149). The substrates degraded by caspase 3 are DNA repair enzymes like poly-(ADP-ribose)-polymerase (PARP) and DNA dependent protein kinase (DNA-PK). The latter is important for the repair of DNA double strand breaks. PARP recognizes single strand disruptions and mediates self-repair of DNA through swift automodification with synthesis of highly negatively charged, long, and branched ADP-ribose molecules. This process utilizes ATP and thus drains the cellular energy pool. ATP consumption by PARP is widely believed to be cytotoxic, in itself. PARP is also capable of inducing caspase independent cellular suicide via the so-called apoptosis inducing factor (AIF) (see later) (150). This might explain the partial failure of caspase inhibitors to protect neurons in some models of cerebral ischemia. In fact, caspase-independent signaling of apoptosis in the penumbra has been described in a rat model of cerebral ischemia (151). The genetic or pharmacological blockade of PARP is neuroprotective in experimental stroke (152–154). Of significance is the cleavage by caspase 3 of the inhibitor of caspase-activated DNase (ICAD). ICAD is activated and causes the characteristic feature of DNA "laddering" that has been described in all stroke models (155). Complete apoptotic laddering leaves DNA-oligomers of about 140 to 180 base pairs in length, which no longer contain any useful genetic information. Besides destroying genetic information, caspases also degrade structural proteins of the nucleus and cytoplasm, like laminin, actin, and gelsolin (143).

Cytochrome C is not only an essential part of the mitochondrial electron transfer chain and, hence, critical for energy production of the cell, but also a central mediator in the caspase activation cascade (156,157). In the extrinsic pathway of apoptosis, ligation of the Fas-receptor leads to the formation of the "death-inducing signaling complex" (DISC). DISC activates caspase 8, which, in turn, activates "Bid," a pro-apoptotic protein of the Bcl-2 family (see later). Bid then liberates cytochrome C from the mitochondrial membrane. Other members of the pro-apoptotic Bcl-2 family are Bad and Bax, which are important members of the intrinsic apoptotic pathway. Their activation leads to their translocation into the outer mitochondrial membrane and to the establishment of the mitochondrial permeability transition pore (MPT) leading to the release of cytochrome C. Cytochrome C can also be released from mitochondria through direct membrane damage by free radicals (155,157). Cytochrome C associates with the cytosolic protein Apaf-1, the caspase precursor protein, and ATP, forming the so-called "apoptosome." The apoptosome cleaves and thereby activates caspase 9 from its precursor (158). Whether cytochrome C is eventually released depends on the balance of pro-apoptotic members of the Bcl-2 family like Bid, Bax, Bad, Bag, and their anti-apoptotic counterparts Bcl-2 and Bcl-x_L (159). Transgenic expression of Bcl-2 and Bcl-x_L results in smaller infarcts after focal cerebral ischemia (160–162). Treatment with a Bcl-x_L fusion protein containing the TAT domain of the human immunodeficiency virus (HIV) for cell penetration protects neurons in models of cerebral ischemia (163,164). Bcl-2 and Bcl-x_L seem to have a stabilizing effect on the mitochondrial membrane; they prevent the formation of the MPT, the ensuing cytochrome C liberation, and the formation of AIF (157).

Members of the IAP-group (inhibitors of apoptosis proteins) also seem important in stroke pathophysiology. The overexpression of the X-chromosome-linked IAP (XIAP) has been demonstrated to be protective in stroke models (165). IAPs act indirectly via the inhibition of the apoptosome, but also by direct interference with caspase 3 (157). Other proteins can themselves block IAPs; such as DIABLO in mice (the human homologue is Smac), which is normally localized in mitochondria. After focal cerebral ischemia, DIABLO is released and binds to XIAP. However, the functional significance of this association in focal ischemia remains unclear (166).

DNA DAMAGE AND REPAIR

In the wake of ischemia and reperfusion, brain tissue is overwhelmed by oxygen free radicals, which cause abundant DNA damage. Particularly, the interaction of hydroxyl radicals with

DNA results in strand breaks and base alterations. Under physiological circumstances, DNA lesions are generated with a frequency of about 10,000 events each day (167). They are efficiently recognized and repaired, provided the repair enzymes are intact and not overloaded. Alterations that are typically caused by free radicals (168) have been found in mouse models of transient focal cerebral ischemia, where a massive increase in DNA damage was observed 10 to 20 minutes after reperfusion. Importantly, 8-hydroxy-deoxy guanosine becomes much more prevalent in both nuclear as well as mitochondrial DNA after ischemia (169–172). These alterations are partially repaired within four to six hours, and this increase in repair activity is proportional to the degree of DNA damage (170,173). Base excision repair (BER) seems to be of particular significance after cerebral ischemia. In BER, DNA glycosylases excise damaged or modified bases. Purine and pyrimidine free sites (AP-sites) are eliminated from the damaged DNA strand by AP-endonucleases (apurinic/apyrimidinic endonucleases) and replaced by DNA-polymerase β and DNA-ligase with a short strand of one to four nucleotides (169), based on the complementary blueprint of the remaining undamaged strand.

In the penumbra, deamination of cytosine to uracil is another mechanism of DNA damage, apart from the one caused by oxidative stress. Such alterations are corrected by uracil-DNA-glycosylase (UDG). We found that mitochondrial UDG-dependent repair activity is massively induced immediately following focal cerebral ischemia. Knockout mice deficient of UDG have larger infarcts than the wild-type controls, suggesting an essential role of UDG in DNA repair during focal cerebral ischemia (174).

DNA repair is neither inexhaustible nor infallible. Erroneous DNA repair may lead to persisting mutations. In models of transient focal cerebral ischemia, a dramatic increase in the frequency of mutations has been shown. The major role of DNA repair is to ensure transcription of mRNA from intact genes. An obvious consequence of mutations is instability of genetic information that may lead to faulty proteins, resulting in either cellular malfunction, disintegration, or the induction of tumors (169,172). The maintenance of swift and effective DNA repair is, therefore, essential in postmitotic cells, like neurons. In order to adapt to an increased demand, the cell may try to increase repair efficiency (173). Another way to avoid erroneous protein synthesis and possibly tumorigenesis is apoptosis (see earlier). Both approaches are encountered in focal cerebral ischemia, and it seems to be the quantity of damage that determines which scenario prevails (169,171). The tumor suppressor protein p53 appears to be the molecular switch on the crossroads of attempted repair and apoptosis (175,176). The induction of p53 has been shown in most models of ischemia (177,178). The fact that p53 knockout mice have, significantly, lower infarct volumes accords with p53s pro-apoptotic function. Interestingly and paradoxically, heterozygous $p53^{+/-}$ mice have even smaller infarcts than homozygous $p53^{-/-}$ mice (179).

ENDOGENOUS NEUROPROTECTION AND CELL REPLACEMENT

In the last two decades, stroke researchers have mainly focused on studying mechanisms of ischemic brain damage to identify promising targets for clinical neuroprotection. More recently, it has become clear that stroke not only damages brain parenchyma, but also initiates complex endogenous protective signaling cascades, involving three supersystems of the organism—the vascular, the immune, and the nervous system.

These mechanisms are currently intensively studied. Central to this research are models of ischemic preconditioning. The principle of ischemic preconditioning is the induction of a protected state of a cell, tissue, or a whole organism by exposure to a noxious stimulus (trigger), which is applied below, but close to the level where it induces damage. The stimulus induces a protective state against insults that normally would be lethal. Short intervals of ischemia ("ischemic tolerance"), hypoxia, reactive oxygen free radicals, inflammation, and so on can serve as tolerance inducing stimuli. After induction, ischemic tolerance occurs within two time windows. Early tolerance exists after about 5 to 120 minutes following stimulation (classical preconditioning). Delayed preconditioning occurs after a latency of about 24 to 72 hours. Seven days after induction, the protected state is no longer detectable (180,181). Studies in patients who had transient ischemic attacks (TIA) before having a persistent stroke indicate that ischemic tolerance does also exist in humans. Subsequent to a TIA, brain infarcts

and neurological deficits were smaller if compared to patients without preceding TIA. As a TIA, by definition, does not lead to infarction, it may thus be considered as a stimulus that induces tolerance (182–184).

Unlike severe ischemia, which leads to stroke, the preconditioning stimulus exclusively induces protective signaling cascades. Conceptually, in delayed preconditioning we can discriminate three stages of this protective signaling. In the induction phase, molecular sensors (mostly receptors, channels, and regulators) are activated by transcription factors. During the transduction phase certain protein kinases, transcription factors, and para- and autocrine mediators, such as growth factors, amplify the signal and thereby prepare the effector phase. In this phase, proteins with a direct protective impact (anti-apoptotic, anti-inflammatory, anti-oxidative) are switched on. These mechanisms are the molecular basis for ischemic tolerance and have been reviewed in detail elsewhere (180–182). As an example for the complex signaling cascades resulting in endogenous neuroprotection we want to give only a brief outline for this concept: In astrocytes, a tolerance-inducing hypoxic stimulus induces the transcription factor hypoxia-inducible-factor-1 (HIF-1). HIF-1 is one of the central sensors of hypoxia and induces the expression of erythropoietin (EPO) (88,185,186). Erythropoietin is released by astrocytes and binds to the neuronal EPO-receptor. Via the activation of a protein kinase cascades, in particular Janus kinase 2 (JAK2), phosphoinositol-3 kinase (PI3K) several transcription factors like NF-κB and STATs kinase are activated. These transciption factors coordinate the induction of anti-apoptotic as well as prosurvival genes like Bcl-X_L (187). In addition, the PI3K/Akt protein kinase cascade can phosphorylate and thus inactivate the pro-apoptotic protein BAD (88). This neuroprotective signaling cascade mediates approximately 50% of the protection observed in this model (188). Besides this paracrine pathway, which is mediated by astrocytes and neurons, a number of other mechanisms have been described. A host of anti-excitotoxic, anti-inflammatory and anti-apoptotic mechanisms, including programs for regeneration and repair, have been implicated in induced tolerance (180–182). Nevertheless, HIF-1 seems to be a central coordinator of the adaptive response to survival during hypoxia and ischemia. HIF-1 not only induces EPO, but also activates the protein synthesis of genes involved in metabolism, vascular processes, and cellular survival or proliferation, such as glucose transporters, glycolytic enzymes, heme oxygenase 1, p21, IGF-2, and VEGF (189).

Understanding these mechanisms may allow, in future, to induce or boost endogenous protection in patients, as a novel strategy to safeguard the brain against hypoxic/ischemic damage. For example, EPO is a promising drug in stroke therapy. There is a solid evidence that exogenously applied EPO is neuroprotective in the in vivo and in vitro models of cerebral ischemia (88,190,191). Clinical phase I and phase II trials suggest that EPO is not only safe but may also be beneficial in the therapy of acute stroke (192). In addition, nonhematopietic variants of EPO become a promising tool. Such variants have been shown to be neuroprotective in models of stroke, spinal cord compression, diabetic neuropathy, and experimental autoimmune encephalomyelitis, and potentially allow long-term treatment (193). In addition, pharmacological inducers of ischemic tolerance, for example desferrioxamine, an approved drug for the treatment of hemosiderosis, are promising in treatment of chronic and acute neurodegenerative diseases (188).

CONCLUSION

The concept of the ischemic penumbra as a highly dynamic tissue volume surrounding the ischemic core is now widely accepted. Core and penumbra are linked to different threshold levels of CBF. In the core, all cells have lost their membrane potential and are undergoing rapid, irreversible damage due to low perfusion. Only hyperacute reperfusion may salvage the core. The penumbra, in which intermediate perfusion prevails, is subjected to a temporospatial evolution. Early, after onset of focal cerebral ischemia, neurons in the penumbra remain structurally intact but functionally silent. In contrast to the core, penumbral tissue is highly active. Complex pathways involving excitotoxicity, oxidative and nitrosative stress, peri-infarct depolarizations, inflammation, and programmed cell death lead to the expansion of damage in the penumbral area—the core is increasing at the expense of the penumbra. Since penumbral tissue is viable for extended time periods, it has the realistic potential to be rescued

by therapeutic intervention: the penumbra is the target for acute stroke therapy. Besides thrombolysis, no therapeutic strategy to protect the brain after a stroke in humans has been convincingly demonstrated so far. However, we believe that the recent advances in stroke pathophysiology, neuroimaging, and clinical trial design, justify cautious optimism, and that within the near future "neuroprotection" will become a reality in stroke therapy.

REFERENCES

1. Ginsberg MD. Adventures in the pathophysiology of brain ischemia: penumbra, gene expression, neuroprotection: the 2002 Thomas Willis lecture. Stroke 2003; 34(1):214–223.
2. Dirnagl U, Iadecola C, Moskowitz MA. Pathobiology of ischemic stroke: an integrated view. Trends Neurosci 1999; 22(9):391–397.
3. Nowicky AV, Duchen MR. Changes in [Ca2+]i and membrane currents during impaired mitochondrial metabolism in dissociated rat hippocampal neurons. J Physiol 1998; 507(1):131–145.
4. Lo EH, Dalkara T, Moskowitz MA. Mechanisms, challenges and opportunities in stroke. Nat Rev Neurosci 2003; 4(5):399–415.
5. Lauritzen M, Hansen AJ. The effect of glutamate receptor blockade on anoxic depolarization and cortical spreading depression. J Cereb Blood Flow Metab 1992; 12(2):223–229.
6. Muller M, Somjen GG. Na(+) dependence and the role of glutamate receptors and Na(+) channels in ion fluxes during hypoxia of rat hippocampal slices. J Neurophysiol 2000; 84(4):1869–1880.
7. Jarvis CR, Anderson TR, Andrew RD. Anoxic depolarization mediates acute damage independent of glutamate in neocortical brain slices. Cereb Cortex 2001; 11(3):249–259.
8. Rossi DJ, Oshima T, Attwell D. Glutamate release in severe brain ischemia is mainly by reversed uptake. Nature 2000; 403(6767):316–321.
9. Nallet H, MacKenzie ET, Roussel S. The nature of penumbral depolarizations following focal cerebral ischemia in the rat. Brain Res 1999; 842(1):148–158.
10. Selman WR, Lust WD, Pundik S, et al. Compromised metabolic recovery following spontaneous spreading depression in the penumbra. Brain Res 2004; 999(2):167–174.
11. Shinohara M, Dollinger B, Brown G, et al. Cerebral glucose utilization: local changes during and after recovery from spreading cortical depression. Science 1979; 203(4376):188–190.
12. Lauritzen M. Pathophysiology of the migraine aura. The spreading depression theory [Review]. Brain 1994; 117(Pt 1):199–210.
13. Leão AAP. Further observations on the spreading depression of activity in the cerebral cortex. J Neurophysiol 1947; 10:409–414.
14. Branston NM, Strong AJ, Symon L. Extracellular potassium activity, evoked potential and tissue blood flow. Relationships during progressive ischemia in baboon cerebral cortex. J Neurol Sci 1977; 32(3):305–321.
15. Aitken PG, Tombaugh GC, Turner DA, et al. Similar propagation of SD and hypoxic SD-like depolarization in rat hippocampus recorded optically and electrically. J Neurophysiol 1998; 80(3):1514–1521.
16. Strong AJ, Smith SE, Whittington DJ, et al. Factors influencing the frequency of fluorescence transients as markers of peri-infarct depolarizations in focal cerebral ischemia. Stroke 2000; 31(1):214–222.
17. Back T, Kohno K, Hossmann KA. Cortical negative DC deflections following middle cerebral artery occlusion and KCl-induced spreading depression: effect on blood flow, tissue oxygenation, and electroencephalogram. J Cereb Blood Flow Metab 1994; 14(1):12–19.
18. Shin HK, Dunn AK, Jones PB, et al. Vasoconstrictive neurovascular coupling during focal ischemic depolarizations. J Cereb Blood Flow Metab 2006; 26(8):1018–1030.
19. Dreier JP, Ebert N, Priller J, et al. Products of hemolysis in the subarachnoid space inducing spreading ischemia in the cortex and focal necrosis in rats: a model for delayed ischemic neurological deficits after subarachnoid hemorrhage? J Neurosurg 2000; 93(4):658–666.
20. Dreier JP, Korner K, Ebert N, et al. Nitric oxide scavenging by hemoglobin or nitric oxide synthase inhibition by N-nitro-L-arginine induces cortical spreading ischemia when K+ is increased in the subarachnoid space. J Cereb Blood Flow Metab 1998; 18(9):978–990.
21. Windmuller O, Lindauer U, Foddis M, et al. Ion changes in spreading ischemia induce rat middle cerebral artery constriction in the absence of NO. Brain 2005; 128(9):2042–2051.
22. Nedergaard M, Hansen AJ. Characterization of cortical depolarizations evoked in focal cerebral ischemia. J Cereb Blood Flow Metab 1993; 13(4):568–574.
23. Dijkhuizen RM, Beekwilder JP, van der Worp HB, et al. Correlation between tissue depolarizations and damage in focal ischemic rat brain. Brain Res 1999; 840(1–2):194–205.
24. Busch E, Gyngell ML, Eis M, et al. Potassium-induced cortical spreading depressions during focal cerebral ischemia in rats: contribution to lesion growth assessed by diffusion-weighted NMR and biochemical imaging. J Cereb Blood Flow Metab 1996; 16(6):1090–1099.

25. Takano K, Latour LL, Formato JE, et al. The role of spreading depression in focal ischemia evaluated by diffusion mapping. Ann Neurol 1996; 39(3):308–318.
26. Back T, Ginsberg MD, Dietrich WD, et al. Induction of spreading depression in the ischemic hemisphere following experimental middle cerebral artery occlusion: effect on infarct morphology. J Cereb Blood Flow Metab 1996; 16(2):202–213.
27. Gill R, Andine P, Hillered L, et al. The effect of MK-801 on cortical spreading depression in the penumbral zone following focal ischemia in the rat. J Cereb Blood Flow Metab 1992; 12(3):371–379.
28. Iijima T, Mies G, Hossmann KA. Repeated negative DC deflections in rat cortex following middle cerebral artery occlusion are abolished by MK-801: effect on volume of ischemic injury. J Cereb Blood Flow Metab 1992; 12(5):727–733.
29. Rawanduzy A, Hansen A, Hansen TW, et al. Effective reduction of infarct volume by gap junction blockade in a rodent model of stroke. J Neurosurg 1997; 87(6):916–920.
30. Hartings JA, Rolli ML, Lu XC, et al. Delayed secondary phase of peri-infarct depolarizations after focal cerebral ischemia: relation to infarct growth and neuroprotection. J Neurosci 2003; 23(37): 11602–11610.
31. Strong AJ, Fabricius M, Boutelle MG, et al. Spreading and synchronous depressions of cortical activity in acutely injured human brain. Stroke 2002; 33(12):2738–2743.
32. Sims NR, Anderson MF. Mitochondrial contributions to tissue damage in stroke. Neurochem Int 2002; 40(6):511–526.
33. Chan PH. Reactive oxygen radicals in signaling and damage in the ischemic brain. J Cereb Blood Flow Metab 2001; 21(1):2–14.
34. Siesjo BK. Acidosis and ischemic brain damage. Neurochem Pathol 1988; 9:31–88.
35. Myers RE, Yamagutchi M. Nervous system effects of cardiac arrest in monkeys. Arch Neurol 1977; 34:65–74.
36. Pulsinelli WA, Waldman S, Rawlinson D, et al. Moderate hyperglycemia augments ischemic brain damage: a neuropathologic study in the rat. Neurology 1982; 32(11):1239–1246.
37. Jorgensen HS, Nakayama H, Raaschou HO, et al. Effect of blood pressure and diabetes on stroke in progression. Lancet 1994; 344 (8916):156–159.
38. Weir CJ, Murray GD, Dyker AG, et al. Is hyperglycaemia an independent predictor of poor outcome after acute stroke? Results of a long-term follow up study. BMJ 1997; 314(7090):1303–1306.
39. Bruno A, Biller J, Adams HP Jr. et al. Acute blood glucose level and outcome from ischemic stroke. Trial of ORG 10172 in Acute Stroke Treatment (TOAST) Investigators. Neurology 1999; 52(2):280–284.
40. Bruno A, Levine SR, Frankel MR, et al. NINDS rt-PA Stroke Study Group. Admission glucose level and clinical outcomes in the NINDS rt-PA Stroke Trial. Neurology 2002; 59(5):669–674.
41. Baird TA, Parsons MW, Phanh T, et al. Persistent poststroke hyperglycemia is independently associated with infarct expansion and worse clinical outcome. Stroke 2003; 34(9):2208–2214.
42. Tracey F, Stout RW. Hyperglycemia in the acute phase of stroke and stress response. Stroke 1994; 25(2):524–525.
43. Counsell C, McDowall M, Dennis M. Hyperglycaemia after acute stroke. Other models find that hyperglycaemia is not independent predictor. BMJ 1997; 315(7111):810.
44. Schurr A. Glucose and the ischemic brain: a sour grape or a sweet treat? Curr Opin Clin Nutr Metab Care 2001; 4(4):287–292.
45. Smith-Swintosky VL, Pettigrew LC, Sapolsky RM, et al. Metyrapone, an inhibitor of glucocorticoid production, reduces brain injury induced by focal and global ischemia and seizures. J Cereb Blood Flow Metab 1996; 16(4):585–598.
46. Tian GF, Baker AJ. Protective effect of high glucose against ischemia-induced synaptic transmission damage in rat hippocampal slices. J Neurophysiol 2002; 88(1):236–248.
47. Seo SY, Kim EY, Kim H, et al. Neuroprotective effect of high glucose against NMDA, free radical, and oxygen-glucose deprivation through enhanced mitochondrial potentials. J Neurosci 1999; 19(20):8849–8855.
48. Ginsberg MD, Prado R, Dietrich WD, et al. Hyperglycemia reduces the extent of cerebral infarction in rats. Stroke 1987; 18(3):570–574.
49. Zasslow MA, Pearl RG, Shuer LM, et al. Hyperglycemia decreases acute neuronal ischemic changes after middle cerebral artery occlusion in cats. Stroke 1989; 20(4):519–523.
50. Parsons MW, Barber PA, Desmond PM, et al. Acute hyperglycemia adversely affects stroke outcome: a magnetic resonance imaging and spectroscopy study. Ann Neurol 2002; 52(1):20–28.
51. Winquist RJ, Kerr S. Cererbal ischemia-reperfusion injury and adhesion. Neurology 1997; 49(S4):S23–S26.
52. Emsley HC, Tyrrell PJ. Inflammation and infection in clinical stroke. J Cereb Blood Flow Metab 2002; 22(12):1399–1419.
53. Becker KJ. Targeting the central nervous system inflammatory response in ischemic stroke. Curr Opin Neurol 2001; 14(3):349–353.
54. del Zoppo G, Ginis I, Hallenbeck JM, et al. Inflammation and stroke: putative role for cytokines, adhesion molecules and iNOS in brain response to ischemia. Brain Pathol 2000; 10(1):95–112.

55. Zhang RL, Chopp M, Zaloga C, et al. The temporal profiles of ICAM-1 protein and mRNA expression after transient MCA occlusion in the rat. Brain Res 1995; 682(1–2):182–188.
56. Fiszer U, Korczak-Kowalska G, Palasik W, et al. Increased expression of adhesion molecule CD1 (LFA-1beta) on the leukocytes of peripheral blood in patients with acute ischemic stroke. Acta Neurol Scand 1998; 97(4):221–224.
57. Zhang L, Zhang ZG, Zhang RL, et al. Effects of a selective CD11b/CD18 antagonist and recombinant human tissue plasminogen activator treatment alone and in combination in a rat embolic model of stroke. Stroke 2003; 34(7):1790–1795.
58. Bitsch A, Klene W, Murtada L, et al. A longitudinal prospective study of soluble adhesion molecule in acute stroke. Stroke 1998; 29(10):2129–2135.
59. Zhang RL, Chopp M, Zaloga C, et al. The temporal profiles of ICAM-1 protein and mRNA expression after transient MCA occlusion in the rat. Brain Res 1995; 682(1–2):182–188.
60. Sanchez-Moreno C, Dashe JF, Scott T, et al. Decreased levels of plasma vitamin C and increased concentrations of inflammatory and oxidative stress markers after stroke. Stroke 2004; 35(1):163–166.
61. Kochanek PM, Hallenbeck JM. Polymorphonuclear leukocytes and monocytes/macrophages in the pathogenesis of cerebral ischemia and stroke. Stroke 1992; 23:1367–1379.
62. Matsuo Y, Onodera H, Shiga Y, et al. Role of cell adhesion molecules in brain injury after middle cerebral artery occlusion in the rat. Brain Res 1994; 656(2):344–352.
63. Hartl R, Schurer L, Schmid-Schonbein GW, et al. Experimental antileukocyte interventions in cerebral ischemia. J of Cereb Blood Flow Metab 1996; 16(6):1108–1119.
64. del Zoppo GJ, Schmid-Schonbein GW, Mori E, et al. Polymorphonuclear leukocytes occlude capillaries following middle cerebral artery occlusion and reperfusion in baboons. Stroke 1991; 22(10):1276–1283.
65. Mori E, del Zoppo GJ, Chambers JD. Inhibition of polymorphonuclear leukocyte adherence suppresses no-reflow after focal cerebral ischemia in baboons. Stroke 1992; 23(5):712–718.
66. Chen H, Chopp M, Zhang RL, et al. Anti-CD11b monoclonal antibody reduces ischemic cell damage after transient focal cerebral ischemia in rat. Ann Neurol 1994; 35:458–463.
67. Zhang RL, Chopp M, Jiang N, et al. Anti-intercellular adhesion molecule-1 antibody reduces ischemic cell damage after transient but not permanent middle cerebral artery occlusion in the Wistar rat. Stroke 1995; 26(8):1438–1442.
68. Soriano SG, Coxon A, Wang YF, et al. Mice deficient in Mac-1 (CD11b/CD18) are less susceptible to cerebral ischemia/reperfusion injury. Stroke 1999; 30(1):134–139.
69. Prestigiacomo CJ, Kim SC, Connolly ES Jr. Cd18-mediated neutrophil recruitment contributes to the pathogenesis of reperfused but not nonreperfused stroke. Stroke 1999; 30(5):1110–1117.
70. Soriano SG, Lipton SA, Wang YF, et al. Intercellular adhesion molecule-1-deficient mice are less susceptible to cerebral ischemia-reperfusion injury. Ann Neurol 1996; 39(5):618–624.
71. Mocco J, Choudhri T, Huan J, et al. HuEP5C7 as a humanized monoclonal anti-E/P-selectin neurovascularprotective strategy in a blinded placebo-controlled trial of non-human primate stroke. Circ Res 2002; 91(10):907–914.
72. Becker K, Kindrick D, Relton J, et al. Antibody to the alpha4 integrin decreases infarct size in transient focal cerebral ischemia in rats. Stroke 2001; 32(1):206–211.
73. Jian N, Chopp M, Chahwala S. Neutrophil inhibitory factor treatment of focal cerebral ischemia in the rat. Brain Res 1998; 788(1–2):25–34.
74. Furuya K, Takeda H, Azhar S, et al. Examination of several potential mechanisms for the negative outcome in a clinical stroke trial of enlimomab, a murine anti-human intercellular adhesion molecule-1 antibody: a bedside-to-bench study. Stroke 2001; 32(11):2665–2674.
75. Becker KJ. Anti-Leukocyte antibodies: Leukarrest (Hu23F2G) and Enlimomab (R6.5) in acute stroke. Curr Med Res Opin 2002; 18:S18–S22.
76. Korematsu K, Goto S, Nagahiro S, et al. Microglial response to transient focal cerebral ischemia: an immunocytochemical study on the rat cerebral cortex using anti-phosphotyrosine antibody. J Cereb Blood Flow Metab 1994; 14(5):825–830.
77. Ueyama T, Ren Y, Sakai N, et al. Generation of a constitutively active fragment of PKN in microglia/macrophages after middle cerebral artery occlusion in rats. J Neurochem 2001; 79(4):903–913.
78. Marks L, Carswell HV, Peters EE, et al. Characterization of the microglial response to cerebral ischemia in the stroke-prone spontaneously hypertensive rat. Hypertension 2001; 38(1):116–122.
79. Tarozzo G, Campanella M, Ghiani M, et al. Expression of fractalkine and its receptor, CX3CR1, in response to ischemia-reperfusion brain injury in the rat. Eur J Neurosci 2002; 15(10):1663–1668.
80. Yrjänheikki J, Tikka T, Keinanen R, et al. A tetracycline derivative, minocycline, reduces inflammation and protects against focal cerebral ischemia with a wide therapeutic window. Proc Natl Acad Sci U S A 1999; 96(23):13496–13500.
81. Gehrmann J, Matsumoto Y, Kreutzberg GW. Microglia: intrinsic immuneffector cell of the brain. Brain Res Rev 1995; 20(3):269–287.
82. Gourmala NG, Buttini M, Limonta S, et al. Differential and time-dependent expression of monocyte chemoattractant protein-1 mRNA by astrocytes and macrophages in rat brain: effects of ischemia and peripheral lipopolysaccharide administration. J Neuroimmunol 1997; 74(1–2):35–44.

83. Priller J, Flugel A, Wehner T. Targeting gene-modified hematopoietic cells to the central nervous system: use of green fluorescent protein uncovers microglial engraftment. Nat Med 2001; 7(12):1356–1361.
84. Eglitis MA, Mezey E. Hematopoietic cells differentiate into both microglia and macroglia in the brains of adult mice. Proc Natl Acad Sci U S A 1997; 94(8):4080–4085.
85. Eglitis MA, Dawson D, Park KW, et al. Targeting of marrow-derived astrocytes to the ischemic brain. Neuroreport 1999; 10(6):1289–1292.
86. Wehner T, Bontert M, Eyupoglu I. Bone marrow-derived cells expressing green fluorescent protein under the control of the glial fibrillary acidic protein promoter do not differentiate into astrocytes in vitro and in vivo. J Neurosci 2003; 23(12):5004–5011.
87. Letterio JJ. Murine models define the role of TGF-beta as a master regulator of immune cell function. Cytokine Growth Factor Rev 2000; 11(1–2):81–87.
88. Ruscher K, Freyer D, Karsch M. Erythropoietin is a paracrine mediator of ischemic tolerance in the brain: evidence from an in vitro model. J Neurosci 2002; 22(23):10291–10301.
89. Trendelenburg G, Prass K, Priller J, et al. Serial analysis of gene expression identifies metallothionein-II as major neuroprotective gene in mouse focal cerebral ischemia. J Neurosci 2002; 22(14):5879–5888.
90. Davies CA, Loddick SA, Toulmond S, et al. The progression and topographic distribution of interleukin-1beta expression after permanent middle cerebral artery occlusion in the rat. J Cereb Blood Flow Metab 1999; 19(1):87–98.
91. Gregersen R, Lambertsen K, Finsen B. Microglia and macrophages are the major source of tumor necrosis factor in permanent middle cerebral artery occlusion in mice. J Cereb Blood Flow Metab 2000; 20(1):53–65.
92. Stoll G. Inflammatory cytokines in the nervous system: multifunctional mediators in autoimmunity and cerebral ischemia. Rev Neurol (Paris) 2002; 158(10 Pt 1):887–891.
93. O'Neill LA, Kaltschmidt C. NF-kappa B: a crucial transcription factor for glial and neuronal cell function. Trends Neurosci 1997; 20(6):252–258.
94. Iadecola C, Alexander M. Cerebral ischemia and inflammation. Curr Opin Neurol 2001; 14(1):89–94.
95. Block F, Peters M, Nolden-Koch M. Expression of IL-6 in the ischemic penumbra. Neuroreport 2000; 11(5):963–967.
96. Tarkowski E, Rosengren L, Blomstrand C, et al. Early intrathecal production of interleukin-6 predicts the size of brain lesion in stroke. Stroke 1995; 26(8):1393–1398.
97. Nawashiro H, Tasaki K, Ruetzler CA. TNF-alpha pretreatment induces protective effects against focal cerebral ischemia in mice. J Cereb Blood Flow Metab 1997; 17(5):483–490.
98. Bruce AJ, Boling W, Kindy MS, et al. Altered neuronal and microglial responses to excitotoxic and ischemic brain injury in mice lacking TNF receptors. Nat Med 1996; 2(7):788–794.
99. Fontaine V, Mohand-Said S, Hanoteau N. Neurodegenerative and neuroprotective effects of tumor necrosis factor (TNF) in retinal ischemia: opposite roles of TNF receptor 1 and TNF receptor 2. J Neurosci 2002; 22(7):RC216.
100. Clark WM, Rinker LG, Lessov NS, et al. Lack of interleukin-6 expression is not protective against focal central nervous system ischemia. Stroke 2000; 31(7):1715–1720.
101. Priller J, Dirnagl U. Inflammation in stroke--a potential target for neuroprotection? Ernst Schering Res Found Workshop 2002; 39:133–157.
102. Bogdan C, Paik J, Vodovotz Y, et al. Contrasting mechanisms for suppression of macrophage cytokine release by transforming growth factor-beta and interleukin-10. J Biol Chem 1992; 267(32): 23301–23308
103. Strle K, Zhou JH, Shen WH, et al. Interleukin-10 in the brain. Crit Rev Immunol 2001; 21(5): 427–449.
104. Prehn JH, Backhauss C, Krieglstein J. Transforming growth factor-beta 1 prevents glutamate neurotoxicity in rat neocortical cultures and protects mouse neocortex from ischemic injury in vivo. J Cereb Blood Flow Metab 1993; 13(3):521–525.
105. Spera PA, Ellison JA, Feuerstein GZ, et al. IL-10 reduces rat brain injury following focal stroke. Neurosci Lett 1998; 251(3):189–192.
106. Becker KJ, McCarron RM, Ruetzler C, et al. Immunologic tolerance to myelin basic protein decreases stroke size after transient focal cerebral ischemia. Proc Natl Acad Sci U. S. A. 1997; 94(20):10873–10878.
107. Becker K, Kindrick D, McCarron R, et al. Adoptive transfer of myelin basic protein-tolerized splenocytes to naive animals reduces infarct size: a role for lymphocytes in ischemic brain injury? Stroke 2003; 34(7):1809–1815.
108. Takeda H, Spatz M, Ruetzler C, et al. Induction of mucosal tolerance to E-selectin prevents ischemic and hemorrhagic stroke in spontaneously hypertensive genetically stroke-prone rats. Stroke 2002; 33(9):2156.
109. Iadecola C. Bright and dark sides of nitric oxide in ischemic brain damage. Trends Neurosci 1997; 20(3):132–138.
110. Crow JP, Beckman JS. The role of peroxynitrite in nitric oxide-mediated toxicity. Curr Top Microbiol Immunol 1995; 196:57–73.

111. Kolb JP. Mechanisms involved in the pro- and anti-apoptotic role of NO in human leukemia. Leukemia 2000; 14(9):1685–1694.
112. Iadecola C, Zhang F, Casey R, et al. Inducible nitric oxide synthase gene expression in vascular cells after transient focal cerebral ischemia. Stroke 1996; 27(8):1373–1380.
113. Forster C, Clark HB, Ross ME. Inducible nitric oxide synthase expression in human cerebral infarcts. Acta Neurpathol 1999; 97(3):215–220.
114. Iadecola C, Zhang F, Casey R, et al. Delayed reduction of ischemic brain injury and neurological deficits in mice lacking the inducible nitric oxide synthase gene. J Neurosci 1997; 17(23):9157–9164.
115. Zhang F, Casey RM, Ross ME, et al. Aminoguanidine ameliorates and L-arginine worsens brain damage from intraluminal middle cerebral artery occlusion. Stroke 1996; 27(2):317–323.
116. Iadecola C, Zhang, Xu X, et al. Inhibition of inducible nitric oxide synthase ameliorates cerebral ischemic damage. Am J Physiol 1995; 268(1 Pt 2):R286–R292.
117. Zhao X, Haensel C, Araki E. Gene-doing effect ad persistence of reduction in ischemic brian injury in mice lacking inducible nitric oxide snythase. Brain Res 2000; 872(1–2):215–218.
118. O´Banion MK. Cyclooxygenase-2: molecular biology, pharmacology, and neurobiology. Crit Rev Neurobiol 1999; 13(1):45–82.
119. Sairanen T, Ristimaki A, Karjalainen-Lindsberg ML, et al. Cyclooxygenase-2 is induced globally in infarcted human brain. Ann Neurol 1998; 43(6):738–747.
120. Iadecola C, Niwa K, Nogawa S, et al. Reduced susceptibility to ischemic brain injury and N-methyl-D-aspartate-mediated neurotoxicity in cyclooxygenase-2-deficient mice. Proc Natl Acad Sci U S A 2001; 98(3):1294–1249.
121. Sugimoto K, Iadecola C. Delayed effect of administration of COX-2 inhibitor in mice with acute cerebral ischemia. Brain Res 2003; 960(1–2):273–276.
122. Nagamaya M, Niwa K, Nagamaya T. The cyclooxygenase-2 inhibitor NS-398 ameliorates cerebral ischemic injury in wild-type mice but not in mice with deletion of the inducible nitric oxide synthase gene. J Cereb Blood Flow Metab 1999; 19(11):1213–1219.
123. Heo JH, Lucero J, Abuiya T. Matrix metalloproteinases increase very early during experimental focal cerebral ischemia. J Cereb Blood Flow Metab 1999; 19(6):624–633.
124. Harkness KA, Adamson P, Sussman JD. Dexamethasone regulation of matrix metalloptroteinase expression in CNS vascular endothelium. Brain 2000; 123(Pt 4):698–709.
125. Fujimara M, Gasche Y, Morita-Fujimara Y. Early appearance of activated matrix metalloproteinase-9 and blood-brain barrier disruption in mice after focal cerebral ischemia and reperfusion. Brain Res 1999; 842(1):92–100.
126. Gasche Y, Fujimura M, Morita-Fujimura Y. Early appearance of activated matrix metalloproteinase-9 after focal cerebral ischemia in mice: a possible role in blood-brain barrier dysfunction. J Cereb Blood Flow Metab 1999; 19(9):1020–1028.
127. Lapchak PA, Chapman DF, Zivin JA. Metalloproteinase inhibition reduces thrombolytic (tissue plasminogen activator)-induced hemorrhage after thromboembolic stroke. Stroke 2000; 31(12):3034–3040.
128. Asahi M, Wang X, Mori T, et al. Effects of matrix metalloproteinase 9 gene knockout on the proteolysis of blood-brain barrier and white matter components after cerebral ischemia. J Neurosci 2001; 21(19):7724–7732.
129. Rosenberg GA, Estrada EY, Dencoff JE. Matrix metalloproteinases and TIMPs are associated with blood-brain barrier opening after reperfusion in rat brain. Stroke 1998; 29(10):2189–2195.
130. Nagai N, Yamamoto S, Tsuboi T, et al. Tissue type plasminogen activator is involved in the process of neuronal death by oxygen-glucose deprivation. J Cereb Blood Flow Metab 2001; 21(6):631–634.
131. Wang YF, Tsirka SE, Strickland S, et al. Tissue plasminogen activator (tPA) increases neuronal damage after focal cerebral ischemia in wild-type and tPA-deficient mice. Nat Med 1998; 4(2):228–231.
132. Tabrizi P, Wang L, Seeds N, et al. Tissue plasminogen activator (tPA) deficiency exacerbates cerebrovascular fibrin deposition and brain injury in a murine stroke model: studies in tPA-deficient mice and wild-type mice on a matched genetic background. Arterioscler Thromb Vasc Biol 1999; 19(11):2801–2806.
133. Wang X, Lee SR, Arai K, et al. Lipoprotein receptor-mediated induction of matrix metalloproteinase by tissue plasminogen activator. Nat Med 2003; 9(10):1313–1317.
134. Lapchak PA. Development of thrombolytic therapy for stroke: a perspective. Expert Opin Investig Drugs 2002; 11:1623–1632.
135. Dijkhuizen RM, Asahi M, Wu O, et al. Rapid breakdown of microvascular barriers and subsequent hemorrhagic transformation after delayed recombinant tissue plasminogen activator treatment in a rat embolic stroke model. Stroke 2002; 33(8):2100–2104.
136. Pfefferkorn T, Rosenberg GA. Closure of the blood-brain barrier by matrix metalloproteinase inhibition reduces rtPA-mediated mortality in cerebral ischemia with delayed reperfusion. Stroke 2003; 34(8):2025–2030.
137. Nicole O, Docagne F, Ali C, et al. The proteolytic activity of tissue-plasminogen activator enhances NMDA receptor-mediated signaling. Nat Med 2001; 7(1):59–64.
138. Matys T, Strickland S. Tissue plasminogen activator and NMDA receptor cleavage. Nat Med 2003; 9(4):371–372.

139. Liberatore GT, Samson A, Bladin C, et al. Vampire bat salivary plasminogen activator (desmoteplase): a unique fibrinolytic enzyme that does not promote neurodegeneration. Stroke 2003; 34(2):537–543.
140. Reddrop C, Moldrich RX, Beart PM. Vampire bat salivary plasminogen activator (desmoteplase) inhibits tissue-type plasminogen activator-induced potentiation of excitotoxic injury. Stroke 2005; 36(6):1241–1246.
141. Hacke W, Albers G, Al-Rawi Y, et al. DIAS Study Group. The Desmoteplase in Acute Ischemic Stroke trial (DIAS): a phase II MRI-based 9-hour window acute stroke thrombolysis trial with intravenous desmoteplase. Stroke 2005; 36(1):66–73.
142. Friedlander RM. Apoptosis and caspases in neurodegenerative diseases. N Engl J Med 2003; 348(14):1365–1375.
143. Endres M, Dirnagl U. Ischemia and stroke. Adv Exp Med Biol 2002; 513:455–473.
144. Ferrer I, Planas AM. Signaling of cell death and cell survival following focal cerebral ischemia: life and death struggle in the penumbra. J Neuropathol Exp Neurol 2003; 62(4):329–339.
145. Mattson MP, Duan W, Pedersen WA, et al. Neurodegenerative disorders and ischemic brain diseases. Apoptosis 2001; 6(1–2):69–81.
146. Katchanov J, Waeber C, Gertz K, et al. Selective neuronal vulnerability following mild focal brain ischemia in the mouse. Brain Pathol 2003; 13(4):452–464.
147. Soriano MA, Ferrer I, Rodriguez-Farre E, et al. Apoptosis and c-Jun in the thalamus of the rat following cortical infarction. Neuroreport 1996; 7(2):425–428.
148. Le DA, Wu Y, Huang Z, et al. Caspase activation and neuroprotection in caspase-3- deficient mice after in vivo cerebral ischemia and in vitro oxygen glucose deprivation. Proc Natl Acad Sci USA 2002; 99(23):15188–15193.
149. Hara H, Friedlander RM, Gagliardini V, et al. Inhibition of interleukin 1beta converting enzyme family proteases reduces ischemic and excitotoxic neuronal damage. Proc Natl Acad Sci USA 1997; 94(5):2007–2012.
150. Yu SW, Wang H, Poitras MF, et al. Mediation of poly (ADP-ribose) polymerase-1-dependent cell death by apoptosis-inducing factor. Science 2002; 297(5579):259–263.
151. Ferrer I, Friguls B, Dalfo E, et al. Caspase-dependent and caspase-independent signaling of apoptosis in the penumbra following middle cerebral artery occlusion in the adult rat. Neuropathol Appl Neurobiol 2003; 29(5):472–481.
152. Endres M, Wang ZQ, Namura S, et al. Ischemic brain injury is mediated by the activation of poly(ADP-ribose) polymerase. J Cereb Blood Flow Metab 1997; 17(11):1143–1151.
153. Eliasson MJ, Sampei K, Mandir AS, et al. Poly(ADP-ribose) polymerase gene disruption renders mice resistant to cerebral ischemia. Nat Med 1997; 3(10):1089–1095.
154. Ying W, Garnier P, Swanson RA. NAD+ repletion prevents PARP-1-induced glycolytic blockade and cell death in cultured mouse astrocytes. Biochem Biophys Res Commun 2003; 308(4):809–813.
155. Love S. Apoptosis and brain ischemia. Prog Neuropsychopharmacol Biol Psychiatry 2003; 27(2):267–282.
156. Mattson MP, Liu D. Mitochondrial potassium channels and uncoupling proteins in synaptic plasticity and neuronal cell death. Biochem Biophys Res Commun 2003; 304(3):539–549.
157. van Gurp M, Festjens N, van Loo G, et al. Mitochondrial intermembrane proteins in cell death. Biochem Biophys Res Commun 2003; 304(3):487–497.
158. Li P, Nijhawan D, Budihardjo I, et al. Cytochrome C and dATP-dependent formation of Apaf-1/caspase-9 complex initiates an apoptotic protease cascade. Cell 1997; 91(4):479–489.
159. Hengartner MO. The biochemistry of apoptosis. Nature 2000; 407(6805):770–776.
160. Linnik MD, Zahos P, Geschwind MD, et al. Expression of bcl-2 from a defective herpes simplex virus-1 vector limits neuronal death in focal cerebral ischemia. Stroke 1995; 26(9):1670–1674.
161. Martinou JC, Dubois-Dauphin M, Staple JK, et al. Overexpression of bcl-2 in transgenic mice protects neurons from naturally occuring cell death and experimental ischemia. Neuron 1994;13:1017–1030.
162. Wiessner C, Allegrini PR, Rupalla K, et al. Neuron-specific transgene expression of Bcl-XL but not Bcl-2 genes reduced lesion size after permanent middle cerebral artery occlusion in mice. Neurosci Lett 1999; 268(3):119–222.
163. Cao G, Pei W, Ge H, et al. Vivo delivery of a Bcl-xL fusion protein containing the TAT protein transduction domain protects against ischemic brain injury and neuronal apoptosis. J Neurosci 2002; 22(13):5423–5431.
164. Kilic E, Dietz GP, Hermann DM, et al. Intravenous TAT-Bcl-Xl is protective after middle cerebral artery occlusion in mice. Ann Neurol 2002; 52(5):617–622.
165. Trapp T, Korhonen L, Besselmann M, et al. Transgenic mice overexpressing XIAP in neurons show better outcome after transient cerebral ischemia. Mol Cell Neurosci 2003; 23(2):302–313.
166. Saito A, Hayashi T, Okuno S, et al. Interaction between XIAP and Smac/DIABLO in the mouse brain after transient focal cerebral ischemia. J Cereb Blood Flow Metab 2003; 23(9):1010–1019.
167. Lindahl T. Instability and decay of the primary structure of DNA. Nature 1993; 362(6422):709–715.
168. Jaruga P, Dizdaroglu M. Repair of products of oxidative DNA base damage in human cells. Nucleic Acids Res 1996; 24(8):1389–1394.

169. Liu PK, Grossman RG, Hsu CY, Robertson CS. Ischemic injury and faulty gene transcripts in the brain. Trends Neurosci 2001; 24(10):581–588.
170. Liu PK, Hsu CY, Dizdaroglu M, et al. Damage, repair, and mutagensis in nuclear genes after mouse forebrain ischemia-reperfusion. J Neurosci 1996; 16(21):6795–6806.
171. Englander EW, Hu Z, Sharma A. Rat MYH, a glycosylase for repair of oxidatively damaged DNA, has brain-specific isoforms that localize to neuronal mitochondria. J Neurochem 2002; 83(6):1471–1480.
172. Chopp M, Chan PH, Hsu CY, et al. DNA damage and repair in central nervous system injury: national institute of neurological disorders and stroke workshop summary. Stroke 1996; 27(3):363–369.
173. Lan J, Li W, Zhang F, et al. Inducible repair of oxidative DNA lesions in the rat brain after transient focal ischemia and reperfusion. J Cereb Blood Flow Metab 2003; 23(11):1324–1339.
174. Endres M, Biniszkiewicz D, Sobol RW, et al. Increased postischemic brain injury in mice deficient in uracil-DNA glycosylase. J Clin Invest 2004; 113(12):1711–1721.
175. Oren M. Decision making by p53: life, death and cancer. Cell Death Differ 2003; 10(4):431–442.
176. Jacks T, Weinberg RA. Cell-cycle control and its watchman. Nature 1996; 381(6584):643–644.
177. Chopp M, Li Y, Zhang ZG, et al. p53 expression in brain after middle cerebral artery occlusion in the rat. Biochem Biophys Res Commun 1992; 182(3):1201–1207.
178. Li Y, Chopp M, Zhang ZG, et al. p53-immunoreactive protein and p53 mRNA expression after transient middle cerebral artery occlusion in rats. Stroke 1994; 25(4):849–855.
179. Crumrine RC, Thomas AL, Morgan PF. Attenuation of p53 expression protects against focal ischemic damage in transgenic mice. J Cereb Blood Flow Metab 1994; 14(6):887–891.
180. Dirnagl U, Simon RP, Hallenbeck JM. Ischemic tolerance and endogenous neuroprotection. Trends Neurosci 2003; 26:248–254.
181. Weih M, Prass K, Ruscher K, et al. Ischemia tolerance; model for research, hope for clinical practice? Nervenarzt 2001; 72:255–260.
182. Kirino T. Ischemic tolerance. J Cereb Blood Flow Metab 2002; 22(11):1283–1296.
183. Weih M, Kallenberg K, Bergk A, et al. Attenuated stroke severity after prodromal TIA: a role for ischemic tolerance in the brain? Stroke 1999; 30(9):1851–1854.
184. Wegener S, Gottschalk B, Jovanovic V, et al. MRI in Acute Stroke Study Group of the German Competence Network Stroke. Transient ischemic attacks before ischemic stroke: preconditioning the human brain? A multicenter magnetic resonance imaging study. Stroke 2004; 35:616–621.
185. Ruscher K, Isaev N, Trendelenburg G, et al.. Induction of hypoxia inducible factor 1 by oxygen glucose deprivation is attenuated by hypoxic preconditioning in rat cultured neurons. Neurosci Lett 1998; 254(2):117–120.
186. Prass K, Ruscher K, Karsch M, et al. Desferrioxamine induces delayed tolerance against cerebral ischemia in vivo and in vitro. J Cereb Blood Flow Metab 2002; 22(5):520–525.
187. Brines M, Cerami A. Emerging biological roles for erythropoietin in the nervous system. Nat Rev Neurosci 2005; 6(6):484–494.
188. Prass K, Scharff A, Ruscher K, et al. Hypoxia-induced stroke tolerance in the mouse is mediated by erythropoietin. Stroke 2003; 34(8):1981–1986.
189. Sharp FR, Bernaudin M. HIF1 and oxygen sensing in the brain. Nat Rev Neurosci 2004; 5(6):437–448.
190. Brines ML, Ghezzi P, Keenan S, et al. Erythropoietin crosses the blood-brain barrier to protect against experimental brain injury. Proc Natl Acad Sci USA 2000; 97(19):10526–10531.
191. Sakanaka M, Wen TC, Matsuda S, et al. In vivo evidence that erythropoietin protects neurons from ischemic damage. Proc Natl Acad Sci USA 1998; 95(8):4635–4640.
192. Ehrenreich H, Hasselblatt M, Dembowski C, et al. Erythropoietin therapy for acute stroke is both safe and beneficial. Mol Med 2002; 8(8):495–505.
193. Leist M, Ghezzi P, Grasso G, et al. Derivatives of erythropoietin that are tissue protective but not erythropoietic. Scienc. 2004; 305(5681):239–242.

6 Multimodal Mapping of the Ischemic Penumbra in Animal Models

Konstantin-A. Hossmann and Günter Mies
Max Planck Institute of Neurological Research, Cologne, Germany

INTRODUCTION

Accurate mapping of the penumbra in animal experiments is an absolute requirement for at least three important research objectives: (*i*) the identification of pathophysiological and pathobiochemical alterations that contribute to the progression of ischemic injury into the peri-infarct surrounding; (*ii*) the evaluation of therapeutic interventions that interfere with this injury; and (*iii*) the validation of surrogate markers of the penumbra, notably of operationally defined noninvasive methods.

As outlined in earlier chapters, the penumbra can be delineated on images of cerebral blood flow by marking the flow range between the beginning functional impairment and the onset of anoxic depolarization (1). However, during the evolution of brain infarction, the thresholds of brain injury steadily increase, and following recirculation the ischemic impact is not necessarily reversed.

A much more reliable approach for the mapping of the penumbra is, therefore, the visualization of biochemical and biophysical alterations underlying the observed functional disturbances (2) (Table 1). From a purely descriptive point of view, this approach requires the demarcation of the penumbra from the nonviable infarct core, on the one hand, and from the undamaged intact tissue, on the other. The most obvious indicator of tissue viability is the maintenance of energy metabolism, which can be readily imaged by pictorial measurements of tissue adenosine tri-phosphate (ATP) content. In fact, the flow threshold of anoxic depolarization closely correlates with the breakdown of the tissue energy state, which, in turn, is associated with the cessation of all anabolic energy-dependent metabolic processes. The demarcation of the penumbra from the intact tissue is less well defined because at declining flow values an increasing number of metabolic processes is impaired. In fact, multimodal imaging methods have greatly contributed to the identification of differential biochemical thresholds and have led to the concept of multiple penumbras (3). In the following sections, the most important penumbra-relevant imaging methods and their applications to animal models will be described.

PENUMBRA-RELEVANT IMAGING METHODS

Imaging of Tissue Sections

The extent and severity of focal ischemic lesions greatly vary, even under standardized experimental conditions. As penumbral mapping requires multimodal imaging, such methods must be applicable to individual animals. This is, in fact, possible by using serial histological brain sections for the measurement of the various parameters of interest; for some variables, multiparametric imaging can even be carried out in the same section, for example, by using multitracer autoradiographic techniques (4,5). As far as measurements of labile substrates such as ATP are concerned, in situ freezing of the brain is necessary to prevent catabolic changes (6). For this reason, multimodal mapping must be applicable to cryostat sections. The following methods have been established to meet these requirements.

Adenosine Triphosphate, Glucose, and Lactate-Induced Bioluminescence

Biochemical substrates that can be measured by enzymatic reactions coupled to a light emitting system are imaged in intact tissue sections by preparing slices of a frozen reaction mix that

TABLE 1 Order of Flow-Dependent Pathophysiological Disturbances Associated with Acute Cerebrovascular Occlusion and Corresponding Imaging Methods

Cerebral blood flow	Pathophysiological disturbances	Penumbra-relevant imaging methods
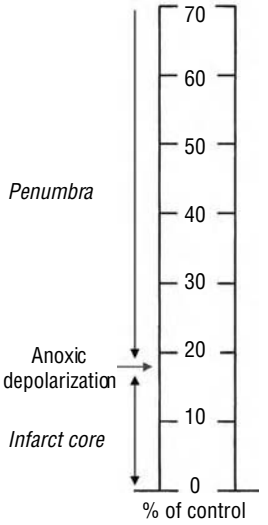	Reduced blood flow	IAP autoradiography, perfusion-weighted MRI
	Increased oxygen extraction	$^{15}O_2$ /$H_2{}^{15}O$ PET, Near infrared spectroscopy
	Increased blood volume	Tc-99m HMPAO SPECT
	Upregulation stress proteins	*hsp70/hsp32* mRNA in situ hybridization
	Suppression protein synthesis	CPS autoradiography, ^{11}C-aminoacid PET
	Increased glycolysis	Deoxyglucose autoradiography, ^{18}FDG PET
	Reduced oxygen use	$^{15}O_2$ PET
	Cellular swelling	Diffusion-weighted MRI, ADC mapping
	Disturbed redox state	NADH fluoroscopy
	Lactacidosis	Lactate bioluminescene imaging, pH fluoroscopy
	Suppressed glucose use	Deoxyglucose autoradiography, ^{18}FDG PET
	ATP depletion	ATP bioluminescence imaging
	Release of potassium	Potassium histochemistry
	Calcium uptake	Calcium histochemistry
	Loss of ligand binding	^{18}F-Flumazenil PET

Note: The penumbra is the mismatch between disturbances that occur only in the infarct core and others, which affect both core and penumbra.
Abbreviations: ADC, apparent diffusion coefficient; CPS, cerebral protein synthesis; FDG, fluorodeoxyglucose; IAP, iodoantipyrine; MRI, magnetic resonance imaging; NADH, reduced nicotinamide adenine dinucleotide; PET, positron emission tomography; SPECT, single-photon emission computed tomography.

contains all the enzymes, coenzymes, and substrates required for the execution of the enzymatic assay. If this slice is placed on the cryostat section and allowed to melt, the reaction mix diffuses into the tissue section and reacts with the substrate of interest. The light emitted by the reaction correlates quantitatively with the tissue concentration of the substrate and can be recorded either with a sensitive charge-coupled device (CCD) camera or by placing the tissue/reaction mix sandwich on a photographic film.

Up to now, practical approaches have been described for the measurements of ATP (7), glucose (8), and lactate (9) (Fig. 1), but the same principle should also be applicable to other

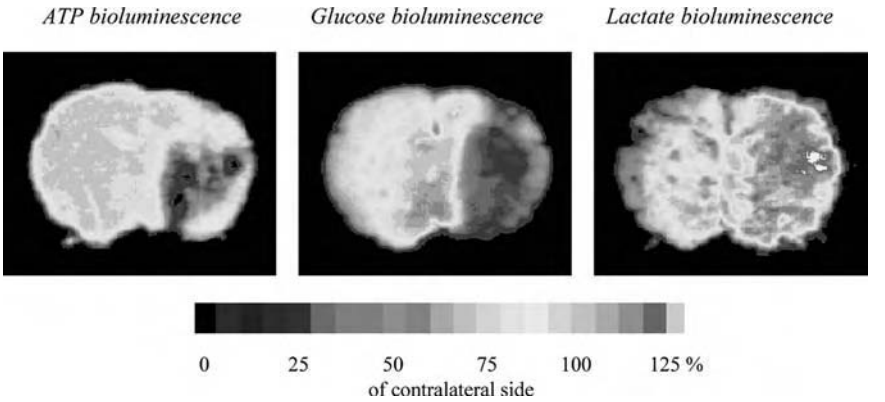

FIGURE 1 (*See color insert.*) Bioluminescence imaging of tissue content of adenosine tri-phosphate (ATP), glucose, and lactate in cryostat sections prepared shortly after occlusion of the middle cerebral artery in rat. Tissue sections were placed on frozen sections of a gelatinized reaction mix containing all the substrates, enzymes, and co-enzymes required to induce substrate-specific bioluminescence. After starting the enzymatic reaction the emitted bioluminescence was recorded on photographic film. Loss of ATP is restricted to the infarct core, whereas the reduction of glucose (due to increased glucose consumption) and the increase of lactate (due to stimulation of anaerobic glycolysis) extend into the penumbra.

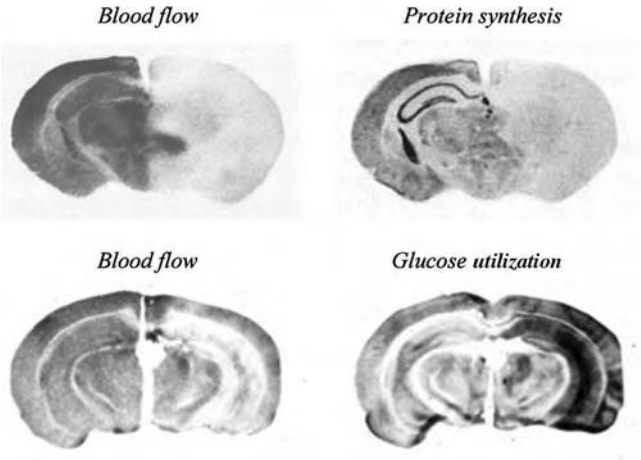

FIGURE 2 Double tracer autoradiographic measurements of blood flow and protein synthesis (*top*) and of blood flow and glucose utilization (*bottom*) after carotid artery occlusion in gerbil. Blood flow was measured with ^{131}I-iodoantipyrine, protein synthesis with ^{14}C-labelled leucine and glucose utilization with ^{14}C-deoxyglucose. Inhibition of protein synthesis or stimulation of (anaerobic) glucose utilization demarcates the penumbra from the intact brain tissue. Simultaneous recording of blood flow permits precise determination of the corresponding flow thresholds.

substrates. Pictorial measurement of ATP is a straightforward way to identify the ischemic core. Due to the threshold relationship between blood flow and energy metabolism, ATP depleted areas are sharply demarcated against the still viable tissue. The penumbra is characterized by the local mismatch between ATP depletion and other metabolic disturbances, which evolve at higher flow thresholds, as described in more detail later.

Blood Flow, Glucose Utilization, and Protein Synthesis

For the pictorial measurement of these variables, quantitative autoradiographic methods have been established, all of which can be used with cryostat sections (10–12) (Fig. 2). These methods have been combined by double or even triple tracer approaches, which take advantage of the differences in the half-life and the radiation intensity of the radioisotopes and the sensitivity of photographic films, to allow measurements in the same tissue section (5,13). The measurements are quantitative and permit precise multipixel threshold analysis between blood flow, on one hand, and the metabolic rates of glucose and protein synthesis, on the other (14). In our hands the double tracer imaging of blood flow and protein synthesis in combination with the pictorial measurement of ATP or pH has become a particularly useful approach to determine the precise localization and the flow thresholds of core and penumbra (Fig. 3).

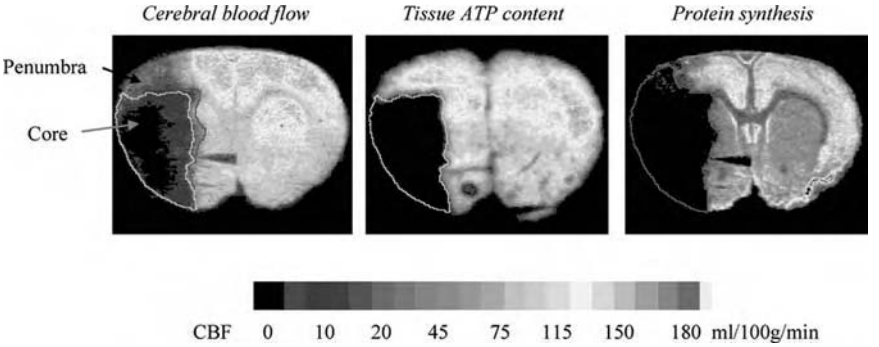

FIGURE 3 (*See color insert.*) Mapping of the mismatch between energy metabolism and protein synthesis at one hour after middle cerebral artery occlusion in rats. Superposition of the outlines of ATP loss and suppressed protein synthesis permits precise anatomical demarcation of the biochemically defined penumbra. *Source*: From Ref. 68. *Abbreviations*: ATP, adenosine tri-phosphate; CBF, cerebral blood flow.

As far as the range of flow values in the penumbra is concerned, different values have been reported, depending mainly on the animal species and the time after the onset of ischemia. In small rodents, the penumbra corresponds at two hours to a flow range of approximately 20% to 40% of control (15), whereas in humans at six hours ischemia the range is about 10% to 30% (16). Mapping of the penumbra on flow images, therefore, requires appropriate determination of flow thresholds and is valid only under experimental conditions in which these thresholds have been established.

pH Imaging

An important parameter for the mapping of the penumbra is tissue pH, which shifts to acidosis with the stimulation of anaerobic glucose utilization. In cryostat sections pH is measured either by placing the section on filter paper soaked with the fluorescent pH indicator umbelliferone (17), or by injecting neutral red into the circulating blood prior to sacrifice (18). For multiparametric mapping, the umbelliferone incubation method is the preferred approach because the systemic application of neutral red may interfere with other imaging modalities (Fig. 4).

NADH Imaging

As first described by Welsh et al., reduced nicotinamide adenine dinucleotide (NADH) imaging is a powerful tool for the pictorial evaluation of the redox state of the brain tissue (19). The method relies on the bright fluorescence of NADH at 450 nm, which can be observed by ultraviolet illumination using the appropriate filter combination. NADH images can be obtained not only ex vivo from frozen brain slices but also in vivo by illuminating the exposed cerebral cortex (20). An inherent problem for quantitative evaluation is the quenching of NADH by hemoglobin. However, under most conditions of experimental ischemia, the focal deterioration of the redox potential is so pronounced, that the increase of NADH can be sharply demarcated against the normoxic tissue, irrespective of blood volume changes (Fig. 4).

Calcium and Potassium Staining

Anoxic depolarization results in massive transmembrane ion fluxes leading to the loss of intracellular potassium and the gain of calcium. Under conditions of complete circulatory

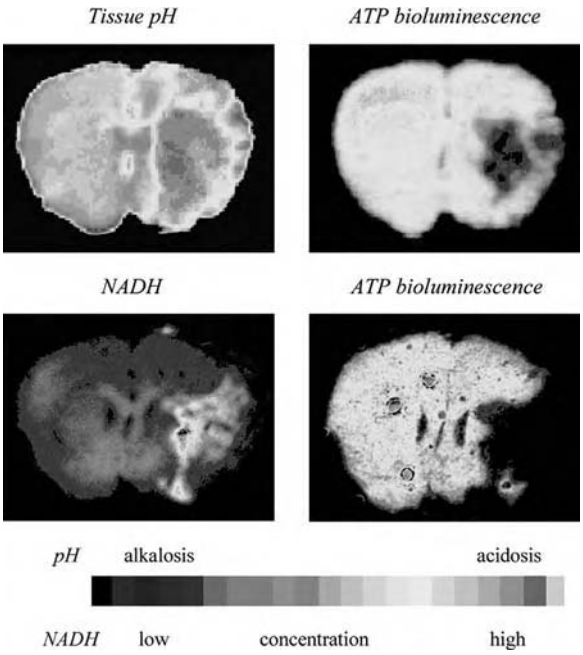

FIGURE 4 (*See color insert.*) Mapping of tissue pH and ATP content (*top*) and of NADH and ATP content (*bottom*) after middle cerebral artery occlusion in rat. Tissue pH was imaged using the fluorescent pH indicator umbelliferone and NADH by recording tissue autofluorescence. Tissue acidosis is observed in core and penumbra, whereas the increase in NADH and the loss of ATP are restricted to the core region.

arrest, these ion shifts do not result in net changes of tissue electrolyte content but if blood flow is resumed or some residual circulation persists, the tissue content equilibrates with that of the blood. These changes can be imaged by histochemical stainings, using cobaltinitrite for the measurement of potassium (21) and fluo-3 solution for calcium content (22). Both methods have been adopted for the use with cryostat sections and, therefore, can be combined with the other imaging methods described here.

An indirect measure of the ischemia-induced disturbance of calcium homeostasis is the imaging of activated ion channels with nimodipine (23) or dizocilpine (24). It has not been established, however, to what extent increased binding colocalizes with the core, or the penumbra, or both.

Mapping of Gene Expression

With the increasing use of high throughput gene expression profiling, a steadily growing number of genes have been associated with the evolution of penumbral injury (25–27). Pictorial evaluation of gene expression can be carried out in cryostat sections both at the transcriptional and translational level, using cDNA in situ hybridization and immunohistochemistry, respectively. So far, only the expression of the stress genes *hsp70* (28,29) and *HO-1*(hsp32) (30) could be clearly colocalized with the penumbra, defined as the mismatch between energy metabolism and protein synthesis (Fig. 5). Genes indirectly linked to the evolution of ischemic injury are activated among others by peri-infarct spreading depression waves, notably the immediate early genes *c-fos*, *c-jun*, and *junB* (31). In accordance with the topical spread of the depolarization waves, these genes are upregulated not only in the penumbra but throughout the ipsilateral hemisphere (29) (Fig. 5). As the protein products of these genes are transcription factors, a great number of other genes are also induced in or outside the ischemic penumbra. Similarly, remote gene expressions associated with edema formation, functional disturbances, and plasticity may affect ischemic and nonischemic tissue and, therefore, are of limited usefulness for penumbral mapping.

Noninvasive Imaging

Positron Emission Tomography

The positron emission tomography (PET) parameters most widely used for imaging of focal ischemia in animal experiments are blood flow, oxygen and glucose consumption, the oxygen extraction fraction, and the binding of various ligands, notably flumazenil, to the corresponding

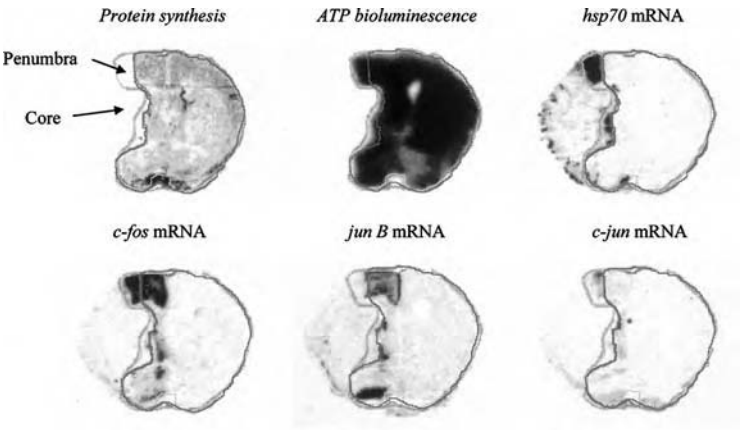

FIGURE 5 Regional allocation of gene expression to the penumbra during permanent MCA occlusion in the mouse. Gene regulation is imaged by in situ hybridization and compared with images of protein synthesis (CPS) and ATP bioluminescence on adjacent cryostat sections. Superposition of the CPS/ATP mismatch on in situ hybridization autoradiograms reveals that only *hsp70* mRNA precisely colocalizes with the biochemically defined penumbra. Upregulation of *c-fos* mRNA and of *jun B* mRNA in the intact tissue outside of the penumbra is due to ischemia-induced spreading depolarization. *Abbreviation*: MCA, middle cerebral artery. *Source*: From Ref. 29.

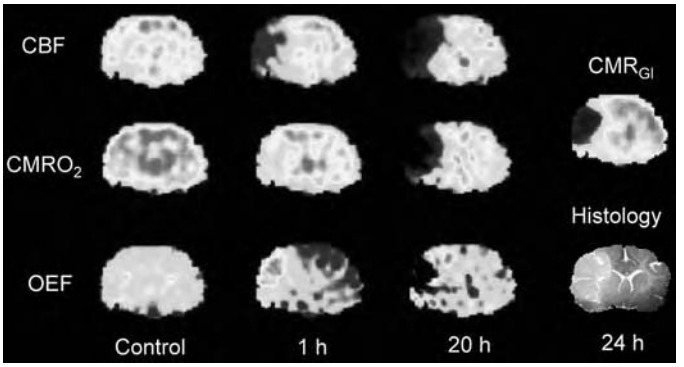

FIGURE 6 Positron emission tomography (PET) mapping of cerebral blood flow (CBF), cerebral metabolic rate of oxygen ($CMRO_2$), oxygen extraction fraction (OEF) and glucose utilization (CMR_{Gl}) after middle cerebral artery occlusion in cat. The ischemic territory is demarcated by the decline in CBF, the penumbra by the increase in OEF and the core by the suppression of $CMRO_2$ and CMR_{Gl}. At 20 to 24 hours after vascular occlusion the histologically documented infarct co-localises with the region in which OEF was increased at one hour, reflecting the progression of the penumbra to infarction. *Source*: From Ref. 59.

viable receptors (32–34). These issues are covered in detail in Chapters 3 and 10. With declining flow values the blood oxygen extraction fraction rises to cover the oxygen requirements of aerobic metabolism but at flow values of less than about 50% of control, the tissue becomes hypoxic, the oxygen consumption begins to decline and anaerobic glycolysis is stimulated. At even lower flow values, also anaerobic glycolysis begins to fail, energy metabolism ceases, the tissue necrotises and ligands no longer bind to their receptors.

According to this scenario, the penumbra is characterized by an increase in glucose utilization or the rise of the oxygen extraction fraction, whereas the ischemic core can be detected by the reduction of oxygen and glucose consumption or by the loss of ligand binding to devitalized receptors (Fig. 6). It should be noted, however, that the thresholds of these variables have been operationally defined by correlating isocontours of a range of values with the outline of ischemic infarcts that evolve after some time. Moreover, due to the low topical resolution of PET and the high scatter of tracer concentrations at low flow values, the demarcation between core and penumbra is much less precise than on biochemical maps obtained from histological sections. Under experimental conditions, PET mapping of the penumbra is, therefore, a surrogate approach restricted to large brains.

Nuclear Magnetic Resonance

This imaging modality is also covered in detail in Chapters 13 and 14, hence an abbreviated comment is given in this chapter. A widely accepted although not rigorously validated magnetic resonance (MR) signature of the ischemic core is the increased signal intensity in diffusion-weighted MR images (DWI). The combination of such images with blood perfusion-weighted images (PWI) has led to the PWI/DWI mismatch concept, which states that the penumbra is the area of reduced blood flow in which DWI-visible alterations are absent (35,36). This assumption, however, is not undisputed (37,38). DWI signal intensity changes inversely to the apparent diffusion coefficient (ADC) of tissue water, which, in turn, reflects the fluid volume of the extracellular compartment. Quantitative ADC measurements revealed that during graded ischemia, ADC begins to decline before energy metabolism fails (39), indicating that the increase in DWI signal intensity is not restricted to the infarct core. Moreover, PWI-detectable flow decreases are pathophysiologically relevant only at flow values that interfere with adequate oxygen supply to the tissue. PWI/DWI mismatch, therefore, includes only the peripheral parts of the penumbra but extends into the surrounding normoxic intact tissue. The prognosis of the PWI/DWI mismatch area is, therefore, better than that of the actual penumbra, which must be considered for the interpretation of therapeutic interventions.

Several laboratories have tried to identify the penumbra by thresholding quantitative ADC maps (39–41). Correlation of such maps with biochemical images revealed that during the

initial few hours of ischemia, the decline of ADC to 90% corresponds to the beginning tissue acidosis, and the further reduction to 77% to the breakdown of energy metabolism. The ADC range between these two thresholds demarcates a region, the volume of which comes close to the actual penumbra (39). However, as these thresholds are statistical values, which may vary with the particular experimental setup, an accurate demarcation of the penumbra is not possible.

Other MR parameters that are potentially useful for penumbral mapping are the measurement of cerebral blood volume (to trace the autoregulatory adjustment of the cerebral vasculature at reduced blood supply) (42), the transverse relaxation time T_2 (to visualize the beginning of edema formation) (43), Mn-enhanced MR imaging (to detect anoxic depolarization) (44), or proton spectroscopical imaging (for mapping the rise of lactate during anaerobic glycolysis) (45,46). However, none of these parameters exhibits a sharp threshold relationship to declining flow values and, therefore, does not provide a clear demarcation of the penumbra from either the core or the intact brain tissue.

Other Noninvasive Methods

In patients single-photon emission computed tomography (SPECT) (see Chapter 12) and near infrared spectroscopy (NIRS) have been used to trace penumbral tissue—SPECT by detecting an increase in blood volume (using Tc-99m HMPAO as a blood tracer) (47), and NIRS to document the reduced oxygen saturation of penumbral blood (48). Both parameters reflect the disturbed hemodynamic situation but are unrelated to the actual biochemical abnormalities within the penumbra. In animal experiments, applications of these methods for penumbral mapping have not been reported.

Selection Guidelines for Penumbral Mapping

Important criteria for the selection of mapping techniques for the visualization of the penumbra are the choice between invasive or noninvasive methods, on the one hand, and between direct and mismatch measurements, on the other. The most widely used noninvasive approach for direct penumbral mapping is the visualization of increased oxygen extraction. This approach systematically overrates the actual penumbra, because at declining flow values oxygen extraction begins to rise before any pathological alterations evolve. Using the appropriate thresholds, the penumbra can also be visualized on quantitative maps of blood flow or ADC. The obvious shortcoming of these maps is the uncertainty about the individual thresholds in different experimental situations; applications are therefore restricted to statistical evaluations.

An invasive but much more precise approach for direct penumbral mapping is the in situ hybridization of *hsp70* mRNA (Fig. 5). HSP-70 is a cytosolic stress protein, which responds to disturbances in protein synthesis but only as long as the energy state of the tissue is preserved. Obviously, the need to prepare histological sections restricts this method to single point measurements. On the other hand, as the dissociation between protein synthesis and energy metabolism characterizes the penumbral tissue at risk both during permanent and after transient vascular occlusion, it can be applied to a wide range of experimental situations.

Other direct mapping approaches include the measurement of cerebral blood volume, the upregulation of HO-1 (hsp-32) and of the hypoxia-induced factor HIF-1, or the binding of the *N*-methyl–D-asperate (NMDA) antagonist MK-801 to activated ionotropic glutamate channels. However, none of these methods have been compared with independent methods and, therefore, require further validation.

The generation of mismatch maps is an extension of the threshold concept of ischemia, which states that penumbral disturbances occur at higher flow thresholds than the loss of viability in the infarct core. Accurate images of the infarct core can be obtained by bioluminescence mapping of ATP or—if some time has elapsed after the induction of ischemia—by triphenyl tetrazolium chloride (TTC) staining. Imageable disturbances that extend into the penumbra include the inhibition of protein synthesis, the accumulation of lactic acid, tissue acidosis, and the increase in NADH (Table 1). As the thresholds of these penumbral disturbances are not the same, the corresponding mismatch areas also differ. This is in line with the concept of multiple penumbras, and has to be considered when different penumbral outcome studies are compared.

A widely used noninvasive mismatch approach for penumbral mapping is the PWI/DWI mismatch. Considering the dependence of neurological symptoms on the localization of flow disturbances, this approach has been recently extended to a "diffusion-clinical mismatch" situation (49). For the reasons given earlier, these mismatches deviate from the true penumbra and must be interpreted with caution. Biochemical mismatches such as the CPS/ATP mismatch, in contrast, are accurate estimates of the actual metabolic situation and can be used as gold standards for the validation of other more indirect approaches (Figs. 3 and 5).

APPLICATIONS TO ANIMAL MODELS OF FOCAL ISCHEMIA

Mappings of the ischemic penumbra have been carried out in various species and different models of focal ischemia. As regards to animal species, a major difference exists between the lissencephalic brains of gerbil and small rodents in which the ischemic territory is well demarcated, and the gyrencephalic brains of larger species such as cat, pig, or primates, where flow reduction is more heterogeneous. This difference is due to the anatomical configuration of Heubner's leptomeningeal network of anastomoses, which is better developed in the gyrencephalic brain. Another major difference is the effect of permanent and transient vascular occlusion. The hemodynamically defined "classical" penumbra of moderately reduced blood flow is a characteristic property of permanent ischemia but the associated biochemical alterations are replicated during reperfusion also in the severely ischemic core, provided reperfusion results in the recovery of energy metabolism and the restoration of cell membrane polarization. In the following, some of the most characteristic animal experimental findings will be reviewed.

Hemispheric Ischemia in Gerbil

In the gerbil unilateral carotid artery occlusion results in hemispheric ischemia, the severity of which varies depending on the anatomical configuration of the anterior communicating artery (Fig. 7). This model produces variable severities of hemispheric ischemia in different animals but not a focal gradient of flow values within the same hemisphere, as after intracerebral vascular occlusion. Blood flow and the associated biochemical changes are, therefore, similar throughout the affected hemisphere. This facilitates tissue sampling for the correlation of blood

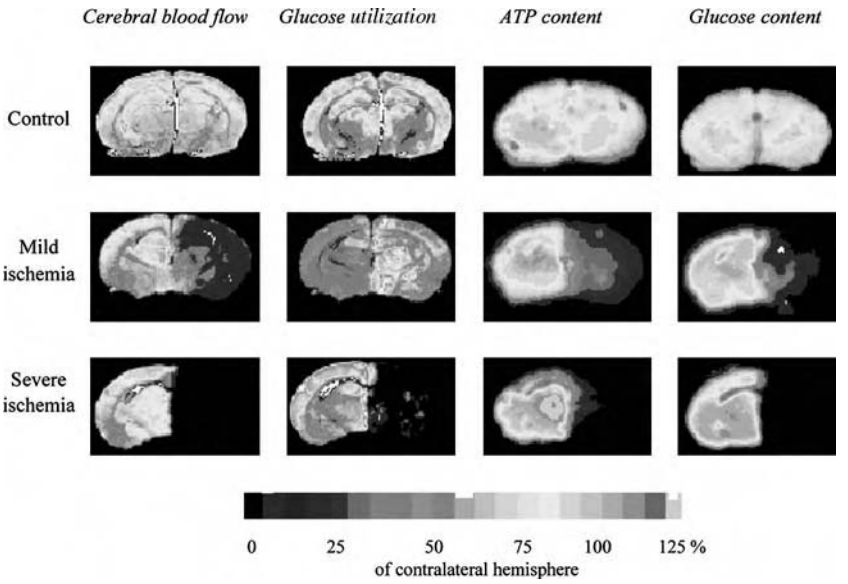

FIGURE 7 (*See color insert*.) Multimodal mapping of the gerbil brain after unilateral carotid artery occlusion. Depending on the caliber of the anterior communicating artery, different severities of hemispheric ischemia are produced. Reduction of blood flow to the penumbra range is reflected by the stimulation of (anaerobic) glucose utilization (*middle*) and reduction to core values by the cessation of glucose utilization and the depletion of ATP and glucose content throughout the ischemic hemisphere (*bottom*). *Source*: From Ref. 69.

flow with biochemical alterations but necessitates multiple experiments to cover the whole range of flow changes.

Rodent Models of Focal Ischemia

Focal ischemia in rodents is usually produced by mechanical or clot occlusion of the middle cerebral artery (MCA). In the mouse, imaging of ATP and cerebral protein synthesis (CPS) revealed that the ischemic core is located in the lateral caudate-putamen and the temporal cortex, whereas the penumbra extends to the medial caudate-putamen and the parietal and fronto-temporal cortex (50). With ongoing ischemia time, the ischemic core gradually expands into the penumbra until, after 6 to 12 hours, most of the penumbra has disappeared (Fig. 8). Multimodal mappings revealed that the CPS-defined penumbra colocalizes precisely with upregulation of *hsp70* mRNA expression (Fig. 5). Upregulation of immediate-early genes (IEG), in contrast, occurs also in the undamaged nonischemic tissue (29,31), in accordance with the spread of peri-infarct depolarizations over the entire ipsilateral hemisphere.

After transient MCA occlusion, mostly induced by withdrawal of an intraluminal thread, protein synthesis recovers in the penumbra, and energy metabolism in the peripheral parts or even throughout the ischemic core (Fig. 9) (50). The resulting CPS/ATP mismatch in the ischemic core colocalizes with a strong postischemic upregulation of *hsp70* mRNA, followed after an interval of a few hours by secondary suppression of energy metabolism and cell death. Postischemic CPS/ATP mismatch thus identifies a region at risk, which despite restoration of blood flow suffers delayed death in a similar way as the penumbra of permanent ischemia.

MCA clot embolism does not differ from MCA thread occlusion but spontaneous or thrombolysis-induced recanalization produces a much less abrupt recirculation than the reversal of mechanical occlusion. As a result, restoration of energy metabolism is more delayed and the CPS/ATP mismatch smaller than after the same duration of mechanical occlusion (51). This difference is of importance for the prediction of outcome, and questions the relevance of transient mechanical occlusion models for the understanding of clinical stroke pathophysiology.

The localization and dynamics of core and penumbra after MCA occlusion in rat are similar to that in the mouse. During permanent MCA occlusion the core is located in the basal ganglia and parts of the temporal cortex, and the penumbra in the parietal and fronto-temporal cortex (Fig. 10). With ongoing ischemia the rat penumbra also disappears within a few hours due to the expansion of the infarct core (52). Penumbral mappings have been carried out mainly by

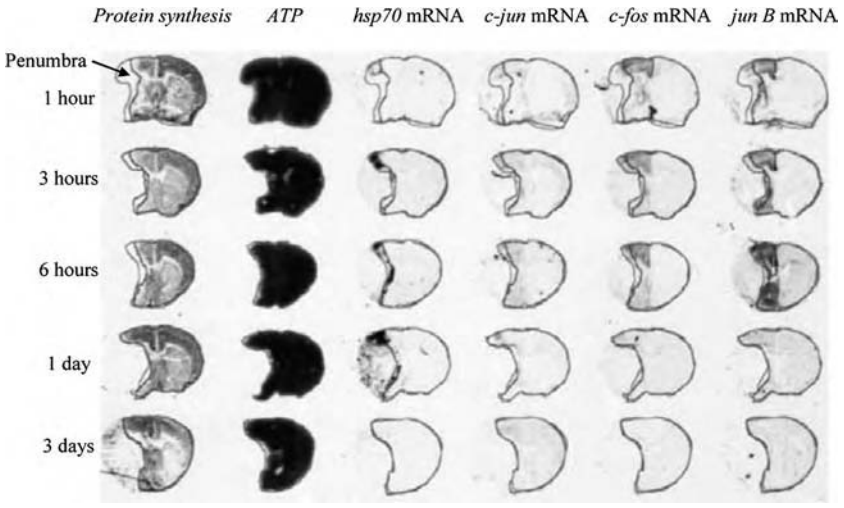

FIGURE 8 Multimodal mapping of the mouse brain during permanent thread occlusion of the middle cerebral artery. The infarct core corresponds to the area of ATP depletion and the penumbra to the mismatch between disturbed protein synthesis and preserved energy metabolism (CPS/ATP mismatch). Note gradual disappearance of the penumbra due to the expansion of the infarct core. Mapping of gene expression on adjacent cryostat sections reveals different allocations to the penumbra and the intact tissue (for higher resolution see Fig. 5). *Source*: From Ref. 70.

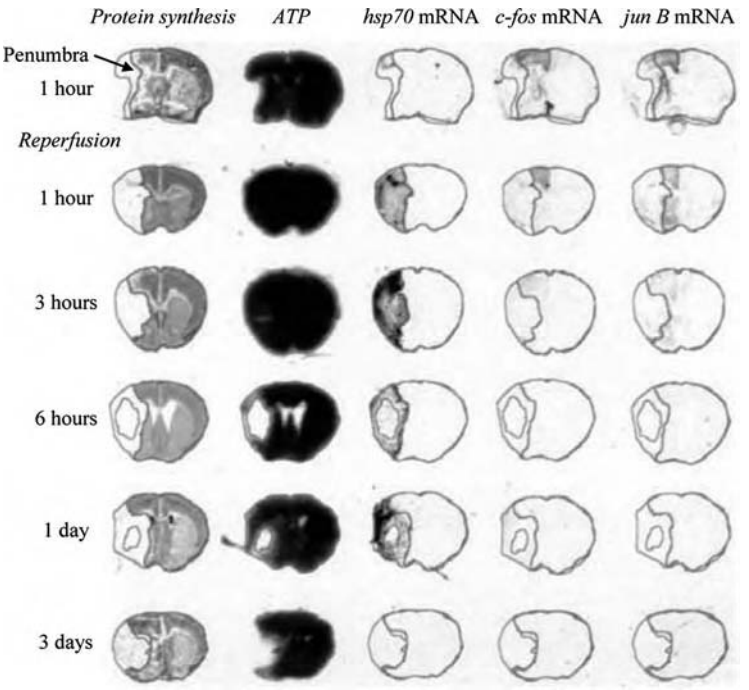

FIGURE 9 Multimodal mapping of the mouse brain during and after one hour transient middle cerebral artery occlusion. Shortly after the beginning of reperfusion ATP but not protein synthesis recovers, resulting in a large CPS/ATP mismatch area which co-localizes with an upregulation of *hsp70* mRNA. The central part of this area progresses to infarction in analogy to the penumbra of permanent ischemia (see Fig. 8). *Source*: From Ref. 50.

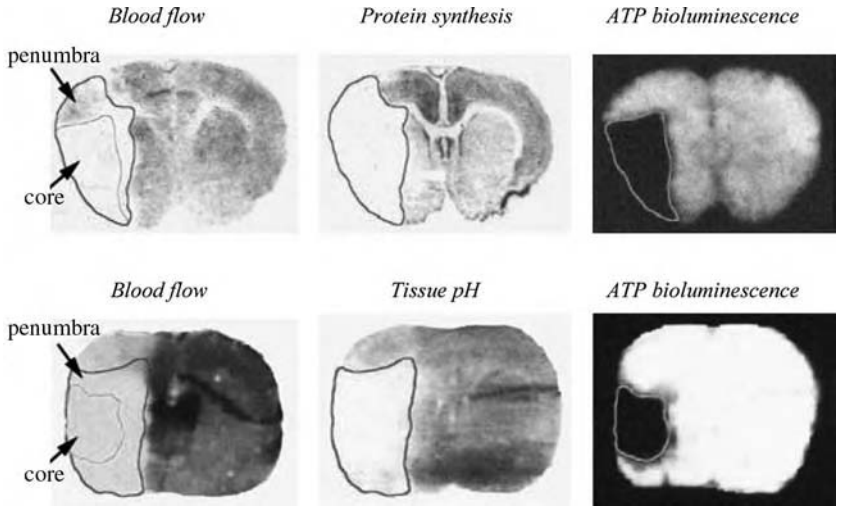

FIGURE 10 Multimodal imaging of the rat brain following middle cerebral artery occlusion. The core is identified by ATP depletion and the penumbra by CPS/ATP mismatch (*top*) or pH/ ATP mismatch (*bottom*).

mismatch approaches, notably between ATP and CPS or pH (2), by PWI/DWI mismatch (40), or the mismatch between the flow tracer iodine-123 N- isopropyl-4-iodoamphetamine (IMP) and the neuronal vitality marker iodine-125 iomazenil (IMZ) (53). Direct visualizations of the penumbra were achieved by imaging the expression of *hsp70* (29,54) or *HO-1* mRNA (30), or by thresholding blood flow and ADC maps (39).

Reversal of transient rat MCA occlusion also replicates the results in mice. ATP, but not CPS recovers and *hsp70* mRNA is strongly expressed in the CPS/ATP mismatch region of the reperfused ischemic core (55). With ongoing recirculation, secondary deterioration of energy metabolism and the associated ADC changes occur, in analogy to delayed neuronal death in the penumbra of permanent ischemia (Fig. 11) (56).

A particular type of penumbra is the center of a cortical photothrombotic ring lesion. This area exhibits a reduced blood flow and overt morphological alterations but different to the peri-infarct penumbra, these disturbances tend to recover spontaneously (57).

Focal Ischemia in Cat and Pig

In both species, MCA occlusion has been carried out by a transorbital approach, which, depending on the individual efficiency of collateral blood supply, leads to greatly varying infarct volumes. In medium sized infarcts, the core is located in the basal ganglia and the ectosylvian gyrus, and the penumbra in the suprasylvian gyrus, but with larger or smaller lesions, the penumbra shifts to either the more central or the more peripheral parts of the MCA supplying territory. Differentiation between core and penumbra has been carried out by MRI (58) and by PET (59), using PWI/DWI mismatch, increased oxygen extraction fraction, or increased glucose

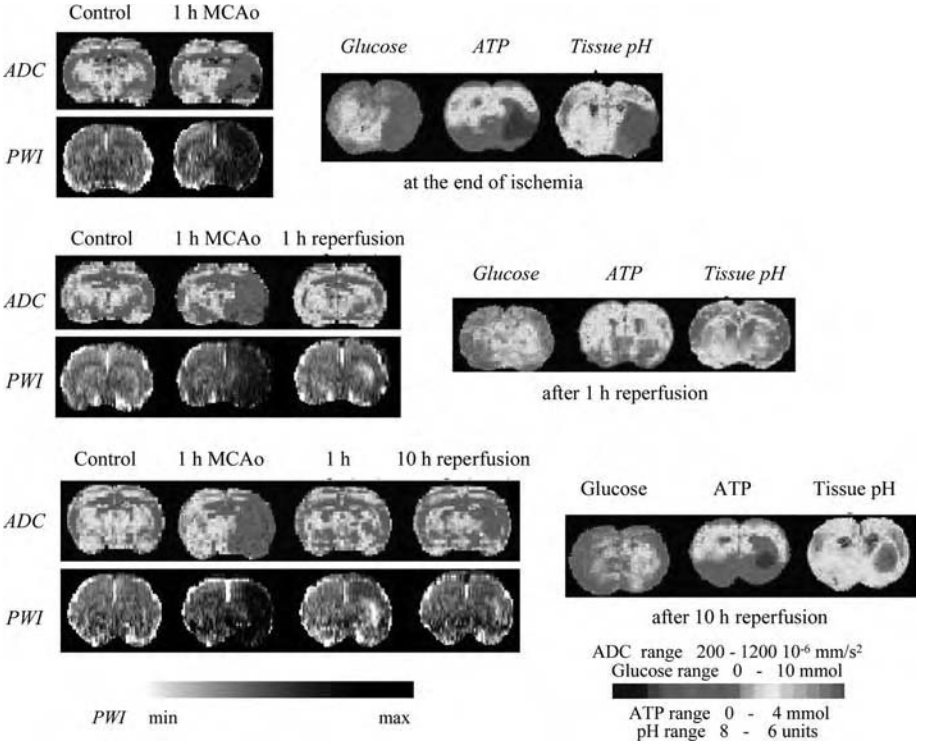

FIGURE 11 (*See color insert.*) Multimodal mapping of rat brains after one-hour middle cerebral artery occlusion without recirculation (*top*), one-hour recirculation (*middle*), and 10 hours recirculation (*bottom*), respectively. Sequential ADC and perfusion-weighted MR imaging (PWI) was followed by terminal invasive imaging of glucose, ATP, and pH. Experiments demonstrate that post-ischemic recirculation promotes primary recovery of ADC and of biochemical variables, which, however, is followed by secondary deterioration of ADC and metabolic injury in the center of the MCA territory. *Source*: From Ref. 56.

consumption as penumbral markers (Fig. 6). Di et al. (24) characterized the penumbra as an area of increased binding of the noncompetitive NMDA antagonist MK-801 but this association has not been validated with independent methods.

In an early application of multiparametric imaging to transorbital MCA occlusion of cat, the simultaneous measurement of a great number of hemodynamic and metabolic parameters revealed a multifocal heterogeneous pattern of areas with low and high blood flow and different kinds of metabolic-biochemical matches and mismatches (Fig. 12) (60). Vascular occlusion led only in one out of four cats to homogenous infarction with the typical distribution of a central core of ATP depletion, surrounded by a slightly larger area of acidosis and suppressed protein synthesis. The multifocal heterogeneous distribution in the other experiments apparently was due to foci of spontaneous reperfusion, which illustrates the difficulty to induce a reproducible pattern of focal ischemia in gyrencephalic brains.

Focal Ischemia in Primates

The preferred model of focal ischemia in primates is the transorbital mechanical occlusion of the proximal segment of the MCA, introduced by Hudgins and Garcia (61). This model was, in fact, used for the early studies on the threshold relationship between blood flow and functional impairment which led to the concept of the ischemic penumbra (1). The infarct core is located in the striato-capsular area of the deep MCA territory, and the penumbra in the overlying cortex, notably the parasylvian gyrus. Similar to cats, homogeneity and volume of the ischemic infarct vary largely, depending on the efficacy of collateral blood supply.

Most of the pictorial information on the ischemic penumbra of primates has been acquired by PET imaging (Fig. 13). Using sequential measurements of the metabolic rate of oxygen ($CMRO_2$) and the oxygen extraction fraction (OEF), the penumbra could be associated with the region in which OEF was increased, and the core with the region in which $CMRO_2$ declined to below 40% of control (62). During permanent MCA occlusion, part of the region of increased OEF progressed to infarction (62) in accordance with the concept of the time-limited viability of the penumbra. When the MCA was reperfused within six hours all of the tissue with increased

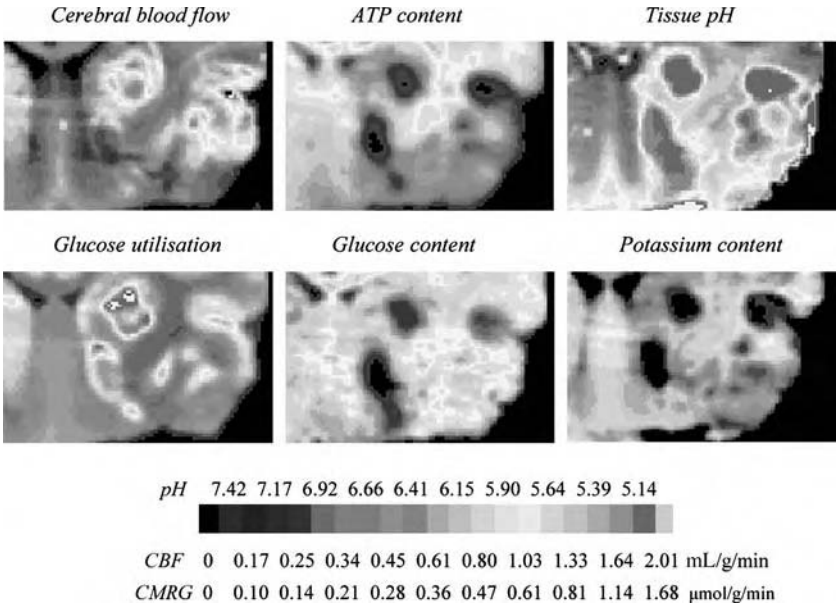

FIGURE 12 Multimodal imaging of cat brain after transorbital middle cerebral artery (MCA) occlusion. Images show the lower right quadrant of coronal cryostat section passing through the center of the MCA territory. Note marked heterogeneity of hemodynamic and biochemical alterations with variable associations and dissociations between flow and metabolism, reflecting focal areas of spontaneous reperfusion. *Abbreviations*: CBF, cerebral blood flow; CMRG, glucose utilization. *Source:* From Ref. 60.

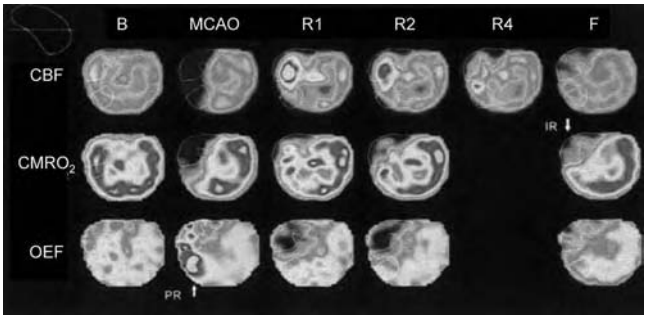

FIGURE 13 Multimodal positron emission tomography (PET) imaging of monkey brain submitted to two hour middle cerebral artery occlusion, followed by 22 hours recirculation. Recording of cerebral blood flow (CBF), cerebral metabolic rate of oxygen ($CMRO_2$), and the oxygen extraction fraction (OEF) before ischemia (B), during vascular occlusion (MCAO), after one hour (R1), two hours (R2) and four hours (R4) recirculation, and before termination of the experiment (F). During middle cerebral artery occlusion the infarct core (IR) corresponds to the region of suppressed $CMRO_2$, and the penumbra (PR) to the region of increased OEF. After recirculation the penumbra survives but the region of depressed $CMRO_2$ progresses to infarction despite transient recovery of $CMRO_2$. *Abbreviation*: MCAO, middle cerebral artery occlusion. *Source*: From Ref. 71.

OEF survived (63), and when recirculation was initiated after 20 hours, still more than 60% remained intact (64). This outcome is much better than the survival of the biochemically defined penumbra in rodents, which supports the view that the region of increased OEF includes intact tissue that is not at risk of infarction (see earlier).

Focal ischemia induced by intracarotid clot embolism led to an increase of the metabolic rate of glucose at flow values between 40% and 80% of control, characterizing the penumbra as an uncoupling between reduced flow and increased (anaerobic) glucose metabolism (65). Autoradiographic measurement of protein synthesis at two hours after clot embolism revealed a highly heterogeneous pattern of severely reduced amino acid incorporation, which was sharply demarcated from the surrounding intact tissue (66). Reduced protein synthesis is a reliable biochemical marker of the penumbra but as this measurement was not supplemented by images of the ischemic core, a differentiation between core and penumbra was not possible. The same restriction applies to a study of Obrenovitch et al. (67) in which pictorial measurements of tissue pH provided an image of both core and penumbra but not a demarcation between the two.

CONCLUSIONS

High spatial resolution mapping of the penumbra on serial cryostat sections provides the opportunity to correlate a wide range of pathophysiological alterations with the evolution of penumbral injury. Similarly, therapeutic interventions can be differentiated into those, which interfere with the hemodynamic or molecular mechanisms pertaining to primary necrosis in the core, and others that may contribute to the amelioration of delayed injury in the penumbra. Finally, surrogate markers of core and penumbra, notably operationally defined noninvasive PET and MRI methods, can be validated to improve prediction of therapeutic outcome under clinical conditions.

According to the concept of multiple penumbras, the topical extension of the penumbra may vary depending on the parameter chosen for penumbral mapping. If the penumbra is defined as the region-at-risk that in the absence of therapeutic intervention progresses to infarction, the most reliable predictor of this outcome is CPS/ATP mismatch. In fact, ATP depletion delineates the region of established injury, and the area of preserved protein synthesis the uninjured intact brain tissue. Using this information, precise topical association of injury pathways can be made to differentiate between those processes that contribute to injury evolution and others that are irrelevant epiphenomena. Multimodal mapping of the penumbra is, therefore, a powerful approach not only for the analysis of disease-relevant injury pathways, but also for the identification of promising therapeutical targets.

REFERENCES

1. Astrup J, Symon L, Siesjö BK. Thresholds in cerebral ischemia—The ischemic penumbra. Stroke 1981; 12:723–725.
2. Hossmann K-A. Viability thresholds and the penumbra of focal ischemia. Ann Neurol 1994; 36(4): 557–565.
3. Sharp FR, Lu AG, Tang Y, Millhorn DE. Multiple molecular penumbras after focal cerebral ischemia. J Cereb Blood Fl Met 2000; 20(7):1011–1032.
4. Sako K, Kato A, Diksic M, Yamamoto LY. Use of short-lived ^{18}F and long-lived ^{14}C in double tracer autoradiography for simultaneous measurement of LCBF and LCGU. Stroke 1984; 15:896–900.
5. Mies G, Bodsch W, Paschen W, Hossmann K-A. Triple-tracer autoradiography of cerebral blood flow, glucose utilization and protein synthesis in rat brain. J Cereb Blood Fl Met 1986; 6:59–70.
6. Pontén U, Ratcheson RA, Salford LG, Siesjö BK. Optimal freezing conditions for cerebral metabolites in rats. J Neurochem 1973; 21:1127–1138.
7. Kogure K, Alonso OF. A pictorial representation of endogenous brain ATP by a bioluminescent method. Brain Res 1978; 154:273–284.
8. Paschen W, Niebuhr I, Hossmann K-A. A bioluminescence method for the demonstration of regional glucose distribution in brain slices. J Neurochem 1981; 36:513–517.
9. Paschen W. Regional quantitative determination of lactate in brain sections. A bioluminescent approach. J Cereb Blood Fl Met 1985; 5(4):609–612.
10. Reivich M, Jehle J, Sokoloff L, Kety SS. Measurement of regional cerebral blood flow with antipyrine-^{14}C in awake cats. J Appl Physiol 1969; 27:296–300.
11. Sokoloff L, Reivich M, Kennedy C, et al. The [^{14}C]deoxyglucose method for the measurement of local cerebral glucose utilization: theory, procedure, and normal values in the conscious and anesthetized albino rat. J Neurochem 1977; 28(5):897–916.
12. Smith CB, Deibler GE, Eng K, Schmidt K, Sokoloff L. Measurement of local cerebral protein synthesis in vivo: influence of recycling of amino acids derived from protein degradation. Proc Natl Acad Sci USA 1988; 85:9341–9345.
13. Mies G, Niebuhr I, Hossmann K-A. Simultaneous measurement of blood flow and glucose metabolism by autoradiographic techniques. Stroke 1981; 12:581–588.
14. Paschen W, Mies G, Hossmann K-A. Threshold relationship between cerebral blood flow, glucose utilization, and energy metabolites during development of stroke in gerbils. Exp Neurol 1992; 117(N3):325–333.
15. Ginsberg MD. Adventures in the pathophysiology of brain ischemia: Penumbra, gene expression, neuroprotection. The 2002 Thomas Willis Lecture. Stroke 2003; 34(1):214–223.
16. Heiss WD, Kracht LW, Thiel A, Grond M, Pawlik G. Penumbral probability thresholds of cortical flumazenil binding and blood flow predicting tissue outcome in patients with cerebral ischaemia. Brain 2001; 124(Part 1):20–29.
17. Csiba L, Paschen W, Hossmann K-A. A topographic quantitative method for measuring brain tissue pH under physiological and pathophysiological conditions. Brain Res 1983; 289:334–337.
18. Veer CAvd, LaManna, JC, Whittingham JC, Selman TS, Lust ED. Metabolic studies of focal ischemic zones in brain defined by neutral red. Fed Proc 1985; 44:1355–1355.
19. Welsh FA, Marcy VR, Sims RE. NADH fluorescence and regional energy metabolites during focal ischemia and reperfusion of rat brain. J Cereb Blood Fl Met 1991; 11:459–465.
20. Strong AJ, Harland SP, Meldrum BS, Whittington DJ. The use of in vivo fluorescence image sequences to indicate the occurrence and propagation of transient focal depolarizations in cerebral ischemia. J Cereb Blood Fl Met 1996; 16(3):367–377.
21. Mies G, Kloiber O, Drewes L, Hossmann K-A. Cerebral blood flow and regional potassium distribution during focal ischemia of gerbil brain. Ann Neurol 1984; 16:232–237.
22. Zhang F, Xie J, Han H. MRI reveals changes in intracellular calcium in ischaemic areas of rabbit brain. Neuroradiology 2003; 45(11):773–779.
23. Hakim AM, Hogan MJ. In vivo binding of nimodipine in the brain. I. The effect of focal cerebral ischemia. J Cereb Blood Fl Met 1991; 11:762–770.
24. Di X, Alves OL, Bullock R. Cytotoxic edema is independent of NMDA ion channel activation following middle cerebral artery occlusion (MCAO). An in vivo autoradiographic and MRI study. Neurol Res 2003; 25(4):329–334.
25. Lipton P. Ischemic cell death in brain neurons [review]. Physiol Rev 1999; 79(4):1431–1568.
26. Carmichael ST. Gene expression changes after focal stroke, traumatic brain and spinal cord injuries. Curr Opin Neurol 2003; 16(6):699–704.
27. Read SJ, Parsons AA, Harrison DC, et al. Stroke genomics: Approaches to identify, validate, and understand ischemic stroke gene expression. J Cereb Blood Fl Met 2001; 21(7):755–778.
28. Kinouchi H, Sharp FR, Koistinaho J, Hicks K, Kamii H, Chan PH. Induction of heat shock hsp70 messenger RNA and HSP70-kDa protein in neurons in the penumbra following focal cerebral ischemia in the rat. Brain Res 1993; 619(1–2):334–338.
29. Hata R, Mies G, Wiessner C, Hossmann K-A. Differential expression of c-fos and hsp72 mRNA in focal cerebral ischemia of mice. Neuroreport 1998; 9(1):27–32.

30. Nimura T, Weinstein PR, Massa SM, Panter S, Sharp FR. Heme oxygenase-1 (HO-1) protein induction in rat brain following focal ischemia. Mol Brain Res 1996; 37(1–2):201–208.
31. Kiessling M, Gass P. Stimulus-transcription coupling in focal cerebral ischemia. Brain Pathol 1994; 4(1):77–83.
32. Heiss W-D. Ischemic penumbra: Evidence from functional imaging in man. J Cereb Blood Fl Met 2000; 20(9):1276–1293.
33. Baron JC. Mapping the ischaemic penumbra with PET: implications for acute stroke treatment [Review]. Cerebrovascular Diseases 1999; 9(4):193–201.
34. Kuhl DE, Phelps ME, Kowell AP, Metter EJ, Selin C, Winter J. Effects of stroke on local cerebral metabolism and perfusion: mapping by emission computed tomography of ^{18}FDG and $^{13}NH_3$. Ann Neurol 1980; 8:47–60.
35. Neumann-Haefelin T, Wittsack HJ, Wenserski F, et al. Diffusion-and perfusion-weighted MRI. The DWI/PWI mismatch region in acute stroke. Stroke 1999; 30(8):1591–1597.
36. Schlaug G, Benfield A, Baird AE, et al. The ischemic penumbra. Operationally defined by diffusion and perfusion MRI. Neurology 1999; 53(7):1528–1537.
37. Kidwell CS, Alger JR, Saver JL. Evolving paradigms in imaging the ischemic penumbra with multimodal magnetic resonance imaging. Stroke 2003; 34(11):2729–2735.
38. Coutts SB, Simon JE, Tomanek AI, et al. Reliability of assessing percentage of diffusion-perfusion mismatch. Stroke 2003; 34(7):1681–1683.
39. Kohno K, Hoehn-Berlage M, Mies G, Back T, Hossmann K-A. Relationship between diffusion-weighted MR images, cerebral blood flow, and energy state in experimental brain infarction. Magn Reson Imaging 1995; 13(1):73–80.
40. Shen Q, Meng TJ, Sotak CH, Duong TQ. Pixel-by-pixel spatiotemporal progression of focal ischemia derived using quantitative perfusion and diffusion imaging. J Cereb Blood Fl Met 2003; 23(12): 1479–1488.
41. Oppenheim C, Grandin C, Samson Y, et al. Is there an apparent diffusion coefficient threshold in predicting tissue viability in hyperacute stroke? Stroke 2001; 32(11):2486–2491.
42. Karonen JO, Nuutinen J, Kuikka JT, et al. Combined SPECT and diffusion-weighted MRI as a predictor of infarct growth in acute ischemic stroke. J Nucl Med 2000; 41(5):788–794.
43. Grohn OHJ, Lukkarinen JA, Oja JME, et al. Noninvasive detection of cerebral hypoperfusion and reversible ischemia from reductions in the magnetic resonance imaging relaxation time, T-2. J Cereb Blood Fl Met 1998; 18(8):911–920.
44. Aoki I, Ebisu T, Tanaka C, et al. Detection of the anoxic depolarization of focal ischemia using manganese-enhanced MRI. Magn Reson Med 2003; 50(1):7–12.
45. Igarashi H, Kwee IL, Nakada T, Katayama Y, Terashi A. H-1 magnetic resonance spectroscopic imaging of permanent focal cerebral ischemia in rat: longitudinal metabolic changes in ischemic core and rim. Brain Res 2001; 907(1–2):208–221.
46. Franke C, Brinker G, Pillekamp F, Hoehn M. Probability of metabolic tissue recovery after thrombolytic treatment of experimental stroke: A magnetic resonance spectroscopic imaging study in rat brain. J Cereb Blood Fl Met 2000; 20(3):583–591.
47. Watanabe Y, Takagi H, Aoki S, Sassa H. Prediction of cerebral infarct sizes by cerebral blood flow SPECT performed in the early acute stage. Ann Nucl Med 1999; 13(4):205–210.
48. Kurth CD, Levy WJ, McCann J. Near-infrared spectroscopy cerebral oxygen saturation thresholds for hypoxia-ischemia in piglets. J Cereb Blood Fl Met 2002; 22(3):335–341.
49. Reineck LA, Agarwal S, Hillis AE. "Diffusion-clinical mismatch" is associated with potential for early recovery of aphasia. Neurology 2005; 64(5):828–833.
50. Hata R, Maeda K, Hermann D, Mies G, Hossmann K-A. Evolution of brain infarction after transient focal cerebral ischemia in mice. J Cereb Blood Fl Met 2000; 20(6):937–946.
51. Hara T, Mies G, Hossmann K-A. Effect of thrombolysis on the dynamics of infarct evolution after clot embolism of middle cerebral artery in mice. J Cereb Blood Fl Met 2000(20):1483–1491.
52. Hoehn-Berlage M, Norris DG, Kohno K, Mies G, Leibfritz D, Hossmann K-A. Evolution of regional changes in apparent diffusion coefficient during focal ischemia of rat brain: The relationship of quantitative diffusion NMR imaging to reduction in cerebral blood flow and metabolic disturbances. J Cereb Blood Fl Met 1995; 15(6):1002–1011.
53. Watanabe Y, Nakano T, Yutani K, et al. Detection of viable cortical neurons using benzodiazepine receptor imaging after reversible focal ischaemia in rats: comparison with regional cerebral blood flow. European J Nucl Med 2000; 27(3):308–313.
54. Kokubo Y, Liu JL, Rajdev S, Kayama T, Sharp FR, Weinstein PR. Differential cerebral protein synthesis and heat shock protein 70 expression in the core and penumbra of rat brain after transient focal ischemia. Neurosurgery 2003; 53(1):186–190.
55. Kokubo Y, Matson GB, Liu JL, et al. Correlation between changes in apparent diffusion coefficient and induction of heat shock protein, cell-specific injury marker expression, and protein synthesis reduction on diffusion-weighted magnetic resonance images after temporary focal cerebral ischemia in rats. J Neurosur 2002; 96(6):1084–1093.

56. Olah L, Wecker S, Hoehn M. Secondary deterioration of apparent diffusion coefficient after 1-hour transient focal cerebral ischemia in rats. J Cereb Blood Fl Met 2000; 20(10):1474–1482.
57. Gu WG, Brannstrom T, Wester P. Cortical neurogenesis in adult rats after reversible photothrombotic stroke. J Cereb Blood Fl Met 2000; 20(8):1166–1173.
58. Roberts TPL, Vexler Z, Derugin N, Moseley ME, Kucharczyk J. High-speed MR imaging of ischemic brain injury following stenosis of the middle cerebral artery. J Cereb Blood Fl Met 1993; 13(6):940–946.
59. Heiss W-D, Graf R, Wienhard K, et al. Dynamic penumbra demonstrated by sequential multitracer PET after middle cerebral artery occlusion in cats. J Cereb Blood Fl Met 1994; 14(6):892–902.
60. Hossmann K-A, Mies G, Paschen W, et al. Multiparametric imaging of blood flow and metabolism after middle cerebral artery occlusion in cats. J Cereb Blood Fl Met 1985; 5:97–107.
61. Hudgins WR, Garcia JH. Transorbital approach to the middle cerebral artery of the squirrel monkey: a technique for experimental cerebral infarction applicable to ultrastructural studies. Stroke 1970; 1:107–111.
62. Touzani O, Young AR, Derlon JM, et al. Sequential studies of severely hypometabolic tissue volumes after permanent middle cerebral artery occlusion: A positron emission tomographic investigation in anesthetized baboons. Stroke 1995; 26(11):2112–2119.
63. Young AR, Sette G, Touzani O, et al. Relationships between high oxygen extraction fraction in the acute stage and final infarction in reversible middle cerebral artery occlusion—an investigation in anesthetized baboons with positron emission tomography. J Cereb Blood Fl Met 1996; 16(6): 1176–1188.
64. Giffard C, Young AR, Kerrouche N, Derlon JM, Baron JC. Outcome of acutely ischemic brain tissue in prolonged middle cerebral artery occlusion: A serial positron emission tomography investigation in the baboon. J Cereb Blood Fl Met 2004; 24(5):495–508.
65. Kuge Y, Yokota C, Tagaya M, et al. Serial changes in cerebral blood flow and flow-metabolism uncoupling in primates with acute thromboembolic stroke. J Cereb Blood Fl Met 2001; 21(3): 202–210.
66. Xie Y, Munekata K, Seo K, Hossm ann K-A. Effect of autologous clot embolism on regional protein biosynthesis of monkey brain. Stroke 1988; 19:750–757.
67. Obrenovitch TP, Garofalo O, Harris RJ, et al. Brain tissue concentrations of ATP, phosphocreatine, lactate, and tissue pH in relation to reduced cerebral blood flow following experimental acute middle cerebral artery occlusion. J Cereb Blood Fl Met 1988; 8:866–874.
68. Mies G, Ishimaru S, Xie Y, Seo K, Hossmann K-A. Ischemic thresholds of cerebral protein synthesis and energy state following middle cerebral artery occlusion in rat. J Cereb Blood Fl Met 1991; 11: 753–761.
69. Paschen W, Djuricic BM, Bosma H-J, Hossmann K-A. Biochemical changes during graded brain ischemia in gerbils. 2. Regional evaluation of cerebral blood flow and brain metabolites. J Neurol Sci 1983; 58:37–44.
70. Hata R, Maeda K, Hermann D, Mies G, Hossmann K-A. Dynamics of regional brain metabolism and gene expression after middle cerebral artery occlusion in mice. J Cereb Blood Fl Met 2000; 20(2): 306–315.
71. Frykholm P, Andersson JLR, Valtysson J, et al. A metabolic threshold of irreversible ischemia demonstrated by PET in a middle cerebral artery occlusion-reperfusion primate model. Acta Neurologica Scandinavica 2000; 102:18–26.

7 Molecular Biology of the Penumbra

Frank R. Sharp, Huichun Xu, Xinshe Liu, and Ruiqiong Ran
Department of Neurology and M.I.N.D. Institute, University of California at Davis, Sacramento, California, U.S.A.

INTRODUCTION

"Clinical" or Treatment Penumbra

Studies of the penumbra have used physiological, imaging, and biochemical methods to define and study the penumbra. These are summarized and critically reviewed in this book. Both positron emission tomography (PET) and magnetic resonance imaging (MRI) have been used to provide evidence of a penumbra in animal models and in humans. Diffusion MRI combined with perfusion MRI appears to provide a reasonable image of the clinical penumbra. The "clinical" penumbra is variously defined, but for the purposes of this chapter represents an area of decreased blood flow, which, if blood flow is not restored, will go on to infarct. The correlates of this definition are that the longer the reduction in flow, the larger the infarct and the smaller the penumbra; the perfect pharmacological treatments for acute stroke would be able to rescue 100% of the penumbra at a given time after the onset of ischemia. For the clinician scientists who study stroke, therefore, the concept of a "penumbra" has been fairly clear but somewhat variously defined since the term was initially coined.

Most Changes of Gene Expression in Brain Unrelated to Penumbra

The role of the various molecular changes that occur following stroke, however, have generally been much less clear in regard to their relation to the "clinical penumbra." There is often uncertainty as to whether changes of gene expression are occurring within the area of infarction itself, are occurring outside the infarct and within an area that sustained decreased blood flow can be defined as the "clinical penumbra," or whether the changes of gene expression are occurring in parts of brain at some distance from where any changes of blood flow occur during a stroke (1–5). An example of the latter is the immediate early gene c-fos, which has been shown to be induced in occipital cortex, thalamus, substantia nigra, and other brain stem regions, all of which are certainly outside the regions of middle cerebral artery ischemia in the rat models used (6). Though c-fos is induced in brain outside areas of infarction, the induction of *c-fos* immediate early gene in brain does not correlate with or indicate the "clinical penumbra." Thus, it is important to emphasize that the vast majority of changes of gene expression described in most animal models represent ischemia-induced changes of gene expression that do not directly correlate spatially with the region of decreased cerebral blood flow. These ischemia-related changes of gene expression will be briefly reviewed in the last half of this chapter. The changes of gene expression that occur outside the clinical penumbra may relate to apoptosis, spreading depression, changes of synaptic transmission between injured brain and interconnected brain regions, changes of trophic support between injured brain and interconnected brain regions, and almost certainly to plastic biochemical and physiological changes that occur in brain regions surrounding an infarct and in brain regions remote from an infarct (7).

Gene Changes Only in the Penumbra

The first part of this chapter will, therefore, focus on molecular changes that occur in brain that are directly contiguous with an area of decreased cerebral blood flow, and for the most part only occur within the region of decreased blood flow. Hence, the changes of gene expression must occur within the middle cerebral artery (MCA) distribution if the ischemia occurs only in the MCA distribution. As a corollary, the changes of gene expression may occur within the region of

the infarction, but they must not extend outside the area of decreased cerebral blood flow. Using this definition, then it turns out that only a few biochemical and molecular studies address the "clinical penumbra," as discussed earlier. The biochemical changes to be briefly reviewed here are related to decreased protein synthesis in areas where there are preserved ATP levels (8,9). Concurrent with the decreased protein synthesis are other molecular changes that are associated with induction of Heat shock protein 70 (Hsp70), other heat shock proteins, and other chaperone proteins that occur in response to denatured proteins and unfolded proteins found in cells in the penumbra, during the period of ischemia (7,10,11). These chaperone proteins are induced when cells are still alive and are attempting to deal with the early periods of ischemia and abnormal protein metabolism and processing. If the cells succeed in the battle of protein denaturation and unfolding, they survive. If they fail, the cells either undergo apoptosis or succumb to necrosis or autophagy (7).

Molecular Penumbras and Outline of Chapter

Immediately surrounding an infarct is a narrow zone of selective neuronal cell death. This selective neuronal cell death can be detected using conventional staining, as well as with more recently described TUNEL staining of brain. Whether these cells die by apoptosis or not is still debated, but apoptosis-related genes are expressed in these cells. This zone of "selective neuronal cell death" is shown schematically in Figures 1 and 12 and is outside the infarct but within the "clinical penumbra."

The next well-defined region outside an infarct is the region of decreased protein synthesis but preserved ATP (Figs. 1,–3, 5–8, and 12). Unfolded proteins are produced during early stages of ischemia and these stimulate the unfolded protein response (UPR) that is associated with activation of PERK (Figs. 2 and 3) and phosphorylation of eIF-2α that blocks translation and decreases protein synthesis (9,11,12). Within the region of decreased protein synthesis denatured proteins occur that stimulate the synthesis of Hsp70 mRNA and Hsp70 protein (Figs. 4–9). The region of decreased protein synthesis coincides with the region of Hsp70 induction (10,13,14), and both appear to correlate best with the "clinical penumbra" that is discussed in most of the chapters in this book.

A number of other molecular changes occur both within the infarct, adjacent to the infarct in the "penumbra," and in regions remote from the infarct. Within the infarct, protein synthesis goes to zero and ATP falls, and cells die via necrosis, apoptosis, and autophagy. There is an inflammatory response that is responsible for clearing dead cells and removal of cell processes even at distant sites connected to the region of infarction (Figs. 12–15). Hypoxia serves as a stimulus for many changes outside the infarction including angiogenesis (Figs. 12 and 13). The zone of HIF-1α induction probably extends well beyond the "clinical penumbra." Finally, spreading depression, deafferentation related to an infarct, and other physiological and synaptic changes must occur in cortex and subcortical regions. These regions would include any region connected directly or indirectly to an infarct. A good example would be cerebellum, where changes of blood flow and metabolism occur following cortical and subcortical infarctions. Changes of immediate-early genes and other transcription factors likely mediate the plastic changes that occur in brain, and are responsible for any degree of recovery that occurs following a stroke (Fig. 15).

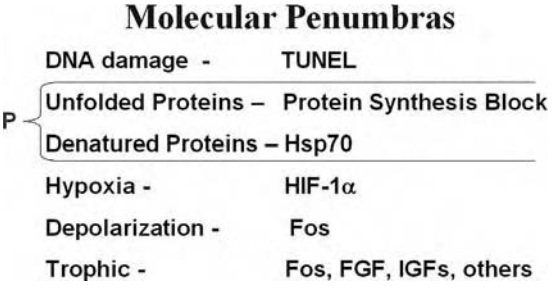

FIGURE 1 Molecular penumbras to be discussed in the chapter are shown on the *left* and their markers are shown on the *right*. *Abbreviation*: P, penumbra.

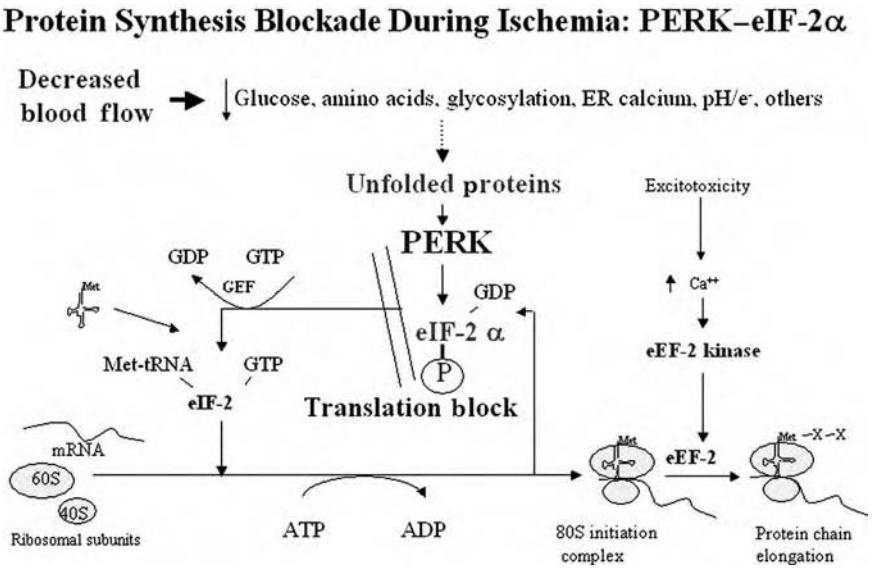

FIGURE 2 Outline of protein synthesis and role of PKR-like endoplasmic reticulum kinase on phosphorylation of eIF-2α and producing a translation block following ischemia.

PENUMBRA

Penumbra: Decreased Protein Synthesis and Preserved Adenosine Triphosphate

Hossmann et al. described a decrease of cerebral protein synthesis following focal cerebral ischemia more than three decades ago (15,16). They and others have replicated the findings multiple times. As flow is progressively lowered (17), the decrease of protein synthesis is one of the first biochemical or molecular changes that can be demonstrated (18–20). Protein synthesis declines when flow is reduced to approximately 50% to 30% of the baseline blood flow (17,21). Though protein synthesis declines in the core of an infarct as well, ATP declines in the core where tissue

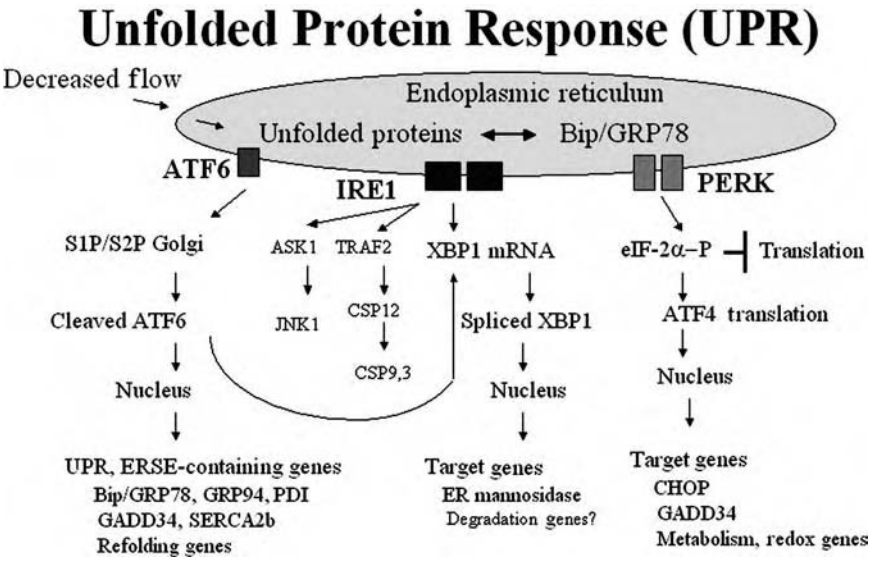

FIGURE 3 The unfolded protein response (UPR) plays a central role in blocking translation following cerebral ischemia. It is also responsible for producing transcriptional changes aimed at either refolding the unfolded proteins or programming the cell for apoptosis.

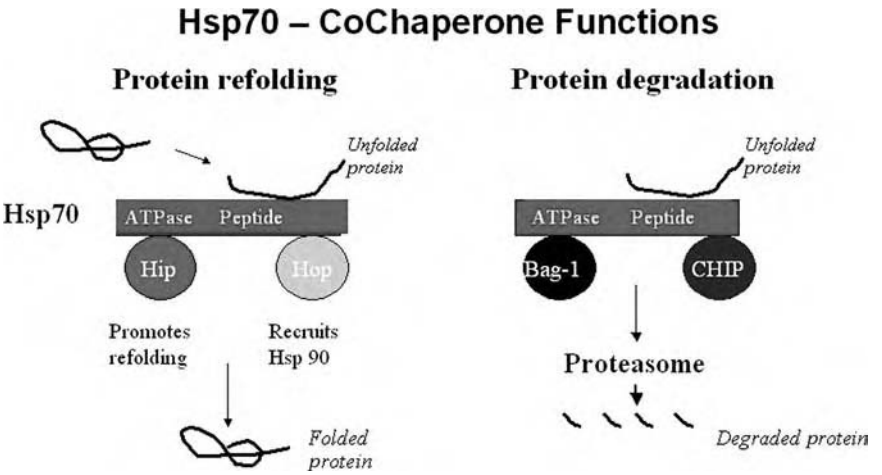

FIGURE 4 Hsp70 plays a role in protein refolding and targeting proteins for degradation depending upon the protein chaperones it associates with.

death occurs. In contrast, in the "penumbra," the protein synthesis rate is depressed, whereas ATP remains normal (16,21).

Protein synthesis decreases in all tissues and virtually all organisms during ischemia, and hence the response of the brain does not appear to be specific (11,22). Protein synthesis decreases can be transient or permanent, since if blood flow is restored, cells will survive and protein synthesis recovers (23). Protein synthesis never recovers in the core (14). Though it has been debated at various levels, the decrease in protein synthesis appears to be protective in a variety of injury models (12,24,25); however, this has not been directly tested in brain ischemia models to date.

Penumbra: Unfolded Protein Response in Endoplasmic Reticulum and Protein Synthesis

The mechanism that decreases protein synthesis appears to be a result of the (UPR) in the endoplasmic reticulum (ER). During translation initiation, the 40S and 60S ribosomal subunits must

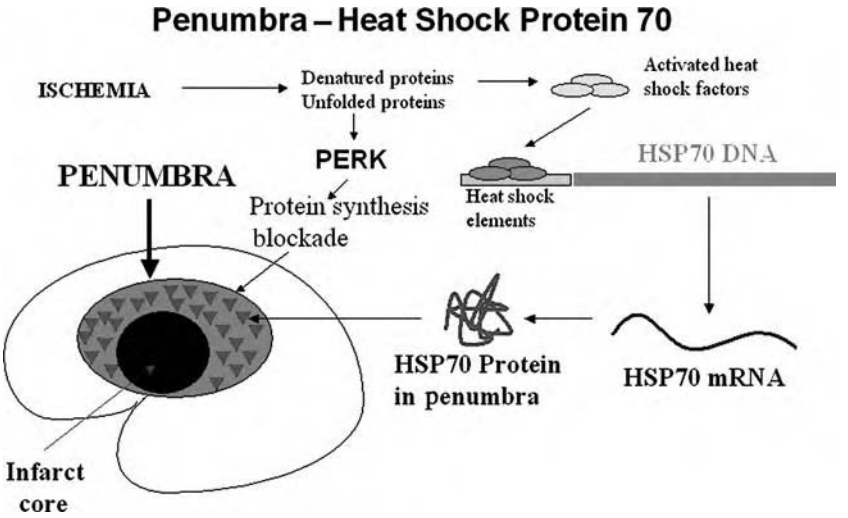

FIGURE 5 Focal ischemia produces denatured proteins that induce Hsp70 and produce unfolded proteins, which induces the UPR and blocks protein synthesis. The Hsp70 and UPR zones are co-incident and probably are the molecular correlates of the "clinical penumbra."

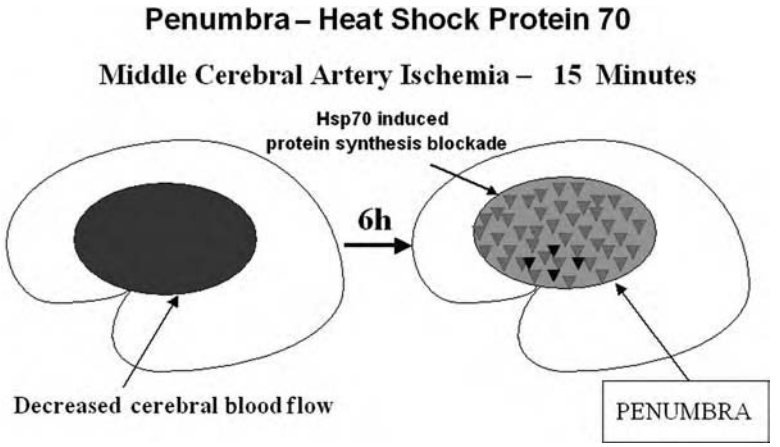

FIGURE 6 With short durations of middle cerebral artery ischemia, the entire middle cerebral artery distribution constitutes the penumbra in which Hsp70 is induced and protein synthesis is suppressed. As ischemia duration increases, infarction occurs and becomes larger, and the penumbra becomes smaller and disappears.

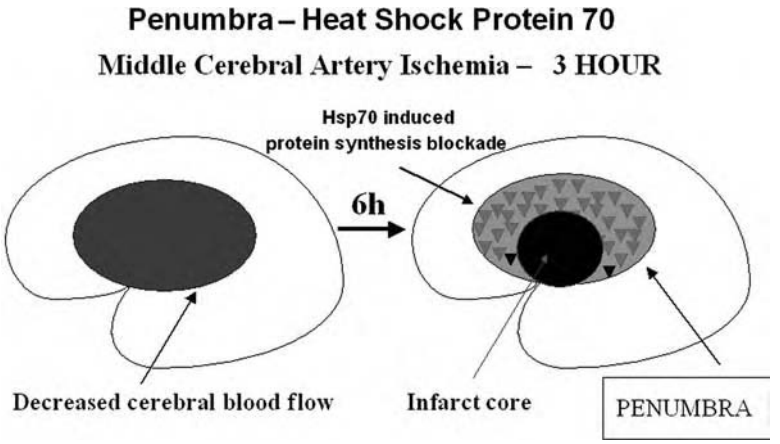

FIGURE 7 With short durations of middle cerebral artery ischemia, the entire middle cerebral artery distribution constitutes the penumbra in which Hsp70 is induced and protein synthesis is suppressed. As ischemia duration increases, infarction occurs and becomes larger, and the penumbra becomes smaller and disappears.

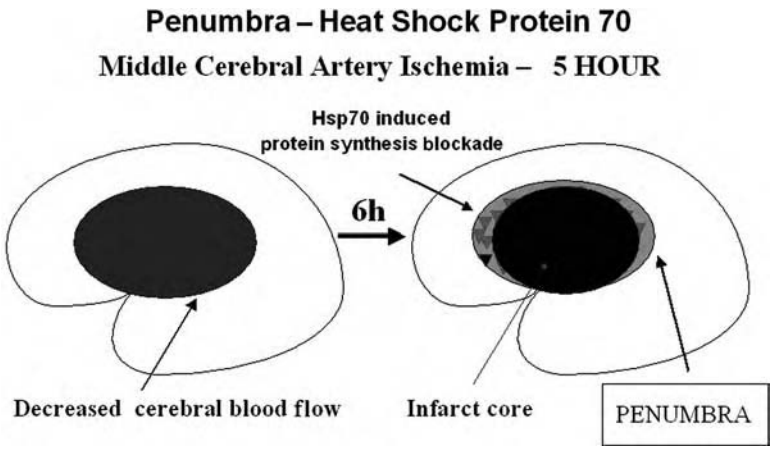

FIGURE 8 With short durations of middle cerebral artery ischemia, the entire middle cerebral artery distribution constitutes the penumbra in which Hsp70 is induced and protein synthesis is suppressed. As ischemia duration increases, infarction occurs and becomes larger, and the penumbra becomes smaller and disappears.

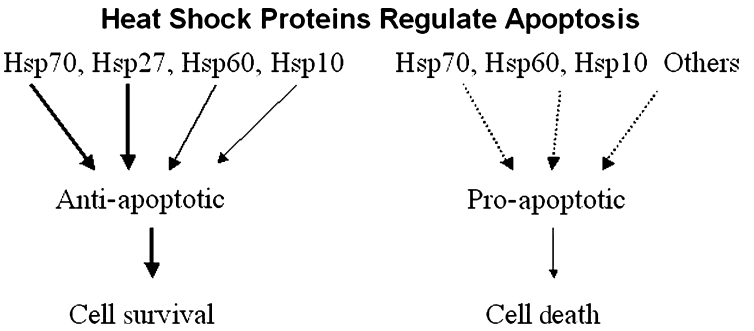

FIGURE 9 A variety of heat shock proteins are induced in response to ischemia and some prevent apoptosis (anti-apoptotic) and some promote apoptosis (pro-apoptotic), and some Hsps do both.

combine with Met-tRNA and the elongation initiation factor -2 (eIF-2α) (Fig. 2). If eIF-2α is phosphorylated, then this complex does not form well and translation is slowed or blocked. Hu and Wieloch first reported dysfunction of the eIF-2α system following cerebral ischemia (26).

It is now known that eIF-2α is phosphorylated by four different kinases including PERK (PKR like endoplasmic reticulum kinase), PKR, GCN2, and HIR (11,12,22). Knockouts of PKR, HRI, and GCN2 did not show any ischemia-induced changes of phosphorylated eIF2α, and hence PERK is the kinase most implicated in ischemia-induced phosphorylation of eIF2α and ischemia-induced translation block in mammalian brain (11,22) (Fig. 2). It is worth pointing out that studies still need to be performed to determine if ischemia suppresses protein synthesis in these knockout mice or not.

The proximal stimulus for the UPR in cerebral ischemia is still unknown. Increased ER calcium has been implicated (27,28). Alternatively, impaired delivery of amino acids or glucose, abnormal glycosylation of proteins, or other factors may account for the appearance of unfolded proteins during synthesis in the ER (12,25,29). Whatever the stimulus is, it must occur when cerebral blood flow is decreased approximately 50% of baseline, and results in severe translation block, when blood flow is decreased to 25% of baseline but when ATP is still preserved (21,30).

The UPR involves much more than suppression of translation (Fig. 3). When unfolded proteins appear in the ER, it is postulated that the glucose regulated protein (GRP78—also called Bip) binds the unfolded proteins. When GRP78 binds the unfolded proteins it releases the lumenal portions of ER membrane associated proteins ATF6, IRE1 and PERK (31). Both

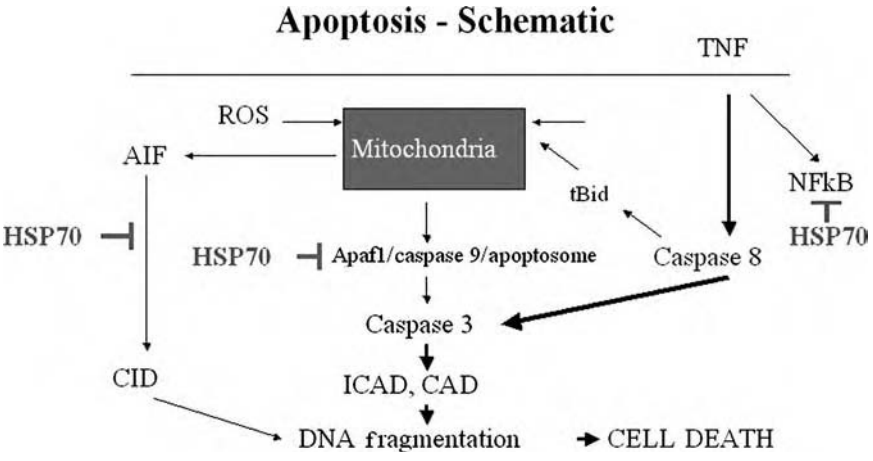

FIGURE 10 Schematic of pathways that produce apoptosis and sites where Hsp70 acts.

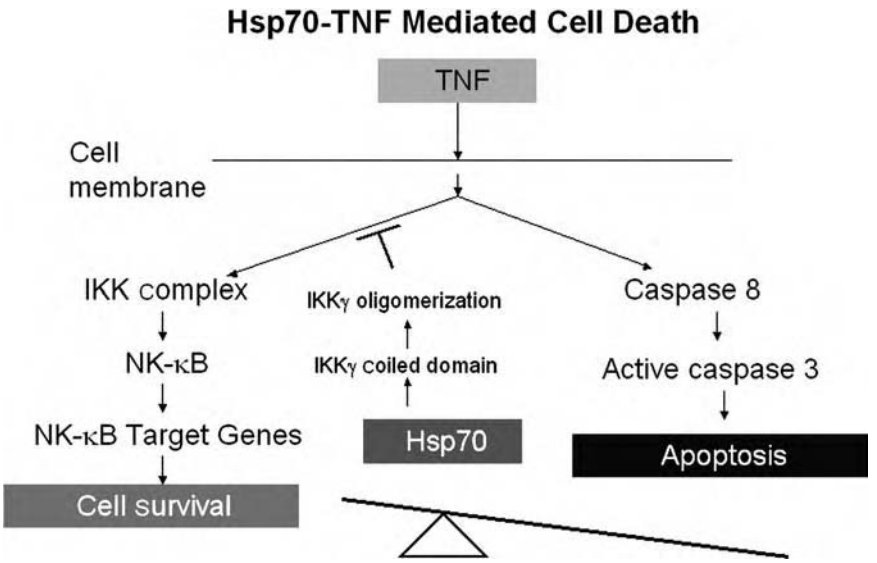

FIGURE 11 Hsp70 promotes apoptosis initiated by TNF by binding IKKgamma and blocking induction of NfkappaB target genes that promote cell survival.

IRE1 and PERK then dimerize and autophosphorylate, and are activated. ATF6 is activated and released from the ER (31). ATF6 transits to the Golgi where it is cleaved by S1P and S2P. The cleaved ATF6 then transits to the nucleus where it binds to the endoplasmic reticulum stress element (ERSE) in the promoter of UPR target genes including GRP78/Bip, GRP94, PDI, GADD34, SERCA2b, and others (12,29,31). These induced genes make proteins that then help to refold the unfolded ER proteins, or help in the disposal of the unfolded ER proteins.

ATF6 also targets XBP1. When IRE1 is activated, it splices full length XBP1 mRNA so that it can be translated. The XBP1 protein then goes to the nucleus to binding ERSE elements in target genes. At least one XBP1 target gene appears to be mannosidase that is involved in the degradation of misfolded glycoproteins (31). Activated IRE1 also appears to dissociate TRAF2 from caspase 12, allowing caspase 12 to be cleaved by calpain. The activated caspase 12 can

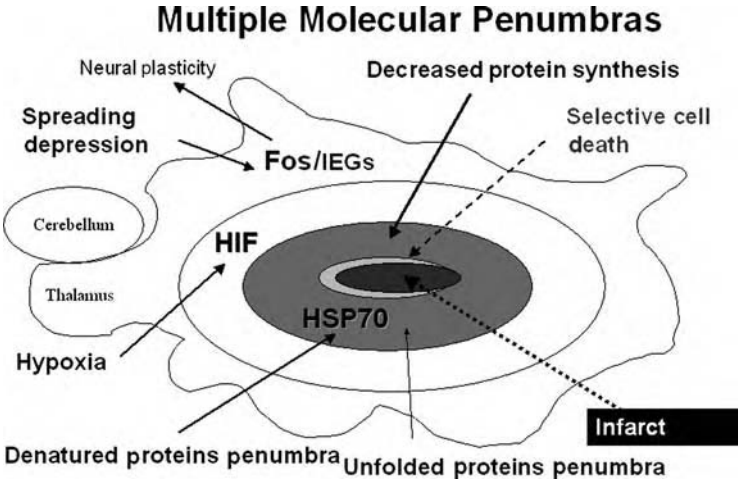

FIGURE 12 (*See color insert.*) Diagram of the molecular penumbras discussed in the chapter. The "clinical penumbra" or penumbra that is closely related to regions of decreased blood flow are located outside the area of infarction and include the region of decreased protein synthesis in which Hsp70 protein is expressed in response to denatured proteins.

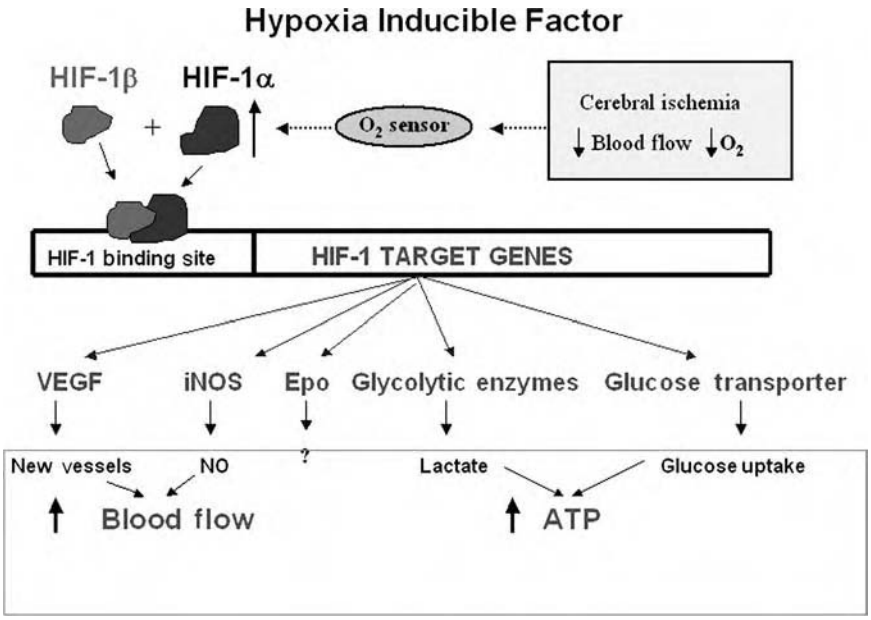

FIGURE 13 HIF is one of the major transcription factors induced by hypoxia that regulates a variety of genes induced in response to the hypoxia associated with ischemia.

cleave caspase 9 that can then activate caspase 3 and lead to cellular apoptosis. Similarly, IRE1 can activate ASK1 and JNK1 (Fig. 3). All of these latter pathways appear to be related to either disposing of unfolded proteins and/or promoting apoptosis in the cell related to inability to cope with the unfolded proteins.

Finally, PERK not only phosphorylates eIF-2α, but it also helps in translating ATF4 message to ATF4 protein. ATF4 protein also binds to ERSE promoter elements to induce genes like CHOP, GADD34, and others involved in metabolism and redox (31) (Fig. 3). It is likely that basic control mechanisms will dictate whether transcription is targeted toward protein folding and whether it

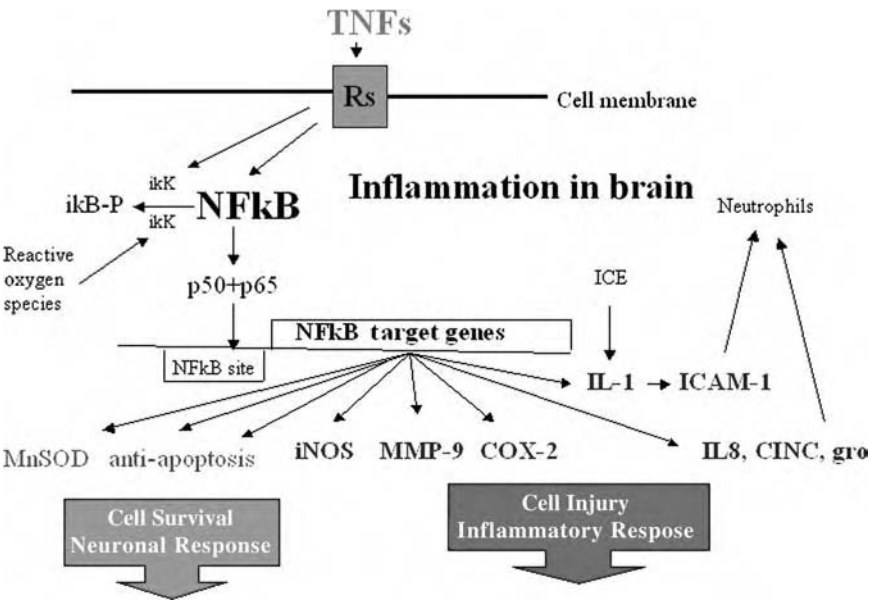

FIGURE 14 Inflammation is a prominent response to cerebral ischemia, and a variety of molecules expressed in blood and in brain mediate this response. It is likely the inflammatory response is targeted to the ischemic core and not the penumbra, at least, initially.

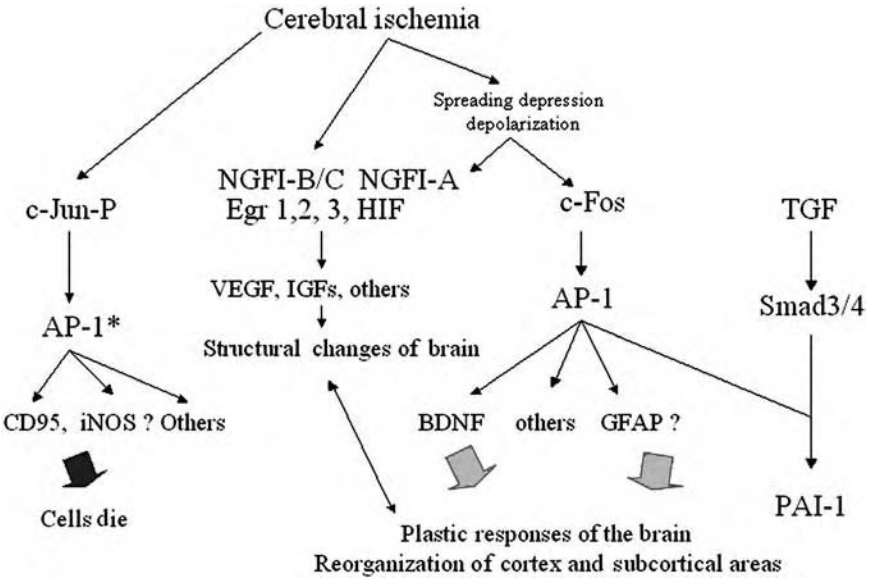

FIGURE 15 Gene expression changes in many brain regions outside the penumbra. Some of these changes are outlined here, and these changes likely regulate plasticity following stroke and guard against future ischemia.

is targeted toward protein degradation and cell apoptosis. Most importantly, with modest decreases of cerebral blood flow for short durations, the UPR results in a translation block, and a UPR transcriptional response is aimed at protein folding in the ER and cell survival (31,11,12).

Penumbra: Heat-Shock Proteins 70 Binds Denatured Proteins and Refolds Proteins or Targets Proteins for Degradation

Heat-shock proteins (HSPs) are related to glucose-regulated proteins (GRPs) in that they both respond to changes of protein conformation. Whereas GRPs are located mainly in the ER and respond to unfolded proteins during their synthesis, in the case of HSPs, these proteins are classically induced in cells during periods of heat stress and similar stresses that produce denatured proteins in cells. The HSPs are expressed in every living organism from plants, to yeast, bacteria, and mammals (32–36). HSC70, constitutively expressed at high levels in all cells, is induced modestly by stress, and chaperones proteins to targets within a cell (37,38).

A related HSP is Hsp70, which is the major inducible heat-shock protein found in all organisms. In mammals and humans, there are several closely related inducible *Hsp70* genes and proteins. Hsp70 is expressed at low levels in normal cells, and with heat shock becomes the most abundant protein in the cell, since it binds denatured proteins directly and attempts to refold them (Fig. 4) (39,40).

The presence of denatured proteins in cells induces Hsp70 via activation of heat-shock factors (HSF) (Fig. 5). The HSF transcription factors bind to heat-shock elements in the Hsp genes and induce the HSP response (Fig. 5), including induction of Hsp70. Hsp70 binds to denatured, unfolded proteins (Figs. 4 and 5). At this point, the cell makes a decision. If Hsp70 promotes refolding, it binds to cochaperones Hip and Hop, recruits Hsp90, and then promotes protein refolding (Fig. 4) (41). Alternatively, if Hsp70 promotes protein degradation, then it binds cochaperones Bag-1 and CHIP that targets the unfolded protein to the proteasome, where the protein is degraded (Fig. 4).

Penumbra: Hsp70 Zone of Protein Denaturation Correlates with Unfolded Protein Response and Zone of Decreased Protein Synthesis

Following both temporary and permanent MCA occlusions hsp70 mRNA is expressed throughout the MCA distribution, both within the areas of infarction and in regions adjacent to the infarction (6,42,43) (Fig. 5). Most importantly, studies by Hata et al. in the Hossmann laboratory

showed that Hsp70 mRNA is induced in the region where there is decreased protein synthesis associated with preserved ATP (10). Thus, the Hsp70 mRNA induction correlated with the penumbra as defined by decreased protein synthesis, but with preserved ATP (10,13,14).

The hsp70 mRNA is induced by the presence of denatured proteins within cells. Injections of denatured proteins into cells induces Hsp70. Plant amino acids when incorporated into mammalian proteins cause abnormalities of tertiary structure that are tantamount to denaturation, and also induce Hsp70 in cells. Hence, the region of hsp70 mRNA induction can be viewed as the zone within and around an infarction where denatured proteins are found within cells.

A schematic diagram is shown of the possible mechanisms of Hsp70 induction following focal ischemia (Fig. 5). Hsp70 mRNA is induced in neurons in the core of the infarct as well as in the penumbra, where denatured proteins within these cells stimulates HSFs that then form a trimer and bind to the heat-shock element on the *Hsp70* gene. This initiates transcription of hsp70 mRNA in these neurons.

In the infarct core, which will continue to infarct, the hsp70 mRNA cannot be translated into protein. The inability of the cells to make Hsp70 protein may contribute to their death. Outside areas of infarction cells that made hsp70 mRNA are able to translate this into Hsp70 protein. Astrocytes and microglia at the periphery of infarcts express high levels of Hsp70 protein. Neurons also express Hsp70 protein outside the areas of infarction (43).

If the MCA occlusion is brief without producing infarction, Hsp70 protein can be expressed in neurons throughout the MCA distribution (Fig. 6). If the MCA occlusion is of an intermediate duration, then there is infarction in the core and Hsp70 expression and decreased protein synthesis in the penumbra surrounding the infarct (Fig. 7). If the MCA occlusion time is prolonged or permanent, then there is an infarct involving most of the MCA distribution, with very little of the penumbra surviving (Fig. 8). Thus, with brief ischemia the penumbra volume is large and associated with widespread Hsp70 expression and suppression of protein synthesis throughout the vascular distribution of decreased blood flow (Fig. 6). As the ischemia duration or severity increases, infarction occurs (Fig. 7) and the volume of the infarction worsens, and the size of the penumbra decreases and eventually disappears (Fig. 8).

Hsp70 expression in the neurons outside areas of infarction is presumed to protect these cells from further protein denaturation. Moreover, the Hsp70 expression may promote protein renaturation and promote cell survival (44). Overexpression of Hsp70 protein in transgenic mice markedly protects the brain against focal ischemic infarction (45).

Role of Heat-Shock Proteins 70 in Apoptosis

Hsp70 has been shown to modulate apoptosis via several direct interactions. Hsp70 binds to Apaf1 and disrupts the formation of the apoptosome. This prevents activation of caspase 9, which in turn prevents activation of caspase 3 (46–48) (Fig. 10). Hsp70 also binds AIF, a molecule released by the mitochondria that directly targets the nucleus and activation of a nuclear DNAase. Hence, Hsp70 decreases mitochondrial-dependent, caspase-independent apoptosis (49) (Fig. 10). Notably, mutant Hsp70 proteins can be engineered that contain DEVD sites within the protein and directly inhibit caspase-3 and improve overall cell survival (50). Though Hsp70 appears to protect against necrosis and apoptosis in a variety of different paradigms (36,48,50,51), Hsp70 also appears to facilitate apoptosis in some circumstances (52). We have shown that coexpression of TNF and Hsp70 prevents NFkappaB survival signaling by binding IKK gamma, and this then promotes TNF mediated, caspase 8 dependent apoptosis (Figs. 10 and 11) (52). This may help explain why Hsp70 is not protective in some systems and could in fact worsen cell survival in some immune-mediated, TNF dependent disease conditions.

Role of Other Heat-Shock Proteins and Other Chaperones

Heat-Shock Proteins 27 (Astrocytes)

There are many known HSPs and other chaperones. For example, Hsp27 is expressed mainly in astrocytes in the injured brain and may be involved in stabilizing actin, GFAP, and cytoskeletal proteins in these cells (53–55). Hsp27 overexpression has consistently been shown to protect brain against ischemic injury (55–57), and can modulate apoptosis pathways including

binding to cytochrome C, as well (58,59). Hsp27 induction appears to occur both inside and outside of the penumbra, and hence probably responds to protein denaturation as well as other stimuli.

HemeOxygenase-1 (Microglia)

HemeOxygenase-1 (HO-1) is induced in brain following hemorrhage and ischemia (51,60–62). HO-1 is induced primarily in microglia in the injured brain, and likely deals with heme chaperoning and heme degradation following brain hemorrhage and cell death and release of heme (61). HO-1 is induced inside and outside of the penumbra, and hence is not a marker of the penumbra as outlined earlier.

Other Heat-Shock Proteins in Various Organelles

Hsp70, Hsp27, and HO-1 are cytoplasmic HSPs. Hsp60, Hsp10, mitochondrial Hsp70, and GRP75 are localized to mitochondria and participate in chaperoning proteins in the mitochondria. Moreover, Hsp60 and Hsp10 have been shown to be both anti-apoptotic and pro-apoptotic in various systems (63–66). Hsp47 interacts with collagen (66).

GENE EXPRESSION UNRELATED TO THE CLINICAL PENUMBRA—MOLECULAR PENUMBRAS DEFINED ON THE BASIS OF GENE EXPRESSION

Selective Neuronal Cell Death–TUNEL/Apoptotic Cell Death–Apoptosis Genes

Selective neuronal cell death has been described following global ischemia, with the death of CA1 pyramidal neurons being particularly well studied (67,68). However, selective neuronal cell death also occurs following focal ischemia. Hematoxylin and eosin staining show eosinophillic neurons within a few millimeters of focal infarction. More recently, TUNEL staining has demonstrated that isolated neurons at the edges of focal infarction can demonstrate DNA fragmentation (69). Figure 12 shows this zone of isolated cell death as being adjacent to the infarction but well within the "clinical penumbra." Whether these cells are apoptotic are not still remains uncertain.

In any case, the TUNEL staining clearly demonstrates that there is selective neuronal cell death in a small rim surrounding a focal infarction. These TUNEL positive cells, generally, do not express Hsp70 protein. However, some of these cells and perhaps other cells outside the infarction express genes and proteins that are involved in apoptotic cascades including caspases, other pro-apoptotic genes, anti-apoptotic genes, as well as genes involved in DNA repair (7,36,69–71).

Hypoxia and Hypoxia Inducible Factors—Hypoxia-Inducible Factor-1α and Hypoxia-Inducible Factor-2α

Hypoxia-inducible factor (HIF) plays a key role in regulating transcriptional responses to hypoxia. The role of HIF in hypoxia responses in brain (72) and other tissues (73,74) has recently been reviewed and will not be repeated here. HIF is clearly a major regulator of transcription and translation following stroke, however.

HIF-1β, also called ARNT, is expressed constitutively. With hypoxia, HIF-1α and HIF-2α are stabilized and bind HIF-1β. This dimer binds to HIF binding sites in target genes. HIF-1α is expressed by neurons and glia and HIF-2α appears to be expressed by vascular cells, and both have different target genes and likely different responses to hypoxia. Following focal ischemia in brain, HIF expression occurs inside as well as outside the area of focal ischemia and likely responds not only to hypoxia but to trophic factors like insulin-like growth factor (75–77). This explains why HIF expression not only occurs in regions that include the penumbra but also well outside the penumbra. This also explains why HIF is induced for some time following global ischemia when blood flow is restored and the brain is no longer hypoxic (77). Even though HIF expression does not correlate with the penumbra, or even the hypoxic penumbra (Fig. 12), HIF does play a role in inducing a variety of hypoxia-inducible genes that are responsible for producing angiogenesis and protecting against subsequent ischemia (Fig. 13) (72,77,78).

Genes Induced by Inflammation, Spreading Depression, Depolarization, and Trophic or Loss of Trophic Factors—c-Fos and Others

There is an enormous literature on the inflammatory response to stroke, and on the genes related to the inflammatory and immune changes (79–82,83). The central role of TNFs and NFkB is shown in Figure 14. The relation of the inflammatory response to the "clinical penumbra" is not entirely clear. For one, the ischemic core is, eventually, removed by microglia and macrophages so that inflammation is mainly a hallmark of the core rather than the penumbra. However, cells that die within the core have processes that often extend into the adjacent cortex or other brain regions, and these dying processes are also subject to scavenging by microglia and other cells (84). Indeed, microglial proliferation can occur for months following stroke in a variety of models, and at some distance even into spinal cord, where cortical pyramidal neurons can project (85).

A consistent finding in all focal ischemia studies has been the induction of c-fos, NGFIA, and other selected transcription factors throughout an ischemic hemisphere (86–89,4). C-fos is induced in the entire MCA territory as well as in cingulated cortex, frontal cortex, and occipital cortex (86). Because of the widespread induction of the gene, it was assumed that it was due to spreading depression. In addition, application of potassium chloride to cortex and focal cortical injuries, similarly, induced c-fos throughout the hemisphere, further supporting spreading depression as the mechanism of c-fos induction (90). Lastly, prior administration of NMDA antagonists, like MK801, was shown to block ischemia-induced spreading depression, and they blocked the whole hemisphere induction of c-fos produced by focal ischemia (86).

Equally importantly, we and others showed that focal ischemia could also induce c-fos and other immediate early genes in hippocampus, thalamus, substantia nigra, contralateral cortex, and in the cerebellum (4,6,7).

This induction in multiple regions outside the areas of middle cerebral ischemia was postulated to be due to activation of pathways in and around the ischemic cortex, and that this activated structures anatomically connected to the ischemic region via NMDA receptors. This was again tested by the prior administration of NMDA antagonists. Prior administration of NMDA antagonists prevented the distant induction of c-fos in hippocampus, thalamus, and contralateral cortex (86). They did not block c-fos induction in substantia nigra. This data suggests that cortical outputs from ischemic and peri-ischemic cortex activated neurons in distant regions via NMDA receptors and induced c-fos in these regions. Such activation was blocked by NMDA receptor antagonists. The failure to block activation in substantia nigra suggests that alternative pathways like GABAergic pathways were involved, that is, loss of GABAergic inhibitory pathways that led to c-fos induction in nigra, cerebellum, and other brain regions.

This distant induction of transcription factors could form the basis for plasticity observed around focal ischemic regions in rodent, primate, and human cortex, and could form a molecular basis for altered patterns of blood flow activation in cortex and subcortical regions following stroke (Fig. 15). Spreading depression does occur in human cortex, though it is not likely that this progresses throughout a hemisphere because of the presence of cortical gyri. However, it is possible that spreading depression could progress down a gyrus, and that activation of corticofugal pathways to adjacent gyri, the opposite cortex, and to subcortical structures could mediate long-term changes of gene expression in those structures and promote the plasticity noted following ischemic brain injury (Fig. 15). Though these changes of gene expression are clearly important in the brain response to injury, they are generally not indicative of the location of the penumbra or even the status of the penumbra.

Penumbra Concept and Biology—Why Is It Important?

Perhaps the most surprising conclusion of this chapter is that though there have been a very large number of studies of gene expression in the brain, relatively few of these have focused on changes of gene expression that occur just in the "clinical penumbra." Though many of the changes of gene expression mentioned earlier occur inside and outside of the penumbra, gene expression studies that are specific for the "salvageable" or "clinical penumbra" might provide better means of salvaging the penumbra during focal ischemia.

REFERENCES

1. Tang Y, Lu A, Aronow BJ, et al. Genomic responses of the brain to ischemic stroke, intracerebral haemorrhage, kainate seizures, hypoglycemia, and hypoxia. Eur J Neurosci 2002; 15:1937–1952.
2. Read SJ, Parsons AA, Harrison DC, et al. Stroke genomics: approaches to identify, validate, and understand ischemic stroke gene expression. J Cereb Blood Flow Metab 2001; 21:755–778.
3. Jin K, Mao XO, Eshoo MW, et al. Microarray analysis of hippocampal gene expression in global cerebral ischemia. Ann Neurol 2001; 50:93–103.
4. Koistinaho J, Hokfelt T. Altered gene expression in brain ischemia. Neuroreport 1997; 8:i–viii.
5. Lu A, Tang Y, Ran R, et al. Genomics of the periinfarction cortex after focal cerebral ischemia. J Cereb Blood Flow Metab 2003; 23:786–810.
6. Kinouchi H, Sharp FR, Chan PH, et al. Induction of c-fos, junB, c-jun, and hsp70 mRNA in cortex, thalamus, basal ganglia, and hippocampus following middle cerebral artery occlusion. J Cereb Blood Flow Metab 1994; 14:808–817.
7. Sharp FR, Lu A, Tang Y, Millhorn DE. Multiple molecular penumbras after focal cerebral ischemia. J Cereb Blood Flow Metab 2000; 20:1011–1032.
8. Hossmann KA. Viability thresholds and the penumbra of focal ischemia. Ann Neurol 1994; 36:557–565.
9. Krause GS, Tiffany BR. Suppression of protein synthesis in the reperfused brain. Stroke 1993; 24: 747–755; discussion 755–746.
10. Hata R, Mies G, Wiessner C, Hossmann KA. Differential expression of c-fos and hsp72 mRNA in focal cerebral ischemia of mice. Neuroreport 1998; 9:27–32.
11. DeGracia DJ, Montie HL. Cerebral ischemia and the unfolded protein response. J Neurochem 2004; 91:1–8.
12. Kaufman RJ. Regulation of mRNA translation by protein folding in the endoplasmic reticulum. Trends Biochem Sci 2004; 29:152–158.
13. Hata R, Maeda K, Hermann D, et al. Dynamics of regional brain metabolism and gene expression after middle cerebral artery occlusion in mice. J Cereb Blood Flow Metab 2000; 20:306–315.
14. Hata R, Maeda K, Hermann D, et al. Evolution of brain infarction after transient focal cerebral ischemia in mice. J Cereb Blood Flow Metab 2000; 20:937–946.
15. Kleihues P, Hossmann K, -A. Protein synthesis in the cat brain after prolonged cerebral ischemia. Brain Research 1971; 35:409–418.
16. Hossmann KA. Disturbances of cerebral protein synthesis and ischemic cell death. Prog Brain Res 1993; 96:161–177.
17. Mies G, Paschen W, Ebhardt G, Hossmann KA. Relationship between of blood flow, glucose metabolism, protein synthesis, glucose and ATP content in experimentally-induced glioma (RG1 2.2) of rat brain. J Neurooncol 1990; 9:17–28.
18. Dienel GA, Pulsinelli WA, Duffy TE. Regional protein synthesis in rat brain following acute hemispheric ischemia. J Neurochem 1980; 35:1216–1226.
19. Bergstedt K, Hu BR, Wieloch T. Postischaemic changes in protein synthesis in the rat brain: effects of hypothermia. Exp Brain Res 1993; 95:91–99.
20. Kiessling M, Dienel GA, Jacewicz M, Pulsinelli WA. Protein synthesis in postischemic rat brain: a two-dimensional electrophoretic analysis. J Cereb Blood Flow Metab 1986; 6:642–649.
21. Hossmann KA. Viability thresholds and the penumbra of focal ischemia [see comments]. Ann Neurol 1994; 36:557–565.
22. DeGracia DJ, Kumar R, Owen CR, et al. Molecular pathways of protein synthesis inhibition during brain reperfusion: implications for neuronal survival or death. J Cereb Blood Flow Metab 2002; 22:127–141.
23. Kiessling M, Auer RN, Kleihues P, Siesjo BK. Cerebral protein synthesis during long-term recovery from severe hypoglycemia. J Cereb Blood Flow Metab 1986; 6:42–51.
24. Boyce M, Bryant KF, Jousse C, et al. A selective inhibitor of eIF2alpha dephosphorylation protects cells from ER stress. Science 2005; 307:935–939.
25. Schroder M, Kaufman RJ. The mammalian unfolded protein response. Annu Rev Biochem 2005; 74:739–789.
26. Hu BR, Wieloch T. Stress-induced inhibition of protein synthesis initiation: modulation of initiation factor 2 and guanine nucleotide exchange factor activities following transient cerebral ischemia in the rat. J Neurosci 1993; 13:1830–1838.
27. Paschen W. Disturbances of calcium homeostasis within the endoplasmic reticulum may contribute to the development of ischemic-cell damage. Med Hypotheses 1996; 47:283–288.
28. Paschen W, Gissel C, Linden T, et al. Activation of gadd153 expression through transient cerebral ischemia: evidence that ischemia causes endoplasmic reticulum dysfunction. Brain Res Mol Brain Res 1998; 60:115–122.
29. Kaufman RJ, Scheuner D, Schroder M, et al. The unfolded protein response in nutrient sensing and differentiation. Nat Rev Mol Cell Biol 2002; 3:411–421.
30. Mies G, Ishimaru S, Xie Y, et al. Ischemic thresholds of cerebral protein synthesis and energy state following middle cerebral artery occlusion in rat. J Cereb Blood Flow Metab 1991; 11:753–761.

31. Rutkowski DT, Kaufman RJ. A trip to the ER: coping with stress. Trends Cell Biol 2004; 14:20–28.
32. Lindquist S, Craig EA. The heat-shock proteins. Annu Rev Genet 1988; 22:631–677.
33. Lindquist S, Kim G. Heat-shock protein 104 expression is sufficient for thermotolerance in yeast. Proc Natl Acad Sci USA 1996; 93:5301–5306.
34. Craig EA, Gambill BD, Nelson RJ. Heat shock proteins: molecular chaperones of protein biogenesis. Microbiol Rev 1993; 57:402–414.
35. Massa SM, Swanson RA, Sharp FR. Stress gene expression in brain. Cerebrovasc Brain Metab Rev 1996; 8:95–158.
36. Yenari MA. Heat shock proteins and neuroprotection. Adv Exp Med Biol 2002; 513:281–299.
37. Beckmann RP, Mizzen LE, Welch WJ. Interaction of Hsp 70 with newly synthesized proteins: implications for protein folding and assembly. Science 1990; 248:850–854.
38. Beckmann RP, Lovett M, Welch WJ. Examining the function and regulation of hsp 70 in cells subjected to metabolic stress. J Cell Biol 1992; 117:1137–1150.
39. Welch WJ. Heat shock proteins functioning as molecular chaperones: their roles in normal and stressed cells. Philos Trans R Soc Lond B Biol Sci 1993; 339:327–333.
40. Welch WJ, Brown CR. Influence of molecular and chemical chaperones on protein folding [published erratum appears in Cell Stress Chaperones 1996; 1(3):207]. Cell Stress Chaperones 1996; 1:109–115.
41. Hohfeld J, Cyr DM, Patterson C. From the cradle to the grave: molecular chaperones that may choose between folding and degradation. EMBO Rep 2001; 2:885–890.
42. Kinouchi H, Sharp FR, Koistinaho J, et al. Induction of heat shock hsp70 mRNA and HSP70 kDa protein in neurons in the 'penumbra' following focal cerebral ischemia in the rat. Brain Res 1993; 619:334–338.
43. Kinouchi H, Sharp FR, Hill MP, et al. Induction of 70-kDa heat shock protein and hsp70 mRNA following transient focal cerebral ischemia in the rat. J Cereb Blood Flow Metab 1993; 13:105–115.
44. Yenari MA, Giffard RG, Sapolsky RM, Steinberg GK. The neuroprotective potential of heat shock protein 70 (HSP70). Mol Med Today 1999; 5:525–531.
45. Rajdev S, Hara K, Kokubo Y, et al. Mice overexpressing rat heat shock protein 70 are protected against cerebral infarction. Ann Neurol 2000; 47:782–791.
46. Beere HM, Wolf BB, Cain K, et al. Heat-shock protein 70 inhibits apoptosis by preventing recruitment of procaspase-9 to the Apaf-1 apoptosome. Nat Cell Biol 2000; 2:469–475.
47. Beere HM, Green DR. Stress management—heat shock protein-70 and the regulation of apoptosis. Trends Cell Biol 2001; 11(1):6–10.
48. Beere HM. "The stress of dying": the role of heat shock proteins in the regulation of apoptosis. J Cell Sci 2004; 117:2641–2651.
49. Ravagnan L, Gurbuxani S, Susin SA, et al. Heat-shock protein 70 antagonizes apoptosis-inducing factor. Nat Cell Biol 2001; 3:839–843.
50. Ran R, Zhou G, Lu A, et al. Hsp70 mutant proteins modulate additional apoptotic pathways and improve cell survival. Cell Stress Chaperones 2004; 9:229–242.
51. Sharp FR, Massa SM, Swanson RA. Heat-shock protein protection. Trends Neurosci 1999; 22:97–99.
52. Ran R, Lu A, Zhang L, et al. Hsp70 promotes TNF-mediated apoptosis by binding IKK gamma and impairing NF-kappa B survival signaling. Genes Dev 2004; 18:1466–1481.
53. Plumier JC, Armstrong JN, Landry J, et al. Expression of the 27,000 mol. wt heat shock protein following kainic acid-induced status epilepticus in the rat. Neuroscience 1996; 75:849–856.
54. Plumier JC, Armstrong JN, Wood NI, et al. Differential expression of c-fos, Hsp70 and Hsp27 after photothrombotic injury in the rat brain. Brain Res Mol Brain Res 1997; 45:239–246.
55. Currie RW, Ellison JA, White RF, et al. Benign focal ischemic preconditioning induces neuronal Hsp70 and prolonged astrogliosis with expression of Hsp27. Brain Res 2000; 863:169–181.
56. Badin RA, Lythgoe MF, van der Weerd L, et al. Neuroprotective effects of virally delivered HSPs in experimental stroke. J Cereb Blood Flow Metab 2006; 26(3): 371–381.
57. Kabakov AE, Budagova KR, Bryantsev AL, Latchman DS. Heat shock protein 70 or heat shock protein 27 overexpressed in human endothelial cells during posthypoxic reoxygenation can protect from delayed apoptosis. Cell Stress Chaperones 2003; 8:335–347.
58. Garrido C, Bruey JM, Fromentin A, et al. HSP27 inhibits cytochrome c-dependent activation of procaspase-9. Faseb J 1999; 13:2061–2070.
59. Garrido C, Gurbuxani S, Ravagnan L, Kroemer G. Heat shock proteins: endogenous modulators of apoptotic cell death. Biochem Biophys Res Commun 2001; 286:433–442.
60. Nimura T, Weinstein PR, Massa SM, et al. Heme oxygenase-1 (HO-1) protein induction in rat brain following focal ischemia. Brain Res Mol Brain Res 1996; 37:201–208.
61. Wagner KR, Sharp FR, Ardizzone TD, et al. Heme and iron metabolism: role in cerebral hemorrhage. J Cereb Blood Flow Metab 2003; 23:629–652.
62. Sharp FR, Kinouchi H, Koistinaho J, et al. HSP70 heat shock gene regulation during ischemia. Stroke 1993; 24:I72–75.
63. Dubaquie Y, Looser R, Rospert S. Significance of chaperonin 10-mediated inhibition of ATP hydrolysis by chaperonin 60. Proc Natl Acad Sci USA 1997; 94:9011–9016.
64. Bukau B, Horwich AL. The Hsp70 and Hsp60 chaperone machines. Cell 1998; 92:351–366.

65. Martin J. Molecular chaperones and mitochondrial protein folding. J Bioenerg Biomembr 1997; 29:35–43.
66. Voos W, Rottgers K. Molecular chaperones as essential mediators of mitochondrial biogenesis. Biochim Biophys Acta 2002; 1592:51–62.
67. Ito U, Spatz M, Walker JT Jr, Klatzo I. Experimental cerebral ischemia in mongolian gerbils. I. Light microscopic observations. Acta Neuropathol (Berl) 1975; 32:209–223.
68. Kirino T. Delayed neuronal death in the gerbil hippocampus following ischemia. Brain Res 1982; 239:57–69.
69. Graham SH, Chen J. Programmed cell death in cerebral ischemia. J Cereb Blood Flow Metab 2001; 21:99–109.
70. Chen D, Minami M, Henshall DC, et al. Upregulation of mitochondrial base-excision repair capability within rat brain after brief ischemia. J Cereb Blood Flow Metab 2003; 23:88–98.
71. Martin LJ. Neuronal cell death in nervous system development, disease, and injury (Review). Int J Mol Med 2001; 7:455–478.
72. Sharp FR, Bernaudin M. HIF1 and oxygen sensing in the brain. Nat Rev Neurosci 2004; 5:437–448.
73. Ratcliffe PJ. New insights into an enigmatic tumour suppressor. Nat Cell Biol 2003; 5:7–8.
74. Semenza GL. Angiogenesis in ischemic and neoplastic disorders. Ann Rev Med 2003; 54:17–28.
75. Bergeron M, Yu AY, Solway KS, Semenza GL, Sharp FR. Upregulation of hypoxia inducible factor-1 (HIF-1) and its target genes following focal ischemia in rat brain. European J Neuroscience 1999; 11(12):4159–4170.
76. Bergeron M, Gidday JM, Yu AY, et al. Role of hypoxia-inducible factor-1 in hypoxia-induced ischemic tolerance in neonatal rat brain [In Process Citation]. Ann Neurol 2000; 48:285–296.
77. Chavez JC, LaManna JC. Activation of hypoxia-inducible factor-1 in the rat cerebral cortex after transient global ischemia: potential role of insulin-like growth factor-1. J Neurosci 2002; 22:8922–8931.
78. Pichiule P, Agani F, Chavez JC, et al. HIF-1 alpha and VEGF expression after transient global cerebral ischemia. Adv Exp Med Biol 2003; 530:611–617.
79. del Zoppo GJ, Becker KJ, Hallenbeck JM. Inflammation after stroke: is it harmful? Arch Neurol 2001; 58:669–672.
80. Dirnagl U, Iadecola C, Moskowitz MA. Pathobiology of ischaemic stroke: an integrated view. Trends Neurosci 1999; 22:391–397.
81. Feuerstein GZ, Liu T, Barone FC. Cytokines, inflammation, and brain injury: role of tumor necrosis factor-alpha. Cerebrovasc Brain Metab Rev 1994; 6:341–360.
82. Hallenbeck JM. Significance of the inflammatory response in brain ischemia. Acta Neurochir Suppl (Wien) 1996; 66:27–31.
83. Iadecola C, Alexander M. Cerebral ischemia and inflammation. Curr Opin Neurol 2001; 14:89–94.
84. Liu J, Lu AG, Sharp FR. Microglia/macrophages proliferate in striatum and neocortex but not hippocampus following brief global ischemia that produces ischemic tolerance in gerbil brain. J Cereb Blood Flow Metab 2001; 21(4):361–373.
The protease thrombin is an e...[PMID:10681455]Related Articles, Links
85. Streit WJ. Microglial response to brain injury: a brief synopsis. Toxicol Pathol 2000; 28:28–30.
86. Kinouchi H, Sharp FR, Chan PH, et al. MK-801 inhibits the induction of immediate early genes in cerebral cortex, thalamus, and hippocampus, but not in substantia nigra following middle cerebral artery occlusion. Neurosci Lett 1994; 179:111–114.
87. Kinouchi H, Sharp FR, Chan PH, et al. Induction of NGFI-A mRNA following middle cerebral artery occlusion in rats: in situ hybridization study. Neurosci Lett 1994; 171:163–166.
88. Honkaniemi J, Sagar SM, Pyykonen I, et al. Focal brain injury induces multiple immediate early genes encoding zinc finger transcription factors. Brain Res Mol Brain Res 1995; 28:157–163.
89. Honkaniemi J, States BA, Weinstein PR, et al. Expression of zinc finger immediate early genes in rat brain after permanent middle cerebral artery occlusion. J Cereb Blood Flow Metab 1997; 17:636–646.
90. Koistinaho J, Pasonen S, Yrjanheikki J, Chan PH. Spreading depression-induced gene expression is regulated by plasma glucose. Stroke 1999; 30:114–119.

8 Selective Neuronal Loss

Anthony J. Strong
Department of Clinical Neuroscience, King's College London, London, U.K.

Anna M. Planas
Institute for Biomedical Research of Barcelona (IIBB)–Spanish Research Council (CSIC), Institut d'Investigacions Biomèdiques August Pi I Sunyer (IDIBAPS), Barcelona, Spain

INTRODUCTION

"Selective neuronal necrosis" is a recurrent theme in studies of the neuropathological effects of cerebral ischemia. There is more than one basis for the term "selective," where a lesion falls short of pan-necrosis, and all of these need to be considered. Selective necrosis may be in the anatomical, cytological, or neurochemical domains, and in the context of ischemic penumbra, each of these requires discussion. In addition, neurones may be lost not only through energy failure (necrosis) but also through execution of cell death pathways—apoptosis. Thus the focus of this chapter is on selective neuronal loss, by either mechanism, occurring in a selected group of contexts in which one or more cellular elements in the region affected are not destroyed by the lesion.

We shall first describe the microscopic appearances obtained from a group of histological methods, and then consider the underlying pathological mechanisms.

HISTOLOGICAL FEATURES OF SELECTIVE NEURONAL NECROSIS IN THE ISCHEMIC PENUMBRA

Acute Changes—"Classical" Staining Methods

A convenient starting point is to review the conventional (hematoxylin and eosin or cresyl fast violet) histopathology of core and penumbral lesions as recorded after, for example, two hours of experimental, permanent occlusion of the middle cerebral artery (MCAO) in the gyrencephalic brain (cat) (Figs. 1 and 2). In cerebral cortex properly perfusion-fixed under these conditions, Tomlinson (1) was able to distinguish clearly between the appearances of core ischemia and changes in the penumbra. In a core gyrus (identified as such by sustained, terminal depolarization for 15–120 minutes, and exemplified by the ectosylvian gyrus) gross ischemic neuronal damage was present. Neuronal cell bodies were shrunken and usually triangular in shape, and the density of nuclei and cytoplasm was increased; there was cytoplasmic microvacuolation, corresponding to severe mitochondrial swelling, which was observed on electron microscopy. There was widespread and intense perineuronal vacuolation, with "scalloping" of neuronal outlines; the appearances suggested swelling of glial processes adjacent to neurons. On the next peripheral gyrus in the MCA territory, there was patchy or scattered ischemic change. Appearances of individual neurones resembled those observed in the proximal core. The appearances in the outer penumbra gyrus were rarely normal. In most experiments, scalloped neurones with perineuronal vacuolation were seen in two types of distribution: either (*i*) isolated or in laminar distribution, or (*ii*) concentrated in foci measuring some 500μm in diameter (Fig. 3). This distribution corresponds closely with that seen in recent studies using ab38 immunocytochemistry (see next section).

Acute Changes: Immunocytochemistry

Patel et al. have had some success, admittedly variable, with the use of immunocytochemical staining with ab38, an antibody to a heptapeptide breakdown product of the subplasmalemmal cytoskeletal protein spectrin (Fig. 4) (2). Immunoreactivity is believed to indicate upregulation

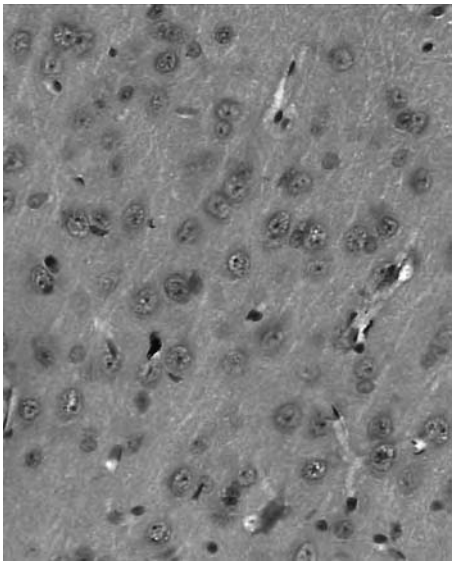

FIGURE 1 20-micron section of control hemisphere after two hours' contralateral middle cerebral artery occlusion (hematoxylin and eosin). Note full staining of neuropil adjacent to essentially all neurons, confirming absence of any perineuronal vacuolation.

of calpains (3). In cats undergoing permanent MCAO, appearances in core and penumbral gyri differed greatly. In the outer and intermediate penumbra, small clusters of pyramidal neurons of layer III were stained, each neuron quite uniformly, together with its axon and apical dendrite. Neurons from other layers were spared, and staining was confined to the clusters, which were present in apparently random foci on the marginal gyrus (outer penumbra in this species). In the ab38-positive neurons, the plasmalemma appeared intact since the reaction was confined to neurons and their processes. In the core territory, all cells and processes were heavily stained, and cell bodies could no longer be distinguished from the extracellular space—implying generalized cell membrane disruption. The interpretation of these appearances is best considered in conjunction with the electrophysiological and hemodynamic substrate for the pathology (see section "Initial Pathophysiological Mechanisms Leading to Morphological Change").

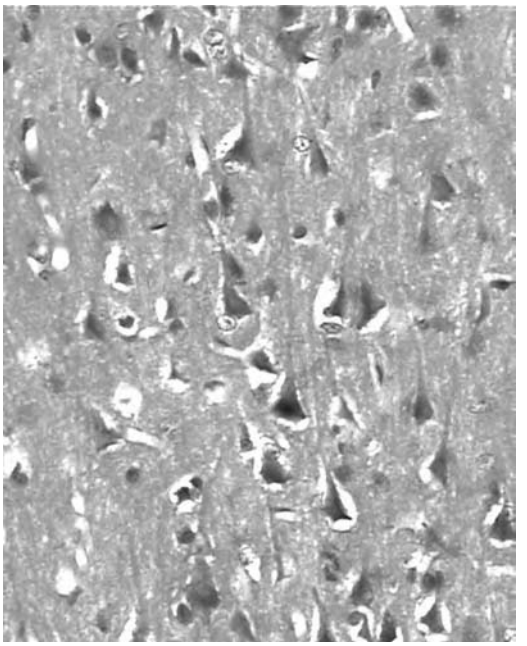

FIGURE 2 Section from core territory two hours after middle cerebral artery occlusion (hematoxylin and eosin). There is widespread intense perineuronal vacuolation, suggesting swelling of glial processes, with shrunken, hyperchromatic cell bodies, and interstitial edema in the neuropil.

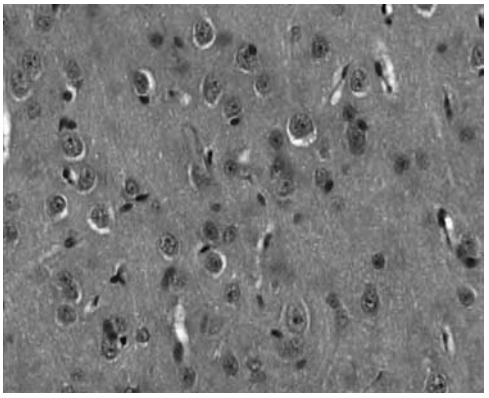

FIGURE 3 Section from outer penumbra two hours after middle cerebral artery occlusion (hematoxylin and eosin), showing several neurons with early perineuronal vacuolation, but no interstitial edema in neuropil.

Immunostaining and in situ hybridization methods have shown that the 70-kDa inducible heat-shock protein (Hsp70) is an excellent marker specifically of penumbral neurons in rodent models of middle cerebral artery occlusion (MCAO). It was first described that neurons with a healthy-looking morphology located at the margin of the ischemic core expressed Hsp70 (4,5). This is a protein to which have been attributed antiapoptotic and protective properties (6). Yet, we now know that expression of Hsp70 does not invariably protect neurons from death (7). Hsp70 mRNA is strongly induced when protein synthesis is inhibited (7,8). Protein synthesis is one of the parameters that is most sensitive to local blood flow (CBF) reductions (9). The process of assembly of amino acids in the ribosomes is rapidly inhibited in response to small CBF reductions, through a complex mechanism regulated, amongst others, by phosphorylation–dephosphorylation of translation initiation and elongation factors (10). This can be a reversible inhibition and can be regarded as a mechanism to prevent the formation of aberrant proteins, as well as a mechanism to save energy—as translation is a highly energy-consuming process. Local rates of cerebral protein synthesis (CPS) are inhibited in the penumbra, while ATP levels are still maintained; according to these findings, the zone of "mismatch" between CPS inhibition and ATP reduction is associated with penumbra (11). It is precisely this "mismatch" zone where expression of Hsp70 mRNA is strongly induced, and thus Hsp70 can be taken as a marker of penumbra. At present Hsp70 expression can only be studied postmortem; therefore, it has to be studied in different groups of animals at different time points. This limitation precludes dynamic studies in single animals. In spite of this, the expression of Hsp70 at different time points in groups of animals shows that positive neurons die with time, and it shows different patterns of Hsp70 expression in different experimental models of ischemia (Fig. 5).

Definitive Infarct Distribution After the Acute Phase: The Penumbra as a Maturation Phenomenon in Permanent Middle Cerebral Artery Occlusion

In postmortem human autopsy material, Nedergaard, Vorstrup, and Astrup (12) assessed the pattern of neuronal loss at the edge of cerebral infarcts that involved cortex, and found little or

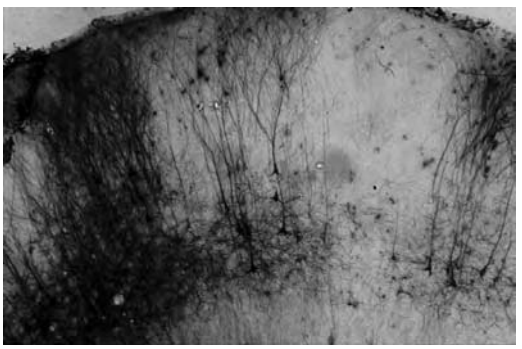

FIGURE 4 Section from outer penumbral cortex four hours after middle cerebral artery occlusion: immunocytochemistry with ab38, for a heptapeptide breakdown product of the subplasmalemmal cytoskeletal protein spectrin (a substrate for calpains). Individual neurones at intermediate depth, and their processes, are clearly stained, whereas islands of healthy (unstained) tissue survive intact at this time point.

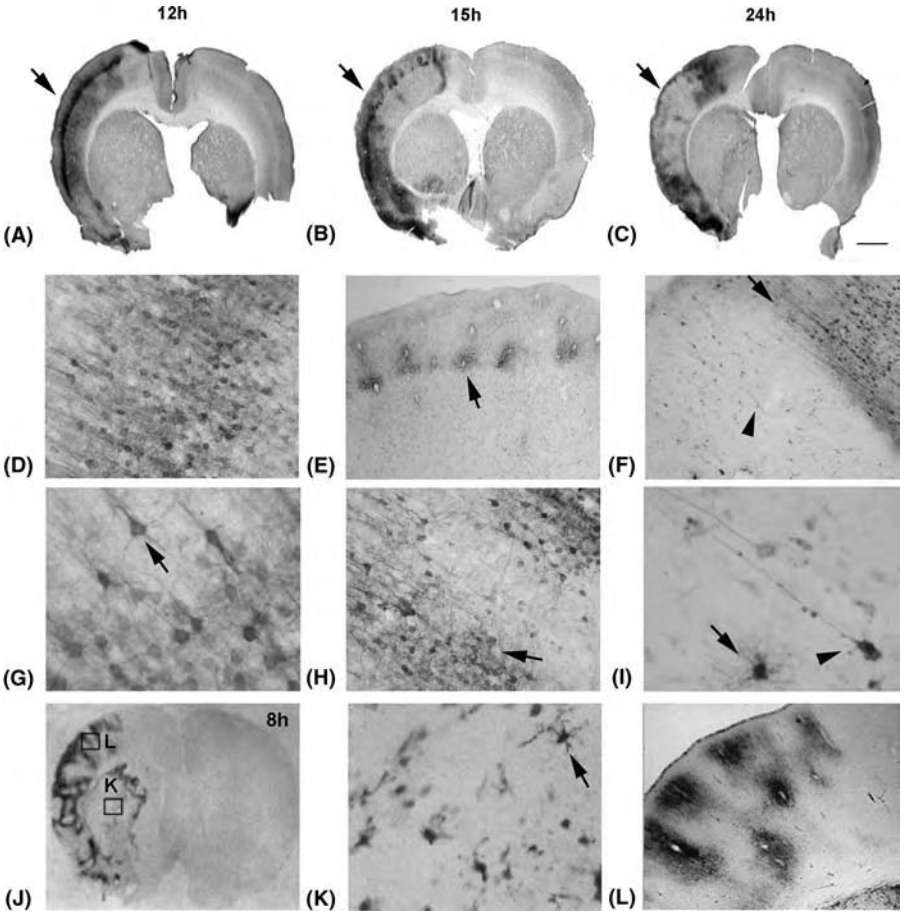

FIGURE 5 Expression of heat-shock proteins 70 at different reperfusion time points following one-hour middle cerebral artery occlusion (MCAO) in rats. Immunohistochemistry against Hsp70 using a mouse monoclonal antibody (Oncogene Research Products) at eight hours (**J–L**), 12 hours (**A,D,G**), 15 hours (**B,E,H**) and 24 hours (**C,F,I**) postischemia. (**A–I**) Intraluminal MCAO. (**J–L**) MCAO with craniectomy. (**A–C**) Macroscopic images of immunostained sections. Immunoreactivity progressively disappears in the ischemic core of the cortex (*arrow*). (**D,E**) Hsp70 immunoreactive neurons with a healthy-looking morphology are seen at 12 hours. (**E,H**) Bunches of immunoreactive neurons are seen, while immunoreactivity is lost in some zones. (**F,I**) A well-defined core area showing immunopositive endothelium (*arrowhead in* **F**), glial cells (*arrow in* **I**) and isolated shrunken neurons (*arrowhead in* **I**), is surrounded by a peripheral zone with strongly immunoreactive neurons (*arrow in* **F**). (**J–L**) Neuronal Hsp70 immunoreactivity affects heterogeneous areas in the cortex (**J,L**), but it is limited to a peripheral rim in the striatum, while its core shows mainly isolated reactive microglia (*arrow in* **K**). Scale bar: A–C, J = 2 mm; L = 750 µm; E = 400 µm; F = 100 µm. D, H = 50 µm; G, I = 25 µm; K = 20 µm.

no evidence of the graded pattern of neuronal loss seen in cats undergoing permanent MCAO for two hours. Rather, there was a sharp transition between core infarct and normal brain—very different from the pattern seen in the experimental penumbra. Several experimental studies have served to resolve this apparent contradiction. Saito et al. (13), studying the effects of pMCAO in cats anesthetized with chloralose, showed that the temporal pattern of recurrent spontaneous depolarizations—"peri-infarct depolarizations" (PIDs)—typical of the penumbra in experimental pMCAO was maintained in the outer penumbra for some 10 hours, but culminated around that time in permanent, "terminal" depolarization. Perfusion of this tissue, while little reduced one hour after occlusion, had fallen to well below the viability perfusion threshold [~16 mL/100 g/min (14)] by 14 hours. This can be considered a form of maturation or progressive degradation, and it has become clear from several experimental studies (reviewed in more detail in section "Initial Pathophysiological Mechanisms Leading to Morphological Change") that infarct size after pMCAO, typically at 24 hours, is a function of

number of PIDs, and that the PID number is the determining variable in this relationship. Conversely, neuroprotection with *n*-methyl–D-aspartate (NMDA) receptor antagonists in experimental pMCAO succeeds (15), very possibly through its capacity to reduce frequency of PIDs (16,17). The transition from laminar or patchy neuronal loss in the pMCAO penumbra to a discrete, stable infarct thus appears to represent a combined temporal and spatial progression, erratic rather than smooth, and not unlike the unsteady progress when the clues in a crossword puzzle are solved—some immediately, some much later, but eventually complete.

Penumbra as a Maturation Phenomenon: Delayed Necrosis as Seen in Rodent Models of Transient Focal Ischemia

Histological and Immunohistochemical Features (Heat Shock Protein 70)

Neuronal Hsp70 expression is hardly detected or it is limited to a very narrow rim surrounding the ischemic cortex and striatum after permanent MCAO in the rat, suggesting that penumbra is restricted to a small zone adjacent to the infarcted core in this model of ischemia. However, richer patterns of Hsp70 expression are observed in models of transient MCAO in the rat, particularly in the cortex. ATP levels recover once CBF is restored, but CPS remains inhibited in peripheral zones showing strong neuronal Hsp70 expression (18). Strictly speaking the area of mismatch between ATP and CPS at reperfusion is no longer the "penumbra," as the concept of penumbra according to the original definition by Astrup et al. (19) specifies loss of electrical activity but preservation of cellular ionic gradients during CBF reduction (see Chapters 2–5). Yet, the area of Hsp70 expression at reperfusion rather conforms to the concept of "tissue at risk" that we will also address in this chapter. This implies that there may be "tissue at risk," once perfusion has been restored, and that cells can progressively die during reperfusion, at least in the rodent model of MCAO. This is an interesting phenomenon that has only a few histological and molecular similarities to delayed neuronal death in the hippocampus after global ischemia. Hsp70 mRNA is abundant in the striatum shortly after one-hour transient MCAO, but after four hours it is restricted to a thin rim of tissue surrounding the ischemic core and resembling the expression pattern seen after permanent MCAO (7). This indicates that while striatal neurons may remain viable when circulation is restored after one-hour ischemia, they die after a few hours of reperfusion. This observation is compatible with the histopathology showing signs of neuronal death in the striatum already at four hours after one-hour MCAO (Fig. 6). A different situation is observed in the cortex, which shows a comparatively more delayed pattern of cell death after transient MCAO (20) (Fig. 6). Cortical Hsp70 expression in the rat brain varies, depending on the experimental model of MCAO. Direct occlusion of the MCA for one hour following craniotomy using the Tamura model (21) leads to a patchy pattern of Hsp70 protein expression in the cortex at 12 hours of reperfusion, while one-hour intraluminal MCAO (22) causes, at this time, a selective pattern of Hsp70 in different cortical layers (Fig. 5). Yet, in both situations by 24 hours Hsp70 is restricted to neurons in the periphery of the ischemic core (Fig. 5). Therefore, potentially viable neurons within the cortex will show delayed cell death mainly ongoing during the first 24 hours of reperfusion. The morphological features of this kind of cell death do not show many differences to typical ischemic necrotic cell death, but it is more delayed. Incomplete reperfusion, influence of a distorted environment caused by signals derived from dying neurons, either in the neighbourhood within the cortex or in the damaged striatum, or intracellular molecular alterations originated during ischemia and progressing with a slower pace, might account for this kind of cell death in the postischemic cortex. Whether this cell death could be prevented by therapeutic intervention remains to be seen. In favour of a possible rescue of these cortical neurons "at risk" is the observation than many drugs administered after transient ischemia can protect the cortex better than the striatum in rodents (23–29).

INITIAL PATHOPHYSIOLOGICAL MECHANISMS LEADING TO MORPHOLOGICAL CHANGE

Very early in studies of the pathophysiology of the penumbra with ion-selective microelectrodes, it became clear that transient increases in extracellular potassium occur spontaneously in the ischemic penumbra in primates: the resemblance of these events with Leão's cortical spreading depression (CSD) was noted (30). Findings in the cat were similar, and it seemed

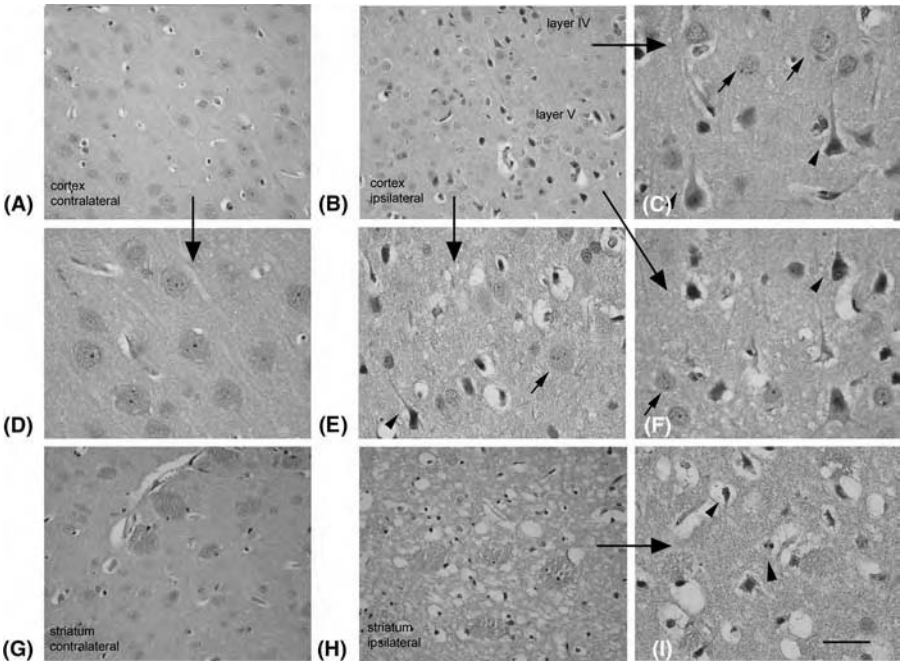

FIGURE 6 Histopathological features at 12 hours after one-hour intraluminal middle cerebral artery occlusion in rats: lesion progresses faster in striatum than in cortex. Hematoxylin and eosin staining of cortex (**A–F**) and striatum (**G–I**). Control cortex is shown in (**A**,**D**) and control striatum in G. (**B**,**C**,**E–F**) The ipsilateral cortex shows morphologically normal neurons (*arrows*) in close vicinity of shrunken neurons (*arrowheads*). The formation of vacuoles around some, but not all, neurons is apparent. (**G–I**) In the ispilateral striatum most neurons (*arrowheads*) are extremely shrunken, scalloped, and pyknotic. Intense vacuolation is seen in the neuropil, and neurons are always surrounded by a large vacuole. *Scale bar*: A–B, G–H = 50 μm; C–F= 25 μm.

possible that a relationship of lesion severity with degree of loss in ion homeostasis might exist and that the ion transients observed in focal cortical ischemia "were not entirely benign" (1). At its simplest, it seemed that recurrent depolarizations necessitate "futile" utilization of ATP, just when it is needed to be preserved the most.

Although the membrane cation conductance changes sustaining both CSD and PIDs, and the associated initial change in local DC or field potential of the cortex are thought to be similar in CSD and PID, their mode of induction and the responses of the microcirculation to these two events differ critically. Thus in healthy cortex, CSD has to be induced—with increasing difficulty in proportion to brain size—whereas PIDs are spontaneous events. Reflecting the energy demand for repolarization, cerebral metabolic glucose consumption rises after CSD by 77% (31), and oxygen consumption by 45% (32). In normally perfused cortex, a striking increase in blood flow—up to 200% to 250% (33)—is coupled to this higher energy utilization, to the extent that, for example, tissue oxygen tension increases (34). A number of gene expression cascades are initiated by CSD, principally immediate early genes such as *c-jun, c-fos*, and *hsp70* (see earlier), and also cytokines such as IL-1β and TNFα. MMP-9 is upregulated, leading to increased blood brain barrier permeability to Evans blue (35). This and IL-1β upregulation (36) suggest a potential adverse effect of CSD through promotion of vasogenic edema. Other work suggests, in contrast, that preconditioning the cerebral cortex of rats by induction of CSD confers protection against later ischemic challenges (37–40).

Since 1983, a very extensive literature on the properties of PIDs has accumulated, and has been reviewed elegantly by Hossmann (41). A cardinal feature of PIDs is the absence or marked attenuation of the hyperemic response that characterizes CSD (17,34), and there are fluctuations in the redox state of the brain during the passage of SD (42) indicating that the oxygen requirements might not be fulfilled, inducing anerobic glycolysis, and causing increased lactate and pH reduction (43). The reduced flow response to depolarization in the penumbra has been attributed

to the limited capacity of the leptomeningeal collateral circulation to compensate for the effects of a major afferent vessel occlusion. Resolution of the DC potential change is delayed, increasingly, so with time (17) and, under conditions of hypoxia and restricted glucose availability, the intracellular calcium transient is prolonged (44). The path is thus opened for initiation of intracellular cytotoxic cascades, and for mitochondrial damage to develop. That infarct size and PID number are related in linear fashion is well established (45). In an elegant subsequent study, Busch et al. induced depolarizations outside the penumbra, which propagated into the region and enlarged the infarct, thus demonstrating that PIDs are a cause rather than simply a marker of infarct expansion (46). Other work supports this concept (47,48). With the onset of anerobic glycolysis, ATP yield per mole glucose utilized falls to some 5% of the aerobic oxidative yield, and glucose utilization in the penumbra increases (49). The same authors predicted marked depletion of the cortical extracellular glucose pool under penumbral conditions, and the dependence of glucose flux into the brain on level of perfusion (50) supports their argument.

What factors initiate PIDs in the penumbra and determine their frequency? Introduction of imaging methods with sufficient temporal resolution to track optically detectable markers of depolarization, such as a change in NADH fluorescence, suggests that most events originate from the edge of a territory or focus that is permanently depolarized, that is, the core (51). It is reasonable to envisage that the high extracellular K^+ concentration in such an area, or perhaps high glutamate, initiates a PID in an adjacent, nondepolarized microfocus in which cation/glutamate homœostasis is unstable on account of energy compromise. Given the dependence of the ATP pool in penumbral cortex on anerobic glycolysis and hence on glucose availability through residual perfusion, the inverse relationship of frequency of PIDs with plasma glucose (52,53) is to be expected, and needs to be borne in mind when clinical management of acute cerebral ischemia with insulin is being considered (54). For the same reason, a further reduction in perfusion must necessarily have a similar, adverse effect on tissue glucose availability as a fall in plasma glucose.

DELAYED NECROSIS MECHANISMS: CORRELATION WITH MRI ALTERATIONS

In rats subjected to transient MCAO, PIDs occur soon after occlusion, but also after reperfusion (55). PIDs begin soon after the onset of ischemia and recur periodically during two-hour MCAO; this activity ceases at reperfusion and does not recur for the following six hours, but at eight hours there is a new wave of PID activity (the peak was at 12 hours and lasted up to 18 hours). The pattern was similar with pMCAO in these studies. According to our experience (56), this is the time-frame when the secondary fall in cortical apparent diffusion coefficient for water (ADC, measured with MRI) takes place in transient MCAO, concomitantly with the overt manifestation of cortical damage (triphenyl tetrazolium chloride, TTC, staining), and with the appearance of invariable histological signs of neuronal and astroglial cell death. It is tempting to hypothesize that this delayed recurrence of cortical PID may contribute to trigger the delayed cortical lesion.

During ischemia, cortical CBF drops and the ADC for water shows deep cortical hypointensity indicating a large area of "ischemic core." Besides the concept of mismatch between diffusion and perfusion as an indicator of tissue at risk during ischemia [taking into account its recognized limitations (57)], we learn from human (58) and rat (59) studies that early reperfusion can completely normalise ADC. Nevertheless, the rat studies have also shown that, after this apparent normalization, ADC can drop again later, and tissue damage becomes evident (60). Therefore, shortly after ischemia there might be "tissue at risk," even within the core zone, showing an ADC drop during ischemia. This tissue might recover some of the MRI alterations with early reperfusion, but it might later show features of cell death, as it occurs in the rat after one-hour MCA occlusion (56). First, MRI disturbances appear in the striatum and later in the cortex, in parallel with the manifestation of overt signs of neuronal and astroglial cell death (56).

It seems that in both permanent and transient ischemia with reperfusion, processes evolve—over a matter of hours in rats—that lead to a second phase of loss of cation or neurotransmitter homœostasis. It is tempting to suggest that this deterioration may be related to cytokine or other inflammatory mechanisms.

INVERSE (VASOCONSTRICTOR) RESPONSES OF PERFUSION TO DEPOLARIZATION: A NEW PROPERTY OF PIDS

Very recently, data from two research groups have appeared, indicating that PIDs are associated with active reductions in perfusion as they propagate in the penumbra both in the gyrencephalic (61) and lissencephalic (62) brains—the opposite of the normal, hyperemic response to CSD. This would indicate that PIDs are a considerably more important player in the evolution of focal cerebral cortical ischemic lesions than previously supposed. The findings resemble the well-documented descriptions of "cortical spreading ischemia" by Dreier et al., studying in rats the effects on cortical perfusion of superfusion with artificial CSF modified to simulate the likely cortical surface environment in patients developing delayed ischemic neurological deficit after aneurysmal subarachnoid hemorrhage (63). There is clear evidence in these papers that the perfusion loss reflects active vasoconstriction in response to the spreading depolarization.

APOPTOSIS AFTER NON-NECROTIC (SUBLETHAL) PERMANENT OR TRANSIENT ISCHEMIA

Focal ischemia leads to the appearance of signs of programmed cell death with some features resembling apoptotic cell death. Permanent focal ischemia involves the delayed (one day) appearance of cells that stain positive with the TUNEL technique, which labels fragmented DNA within the ischemic core (11). We now know that not all TUNEL+ cells comply with the criteria of apoptosis, as necrotic cells can also stain positive with this technique. Yet, the combination of this staining with signs of nuclear fragmentation and condensation are also apparent after focal ischemia in rodents (64). There appears to be a small fraction of cells with some features of apoptosis accompanying necrosis (11,18,64–66). For this reason it is feasible that necrotic cell death can itself induce changes in the environment contributing to secondary damage affecting more resistant cells, which would then develop cell death with features of apoptosis. Garcia et al. (20) described the presence of delayed (4–7 days) and selective neuronal necrosis after short (<25 minutes) episodes of transient MCAO, indicating that neuronal cell death is more discrete and progresses more slowly after mild ischemic insults, particularly in the cortex. The abundance of cells with signs of programmed cell death is inversely proportional to the duration of ischemia, that is, apoptotic-like cell death is more predominant after short periods of MCAO (10–30 minutes) than after longer occlusion times (67,68). Therefore, it appears that mild ischemic insults will predominantly cause programmed cell death, while more severe insults will predominantly cause necrosis, as can be seen with the differential rises of intracellular calcium (69). Also, in vitro observations under various circumstances suggest that the mode of cell death might depend on the energy supply and the intracellular ATP levels, as glucose can induce a switch from necrosis to apoptosis (70), while ATP depletion can induce a switch from apoptosis to necrosis (71).

Blood flow reductions compatible with penumbra flow (20–35 mL/100 g^{-1}/min^{-1}) lead to the appearance of cells with morphological features of programmed cell death (68); and signs of this form of cell death are observed shortly after ischemia in perifocal areas associated with penumbra (66). One of the classical signs of apoptosis is release of cytochrome-*c* from mitochondria to the cytoplasm, which leads to activation of caspase-9, followed by activation of the executor caspase-3 causing DNA cleavage. We found activation of this caspase-dependent intrinsic form of cell death in perifocal zones of the cortex at four hours, after one-hour MCAO (66,72), in agreement with other reports (73–77). The contribution of caspases to ischemic injury has been shown by administering caspase-inhibitors after transient ischemia (78), and in deficient mice (79). Also, we found that caspase-independent modes of programmed cell death, such as activation of the apoptosis-inducing factor (AIF) after mitochondrial release and translocation to cytosol and nucleus, occur in the PIA at early reperfusion times (66,72), in agreement with other reports (80,81).

Important modulators of mitochondrial cell death are members of the Bcl-2 family of proteins. Expression of Bcl-2 and Bcl-$_{XL}$ promotes cell survival and prevents apoptosis by preserving the integrity of the mitochondrial membrane (82). Bcl-2 can block the translocation of AIF and subsequent apoptosis after focal ischemia in the rat (83), while mitochondrial translocation of Bax and Bim promotes release of cytochrome-c and apoptosis (84–86). Because

of the extreme complexity of signals being activated in the PIA, including death and survival molecules, we envisage that a struggle between cell death and survival signals takes place in this zone and the final cellular outcome will likely depend on the fine balance amongst all of them (66). According to these findings, the evidence that mitochondrial release of pro-apoptotic factors that plays a role in neuronal cell death after ischemia is now growing (87–89), thus suggesting that programmed cell death might be an effective therapeutic target in cerebral ischemia. Yet, it is likely that the usefulness of this strategy in the acute phase might be limited to those situations where apoptosis plays a fundamental role, such as after mild episodes of transient ischemia. However, we now know that signs of programmed cell death, such as caspase-3 activation, occur in peri-infarct zones even at seven days after severe focal ischemia in rats (AMP: personal unpublished observations), suggesting that targeting apoptosis might prevent the progression of the necrotic injury toward the surrounding tissue over time.

REGIONAL AND NEUROCHEMICAL SELECTIVE VULNERABILITY

The clearest example of regional selectivity is neuronal cell death after global ischemia. A short episode of transient global ischemia causes selective neuronal death, particularly, affecting neurons in the CA1 and hilus of the hippocampus in the rat (90–92), in the Mongolian gerbil (93–96), and also in the cat (97). This particular kind of delayed cell death involves nuclear DNA fragmentation and shows some features of programmed cell death (98). Yet, the increase of extracellular glutamate after ischemia is similar in vulnerable CA1 and resistant CA3 regions (99), and the distribution of NMDA receptors cannot account for selective vulnerability either (100). CA1 neurons are selectively vulnerable to the damaging effect of superoxide (101), and have a low content of superoxide scavenging enzymes (102,103). Also, the CA1 sector has low activity of the mitochondrial respiratory enzyme succinate dehydrogenase (104), and a reduction of pyruvate-supported oxidative metabolism develops in mitochondria from areas sensitive to ischemia (105). All these particular features of CA1 pyramidal neurons might account for its selective vulnerability to ischemia. In addition, the activation of synaptic afferent pathways, particularly the septo-hippocampal pathway, is determinant for the ischemic CA1 lesion (106).

In animals, there is some further selectivity within CA1 neurons, as the most vulnerable cells are pyramidal projection neurons while GABAergic local-circuit neurons, which express the calcium-binding protein parvalbumin, are more resistant to ischemia in the gerbil (107–109), and some resistance has also been found in GABA interneurons of the rat hippocampus (110). Differential regional distribution and cellular density of excitatory amino acid receptors might account for this variability (111,112). Also, CA1 neurons surviving the ischemic insult coexpress the neurotrophin brain-derived neurotrophic factor (BDNF) and its receptor tyrosine protein kinase B (TrkB), suggesting that the BDNF/TrkB autocrine regulatory loop may be involved in cell survival after ischemia (113).

We have seen in previous sections that neuronal cell death after transient MCAO affecting cortex and striatum does not cause the same mode of cell death in both regions, as cortical neuronal death progresses more slowly than death of striatal neurons. This has been attributed to regional differences in vascular anatomy, allowing that collateral circulation results in a less dramatic perfusion deficit in the cortex than in the striatum during MCAO (114). However, the contribution of a particular intrinsic sensitivity of striatal tissue to ischemia cannot be excluded. Cortical GABAergic interneurons are resistant to ischemia induced by photothrombosis in rats (115). GABAergic and somatostatin-containing interneurons in the striatum are also more resistant to ischemia after 30-minutes MCAO in mice (116), and the proposed explanations are also related to the presence of calcium binding proteins and low density of glutamate receptors. Neurons containing NADPH-diaphorase, neuropeptide-Y, or somatostatin in the striatum are spared from the ischemic lesion in the gerbil after global ischemia (117). Furthermore, vulnerable (118) spiny neurons in the striatum show a pathological form of postischemic long-term synaptic potentiation (iLTP), which is triggered by energy deprivation. This is dependent on the activation of NMDA and AMPA receptors and the MAP kinase signaling pathway, and it might contribute to selective neuronal death as it does not occur in resistant (119) striatal cholinergic interneurons (120). These authors proposed that iLTP might be a synaptic mechanism causing a controlled long-term rise of intracellular calcium in spiny striatal neurons that might be

compatible with the induction of apoptosis. Taken altogether, the present findings suggest that there is an intrinsic cellular sensitivity depending on particular metabolic and neurochemical features, and on the availability of protective resources against the ischemic insult. Besides intrinsic cellular characteristics, the specific synaptic connections can also influence the cellular responses and may be involved in the generation of damage.

ANALOGUES OF PENUMBRA IN ISCHEMIC AND TRAUMATIC BRAIN INJURY IN HUMANS

Other chapters address the detection and characterization of the penumbra in patients with occlusive stroke. Subarachnoid hemorrhage from ruptured intracranial aneurysm (aSAH) and traumatic brain injury (TBI), especially when contusion or focal intracerebral hematoma is present, are additional clinical conditions in which it now seems that many of the lessons from experimental studies of the penumbra can be applied quite directly in clinical management of these conditions.

The basis for this statement is the recent emergence of clear evidence for the occurrence of SD in the injured brain. Strong et al. monitored the electrocorticogram (ECoG) for periods of up to five days, using subdural strips with a linear array of six electrodes placed on pericontusional cortex, in 14 patients undergoing surgery for evacuation of an intracerebral hematoma (121). They recorded spreading or synchronous, but transient episodes of complete ECoG suppression in 10 patients: the velocity of spread was close to that originally described by Leão (122). Subsequent development of the technology has allowed deconvolution of the ECoG signal to reveal underlying slow potential changes characteristic of a depolarization event—the cardinal feature of SD: in addition, features were identified, which serve to distinguish PID-like events from more normal SD (123). Most recently, the work has been extended to study patients requiring surgery for aSAH, with detection of SD or PID in the majority of patients (124) however, patients were selected partly on the basis of an urgent indication for surgery, and may not be entirely representative of good grade aSAH. The emerging data, if confirmed, amount to a demonstration of penumbral conditions in the (very restricted) area monitored, and raise the possibility that such conditions may apply wherever there is a significant accumulation of products of hemolysis, especially when spasm of the major branches of the Circle of Willis is also present. On the other hand, in the case of contusional brain injury, traumatic SAH is less common, and despite evidence for ischemia in this type of TBI (125), more recent quantitative imaging, of perfusion (126), or of selective fall in ADC for water (without an increase in the T_2-weighted signal) (127) in similar cases suggests that any ischemic penumbra surrounding a focus of contusion may be relatively narrow.

The group of investigators conducting these studies, (Co-Operative Study of Brain Injury Depolarizations, COSBID, www.cosbid.org), believe that results now emerging from the work will lead to adoption of monitoring and, perhaps, treatment routines in neurological critical care that target evolving pathophysiological processes with a new level of accuracy. The results increasingly confirm that many of the concepts that have been developed using in vivo experimental models can be applied in specific patients, if the pathophysiology has been properly defined with the new monitoring methods.

Acknowledgments

We thank Dr. Sara Patel for her substantial contribution to the ab38 work. AJS has received support from the UK Medical Research Council, The Wellcome Trust, The Community Fund (UK), GlaxoSmithKline, the Rosetrees Trust, and HeadFirst during the period covered by this review. AMP acknowledges grants from the Spanish "Comisión Interministerial de Ciencia y Tecnología" (SAF2002-01963) and "Fondo de Investigaciones Sanitarias" (FS041104-O and Red CIEN: IDIBAPS-ISCIII RTIC, C03/06).

REFERENCES

1. Strong AJ, Tomlinson BE, Venables GS, Gibson G, Hardy JA. The cortical ischaemic penumbra associated with occlusion of the middle cerebral artery in the cat: 2. Studies of histopathology, water content, and in vitro neurotransmitter uptake. J Cereb Blood Flow Metab 1983; 3:97–108.
2. Patel S, Charles K, Smith SE, et al. Calpain 1 activation and neuronal cell death in cats after 4 hours of unilateral permanent middle cerebral artery occlusion. J Cereb Blood Flow Metab 1997; 17(suppl 1):S256.

3. Roberts Lewis JM, Savage MJ, Marcy VR, Pinsker LR, Siman R. Immunolocalization of calpain I-mediated spectrin degradation to vulnerable neurons in the ischemic gerbil brain. J Neurosci 1994; 14:3934–3944.
4. Kinouchi H, Sharp FR, Hill MP, Koistinaho J, Sagar SM, Chan PH. Induction of 70-kDa heat shock protein and hsp70 mRNA following transient focal cerebral ischemia in the rat. J Cereb Blood Flow Metab 1993; 13:105–115.
5. Sanz O, Estrada A, Ferrer I, Planas AM. Differential cellular distribution and dynamics of HSP70, cyclooxygenase-2, and c-Fos in the rat brain after transient focal ischemia or kainic acid. Neurosci 1997; 80(1):221–232.
6. Lee SH, Kim M, Yoon BW, et al. Targeted hsp70.1 disruption increases infarction volume after focal cerebral ischemia in mice. Stroke 2001; 32(12):2905–2912.
7. Planas AM, Soriano MA, Estrada A, Sanz O, Martin F, Ferrer I. The heat shock stress response after brain lesions: induction of 72 kDa heat shock protein (cell types involved, axonal transport, transcriptional regulation) and protein synthesis inhibition. Prog Neurobiol 1997; 51:607–636.
8. Nowak TS Jr. Protein synthesis and the heart shock/stress response after ischemia. Cerebrovasc Brain Metab Rev 1990; 2(4):345–366.
9. Mies G, Ishimaru S, Xie Y, Seo K, Hossmann KA. Ischemic thresholds of cerebral protein synthesis and energy state following middle cerebral artery occlusion in rat. J Cereb Blood Flow Metab 1991; 11(5):753–761.
10. Krause GS, Tiffany BR. Suppression of protein synthesis in the reperfused brain. Stroke 1993; 24:747–755.
11. Hata R, Maeda K, Hermann D, Mies G, Hossmann KA. Dynamics of regional brain metabolism and gene expression after middle cerebral artery occlusion in mice. J Cereb Blood Flow Metab 2000; 20(2):306–315.
12. Nedergaard M, Vorstrup S, Astrup J. Cell density in the border zone around old small human brain infarcts. Stroke 1986; 17(6):1129–1137.
13. Saito R, Graf R, Hubel K, Fujita T, Rosner G, Heiss WD. Reduction of infarct volume by halothane: effect on cerebral blood flow or perifocal spreading depression-like depolarizations. J Cereb Blood Flow Metab 1997; 17(8):857–864.
14. Strong AJ, Venables GS, Gibson G. The cortical ischaemic penumbra associated with occlusion of the middle cerebral artery in the cat: 1. Topography of changes in blood flow, potassium ion activity, and EEG. J Cereb Blood Flow Metab 1983; 3:86–96.
15. Ozyurt E, Graham DI, Woodruff GN, McCulloch J. Protective effect of the glutamate antagonist, MK-801 in focal cerebral ischemia in the cat. J Cereb Blood Flow Metab 1988; 8:138–143.
16. Gill R, Andine P, Hillered L, Persson L, Hagberg H. The effect of MK-801 on cortical spreading depression in the penumbral zone following focal ischaemia in the rat. J Cereb Blood Flow Metab 1992; 12:371–379.
17. Iijima T, Mies G, Hossmann KA. Repeated negative DC deflections in rat cortex following middle cerebral artery occlusion are abolished by MK-801: effect on volume of ischemic injury. J Cereb Blood Flow Metab 1992; 12:727–733.
18. Hata R, Maeda K, Hermann D, Mies G, Hossmann KA. Evolution of brain infarction after transient focal cerebral ischemia in mice. J Cereb Blood Flow Metab 2000; 20:937–946.
19. Astrup J, Symon L, Branston NM, Lassen NA. Cortical evoked potential and extracellular K+ and H+ at critical levels of brain ischaemia. Stroke 1977; 8:51–57.
20. Garcia JH, Liu KF, Ye ZR, Gutierrez JA. Incomplete infarct and delayed neuronal death after transient middle cerebral artery occlusion in rats. Stroke 1997; 28:2303–2309.
21. Tamura A, Graham DI, McCulloch J, Teasdale GM. Focal cerebral ischaemia in the rat: 1. Description of technique and early neuropathological consequences following middle cerebral artery occlusion. J Cereb Blood Flow Metab 1981; 1:53–60.
22. Longa EZ, Weinstein PR, Carlson S, Cummins R. Reversible middle cerebral artery occlusion without craniectomy in rats. Stroke 1989; 20:84–91.
23. Belayev L, Khoutorova L, Zhang Y, et al. Caffeinol confers cortical but not subcortical neuroprotection after transient focal cerebral ischemia in rats. Brain Res 2004; 1008(2):278–283.
24. Harukuni I, Bhardwaj A, Shaivitz AB, et al. Sigma(1)-receptor ligand 4-phenyl-1-(4-phenylbutyl)-piperidine affords neuroprotection from focal ischemia with prolonged reperfusion. Stroke 2000; 31(4):976–982.
25. Iwashita A, Maemoto T, Nakada H, Shima I, Matsuoka N, Hisajima H. A novel potent radical scavenger, 8-(4-fluorophenyl)-2-((2E)-3-phenyl-2-propenoyl)-1,2,3,4-tetrahydropyrazol o[5,1-c] [1,2,4]triazine (FR210575), prevents neuronal cell death in cultured primary neurons and attenuates brain injury after focal ischemia in rats. J Pharmacol Exp Ther 2003; 307(3):961–968.
26. Justicia C, Perez-Asensio FJ, Burguete MC, Salom JB, Planas AM. Administration of transforming growth factor-alpha reduces infarct volume after transient focal cerebral ischemia in the rat. J Cereb Blood Flow Metab 2001; 21:1097–1104.
27. Schmid-Elsaesser R, Hungerhuber E, Zausinger S, Baethmann A, Reulen HJ. Neuroprotective effects of the novel brain-penetrating antioxidant U-101033E and the spin-trapping agent alpha-phenyl-N-tert-butyl nitrone (PBN). Exp Brain Res 2000; 130(1):60–66.

28. Shimizu K, Rajapakse N, Horiguchi T, Payne RM, Busija DW. Protective effect of a new nonpeptidyl mimetic of SOD, M40401, against focal cerebral ischemia in the rat. Brain Res 2003; 963(1–2):8–14.
29. Zausinger S, Lumenta DB, Pruneau D, Schmid-Elsaesser R, Plesnila N, Baethmann A. Therapeutical efficacy of a novel non-peptide bradykinin B2 receptor antagonist on brain edema formation and ischemic tissue damage in focal cerebral ischemia. Acta Neurochir Suppl 2003; 86:205–207.
30. Branston NM, Strong AJ, Symon L. Extracellular potassium activity, evoked potential and tissue blood flow: relationships during progressive ischaemia in baboon cerebral cortex. J Neurol Sci 1977; 32:305–321.
31. Kocher M. Metabolic and hemodynamic activation of postischemic rat brain by cortical spreading depression. J Cereb Blood Flow Metab 1990; 10(4):564–571.
32. Mayevsky A, Weiss HR. Cerebral blood flow and oxygen consumption in cortical spreading depression. J Cereb Blood Flow Metab 1991; 11(5):829–836.
33. Lauritzen M, Jorgensen MB, Diemer NH, Gjedde A, Hansen AJ. Persistent oligemia of rat cerebral cortex in the wake of spreading depression. Ann Neurol 1982; 12:469–474.
34. Back T, Kohno K, Hossmann KA. Cortical negative DC deflections following middle cerebral artery occlusion and KCl-induced spreading depression: effect on blood flow, tissue oxygenation, and electroencephalogram. J Cereb Blood Flow Metab 1994; 14:12–19.
35. Gursoy-Ozdemir Y, Qiu J, Matsuoka N, et al. Cortical spreading depression activates and upregulates MMP-9. J Clinic Invest 2004; 113(10):1447–1455.
36. Jander S, Schroeter M, Peters O, Witte OW, Stoll G. Cortical spreading depression induces proinflammatory cytokine gene expression in the rat brain. J Cereb Blood Flow Metab 2001; 21(3):218–225.
37. Kobayashi S, Harris VA, Welsh FA. Spreading depression induces tolerance of cortical neurons to ischemia in rat brain. J Cereb Blood Flow Metab 1995; 15:721–727.
38. Otori T, Greenberg JH, Welsh FA. Cortical spreading depression causes a long-lasting decrease in cerebral blood flow and induces tolerance to permanent focal ischemia in rat brain. J Cereb Blood Flow Metab 2003; 23(1):43–50.
39. Muramatsu H, Kariko K, Welsh FA. Induction of tolerance to focal ischemia in rat brain: dissociation between cortical lesioning and spreading depression. J Cereb Blood Flow Metab 2004; 24(10): 1167–1171.
40. Kariko K, Weissman D, Welsh FA. Inhibition of toll-like receptor and cytokine signaling—a unifying theme in ischemic tolerance. [Review] [170 refs]. J Cereb Blood Flow Metab 2004; 24(11):1288–1304.
41. Hossmann KA. Periinfarct depolarizations. [Review] [81 refs]. Cerebrovasc, Brain Metabol Rev 1996; 8(3):195–208.
42. Mayevsky A, Sclarksy DL. Correlation of brain NADH redox state, K+, PO2 and electrical activity during hypoxia, ischemia and spreading depression. Adv Exp Med Biol 1983; 159:129–141.
43. Csiba L, Paschen W, Mies G. Regional changes in tissue pH and glucose content during cortical spreading depression in rat brain. Brain Res 1985; 336:167–170.
44. Gido G, Katsura K, Kristian,T, Siesjo BK. Influence of plasma glucose concentration on rat brain extracellular calcium transients during spreading depression. J Cereb Blood Flow Metab 1993; 13:179–182.
45. Mies G, Iijima T, Hossmann KA. Correlation between peri-infarct DC shifts and ischaemic neuronal damage in rat. Neuroreport 1993; 4:709–711.
46. Busch E, Gyngell ML, Eis M, Hoehn Berlage M, Hossmann KA. Potassium-induced cortical spreading depressions during focal cerebral ischemia in rats: contribution to lesion growth assessed by diffusion-weighted NMR and biochemical imaging. J Cereb Blood Flow Metab 1996; 16:1090–1099.
47. Back T, Ginsberg MD, Dietrich WD, Watson BD. Induction of spreading depression in the ischemic hemisphere following experimental middle cerebral artery occlusion: effect on infarct morphology. J Cereb Blood Flow Metab 1996; 16(2):202–213.
48. Takano K, Latour LL, Formato JE, et al. The role of spreading depression in focal ischemia evaluated by diffusion mapping. Ann Neurol 1996; 39(3):308–318.
49. Nedergaard M, Astrup J. Infarct rim: effect of hyperglycemia on direct current potential and [14C]2-deoxyglucose phosphorylation. J Cereb Blood Flow Metab 1986; 6:607–615.
50. Betz AL, Gilboe DD, Yudilevich DL, Drewes LR. Kinetics of unidirectional glucose transport into the isolated dog brain. Am J Physiol 1973; 225(3):586–592.
51. Strong AJ, Harland SP, Meldrum BS, Whittington DJ. The use of in vivo fluorescence image sequences to indicate the occurrence and propagation of transient focal depolarizations in cerebral ischemia. J Cereb Blood Flow Metab 1996; 16:367–377.
52. Strong AJ, Smith SE, Whittington DJ, et al. Factors influencing the frequency of fluorescence transients as markers of peri-infarct depolarizations in focal cerebral ischemia. Stroke 2000; 31(1):214–222.
53. Hopwood SE, Parkin MC, Bezzina EL, Boutelle MG, Strong AJ. Transient changes in cortical glucose and lactate levels associated with peri-infarct depolarisations, studied with rapid-sampling microdialysis. J Cereb Blood Flow Metab 2005; 25(3):391–401.
54. Strong AJ, Boutelle MG, Vespa PM, Bullock MR, Bhatia R, Hashemi P. Treatment of critical care patients with substantial acute ischemic or traumatic brain injury [comment]. Critic Care Med 2005; 33(9):2147–2149.

55. Hartings JA, Rolli ML, Lu XC, Tortella FC. Delayed secondary phase of peri-infarct depolarizations after focal cerebral ischemia: relation to infarct growth and neuroprotection. J Neurosci 2003; 23(37):11602–11610.
56. Rojas S, Martin A, Justicia C, et al. Modest MRI signal intensity changes precede delayed cortical necrosis after transient focal ischemia in the rat. Stroke 2006; 37(6):1525–1532.
57. Kidwell CS, Alger JR, Saber JL. Evolving paradigms in neuroimaging of the ischemic penumbra. Stroke 2004; 35(11 suppl 1):2662–2665.
58. Kidwell CS, Alger JR, Saber JL. Beyond mismatch: evolving paradigms in imaging the ischemic penumbra with multimodal magnetic resonance imaging. Stroke 2003; 34(11):2729–2735.
59. Ringer TM, Neumann-Haefelin T, Sobel RA, Moseley ME, Yenari MA. Reversal of early diffusion-weighted magnetic resonance imaging abnormalities does not necessarily reflect tissue salvage in experimental cerebral ischemia. Stroke 2001; 32(10):2362–2369.
60. Neumann-Haefelin T, Kastrup A, de Crespigny A, et al. Serial MRI after transient focal cerebral ischemia in rats: dynamics of tissue injury, blood-brain barrier damage, and edema formation. Stroke 2000; 31(8):1965–1972.
61. Strong AJ, Anderson PJB, Watts H, et al. Peri-infarct depolarizations lead to loss of perfusion in ischaemic gyrencephalic cortex. Brain. In press.
62. Shin HK, Dunn AK, Jones PB, Boas DA, Moskowitz MA, Ayata C. Vasoconstrictive neurovascular coupling during focal ischemic depolarizations. J Cereb Blood Flow Metab 2006; 26(8):1018–1030.
63. Dreier JP, Ebert N, Priller J, et al. Products of hemolysis in the subarachnoid space inducing spreading ischemia in the cortex and focal necrosis in rats: a model for delayed ischemic neurological deficits after subarachnoid hemorrhage? J Neurosurg 2000; 93(4):658–666.
64. Guegan C, Ceballos-Picot I, Nicole A, Kato H, Onteniente B, Sola B. Recruitment of several neuroprotective pathways after permanent focal ischemia in mice. Exp Neurol 1998; 154(2):371–380.
65. Li Y, Chopp M, Jiang N, Zhang ZG, Zaloga C. Induction of DNA fragmentation after 10 to 120 minutes of focal cerebral ischemia in rats. Stroke 1995; 26(7):1252–1257.
66. Ferrer I, Planas AM. Signaling of cell death and cell survival following focal cerebral ischemia: life and death struggle in the penumbra. J Neuropathol Exp Neurol 2003; 62(4):329–339.
67. Lee SH, Kim M, Kim YJ, et al. Ischemic intensity influences the distribution of delayed infarction and apoptotic cell death following transient focal cerebral ischemia in rats. Brain Res 2002; 956(1):14–23.
68. Kametsu Y, Osuga S, Hakim AM. Apoptosis occurs in the penumbra zone during short-duration focal ischemia in the rat. J Cereb Blood Flow Metab 2003; 23(4):416–422.
69. Choi DW. Calcium: still center-stage in hypoxic-ischemic neuronal death. [Review] [32 refs]. Trends Neurosci 1995; 18(2):58–60.
70. Fujita R, Ueda H. Protein kinase C-mediated cell death mode switch induced by high glucose. Cell Death Differ 2003; 10(12):1336–1347.
71. Eguchi Y, Shimizu S, Tsujimoto Y. Intracellular ATP levels determine cell death fate by apoptosis or necrosis. Cancer Res 1997; 57(10):1835–1840.
72. Ferrer I, Friguls B, Dalfo E, Justicia C, Planas AM. Caspase-dependent and caspase-independent signalling of apoptosis in the penumbra following middle cerebral artery occlusion in the adult rat. Neuropathol Appl Neurobiol 2003; 29(5):472–481.
73. Cao G, Pei W, Lan J, et al. Caspase-activated DNase/DNA fragmentation factor 40 mediates apoptotic DNA fragmentation in transient cerebral ischemia and in neuronal cultures. J Neurosci 2001; 21(13):4678–4690.
74. Fujimura M, Morita-Fujimura Y, Murakami K, Kawase M, Chan PH. Cytosolic redistribution of cytochrome c after transient focal cerebral ischemia in rats. J Cereb Blood Flow Metab 1998; 18(11):1239–1247.
75. Krajewski S, Krajewska M, Ellerby LM, et al. Release of caspase-9 from mitochondria during neuronal apoptosis and cerebral ischemia. Proc Natl Acad Sci USA 1999; 96(10):5752–5757.
76. Namura S et al. Activation and cleavage of caspase-3 in apoptosis induced by experimental cerebral ischemia. J Neurosci 1998; 18(10):3659–3668.
77. Manabat C, Han BH, Wendland M, et al. Reperfusion differentially induces caspase-3 activation in ischemic core and penumbra after stroke in immature brain. Stroke 2003; 34(1):207–213.
78. Endres M, Namura S, Shimizu-Sasamta M, et al. Attenuation of delayed neuronal death after mild focal ischemia in mice by inhibition of the caspase family. J Cereb Blood Flow Metab 1998; 18(3):238–247.
79. Le DA, Wu Y, Huang Z, et al. Caspase activation and neuroprotection in caspase-3-deficient mice after in vivo cerebral ischemia and in vitro oxygen glucose deprivation. Proc Natl Acad Sci USA 2002; 99(23):15188–15193.
80. Cao G, Clark RS, Pei W, et al. Translocation of apoptosis-inducing factor in vulnerable neurons after transient cerebral ischemia and in neuronal cultures after oxygen-glucose deprivation. J Cereb Blood Flow Metab 2003; 23(10):1137–1150.
81. Plesnila N, Zhu C, Culmsee C, Groger M, Moskowitz MA, Blomgren K. Nuclear translocation of apoptosis-inducing factor after focal cerebral ischemia. J Cereb Blood Flow Metab 2004; 24(4): 458–466.

82. Graham SH, Chen J, Clark RS. Bcl-2 family gene products in cerebral ischemia and traumatic brain injury. J Neurotrauma 2000; 17(10):831–841.
83. Zhao H, Yenari MA, Cheng D, Barreto-Chang OL, Sapolsky RM, Steinberg GK. Bcl-2 transfection via herpes simplex virus blocks apoptosis-inducing factor translocation after focal ischemia in the rat. J Cereb Blood Flow Metab 2004; 24(6):681–692.
84. Cao G, Minami M, Pei W, et al. Intracellular Bax translocation after transient cerebral ischemia: implications for a role of the mitochondrial apoptotic signaling pathway in ischemic neuronal death. J Cereb Blood Flow Metab 2001; 21(4):321–333.
85. Plesnila N, Zinkel S, Le DA, et al. BID mediates neuronal cell death after oxygen/glucose deprivation and focal cerebral ischemia. Proc Natl Acad Sci USA 2001; 98(26):15318–15323.
86. Yin XM, Luo Y, Cao G, et al. Bid-mediated mitochondrial pathway is critical to ischemic neuronal apoptosis and focal cerebral ischemia. J Biol Chem 2002; 277(44):42074–42081.
87. Fujimura M, Morita-Fujimura Y, Kawase M, et al. Manganese superoxide dismutase mediates the early release of mitochondrial cytochrome C and subsequent DNA fragmentation after permanent focal cerebral ischemia in mice. J Neurosci 1999; 19(9):3414–3422.
88. Graham SH, Chen J. Programmed cell death in cerebral ischemia. J Cereb Blood Flow Metab 2001; 21(2):99–109.
89. Plesnila N. Role of mitochondrial proteins for neuronal cell death after focal cerebral ischemia. Acta Neurochir Suppl 2004; 89:15–19.
90. Petito CK, Pulsinelli WA. Delayed neuronal recovery and neuronal death in rat hippocampus following severe cerebral ischemia: possible relationship to abnormalities in neuronal processes. J Cereb Blood Flow Metab 1984; 4:194–205.
91. Petito CK, Pulsinelli WA. Sequential development of reversible and irreversible neuronal damage following cerebral ischemia. J Neuropath Exptl Neurol 1984; 43(2):141–153.
92. Schmidt-Kastner R, Freund TF. Selective vulnerability of the hippocampus in brain ischemia. Neuro Sci 1991; 40(3):599–636.
93. Ito U, Spatz M, Walker JT Jr, Klatzo I. Experimental cerebral ischemia in mongolian gerbils. I. Light microscopic observations. Acta Neuropathol (Berl) 1975; 32(3):209–223.
94. Kirino T. Delayed neuronal death in the gerbil hippocampus following ischemia. Brain Res 1982; 239:57–69.
95. Kirino T, Sano K. Selective vulnerability in the gerbil hippocampus following transient ischemia. Acta Neuropathol (Berl) 1984; 62:201–208.
96. Crain BJ, Westerkam WD, Harrison AH, Nadler JV. Selective neuronal death after transient forebrain ischemia in the Mongolian gerbil: a silver impregnation study. Neuro Sci 1988; 27(2):387–402.
97. Schmidt-Kastner R, Ophoff BG, Hossmann KA. Pattern of neuronal vulnerability in the cat hippocampus after one hour of global cerebral ischemia. Acta Neuropathol (Berl) 1990; 79(4):444–455.
98. Ferrer I, Tortosa A, Macaya A, et al. Evidence of nuclear DNA fragmentation following hypoxia-ischemia in the infant rat brain, and transient forebrain ischemia in the adult gerbil. Brain Pathol 1994; 4(2):115–122.
99. Mitani A, Andou Y, Kataoka K. Selective vulnerability of hippocampal CA1 neurons cannot be explained in terms of an increase in glutamate concentration during ischemia in the gerbil: brain microdialysis study. Neuro Sci 1992; 48(2):307–313.
100. Lee KS. Selective neuronal vulnerability and the distribution of N-methyl-D-aspartate (NMDA) receptors. Neurobiol Aging 1989; 10(5):609–611.
101. Wilde GJ, Pringle AK, Wright P, Iannotti F. Differential vulnerability of the CA1 and CA3 subfields of the hippocampus to superoxide and hydroxyl radicals in vitro. J Neurochem 1997; 69(2): 883–886.
102. Matsuyama T, Shimizu S, Nakamura H, Michishita H, Tagaya M, Sugita M. Effects of recombinant superoxide dismutase on manganese superoxide dismutase gene expression in gerbil hippocampus after ischemia. Stroke 1994; 25(7):1417–1423.
103. Kato H, Kogure K, Araki T, Liu XH, Kato K, Itoyama Y. Immunohistochemical localization of superoxide dismutase in the hippocampus following ischemia in a gerbil model of ischemic tolerance. J Cereb Blood Flow Metab 1995; 15(1):60–70.
104. Kuroiwa T, Terakado M, Yamaguchi T, Endo S, Ueki M, Okeda R. The pyramidal cell layer of sector CA 1 shows the lowest hippocampal succinate dehydrogenase activity in normal and postischemic gerbils. Neurosci Lett 1996; 206(2–3):117–120.
105. Sims NR. Energy metabolism and selective neuronal vulnerability following global cerebral ischemia. Neurochem Res 1992; 17(9):923–931.
106. Buchan AM, Pulsinelli WA. Septo-hippocampal deafferentation protects CA1 neurons against ischemic injury. Brain Res 1990; 512(1):7–14.
107. Nitsch C, Goping G, Klatzo I. Preservation of GABAergic perikarya and boutons after transient ischemia in the gerbil hippocampal CA1 field. Brain Res 1989; 495:243–252.
108. Tortosa A, Ferrer I. Parvalbumin immunoreactivity in the hippocampus of the gerbil after transient forebrain ischaemia: a qualitative and quantitative sequential study. Neuro Sci 1993; 55(1):33–43.

109. Ferrer I, Soriano MA, Vidal A, Planas AM. Survival of parvalbumin-immunoreactive neurons in the gerbil hippocampus following transient forebrain ischemia does not depend on HSP-70 protein induction. Brain Res 1995; 692(1–2):41–46.
110. Johansen FF. Interneurons in rat hippocampus after cerebral ischemia. Morphometric, functional, and therapeutic investigations. Acta Neurol Scand 1993; 150:1–32.
111. Siegel SJ, Brose N, Janssen WG, et al. Regional, cellular, and ultrastructural distribution of N-methyl-D-aspartate receptor subunit 1 in monkey hippocampus. Proc Natl Acad Sci USA 1994; 91(2):564–568.
112. Sugimoto A, Takeda A, Kogure K, Onodera H. NMDA receptor (NMDAR1) expression in the rat hippocampus after forebrain ischemia. Neurosci Lett 1994; 170(1):39–42.
113. Ferrer I, Ballabriga J, Marti E, Pozas E, Planas AM, Blasi J. BDNF and TrkB co-localize in CA1 neurons resistant to transient forebrain ischemia in the adult gerbil. J Neuropath Exptl Neurol 1997; 56(7):790–797.
114. Wang L, Yushmanov VE, Liachenko SM, Tang P, Hamilton RL, Xu Y. Late reversal of cerebral perfusion and water diffusion after transient focal ischemia in rats. J Cereb Blood Flow Metab 2002; 22(3):253–261.
115. Frahm C, Haupt C, Witte OW. GABA neurons survive focal ischemic injury. Neuro Sci 2004; 127(2):341–346.
116. Katchanov J, Waeber C, Gertz K, et al. Selective neuronal vulnerability following mild focal brain ischemia in the mouse. Brain Pathol 2003; 13(4):452–464.
117. Uemura Y, Kowall NW, Beal MF. Selective sparing of NADPH-diaphorase-somatostatin-neuropeptide Y neurons in ischemic gerbil striatum. Ann Neurol 1990; 27(6):620–625.
118. Pulsinelli WA. Selective neuronal vulnerability: morphological and molecular characteristics. Prog Brain Res 1985; 63:29–37.
119. Chesselet MF, Gonzales C, Lin CS, Polsky K, Jin BK. Ischemic damage in the striatum of adult gerbils: relative sparing of somatostatinergic and cholinergic interneurons contrasts with loss of efferent neurons. Exptl Neurol 1990; 110(2):209–218.
120. Calabresi P, Saulle E, Centonze D, Pisani A, Marfia GA, Bernardi G. Post-ischaemic long-term synaptic potentiation in the striatum: a putative mechanism for cell type-specific vulnerability. Brain 2002; 125(Pt 4):844–860.
121. Strong AJ, Fabricius M, Boutelle MG, et al. Spreading and synchronous depressions of cortical activity in acutely injured human brain. Stroke 2002; 33(12):2738–2743.
122. Leao AAP. Spreading depression of activity in cerebral cortex. J Neurophysiol 1944; 7:359–390.
123. Fabricius M, Fuhr S, Bhatia R, et al. Cortical spreading depression and peri-infarct depolarization in acutely injured human cerebral cortex. Brain 2006; 129(3):778–790.
124. Dreier JP, Woitzik J, Fabricius M, et al. Delayed ischaemic neurological deficits after subarachnoid haemorrhage are associated with clusters of cortical spreading depression. Brain 2006; 129(12): 3224–3237.
125. Bouma GJ, Muizelaar JP, Stringer WA, Choi SC, Fatouros P, Young HF. Ultra-early evaluation of regional cerebral blood flow in severely head-injured patients using xenon-enhanced computerized tomography [see comments]. J Neurosurg 1992; 77(3):360–368.
126. von Oettingen G, Bergholt B, Gyldensted C, Astrup J. Blood flow and ischemia within traumatic cerebral contusions. Neurosurgery 2002; 50(4):781–788.
127. Jones DK, Dardis R, Ervine M, et al. Cluster analysis of diffusion tensor magnetic resonance images in human head injury. Neurosurgery 2000; 47(2):306–313.

9 Inflammation and Reperfusion Injury Within the Penumbra

Adrian Parry-Jones
Faculty of Life Sciences, University of Manchester, Manchester, U.K.

Johann R. Selvarajah and Pippa J. Tyrrell
Faculty of Medical and Human Sciences, University of Manchester, Manchester, and Salford Royal Hospitals NHS Foundation Trust, Salford, U.K.

Nancy J. Rothwell
Faculty of Life Sciences, University of Manchester, Manchester, U.K.

INTRODUCTION

Inflammation manifests in most tissues through the cardinal features of swelling, redness, pain, and raised local temperature. The brain differs somewhat in its inflammatory response to other tissues. For example, edema is limited by the cranium, and leukocyte invasion is often modest and delayed. Nevertheless, inflammatory responses within the central nervous system (CNS) are being recognized, and their contribution to brain disorders such as multiple sclerosis and infections (e.g., measles, malaria, and more recently HIV) has been long recognized. Indeed, classical anti-inflammatory drugs have been the first approach to treat some CNS disorders. Realization that inflammation and specific inflammatory mediators contribute to ischemic injury has been more recent. Even in severe cerebral ischemia, leukocyte invasion is often delayed until after the primary injury, suggesting that inflammation may play a minor role. However, an array of inflammatory mediators and pathways is activated or expressed rapidly and there is growing evidence for their contribution to infarction and reperfusion injury.

The key mediators of inflammation are cytokines, complement, kinins, and cyclooxygenase (COX) products. These have provided targets for therapeutic intervention in peripheral inflammatory diseases, and more recently in CNS disorders, including stroke. Particular attention has focused on the pro-inflammatory cytokines of which interleukin-1 (IL-1), tumor necrosis factor α (TNFα), and IL-6 are most prominent. These proteins act locally to mediate inflammation and more generally to activate the best defense response. They are all induced in the CNS in response to distant, peripheral infection, injury, ischemia and immune activation, and rapidly after diverse forms of brain injury (1). Brain expression of cytokines in response to systemic disease is probably mediated by neural and humoral afferents, and contributes to key features of the host defense response to disease, including fever, loss of appetite, changes in metabolism, and alterations in neuroendocrine, cardiovascular, and immune function (2). Systemic influences on CNS inflammation may also be important in determining the incidence and outcome from cerebral ischemia. Infection is a risk factor for both the development of cerebral ischemia and poor outcome, but it is also now recognized that atherosclerosis—the underlying cause of stroke—is an inflammatory condition (3).

INFLAMMATION AS A CAUSE OF ISCHEMIC BRAIN DISEASE

Clinical Evidence

There is increasing evidence that inflammation is involved in the pathogenesis of cerebral ischemia following ischemic and hemorrhagic stroke, brain injury, cardiac arrest, and subarachnoid hemorrhage (4–7). Inflammation is also implicated in the pathogenesis of a number of other CNS diseases including Alzheimer's disease, epilepsy, Parkinson's disease, and multiple sclerosis. Inflammation is a central mechanism in atherosclerosis (3,8) which mediates most

strokes. Even in the absence of atherosclerosis, for example, in pediatric stroke, inflammatory mechanisms are important (9,10). Preceding systemic infection is linked to stroke risk, as are other noninfective inflammatory conditions (11,12).

Plasma levels of inflammatory markers such as the important acute phase protein C-reactive protein (CRP) (13) are predictors of ischemic heart disease and may be an additional risk factor in the development of ischemic stroke and transient ischemic attack (TIA). Plasma levels of CRP and IL-6 predict for clinical and radiological outcome after stroke (14). Clinical investigations in ischemic brain disease are usually limited to blood or cerebrospinal fluid sampling after the event, or postmortem histopathological studies, but novel imaging techniques facilitate in vivo observations of the inflammatory process and their relationship with brain tissue damage and clinical outcome. Magnetic resonance (MR) and positron emission tomography (PET) measures of brain inflammation in vivo may provide more information on the time course of central inflammatory processes in the penumbra after ischemia and its modulation, by therapy. Techniques have been developed both in experimental models (15) and in patients with stroke (16), as they have in other neuroinflammatory disorders such as multiple sclerosis (17). Early endothelial activation can be imaged using a novel MR agent that binds to E- or P-selectin expressed on activated endothelial cells (18), whereas 11-C-PK1115 PET has been used to image activated microglia, following ischemic stroke (19) (Fig. 1). To date, most data on the role of inflammation in the ischemic penumbra come from experimental and histopathological studies.

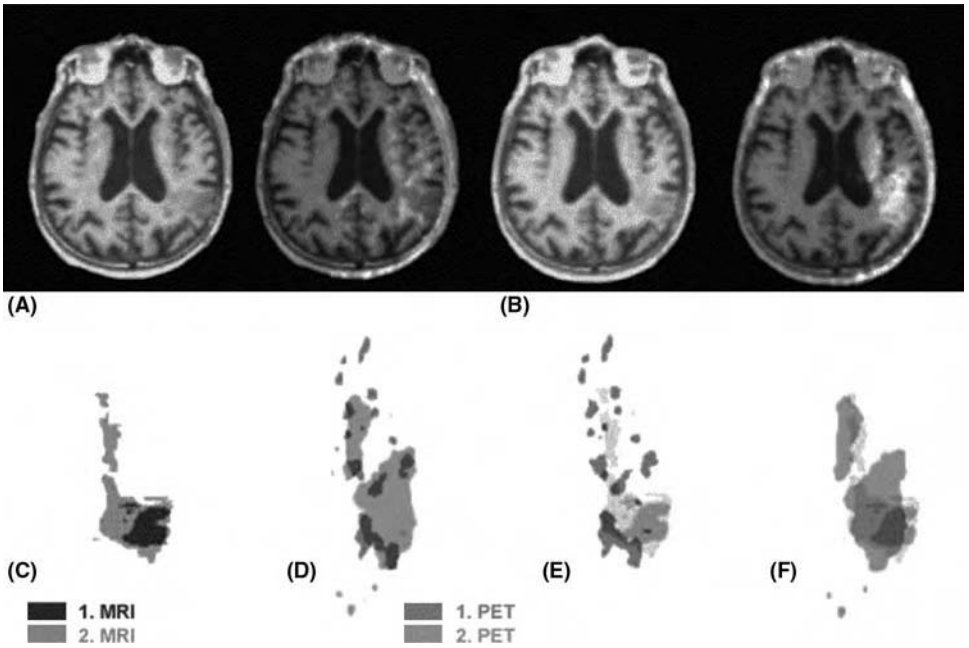

FIGURE 1 (*See color insert*.) Evolution of PK11195 signal at five days and 13 days after stroke. [^{11}C](*R*)-PK11195 PET and MRI scans for patient two at different time points: Patient two was examined five (**A**) and 13 (**B**) days after the infarct. T1-weighted MRI and the [^{11}C](*R*)-PK11195 binding potential map coregistered to the MRI are shown on a representative transverse plane. After five days, there is only minimal overlap between the hypointensity in the MRI and the area of increased [^{11}C](*R*)-PK11195 binding, the latter being largely confined to the area surrounding the T1 lesion. Thirteen days after the infarct, both the area of increased [^{11}C](*R*)-PK11195 binding and T1-weighted MRI hypointensity have extended in size now showing considerable overlap. The spatial relationship between the different imaging modalities in the same transverse slice at the two time points is further illustrated in the second row (**C–F**) with (**C**) showing the area of T1-weighted MRI changes and (**D**) of increased [^{11}C](*R*)-PK11195 binding at the two time points. (**E**) and (**F**) illustrate the relationship between the increasing size of the postischemic lesion delineated by T1-weighted MRI hypointensity and the changes in the distribution pattern of increased [^{11}C](*R*)-PK11195 binding after five (**E**) and 13 (**F**) days, respectively. *Source*: From Ref. 19.

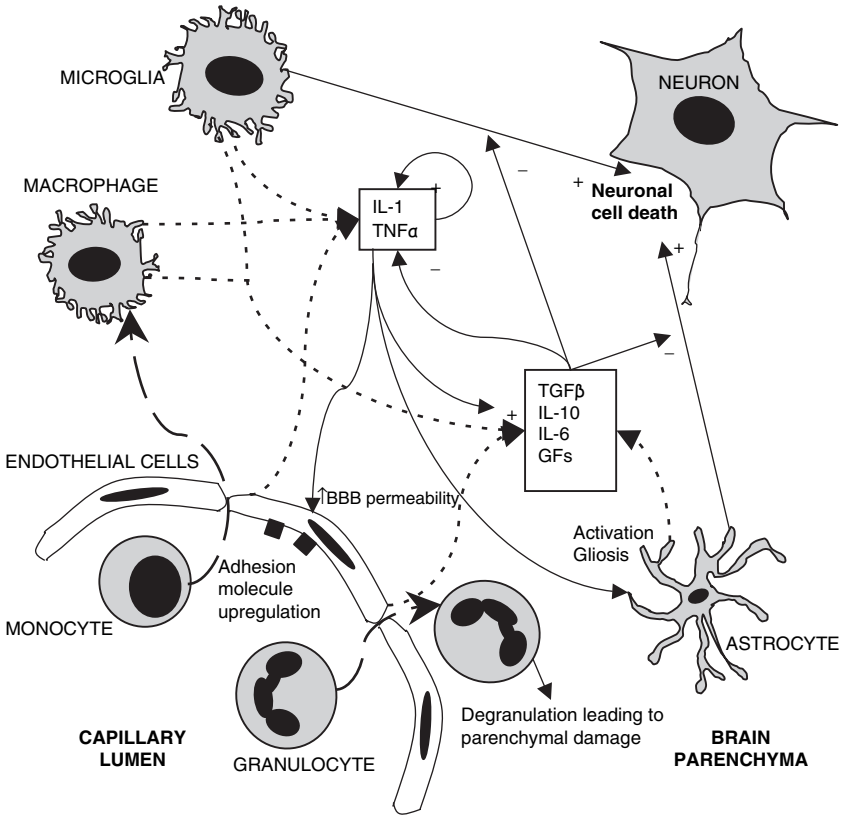

FIGURE 2 A simplified schematic representation of the principal cells and cytokines involved in the neuroinflammatory response to acute cerebral ischemia. *Dotted lines* represent cytokine production and *dashed lines* represent immune cell extravazation. *Abbreviations*: BBB, blood–brain barrier; GFs, growth factors; IL, interleukin; TGFβ, transforming growth factor beta, TNFα, tumor necrosis factor alpha.

Experimental Evidence

Much of the evidence implicating inflammation as a contributor to ischemic brain injury is derived from work in rodent models of focal ischemia. Although studies have often focused on individual cellular or molecular mediators of inflammation, it is important to stress that each does not act in isolation, but a complicated interplay is likely to occur between the many factors involved (Fig. 2). Cellular components can produce inflammatory mediators, and such mediators are also capable of activating and/or recruiting immune and other cells within the CNS. Precisely how each factor interacts with others and the sequence in which events occur remains unclear. However, evidence supporting the involvement of some of the major components of the inflammatory response will be summarized later.

Glia play a key role in determining the outcome of neuronal ischemic injury. Microglia respond rapidly to subtle and transient molecular signals of injury with morphological change, acquisition of macrophage differentiation markers, effector properties, and increased expression of many receptor molecules mediating antigen-recognition, cellular interaction, and migration (20,21). Activated microglia are the primary endogenous brain macrophages and also secrete various inflammatory molecules, including many cytokines. These properties define microglia as major resident immune cells within the brain (22,23).

Following ischemic injury, pathological signals for microglial activation may arise from the cytosol or plasma membranes of stressed cells, molecules coreleased with neurotransmitters, or inflammatory molecules secreted locally by both resident and infiltrating cells (24–26). Microglial activation is apparent within one hour after reperfusion in transient forebrain ischemia, thus preceding any detectable neuronal death, which increases in number to cover the entire ischemic

lesion by 70 hours (27,28). Activity of microglial cytotoxins and pro-inflammatory cytokines such as IL-1 and TNFα become prominent in the neuronal injury that follows. Subsequently, over a period of several hours microglia phagocytose nonviable and dead neurons (29,30). Macrophage, neutrophil natural killer cell, and B and differential T lymphocyte recruitment into the ischemic brain may be directly or indirectly shaped by a changing microglial secretory profile. Microglial surface receptors may also serve as a major target for the effector molecules, including cytokines, of other resident or infiltrating immune cells. Consequently, microglia are ascribed a central role in the reciprocal interactions of peripheral and central immune processes (23,24,31).

Astrocytes, like microglia, also transform into activated cells following ischemic injury with secretion of various mediators including reactive oxygen species, inflammatory molecules, neurotrophic factors, and neuromodulators (32,33). Astrocytic nitric oxide synthase (NOS) expression is increased within hours of experimental ischemia, reaching peak at two to three days (34,35). Various pro-, anti-, and immunomodulatory cytokines are produced by activated astrocytes including TNFα and β, IL-1, IL-6, IL-10, matrix metalloproteinases (MMP), and interferon. Several of these mediators have been implicated in either delayed neuronal death or supportive mechanisms following experimental ischemic injury. Furthermore, astrocyte-mediated effects at the blood–brain barrier may have particular importance for penumbral neuronal survival, reperfusion injury, and the pathogenesis of vasogenic edema. For example, astrocyte MMP production contributes to physical disruption of blood–brain barrier matrix proteins (36–38). Astrocytic gap junction interactions are associated with the spread of hypoxic neuronal injury but also reduced penumbral apoptosis with anti-inflammatory effects in various models of cerebral ischemia (33,39).

The net neurotoxic, neuroprotective, or neurotrophic effects of both microglia and astrocyte activities are likely to reflect the pathophysiology of injury, the profile of inflammatory mechanisms deployed, and the prevailing cytokine milieu. The concept of facilitative neurotoxicity argues that the glial cytotoxic response is highly targeted rather than indiscriminate, with the overall aims of maintaining tissue integrity and promoting neuronal recovery. Neurones that are compromised beyond viability by the primary injury become the specific targets of locally activated glia. The production of cytotoxic and pro-inflammatory molecules, and subsequent phagocytosis by glia, particularly microglia, removes these nonviable neurones. This process reflects an attempt to maintain tissue homeostasis by reorganization of synaptic communication, restoration of tissue integrity, and protection of viable neurones from further injury (21,31,40).

However, this model assumes that activated glia accurately distinguish viable from nonviable neuronal tissue and deploy cytotoxic effector properties with specificity. If glial sensory and effector properties lack the required sensitivity and/or specificity, or if microglia undergo pathological transformation into dysfunctional auto-aggressor cells, bystander damage ensues with the spread of injury to viable neurons (21,31). The challenge lies in identifying the pathophysiological signals that determine these alternate outcomes, and whether therapeutic intervention can skew the glial response toward supportive effects (35).

Polymorphonuclear leucocytes have been detected in cerebral microvessels as early as 30 minutes after the onset of ischemia and reach peak numbers in the parenchyma at approximately 24 hours (41). Although it has proved difficult to clearly differentiate resident microglia from monocytes/macrophages recruited from the circulation, the work comparing naïve and peripheral monocyte depleted rats has identified an infiltration of circulating monocytes from day six onward (42). Whether invading immune cells contribute to damage or are part of reparative processes in response to damage has been a subject of debate (43,44). Inflammatory responses may help in clearing and healing damaged tissue during long-term recovery, but compelling evidence exists for a damaging role for leucocytes in the early stages of cerebral ischemia. For example, depletion of peripheral leucocytes leads to a 40% to 45% reduction in infarct size in various experimental models (4), and microglia are responsible for the production of inflammatory mediators which may, in turn, exacerbate ischemic damage. Adhesion molecules [P-selectin, intracellular adhesion molecule-1 (ICAM-1), E-selectin] promote margination and recruitment of leucocytes into the area of damage, and although anti-ICAM-1 antibodies reduce infarct volumes by up to 40% in models of transient middle cerebral artery occlusion (MCAO), a large clinical trial has proved negative (45,46).

Cytokines are important inflammatory mediators with multiple and overlapping actions (both neurotoxic and neuroprotective) and are central to the inflammatory response in the CNS. The classically pro-inflammatory cytokines IL-1 and TNFα have been shown to have central neurotoxic roles in acute ischemia. Exogenous IL-1 increases infarct volumes and cerebral edema following experimental ischemia when administered centrally or peripherally. More compelling evidence comes from blocking the actions of endogenous IL-1 with antibodies against IL-1, inhibition of caspase-1 (which activates the precursor of IL-1β), or with the naturally occurring IL-1 receptor antagonist, which all reduce infarct volumes in rodent models of cerebral ischemia (47). This is further supported by a 70% reduction in damage observed following deletion of the IL-1α and β genes in the mouse. The exact mechanisms of action of IL-1 in ischemic injury are not known but are likely to include effects on glial and other cells, alteration of physiological parameters (temperature/blood flow/pH), and increase in seizure activity (48).

TNF-α is expressed in ischemic brain soon after the onset of ischemia, and as with IL-1, inhibition of endogenous TNF-α using soluble receptor or antibodies leads to a reduction on damage. However, unlike IL-1 deficient mice, TNF-α receptor knockout mice show enhanced ischemic damage suggesting a neuroprotective role under certain conditions (47).

Overall, experimental studies on IL-6 in rodents present a predominantly neuroprotective picture. An increase in the bioactivity of IL-6 within two hours of onset of permanent MCAO is seen in the ischemic hemisphere of the rat brain with a further increase over 24 hours. Central administration of exogenous IL-6 is neuroprotective, leading to a 65% reduction in ischemic damage at higher doses when compared to controls (49). Early studies in IL-6 deficient mice cast doubt on whether IL-6 is really neuroprotective as no difference in ischemic damage was seen when compared with wild-type mice (50). However, a more recent study shows that this lack of difference may be due to the role of IL-6 in fever and thermoregulation. Low body temperature is well known to be neuroprotective and it has been shown that IL-6 deficient mice become hypothermic during cerebral ischemia. When temperature was controlled carefully during MCAO, IL-6 deficient mice had reduced survival, worse neurological status, and larger infarcts than control animals, explaining the seemingly conflicting evidence obtained from earlier studies (51).

Other downstream mediators of inflammation known to be central in the damage occurring after cerebral ischemia include nitric oxide (NO), COX-2, bradykinin, and the complement cascade. NO production occurs from constitutive neuronal and endothelial NOS (nNOS/eNOS), requiring a rise in intracellular calcium to increase release of NO from L-arginine. Early production of NO by endothelial cell (Enos) may lead to neuroprotection by enhancing blood flow through vasodilatation (52). However, invading neutrophils express inducible (or immunological) NOS, which is not normally present in most cells but is expressed in inflammation. iNOS expression peaks at 12 to 48 hours and is found in inflammatory cells invading the injured brain and in cerebral microvessels (53). Unlike nNOS and eNOS, INOS is not dependent on intracellular calcium for activation, and produces NO continuously. Animal studies have demonstrated the deleterious effect of INOS in cerebral ischemia; selective INOS inhibition 12 to 24 hours after the onset of ischemia leads to a 30% to 40% reduction in infarct volume (54) and improvement in neurological outcome (55); and iNOS gene knockout mice show a similar reduction in ischemic damage (56). An NO modulator, *S*-nitrosoglutathione (GSNO), administered after the onset of ischemia reduces infarction and improves cerebral blood flow with reduction in the expression of TNF-α, IL-1β, and INOS, inhibition of the activation of microglia/macrophages, and reduction in the number of apoptotic cells (including neurons) and caspase-3 activity (57). COX-2 catalyzes the conversion of arachidonic acid into various prostanoids and is normally expressed in the dendritic spines of glutamatergic neurones in the CNS, where it is thought to play a role in normal synaptic function. However, in cerebral ischemia COX-2 is upregulated in response to inflammatory mediators in neurones, glia, vascular cells, and invading inflammatory cells with a similar time profile to that seen for iNOS (peaking at 12–24 hours) (58). COX-2 leads to the production of toxic prostanoids and free radicals, and delayed COX-2 inhibition leads to a reduction in infarct volume (59) as does deletion of the COX-2 gene in mice (60).

Another important facet of the immune response to ischemia in the CNS is activation of the complement system. Complement activation via the classical, lectin or alternative pathways

leads to production of opsonins and the membrane attack complex, which are important in clearing microorganisms and damaged cells. Anaphylatoxin peptides (C3a and C5a) are also produced and are potent chemo-attractants and activators of granulocytes. The complement system is known to be rapidly activated in experimental focal ischemia (61,62), but inhibition of the pathway has provided mixed results, perhaps due to the use of different inhibitors in different models of ischemia in the studies undertaken (61,63–65). However, a more recent study using a C1 inhibitor (C1-INH) in a murine model of ischemia–reperfusion shows a marked reduction in infarct volume and improvement in neurological outcomes in the treated group (66). The mechanism of action of C1-INH has been investigated in more detail using mice subjected to two-hour ischemia and early or late reperfusion. C1-INH significantly dampened the mRNA expression of the adhesion molecules P-selectin and ICAM-1 induced by the ischemic insult. It significantly decreased the pro-inflammatory cytokine (TNFα, IL-18) and increased the protective cytokine (IL-6, IL-10) gene expression. It prevented the decrease of *NFH* gene, a marker of cellular integrity and counteracted the increase of procaspase 3, an apoptosis index. Furthermore, C1-INH markedly inhibited the activation and/or recruitment of microglia/macrophages, demonstrated by immunohistochemistry, suggesting both an anti-inflammatory and antiapoptotic action on ischemia–reperfusion injury (67).

Bradykinin is a nonapeptide inflammatory mediator that is important in both central and peripheral inflammation and has attracted interest as a potential mediator of brain injury following stroke. The kallikrein/kinin system is fully expressed in the CNS and leads to vascular dilatation and increased permeability with subsequent edema formation (68). Bradykinin is thought to act via B_2 receptors to activate COX-2, as well as acting as a potent stimulator of cytokines and as a leucocyte chemoattractant. Evidence for the damaging effects of bradykinin after experimental ischemia is provided by studies where B_2 receptor antagonists have been shown to improve histological and neurological outcomes in rodents (69,70).

The importance of peripherally derived cells in the pathogenesis of cerebral ischemia has been demonstrated by the attenuation of ischemic injury to the selective inactivation of adenosine A2 receptors on bone marrow derived cells, suggesting that cerebral ischemia is dependent upon a complex balance between inflammatory cells not only in the brain and endothelium, but also in the periphery (71). It is noteworthy that IL-1β controls the production of both secreted and cytosolic A2 enzymes (72).

THERAPEUTIC OPPORTUNITIES

Previous trials of neuroprotective agents have focused on inhibiting components of the ischemic cascade that are expressed mainly in the first few hours after the onset of cerebral ischemia (4). Numerous such agents (including calcium channel blockers and glutamate antagonists) have been tested in large phase III trials with negative outcomes. Differences between studies at preclinical and clinical stages (such as dose and time of drug administration) are likely to have contributed to this. Indeed, it has been noted that clinical trials that have closely replicated conditions in successful preclinical studies [e.g., tissue plasminogen activator (73), ancrod (74), and intra-arterial prourokinase (75)] have led to successful outcomes (76). Based on experience from previous negative trials of neuroprotective agents, it has been recommended that preclinical studies should clearly identify the dose–response relationship and therapeutic window of novel agents. These should be further investigated in early phase I and II studies and adhered to in subsequent clinical trials. Preclinical experimental design should incorporate physiological monitoring and utilize histological infarct volume and functional outcome in both short and long-term studies (77,78). Future investigations targeting neuroinflammation should closely follow these recommendations to maximize the chances of detecting any potential new therapy for stroke.

Deleterious neuroinflammation occurring after stroke has a relatively delayed onset, and the extended therapeutic window resulting from this would allow a greater proportion of patients to benefit from anti-inflammatory treatments. Inflammation involves a wide array of cellular and molecular components with multiple and overlapping actions, and at present, it is not clear which component(s) should be targeted for intervention. Preventing hematogenous leucocyte infiltration represents an obvious target; however, a large trial investigating a murine

derived anti-ICAM antibody (enlimomab) within six hours of onset in a double-blind, placebo-controlled trial actually worsened the outcome in the treatment group (79). The reasons for this were subsequently investigated in the rat, using a murine antibody to rat ICAM-1 (similar to enlimomab). It was found to activate the rat immune system, leading to host antibody production against the murine antibody, activation of circulating neutrophils, complement activation and microvascular activation, providing a possible explanation for the poor outcome of patients treated with enlimomab (80). However, other approaches to preventing neutrophil adhesion/infiltration may bear fruit after careful preclinical assessment.

Resident microglia are also of interest as cellular targets for anti-inflammatory intervention. Minocycline and doxycycline are second generation, semisynthetic tetracycline derivatives with significant brain and cerebrospinal fluid penetration. In addition to their wide clinical application as antimicrobial agents, they demonstrate various anti-inflammatory biological properties. In rodent, global and focal cerebral ischemia, these agents are neuroprotective by inhibition of microglial (but not astrocytic) activitation and proliferation (81–84). These effects are associated with reduced microglial production of pro-inflammatory mediators such as TNFα, IL-1β, and NO, and may in part reflect inhibition of microglial signal transduction pathways. Furthermore, this neuroprotection is achieved at relatively low doses within clinically relevant therapeutic time windows.

Considerable interest also exists in targeting NO production and animal studies suggesting that the therapeutic window for this may extend to 12 to 24 hours after symptom onset (85). Although relatively selective inhibitors of iNOS are available, it will be important to minimize inhibition of eNOS, which may have a neuroprotective role, and of nNOS, which may play an important role in normal neuronal function.

Inhibition of COX-2 shows a considerable benefit in studies of experimental stroke. However, it is likely to be involved in excitatory synaptic transmission (86), and inhibition of the enzyme may have deleterious effects on functional recovery from stroke. Furthermore, it has recently become apparent that previously approved COX-2 inhibitors are associated with an increase in risk of thrombotic cardiovascular events compared with more established non-steroidal anti-inflammatory drugs, and this has lead to the withdrawal of rofecoxib from the market (87). These factors will need to be closely addressed and current issues overcome before proceeding to studies in clinical stroke.

The central coordinating role of cytokines in inflammation makes them a promising target for developing novel treatments. Inhibition of IL-1 in animal models has been comprehensively shown to reduce damage from focal or global ischemia, traumatic injury, and excitotoxicity. IL-1ra (given centrally or peripherally) leads to both improved histological and neurological outcome in permanent and transient focal ischemia, even when given three hours after onset (47,88). Moreover, IL-1ra is a naturally occurring treatment that is fully licensed for rheumatoid arthritis and has been given to many thousands of patients with no significant adverse events. A recent small, double-blinded, randomized, controlled safety study of IL-1ra given to acute stroke patients within six hours of symptom onset by intravenous infusion provides preliminary data supporting the safety of IL-1ra in stroke patients. Evidence for biological activity was seen with a reduced peripheral CRP, IL-6, neutrophil, and white cell count in the circulation of patients receiving IL-1ra (89). Exploratory efficacy analysis suggested an improvement in clinical outcome at three months in patients with cortical stroke receiving IL-1ra compared to placebo**.** Further investigations of efficacy using surrogate imaging markers of outcome and studies to determine the optimal dose in stroke will be required before proceeding to any definitive phase III trial of IL-1ra. Other cytokines (IL-6, TNFα) do not have such a clearly defined neurotoxic role, and further basic research will be required to clarify their role before proceeding to further studies.

CONCLUSION

The ischemic penumbra is a key target for intervention after stroke. Extensive experimental evidence, together with an increasing accumulation of clinical data, suggests that inflammatory responses, both cellular and humoral, play a major role in the development of brain injury after ischemia and reperfusion. Strategies that target the modulation of the inflammatory response

provide a feasible and rational approach to therapeutic trials. There are a number of potential anti-inflammatory treatments in addition to IL-1ra, including molecules that target the production of biologically active IL-1 ligands or downstream signaling events. The peripheral inflammatory response to cerebral ischemia is a potentially exciting area to study, as potential therapeutic agents would not necessarily have to penetrate the blood–brain barrier.

REFERENCES

1. Allan SM, Tyrrell PJ, Rothwell NJ. Interleukin-1 and neuronal injury. Nat Rev Immunol 2005; 5(8):629–640.
2. Dantzer R. Cytokine-induced sickness behaviour: a neuroimmune response to activation of innate immunity. Eur J Pharmacol 2004; 500(1–3):399–411.
3. Paoletti R, Gotto AM, Hajjar DP. Inflammation in atherosclerosis and implications for therapy. Circulation 2004; 109(23 suppl 1):III20–III26.
4. Barone FC, Feuerstein GZ. Inflammatory mediators and stroke: new opportunities for novel therapeutics. J Cereb Blood Flow Metab 1999; 19(8):819–834.
5. Bramlett HM, Dietrich WD. Pathophysiology of cerebral ischemia and brain trauma: similarities and differences. J Cereb Blood Flow Metab 2004; 24(2):133–150.
6. Dumont AS, Dumont RJ, Chow MM, et al. Cerebral vasospasm after subarachnoid hemorrhage: putative role of inflammation. Neurosurgery 2003; 53(1):123–133.
7. Mussack T, Biberthaler P, Gippner-Steppert C, et al. Early cellular brain damage and systemic inflammatory response after cardiopulmonary resuscitation or isolated severe head trauma: a comparative pilot study on common pathomechanisms. Resuscitation 2001; 49(2):193–199.
8. Ross R. Atherosclerosis—an inflammatory disease. N Engl J Med 1999; 340(2):115–126.
9. Takeoka M, Takahashi T. Infectious and inflammatory disorders of the circulatory system and stroke in childhood. Curr Opin Neurol 2002; 15(2):159–164.
10. Ganesan V, Prengler M, McShane MA, et al. Investigation of risk factors in children with arterial ischemic stroke. Ann Neurol 2003; 53(2):167–173.
11. Emsley HC, Tyrrell PJ. Inflammation and infection in clinical stroke. J Cereb Blood Flow Metab 2002; 22(12):1399–1419.
12. Lindsberg PJ, Grau AJ. Inflammation and infections as risk factors for ischemic stroke. Stroke 2003; 34(10):2518–2532.
13. Ridker PM, Hennekens CH, Buring JE, et al. C-reactive protein and other markers of inflammation in the prediction of cardiovascular disease in women. N Engl J Med 2000; 342(12):836–843.
14. Smith CJ, Emsley HC, Gavin CM, et al. Peak plasma interleukin-6 and other peripheral markers of inflammation in the first week of ischaemic stroke correlate with brain infarct volume, stroke severity and long-term outcome. BMC Neurol 2004; 4:2.
15. Sironi L, Guerrini U, Tremoli E, et al. Analysis of pathological events at the onset of brain damage in stroke-prone rats: a proteomics and magnetic resonance imaging approach. J Neurosci Res 2004; 78(1):115–122.
16. Saleh A, Schroeter M, Jonkmanns C, et al. In vivo MRI of brain inflammation in human ischaemic stroke. Brain 2004; 127(Pt 7):1670–1677.
17. Versijpt J, Debruyne JC, Van Laere KJ, et al. Microglial imaging with positron emission tomography and atrophy measurements with magnetic resonance imaging in multiple sclerosis: a correlative study. Mult Scler 2005; 11(2):127–134.
18. Barber PA, Foniok T, Kirk D, et al. MR molecular imaging of early endothelial activation in focal ischemia. Ann Neurol 2004; 56(1):116–120.
19. Gerhard A, Schwarz J, Myers R, et al. Evolution of microglial activation in patients after ischemic stroke: a [11C](R)-PK11195 PET study. Neuroimage 2005; 24(2):591–595.
20. Stoll G, Jander S, Schroeter M. Inflammation and glial responses in ischemic brain lesions. Prog Neurobiol 1998; 56(2):149–171.
21. Kreutzberg GW. Microglia: a sensor for pathological events in the CNS. Trends Neurosci 1996; 19(8):312–318.
22. Rothwell NJ. Annual review prize lecture cytokines—killers in the brain? J Physiol 1999; 514(Pt 1): 3–17.
23. Aloisi F. Immune function of microglia. Glia 2001; 36(2):165–179.
24. Hanisch UK. Microglia as a source and target of cytokines. Glia 2002; 40(2):140–155.
25. Streit WJ, Walter SA, Pennell NA. Reactive microgliosis. Prog Neurobiol 1999; 57(6):563–581.
26. Streit WJ, Hurley SD, McGraw TS, et al. Comparative evaluation of cytokine profiles and reactive gliosis supports a critical role for interleukin-6 in neuron-glia signaling during regeneration. J Neurosci Res 2000; 61(1):10–20.
27. Zhang Z, Chopp M, Powers C. Temporal profile of microglial response following transient (2 h) middle cerebral artery occlusion. Brain Res 1997; 744(2):189–198.

28. Morioka T, Kalehua AN, Streit WJ. The microglial reaction in the rat dorsal hippocampus following transient forebrain ischemia. J Cereb Blood Flow Metab 1991; 11(6):966–973.
29. Boje KM, Arora PK. Microglial-produced nitric oxide and reactive nitrogen oxides mediate neuronal cell death. Brain Res 1992; 587(2):250–256.
30. Lees GJ. The possible contribution of microglia and macrophages to delayed neuronal death after ischemia. J Neurol Sci 1993; 114(2):119–122.
31. Schwartz M. Macrophages and microglia in central nervous system injury: are they helpful or harmful? J Cereb Blood Flow Metab 2003; 23(4):385–394.
32. Chen Y, Swanson RA. Astrocytes and brain injury. J Cereb Blood Flow Metab 2003; 23(2):137–149.
33. Swanson RA, Ying W, Kauppinen TM. Astrocyte influences on ischemic neuronal death. Curr Mol Med 2004; 4(2):193–205.
34. Iadecola C, Xu X, Zhang F, et al. Marked induction of calcium-independent nitric oxide synthase activity after focal cerebral ischemia. J Cereb Blood Flow Metab 1995; 15(1):52–59.
35. Nakashima MN, Yamashita K, Kataoka Y, et al. Time course of nitric oxide synthase activity in neuronal, glial, and endothelial cells of rat striatum following focal cerebral ischemia. Cell Mol Neurobiol 1995; 15(3):341–349.
36. Rosenberg GA, Estrada EY, Dencoff JE. Matrix metalloproteinases and TIMPs are associated with blood–brain barrier opening after reperfusion in rat brain. Stroke 1998; 29(10):2189–2195.
37. Rosenberg GA, Cunningham LA, Wallace J, et al. Immunohistochemistry of matrix metalloproteinases in reperfusion injury to rat brain: activation of MMP-9 linked to stromelysin-1 and microglia in cell cultures. Brain Res 2001; 893(1–2):104–112.
38. del Zoppo GJ, Mabuchi T. Cerebral microvessel responses to focal ischemia. J Cereb Blood Flow Metab 2003; 23(8):879–894.
39. Nakase T, Fushiki S, Sohl G, et al. Neuroprotective role of astrocytic gap junctions in ischemic stroke. Cell Commun Adhes 2003; 10(4–6):413–417.
40. Streit WJ. Microglia as neuroprotective, immunocompetent cells of the CNS. Glia 2002; 40(2): 133–139.
41. Garcia JH, Liu KF, Yoshida Y, et al. Influx of leukocytes and platelets in an evolving brain infarct (Wistar rat). Am J Pathol 1994; 144(1):188–199.
42. Schroeter M, Jander S, Huitinga I, et al. Phagocytic response in photochemically induced infarction of rat cerebral cortex. The role of resident microglia. Stroke 1997; 28(2):382–386.
43. Hayward NJ, Elliott PJ, Sawyer SD, et al. Lack of evidence for neutrophil participation during infarct formation following focal cerebral ischemia in the rat. Exp Neurol 1996; 139(2):188–202.
44. Matsuo Y, Onodera H, Shiga Y, et al. Correlation between myeloperoxidase-quantified neutrophil accumulation and ischemic brain injury in the rat. Effects of neutrophil depletion. Stroke 1994; 25(7):1469–1475.
45. Chopp M, Li Y, Jiang N, et al. Antibodies against adhesion molecules reduce apoptosis after transient middle cerebral artery occlusion in rat brain. J Cereb Blood Flow Metab 1996; 16(4): 578–584.
46. DeGraba TJ. The role of inflammation after acute stroke: utility of pursuing anti-adhesion molecule therapy. Neurology 1998; 51(3 suppl 3):S62–S68.
47. Allan SM, Rothwell NJ. Cytokines and acute neurodegeneration. Nat Rev Neurosci 2001; 2(10):734–744.
48. Touzani O, Boutin H, Chuquet J, et al. Potential mechanisms of interleukin-1 involvement in cerebral ischaemia. J Neuroimmunol 1999; 100(1–2):203–215.
49. Loddick SA, Turnbull AV, Rothwell NJ. Cerebral interleukin-6 is neuroprotective during permanent focal cerebral ischemia in the rat. J Cereb Blood Flow Metab 1998; 18(2):176–179.
50. Clark WM, Rinker LG, Lessov NS, et al. Lack of interleukin-6 expression is not protective against focal central nervous system ischemia. Stroke 2000; 31(7):1715–1720.
51. Herrmann O, Tarabin V, Suzuki S, et al. Regulation of body temperature and neuroprotection by endogenous interleukin-6 in cerebral ischemia. J Cereb Blood Flow Metab 2003; 23(4):406–415.
52. Huang Z, Huang PL, Ma J, et al. Enlarged infarcts in endothelial nitric oxide synthase knockout mice are attenuated by nitro-L-arginine. J Cereb Blood Flow Metab 1996; 16(5):981–987.
53. Iadecola C, Zhang F, Casey R, et al. Inducible nitric oxide synthase gene expression in vascular cells after transient focal cerebral ischemia. Stroke 1996; 27(8):1373–1380.
54. Iadecola C, Li J, Ebner TJ, et al. Nitric oxide contributes to functional hyperemia in cerebellar cortex. Am J Physiol 1995; 268(5 Pt 2):R1153–R1162.
55. Nagayama M, Aber T, Nagayama T, et al. Age-dependent increase in ischemic brain injury in wild-type mice and in mice lacking the inducible nitric oxide synthase gene. J Cereb Blood Flow Metab 1999; 19(6):661–666.
56. Iadecola C, Zhang F, Casey R, et al. Delayed reduction of ischemic brain injury and neurological deficits in mice lacking the inducible nitric oxide synthase gene. J Neurosci 1997; 17(23):9157–9164.
57. Khan M, Sekhon B, Giri S, et al. S-Nitrosoglutathione reduces inflammation and protects brain against focal cerebral ischemia in a rat model of experimental stroke. J Cereb Blood Flow Metab 2005; 25(2):177–192.

58. Nogawa S, Zhang F, Ross ME, et al. Cyclo-oxygenase-2 gene expression in neurons contributes to ischemic brain damage. J Neurosci 1997; 17(8):2746–2755.
59. Sugimoto K, Iadecola C. Delayed effect of administration of COX-2 inhibitor in mice with acute cerebral ischemia. Brain Res 2003; 960(1–2):273–276.
60. Iadecola C, Niwa K, Nogawa S, et al. Reduced susceptibility to ischemic brain injury and N-methyl-D-aspartate-mediated neurotoxicity in cyclooxygenase-2-deficient mice. Proc Natl Acad Sci U.S.A. 2001; 98(3):1294–1299.
61. Huang J, Kim LJ, Mealey R, et al. Neuronal protection in stroke by an sLex-glycosylated complement inhibitory protein. Science 1999; 285(5427):595–599.
62. Van BJ, Bernaudin M, Petit E, et al. Expression of receptors for complement anaphylatoxins C3a and C5a following permanent focal cerebral ischemia in the mouse. Exp Neurol 2000; 161(1):373–382.
63. Heimann A, Takeshima T, Horstick G, et al. C1-esterase inhibitor reduces infarct volume after cortical vein occlusion. Brain Res 1999; 838(1–2):210–213.
64. Lew SM, Gross CE, Bednar MM, et al. Complement depletion does not reduce brain injury in a rabbit model of thromboembolic stroke. Brain Res Bull 1999; 48(3):325–331.
65. Vasthare US, Barone FC, Sarau HM, et al. Complement depletion improves neurological function in cerebral ischemia. Brain Res Bull 1998; 45(4):413–419.
66. De Simoni MG, Storini C, Barba M, et al. Neuroprotection by complement (C1) inhibitor in mouse transient brain ischemia. J Cereb Blood Flow Metab 2003; 23(2):232–239.
67. Storini C, Rossi E, Marrella V, et al. C1-inhibitor protects against brain ischemia-reperfusion injury via inhibition of cell recruitment and inflammation. Neurobiol Dis 2005; 19(1–2):10–17.
68. Sobey CG. Bradykinin B2 receptor antagonism: a new direction for acute stroke therapy? Br J Pharmacol 2003; 139(8):1369–1371.
69. ng-Zhou L, Margaill I, Palmier B, et al. LF 16-0687 Ms, a bradykinin B2 receptor antagonist, reduces ischemic brain injury in a murine model of transient focal cerebral ischemia. Br J Pharmacol 2003; 139(8):1539–1547.
70. Relton JK, Beckey VE, Hanson WL, et al. CP-0597, a selective bradykinin B2 receptor antagonist, inhibits brain injury in a rat model of reversible middle cerebral artery occlusion. Stroke 1997; 28(7):1430–1436.
71. Yu L, Huang Z, Mariani J, et al. Selective inactivation or reconstitution of adenosine A2A receptors in bone marrow cells reveals their significant contribution to the development of ischemic brain injury. Nat Med 2004; 10(10):1081–1087.
72. Stella N, Estelles A, Siciliano J, et al. Interleukin-1 enhances the ATP-evoked release of arachidonic acid from mouse astrocytes. J Neurosci 1997; 17(9):2939–2946.
73. The National Institute of Neurological Disorders and Stroke rt-PA Stroke Study Group. Tissue plasminogen activator for acute ischemic stroke. N Engl J Med 1995; 333(24):1581–1587.
74. Sherman DG, Atkinson RP, Chippendale T, et al. Intravenous ancrod for treatment of acute ischemic stroke: the STAT study: a randomized controlled trial. Stroke Treatment with Ancrod Trial. JAMA 2000; 283(18):2395–2403.
75. Furlan A, Higashida R, Wechsler L, et al. Intra-arterial prourokinase for acute ischemic stroke. The PROACT II study: a randomized controlled trial. Prolyse in acute cerebral thromboembolism. JAMA 1999; 282(21):2003–2011.
76. Grotta J. Neuroprotection is unlikely to be effective in humans using current trial designs. Stroke 2002; 33(1):306–307.
77. Recommendations for standards regarding preclinical neuroprotective and restorative drug development. Stroke 1999; 30(12):2752–2758.
78. Recommendations for clinical trial evaluation of acute stroke therapies. Stroke 2001; 32(7): 1598–1606.
79. Use of anti-ICAM-1 therapy in ischemic stroke: results of the Enlimomab Acute Stroke Trial. Neurology 2001; 57(8):1428–1434.
80. Furuya K, Takeda H, Azhar S, et al. Examination of several potential mechanisms for the negative outcome in a clinical stroke trial of enlimomab, a murine anti-human intercellular adhesion molecule-1 antibody: a bedside-to-bench study. Stroke 2001; 32(11):2665–2674.
81. Suk K. Minocycline suppresses hypoxic activation of rodent microglia in culture. Neurosci Lett 2004; 366(2):167–171.
82. Tikka T, Fiebich BL, Goldsteins G, et al. Minocycline, a tetracycline derivative, is neuroprotective against excitotoxicity by inhibiting activation and proliferation of microglia. J Neurosci 2001; 21(8):2580–2588.
83. Yrjanheikki J, Keinanen R, Pellikka M, et al. Tetracyclines inhibit microglial activation and are neuroprotective in global brain ischemia. Proc Natl Acad Sci U.S.A. 1998; 95(26):15769–15774.
84. Yrjanheikki J, Tikka T, Keinanen R, et al. A tetracycline derivative, minocycline, reduces inflammation and protects against focal cerebral ischemia with a wide therapeutic window. Proc Natl Acad Sci U.S.A. 1999; 96(23):13496–13500.
85. Parmentier S, Bohme GA, Lerouet D, et al. Selective inhibition of inducible nitric oxide synthase prevents ischaemic brain injury. Br J Pharmacol 1999; 127(2):546–552.

86. Kaufmann WE, Worley PF, Pegg J, et al. COX-2, a synaptically induced enzyme, is expressed by excitatory neurons at postsynaptic sites in rat cerebral cortex. Proc Natl Acad Sci U.S.A. 1996; 93(6):2317–2321.
87. Iadecola C, Gorelick PB. The Janus face of cyclooxygenase-2 in ischemic stroke: shifting toward downstream targets. Stroke 2005; 36(2):182–185.
88. Mulcahy NJ, Ross J, Rothwell NJ, et al. Delayed administration of interleukin-1 receptor antagonist protects against transient cerebral ischaemia in the rat. Br J Pharmacol 2003; 140(3):471–476.
89. Emsley HCA, Smith CJ, Georgiou RF, et al. A randomised phase II study of interleukin-1 receptor antagonist in acute stroke patients. J Neurol Neurosurg Psychiatry 2005. In Press.

10 Imaging Penumbra and Neuronal Loss: Positron Emission Tomography with Flumazenil

Wolf-Dieter Heiss
Max Planck Institute for Neurological Research, Cologne, Germany

Jan Sobesky, Alexander Thiel, and Christian Dohmen
Department of Neurology, University of Cologne, Cologne, Germany

Bernd Bauer, Karl Wienhard, and Rudolf Graf
Max Planck Institute for Neurological Research, Cologne, Germany

INTRODUCTION

Inhibitory glutamate and γ-amino-butyric acid (GABA) ergic synapses are present in high concentrations on cortical neurons (1) and found in lesser density in basal ganglia and cerebellum, but lacking in white matter (2). There is ample evidence that cerebral ischemia impairs GABAergic neurotransmission (3): downregulation of GABA receptors in the hippocampus and cerebral cortex can be observed as early as 30 minutes after transient global ischemia (4), and inhibitory postsynaptic potentials disappear earlier than excitatory postsynaptic potentials in hippocampal cornu ammonis section 1 (CA1) pyramidal neurons of rats subjected to cerebral ischemia (5). These alterations of GABA transmission are accompanied or even may be the cause of various cellular events including changes in the Cl^- gradient, increase in intracellular Ca^{2+} concentration, reduction of ATP, and generation of reactive oxygen species, to name a few, which lead to synaptic disruption that can be demonstrated at the microscopic or ultrastructural level before the neuronal somata are disintegrated (6,7). The early disruption of GABAergic transmission formed the rationale for studies of neuroprotection by GABAergic drugs, which were successful in animal models providing additional evidence for the role of this transmitter system in the evolution of ischemic neuronal damage (3). However, a first clinical trial with the GABA modulator clomethiazole has not proven a convincing benefit of this neuroprotective strategy (8).

The central benzodiazepine receptor (BZR) is a subunit of the postsynaptic GABAergic complex (9,10) and can be detected by radioligands, for example, 11C-flumazenil (FMZ) and 123I-iomazenil (IMZ) (11–13). The regional specific binding determined by dose-dependent saturation with coinjection of the cold ligand was in good agreement with postmortem data of receptor density (14), and consequently, radiolabelled ligands of BZR were successfully applied to detect neuronal loss in various brain disorders affecting predominantly cortical cells, including focal epilepsy (13,15–18) and Alzheimer's disease (19), but also in degenerative disorders of basal ganglia and cerebellum (20,21). Compared to a peripheral-type BZR ligand, the binding of which was increased in the peri-infarcted area due to glial macrophage reaction, Sette et al. (22) observed a marked depression of FMZ specific binding in ischemically damaged tissue in the baboon, suggesting the suitability of this tracer for early assessment of ischemia-induced brain damage in humans. These findings were confirmed in auto-radiographic studies of BZR availability, which was reduced equal to (23) or less pronounced than (24) regional blood flow in experimental focal ischemia. The single-photon emission computed tomography (SPECT) tracer IMZ was successfully used to delineate the extensions of cortical infarcts (25,26) and also to detect incomplete infarction of reperfused cortex appearing structurally intact on CT or MRI (27). These findings formed the basis to test the value of FMZ for early detection of irreversible ischemic damage and for differentiation to potentially salvageable penumbra tissue.

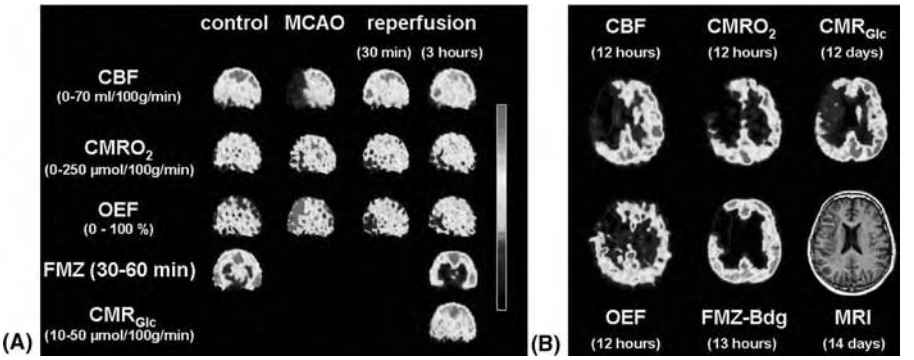

FIGURE 1 (*See color insert.*) (**A**) Sequential coronal positron emission tomography (PET) images of cerebral blood flow (CBF), cerebral metabolic rate O_2 ($CMRO_2$), oxygen extraction fraction (OEF), and flumazenil (FMZ) binding before, during one-hour occlusion, and ~30 minutes respectively ~3 hours after reperfusion of the middle cerebral artery in an individual cat. CMR of glucose (CMRGlc) was measured ~9 hours after reperfusion. In this cat, CBF reduction was severe, and the FMZ binding defect was prominent. (**B**) Coregistered transaxial PET images of CBF, $CMRO_2$, OEF, and FMZ binding (Bdg) at 12 to 13 hours and CMRGlc and MRI at 14 days after stroke onset in a 52-year old male patient. The large territorial defect is visible in all PET modalities with different extensions. The contour delineates the cortical infarct as determined on late MRI. FMZ binding precisely predicts the extension of the final infarct, whereas CBF delineates a considerably larger volume of disturbed perfusion. *Abbreviation*: MCAO, middle cerebral artery occlusion.

VALIDATION OF FLUMAZENIL IN ANIMAL MODELS

Based on the study of Sette et al. (22), who recommended FMZ as a tracer for early assessment of ischemic damage, we performed a multitracer positron emission tomography (PET)-study on binding of FMZ, regional cerebral blood flow (rCBF), regional cerebral metabolic rate of oxygen ($CMRO_2$), regional oxygen extraction fraction (OEF), and regional cerebral metabolic rate of glucose (CMRGlu) in the cat middle cerebral artery occlusion (MCAO) model (28). The development of defects in energy metabolism were related to the defects in FMZ binding in the course after transient MCAO (30–120 minutes) and to the size of the infarcts determined 15 hours after MCAO in 11 cats.

Irrespective of the level of reperfusion, deficits of FMZ binding two to three hours after MCAO were closely related to areas with severely depressed oxygen consumption (Fig. 1A) and predicted the size of the final infarcts (Fig. 2A), whereas preserved FMZ binding indicated intact cortex. In all animals, depression of glucose metabolism was larger than the defects in FMZ binding and the infarcts, indicating functional deactivation of brain areas beyond the

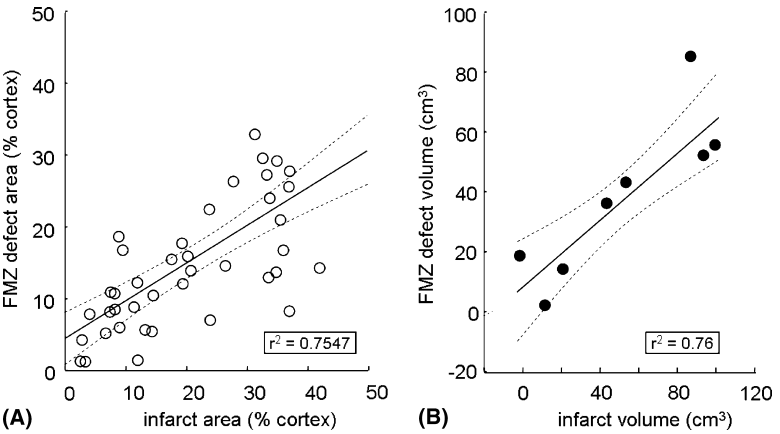

FIGURE 2 **(A)** Linear regression between matched areas showing defects in flumazenil (FMZ) binding three hours after middle cerebral artery occlusion (MCAO) respectively infarct areas assessed in histological sections 15 hours after MCAO. Data derived from matched coronal planes obtained in six cats. (**B**) Linear regression between final infarct volume on MRI/CT and volume of decreased FMZ binding on initial PET in 10 patients. *Broken lines* indicate 95% confidence limits.

permanent morphological damage. In addition, FMZ distribution within two minutes after injection was significantly correlated to flow and yielded reliable perfusion images.

These results demonstrate that the reduction of FMZ binding early after focal ischemia reflects irreversible neuronal damage that can otherwise only be detected by multitracer studies requiring arterial blood sampling. Independently of the binding of the tracer at steady state, imaging of perfusion is feasible by following the early distribution of FMZ (29). As confirmed in a succeeding autoradiographic study (30), the uptake of the BZR ligand is decreased in ischemic areas progressing to necrosis irrespective of reperfusion. A further support of the early irreversible impairment of the BZR receptor is yielded by Kaji et al. (31) who observed that neuronal DNA is still intact and cellular integrity is maintained in ischemic regions with preserved IMZ accumulation, whereas the impairment of this accumulation precedes DNA fragmentation and denaturation of cellular integrity. The only contradictory results were reported by Abe et al. (32) who observed vulnerability of the D1 dopamine and the muscarinic acetylcholine receptors to ischemia and reperfusion, but did not find a correlation of the reduced BZR binding with cell injury. In their model of transient MCAO in rats FMZ binding was not decreased in the striatum and cerebral cortex, suggesting that the BZR might be essentially stable to neuronal cell injury by transient ischemia. This discrepancy between this and the other autoradiographic and our in vivo imaging studies might be explained by differences in the experimental models where in the study by Abe et al. (32), the ischemic changes in the initial phase mainly affect the basal ganglia—where striatal interneurons might be remarkably resistant against mild ischemic brain injury (33) and later on spread to the cortex; however, rCBF was not measured to document the propagation of ischemia. It is one of the main disadvantages of BZR ligands for the demonstration of early neuronal injury that BZR are abundant in the cerebral cortex, but of low density in basal ganglia and brain stem, and practically missing in the white matter (2,34). Most data also stress the high sensitivity of functioning of GABA and 5HT receptors to ischemia (35,36) compared to the relative resistance of the glutamate receptors (37,38).

DETECTION OF IRREVERSIBLE DAMAGE IN ACUTE STROKE

With the aim to transfer the results obtained with FMZ in the experimental model of focal ischemia into clinical application, a similar multitracer PET study was performed in 10 patients with acute ischemic stroke. CBF, $CRMO_2$, OEF, and FMZ binding were studied by PET 3.5 to 16 hours after onset of symptoms, and the early changes in flow, oxygen metabolism, and BZR activity were compared with permanent disturbances in glucose metabolism and the size of the final infarcts determined on MRI or CT 12 to 22 days after the attack (39). In all patients except one rCBF was disturbed with marked decreases in eight and a hyperperfusion in one patient in areas corresponding to the location of neurological deficits. In these areas $CMRO_2$ was also reduced but to a variable degree, inducing highly variable OEF. FMZ binding in the normal cortex is 5.5 times higher than in the white matter. A threshold was operationally defined as 2 standard deviations below the mean value at four times the FMZ binding in white matter. Areas with FMZ binding decreased below this threshold corresponded to regions with markedly decreased $CMRO_2$ (<60 mmol/100 g/min) (Fig. 1B). In all cases, the permanent lesions were predicted by defects in early FMZ binding, the extent of which correlated significantly to the size of the final infarcts (with a slight underestimation) (Fig. 2B). The extents of critical hypoperfusion and of altered OEF were poor predictions of the final infarction. In finally hypometabolic cortex FMZ binding was initially decreased or normal, with OEF covering a wide range; FMZ below threshold indicated neuronal loss, whereas FMZ values above threshold suggested deactivation as the cause of metabolic disturbance in these areas (Fig. 1B). Additionally, a highly significant correlation was found between FMZ distribution within the first two minutes after injection and rCBF. These results demonstrate that permanently and irreversibly damaged cortex can be detected by reduced FMZ binding early after stroke. As an example of translational research, this study replicated and confirmed the experimental findings in the clinical setting and proved that irreversible tissue damage can be detected early after stroke without the necessity of multitracer injection and invasive (arterial) blood sampling.

In a further study, the probability threshold of final infarction was defined by comparing regional FMZ binding determined 2 to 12 hours after onset of symptoms to the final state of the

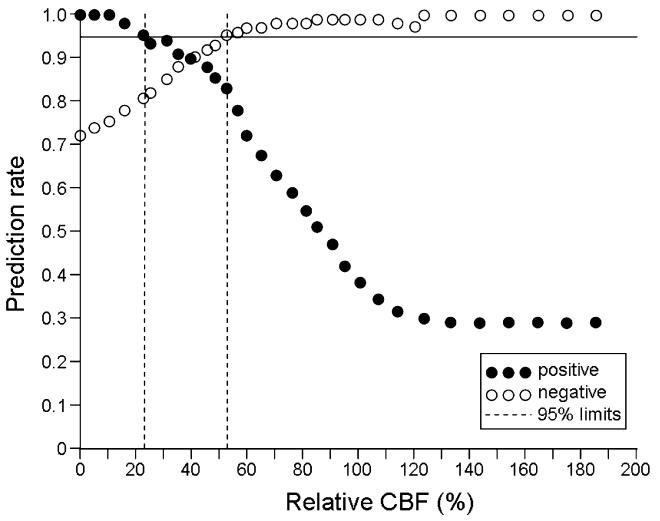

FIGURE 3 Weighted mean curves across 10 patients' volumes of interest and corresponding 95% probability limits, predicting cortical infarction (positive prediction curve) or negative infarction (negative prediction curve) from early relative cerebral blood flow. Lower endpoints of curves denote proportion of non-infarcted and infarcted tissue, respectively, as present in the analyzed sample. *Abbreviation*: CBF, cerebral blood flow.

tissue (infarcted or noninfarcted) three weeks later in 10 stroke patients (40). Using initial FMZ binding data from volumes of interest (3 mm radius) finally located within or outside the cortical infarct, cumulative probability curves were computed to predict eventual infarction or noninfarction. Positive (at least 95% chance of infarct) and negative (at least 95% chance of noninfarct) prediction limits for FMZ binding were determined at 3.4 and 5.5 times the mean of normal white matter (Fig. 3). Additionally, CBF probability curves for infarction were computed and positive and negative prediction limits were defined at 4.8 and 14.1 mL/100 g/min. Using the lower FMZ binding threshold of 3.4 for irreversible tissue damage and the upper CBF value of 14.1 mL/100 g/min for the threshold of critical perfusion at or above which tissue will likely be preserved, various cortical subcompartments could be identified: of the final cortical infarct a major portion (median 55.1%) showed FMZ binding critically decreased, thus predicting necrosis. In 20.15% of the final infarct, on average, CBF was in the penumbral range (<14.1 mL/100 g/min) and FMZ binding was above the critical threshold of irreversible damage, at the time of the study, thereby indicating morphologically intact but critically perfused tissue, that is, penumbra. Only 12.9% of the final infarct exhibited neuronal integrity and CBF values above the penumbral range—this tissue turned into necrosis despite sufficient blood supply and could benefit from neuroprotective or other measures targeted at secondary mechanisms. The penumbra (in this study 20.15% of final infarction) could be salvaged by effective reperfusion, whereas the largest portion (55.1% of the final infarct) is not amenable to any therapeutic strategy, since it is already irreversibly damaged at initial evaluation. The identification of the area of irreversible damage and its distinction from the penumbral zone, as it can be achieved by imaging of BZR binding and flow, therefore, not only may help to predict the clinical course after stroke, but also can estimate the potential efficacy of therapeutic strategies.

COMPARISON OF FLUMAZENIL-POSITRON EMISSION TOMOGRAPHY TO DIFFUSION WEIGHTED MAGNETIC RESONANCE IMAGING

Diffusion-weighted magnetic resonance imaging (DWI) has been the method of choice to detect ischemic lesions early after onset of symptoms (41) and, in combination with perfusion-weighted imaging, is widely applied for the selection of patients amenable for acute therapy, if a mismatch between these procedures suggests viable penumbral tissue. However, it has been shown repeatedly that an area with increased DWI signal does not necessarily turn into infarction but may finally normalize with spontaneous or treatment-induced recovery of neurological deficits

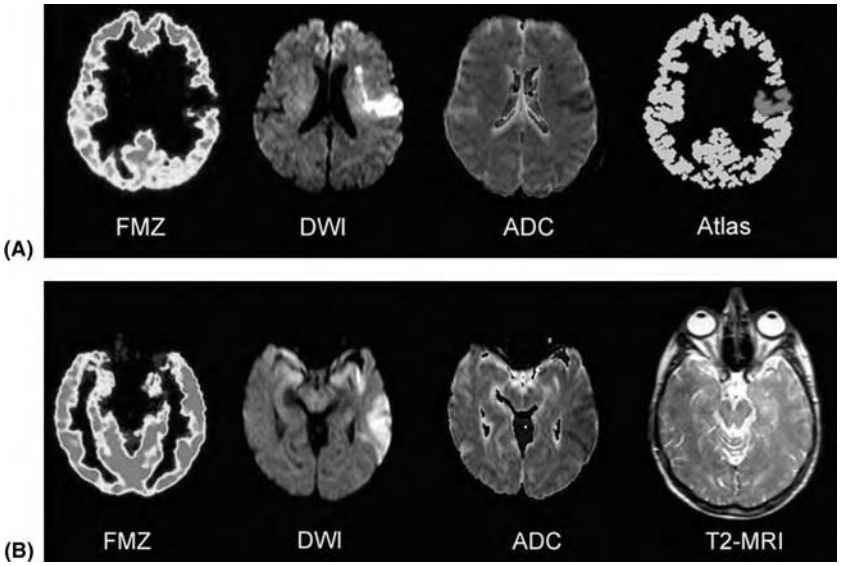

FIGURE 4 (*See color insert.*) (**A**) Coregistrated images in a patient seven hours after symptom onset showing decreased flumazenil (FMZ) binding, diffusion weighted imaging (DWI) hyperintensity, and decreased apparent diffusion coefficient (ADC) values in the left central region. Lesion volumes are transferred into T1-MRI-based cortical atlas (gray) for a voxel-by-voxel analysis of subcompartments with respect to final infarct volume (red). (**B**) DWI hyperintensity and decreased ADC values in the left temporal cortex of another patient three hours after symptom onset. The FMZ-positron emission tomography shows no decrease of tracer binding, and no final infarct is seen on the follow-up T2-MRI.

(42) limiting the prediction of infarcted and the definition of potentially viable penumbral tissue. These uncertainties and limitations of DWI may be better understood by comparing the results in individual patients with those from studies, applying a different approach for identification of tissue integrity. Therefore, DWI was compared to FMZ–PET with respect to the probability to predict infarction in 12 patients with early ischemic stroke (43). The patients were studied by DWI (median 6.5 hours after symptoms onset) and FMZ–PET (median interval 85 minutes between DWI and PET) and the extension of the final infarcts was determined on T2 weighted MRI 24 to 48 hours later. Probability curves predictive of eventual infarction were computed using respective FMZ, DWI, and apparent diffusion coefficient (ADC) values for voxels of interest, later classified as representing infarcted or noninfarcted tissue. Ninety-five percent limits predictive of cortical infarction were determined for relative FMZ binding ≤3.2 times the mean in white matter, DWI signal intensity ≥1.18 the contralateral value, and ADC ≤0.83 the contralateral value. Cortical regions with values beyond these 95% limits did not necessarily overlap nor were fully congruous with final cortical infarct volumes (Fig. 4A). Overall, 83.5 % of the final infarct volume, on average, was predicted by decreased FMZ binding, 84.7% by increased DWI signal intensity, and 70.9% by decreased ADC value. The portions of the final infarct not predicted in the early investigation (false-negatives) were 16.5% (median) for FMZ, 15.3% for DWI, and 29.1% for ADC. False-positive areas not included in the final infarct were negligible (median 0%) for FMZ, but relatively large for DWI (25.9%) and ADC (22.3%) (Fig. 4B). These results indicate that FMZ–PET and DWI are comparable in the prediction of probability of ischemic cortical infarction. However, FMZ–PET carries a lower probability of false-positive prediction. The final infarcts include tissue not identified by these imaging modalities; at the time of the study, these tissue compartments are viable and could benefit from treatment. Further insight can be obtained by extending the examinations to include perfusion-weighted magnetic resonance imaging (PWI) and $CBF/CMRO_2$ determination, respectively. The DW–PWI mismatch, as it is detected in many cases and considered as a surrogate of the penumbra, however, imprecisely depicts and overestimates the area of misery perfusion as it is obtained by PET (44) and, therefore, might not represent a fully reliable correlate of the penumbra.

THE VALUE OF FLUMAZENIL BINDING STUDIES FOR TREATMENT DECISIONS

Therapeutic strategies in acute ischemic stroke are targeted at rescuing from infarction ischemic but potentially viable tissue, the penumbra. As treatment can only be effective as long as tissue has not become necrotic, indicators of irreversible tissue damage or markers of neuronal integrity would be helpful for the selection of patients who might benefit from reperfusion induced by thrombolysis or other therapeutic approaches with a potential to salvage penumbra tissue but also with the hazard to further threaten patients with large infarction. In order to prove the validity of this concept, CBF and FMZ binding were assessed by PET in 11 patients with acute hemispheric ischemic stroke at the beginning of thrombolytic therapy [0.9 mg/kg recombinant tissue plasminogen activator (rt PA) 10% as i.v. bolus, 90 % as i.v. infusion over 60 minutes] initiated within three hours of onset of symptoms (45). The early PET findings were related to the change in neurological deficit (NIHSS) and to the extent of cortical damage on MRI or CT, three weeks after the stroke. Initial hypoperfusion was observed in all cases, and in eight patients the values were below critical thresholds estimated at 12 mL/100 g/min, comprising 1 to 174 cm^3 of cortical tissue. In four cases, distinct areas of decreased FMZ binding were detected within the severely hypoperfused regions, and corresponding infarcts have developed on final CT/MRI. In the other cases, the hypoperfusion could be reversed by thrombolysis to values above the upper threshold of the penumbra 24 hours after the stroke, and no cortical defects on morphological images were found (Fig. 5). Therefore, severe decreases in early FMZ binding, significantly ($P < 0.005$ by Fisher's exact test) predicted irreversible cortical damage. It was of interest to note that deficits in FMZ were not related to the size of the critically hypoperfused area: in small ischemic areas of two patients, irreversible damage was indicated by early loss of FMZ binding. In contrast, fairly large hypoperfused regions could also benefit from reperfusion and did not become infarcted, as long as reperfusion began before decreased FMZ binding indicated irreversible damage (Fig. 5B). The largest and most severely hypoperfused cortical area (174 cm^3), however, included a rather large region of decreased FMZ binding (112 cm^3). This finding suggested widespread neuronal damage at this early stage with

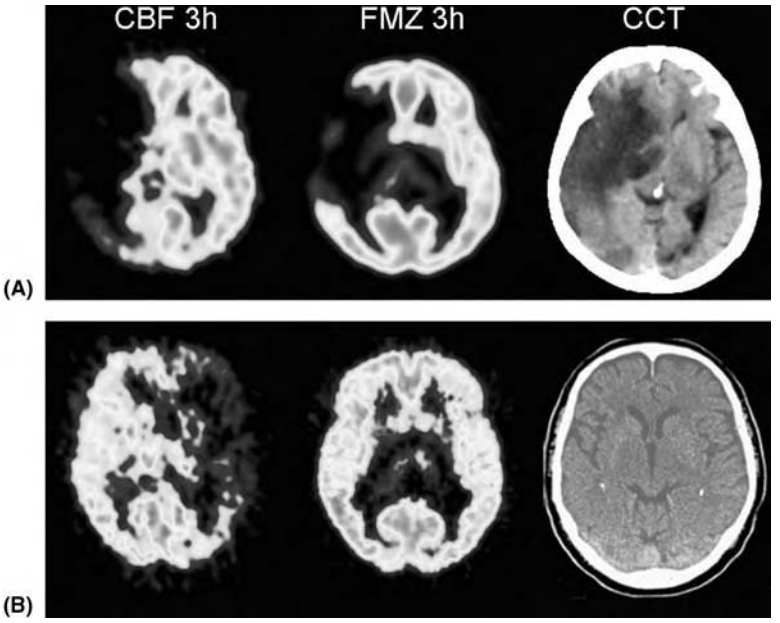

FIGURE 5 (*See color insert.*) Two patients with acute hemispheric stroke at the beginning of thrombolytic therapy demonstrate large ischemic areas on cerebral blood flow images. (**A**) Individual patient with an area of decreased flumazenil (FMZ) binding early (three hours) after symptom onset shows a corresponding large infarction on late cranial CT (CCT). (**B**) This individual patient does not show a defect in early FMZ binding. Thrombolytic therapy was effective in this patient, and infarction was not seen on late cranial CT. *Abbreviation*: CBF, cerebral blood flow.

subsequent infarct growth as indicated by late CT (Fig. 5A). This study proves the potential of BZR ligands to identify early after the attack irreversibly damaged cortical tissue which is not amenable for therapy and to differentiate the permanent lesion from the penumbra, which might benefit from reperfusion or neuroprotective treatment. Studies of the BZR are not limited to the complex logistics required by 11C tracer and PET, since similar results can be obtained with IMZ and SPECT (27,46,47), which might be of value for therapeutic decisions if appropriate investigations are carried out in the first hours after onset of symptoms.

The early assessment of large irreversible tissue damage is also important for the prediction of the further course and for the decision to interventional treatment to ameliorate the final outcome. This might be relevant for malignant brain infarcts, which result from space-occupying brain edema after ischemic stroke in the MCA territory, and carry a risk of mortality of ~ 80% under conservative treatment (48). To improve outcome with acceptable neurological impairment, invasive strategies such as decompressive hemicraniectomy or induced hypothermia might be justified, but patients who might benefit from these interventions must be selected and the time point must be determined when the intervention must be performed to prevent large lesions not compatible with a minimal quality of life. In 18 patients of a prospective study comprising 34 patients with acute infarcts, more than 50% of the MCA territory on CT performed <12 hours after onset of symptoms (49) PET of FMZ distribution [as a marker of flow (29)] and FMZ binding (as a marker of neuronal integrity) were performed 3 to 24 hours (mean 17.2 hours) after the onset of clinical symptoms (Table 1, Fig. 6). Of these patients, eight had a malignant course with transtentorial herniation, leading to death or severe permanent neurological deficits. In the other 10 cases, malignant brain swelling did not develop and these patients survived with mild to moderate handicap. The early PET investigations revealed significant differences between these two groups: The volume of the ischemic core region (CBF values determined by FMZ distribution <50% of the mean of the unaffected hemisphere) was larger in the malignant (144.5 cm^3) than in the benign group (62.2 cm^3, $P < 0.01$), and CBF was decreased to 21.5% in the malignant versus to 34.7% in the benign group ($P < 0.01$). The volume of irreversible neuronal damage assessed by FMZ binding (threshold 3.4 times the mean value of white matter) was significantly larger in the malignant (157.9 cm^3) than in the benign group (47.0 cm^3, $P < 0.01$). The penumbra zone, defined by flow reduction to 50% to 70% of the contralateral mean and by preserved FMZ binding, was smaller in the malignant than in the benign group (42.6 vs. 58.0 cm^3). The volume of irreversible neuronal damage, volume of ischemic core, and mean CBF within the core region correlated significantly with the clinical outcome of the patients, expressed by the modified Rankin Scale after three months. For the prediction of malignant infarction a cutoff value for irreversible neuronal damage that amounted to 95 cm^3 was determined; for the ischemic core region a cutoff value of 105.0 cm^3 and for mean CBF within the hypoperfused tissue a value of 25.5% was assessed. In the patients who died as a result of brain edema PET scans were performed 54.2 hours (mean) before patients showed clinical signs of brain death. In all cases with malignant course, the deteriorations of neurological deficits and the changes in neuromonitoring (intracranial pressure, tissue oxygen tension, concentration of glutamate, aspartate, GABA, glycerol, lactate, and pyruvate) occurred many hours after the PET studies, and peak values were reached 74.2 to 100.6 hours after stroke onset. Even transtentorial herniation was indicated later by abrupt deflections of the various neuromonitoring parameters.

TABLE 1 Neuronal Damage in Flumazenil-Positron Emission Tomography and Cerebral Blood Flow in Patients Developing Malignant Respectively Benign Courses of Stroke

	Volume of irreversible damage (cm^3)	Volume of ischemic core (cm^3)	Mean CBF in ischemic core (% unaffected hemisphere)	Volume of ischemic penumbra (cm^3)
Malignant ($n = 8$)	157.9 (± 37.9)	144.5 (± 27.6)	21.5 (± 3.7)	42.6 (± 14.4)
Benign ($n = 10$)	47.0 (± 46.9)	62.2 (± 37.2)	34.7 (± 6.6)	58.0 (± 30.8)
	$p < 0{,}01$	$p < 0{,}01$	$p < 0{,}01$	NS

Note: Values are mean ± SD. Note that in malignant stroke, larger irreversible damage correlates with larger ischemic core and deeper cerebral blood flow reduction in the ischemic core, while the penumbra is smaller than in benign stroke.
Abbreviation: CBF, cerebral blood flow.

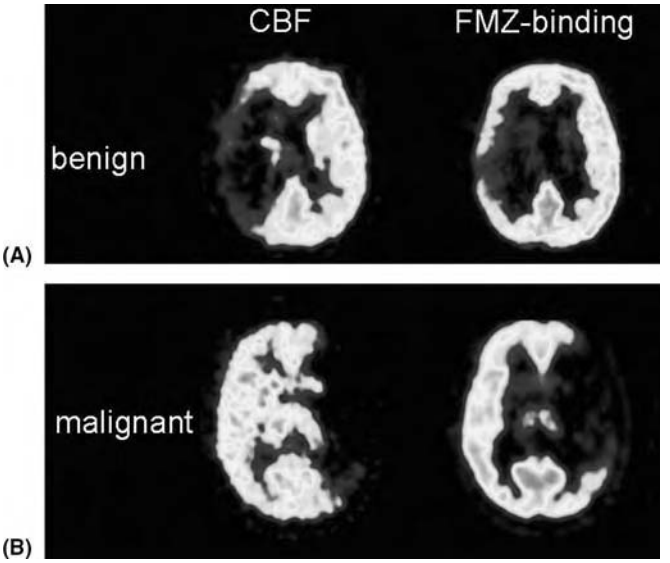

FIGURE 6 (*See color insert.*) (**A**) In a patient with benign course, the volume of severe cerebral blood flow (CBF) reduction is much larger than the volume of reduced flumazenil (FMZ) binding. (**B**) In another patient with malignant course, the volume of reduced FMZ binding is almost as large as the volume of severe CBF reduction. CBF and FMZ binding were determined early after stroke onset.

The important conclusion from the comparison of early PET studies with continuous neuromonitoring in large MCA infarction is the predictive value of the identified volume of critically hypoperfused tissue and of reduced uptake of a marker of neuronal integrity for the development of malignant infarction. In this context, PET results precede the clinical impairment and changes observed by monitoring, and this observation again is supported by comparable results in the experimental model of MCAO in cats (50), where large critically ischemic volumes predicted a malignant course characterized by progressive deterioration, extension of hypoperfusion, increase of intracranial pressure, and increase of extra cellular biochemical markers of ischemic damage. Therefore, the assessment of critically hypoperfused areas and of reduced receptor binding is useful for the identification of patients at risk for formation of space-occupying edema and for selection of patients who might benefit from invasive interventional therapeutic strategies; the time point of significant changes in neuromonitoring is coincident with severe clinical deterioration, often caused by transtentorial herniation, and might be too late for successful prevention of massive tissue destruction.

ANNEX: FLUMAZENIL AS A TRACER FOR CENTRAL BENZODIAZEPINE RECEPTORS

Carbon 11-labelled FMZ, which is regarded as the radioligand of choice for the in vivo quantification of central BZRs (12), was prepared by a modification of the method of Maziere et al. (51): [N-methyl-^{11}C]FMZ is methylated by reaction of the precursor desmethyl FMZ (Ro 15-5528 from Hoffmann-La Roche, Basel, Switzerland) with [^{11}C]methyl iodide, which in turn is produced from [^{11}C]carbon dioxide and lithium aluminium hydride in THF and subsequent reaction with 1 mL 57% hydriodic acid.

[^{11}C]methyl iodide is bubbled by a nitrogen flow into a solution of 0.5 to 1 mg desmethyl FMZ in 800 µL of dry acetonitrile activated by 15 µL of 5 M NaOH. After heating the closed reaction vial for 5 minutes in an oil bath of 70°C the reaction mixture is neutralized by 150 µL of 0.5 M hydrogen chloride. It is injected into a semipreparative HPLC system (column: Phenomenex Luna, silica, 10 µm, 100A, 250 × 10 mm; eluent: dichloromethane with 1.5% of solution A, A = ethanol, 2% water, 0.03% ethyl amine; UV detection at 254 nm; flow 8 mL/min). The product fraction is collected from about six to seven minutes in a rotary evaporator and the

solvent is removed under reduced pressure. The residue is dissolved in 8 mL of 0.9% saline and transferred into a sterile evacuated vial by suction through a sterile filter. Activity of the solution ready for injection: Up to about 7 GBq (conditions of irradiation of target gas for [^{11}C]carbon dioxide production: 40 µA with 17 MeV protons during 40 minutes), radiochemical purity is ≥95%. Synthesis is completed in 35 minutes and specific activity at that time (EOS) is 20 to 100 GBq/µmol.

After intravenous injection of 20 mCi (740 MBq), the distribution and accumulation of this tracer was followed for 60 minutes by serial scanning on the ECAT EXACT HR scanner (Siemens/CTI) using three-dimensional data acquisition mode providing 47 contiguous 3 mm slices of 5 mm full width at half maximum in-plane reconstructed resolution (52). The multiple brain activity frames after FMZ injection were corrected for decay, attenuation, and scatter and quantified to Bq/cm^3. The initial tracer distribution reached within two minutes after injection served as an indicator of the perfusion pattern as it was calibrated to the flow values determined by $H_2{}^{15}O$ and arterial blood sampling (29). BZR density was estimated from the distribution of FMZ 30 to 60 minutes after the bolus injection. In a few cases in which arterial blood samples were available, a two-compartment, two-parameter model could be applied to estimate regional receptor distribution (53,54). The ratio of distribution volume between cortical and white matter regions compared well with corresponding values of activity distribution between 30 and 60 minutes. Since the quantification of receptor density was not generally feasible—and arterial blood sampling was especially prohibited in cases amenable for thrombolysis—relative values of FMZ binding in comparison to averaged white matter activity were used for further analysis. This approach is also justified by the binding equilibrium achieved 20 minutes after injection and the lack of specific receptors in the white matter which can serve as the reference region (14). However, a quantification of the density and affinity of central BZRs in different brain regions cannot be obtained by this procedure; the determination of B_{max} and K_d requires multiple injections of FMZ at different specific radioactivity and arterial blood sampling (54,55).

REFERENCES

1. Krnjevic K. Neurotransmitters in cerebral cortex. In: Jones E, Peters A, eds. Cerebral Cortex. Vol. 2. Functional Properties of Cortical Cells. New York: Plenum Press, 1984:39–61.
2. Braestrup C, Nielsen M. Benzodiazepine receptors. In: Iversen Ll, Iversen SD, Snyder SH, eds. Handbook of Psychopharmacology. Vol. 17. New York: Plenum Press, 1983:285–384.
3. Schwartz-Bloom RD, Sah R. Gamma-aminobutyric acid (A) neurotransmission and cerebral ischemia. J Neurochem 2001; 77:353–371.
4. Alicke B, Schwartz-Bloom RD. Rapid down-regulation of gabaa receptors in the gerbil hippocampus following transient cerebral ischemia. J Neurochem 1995; 65:2808–2811.
5. Xu ZC, Pulsinelli WA. Responses of ca1 pyramidal neurons is rat hippocampus to transient forebrain ischemia: an in vivo intracellular recording study. Neurosci Lett 1994; 171:187–191.
6. Garcia JH, Mitchem Hl, Briggs L, et al. Transient focal ischemia in subhuman primates. neuronal injury as a function of local cerebral blood flow. J Neuropathol Exp Neurol 1983; 42:44–60.
7. Garcia JH, Liu KF, Ye ZR, et al. Incomplete infarct and delayed neuronal death after transient middle cerebral artery occlusion in rats. Stroke 1997; 28:2303–2309.
8. Lyden P, Shuaib A, Ng K, et al. Clomethiazole acute stroke study in ischemic stroke (class-I): final results. Stroke 2002; 33:122–128.
9. Müller WE. The Benzodiazepine Receptor. Cambridge, England: Cambridge University Press, 1987.
10. Olsen RW, Tobin AJ. Molecular Biology Of Gabaa Receptors. FASEB J 1990; 4:1469–1480.
11. Hantraye P, Kaijima M, Prenant C, et al. Central type benzodiazepine binding sites: a positron emission tomography study in the baboon's brain. Neurosci Lett 1984; 48:115–120.
12. Abadie P, Baron JC. In vivo studies of the central benzodiazepine receptors in the human brain with positron emission tomography. In: Diksic M, Reba RC, eds. Radiopharmaceuticals and Brain Pathology Studies with PET and Spect. Boca Raton: CRC Press, 1991:357–379.
13. Sadzot B, Franck G. Non-invasive methods to study drug disposition: positron emission tomography detection and quantification of brain receptors in man. Eur J Drug Metab Pharmacokinet 1990; 15:135–142.
14. Pappata S, Samson Y, Chavoix C, et al. Regional specific binding of (11c)Ro 15 1788 to central type benzodiazepine receptors in human brain: quantitative evaluation by PET. J Cereb Blood Flow Metab 1988; 8:304–313.
15. Duncan JS. Modern treatment strategies for patients with epilepsy: a review. J R Soc Med 1991; 84:159–162.

16. Szelies B, Weber-Luxenburger G, Pawlik G, et al. Mri-guided flumazenil- and FDG-PET in temporal lobe epilepsy. Neuroimage 1996; 3:109–118.
17. Savic I, Ingvar M, Stone-Elander S. Comparison of [11c] flumazenil and [18f] FDG as PET markers of epileptic foci. J Neurol Neurosurg Psychiatry 1993; 56:615–621.
18. Henry TR, Frey KA, Sackellares JC, et al. In vivo cerebral metabolism and central benzodiazepine receptor binding in temporal lobe epilepsy. Neurology 1993; 43:1998–2006.
19. Fukuchi K, Hashikawa K, Seike Y, et al. Comparison of iodine-123-iomazenil spect and technetium-99m-hmpao-spect in Alzheimer's disease. J Nucl Med 1997; 38:467–470.
20. Holthoff VA, Koeppe RA, Frey KA, et al. Positron emission tomography measures of benzodiazepine receptors in Huntington's disease. Ann Neurol 1993; 34:76–81.
21. Ishibashi M, Sakai T, Matsuishi T, et al. Decreased benzodiazepine receptor binding in Machado-Joseph disease. J Nucl Med 1998; 39:1518–1520.
22. Sette G, Baron JC, Young AR, et al. In vivo mapping of brain benzodiazepine receptor changes by positron emission tomography after focal ischemia in the anesthetized baboon. Stroke 1993; 24:2046–2057.
23. Al-Tikriti MS, Dey HM, Zoghbi SS, et al. Dual isotope autoradiographic measurement of regional blood flow and benzodiazepine receptor availability following unilateral middle cerebral artery occlusion. Eur J Nucl Med 1994; 21:196–202.
24. Matsuda H, Tsuji S, Kuji I, et al. Dual-tracer autoradiography using I-125 iomazenil and TC- 99m-hmpao in experimental brain ischemia. Nucl Med Commun 1995; 16:581–590.
25. Hatazawa J, Satoh T, Shimosegawa E, et al. Evaluation of cerebral infarction with iodine-123-iomazenil spect. J Nucl Med 1995; 36:2154–2161.
26. Hayashida K, Hirose Y, Tanaka Y, et al. Reduction of 123I iomazenil uptake in hemodynamically and metabolically impaired brain areas in patients with cerebrovascular disease. Nucl Med Commun 1996; 17:701–705.
27. Nakagawara J, Sperling B, Lassen NA. Incomplete brain infarction of reperfused cortex may be quantitated with iomazenil. Stroke 1997; 28:124–132.
28. Heiss W-D, Graf R, Fujita T, et al. Early detection of irreversibly damaged ischemic tissue by flumazenil positron emission tomography in cats. Stroke 1997; 28:2045–2051.
29. Thiel A, Löttgen J, Grond M, et al. Estimation of regional cerebral blood flow levels in ischemia using [15o]water or [11c]flumazenil PET without arterial input function. J Comput Assist Tomogr 2001; 25:446–451.
30. Watanabe Y, Nakano T, Yutani K, et al. Detection of viable cortical neurons using benzodiazepine receptor imaging after reversible focal ischaemia in rats: comparison with regional cerebral blood flow. Eur J Nucl Med 2000; 27:308–313.
31. Kaji T, Kuge Y, Yokota C, et al. Characterisation of [123i] iomazenil distribution in a rat model of focal cerebral ischaemia in relation to histopathological findings. Eur J Nucl Med Mol Imaging 2004; 31:64–70.
32. Abe K, Kashiwagi Y, Tokumura M, et al. Discrepancy between cell injury and benzodiazepine receptor binding after transient middle cerebral artery occlusion in rats. Synapse 2004; 53:234–239.
33. Katchanov J, Waeber C, Gertz K, et al. Selective neuronal vulnerability following mild focal brain ischemia in the mouse. Brain Pathol 2003; 13:452–464.
34. Olsen RW. The gaba postsynaptic membrane receptor-ionophore complex. Site of action of convulsant and anticonvulsant drugs. Mol Cell Biochem 1981; 39:261–279.
35. Schwartz RD, Yu X, Wagner J, et al. Cellular regulation of the benzodiazepine/gaba receptor: arachidonic acid, calcium, and cerebral ischemia. Neuropsychopharmacology 1992; 6:119–125.
36. Brown CM, Kilpatrick AT, Martin A, et al. Cerebral ischaemia reduces the density of 5-Ht2 binding sites in the frontal cortex of the gerbil. Neuropharmacology 1988; 27:831–836.
37. Westerberg E, Monaghan DT, Cotman CW, et al. Excitatory amino acid receptors and ischemic brain damage in the rat. Neurosci Lett 1987; 73:119–124.
38. Dewar D, Wallace MC, Kurumaji A, et al. Alterations in the N-methyl-D-aspartate receptor complex following focal cerebral ischemia. J Cereb Blood Flow Metab 1989; 9:709–712.
39. Heiss W-D, Grond M, Thiel A, et al. Permanent cortical damage detected by flumazenil positron emission tomography in acute stroke. Stroke 1998; 29:454–461.
40. Heiss W-D, Kracht LW, Thiel A, et al. Penumbral probability thresholds of cortical flumazenil binding and blood flow predicting tissue outcome in patients with cerebral ischaemia. Brain 2001; 124:20–29.
41. Donnan GA, Davis SM. Neuroimaging, the ischaemic penumbra, and selection of patients for acute stroke therapy. Lancet Neurol 2002; 1:417–425.
42. Kidwell CS, Alger JR, Saver JL. Beyond mismatch: evolving paradigms in imaging the ischemic penumbra with multimodal magnetic resonance imaging. Stroke 2003; 34:2729–2735.
43. Heiss W-D, Sobesky J, Smekal U, et al. Probability of cortical infarction predicted by flumazenil binding and diffusion-weighted imaging signal intensity: a comparative positron emission tomography/magnetic resonance imaging study in early ischemic stroke. Stroke 2004; 35:1892–1898.

44. Sobesky J, Zaro-Weber O, Lehnhardt FG, et al. Does the mismatch match the penumbra? magnetic resonance imaging and positron emission tomography in early ischemic stroke. Stroke 2005; 36:980–985.
45. Heiss W-D, Kracht L, Grond M, et al. Early [11c]flumazenil/H2o positron emission tomography predicts irreversible ischemic cortical damage in stroke patients receiving acute thrombolytic therapy. Stroke 2000; 31:366–369.
46. Dong Y, Fukuyama H, Nabatame H, et al. Assessment of benzodiazepine receptors using iodine-123-labeled iomazenil single photon emission computed tomography in patients with ischemic cerebrovascular disease. A comparison with PET study. Stroke 1997; 28:1776–1782.
47. Müller V, Saur D, Klutmann S, et al. Experience with 123i-iomazenil spect in acute cerebral infarction. Nucl Med Commun 2002; 23:1191–1196.
48. Hacke W, Schwab S, Horn M, et al. "Malignant" middle cerebral artery territory infarction: clinical course and prognostic signs. Arch Neurol 1996; 53:309–315.
49. Dohmen C, Bosche B, Graf R, et al. Prediction of malignant course in mca infarction by PET and microdialysis. Stroke 2003; 34:2152–2158.
50. Heiss WD, Dohmen C, Sobesky J, et al. Identification of malignant brain edema after hemispheric stroke by PET-imaging and microdialysis. Acta Neurochir Suppl 2003; 86:237–240.
51. Maziere M, Hantraye P, Prenant C, et al. Synthesis of ethyl 8-fluoro-5,6-dihydro-5-(11c)methyl-6-oxo- 4h-imidazo(1,5-A) (1,4)benzodiazepine-3-carboxylate (Ro 15.1788-11c): a specific radioligand for the in vivo study of central benzodiazepine receptors by positron emission tomography. Int J Appl Radiat Isot 1984; 35:973–976.
52. Wienhard K, Dahlbom M, Eriksson L, et al. The ECAT exact HR: performance of a new high resolution positron scanner. J Comput Assist Tomogr 1994; 18:110–118.
53. Frey KA, Holthoff VA, Koeppe RA, et al. Parametric in vivo imaging of benzodiazepine receptor distribution in human brain. Ann Neurol 1991; 30:663–672.
54. Abadie P, Baron JC, Bisserbe JC, et al. Central benzodiazepine receptors in human brain: estimation of regional Bmax and Kd values with positron emission tomography. Eur J Pharmacol 1992; 213:107–115.
55. Koeppe RA, Holthoff VA, Frey KA, et al. Compartmental analysis of [11c]flumazenil kinetics for the estimation of ligand transport rate and receptor distribution using positron emission tomography. J Cereb Blood Flow Metab 1991; 11:735–744.

11 Imaging the Penumbra: Positron Emission Tomography Fluoromisonidazole

Neil J. Spratt and David W. Howells
Department of Medicine, University of Melbourne, National Stroke Research Institute, Austin Health, Melbourne, Victoria, Australia

Geoffrey A. Donnan
National Stroke Research Institute, Austin Health, University of Melbourne, Melbourne, Victoria, Australia

INTRODUCTION

One of the disadvantages of many penumbral imaging methods used, both in humans and experimental animals, is that they rely on cerebral blood flow (CBF) at a single point in time to assess the degree of ischemia. This neglects the important considerations of tissue/cellular metabolic rate and time in the assessment of penumbra. An appealing alternative approach is to use a marker of cellular hypoxia, thereby directly assessing the combination of oxygen delivery and use. Several compounds and methods have been tested as hypoxic markers, of which fluoromisonidazole (FMISO) is the best established.

Fluorine-18 FMISO (^{18}F-FMISO) positron emission tomography (PET) uses as a radioligand the nitroimidazole compound FMISO that is trapped within hypoxic cells (1). As FMISO is a marker of intracellular hypoxia rather than tissue perfusion, it may provide a more direct measure of threatened tissue than other available techniques. This may be particularly relevant for tissues with lower baseline metabolic rate and CBF such as cerebral white matter. FMISO has been used extensively as a marker of hypoxic tissue within tumor cells (2). It has also been shown to localize to hypoxic myocardium, which retained glucose catabolic function but had lost contractile function (3). This chapter will briefly outline the mechanism of binding of hypoxic markers such as FMISO within hypoxic cells, what is known about the characteristics of FMISO binding in animals and humans, and then summarize the available data regarding the use of FMISO in stroke.

HISTORY OF THE DEVELOPMENT OF HYPOXIC MARKERS

FMISO belongs to the class of compounds known as nitroimidazoles. These compounds were first used therapeutically as antibiotics (e.g., metronidazole "Flagyl™"). Nitroimidazoles have antiparasitic and antimicrobial actions against anaerobic organisms, due to their selective reduction and binding in hypoxic environments. The chemically reactive reduced forms, which are generated in the presence of hypoxia, lead to formation of cytotoxic products that inhibit DNA synthesis and cause degradation of existing DNA within microorganisms (4,5). During the 1970s interest focused on this class of compounds as potential therapeutic agents for use in radiation oncology, allowing targeting of hypoxic regions within tumors. The rate of killing of tumor cells by radiation is 2.5 to 3.0 times higher in the presence of oxygen (6). Since solid tumors often have zones of hypoxia, and these radioresistant regions are thought to be responsible for tumor recurrence, the electron affinity of nitroimidazoles appeared well suited to a radiosensitizing role for these compounds, and misonidazole (MISO) initially showed promise as a radiosensitizing agent. It was quickly discovered, however, that toxicity in the form of peripheral neuropathy became dose limiting before maximum radiosensitization. These doses (approximately 12 g/m^2) are several orders of magnitude greater than those used in imaging studies.

Despite the impracticality of this compound as a radiosensitizer, it was the obvious candidate to develop imaging of hypoxic regions within tumors. Safety had been demonstrated for doses much greater than the tracer amounts required for imaging. Moreover, the chemical structure was well suited for radiolabeling with positron and gamma-emitting radioisotopes (7–9). Once the ability to safely image hypoxic regions in vivo using PET or single-photon emission computed tomography (SPECT) was realized, alternative applications in cardiac and cerebral ischemia quickly became apparent.

CHARACTERISTICS OF NITROIMIDAZOLES AS HYPOXIC MARKERS

The commonly used nitroimidazole antibiotics such as metronidazole ("Flagyl") have reduction potentials of approximately –415 mV, and so are efficiently reduced in anaerobic bacteria, with redox potentials of –430 to –460 mV (1). The most negative redox potentials in aerobic cells, however, are only about –320 mV (NAD/NADH and NADP/NADPH couples), so metronidazole is not efficiently reduced in these cells. This selectivity is the basis for the efficient activity of these antibiotics against anaerobic organisms; however, a molecule with lower reduction potential is necessary to obtain useful reduction in hypoxic aerobic cells. Changing the substitution pattern from the 5-nitro of metronidazole to the 2-nitro produces MISO, which has a more suitable reduction potential of –389 mV. Lipophilicity of the compounds is the major factor affecting their diffusion into cells; however increasing lipophilicity also prolongs the clearance time from blood. Blood clearance is important for imaging applications, because adequate clearance (reduction of nonspecific background signal) must occur before a sufficient hypoxic—normoxic tissue ratio is achieved for imaging.

Suitability of nitroimidazoles for imaging of hypoxic tissue is dependent on four factors (1):

1. Delivery to hypoxic cells—dependent on dose and diffusibility.
2. The fraction becoming irreversibly reduced—dependent on the oxygen concentration at which trapping occurs.
3. Speed of clearance from normoxic tissues—adequate contrast between hypoxic and normoxic tissues is necessary for imaging.
4. Duration retained in hypoxic cells—sufficient to allow imaging.

Preliminary in vitro studies established that MISO, and its fluorinated congener FMISO, had suitable characteristics and these agents were the first chosen for further investigation as PET hypoxia imaging agents. The two compounds were retained similarly in hypoxic cells within in vitro tumor cell spheroids; however, FMISO uptake was greater than that of MISO under similar conditions when assessed in a mouse tumor model (10). As FMISO is labeled with a positron emitter suited to the process of imaging applications (^{18}F), it was the primary compound investigated for PET studies.

Nitroimidazoles diffuse freely across cell membranes (1), and are bound within hypoxic cells (Fig. 1) (11,12). Binding is in inverse proportion to pO_2 in living cells (10,13). The proposed mechanism of binding in hypoxic tissue is through a series of reduction steps resulting in binding to intracellular molecules (12,14). The initial reduction to the nitro anion radical occurs in all metabolically active cells, however, in the presence of oxygen reoxidation is favored. The resultant parent compound is freely diffusible, and will, therefore, equilibrate with plasma and be cleared from the tissues. In hypoxic tissues the reactive metabolite is bound to intracellular molecules. Nitroreductase activity in cells is not inhibited by a range of standard inhibitors, implying that these compounds are plentiful and therefore unlikely to limit hypoxic binding (15). The labelling partition for MISO between cytoplasm and nucleus is proportional to the

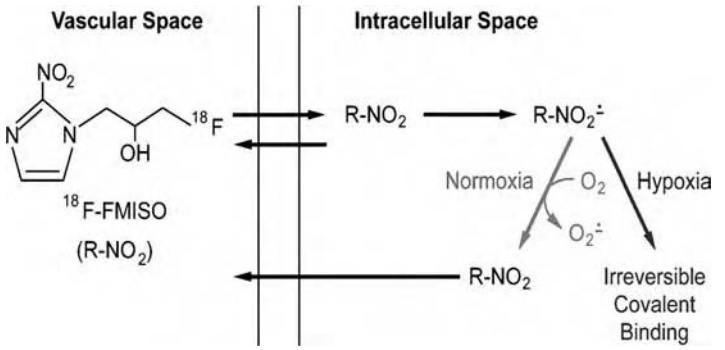

FIGURE 1 Proposed mechanism of nitroimidazole binding within hypoxic cells. *Source*: From Ref. 78.

relative volume of each compartment (16), suggesting that binding occurs in a nonspecific fashion to a range of intracellular molecules. This binding is only very slowly reversible, with a half-life of approximately 55 hours (13). Because the initial reduction reaction relies on active metabolism, no trapping occurs in necrotic cells (10). In addition binding of tracer is relatively independent of blood flow, when assessed in models of cerebral or myocardial ischemia (3,17). In a dog myocardial occlusion model, concentrations of tracer in the lowest flow areas (necrotic core) were equal to that in plasma, suggesting adequate delivery but no binding (12). Certain factors other than hypoxia have been shown to affect rate of binding during in vitro studies. This included cell growth state (tumor cell lines), glucose concentration, and nonprotein sulfhydryl concentrations (11). Overexpression of the cytochrome P450 reductase system, by recombinant plasmid transfection, was shown to influence the rate of binding to a greater extent than other reductase enzymes, suggesting that this is the most important enzyme in the reduction and binding of these compounds, and that intracellular enzyme concentration may influence hypoxic binding (18). The effect of any of these factors was small compared to that of varying oxygen concentrations, which produced a 12- to 28-fold increase in bound activity in four different cell lines (11).

ANIMAL/HUMAN STUDIES OF FLUOROMISONIDAZOLE

Fluoromisonidazole for Imaging Hypoxic Regions Within Tumors

Initial characterization of FMISO as a hypoxia imaging agent was performed in tumor cell lines and in rodent tumor models using autoradiography (10,11,19,20). Dogs with spontaneous tumors were used for initial development of a PET imaging protocol, which could then be modified for clinical use (21). Autoradiographic and PET studies in rat intracerebral glioma models have demonstrated that uptake occurs in cerebral tumors (22,23). Rasey et al. manipulated the inspired oxygen concentration to determine the effect on the radiobiologically hypoxic fraction as determined by modeling of FMISO uptake or by radiation response data. At low inspired oxygen concentrations there was a discrepancy between the techniques, which the authors felt was likely due to the failure of FMISO to label cells with an oxygen level at or above 2 to 3 mmHg—these cells may nevertheless be substantially protected against the effects of radiation. This suggests that there is quite a tight threshold of oxygen concentration for FMISO binding in cells, which in a stroke context reduces the likelihood of significant binding in nonthreatened oligemic tissue.

PET studies using FMISO were then used for imaging of hypoxia in human tumors (24,25), providing a less invasive method than previously used Eppendorf electrodes. Based on data from normal tissue distribution in animal models and on the first six patients with FMISO binding areas within tumors, a tumor:plasma ratio ≥1.4, two hours after administration was defined as hypoxic (24). Interestingly, in this initial study the three patients who returned for a repeat PET scan after a course of fractionated radiotherapy no longer had hypoxic regions detectable. Hypoxic regions have been demonstrated in a wide range of tumor types using FMISO PET, with significant heterogeneity seen within tumor types and within patients (24,25). Eliciting the prognostic value of tumor hypoxia in predicting tumor recurrence has proved difficult in human studies due to difficulties achieving follow-up in these patients, and the fact that many die from metastatic disease before experiencing failure of local control (25). FMISO has also been used to image hypoxia in human cerebral gliomas (26). Interestingly, all three patients studied showed increased tumor uptake compared to normal cerebral cortex, when imaged only five minutes after tracer injection. This likely represents an effect of increased tumor perfusion, and only two of the three patients showed increased uptake (representing tumor hypoxia) at two hours.

Fluoromisonidazole for the Investigation of Infection

There is a limited literature on the use of FMISO to study infection. In a rat peritonitis model of sepsis, FMISO uptake was not increased, suggesting that hypoxia was not a significant factor in the resultant organ injury (27). Interestingly, when the femoral artery was ligated, there was increased uptake of FMISO in the skeletal muscle of septic rats, with concomitant perfusion

studies showing a much more dramatic reduction of perfusion to the affected limb in septic than in control animals. A study of periodontal infection in patients with nasopharyngeal carcinoma undergoing FMISO PET revealed this to be a very sensitive and specific technique for the detection of these infections (by predominantly anaerobic organisms) (28). All 14 of 14 cases of dental caries with root canal infection, 15/15 cases of periodontal abscess, and 45/51 cases of periodontitis were successfully detected, with no false positives in healthy teeth or control patients.

Fluoromisonidazole for the Investigation of Myocardial Ischemia

FMISO has also been utilized for the investigation of hypoxia in myocardial infarction. Studies in isolated myocytes demonstrated avid uptake under conditions of anoxia or hypoxia, and that this occurred in the absence of significant cellular injury as measured by creatine kinase release or morphological change (29). Initial studies in rabbits and dogs showed selective retention in conditions of low flow ischemia or normal flow hypoxia, but not in hearts subject to 35 minutes of ischemia followed by 20 minutes of reperfusion (30). In a circumflex coronary artery occlusion model, accumulation of tracer occurred in inverse proportion to blood flow, indicating increased binding in hypoxic tissue (12). Similar results were demonstrated in studies of isolated perfused hearts subject to either hypoxia or ischemia (30). Importantly, continuous monitoring of developed left ventricular pressure (30), or contractile function (31) demonstrated resumption of normal cardiac function in reperfusion groups, suggesting the potential for functional recovery in tissue retaining tracer. In a permanent coronary occlusion model, the fractional extraction of ^{18}F-FMISO was maximal with tracer administration early after coronary occlusion. When tracer was administered at 24 hours, fractional extraction was only marginally higher than that in nonischemic myocardium (32), providing in vivo evidence for the lack of binding in necrotic tissue.

The feasibility of ^{18}F-FMISO PET in myocardial ischemia was also established using a dog coronary artery occlusion model (31,33). Scans showed specific uptake within the ischemic anterior wall, which was observed from two to four hours after tracer administration (31). Histochemical and histological studies suggested uptake occurring in areas without evidence for infarction, as well as in tissue with more clear-cut ischemic damage. A comparison of binding of tritiated FMISO and ^{18}F-Fluorodeoxyglucose (^{18}F-FDG) uptake (used in FDG/flow mismatch studies) in the same model showed greater uptake of FMISO in regions of low flow. The authors suggest that FMISO is as sensitive as FDG for detecting ischemia, and could be used to detect viable myocardium (33).

The positron-emitting ^{18}F-labeled FMISO is used for PET studies, while the beta particle-emitting ^{3}H-label is more suitable for animal and in vitro autoradiographic studies. Concurrent injection of ^{3}H- and ^{18}F-FMISO in a coronary occlusion model has confirmed excellent agreement in the deposition of the two tracers with a slope of 1.01 and $R^2 = 0.98$ (31), suggesting that addition of tritium does not result in any significant change in binding characteristics.

FLUOROMISONIDAZOLE AND STROKE

Relatively early in the development of the nitroimidazole hypoxic markers, their potential for use in stroke was recognized. Intracellular binding occurs in proportion to the degree of cellular hypoxia (10,11), yet is dependent on active cellular metabolism and so does not occur in necrotic tissue (10). Therefore they appeared to be ideal candidates to image the ischemic penumbra. Because these agents are bound in proportion to intracellular hypoxia, which is probably the critical factor in cell death, they may also avoid some of the difficulties inherent in perfusion imaging methods due to different rates of metabolism (and therefore oxygen utilization) in some tissues. For example, cerebral white matter has lower metabolic activity and perfusion than cortical grey matter, and may have a different blood flow threshold for infarction (34). FMISO uptake is proportional to degree of intracellular hypoxia (10,13), so may be more applicable to the investigation of threatened white matter than perfusion-based penumbral imaging methods. Because the technique for FMISO PET studies is simpler to apply than that for the more standard oxygen–water PET, and FMISO autoradiography is easily applied to the study of small animal models, FMISO imaging seems ideal to further our understanding of stroke and the ischemic penumbra.

Animal Studies

Much of our knowledge about the pathophysiology of ischemic brain comes from nonhuman studies using cell culture, tissue slice preparations and in vivo models of stroke. Being able to correlate the findings in human imaging studies with the pathophysiological events occurring in these models is an important goal to further our understanding of human stroke. The previously discussed studies in the fields of oncology and cardiology have established that FMISO is wellsuited to studies in both small and large animals, as well as in vitro systems; however, the use of this marker in stroke models has been limited to date.

The nonfluorinated congener ^{3}H-MISO was used in a small study using a gerbil carotid occlusion model (17). Increased uptake was seen in the ipsilateral hemisphere and this correlated with stroke severity at six to nine hours postocclusion. Microscopic autoradiography showed widespread diffuse labeling within the ischemic hemisphere, some over areas of histological damage, and some over areas that appeared intact. MISO and FMISO have very similar in vivo characteristics. FMISO has a marginally slower rate of tissue uptake and blood clearance, however brain uptake at two hours is higher than for MISO (8). FMISO is more commonly utilized because of its suitability for PET imaging studies using ^{18}F.

^{18}F-FMISO autoradiography has been used in the commonly used temporary rat middle cerebral artery (MCA) thread-occlusion model (35). Binding was most intense and widespread soon after thread occlusion, in the entire ipsilateral MCA territory (Fig. 2). A smaller volume of bound tissue was seen at later time points (two to three hours) and surrounded the infarct core. Binding was negligible in the subacute phase (6 to 24 hours). The degree of binding decreased inversely with the evolution of ischemic change as assessed by the vital stain

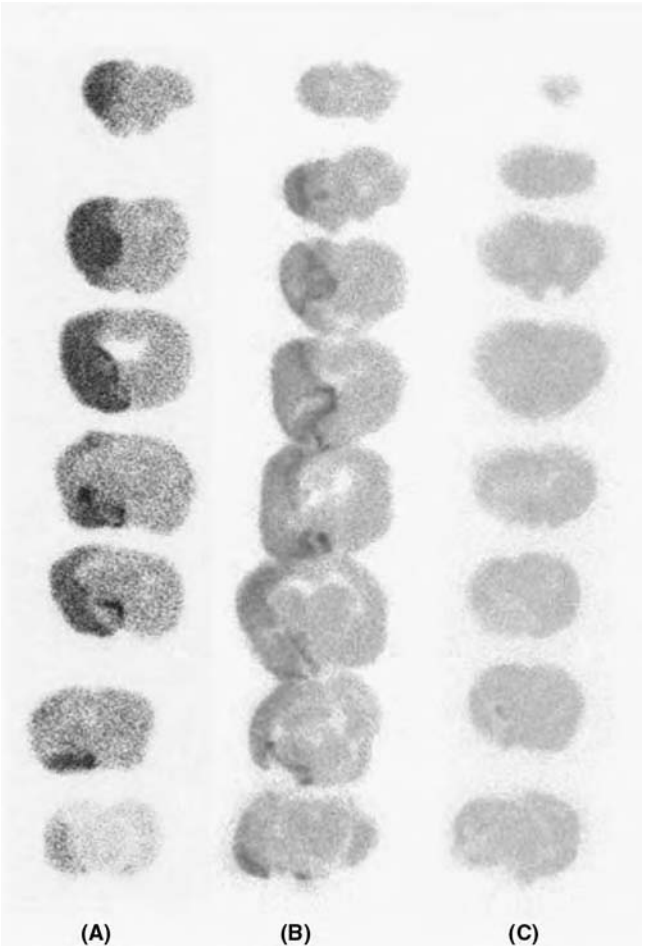

FIGURE 2 Representative ^{18}F-fluoromisonidazole (FMISO) autoradiographs at different time points post onset of two hour transient middle cerebral artery occlusion. ^{18}F-FMISO injection times: (**A**) 0.5 hour; (**B**) three hour; and (**C**) 22 hour (autoradiography two hours later). *Source*: From Ref. 35.

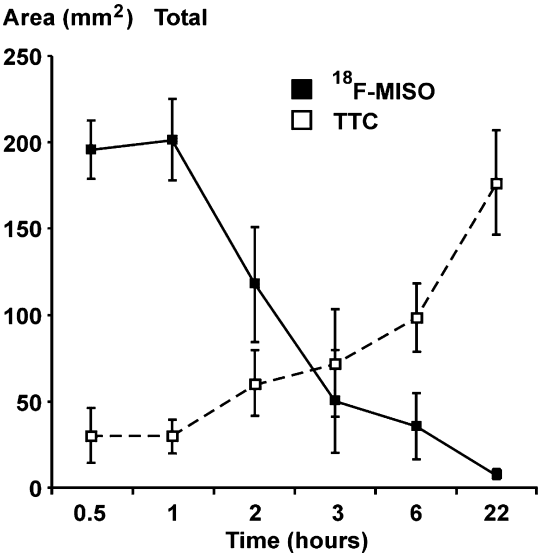

FIGURE 3 Total ^{18}F-fluoromisonidazole uptake and triphenyltetrazolium chloride pallor at different times after onset of two hours middle cerebral artery occlusion. Areas (mean ± SEM) = sum totals of all 2 mm sections for each rat (0.5, 6, and 22 hour cohorts n = 4 each; two, three hour cohorts n = 5; one hour cohort n = 8). *Source*: From Ref. 35.

triphenyltetrazolium chloride (TTC) (Fig. 3). The pattern of binding in the rat after temporary MCA occlusion reproduced that seen in human PET studies, and established the suitability of ^{18}F-FMISO for autoradiographic studies in animal stroke models.

The tritiated congener ^{3}H-FMISO is more suited to animal studies and is currently the preferred form in our laboratory for use in animal studies (Fig. 4). This allows vastly superior resolution for autoradiographic studies than is possible using ^{18}F-FMISO; and due to the prolonged half-life of tritium (^{3}H t/2 = 11 years), autoradiography can be performed on fixed, slide-mounted sections rather than fresh tissue slices (36). This allows direct correlation of

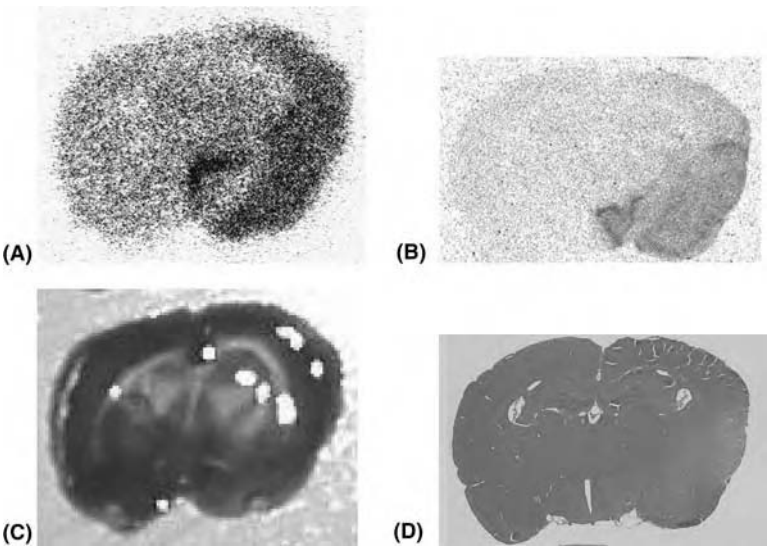

FIGURE 4 Comparison of binding patterns of (**A**) ^{18}F-fluoromisonidazole (FMISO) and (**B**) 3H-FMISO, with corresponding triphenyltetrazolium chloride (**C**), and hematoxylin and eosin (H&E) (**D**) tissue slices. Rats in both groups received injection of radiotracer half an hour following middle cerebral artery (MCA) occlusion, and the MCA was reperfused two hours after occlusion, with animals killed for tissue processing half an hour later. The short half-life of fluorine-18 precludes the use of tissue fixation and H&E staining. The superior resolution obtained with 3H-FMISO can also be appreciated. *Source*: From Ref. 36.

histology with autoradiographs obtained from the same sections. Reperfusion experiments using the rat temporary MCA occlusion model with laser Doppler monitoring of CBF have demonstrated persistence of binding within the previously hypoxic region after reperfusion (36). This confirms in brain the prolonged nature of the hypoxic binding, previously demonstrated in tumor cells and heart (13,30). Exploiting the prolonged nature of FMISO binding we have also demonstrated the feasibility of delaying animal sacrifice for 24 hours after tracer injection even after relatively short duration (45 minutes) hypoxic exposure. Due to the delayed nature of the evolution of histological change this allows correlation of tracer binding with the histological fate of the tissues. This is not possible using conventional techniques, where animals are sacrificed within a few hours of stroke induction (37,38). Because of the increased washout of tracer from contralateral normoxic tissues, the relative intensity and volume of FMISO binding are not significantly altered by the delay in tissue processing for autoradiography (36). Studies using this model suggest that the process of FMISO uptake is relatively prolonged, with at least 45 minutes of ischemia necessary to produce detectable autoradiographic signal and progressively increasing volumes of binding seen with lengthening arterial occlusion duration out to at least 90 minutes (39). This binding is however, specific to hypoxic tissue—no binding was seen in previously ischemic tissue when FMISO was administered one hour after arterial reperfusion, despite confirmed histological injury from the ischemia (36).

Human Studies

FMISO has been more extensively used in PET studies of the evolution of hypoxia in human stroke. Because of the "positive" image generated, it has been particularly useful for identifying the small volumes of hypoxic tissue (putative penumbra) that occur at the periphery of the infarct, relatively late after stroke onset, and for tracing the evolution and temporal extent of hypoxic tissue in evolving stroke.

In a preliminary study in human stroke, selective uptake of ^{18}F-FMISO was shown in a peri-infarct distribution in three of six patients with acute stroke. There was no uptake seen in patients imaged at one month in the chronic state (40). Subsequent studies have demonstrated that there is binding surrounding the infarct core in the acute phase, that binding is not seen in the subacute phase (Fig. 5) (41), and that some of the hypoxic tissue progresses to infarction,

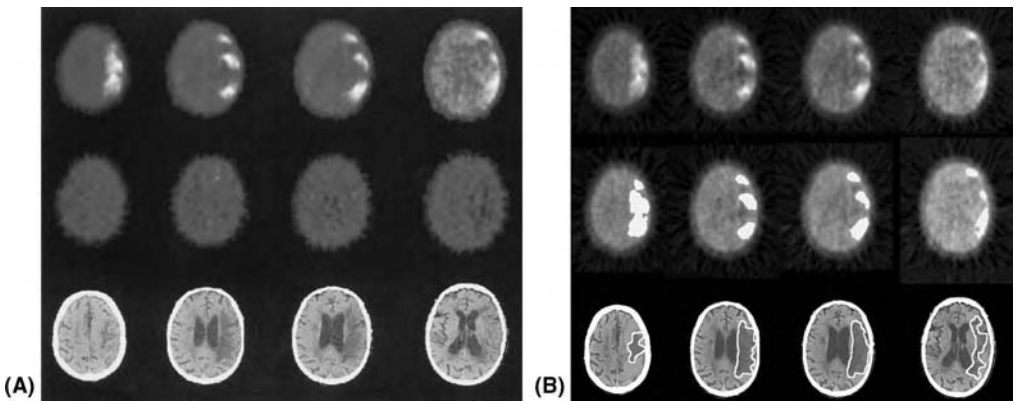

FIGURE 5 (*See color insert.*) (**A**) Serial ^{18}F-fluoromisonidazole (^{18}F-FMISO) positron emission tomography studies from patient five performed at 22 hours (*top row*) and 10 days (*middle row*) after acute ischemic stroke. The CT images (*bottom row*) show the final area of infarction. Extensive areas of increased ^{18}F-FMISO activities are seen in the peripheries of the infarct region on the early study, but these are no longer present at the time of the late study. (**B**) The same patient in (**A**), with PET image thresholded showing area of increased binding (activity >3 SDs above the mean value for the contralateral hemisphere) in yellow. The bottom panel shows this thresholded image superimposed on the late CT, with bound area which progressed to infarction shown in red, and those which survived shown in green. *Source*: From Ref. 42.

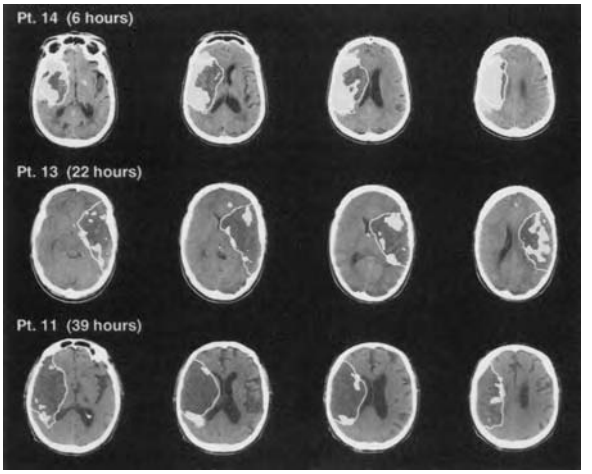

FIGURE 6 (*See color insert.*) Representative images from three patients with large middle cerebral artery infarcts imaged at different times after stroke onset. Areas of ^{18}F-fluoromisonidazole trapping, defined as pixels with activity >3 SDs above the mean value for the contralateral (nonischemic) hemisphere (shown in yellow) are superimposed on the coregistered late CT image. The distribution of hypoxic tissue in the periphery of the infarct and adjacent noninfarcting tissue, and its declining volume with time are consistent with this tissue representing the ischemic penumbra. *Source*: From Ref. 42.

while some does not (42). The distribution of FMISO binding at the periphery of the infarct and adjacent peri-infarct regions, as well as the decrease in binding with time suggested that this tissue was penumbra (Fig. 6). Interestingly, there was increased uptake in some patients up to 42 hours after stroke onset, but no uptake seen in patients imaged 6 to 11 days poststroke. Additionally, areas of ^{18}F-FMISO retention were not seen in all patients imaged <24 hour postonset, consistent with the concept that some patients may not have penumbra even relatively early poststroke, either due to reperfusion or completed infarction. For example, the striatocapsular region has poor collateral supply, and may progress to infarction more rapidly than other regions (43–46). Read et al. also found a correlation between neurological deterioration in the week following stroke and the proportion of the initially hypoxic region labeled by FMISO that progressed to infarction—a finding that has been confirmed and elaborated on with subsequent studies (47).

Markus et al. studied patients within 0 to 48 hours of symptom onset with ^{18}F-FMISO PET to assess the volume of hypoxic tissue, and with CT or T2-MRI, initially; and again at 7 to 10 days to assess initial and final infarct size (47). Patients were dichotomized by the time of symptom onset, less than or greater than 12 hour before PET imaging. This and subsequent studies by the Austin group used a statistical parametric mapping technique rather than the conventional region-of-interest (ROI) analysis used in many PET studies. A system of automated image registration of PET and CT scans was developed. Using pooled variance from normal subjects and contralateral hemisphere normalization, they were able to assess area of FMISO binding objectively and also demonstrated significantly lower variability than using ROI analysis (48). As a further validation, the outcomes were compared with those obtained using nonparametric techniques—the correlation between the two techniques was very high ($r = 0.99$). Using these techniques associations were found between time of onset and presence of hypoxic tissue (84% of those <12 hour vs. 41% in those >12 hour postsymptom onset had hypoxic tissue) and proportion of the total ischemic volume (hypoxic + infarct volumes), which was hypoxic (58% in the <12 hour group vs. 24% in the >12 hour group) (Fig. 7). In those patients with hypoxic tissue, there was no association between the time since stroke onset and proportion of initially hypoxic tissue that survived. There was a strong association between the proportion of initially hypoxic tissue that survived and functional outcome at 7 or 30 days, irrespective of the clinical rating scale used (Table 1). There was no significant interaction of time since stroke onset with this association. The relatively small sample size inherent in this type of study may have limited the power to detect such an interaction; however, the fact that in some patients, clinically meaningful recovery appeared to be associated with spontaneous penumbral salvage occurring 12 to 48 hours after onset, is very exciting. It suggests that there is still potential for meaningful therapeutic intervention after a much greater time interval than what the current thrombolysis guidelines would suggest.

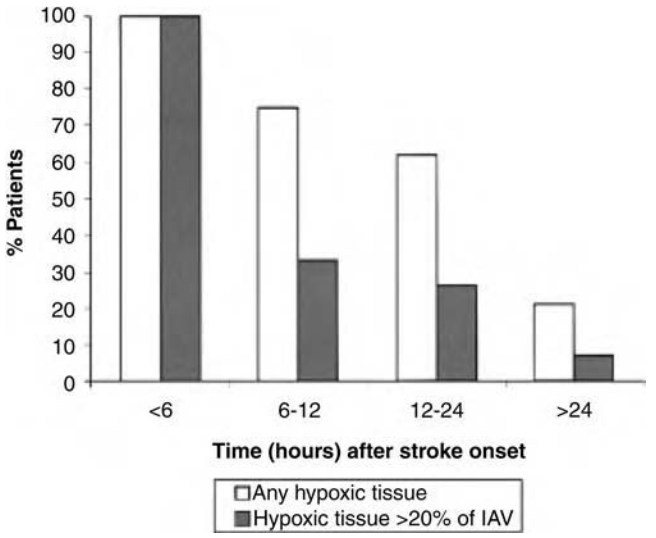

FIGURE 7 Prevalence of hypoxic tissue related to time of study in patients studied with fluoromisonidazole positron emission tomography after presentation with acute hemispheric stroke. *Source*: From Ref. 48.

^{18}F-FMISO PET has also been used to map the spatial evolution of ischemic changes in human stroke (43) (Fig. 8). Infarct expansion occurred at the expense of hypoxic tissue (penumbra) from the center to the periphery of the infarct, analogous to the pattern of evolution in animal models (45,49–51). In addition, a greater proportion of the hypoxic tissue was located superior, medial, and posterior to the infarct core (44).

The differential effects of ischemia in the white and grey matter in human stroke have also been examined using FMISO PET (52). This is an important problem given the failure of many neuroprotectant trials and the hypothesis that this may in part be due to the much greater proportion of white matter in human than in rodent brain (where most putative neuroprotectants have been tested). Twenty-seven patients had FMISO PET performed within 48 hour of stroke onset, with final infarct defined by CT at day 7 to 10. A greater proportion of the "at-risk" tissue (either FMISO-bound or infarcted) bound FMISO within white matter than grey (41% vs. 24%). Although a greater proportion of the final infarct was within the grey matter, much of this tissue did not bind FMISO—implying that it had already progressed to infarction at the time of PET scanning. Of the FMISO-bound tissue, a similar proportion progressed to infarction in both grey and white matter (47% and 55%, no significant difference). This is indirect evidence for the more rapid progression of grey matter to infarction, a plausible argument given its greater metabolic rate. The finding that a greater proportion of the ischemic tissue within white matter remained potentially salvageable at the time of PET scanning was used to argue that neuroprotectant strategies should focus more on white matter ischemia, which has often been neglected in the past. It has only been relatively recently, that techniques to examine white matter damage

TABLE 1 The Correlations Between the Proportion of the Total Ischemic Volume that Survives Spontaneously (SHVR) and Early and Late Neurological Outcome in Patients Studied ≤12 and >12 Hours After Stroke Onset

	Correlation with SHVR			
	≤12 h		>12 h	
Measure	***r*[a]**	***P* value**	***r*[a]**	***P* value**
ΔNIHSS	0.85	<0.01	0.59	<0.01
Day 90 mRS	−0.89	<0.01	−0.46	<0.05
Day 90 BI	0.86	<0.01	0.37	0.12

[a]Spearman's rank correlation coefficient.
Abbreviations: BI, Barthel index; mRS, modified Rankin Score; NIHSS, National Institutes of Health Stroke Scale; SHVR, surviving hypoxic volume ratio.
Source: From Ref. 48.

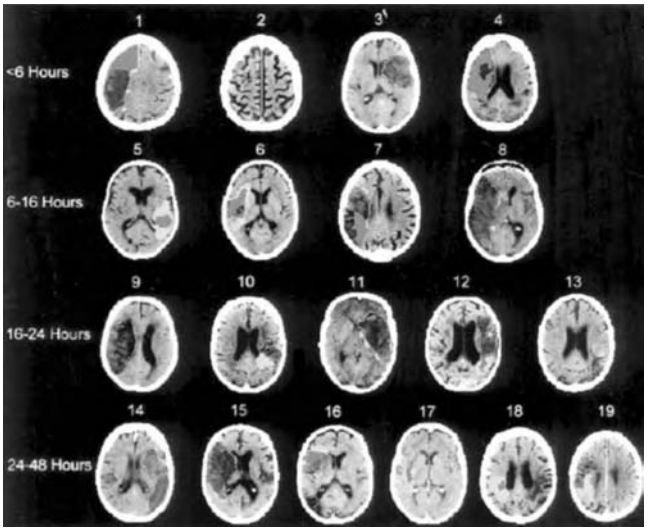

FIGURE 8 (*See color insert.*) Representative image slices from each patient showing the region of hypoxic tissue identified by acute-stage ^{18}F-fluoromisonidazole positron emission tomography (FMISO PET) superimposed on the final infarct defined on late CT. Infarct boundary is outlined in yellow. Hypoxic tissue that was viable at the time of acute PET but subsequently infarcted is shown in red; areas that survived are shown in green. Tissue without ^{18}F-FMISO uptake within the final infarct is presumed to have infarcted by the time of the acute PET study. Representative image slice for each patient was chosen to show the maximal extent of hypoxic tissue and therefore does not correspond to center of the final infarct. *Source*: From Ref. 44.

in experimental models of stroke have been developed, and as yet they are not routinely applied (53–57). The neglect of this important aspect of ischemic injury has been hypothesized to be a possible mechanism for the failure to translate neuroprotection in animals to the clinical setting (58). Therefore, methods such as FMISO PET and autoradiography, which can provide insights into threatened tissue in patients and experimental stroke models, are an additional important tool to address the issue of white matter ischemia.

The FMISO PET studies described earlier have not examined the effect of therapeutic interventions. Nevertheless, the observations that infarct grows into hypoxic tissue in humans, that there is still significant volumes of hypoxic tissue >12 hours post stroke onset, and that spontaneous survival of hypoxic tissue is associated with meaningful neurological improvement are exciting in their implications for care of stroke patients. In addition, FMISO was used to demonstrate that there is threatened, but potentially viable tissue within white matter in humans, with important implications for the design of neuroprotectant strategies. The volume of hypoxic tissue was greater in those studied within 12 hours of stroke onset, and this subgroup presumably has the greatest potential to benefit from any interventions. However, it appears that in some patients there may be the potential for tissue salvage and improved functional outcomes, well beyond this time threshold.

The role of hypoxia in hemorrhagic stroke has also been examined using FMISO PET (59). None of the six patients studied 24 to 43 hours after stroke had areas of FMISO binding, in contrast to ischemic stroke studies in which approximately 58% of patients imaged 24 to 48 hours after onset had areas of binding (42,47).

Radiation Dosimetry

Radiation doses have been calculated for patients undergoing imaging studies with ^{18}F-FMISO at a standard radiopharmaceutical dose of 3.7 MBq/kg, and time dependent concentration of radioactivity determined from blood samples and PET images (60). The effective dose equivalent was 0.013 mSv/MBq in men and 0.014 mSv/MBq in women. The critical organ receiving the highest dose was the urinary bladder (0.029 MGy/MBq using an assumed voiding

interval of four hours). These values are comparable to other commonly performed nuclear medicine studies, suggesting that the radiation risks from studies using ^{18}F-FMISO are within acceptable limits.

OTHER HYPOXIC MARKERS IN STROKE

MISO, a nitroimidazole closely related to FMISO, has been used in a small study using a gerbil stroke model (17). Uptake in the ischemic hemisphere correlated positively with the severity of the stroke, and emulsion-dipping autoradiography showed heavy labeling only in the ischemic hemisphere. Concurrent ^{14}C-Iodoantipyrine blood flow studies indicated that flow was not a major determinant of MISO retention.

A technetium-99 m labeled 2-nitroimidazole-derivatized propylene amine oxime (BMS-181321) has been studied in rat and cat models of ischemic stroke, and also in a small SPECT study in human stroke. Using dual label autoradiography with a perfusion marker in a rat MCA occlusion model, it was selectively retained in ischemic brain, but not in infarct, and retention occurred before blood–brain barrier (BBB) breakdown (61). Combined autoradiographic/SPECT experiments in cats showed early tracer distribution approximating CBF, but subsequent selective retention within the ischemic territory. The small clinical SPECT study demonstrated selective uptake in a stroke patient imaged 11 hour postonset of symptoms, in the same distribution as the CT hypodensity, which developed by 36 hours after onset (62). Two patients imaged more than 22 hours after symptom onset did not show selective uptake.

A SPECT-suitable nitroimidazole, ^{125}I-iodoazomycin arabinoside (^{125}I-IAZA), was administered concurrently with a perfusion marker, ^{99m}Tc-hexamethylpropylene amine oxime (^{99m}Tc-HMPAO), in a dual autoradiographic study in a rat MCAO model (63). Three distinct binding patterns were reported—mildly reduced CBF with no increased ^{125}I-IAZA uptake, moderately reduced CBF with increased ^{125}I-IAZA uptake, and severely reduced CBF with no ^{125}I-IAZA uptake. These results suggest that ^{125}I-IAZA is bound to penumbra, without increased binding in either core or the oligaemic zone. The same group also studied MRI imaging in combination with dual autoradiography using the same paradigm (64). Coregistration of autoradiographs and MR images was not performed due to differences in spatial orientation, however, analysis of lesion volumes by hemispheric lesion area indicated good correlation between reduced apparent diffusion coefficient$_{av}$ (ADC_{av}), seven-hour T2, seven-hour histology, and increased IAZA uptake. One potential difficulty arising from these results is in the interpretation of the seven-hour histology data. Previous studies of sequentially timed histology in permanent MCA occlusion in the rat suggest that the lesion area continues to grow out to 24 hours or beyond (49). If this is the case it would imply that ADC, T2, and IAZA are underestimating the final area of infarction.

Technetium-99 m-labeled metronidazole SPECT was used in a study of subacute stroke patients (10 ± 2.5 days). Hypoxic tissue was defined as tissue showing an uptake of ^{99m}Tc-ethylene dicysteine-Metronidazole (^{99m}Tc-EC-MN) that was greater than 30% of that in the contralateral normal brain. Using this definition, hypoxic volumes were demonstrated in all eight patients (65). Used in combination with the perfusion tracer, ^{99m}Tc-ethyl cysteinate dimer, a correlation with National Institutes of Health (NIH) stroke score was shown. The interpretation of these results is difficult, given that the improvement in NIH stroke score had already occurred at the time of imaging in most patients. This late uptake (in contrast to the lack of late uptake seen with FMISO) suggests that ^{99m}Tc-EC-MN may, in fact, be imaging processes involved in inflammation or repair. The difference between the two agents is not surprising, given the large differences in their reduction potentials, as discussed previously.

Fluorescence immunohistochemical methods have been used to label hypoxic regions within tumors (66), and a kit is available commercially (Hypoxyprobe™, Chemicon, U.S.A.). This method is suitable for use with biopsy specimens and in animal studies, not for human stroke studies. However, to date, there is no published data on its use in stroke models.

Within the nuclear medicine community, there has been a concerted effort to develop agents with imaging characteristics more suitable for rapid imaging (67). The focus of most of this work has been the imaging of tumor hypoxia; however, there are some recent preliminary studies on the development of new agents for use in stroke (68,69).

ADVANTAGES/DISADVANTAGES OF FLUOROMISONIDAZOLE

Tissue outcome is dependent on four factors—time, hemodynamics, tissue, and intervention (70). Perfusion methods provide an image of only the hemodynamic factor. On the other hand, intracellular hypoxia, as imaged by hypoxic markers, is dependent on both blood flow (hemodynamics) and cellular metabolism (tissue). In fact, because binding occurs over time and in proportion to degree of hypoxia, these agents provide an image representative of cellular hypoxia over a window of time, rather than a snapshot in time. The technique is much less cumbersome than other PET-based techniques, and a great advantage is the ability to perform animal autoradiographic studies, which have the potential for resolution down to the cellular level.

Obviously, the time lag before imaging is one of the major drawbacks of FMISO. This is particularly true for acute decision-making in stroke. Other hypoxic markers are in development with the aim of reducing the time from injection to imaging. There is also the potential to develop agents that can be used with other imaging techniques, such as SPECT or MR, which are more widely available than PET. Unfortunately, the current situation is that agents with more rapid clearance suffer from contamination of the hypoxic imaging with blood flow effects (2,67,71–73). For this reason, FMISO still provides arguably the best reflection of regional oxygen concentration (71).

The advantages of ^{18}F-FMISO PET are that it is less demanding than the current gold-standard multitracer technique, and is therefore more feasible in acute stroke patients. The radiotracer is also suitable for use in autoradiographic experiments, greatly facilitating animal studies. Using photographic emulsion-dipped histology sections very high resolution is achievable, providing a powerful tool for understanding the varying susceptibilities of different cell types in an in vivo model.

Recent Studies

Our team has been undertaking further work in order to try to demonstrate that the tissue bound by this tracer does indeed fulfil the criteria for the presence of penumbra, as proposed by Baron (74), and modified by Donnan and Davis (75) (Table 2). Most of these criteria have been fulfilled for FMISO. By its nature FMISO is bound only to tissues with altered biochemical characteristics. This is because in the presence of oxygen the initial reduction reaction is rapidly reversed, and there is no progression to further reduction and subsequent binding to intracellular molecules. It remains to be conclusively demonstrated that this bound tissue has reduced function, most commonly taken as reduced electrical activity. However, it has been shown that spontaneous salvage of FMISO-bound tissue is associated with neurological improvement (47). Topographic association with the infarct has been well demonstrated in both the human and animal studies, as discussed above (35,36,41–43,47,76). Human studies have demonstrated that some of the initially FMISO-bound tissue progresses to infarction as measured by late CT or MRI, while some does not (41–43,47). This remains to be demonstrated in the animal model, in which the need to prepare tissues promptly for autoradiography means that obtaining a sufficiently late assessment of histology to demonstrate the final infarct has until recently been problematic. Demonstration of the potential for either survival or death in all FMISO-bound tissue is critical to demonstrate that it is indeed penumbral, and this is probably only feasible using animal models. An alternative terminology is that establishing this duality of possible outcomes

TABLE 2 Criteria for the Presence of the Ischemic Penumbra

Area of abnormal brain tissue with physiological and/or biochemical characteristics consistent with cellular dysfunction but not death.
This area topographically associated with the infarct.
Demonstration that this tissue either may survive or die.
Salvage of this tissue correlates with better clinical outcomes.

Source: From Ref. 63.

will require the demonstration that none of the bound tissue is either oligaemic (i.e., under no threat of dying), or already irreversibly injured.

Recent data from our laboratory casts some doubt over the utility of FMISO as a clinically useful marker of penumbra. In the rat stroke model, animals were administered FMISO six hours after the onset of permanent arterial occlusion. Intense binding was seen consistently within the striatum (lesion core). Even an optimistic reading of current animal neuroprotection literature would suggest that after six hours of vessel occlusion, the infarct core is irreversibly damaged in the rat MCA thread occlusion model. Therefore we conclude from this finding that significant uptake of FMISO can occur in tissue that is already irreversibly injured. We believe that this may occur because the intracellular reductase enzymes responsible for FMISO binding are both ubiquitous and robust, such that enzyme activity continues after the cell is irreversibly committed to a death pathway. It should be born in mind that these findings are from rats, not humans. Nevertheless we feel the results are sufficiently disquieting to prompt a review of the role of FMISO and other hypoxic imaging agents as penumbral imaging agents. In particular, the possibility that significant FMISO binding may occur in tissues that by all current criteria are irreversibly injured suggests that this marker may not be helpful for clinical decision making—where the aim is to identify patients with salvageable tissue who may benefit from therapies. In addition, a cautionary note must be sounded regarding the use of other hypoxic imaging agents as penumbral markers. If these agents are to be clinically useful, it must first be established that binding does not occur in irreversibly injured tissue.

SUMMARY

- FMISO is a nitroimidazole hypoxic marker selectively bound in hypoxic but metabolically active tissue.
- This class of compounds has also been used to image hypoxia in tumors, anaerobic infections, and myocardial ischemia.
- Due to its dependence on cellular hypoxia it provides an image of penumbra less dependent on CBF than perfusion-based techniques.
- This may be more reflective of the degree of threat to the tissue as this is dependent on a combination of blood flow, metabolism, and time.
- Studies in a rat model of stroke have established that the pattern of binding mimics that seen in humans, providing a powerful tool for understanding some of the basic mechanisms of hypoxic tissue injury.
- Studies in human stroke patients have established that the tracer surrounds the infarct core in the acute phase of stroke, and is not bound in the subacute phase.
- On average, patients studied at times < 12hours from onset have greater volumes of hypoxic tissue—however some patients have persistence of hypoxic tissue as late as 48 hours.
- A strong association has been shown in stroke patients between the proportions of FMISO bound tissue that spontaneously survives and functional outcome (NIH stroke score, modified Rankin Score or Barthel Index).
- FMISO has been used to map the evolution of ischemic change in patients—demonstrating that infarct expands from the center at the expense of the hypoxic tissue.
- A comparison of binding within white and grey matter suggests that infarct may progress more rapidly in grey matter, and therefore in many patients by the time they receive treatment white matter may be the more important target for neuroprotectant strategies.
- Studies in patients with hemorrhagic stroke show no areas of hypoxic binding, suggesting that hypoxia is not a major factor in tissue injury in hemorrhage.
- Currently FMISO is a powerful research tool with applicability both in patients and animal models of stroke.
- Recently performed and as yet unpublished studies from our laboratory using a rat model of stroke suggest that in the rat model significant degrees of FMISO binding appears to occur in tissue which is already irreversibly injured.
- As the prototype hypoxic marker it may pave the way for the development of new compounds with the potential for broad clinical application.

REFERENCES

1. Nunn A, Linder K, Strauss HW. Nitroimidazoles and imaging hypoxia. Eur J Nucl Med 1995; 22:265–280.
2. Lewis J, Welch M. PET imaging of hypoxia. Q J Nucl Med 2001; 45(2):183–188.
3. Strauss HW, Nunn A, Linder K. Nitroimidazoles for imaging hypoxic myocardium. J Nucl Cardiol 1995; 2(5):435–437.
4. Webster LT. Drugs used in the chemotherapy of protozoal infections—amebiasis, giardiasis, and trichomoniasis. In: Gilman AG, Rall TW, Nies AS, Taylor P, eds. Goodman and Gilman's The Pharmacological Basis of Therapeutics. Singapore: McGraw-Hill Book Co., 1991:999–1008.
5. LaRusso NF, Tomasz M, Muller M, et al. Interaction of metronidazole with nucleic acids in vitro. Mol Pharmacol 1977; 13(5):872–882.
6. Chapman JD. Hypoxic sensitizers—implications for radiation therapy. N Engl J Med 1979; 301(26): 1429–1432.
7. Martin GV, Biskupiak JE, Caldwell JH, et al. Characterization of iodovinylmisonidazole as a marker for myocardial hypoxia. J Nucl Med 1993; 34(6):918–924.
8. Grunbaum Z, Freauff SJ, Krohn KA, et al. Synthesis and characterization of congeners of misonidazole for imaging hypoxia. J Nucl Med 1987; 28(1):68–75.
9. Mathias CJ, Welch MJ, Kilbourn MR, et al. Radiolabeled hypoxic cell sensitizers: tracers for assessment of ischemia. Life Sci 1987; 41(2):199–206.
10. Rasey JS, Grunbaum Z, Magee S, et al. Characterization of radiolabeled fluoromisonidazole as a probe for hypoxic cells. Radiat Res 1987; 111(2):292–304.
11. Rasey JS, Nelson NJ, Chin L, et al. Characteristics of the binding of labeled fluoromisonidazole in cells in vitro. Radiat Res 1990; 122(3):301–308.
12. Martin GV, Caldwell JH, Rasey JS, et al. Enhanced binding of the hypoxic cell marker [3H]fluoromisonidazole in ischemic myocardium. J Nucl Med 1989; 30(2):194–201.
13. Chapman JD, Baer K, Lee J. Characteristics of the metabolism-induced binding of misonidazole to hypoxic mammalian cells. Cancer Res 1983; 43(4):1523–1528.
14. Moreno SN, Docampo R. Mechanism of toxicity of nitro compounds used in the chemotherapy of trichomoniasis. Environ Health Perspect 1985; 64:199–208.
15. Prekeges JL, Rasey JS, Grunbaum Z, et al. Reduction of fluoromisonidazole, a new imaging agent for hypoxia. Biochem Pharmacol 1991; 42(12):2387–2395.
16. MillerGG, Ngan-Lee J, Chapman JD. Intracellular localization of radioactively labeled misonidazole in EMT-6-tumor cells in vitro. Int J Rad Oncol Biol Phys 1982; 8(3–4):741–744.
17. Hoffman JM, Rasey JS, Spence AM, et al. Binding of the hypoxia tracer tritiated misonidazole in cerebral ischemia. Stroke 1987; 18(1):168–176.
18. Joseph P, Jaiswal AK, Stobbe CC, et al. The role of specific reductases in the intracellular activation and binding of 2-nitroimidazoles. Int J Radiat Oncol Biol Phys 1994; 29(2):351–355.
19. Kubota K, Tada M, Yamada S, et al. Comparison of the distribution of fluorine-18 fluoromisonidazole, deoxyglucose and methionine in tumour tissue. Eur J Nucl Med 1999; 26(7):750–757.
20. Casciari JJ, Rasey JS. Determination of the radiobiologically hypoxic fraction in multicellular spheroids from data on the uptake of [3H]fluoromisonidazole. Radiat Res 1995; 141(1):28–36.
21. Rasey JS, Koh WJ, Grierson JR, et al. Radiolabelled fluoromisonidazole as an imaging agent for tumour hypoxia. Int J Radiat Oncol Biol Phys 1989; 17:985–991.
22. Tochon-Danguy H, Sachinidis J, Chan F, et al. Imaging and quantitation of the hypoxic cell fraction of viable tumour in and animal model of intracerebral high grade glioma using [18F]fluoromisonidazole (FMISO). Nucl Med Biol 2002; 29: 191–197.
23. Rasey JS, Casciari JJ, Hofstrand PD, et al. Determining hypoxic fraction in a rat glioma by uptake of radiolabeled fluoromisonidazole. Radiat Res 2000; 153(1): 84–92.
24. Koh WJ, Rasey JS, Evans ML, et al. Imaging of hypoxia in human tumors with [F-18]fluoromisonidazole. Int J Radiat Oncol Biol Phys 1992; 22(1):199–212.
25. Rasey JS, Koh WJ, Evans ML, et al. Quantifying regional hypoxia in human tumors with positron emission tomography of [18F]fluoromisonidazole: a pretherapy study of 37 patients. Int J Radiat Oncol Biol Phys 1996; 36(2):417–428.
26. Valk PE, Mathis CA, Prados MD, et al. Hypoxia in human gliomas: demonstration by PET with fluorine-18-fluoromisonidazole. J Nucl Med 1992; 33(12):2133–2137.
27. Hotchkiss RS, Rust RS, Dence CS, et al. Evaluation of the role of cellular hypoxia in sepsis by the hypoxic marker [18F]fluoromisonidazole. Am J Physiol 1991; 261(4 pt. 2):R965–972.
28. Liu RS, Chu LS, Yen SH, et al. Detection of anaerobic odontogenic infections by fluorine-18 fluoromisonidazole. Eur J Nucl Med 1996; 23(10):1384–1387.
29. Martin GV, Cerqueira MD, Caldwell JH, et al. Fluoromisonidazole. A metabolic marker of myocyte hypoxia. Circ Res 1990; 67(1):240–244.
30. Shelton ME, Dence CS, Hwang DR, et al. Myocardial kinetics of fluorine-18 misonidazole: a marker of hypoxic myocardium. J Nucl Med 1989; 30(3):351–358.

31. Martin GV, Caldwell JH, Graham MM, et al. Noninvasive detection of hypoxic myocardium using fluorine-18-fluoromisonidazole and positron emission tomography. J Nucl Med 1992; 33(12): 2202–2208.
32. Shelton ME, Dence CS, Hwang DR, et al. In vivo delineation of myocardial hypoxia during coronary occlusion using fluorine-18 fluoromisonidazole and positron emission tomography: a potential approach for identification of jeopardized myocardium. J Am Coll Cardiol 1990; 16(2):477–485.
33. Caldwell JH, Revenaugh JR, Martin GV, et al. Comparison of fluorine-18-fluorodeoxyglucose and tritiated fluoromisonidazole uptake during low-flow ischemia. J Nucl Med 1995; 36(9):1633–1638.
34. Marcoux FW, Morawetz RB, Crowell RM, et al. Differential regional vulnerability in transient focal cerebral ischemia. Stroke 1982; 13(3):339–346.
35. Saita K, Chen M, Spratt NJ, et al. Imaging the ischemic penumbra with 18F-fluoromisonidazole in a rat model of ischemic stroke. Stroke 2004; 35(4):975–980.
36. Spratt NJ, Ackerman U, Tochon-Danguy HJ, et al. Characterization of Fluoromisonidazole Binding in Stroke. Stroke 2006; 37(7):1862–1867.
37. Fisher M. Characterizing the target of acute stroke therapy. Stroke 1997; 28(4):866–872.
38. Garcia JH, Yoshida Y, Chen H, et al. Progression from ischemic injury to infarct following middle cerebral artery occlusion in the rat. Am J Pathol 1993; 142(2):623–635.
39. Spratt NJ, Donnan GA, Howells DW. What time epoch is imaged using Fluoromisonidazole? Int Med J 2006; 36(2):A6.
40. Yeh SH, Liu RS, Hu HH, et al. Ischemic Penumbra in acute stroke: demonstration by PET with fluorine-18 fluoromisonidazole [Abstr]. J Nucl Med 1994; 35:205P.
41. Read SJ, Hirano T, Abbott DF, et al. Identifying hypoxic tissue after acute ischemic stroke using PET and 18F-fluoromisonidazole. Neurology 1998; 51(6):1617–1621.
42. Read SJ, Hirano T, Abbott DF, et al. The fate of hypoxic tissue on 18F-fluoromisonidazole positron emission tomography after ischemic stroke. Ann Neurol 2000; 48(2):228–235.
43. Markus R, Reutens DC, Kazui S, et al. Topography and temporal evolution of hypoxic viable tissue identified by 18F-fluoromisonidazole positron emission tomography in humans after ischemic stroke. Stroke 2003; 34(11):2646–2652.
44. Wise R, Bernardi S, Frackowiak R, et al. Serial observations on the pathophysiology of acute stroke. The transition from ischaemia to infarction as reflected in regional oxygen extraction. Brain 1983; 106(1):197–222.
45. Pappata S, Fiorelli M, Rommel T, et al. PET study of changes in local brain hemodynamics and oxygen metabolism after unilateral middle cerebral artery occlusion in baboons. J Cereb Blood Flow Metab 1993; 13(3):416–424.
46. Bozzao L, Bastianello S, Fantozzi LM, et al. Correlation of angiographic and sequential CT findings in patients with evolving cerebral infarction. Am J Neuroradiol 1989; 10(6):1215–1222.
47. Markus R, Reutens DC, Kazui S, et al. Hypoxic tissue in ischaemic stroke: persistence and clinical consequences of spontaneous survival. Brain 2004; 127(6):1427–1436.
48. Markus R, Donnan GA, Kazui S, et al. Statistical parametric mapping of hypoxic tissue identified by [(18)F]fluoromisonidazole and positron emission tomography following acute ischemic stroke. Neuroimage 2002; 16(2):425–433.
49. Garcia JH, Liu K-F, Ho K-L. Neuronal necrosis after middle cerebral artery occlusion in Wistar rats progresses at different time intervals in the caudoputamen and the cortex. Stroke 1995; 26(4): 636–643.
50. Hakim AM, Hogan MJ, Carpenter S. Time course of cerebral blood flow and histological outcome after focal cerebral ischemia in rats. Stroke 1992; 23(8):1138–1143.
51. Baron JC, von Kummer R, del Zoppo GJ. Treatment of acute ischemic stroke: challenging the concept of a rigid and universal time window. Stroke 1995; 26(12):2219–2221.
52. Falcao AL, Reutens DC, Markus R, et al. The resistance to ischemia of white and gray matter after stroke. Ann Neurol 2004; 56(5):695–701.
53. Yam PS, Patterson J, Graham DI, et al. Topographical and quantitative assessment of white matter injury following a focal ischaemic lesion in the rat brain. Brain Res Protocols 1998; 2(4):315–322.
54. Dietrich WD, Kraydieh S, Prado R, et al. White matter alterations following thromboembolic stroke: a beta-amyloid precursor protein immunocytochemical study in rats. Acta Neuropathologica 1998; 95(5):524–531.
55. Imai H, McCulloch J, Graham DI, et al. New method for the quantitative assessment of axonal damage in focal cerebral ischemia. J Cereb Blood Flow Metab 2002; 22(9):1080–1089.
56. Irving EA, Bentley DL, Parsons AA. Assessment of white matter injury following prolonged focal cerebral ischaemia in the rat. Acta Neuropathol (Berl) 2001; 102(6):627–635.
57. Valeriani V, Dewar D, McCulloch J. Quantitative assessment of ischemic pathology in axons, oligodendrocytes, and neurons: attenuation of damage after transient ischemia. J Cereb Blood Flow Metab 2000; 20(5):765–771.
58. Dewar D,Yam P, McCulloch J. Drug development for stroke: importance of protecting cerebral white matter. Eur J Pharmacol 1999; 375(1–3):41–50.

59. Hirano T, Read SJ, Abbott DF, et al. No evidence of hypoxic tissue on 18F-fluoromisonidazole PET after intracerebral hemorrhage. Neurology 1999; 53(9):2179–2182.
60. Graham MM, Peterson LM, Link JM, et al. Fluorine-18-fluoromisonidazole radiation dosimetry in imaging studies. J Nucl Med 1997; 38(10):1631–1636.
61. Di Rocco RJ, Kuczynski BL, Pirro JP, et al. Imaging ischemic tissue at risk of infarction during stroke. J Cereb Blood Flow Metab 1993; 13(5):755–762.
62. Barron B,Grotta JC, Lamki L, et al. Preliminary experience with technetium-99m BMS-181321, a Nitroimidazole, in the detection of cerebral ischemia associated with acute stroke. J Nucl Med 1996; 5(Suppl):1218.
63. Lythgoe MF, Williams SR, Wiebe LI, et al. Autoradiographic imaging of cerebral ischaemia using a combination of blood flow and hypoxic markers in an animal model. Eur J Nucl Med 1997; 24(1):16–20.
64. Lythgoe MF, Williams SR, Busza AL, et al. The relationship between magnetic resonance diffusion imaging and autoradiographic markers of cerebral blood flow and hypoxia in an animal stroke model. Magn Reson Med 1999; 41(4):706–714.
65. Song H-C, Bom H-S, Cho KH, et al. Prognostication of recovery in patients with acute ischemic stroke through the use of bBrain SPECT with technetium-99m-labeled metronidazole. Stroke 2003; 34(4):982–986.
66. Raleigh JA, Miller GG, Franko AJ, et al. Fluorescence immunohistochemical detection of hypoxic cells in spheroids and tumours. Br J Cancer 1987; 56(4):395–400.
67. Rajendran JG, Krohn, KA. Imaging hypoxia and angiogenesis in tumors. Radiol Clin North Am 2005; 43(1):69–187.
68. Falzon CL, Ackermann U, Spratt, N, et al. F-18 labelled N,N-Bis-haloethylamino- henylsulfoxides. A new class of compounds for the imaging of hypoxic tissue. J Lab Comp Radiopharm 2006; 49:1089–1103.
69. Falzon CL, Ackermann U, White JM, et al. Synthesis and Radiolabelling of Novel Nitrogen Mustards for the Imaging of Hypoxic Tissue (Abstract). ISMC/RACIOC Chemistry Conference.Cairns, Australia, 2004.
70. Warach S. Tissue viability thresholds in acute stroke: The 4-factor model. Stroke 2001; 32(11): 2460–2461.
71. Gronroos T, Bentzen L, Marjamaki P, et al. Comparison of the biodistribution of two hypoxia markers [18F]FETNIM and [18F]FMISO in an experimental mammary carcinoma. European Journal of Nuclear Medicine and Molecular Imaging 2004; 31(4):513–520.
72. Lewis JS, McCarthy DW, McCarthy TJ, et al. Evaluation of 64Cu-ATSM in vitro and in vivo in a hypoxic tumor model. J Nucl Med 1999; 40(1):177–183.
73. Rasey JS, Hofstrand PD, Chin LK, et al. Characterization of [18F]fluoroetanidazole, a new radiopharmaceutical for detecting tumor hypoxia. J Nucl Med 1999; 40(6):1072–1079.
74. Baron JC. Mapping the ischaemic penumbra with PET: implications for acute stroke treatment. Cerebrovasc Dis 1999; 9(4):193–201.
75. Donnan GA, Davis SM. Neuroimaging, the ischaemic penumbra and selection of patients for acute stroke therapy. Lancet Neurol 2003; 1:417–425.
76. Markus R, Donnan G, Kazui S, et al. Penumbral topography in human stroke: methodology and validation of the "Penumbragram." Neuroimage 2004; 21(4):1252–1259.

12 Can the Penumbra Be Imaged Using Single-Photon Emission Computed Tomography?

Toshihiro Ueda
Department of Neuroendovascular Therapy, Stroke Center, Tokyo Saiseikai Central Hospital, Tokyo, Japan

INTRODUCTION

Single-photon emission computed tomography (SPECT) is a readily available noninvasive imaging tool for the management of patients with acute or chronic ischemia. SPECT was introduced in the late 1970s and has been proven as an established and cost-effective mean for the evaluation of regional cerebral blood flow (CBF) and cerebrovacular reserve. The study of CBF using SPECT has become more widespread and accessible with the commercial availability of tracers that cross the blood-brain barrier (BBB) and are retained by the cells of the central nervous system.

One of the major reasons for the interest in using SPECT to manage ischemia is that it represents a less expensive functional neuroimaging. The technique is also safe and can easily be repeated for series measurements. Unlike positron emission tomography (PET), SPECT cannot routinely measure the absolute CBF value and cerebral metabolism. However, SPECT can be routinely used in clinical practice and can promptly provide functional information that is not available by conventional computed tomography (CT) or magnetic resonance imaging (MRI) and PET. Therefore, SPECT is useful for the diagnosis of acute or chronic ischemia, assessment of ischemic tissue viability, and reversibility in acute ischemia or cerebrovacular reserves in chronic ischemia and post-treatment evaluation.

Can the penumbra be imaged using SPECT? The consequence of cerebral artery occlusion can be imaged by SPECT from the very first minute. SPECT imaging can visualize the entire hypoperfused area, including the dense ischemic area that inevitably develops into tissue necrosis, and the surrounding less pronounced hypoperfused area representing the still living ischemic penumbra. The visualization of only the ischemic penumbra may be impossible by SPECT imaging. However, the ischemic CBF thresholds estimated using SPECT provide us important information that distinguish ischemic penumbra from ischemic core.

RADIOPHARMACEUTICALS

SPECT imaging requires radiotracers such as xenon-133(^{133}Xe), radioiodine-labeled amines *N*-isopropyl-[^{123}I]iodoamphetamine (IMP), Technitium-99m(^{99m}Tc) hexamnethylpropyleneamineoxime (HMPAO), or ^{99m}Tc-ethyl cysteinate dimmer (ECD).

^{133}Xe-SPECT can measure CBF quantitatively with inert gas clearance technique and without arterial sampling. ^{133}Xe-SPECT is well suitable for repeated studies within a short time in the same patients. The limitation of ^{133}Xe-SPECT includes poor spatial resolution due to the low energy and its rapid clearance from brain (1). This technique needs relatively high cost and is difficult to apply as an emergency examination.

IMP crosses the BBB easily and is extracted almost completely during a single passage through cerebral circulation (2). It remains trapped in proportion to CBF in brain tissue and has a short brain retention time and follows higher CBF levels more accurately than either ^{99m}Tc-HMPAO or ^{99m}Tc-ECD. However, it is not constantly available and limiting for emergency events.

^{99m}Tc- HMPAO is a lipid-solute, macrocyclic amine available for routine clinical use. HMPAO has a high first-pass extraction fraction and its brain uptake reaches its maximum within five

minutes after intravenous injection (3). The initial distribution of this tracer remains constant for several hours (4). In contrast to ^{133}Xe-SPECT, it is not possible to quantify CBF with ^{99m}Tc- HMPAO. A nonlinear relationship has been noted between the retention of HMPAO and CBF measured by PET, owing to flow-dependent back diffusion. Therefore, a correction algorithm has been proposed for HMPAO SPECT by Lassen et al. (5) to compensate for the nonlinearity.

ECD has rapid brain uptake and very slow clearance from the brain. ECD level stabilized 7 to 20 minutes after intravenous injection. Blood clearance is rapid, resulting in higher brain-to-background activity ratio than with HMPAO (6). Therefore, the imaging quality of ECD is slightly better than that of HMPAO. In addition, a "hypofixation" of ECD was described by Lassen and Sperling (7) in patients with subacute stroke, where reperfusion of the infarcted area was not detected. This is explained by a slow de-esterification of the compound and consequent low conversion to the trapped hydrophilic form. When flow and metabolism are uncoupled as in subacute stroke, ECD uptake reflects cell functional status rather than perfusion and especially so when perfusion is high relative to metabolism. Shishido et al. (8) reported that in patients with subacute stroke and "luxury perfusion" confirmed by PET, a focal decreased ECD uptake in the infarcted lesion, corresponding with a decreased cerebral metabolic rate of oxygen ($CMRO_2$), increased CBF, and increased HMPAO uptake. However, similar discrepancies were not indicated in the acute and chronic phases of stroke.

ACUTE ISCHEMIC STROKE AND SINGLE-PHOTON EMISSION COMPUTED TOMOGRAPHY

Numerous reports describe the usefulness of SPECT in the management of acute ischemic stroke. Perfusion status evaluated by SPECT is important for the differential diagnosis, early detection of ischemia, assessment of the viability, and reversibility of the ischemic tissue, and decisions making for early treatment in patients with acute ischemic stroke. Hypoperfusion on SPECT indicates cerebral ischemia and suggests hemodynamically significant arterial stenosis in chronic stroke or occlusion in acute stroke from the very first minutes (9). CT scan is positive during eight hours after the onset in approximately 20% of acute ischemic stroke patients, but nearly 90% of SPECT is positive (10,11). Two large, prospective, blind trials tested the ability of SPECT to localize acute ischemic stroke. Sensitivities of 61% to 74% (about 85% for nonlacunar strokes) and specificities of 88% to 98% were reported (12). Diffusion and perfusion MRI may be another potentially useful means to assess tissue viability and reversibility in acute ischemia. Karonen et al. (13,14) reported that a clinically relevant ischemic penumbra estimated by diffusion–perfusion mismatch could be detected in most acute stroke patients by using the combination of SPECT and diffusion MRI.

Although a number of studies have reported the relation between SPECT findings and outcome in acute stroke patients, most reports were the natural history studies in the acute stroke setting. SPECT findings correlated with the severity of neurological deficit and clinical outcome. In stroke patients within six hours, early severe hypoperfusion on SPECT were highly predictive (92%) of poor neurologic outcome (15). Other studies have demonstrated a good correlation, especially when the three-dimensional volume of the perfusion defects used. Laloux et al. (16) reported that there was a strong correlation between CBF measured by the degree and size of hypoperfusion and clinical outcome. Alexandrov et al. (17) indicated that SPECT was statistically better than the neurological deficit scores in predicting short-term outcome of ischemic stroke if performed within the first 72 hours after stroke onset compared with SPECT studies performed later during the first week. Watanabe et al. (18) reported that there was a strong correlation between the infarct size predicted by SPECT and that measured by CT scan. Other recent reports also suggested that SPECT had a significant added predictive value even when compared to admission neurological scores and, although not as reliable as PET, was a strong predictor of neurological recovery (19). In the thrombolysis study, Grotta and Alexandrov (20) suggested that SPECT measurement of cerebral perfusion before and after intravenous recombinant tissue plasminogen activator (rt-PA) infusion correlated with outcome and response to therapy.

Earlier HMPAO-SPECT studies showed that severely reduced tracer uptake over a large area is associated with poor outcome, while normal or increased uptake is predictive of good

clinical outcome. Reviewing the literature, Baron (21) concluded that there were highly significant relationships between hypoperfusion scores (which express both the volume and the severity of tracer hypofixation) and clinical outcome/recovery measures, such that the smaller the score, the better the clinical prognosis. Markedly reperfusion of previously hypoperfused ischemic tissue detected by SPECT after 24 to 36 hours was associated with better outcome (22–24). Early hyperperfusion that indicates recanalization of the occluded artery (25) and is detected by PET has been observed in up to one-third of cases studied between 15 and 18 hours after the onset (26). As HMPAO-SPECT is poorly sensitive to focal hyperperfusion (27), some cases may represent overlooked mild hyperperfusion. HMPAO measures may overestimate hyperemia especially in subacute state after stroke. A "hyperfixation" of HMPAO in patients with subacute stroke may not represent hyperperfusion, but abnormal penetration in parenchyma due to altered BBB in already necrotic tissue may be possible (28).

Diagnosis of stroke subtypes is important for therapeutic decision making and prediction of recovery. Small-vessel disease such as lacunar infarction should be separated from large-vessel disease such as atherothromboembolic infarction. Brass et al. (29) reported that ECD-SPECT demonstrated a specificity of 98% and a sensitivity of 86% for localization of strokes. A normal image or small deep perfusion defect was highly predictive of a lacunar infarction, and defects involving the cortical surface were strongly associated with nonlacunar infarction.

SINGLE-PHOTON EMISSION COMPUTED TOMOGRAPHY AND ISCHEMIC THRESHOLDS

The treatment of acute ischemic stroke has recently become a medical emergency with the advent of effective therapy such as endovascular recanalization treatment using mechanical disruption and/or thrombolysis. The goals for the acute treatment are two folds: salvaging the reversible ischemic tissue and avoiding reperfusion of dead (nonviable) tissue. The target of these therapies should be the ischemic tissue that can respond to treatment (30). Rapid diagnostic modalities that distinguish reversible ischemic tissue from irreversibly damaged or nonviable tissue are needed, because of the risk for reperfusion injury such as hemorrhagic transformation with early intervention. Although the therapeutic time window in humans is generally thought to be the first few hours after the onset of symptoms, there could be variability among different individuals. The therapeutic window for potentially salvageable ischemic tissue is likely dependent on the degree of collateral flow and metabolic status. Each individual patient could have his or her own therapeutic time window for potentially effective interventional treatment. Fisher (31) suggests that individual stroke patients have their own therapeutic time windows based on factors such as residual collateral CBF, temperature, blood pressure, and the systemic metabolic milieu. However, a rapid assessment of status of the collateral circulation and associated tissue reversibility before treatment has not been emphasized or considered in recent clinical trials of thrombolytic therapy.

In animal studies, it is well known that the reversibility of ischemic tissue depends fundamentally on the severity and duration of ischemia. Ischemic tissue with a very low CBF (<10 mL/100 g/min), as the ischemic core, rapidly suffered irreversible damage. The concept of an ischemic penumbra surrounding the ischemic core was defined originally as a region of blood flow below that needed to sustain electric activity, but above that required to maintain cellular ionic gradient, which may in time lead to irreversible cellular damage (32–34). Recently, the ischemic penumbra has been reported to be indicative of potentially reversible ischemic tissues with early and appropriate therapeutic intervention (35). The classic CBF ranges for the penumbra are known to be around 10 to 20 mL/100 g/min in animal studies (36) (see Chapter 4 for details on the penumbra threshold). The penumbra provides a realistic target for intervention in the acute phases of ischemic stroke. If each patient's penumbra could be detected by rapid pretreatment neuroimaging techniques, it would improve patient selection and increase the efficacy of therapy. However, the relation between CBF and tissue viability (or reversibility) during acute ischemia is complicated. Accurate quantitative measurement of regional CBF may not be necessarily useful for predicting tissue viability in acute ischemic stroke.

There is a threshold relationship between CBF and irreversible ischemic tissue damage and infarction. This has been variously estimated using different modalities. SPECT has

advantages in that it is readily available and can be performed quickly in emergency cases. The fixation of HMPAO, within two minutes after intravenous injection with minimal washout from the brain, permits the scanning up to four hours after injection. SPECT scanning with triple head cameras can be completed within 15 to 20 minutes. Several studies have reported SPECT to be potentially useful in the diagnosis of acute ischemic stroke patients. The perfusion abnormality of SPECT correlates with the extent, severity, and short-term outcome of acute stroke patients (37). Laloux et al. (38) indicated that there was a strong correlation between CBF measured by the degree and size of hypoperfusion and clinical outcome. Nakano et al. (39) reported that the infarcted and symptomatic CBF threshold using IMP-SPECT were 39% to 48% and 65% to 72% of contralateral presumed normal CBF values, respectively. The infarcted and symptomatic CBF thresholds by ^{133}Xe-SPECT were 19 to 23 and 33 to 36 mL/100 g/min, respectively. Although SPECT cannot routinely measure an absolute value of regional CBF, semiquantitative analysis of CBF may provide important information that identifies threshold values for the severity of ischemic brain tissue.

Shimosegawa et al. (40) reported that the lesion-to-contralateral radioactivity ratios (L/C ratio) on HMPAO-SPECT for the infarct and peri-infarct regions were respectively 0.48 ± 0.14 and 0.75 ± 0.10 in acute stroke patients within six hours from the onset. They suggested that considering the lowest L/C ratio of the peri-infarct area, a decrease of approximately 40% in CBF compared to the contralateral normal brain appears to represent the borderzone between reversible and irreversible structural brain damage. Sasaki et al. (41) demonstrated that reperfusion in only nine patients within 7.25 hours from onset significantly reduced the development of infarction in an ischemic regional activity to cerebellar activity ratio (R/CE ratio) between 0.55 and 0.75 (35). Furthermore, Hatazawa et al. (42) reported that in patients with acute stroke within six hours after onset, relative cerebral blood volume (CBV) was significantly increased in the noninfarcted area in the territory of the occluded artery and was significantly reduced in the core of infarction. A relative CBV of less than 70% was indicative of evolving into infarction. Although the relative CBF estimated by HMPAO-SPECT is a better predictor of infarction than the relative CBV, the CBV measurement provided the new information that the probability of infarction in the hypervolemic regions is lower than that in the hypovolemic regions. They also speculated that the brain regions in the relative CBV range between 0.40 and 0.60, where 75% of regions were infarcted, while others were not, may correspond to an "ischemic penumbra." The penumbra tissue may consist of both hypervolemic and hypovolemic regions associated with the delayed bolus transit.

There are a number of other reports which show ischemic CBF thresholds estimated by HMPAO-SPECT. Giubilei et al. (15) reported that patients who had an asymmetry index (affected vs. contralateral area) of less than 60% measured by HMPAO-SPECT within six hours from onset had a poor prognosis, whereas patients with an asymmetry index of more than 60% had a good outcome. Hirano et al. (43) showed that in a patient studied within six hours of stroke onset, under conditions of stable CBF reduction on HMPAO-SPECT, identifying tissue with CBF below a threshold value of 63.7% of the contralateral mean CBF value reliably predicts the final infarct volume.

On the other hand, current clinical studies demonstrated various ischemic thresholds estimated by ECD-SPECT. Berrouschot et al. (44) demonstrated that ECD-SPECT allows transient ischemia to be distinguished from cerebral infarction using relative activity thresholds within six hours after onset. All patients with transient ischemia had count rate densities more than 70% of the respective contralateral region-of-interest (ROI), whereas all patients with subsequent infarction had values less than 70%. Mahagne et al. (45) indicated that the degree of ECD cortical uptake reduction, measured on early brain SPECT, is a strong predictor of spontaneous neurological recovery and functional outcome. They found a strong correlation between the extent of irreversibly damaged cortex defined as ECD uptake below 40% of maximal uptake. The apparently better predictive value of ECD over HMPAO may reflect this tracer's brain retention mechanisms which are weighted more toward cell function than toward perfusion.

Liu et al. (46) reported that the relative (ischemic vs. contralateral control) CBF of ECD-SPECT for the corresponding tissues were 45 ± 26% (mean CBF of the ischemic core and the area of infarct growth) and 87 ± 7% (the eventually viable ischemic tissue), respectively. These values were somewhat higher than those measured using HMPAO-SPECT, reported by Shimosegawa

et al. (40). The effect of metabolism on the uptake of ECD may play a role in this discrepancy. Iseda et al. (47) showed statistically analyzed discriminant lines between reversible and irreversible ischemia. The discriminant line rapidly rose to 45.5% of contralateral presumed normal CBF on ECD-SPECT within the first three hours after stroke onset, which suggests urgency for treatment and less need for triage based on CBF measurements. Thereafter, it very gradually increases from 49.8% to 52.3% of contralateral presumed normal CBF between three and eight hours, which suggests the possibility of triage based on CBF measurement.

Mahagne et al. (48) indicated that ECD uptake can reflect neuronal viability and that ECD-SPECT can be useful for the early detection of potentially salvageable tissue and irreversible damage. They showed that the majority of irreversibly damaged tissue voxels (average 84%), defined by ECD uptake less than 40%, evolved toward infarction, and 51.8% to 100% of at-risk voxels (average 89%) escaped infarction. Normally perfused voxels (ECD uptake >80%) were consistently found in noninfarcted area, and the penumbral voxels (ECD uptake between 40% and 80%) exhibited the expected variable fate. These results supported the validity of the 40% threshold for ECD-SPECT in acute stroke management and of applying this threshold for a convenient visual analysis of the data.

Currently, Patlak plot graphical analysis was applied to the time activity curves of aortic arch and brain in this protocol without arterial blood sampling method (49). This quantitative approach has been reported to be useful for routine clinical studies, and ECD might have several advantages over HMPAO. Matsuda et al. (50) suggested that a limitation of this method might have existed in radionuclide angiography of the anterior view, which could not adequately reflect reduced perfusion in the posterior region. Watanabe et al. (51) reported that in patients who had acute stroke within six hours from onset, the CBF in the region of severe ischemia and the surrounding region was determined by Patlak plot method, and the affected/nonaffected (A/NA) ratio was calculated. In severe ischemic regions the CBF ranged from 1.7 to 20 mL/100 g/min (mean, 11 ± 5 mL/100 g/min), whereas the A/NA ratio ranged from 4% to 45% (mean 26 ± 11%). On the other hand, the CBF in the surrounding regions ranged from 20 to 52 mL/100 g/min (mean, 34 ± 8 mL/100 g/min), whereas the A/NA ratio ranged from 52% to 104% (mean 77 ± 11%). Umemura et al. (52) showed that the regions where residual CBF measured by the Patlak plot method using HMPAO-SPECT was preserved over 35 mL/100 g/min had a low possibility of infarction without recanalization and regions where residual CBF was preserved over 25 mL/100 g/min could be recovered by early recanalization. However, regions where residual CBF was severely decreased (<20 mL/100 g/min) had a risk of intracerebral hemorrhage and severe edema.

SINGLE-PHOTON EMISSION COMPUTED TOMOGRAPHY AND THROMBOLYTIC THERAPY

SPECT was also useful to evaluate ischemic tissue reversibility and the risk of hemorrhagic transformation in acute ischemic patients who had thrombolytic therapy (Figs. 1–4). Ueda et al. (53) suggested that patients who had residual CBF values of an ischemic R/CE ratio of less than 0.35 had a significantly high risk of hemorrhagic transformation, after successful intra-arterial thrombolysis. This semiquantitative analysis of residual CBF in ischemic tissue is quite simple and prompt, and can be readily implemented by any institution without using a special computer setting or protocol. After one axial section showing the ischemic region most clearly is selected, three regions such as (*i*) the ischemic region, (*ii*) the corresponding region on the contralateral side, and (*iii*) the whole cerebellar hemisphere on the ischemic side are set and the mean count is determined in each region of interest. The residual CBF is assessed by calculating two parameters: (*i*) R/CE ratio = a/c, and (*ii*) asymmetry index = 1 + (b − a)/(a + b). In addition, Ueda et al. (54) showed also that outcomes of acute ischemia with early and successful recanalization after intra-arterial thrombolysis were significantly different and are influenced markedly by pretreatment CBF assessed by HMPAO-SPECT. Thirty patients who had complete recanalization by intra-arterial thrombolysis after pretreatment SPECT were analyzed retrospectively. Outcomes of acute cerebral ischemia with early and complete recanalization using intra-arterial thrombolytic therapy are significantly different and are influenced markedly by pretreatment CBF assessed by SPECT. Furthermore, CBF thresholds evaluated by SPECT provide important

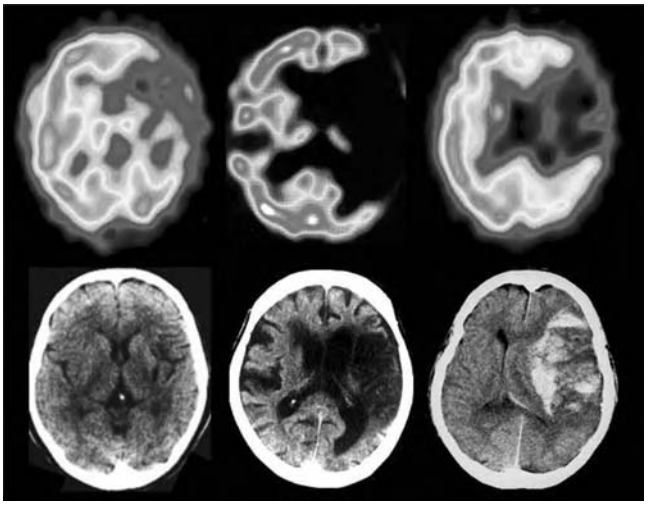

FIGURE 1 (*See color insert*.) Pretreatment single-photon emission computed tomography (SPECT) and posttreatment computerized tomography (CT) in acute ischemic patients with intra-arterial thrombolytic therapy. (*Upper left*) Pretreatment SPECT in a patient who had complete recanalization of the left middle cerebral artery occlusion four hours after onset of symptoms, shows left frontotenporoparietal perfusion deficit. The ratio of ischemic region to cerebellar flow [regional activity to cerebellar activity ratio (R/CE ratio)] was 0.51. (*Lower left*) Posttreatment CT scan one month later shows no new apparent infarction.(*Upper middle*) Pretreatment SPECT in a patient, who had complete recanalization of the left middle cerebral artery occlusion six hours after onset of symptoms, shows left frontotenporoparietal perfusion deficit. The R/CE ratio was 0.45. (*Lower middle*) Posttreatment CT scan one month later shows a large infarction in the territory of the left middle cerebral artery. (*Upper right*) Pretreatment SPECT in a patient who had near complete recanalization of the left middle cerebral artery occlusion 4 hours after onset of symptoms, shows left frontotenporoparietal perfusion deficit. The R/CE ratio was 0.21. (*Lower right*) Posttreatment CT scan shows hemorrhagic transformation in the territory of the left middle cerebral artery.

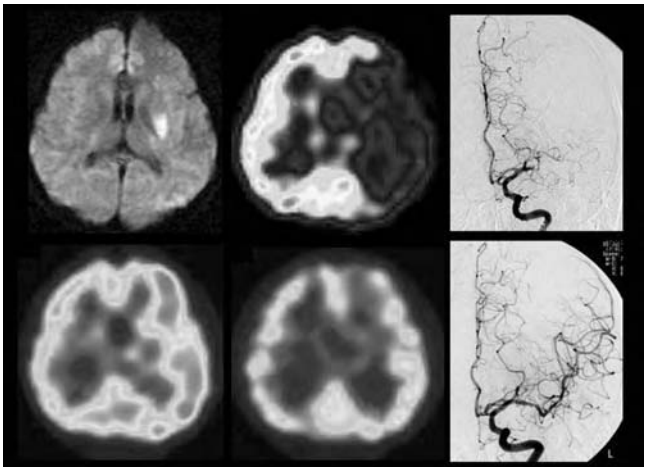

FIGURE 2 A 46-year-old male with atherothrombotic infarction due to left middle cerebral artery (MCA) occlusion. (*Upper left*) Diffusion magnetic resonance imaging at six hours from the onset shows small high intensity area in left basal ganglia. (*Upper middle*) Pretreatment single-photon emission computed tomography (SPECT) demonstrates perfusion deficit in left MCA territory. (*Upper right*) Pretreatment cerebral angiography shows occlusion of M1 portion of the left MCA. (*Lower left*) Posttreatment SPECT 24 hours after recanalization demonstrates mild hyperperfusion in left MCA territory. (*Lower middle*) Follow-up SPECT one week later shows improvement of hyperperfusion and almost normal perfusion in left MCA territory. (*Lower right*) Posttreatment cerebral angiography shows complete recanalization of M1 portion of the left MCA due to intra-arterial administration of urokinase and balloon angioplasty.

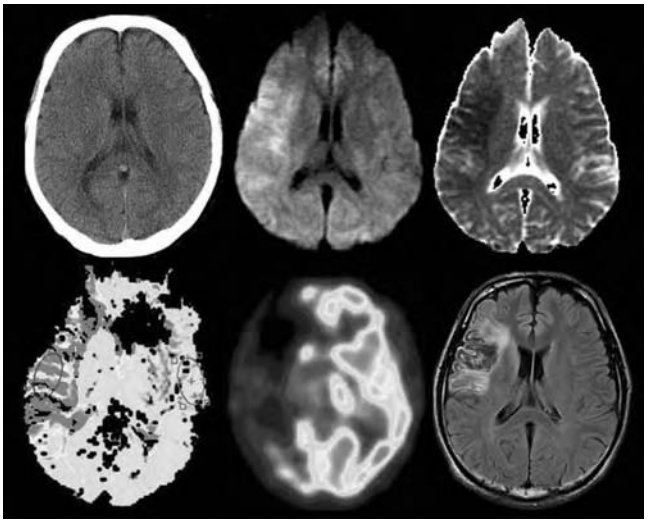

FIGURE 3 A 48-year-old male with cardioembolic infarction due to right middle cerebral artery (MCA) occlusion at four hours from the onset. (*Upper left*) computed tomography (CT) scan at four hours from the onset shows no abnormal lesions. (*Upper middle*) Diffusion magnetic resonance imaging (MRI) at 4.5 hours from the onset demonstrates abnormal high intensity area in right MCA territory. (*Upper right*) The apparent diffusion coefficient map demonstrates mild abnormal intensity area in right MCA territory. (*Lower left*) Perfusion MRI demonstrates low perfusion area in left MCA territory. (*Lower middle*) Pretreatment single-photon emission CT demonstrates perfusion deficit in left MCA territory. The residual cerebral blood flow values (R/CE ratio) are 0.25 in anterior portion and 0.50 in posterior portion of left MCA territory, respectively. (*Lower right*) Flair image at one month after intra-arterial thrombolytic therapy which demonstrated partial recanalization shows cerebral infarction in anterior portion of left MCA territory.

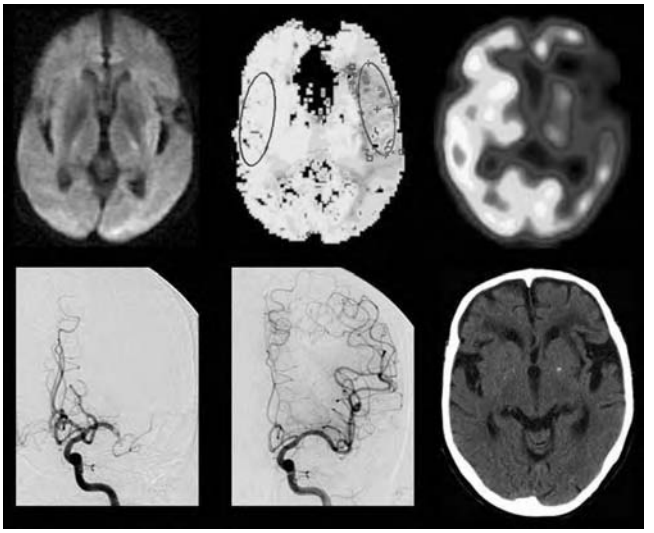

FIGURE 4 A 72-year-old female with cardioembolic infarction due to left middle cerebral artery (MCA) occlusion at two hours from the onset. (*Upper left*) Diffusion magnetic resonance imaging (MRI) at two hours from the onset shows no abnormal lesions. (*Upper middle*) Perfusion MRI demonstrates low perfusion area in whole left MCA territory. (*Upper right*) Pretreatment single-photon emission computed tomography (CT) demonstrates perfusion deficit in left MCA territory, that is, same as perfusion MRI finding. (*Lower left*) Pretreatment cerebral angiography shows occlusion of M1 portion of the left MCA. (*Lower middle*) Posttreatment cerebral angiography shows complete recanalization of M1 portion of the left MCA due to intra-arterial administration of urokinase. (*Lower right*) CT scan at one month after intra-arterial thrombolytic therapy shows small cerebral infarction in left basal ganglia.

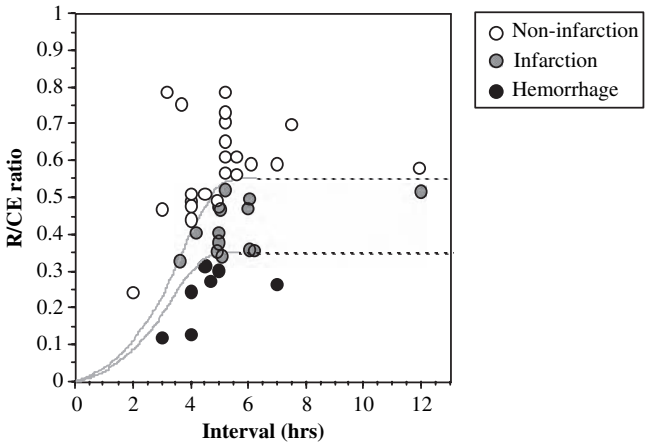

FIGURE 5 Outcome versus severity and duration of ischemia. *Source*: From Ref. 54.

information that can be potentially useful in the management of acute stroke patients with intra-arterial thrombolysis: (*i*) ischemic tissue with a flow index greater than 0.55 may still be salvageable even if treatment is initiated six hours after onset of symptoms; (*ii*) ischemic tissue with a flow index greater than 0.35 may still be salvageable with early treatment (<5 hours); and (*iii*) ischemic tissue with a flow index below 0.35 may be at risk for hemorrhage even if treatment is started within the critical time window. (Fig. 5) Therefore, CBF thresholds evaluated by SPECT provide important information that can be potentially useful in the management of acute stroke patients who are being considered for intra-arterial thrombolysis. That means, the tissue was kept viable with collateral circulation distal to the occluding thromboembolism so that it could be salvaged with recanalization, even if many hours had spent from stroke onset. This study gave validity to the concept that the determination of the state of tissue perfusion from collateral circulation is more important than the initial time from stroke onset. Such observation is further supported by Sasaki et al. (41) that significant reduction of infarction is observed for reperfusion of ischemic tissue having the R/CE ratio between 0.55 and 0.75 within 7.25 hours.

Ogasawara et al. (55) demonstrated that CBF parameters obtained by pretreatment ECD-SPECT could be used to differentiate patients with reversible ischemia from those with irreversible brain damage. However, pretreatment ECD-SPECT did not always predict the occurrence of hemorrhagic transformation, whereas dynamic ECD-SPECT performed immediately after thrombolysis allowed clear identification of patients at risk for hemorrhagic transformation. They speculated that possible sources of this inconsistency are a difference in the tracers used for SPECT, the methods of establishing ROIs, and the change or the regional CBF due to the efficacy of collateral supply and the influence of migration of emboli. They also suggested that the relative retention ratio of ECD obtained by dynamic SPECT is presumably influenced only by the activity of cytosolic esterase and the severity of BBB breakdown. The extremely decreased relative retention ratio of ECD in the reperfused area thus may indicate ongoing irreversible brain damage, which in turn leads to hemorrhagic transformation. Nakano et al. (56) indicated that in stroke patients who had intravenous rt-PA therapy, pretreatment residual CBF using ECD-SPECT for irreversible lesions ranged from 15% to 53.4% (37 ± 12%), whereas that for reversible lesions ranged from 45% to 83% (69 ± 8.6%). Therefore, the ischemic tissue with residual CBF of more than 53.4% was reversible and thatless than 45% could not escape cerebral infarction with intravenous rt-PA therapy.

CONCLUSIONS

The potential for application of SPECT study warrants further evaluation as it may help to improve the assessment of acute ischemic stroke and to choose the most appropriate therapeutic strategy. Since the penumbra is a hypoperfused but viable tissue, it represents an ideal

therapeutic target of acute ischemic stroke. The ischemic penumbra is able to regain its function if promptly reperfused. SPECT have the advantage of giving semiquantitative estimate of CBF as well as various ischemic thresholds. Although the hypoperfused area visualized by SPECT imaging shows not only the ischemic core (irreversible tissue) but also the penumbra area (reversible tissue), we are able to identify the different CBF thresholds such as penumbra, infarction, and hemorrhage. Therefore, SPECT can provide important information to allow the most appropriate candidate for the thrombolytic therapy and neurointerventional treatment to be selected.

REFERENCES

1. Holman BL, Devous MD. Functional brain SPECT: the emergence of a powerful clinical method. J Nucl Med 1992; 33:1888–1904.
2. Winchell HS, Baldwin RM, Lin TH. Development of ^{123}I-labeled amines for brain studies: localization of ^{123}I iodophenyllalkylamines in rat brain. J Nucl Med 1980; 21:940–946.
3. Neirinckx RD, Canning LR, Piper IM, et al. Technetium-99m d, l -HM-PAO: a new radiopharmaceutical for SPECT imaging of regional cerebral blood perfusion. J Nucl Med 1987; 28:191–202.
4. Devous MD. SPECT instrumentation, radiopharmaceuticals, and technical factors. Functional Cerebral SPECT and PET Imaging, 3rd ed. Van Heertum RL and Tikofsky RS, eds. Philadelphia: Lippincott Williams & Wilkins, 2000:3–22.
5. Lassen N, Anderson A, Friberg L, Paulson O. The retention of [99mTc]-d,l-HM-PAO in the human brain after intracarotid bolus injection: a kinetic analysis. J Cereb Blood Flow Metab 1988; 8:S13–S22.
6. Leveille J, Demonceau G, Walovitch RC. Intrasubject comparison between technitium-99m-ECD and technetium-99m-HMPAO in healthy human subjects. J Nucl Med 1992; 33:480–484.
7. Lassen NA, Sperling B. ^{99m}Tc-Bicisate reliably images CBF in chronic brain diseases but fails to show reflow hyperemia in subacute stroke: report of a multicenter trial of 105 cases comparing ^{133}Xe and ^{99m}Tc-Biciste (ECD, Neurolite) measured by SPECT on same day. J Cereb Blood Flow Metab 1994; 14(suppl):44–48.
8. Shishido F, Uemura K, Inugami A, et al. Discrepant 99m Tc-ECD images of CBF in patients with subacute cerebral infarction: a comparison of CBF, CMRO2 and 99m Tc-HMPAO imaging. Ann Nucl Med 1995; 3:161–166.
9. Raynaud C, Rancurel G, Tzourio N, et al. SPECT analysis of recent cerebral infarction. Stroke 1989; 20:192–204.
10. Fieschi C, Argentino C, Lenzi GL, Sacchetti ML, Toni D, Bozzao L. Clinical and instrumental evaluation of patients with ischemic stroke within the first six hours. J Neurol Sci 1989; 91:311–321.
11. De Roo M, Mortelmans L, Devos P, et al. Clinical experience with Tc-99m HMPAO high resolution SPECT of the brain in patients with cerebrovascular accidents. Eur J Nucl Med 1989; 15:9–15.
12. Brass LM, Walvitch RC. Two prospective, blinded, controlled trials of Tc99m bicisate brain SPECT and standard neurological evaluation for identifying and localizing and ischemic strokes. J Stroke Cerebrovasc Dis 1992; 1(suppl 1):S59.
13. Karonen JO, Vanninen RL, Liu Y, et al. Combined diffusion and perfusion MRI with correlation to single-photon emission CT in acute ischemic stroke: ischemic penumbra predicts infarct growth. Stroke 1999; 30:1583–1590.
14. Karonen JO, Nuutinen J, Kuikkla JT, et al. Combined SPECT and diffusion-weighted MRI as a predictor of infarct growth in acute ischemic stroke. J Nucl Med 2000; 41:788–794.
15. Giubilei F, Lenzi GL, Di Piero V, et al. Predictive value of brain perfusion single-photon emission computed tomography in acute stroke. Stroke 1990; 21:895–900.
16. Laloux P, Richelle F, Jamart J, Coster PD, Laterre C. Comparative correlations of HMPAO SPECT indices, neurological score, and stroke subtypes with clinical outcome in acute carotid infarcts. Storke 1995; 26:816–821.
17. Alexandrov AV, Black SE, Ehrlich LE, et al. Simple visual analysis of brain perfusion on HMPAO SPECT predicts early outcome in acute stroke. Stroke 1996; 27:1537–1542
18. Watanabe Y, Takagi H, Aoki S, Sassa H. Prediction of cerebral infarct sizes by cerebral blood flow SPECT performed in the early acute stage. Ann Nucl Med 1999; 13:205–210.
19. Marchal G, Bouvard G, Iglesias S, et al. Predictive value of ^{99m}Tc-HMPAO SPECT for neurological outcome/recovery in the acute stage of stroke. Cerebrovasc Dis 2000; 10:8–17.
20. Grotta JC, Alexandrov AV. t-PA-associated reperfusion after acute stroke demonstrated by SPECT. Stroke 1998; 29:429–432.
21. Baron JC. Perfusion thresholds in human cerebral ischemia: historical perspective and therapeutic implications. Cerebrovasc Dis 2001; 11(suppl 1):2–8.
22. Baird AE, Donnan GA, Austin MC. Early reperfusion in the "spectacular shrinking deficits demonstrated by single-photon emission computed tomography. Neurology 1995; 45:1335–1339.

23. Herderschee D, Limburg M, van Royen EA, et al. Thrombolysis with recombinant tissue plasminogen activator in acute ischemic stroke: evaluation with rCBF-SPECT. Acta Neurol Scand 1991; 83: 317–322.
24. Overgaard K, Sperling B, Boysen G, et al. Thrombolytic therapy in acute ischemic stroke. A Danish pilot study. Stroke 1993; 24:1439–1446.
25. Lassen NA. The luxury perfusion syndrome and its possible relation to acute metabolic acidosis localized within the brain. Lancet 1966; 2:1113–1115.
26. Marchal G, Rioux R, Serrati C, et al. Value of acute-stage PET in predicting neurological outcome after ischemic stroke: further assessment. Stroke 1995; 26:524–525.
27. Gartshore G, Bannan P, Patterson J, et al. Evaluation of technetium-99m exametazime stabilized with cobalt chloride as a blood flow tracer in focal cerebral ischemia. Eur J Nucl Med 1994; 21:913–923.
28. Sperling B, Lassen LA. Hyperfixation of HMPAO in subacute ischemic stroke leading to spuriously high estimates of cerebral blood flow by SPECT. Stroke 1993; 24:193–194.
29. Brass LM, Walovitch RC, Joseph JL, et al. The role of single photon emission computed tomography brain imaging with 99mTc-bicisate in the localization and definition of mechanism of ischemic stroke. J Cereb Blood Flow Metab 1994; 14:S91–S98.
30. Yuh WTC, Maeda M, Wang A, et al. Fibrinolytic treatment of acute stroke: are we treating reversible cerebral ischemia? AJNR 1995; 16:1994–2000.
31. Fisher M. Characterizing the target of acute stroke therapy. Stroke 1997; 28:866–872.
32. Symon L, Branston N, Strong A, Hope T. The concept of thresholds of ischaemia in relation to brain structure and function. J Clin Pathol 1977; 30(suppl 11):149–154.
33. Astrup J, Symon L, Siesjö B. Thresholds in cerebral ischemia - the ischemic penumbra. Stroke 1981; 12:723–725.
34. Hossmann K. Viability thresholds and the penumbra of focal ischemia. Ann Neurol 1994; 36:557–565.
35. Fisher M, Garcia J. Evolving stroke and the ischemic penumbra. Neurology 1996; 47:884–888.
36. Jones T, Morawetz R, Crowell R, et al. Thresholds of focal cerebral ischemia in awake monkeys. J Neurosurg 1981; 54:773–782.
37. Alexandrov A, Masdeu J, Devous M, Black S, Grotta J. Brain single-photon emission CT with HMPAO and safety of thrombolytic therapy in acute ischemic stroke Stroke 1997; 28:1830–1834.
38. Laloux P, Richelle F, Jamart J, Coster PD, Laterre C. Comparative correlations of HMPAO SPECT indices, neurological score, and stroke subtypes with clinical outcome in acute carotid infarcts. Storke 1995; 26:816–821.
39. Nakano S, Kinoshita K, Jinnouchi S, et al. Comparative study of regional cerebral blood flow images by SPECT using Xenon-133, Iodine-123 IMP, and technetium-99m, HMPAO. J Nucl Med 1989; 30:337–342.
40. Shimosegawa E, Hatazawa J, Inugami A, et al. Cerebral infarction within six hours of onset: prediction of completed infarction with technetium-99m-HMPAO SPECT. J Nucl Med 1994; 35:1097–1103.
41. Sasaki O, Takeuchi S, Koizumi T, Koike T, Tanaka R. Complete recanalization via fibrinolytic therapy can reduce the number of ischemic territories that progress to infarction. AJNR 1996; 17:1661–1668.
42. Hatazawa J, Shimosegawa E, Toyoshima H, et al. Cerebral blood volume in acute brain infarction: a combined study with dynamic susceptibility contrast MRI and ^{99m}Tc-HMPAO-SPECT. Stroke 1999; 30:800–806.
43. Hirano T, Read SJ, Abbott DF, et al. Prediction of the final infarct volume within 6 h of stroke using single photon emission computed tomography with technetium-99m hexamethylpropylene amine oxime. Cerebrovasc Dis 2001; 11:119–127.
44. Berrouschot J, Barthel H, Hesse SH, et al. Differentiation between transient ischemic attack and ischemic stroke within the first 6 hours after onset of symptoms by using ^{99m}Tc-ECD SPECT. J Cereb Blood Flow Metab 1998; 18:921–929.
45. Mahagne MH, Darcourt J, Migneco O, et al. Early 99m Tc-ethylcysteinase dimmer brain SPECT patterns in the acute phase of stroke as predictors of neurological recovery. Cerebrovasc Dis 2000; 10:364–373.
46. Liu Y, Karonen JO, Vanninen RL, et al. Cerebral hemodynamics in human acute ischemic stroke: a study with diffusion- and perfusion-weighted magnetic resonance imaging and SPECT. J Cereb Blood Flow Metab 2000; 20:910–920.
47. Iseda T, Nakano S, Yano T, et al. Time-threshold curve determined by single photon emission CT in patients with acute middle cerebral artery occlusion. AJNR 2002; 23:572–576.
48. Mahagne MH, David O, Darcourt J, et al. Voxel-basec mapping of cortical ischemic damage using Tc 99m L, L-ethylcysteinate dimmer SPECT in acute stroke. J Neuroimaging 2004; 14:23–32.
49. Patlak CS, Blasberg RG, Fenstermacher JD. Graphical evaluation of blood-to-brain transfer constants from multiple-time uptake data. J Cereb Blood Metab 1983; 3:1–7.
50. Matsuda H, Tsuji S, Shuke N, Sumiya H, Tonami N, Hisada K. Noninvasive measurements of regional cerebral blood flow using technetium-99m hexamethylprophylene amine oxime. Eur J Nucl Med 1993; 20:391–401.

51. Watanabe Y, Takagi H, Aoki S, et al. Prediction of cerebral infarct sizes by cerebral blood flow SPECT performed in the early acute stage. Ann Nucl Med 1999; 13:205–210.
52. Umemura A, Suzuka T, Yamada K. Quantitative measurement of cerebral blood flow by 99mTc-HMPAO SPECT in acute ischaemic stroke: usefulness in determining therapeutic options. J Neurol Neurosurg Psychiatry 2000; 69:472–478.
53. Ueda T, Hatakeyama T, Kumon Y, Sakaki S, Uraoka T. Evaluation of risk of hemorrhagic transformation in local intra-arterial thrombolysis in acute ischemic stroke by initial SPECT. Stroke 1994; 25:298–303.
54. Ueda T, Sakaki S, Yuh WTC, Nochide I, Ohta S. Outcome in acute stroke with successful intra-arterial thrombolysis and predictive value of initial single-photon emission-computed tomography. J Cereb Blood Flow Metab 1999; 19:99–108.
55. Ogasawara K, Ogawa A, Doi M, et al. Prediction of acute embolis stroke outcome after local intra-arterial thrombolysis: value of pretreatment and posttreatment ^{99m}Tc-ECD single photon emission computed tomography. J Cereb Blood Flow Metab 2000; 20:1579–1586.
56. Nakano S, Iseda T, Ikeda T, et al. Thresholds of ischemia salvageable with intravenous tissue plasminogen activator therapy: evaluation with cerebral blood flow single-photon emission computed tomographic measurements. Neurosurgery 2000; 47:68–73.

13 Magnetic Resonance Imaging Assessment of the Ischemic Penumbra in Experimental Stroke

Timothy Q. Duong
Yerkes Imaging Center, Division of Neuroscience and Department of Neurology, Emory University, Atlanta, Georgia, U.S.A.

Marc Fisher
University of Massachusetts/Memorial Healthcare, Worcester, Massachusetts, U.S.A.

QUANTITATIVE PERFUSION AND DIFFUSION IMAGING

Diffusion-weighted magnetic resonance imaging (MRI) has become an established method for noninvasive evaluation of cerebral ischemia in both humans and animal models. Although the biophysical mechanism(s) underlying apparent diffusion coefficient (ADC) reduction in ischemic tissue remains poorly understood (1–4), diffusion-weighted imaging (DWI) (1) is widely recognized for its ability to noninvasively detect ischemic brain injury within minutes after its onset, whereas other conventional imaging techniques [such as T_1-, T_2-weighted MRI, Computed Tomography (CT)] fail to detect such injury for at least several hours (1). Brain tissues with perfusion deficits below a critical threshold level [e.g., a cerebral blood flow (CBF) value of ~20 mL/100 g/min in rat or gerbil brain] (5,6) experience metabolic energy failure, membrane depolarization, and subsequent cellular swelling (cytotoxic edema). These changes precipitate a reduction in the ADC of brain water that is manifested as a hyperintense region on a DWI (1). Perfusion-weighted imaging (PWI) evaluates blood flow in the microcirulation of the brain and can be performed with either a bolus contrast technique or an arterial spin labeling technique (7,8). The latter approach provides relatively higher sensitivity and allows repeated measures for increased spatial resolution, but is less widely used because it is relatively more difficult to perform. During the first few hours after stroke onset (i.e., the acute phase), the anatomic region encompassed by the DWI abnormality is typically smaller than the volume of the perfusion deficit, but it usually expands and eventually coincides with the PWI volume (6,9). The difference in the regions of the PWI and DWI abnormality during the acute phase of stroke has been termed the "perfusion–diffusion" mismatch (PWI/DWI mismatch), and it was suggested that this region of mismatch approximates potentially salvageable ischemic tissue or the ischemic penumbra (10).

In humans, a "perfusion–diffusion mismatch" has been widely observed and it persists for many hours after stroke onset (10). Although the precise imaging identification of the ischemic penumbra requires correlation with regions of disturbed energy metabolism [as rigorously investigated on animal models (11–13)], such correlation is generally not possible in humans. Therefore, identification of the ischemic penumbra and viability thresholds have been operationally defined based on DWI, PWI, and other equivalent imaging modalities (14–16). The transition from potentially reversible to irreversible ischemic injury is a complex process that is highly dependent on the duration and severity of ischemia, and as such different subsets of the ischemic penumbra could have variable outcomes. Re-establishing tissue perfusion and/or administering neuroprotective drugs in a timely fashion could be expected to salvage some portions of the ischemic penumbra (17,18). For example, clinical trials have demonstrated the benefits of thrombolytic therapy using recombinant tissue plasminogen activator (t-PA) within three hours after the onset of ischemia and the clinical benefit was associated with smaller late infarcts on CT (18). It is therefore plausible to presume that early intravenous t-PA use likely salvages a portion of the ischemic penumbra, and preliminary studies support this hypothesis. To potentially help to

expand the time window for thrombolytic therapy, it will be important to have the means to identify the "tissue signature" and "clock window" of ischemic tissues in order to achieve the maximum benefit and to avoid devastating, intraparenchymal hemorrhage (17). Using DWI/PWI to identify potential candidates for i.v. or intra-arterial (i.a.) thrombolysis, especially beyond the currently approved three-hour time window should provide a mechanism to enhance patient selection that could lead to a greater chance for therapeutic benefit. Preliminary open-label studies support this hypothesis as patients treated with thrombolytic therapy beyond three hours, who have a PWI/DWI mismatch, appear to have a reasonably favorable outcome that may even exceed the benefits observed without penumbral imaging, during the three-hour window (19).

Similar observations of a PWI/DWI mismatch in animal stroke models have been limited and the temporal evolution of the mismatch on a pixel-by-pixel basis in animal models has yet to be systematically investigated. Animal models in which focal ischemia can be reproducibly studied under controlled conditions are important for identifying and predicting the severity of ischemic injury and for evaluating the efficacy of therapeutic interventions. Characterizing the natural history and predictive value of the PWI/DWI mismatch in animal stroke models is, particularly, important because the PWI/DWI mismatch is being used as an indicator of "ischemic penumbra" in the clinical trial setting. In animal studies, the PWI/DWI mismatch approach could be used to determine the potential therapeutic window for interventions, and to assess the effects of interventions on different components of the ischemic region. It is highly likely that each type of animal stroke model has a different temporal profile for the evolution of the ischemic penumbra and, therefore, the potential for therapeutic intervention. It is even possible that the same model may vary among different laboratories related to subtle differences in technique. Therefore, investigating the PWI/DWI mismatch in different models and locations should prove highly valuable for better characterizing stroke models.

The application of DWI and PWI in stroke animal models has a long history and helped to guide their application in human stroke (20). DWI was used to characterize the temporal and spatial evolution of experimental ischemic injury. It was also used as an in vivo assessment tool for both reperfusion and neuroprotective therapy, providing invaluable information about the location and characteristics of ischemic tissue responses to a variety of therapeutic interventions (21). PWI has also been applied to the study of ischemic lesion development and its response to therapy, primarily reperfusion, in several different types of animal stroke models (22). It is particularly useful for evaluating the effect of i.v. or i.a. thrombolysis on the brain's microcirculation. These animal DWI and PWI studies have helped to lead the way for the application of these MRI techniques in human stroke studies and trials. Little experimental work has been performed using the PWI/DWI mismatch in animal stroke models to approximate the ischemic penumbra and to characterize the effects of treatment on this tissue.

Over the past few years, we and others have developed and applied high-resolution quantitative perfusion and diffusion imaging protocols in rat stroke models. Figure 1A shows a representative high-resolution quantitative perfusion and diffusion maps obtained at approximately 30 minutes postischemic occlusion in Sprague-Dawley rats. The anatomic area defined by ADC reduction is initially smaller than the area of CBF reduction. The perfusion–diffusion mismatch is clearly delineated. The areas defined by ADC reduction expand over time and eventually coincides with the area defined by PWI abnormality, if left untreated. The temporal evolution of the permanent and transient (60 minutes) cerebral ischemia is shown in Figure 1B. The lesion volumes were defined based on ADC and CBF viability thresholds validated previously by our laboratory (23). As would be expected, in the permanent occlusion group, the perfusion-defined lesion volume remained relatively constant over time. The diffusion imaging-defined lesion volume was initially small and grew over time to match the perfusion-defined lesion volume. The ADC- and CBF-defined lesion volumes at 180 minutes after stroke onset were similar to the histologically defined triphenyltetrazolium chloride (TTC) infarct volume at 24 hours.

In an experiment using Sprague–Dawley rats, reperfusion at 60 minutes immediately reduced the CBF- and ADC-defined lesion volumes. However, the ADC-defined lesion volume grew slightly over time after reperfusion and the infarct volume at 24 hours was slightly larger than the DWI-defined lesion volume at 180 minutes, probably a result of delayed cell death or secondary injury in reperfused tissue. Both the ADC-defined lesion volume at 180 minutes and TTC infarct volume at 24 hours were significantly smaller than those observed with permanent

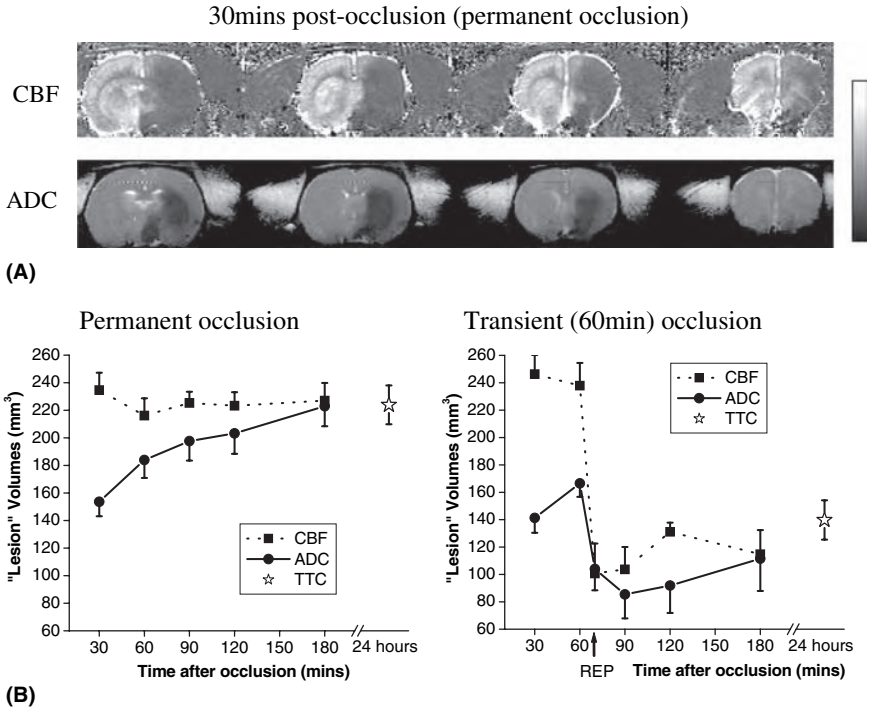

FIGURE 1 (**A**) Representative apparent diffusion coefficient (ADC) and cerebral blood flow (CBF) maps from one animal at 30 minutes postocclusion. The grayscale bar indicates ADC ranges from 0 to 0.001 mm^2/sec and CBF ranges from 0 to 2 mL/g/min. (**B**) Temporal progression of ADC- and CBF-defined lesion volumes of permanent ($n = 6$) and transient (60 minutes, $n = 6$) occlusion determined by using the group-average viability thresholds 57% and 30% reduction for CBF and ADC thresholds, respectively. Histological triphenyltetrazolium chloride infarction volumes are also displayed. *Source*: From Ref. 17.

occlusion, supporting the concept that early reperfusion will salvage a portion of the ischemic region.

We had also investigated the dynamic evolution of ischemic injury in a different rat strain, Wistar rats, which are known to have better collateral blood flow (24). In the Wistar rats that underwent permanent occlusion, a significant mismatch of PWI to DWI volume was observed up to 90 minutes after middle cerebral artery occlusion (MCAO) (25). At this time point, in the Sprague–Dawley group, the mismatch volume was no longer statistically significant. The experiments were performed under identical conditions so that the only difference was the rat strain employed and appear to demonstrate that the strain of rats used in an experiment can influence the dynamics of penumbral evolution. These studies together demonstrate how DWI and PWI can be used to follow the evolution of ischemic injury, the PWI/DWI mismatch region, and the effects of mechanical reperfusion on in vivo tissue injury and how differences in experimental conditions can be used to follow the evolution of the PWI/DWI mismatch.

AUTOMATED CLUSTER ANALYSIS

Most of the analysis of stroke data were carried out using a volumetric approach and involved the use of a region-of-interest (ROI) analysis. Although ROI analysis is helpful in simplifying a complex analysis problem, these contain tissues with different ADC and CBF characteristics, thereby inadvertently mixing the characteristics that one is trying to resolve and oversimplifying the complex task of assessing tissue viability. The complex temporal and spatial evolution of focal cerebral ischemia has recently prompted the use of various combinations of MR parameters and more sophisticated analysis methods (26–31) for performing multiparametric segmentation on a pixel-by-pixel basis to predict stroke outcome. These methods could significantly enhance the use of MRI for accurate diagnosis and prognosis of stroke. One of the most well-known

multiparametric segmentation approaches is the iterative self-organizing data analysis technique (ISODATA). Jacobs et al. (27) employed the ISODATA technique to analyze T_2, T_1, and DWI stroke data in both animals (26) and humans, during the subacute phase where T_1 and T_2 were informative. Wu et al. (30) used generalized linear model algorithms to analyze DWI and PWI data to predict tissue outcome in human stroke patients scanned within 12 hours of symptom onset. Essentially, all of the studies, mentioned earlier, focused on the subacute stage when the DWI-defined ischemic lesions had essentially stopped evolving. Furthermore, qualitative PWI and DWI were often used due to time constraint and/or technical limitations in the MRI data acquisition. Cluster analysis of quantitative perfusion and diffusion imaging could potentially yield a finer discrimination of tissue status based on their intrinsic diffusion and perfusion characteristics during the acute phase.

Our lab recently implemented a modified ISODATA technique with some improved figures (32). Figure 2 shows the results of the modified ISODATA analysis in a stroke rat. In contrast to

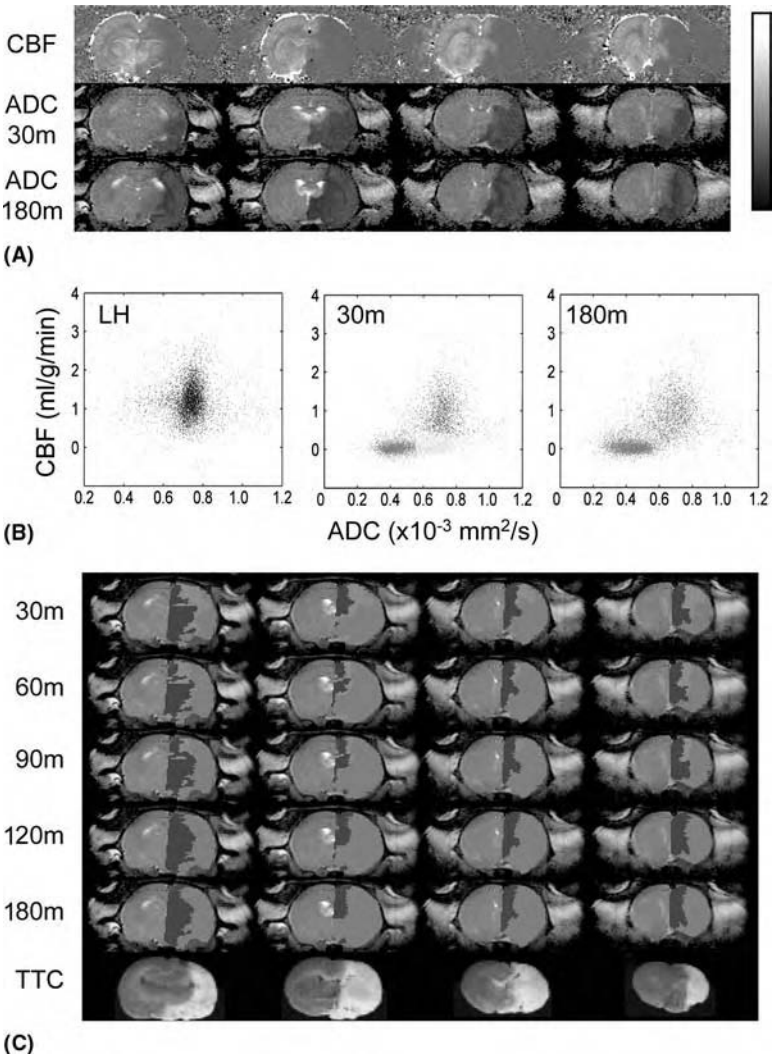

FIGURE 2 (*See color insert.*) Iterative self-organizing data analysis technique (ISODATA) analysis of different ischemic tissue types. (**A**) cerebral blood flow (CBF) maps, and apparent diffusion coefficient (ADC) maps at 30 minutes and 180 minutes. The greyscale bar: ADC ranges from 0 to 0.001 mm^2/sec, CBF ranges from 0 to 2 mL/g/min. (**B**) CBF–ADC scatterplots of the normal left hemisphere at 30 minutes, ISODATA cluster analysis results of the right hemisphere at 30 and 180 minutes. (**C**) Pixel clusters from the CBF–ADC scatterplots were overlaid on the image space at 30, 60, 90, 120, and 180 minutes. In the right hemisphere, blue, green, and red are assigned as "normal," "perfusion–diffusion" mismatch, and "ischemic core" clusters, respectively. Triphenyltetrazolium chloride slides at 24 hours are also shown.

the normal left hemisphere that exhibited a single cluster, the right ischemic hemisphere showed three distinct clusters at 30 minutes, namely: the normal (blue), core (red), and mismatch cluster (green). At 180 minutes, the scatterplots showed that the mismatch had largely disappeared. Different pixel clusters resolved on the scatterplots were mapped onto the image spaces. Mismatch was located peripheral to the ischemic core. The ischemic "core" volumes grew and the "mismatch" volumes decreased as ischemia progressed. The ISODATA-derived lesion volumes showed excellent slice-by-slice correspondence with the TTC infarct volumes. A correlation analysis was performed between the ISODATA-derived lesion volumes and TTC infarct volumes for each animal, at each time point postocclusion. The correlation coefficients with respect to the unity line for 30, 60, 90, 120, and 180 minutes postischemia were 0.62, 0.74, 0.83, 0.94, 0.99, respectively. These results demonstrated that the automated cluster analysis yielded objective classification of different ischemic tissue types.

PREDICTING ISCHEMIC TISSUE FATES

In addition to ischemic tissue characterization, MRI data obtained early after stroke onset also offers the unique opportunity to statistically predict ischemic tissue fate. Jacobs et al. (27) used a threshold-based analysis and demonstrated that the combination of T_2 and ADC data provided improved prediction of infarction relative to either parameter alone, in subacute stroke in humans. Wu et al. (30) reported the eloquent use of a generalized linear model to predict stroke outcomes based on DWI, PWI, and T_2 data in humans. Lesions were defined using a threshold-based method to generate the training set. However, this approach appears less intuitive as the contribution of various parameters is difficult to assess. We developed and validated a simple and intuitive statistical algorithm for predicting ischemic tissue fate after acute ischemic stroke in a well-characterized rat stroke (permanent suture occlusion) model (32). Quantitative high-resolution perfusion and diffusion imaging were obtained. A modified ISODATA cluster analysis (as opposed to a threshold-based analysis) was used to classify tissue types. Prediction of tissue infarct was made for overall tissue fate as well as for individual ISODATA-defined pixel clusters (such as normal tissue, ischemic "penumbra," and ischemic core) by comparing the in vivo MRI data to TTC-confirmed infarction at 24 hours. Probability profiles were derived. Prediction using ADC data alone, CBF data alone, and CBF + ADC data were compared and correlated with endpoint imaging and histology. The resultant prediction maps were not used to identify tissue infarction but to predict risk of future infarction. Performance measures of the prediction, such as sensitivity, specificity, and receiver operating characteristic, were also evaluated.

Two-dimensional probability of infarct (P_I) contour plots based on the combined ADC + CBF data at different time points postischemia were computed (Fig. 3A). Pixels with low ADC and low CBF showed high P_I. The "mismatch" zone, in which the ADC was normal or near normal but the CBF was reduced, dynamically evolved and showed a nonzero P_I (>20%). The P_D contour plot showed two modes at 30 minutes postischemia and a single mode at subsequent time points. As ischemia progressed, the P_I contour plots became sharper with the highest probability density remained relatively time invariant (ADC ~ 0.42×10^{-3} mm^2/sec and CBF ~ 0 mL/g/min).

Probability maps of risk of subsequent infarction were computed on a separate group of animals. Figure 3B shows the probability maps of future infarction based on the 30-minute ADC, CBF, and ADC + CBF data from one animal. For comparison, ADC and CBF maps at 30 and 180 minutes, ISODATA analysis of the 180-minute data, and 24-hour TTC histology are also displayed. Prediction made with ADC data alone underestimated infarct volume, whereas predictions made with CBF data alone overestimated infarct volume. With the combined ADC + CBF data, most of the mismatch pixels (circular ROI in the inset) were predicted correctly to go into infarct (i.e., correlated with histology and ISODATA results), whereas with ADC data alone, the mismatch was incorrectly predicted not to go into infarct. Furthermore, with the combined ADC + CBF information, most of the "normal" pixels in the right hemisphere (rectangular ROI in the inset) was predicted to remain normal with significantly higher certainty (P_I ~ 0), whereas with CBF data alone, most of the "normal" pixels were incorrectly predicted to have substantial nonzero probability of going into infarct. Predicted infarct volumes based on the ADC + CBF data showed the best correspondence with the ISODATA maps and the 24-hour TTC infarct volumes.

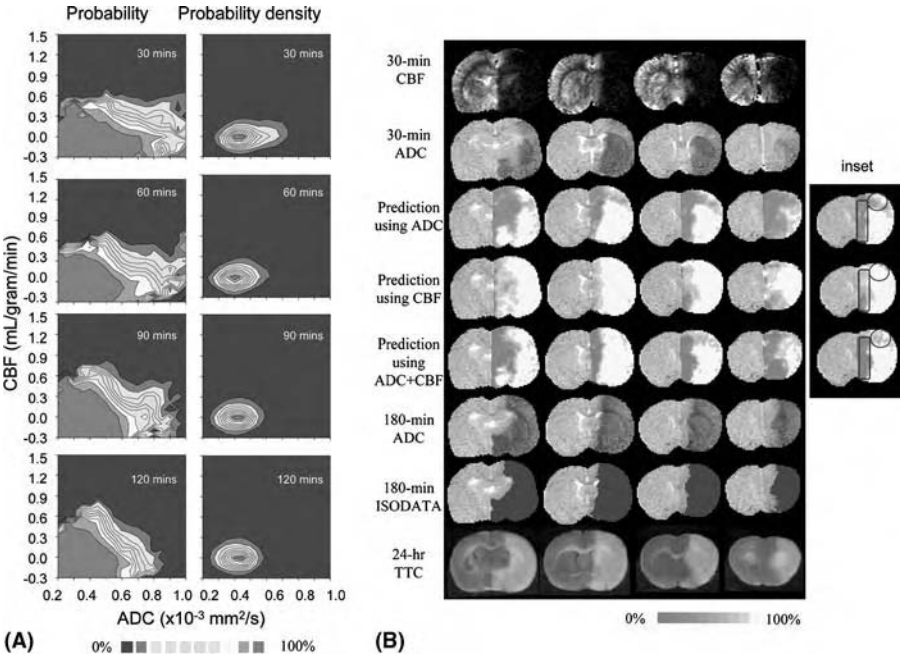

FIGURE 3 (*See color insert*.) Profiles of probability of infarct and probability density of infarct as a function of (**A**) apparent diffusion coefficient (ADC) + cerebral blood flow (CBF) at different time points postischemia (training Group A, $n = 6$). Blue–red color bar indicates the probability ranging from 0% to 100% in steps of 10%. Probability density profiles were normalized from 0% to 100%. Probability maps of risk of future infarction (**B**) determined based on the 30-minutes ADC data alone, CBF data alone, and ADC+CBF data from a representative animal (experimental Group B). Multislice images are displayed from left to right as posterior to anterior slices. Also shown are the 30-minute ADC and CBF maps, 180-minute ADC maps, iterative self-organizing data analysis technique analysis at 180 minutes, and 24-hour triphenyltetrazolium chloride staining. Hypointensities in the ADC and CBF maps indicate regions of reduced ADC and CBF values, respectively. Red–yellow color bar indicates the probability of infarct ranging from 0% to 100% in steps of 10%. The inset shows prediction using ADC alone underestimated infarct volume whereas CBF alone overestimated infarct volume [circular region-of-interest (ROI)]. Prediction using ADC+CBF showed "normal" tissues having a high degree of certainty of not going into infarct (low probability, rectangular ROI) relative ADC or CBF alone.

Receiver-operating-characteristic (ROC) curves were used to evaluate the accuracy of the predictions made by using ADC alone, CBF alone, and ADC + CBF (Fig. 4A). Predictions made using ADC + CBF data showed slightly higher sensitivity and specificity than those using ADC alone or CBF alone. At the optimal operating points, combined ADC + CBF predicted tissue infarction with $86 \pm 4\%$ sensitivity and $89 \pm 6\%$ specificity.

Although performance measures of overall tissue fate prediction made with ADC+CBF, generally, showed improvement over those made with ADC or CBF alone, the improvement was surprisingly small. This is because the performance measures based on the prediction of overall tissue fate have a poor dynamic range (i.e., good performance is clustered at the very high percentage of sensitivity and specificity) and are dominated by the fate of the "core" pixels. A partial area index was helpful because it samples specific region of under the ROC curve region with a larger dynamic range. However, the choice of the ranges over which the area is integrated is subjective and such ranges could depend on diseases and/or disease stages. The combined automated tissue classification and statistical prediction proposed herein are important because it allowed the performance measures of individual tissue types to be assessed, avoiding the aforementioned drawbacks. Indeed, performance analysis confirmed that the poor dynamic ranges of the ROC curves were dominated by the fate of the already infarcted pixels. Performance measures of individual tissue types should provide a more sensitive and appropriate assessment of the prediction accuracy compared to those of the overall tissue fates. Figure 4B shows the prediction of individual tissue types. Modified ISODATA clustering was used to resolve "normal," "mismatch," and "core" pixels and probability of infarct were

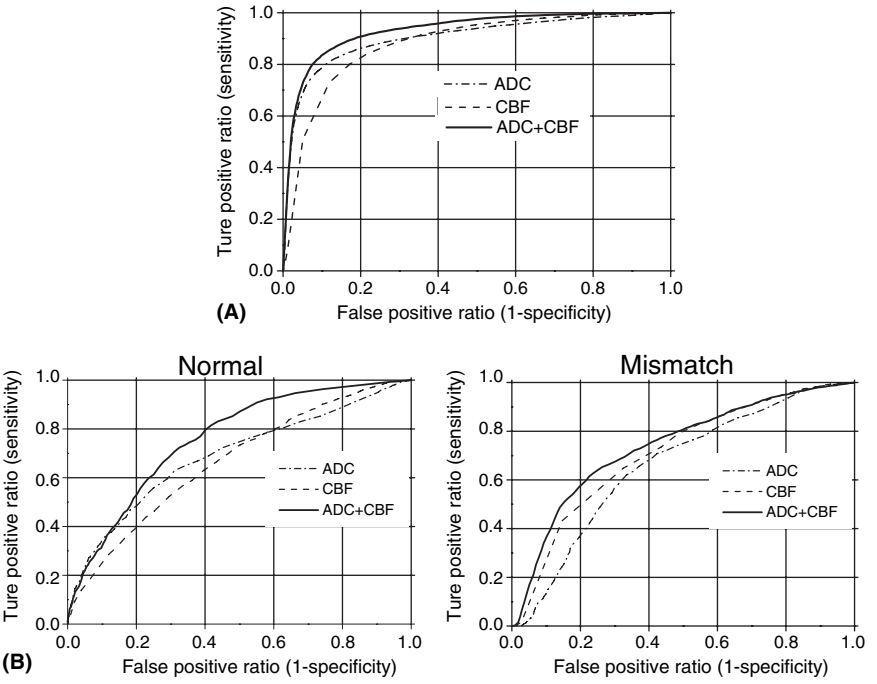

FIGURE 4 Receiver-operating-characteristic curves of sensitivity versus (1-specificity) of the prediction of (**A**) overall tissue fates and (**B**) tissue fates of individual iterative self-organizing data analysis technique-derived (normal, mismatch) clusters. Data were derived from incorporating the ADC data, CBF data, and ADC + CBF data (Group B, $n = 6$). All standard deviation error bars were <0.05 and are not displayed for clarity.

evaluated for individual tissue types. Prediction of infarct for each tissue type was made and the results were as follows: (*i*) For the P_1 of the right-hemisphere normal cluster, combined ADC + CBF data correctly showed low probability of infarct, whereas ADC data alone and CBF data alone showed substantial probability of infarct. (*ii*) For the mismatch cluster, combined ADC + CBF data correctly predicted the infarct probability, whereas ADC underestimated the infarct probability and CBF overestimated the infarct probability. The dynamic ranges of sensitivity and specificity of the prediction algorithm made for individual tissue types were larger than those the prediction algorithm made for overall tissue fates. To the best of our knowledge, this is the first statistical prediction of tissue infarction for individual ischemic tissue types.

APPLICATIONS TO THERAPY

Based upon our observations for penumbral survival using the PWI/DWI mismatch temporal profile, we predicted that initiation of therapy at 60 minutes after MCAO in the permanent suture occlusion model could yield substantial tissue salvage with neuroprotection. Dimethyl sulfoxide (DMSO) was evaluated and compared to a saline control group (33). A 33% solution of DMSO or saline was initiated at 60 minutes and then infused for three hours for a total dose of 1.5 g/kg of DMSO. Serial DWI and PWI studies were performed and demonstrated a large initial region of PWI abnormality that persisted over time (Fig. 5). The DWI abnormal region initially increased but when the DMSO infusion was started no further growth occurred over the subsequent three hours and the TTC-confirmed infarct volume at 24 hours was reduced by more than 40% in the DMSO group compared to the control group ($P = 0.002$). The absolute ADC values in the PWI/DWI mismatch region were characterized in the DWSO-treated and control groups. The ADC values progressively declined in the mismatch region over time in the control group but declined only slightly in the DMSO group. This study demonstrates that DMSO, initiated 60 minutes after MCAO in this permanent occlusion model, was highly protective and prevented the PWI/DWI mismatch region, probably representing the ischemic

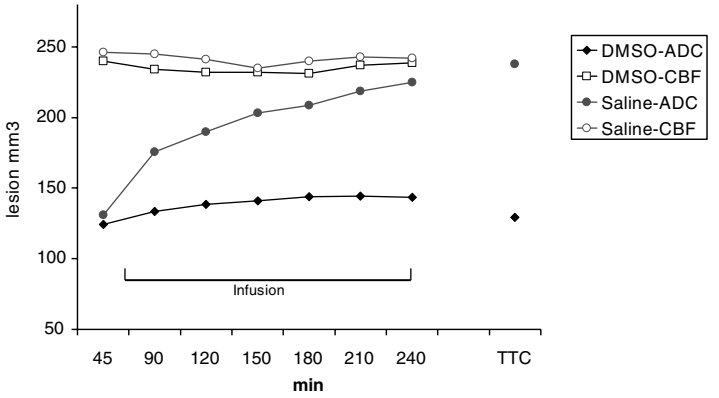

FIGURE 5 The perfusion and diffusion lesion volumes evolve differently over time in DMSO and saline vehicle treated animals with dimethyl sulfoxide treatment essentially preventing further enlargement of the diffusion lesion volume.

penumbra from evolving into infarction. Follow-up benchtop studies with DMSO demonstrated that three-day survival with the same treatment paradigm maintained the protective effect and that initiation of the therapy at two hours after MCAO did not demonstrate a significant effect on infarct volume reduction. Interestingly, the infarct volume observed in the two-hour DMSO treatment group was almost identical to the DWI lesion volume observed at two hours in the control group of the MRI experiment.

In a second preliminary MRI experiment using normobaric hyperoxia as the therapeutic intervention, the initial results appear to be somewhat different. Prior studies with normobaric hyperoxia suggested that this therapy is effective in reducing infarct size in temporary MCAO models but not with permanent occlusion (34). Additionally, normobaric hyperoxia was shown to extend the time window for successful treatment with i.v. t-PA in a rat stroke model (35). We observed that normobaric hyperoxia, when initiated 30 minutes after initiation of permanent MCAO, dramatically reduced the expansion of the DWI-determined lesion volume during the three hours of treatment without any effect on the PWI-lesion volume. However, after stopping treatment, the DWI lesion volume began to grow again within 30 minutes of cessation and the TTC-determined infarct volume at 24 hours was almost the same as untreated animals. This preliminary MRI experiment appears to also show that normobaric hyperoxia is effective in the PWI/DWI mismatch region but the effect is lost when treatment stops—a different pattern than that observed with DMSO.

CONCLUSIONS

High-resolution quantitative perfusion and diffusion imaging offers a useful means to evaluate ischemic brain injury. An automated ISODATA analysis of the ADC and CBF tissue characteristics during the acute phase provides a powerful and unbiased means to characterize tissue fates in ischemic brain injury, and to monitor therapeutic intervention. Combined with the probabilistic prediction algorithm, risk of future infarction could be statistically estimated. These advances are expected to be useful for staging and monitoring the spatiotemporal dynamics of ischemic brain injury on a pixel-by-pixel basis as a function of therapeutic intervention in both animals and, eventually, humans. In treatment experiments, the mismatch-defined penumbra could be persistently salvaged with DMSO and transiently prevented from evolving with normobaric hyperoxia.

REFERENCES

1. Moseley ME, Cohen Y, Mintorovitch J, et al. Early detection of regional cerebral ischemia in cats: comparison of diffusion- and T2-weighted MRI and spectroscopy. Magn Reson Med 1990; 14:330–346.
2. Zhong J, Petroff AC, Prichard JW, Gore JC. Changes in water diffusion and relaxation properties of rat cerebrum during status epilepticus. Magn Reson Med 1993; 30:241–246.

3. van der Toorn A, Dijkhuizen RM, Tulleken CAF, Nicolay K. Diffusion of metabolites in normal and ischemic rat brain measured by localized 1H MRS. Magn Reson Med 1996; 36:914–922.
4. Duong TQ, Ackerman JJH, Ying HS, Neil JJ. Evaluation of extra- and intracellular apparent diffusion in normal and globally ischemic rat brain via 19F NMR. Magn Reson Med 1998; 40:1–13.
5. Busza AL, Allen KL, King MD, van Bruggen N, Williams SR, Gadian DG. Diffusion-weighted imaging studies of cerebral ischemia in gerbils: Potential relevance to energy failure. Stroke 1992; 23:1602–1612.
6. Mancuso A, Karibe H, Rooney WD. Correlation of early reduction in the apparent diffusion coefficient of water with blood flow reduction during middle cerebraal artery occlusion in rats. Magn Reson Med 1995; 34:368–377.
7. Calamante F, Thomas DL, Pell GS, Wiersma J, Turner R. Measuring cerebral blood flow using magnetic resonance imaging techniques. J Cereb Blood Flow Metab 1999; 19:701–735.
8. Williams DS, Detre JA, Leigh JS, Koretsky AP. Magnetic resonance imaging of perfusion using spin inversion of arterial water. Proc Natl Acad Sci U S A 1992; 89:212–216.
9. Roussel SA, van Bruggen N, King MD, Housemen J, Williams SR, Gadian DG. Monitoring the intitial expansion of focal ischemic changes by diffusion-weighted MRI using a remote controlled method of occlusion. NMR in Biomed 1994; 7:21–28.
10. Warach S, Dashe J, Edelman R. Clinical outcome in ischemic stroke predicted by early diffusion-weighted and perfusion magnetic resonance imaging. J Cereb Blood Flow Metab 1996; 16:53–59.
11. Hoehn-Berlage M, Norris DG, Kohno K, Mies G, Leibfritz D, Hossmann K-A. Evolution of regional changes in apparent diffusion coefficient during focal ischemia of rat brain: The relationship of quantitative diffusion NMR imaging to reduction in cerebral blood flow and metabolic disturbances. J Cereb Blood Flow Metab 1995; 15:1002–1011.
12. Back T, Hoehn-Berlage M, Kohno K, Hossmann K-A. Diffusion nuclear magnetic resonance imaging in experimental stroke correlation with cerebral metabolites. Stroke 1994; 25:494–500.
13. Kohno K, Hoehn-Berlage M, Mies G, Back T, Hossmann KA. Relationship between diffusion-weighted MR images, cerebral blood flow, and energy state in experimental brain infarction. Magn Reson Imag 1995; 13:73–80.
14. Parsons MW, Yang Q, Barber A, et al. Perfusion magnetic resonance imaging maps in hyperacute stroke relative cerebral blood flow most accurately identifies tissue destined to infarct. Stroke 2001; 32:1581–1587.
15. Schlaug G, Benfield A, Baird AE, et al. The ischemic penumbra: operationally defined by diffusion and perfusion MRI. Neurology 1999; 53:1528–1537.
16. Kaufmann AM, Firlik AD, Fukui MB, Weshsler LR, Jungries CA, Yonas H. Ischemic core and penumbra in human stroke. Stroke 1999; 30:93–99.
17. Albers GW. Expanding the window for thrombolytic therapy in acute stroke: The potential role of acute MRI for patient selection. Stroke 1999; 30:2230–2237.
18. NINDS. Tissue plasminogen activator for acute ischemic stroke. The National Institute of Neurological Disorder, and Stroke rt-PA Stroke Study Group. N Engl J Med 1995; 333:1581–1587.
19. Ribo M, Molina CA, Rovira A, et al. Safety and efficacy of intravenous tissue plasminogen activator stroke treatment in the 3- to 6- hour window using multimodal transcranial/doppler MRI selection protocol. Stroke 2005; 36:602–606.
20. van Bruggen N, Roberts TP, Cremer JE. The application of magnetic resonance imaging to the study of experimental cerebral ischemia. Cerebrovasc Brain Metab Rev 1994; 6:180–210.
21. Li F, Carano RAD, Irie K, et al. Neuroprotective effects of a novel broad spectrum cation channel blocker LOE 908M5 on experimental focal ischemia. JMRI 1999; 10:138–145.
22. Takano K, Carano RAD, Tatlisumak T, et al. The efficacy of intraarterial and intravenous Prourokinase in an embolic stroke model evaluated by diffusion-perfusion magnetic resonance imaging. Neurology 1998; 50:870–875.
23. Shen Q, Meng X, Fisher M, Sotak CH, Duong TQ. Pixel-by-pixel spatiotemporal progression of focal ischemia derived using quantitative perfusion and diffusion imaging. J Cereb Blood Flow Metab 2003; 23:1479–1488.
24. Oliff HS, Coyle P, Weber E. Rat strain and vendor differences in collateral anastomoses. J Cereb Blood Flow Metab 1997; 17:571–578.
25. Bardutzky J, Shen Q, Ren H, et al. Differences in ischemic lesion evolution in different rat strains using diffusion and perfusion imaging. Stroke 2005; 36:2000–2005.
26. Welch KM, Windham J, Knight RA, et al. A model to predict the histopathology of human stroke using diffusion and T2-weighted magnetic resonance imaging. Stroke 1995; 26:1983–1989.
27. Jacobs MA, Mitsias P, Soltaniaan-Zadeh H, et al. Multiparametric MRI tissue characterization in clinical stroke with correlation to clinical outcome: part 2. Stroke 2001; 32:950–957.
28. Mitsias PD, Jacobs MA, Hammound R, et al. Multiparametric MRI ISODATA ischemic lesion analysis correlation with the clinical neurological deficit and single-parameter MRI techniques. Stroke 2002; 33:2839–2844.
29. Carano RA, Li F, Irie K, et al. Multispectral analysis of the temporal evolution of cerebral ischemia in the rat brain. J Magn Reson Imag 2000; 12:842–858.

30. Wu O, Koroshetz WJ, Ostergard L, et al. Predicting tissue outcome in acute human cerebral ischemia using combined diffusion-and perfusion-weighted MR imaging. Stroke 2001; 32:933–942.
31. Jacobs MA, Zhang ZG, Knight RA, et al. A model for multiparametric mri tissue characterization in experimental cerebral ischemia with histological validation in rat: part 1. Stroke 2001; 32:943–949.
32. Shen Q, Ren H, Bouley J, Fisher M, Duong TQ. Dynamic tracking of acute ischemic tissue fates using improved unsupervised ISODATA analysis of high-resolution quantitative perfusion and diffusion data. J Cereb Blood Flow Metab 2004; 24:887–897.
33. Bardutzky J, Meng X, Bouley J, Duong TQ, Ratan R, Fisher M. Effects of IV dimethyl sulfoxide on ischemia evolution in permanently occluded rats. J Cereb Blood Flow Metab 2005; 25:968–977.
34. Singhal AB, Dijkhuizen RM, Rosen BR, Lo EH. Normobaric hyperoxia reduces MRI diffusion abnormalities and infarct size in experimental stroke. Neurology 2002; 58:945–952.
35. Kim HY, Singhal AB, Lo EH. Normobaric hyperoxia extends the reperfusion window in focal cerebral ischemia. Ann Neurol 2005; 57:571–575.

14 Penumbra Imaged with Magnetic Resonance Imaging in Humans

Chelsea S. Kidwell
Department of Neurology, Georgetown University and Washington Hospital Center, Washington, D.C., U.S.A.

Steven Warach
Section of Stroke Diagnostics and Therapeutics, National Institutes of Neurological Disorders and Stroke, National Institutes of Health, Bethesda, Maryland, U.S.A.

HISTORICAL OVERVIEW AND BACKGROUND

The advent of novel magnetic resonance imaging techniques in the 1990s opened the door for magnetic resonance imaging (MRI) of the ischemic penumbra in the acute stroke clinical setting. The first diffusion-weighted MRI study in a human was reported in 1992 (1). In the mid-1990s as studies of perfusion-weighted imaging findings appeared in the literature (2), a new concept for defining the penumbra with MRI using the diffusion–perfusion mismatch model emerged (3). Reports of the natural history of diffusion and perfusion lesions were followed by studies describing the effect of therapies on these imaging findings. In the early 2000s, it became apparent that the mismatch model faced a number of challenges in defining the penumbra, and a new era of research attempting to better define the penumbra was born. While there are a number of approaches to define the ischemic penumbra, for the purposes of this chapter, we will use the following definition, which is most practical and relevant to MRI of the penumbra—tissue that is at risk of infarction, but still salvageable (Fig. 1). This chapter will review the general principles of MRI of the penumbra, the results of natural history, and treatment studies and their impact on the MRI defined penumbra. The current role and future directions of MRI of the penumbra will then be discussed.

MAGNETIC RESONANCE IMAGING AND THE ISCHEMIC PENUMBRA—GENERAL PRINCIPLES

Until the 1990s, MRI was not routinely employed for the evaluation of acute stroke patients. This was due mainly to the fact that within the first 6 to 12 hours from symptom onset, conventional structural MRI techniques such as T1-weighted imaging (T1WI), T2-weighted imaging (T2WI), and fluid-attenuated inversion recovery (FLAIR) imaging sequences are relatively insensitive to ischemic changes. However, the recent advent of diffusion and perfusion-weighted MRI within the clinical setting revolutionized the role of MRI for the evaluation of acute ischemic stroke. These techniques became feasible for routine clinical use with the development of echo-planar imaging techniques, which allow for short acquisition times, thus minimizing the effects of motion due either to head movement or physiological pulsations of the brain.

Diffusion-weighted imaging (DWI) detects the self-diffusion of water, allowing visualization of regions of ischemia within minutes of symptom onset (4,5). Decreased water diffusion associated with cytotoxic edema causes an increased (bright) signal on DWI sequences, which can be quantitatively measured on the apparent diffusion coefficient (ADC) maps, where darker areas represent decreased diffusion. The increase in signal on DWI may persist for several weeks or longer, partially due to a T2 effect. The average ADC, however, typically remains reduced for only four to seven days, then returns to normal or supranormal levels within 7 to 10 days from ischemia onset (6). While the average ADC generally follows this pattern, studies

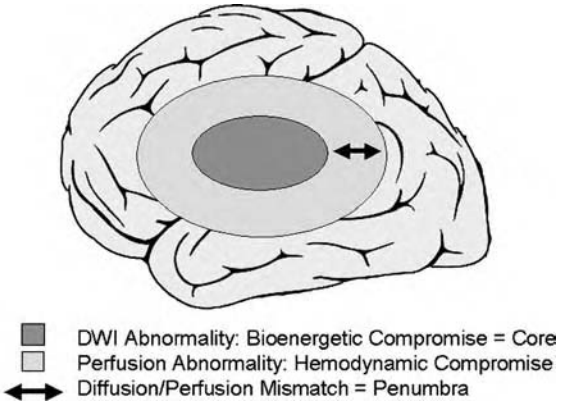

FIGURE 1 Diffusion–perfusion mismatch model of the ischemic penumbra. According to this model, the perfusion deficit appears in light gray, the diffusion in dark gray with the penumbra equaling the mismatch between the two. *Abbreviation*: DWI, diffusion weighted imaging. *Source*: Courtesy of UCLA.

have now clearly demonstrated that marked heterogeneity of the ADC value can occur within the ischemic lesion, even in the hyperacute time window (7).

Perfusion-weighted imaging is most commonly performed using dynamic contrast-enhanced imaging (8). Following a bolus injection of intravenous gadolinium, a series of susceptibility-weighted gradient echo images is rapidly acquired. The intravascular passage of gadolinium in sufficiently high concentration distorts the local magnetic field due to magnetic susceptibility effects, causing signal loss. During ischemia with hemodynamic compromise, decreased and/or delayed passage of the contrast agent compared to normal regions is then detected.

The amount of signal loss over time in a series of rapidly acquired images (area under the signal intensity–time curve) has been shown to be proportional to cerebral blood volume (CBV), in healthy brain tissue. The time it takes for the change in signal intensity to reach a maximum (time to peak—TTP) is related to the mean transit time (MTT) of an idealized bolus of contrast. Since cerebral blood flow (CBF) equals the ratio CBV/MTT, information about CBF can potentially be inferred with this technique. In acute stroke patients, qualitative perfusion

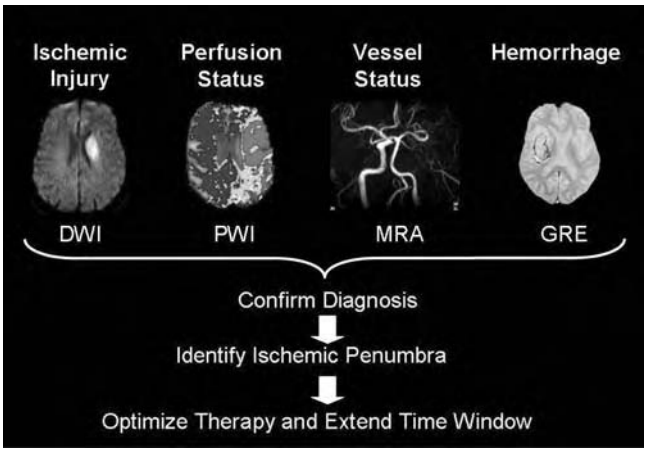

FIGURE 2 (*See color insert*.) Multimodal magnetic resonance imaging approach. Ischemic tissue injury is assessed with diffusion weighted imaging, hemodynamic compromise with perfusion-weighted magnetic resonance imaging, vessel status with MRA, and hemorrhage with GRE sequences. This information can be combined to confirm the diagnosis and stroke mechanism, as well as to identify patients who have an ischemic penumbra and a target vessel occlusion and therefore may benefit from therapy. In this way, acute therapies may be optimized and the time window for treatment extended. *Abbreviations*: DWI, diffusion weighted imaging; MRA, magnetic resonance imaging pathology; PWI, perfusion-weighted magnetic resonance imaging. *Source*: Courtesy of UCLA.

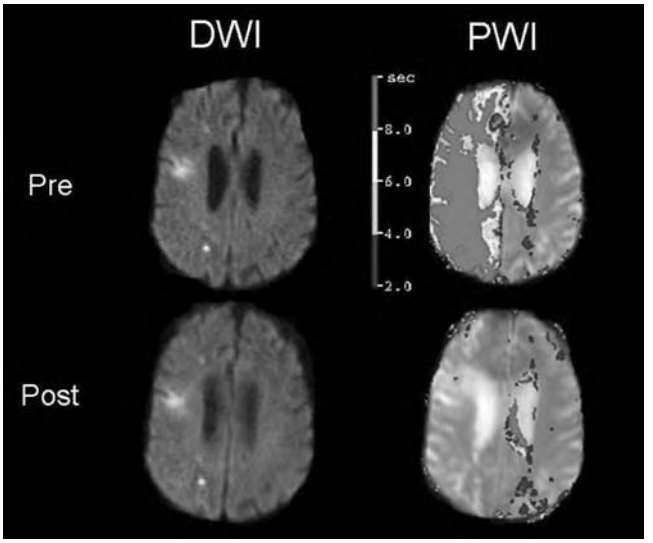

FIGURE 3 (*See color insert*.) Example of diffusion-perfusion mismatch with therapeutic salvage of mismatch region following intra-arterial thrombolysis. The top row shows the baseline diffusion weighted imaging (*left panel*) and perfusion-weighted magnetic resonance imaging images from a color-coded Tmax image (*right panel*, time to peak of the residue function with red indicating greater than eight seconds, yellow greater than six seconds, green greater than four seconds, and blue greater than two seconds). These images show small diffusion lesions in the right middle cerebral artery territory with a much larger perfusion deficit in the right internal carotid artery territory. Following vessel recanalization, there is no substantial change in the diffusion lesions, however the perfusion deficit is largely resolved. *Abbreviations*: DWI, diffusion weighted imaging; PWI, perfusion-weighted magnetic resonance imaging. *Source*: Courtesy of UCLA.

maps of the relative MTT (rMTT), relative CBF, and relative CBV have been generated and have permitted visualization of perfusion changes in patients with cerebrovascular disease. Absolute quantification of CBF parameters with bolus tracking MRI perfusion may be possible, but is not currently routinely applied in clinical practice, and questions persist about the accuracy of the quantification algorithms (9–11). Many different approaches to absolute and relative estimates of these parameters are in the literature, with none clearly superior in accuracy or predictive validity. Modeling of CBF with MRI is more straightforward using arterial spin labeling techniques (12–14), but at present the longer acquisition times and sensitivity to motion artifacts limit the clinical utility of this approach in acute stroke.

MRI is typically applied as a multimodal exam (Fig. 2) to evaluate the stroke patient for arterial pathology magnetic resonance angiography (MRA), hemodynamic changes [perfusion-weighted magnetic resonance imaging (PWI)], hyperacute parenchymal injury (DWI), subacute and chronic infarct (FLAIR), and evidence of acute or chronic hemorrhage gradient echo (GRE). Numerous studies have demonstrated the sensitivity of these techniques in confirming the diagnosis of cerebrovascular disease (15–18) However, the potential of MRI to identify individual patient pathophsyiology, including the presence of ischemic penumbra, in the acute stroke setting has sparked enormous interest in this technique. Perhaps the most promising application of current MRI methodology is as a patient selection tool for acute therapies and as a biomarker of therapeutic response in clinical trials.

NATURAL HISTORY OF DIFFUSION AND PERFUSION LESIONS

Information on the natural history of diffusion and perfusion imaging lesion evolution comes from a growing number of clinical trials and case series. Warach et al. (19) analyzed serial imaging studies from patients enrolled in the placebo arm of a neuroprotective trial and demonstrated that the natural history of untreated diffusion lesions is to grow over time during the acute and subacute period. Ischemic lesions follow a relatively consistent pattern of growth during the first three days, followed by subsequent decrease in size to day five to seven (3,20,21). The extent of growth depends on a number of factors including time from symptom onset,

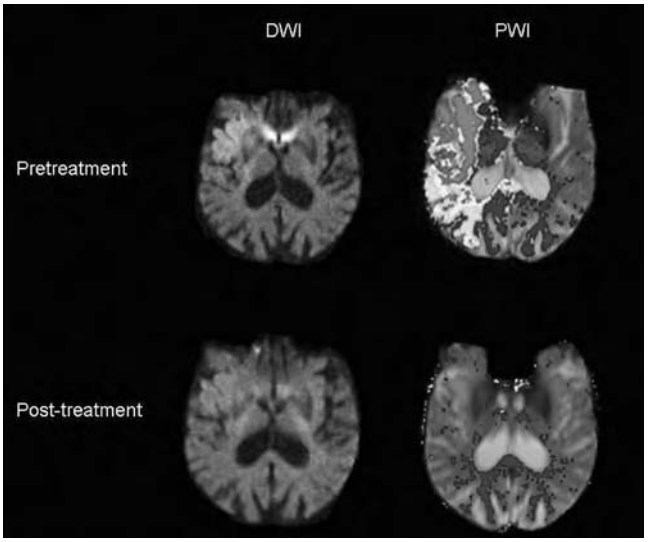

FIGURE 4 (*See color insert*.) Example of reversal of diffusion lesion. The top row shows the baseline diffusion weighted imaging (DWI) (*left panel*) and perfusion-weighted magnetic resonance imaging (PWI) images from a color-coded Tmax image (*right panel*, time to peak of the residue function with red indicating greater than eight seconds, yellow greater than six seconds, green greater than four seconds and blue greater than two seconds). These images show a diffusion lesion in the right middle cerebral artery territory with a larger perfusion deficit. Following vessel recanalization, both the DWI and PWI lesions have resolved. *Source*: Courtesy of UCLA

vascular territory involved, collateral blood supply, and as discussed later, the extent of the perfusion deficit.

These and other studies have shown that both the initial diffusion and perfusion lesion volumes correlate well both with final infarct volume as well as neurological and functional outcomes in stroke patients, suggesting that diffusion MR can provide important early prognostic information (22–24). While these correlations have been repeatedly demonstrated in anterior circulation ischemia, several small case series have suggested that acute DWI lesion volumes correlate poorly with clinical measures in the posterior circulation, since small strategic brainstem infarcts can lead to devastating clinical syndromes, while large cerebellar infarcts may cause minimal symptomatology (25,26).

DEFINING THE PENUMBRA WITH MAGNETIC RESONANCE IMAGING

The diffusion–perfusion mismatch model (Fig. 1) developed from these natural history observations that diffusion lesions tend to grow over time into the region of perfusion deficit, if reperfusion is not established at an early time point. In approximately 70% of patients studied within 24 hours of symptom onset, there is a "perfusion–diffusion mismatch," in which the area

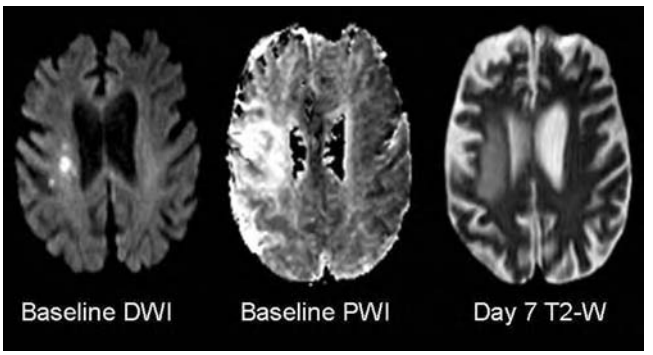

FIGURE 5 Example of natural history of diffusion lesion evolution and benign oligemia. The baseline diffusion weighted imaging (DWI) image (*left panel*) shows a moderate sized lesion in the right middle cerebral artery territory. The baseline perfusion-weighted magnetic resonance imaging (PWI) image (*middle panel*) shows a much larger perfusion deficit. The day seven T2-weighted image (*right panel*) shows a infarct intermediate in size between the baseline DWI and PWI lesions suggested that a portion of the initial PWI deficit was due to benign oligemia. *Source*: Figure belongs to NIH and cannot be copyrighted.

of DWI abnormality is surrounded by a larger area of hypoperfusion, most commonly measured by the rMTT perfusion map (27). It has been suggested that the ischemic penumbra is the region of tissue that is hypoperfused but has a normal DWI signal (i.e., blood flow is reduced, but tissue bioenergetic failure as evidenced by cytotoxic edema has not yet developed). Thus, according to this model, the diffusion lesion represents core irreversibly infarcted tissue. In other patients, the DWI lesion is larger than the perfusion lesion in approximately 10% (presumed partial or total reperfusion) and in 10% to 15% the DWI and perfusion lesions are of equivalent size (probably little viable tissue, operationally defined as a completed infarct). Serial MRI studies, performed in patients with mismatch, have confirmed that infarct growth occurs primarily in patients with large regions of mismatch, suggesting gradual failure of the ischemic penumbra within the region of mismatch as it is incorporated into the infarct core.

A second important concept arose from these early studies of diffusion and perfusion abnormalities in acute stroke. Darby et al. (27) demonstrated that while the presence and volume of mismatch progressively decreases over time, approximately 60% to 70% of patients up to 24 hours still have substantial regions of mismatch. This finding is supported by studies previously performed in stroke patients employing positron emission tomography (28,29) and suggests that the time window available for salvage of the penumbra in selected patients identified by MRI may be longer than the traditional three to six hour window.

Several groups have reported that an altered evolution of infarction can be visualized on serial diffusion and perfusion imaging studies in patients undergoing intravenous thrombolytic therapy. Inhibition of lesion growth has been clearly demonstrated in patients experiencing reperfusion compared with patients with persistent perfusion deficits or vessel occlusions (30). Schellinger et al. (31) studied patients with mismatch and evidence of a vessel occlusion at baseline and found that patients with subsequent early recanalization had substantially smaller final infarct lesions than those without recanalization and better clinical outcome (31). Other groups have found regions of higher ADC within the initial ischemic field on follow-up imaging in patients undergoing reperfusion within 36 hours of onset compared to nonreperfusers, suggesting tissue salvage (32,33). Further compelling data come from Parsons et al. (34), who compared MRI signatures in patients treated with IV tissue plasminogen activator (tPA) within six hours of onset to a group of matched controls. They found a significant decrease in the amount of mismatch tissue proceeding to infarction as well as less infarct expansion in the thrombolysis treated group. These studies demonstrating therapeutic salvage of the mismatch region provide compelling support for this model of the MRI defined penumbra (Fig. 3).

While the mismatch model was particularly appealing as a means to identify the penumbra in the acute stroke clinical setting, growing experience with this technique revealed several limitations to this definition of the penumbra. Prior animal studies and recent case series in humans undergoing thrombolytic therapy have now shown that diffusion abnormalities can be partially or even completely reversed with early reperfusion (35–38) (Fig. 4). Thus, the diffusion lesion does not always represent the ischemic core of irreversibly injured tissue, as suggested by the mismatch model. In addition, studies have now also demonstrated that not all of the mismatch region is true penumbra—a portion of the perfusion deficit includes a region of benign oligemia where blood flow is reduced below the normal range but not to the critical level of ischemia (39–41) (Fig. 5).

To address these shortcomings, efforts have been underway to identify perfusion and ADC thresholds to predict tissue that will proceed to infarction versus salvageable, penumbral tissue. Several groups have found that relative ADC values could differentiate regions that would proceed to infarction compared to those that would not, within the initial hypoperfused region (42–44). These findings are in accord with those of Schlaug et al. (45) who found ADC values of 56.4% of normal in the core, and values of 91.3% in the penumbra. However, these findings apply generally to untreated patients or patients in whom early recanalization does not occur. In patients with early vessel recanalization, ADC decreases may not reliably indicate tissue infarction independent of the duration and severity of ischemia. ADC thresholds for infarct progression, malignant middle cerebral artery infarct, and risk of hemorrhagic transformation may be identified by quantitative diffusion MRI, but these thresholds are not absolute, and instead, are dependent on the technique of measurement and analysis, the time from onset, the therapeutic intervention, and interactions with other physiological and clinical variables.

A number of researchers have developed multivariate models incorporating data from a number of sequences in an attempt to predict tissue fate over time. Several natural history studies provide predictive models of tissue outcome assuming that early recanalization does not occur. Schlaug et al. (45) used a logistic regression model to differentiate regions of ultimate infarction versus Noninfarction, based on the baseline perfusion measures to operationally define the ischemic penumbra. Other groups have employed generalized linear model algorithms, multiparametric iterative self-organizing data analysis technique (ISODATA) and other automated strategies to predict final tissue status (46–48). Multivariate models predicting tissue fate assuming recanalization are also under development. All of these approaches have demonstrated relatively good overall accuracy but have not reached widespread adoption in the acute clinical setting.

OPERATIONAL DEFINITION AND ITS VALIDITY

Based on the data available to date, an operational definition of the MRI defined ischemic penumbra has begun to emerge (49). According to this definition, the penumbra includes not only diffusion–perfusion mismatch but also portions of the initial diffusion abnormality itself (Fig. 6). In addition, it is recognized that portions of the perfusion deficit may represent benign oligemia and, thus, the outer rim of the perfusion deficit may overestimate the true extent of the penumbra. An important implication of this modified view is that even select patients without diffusion–perfusion mismatch may still derive benefit from reperfusion therapies. It remains to be seen whether the simple mismatch model, the modified mismatch model, or more sophisticated multivariate predictive models will ultimately best meet the clinical and/or research needs in the acute stroke setting. In the meantime, the simple mismatch model remains a simple and practical approach for identifying patients with penumbra, and provides a rough estimation of the extent of the penumbra.

MAGNETIC RESONANCE IMAGING: THE PENUMBRA AND ACUTE STROKE CLINICAL TRIALS

The most exciting potential application of MRI in acute stroke is its use as a selection tool for acute stroke therapies. The National Institute of Neurological Disorders and Stroke (NINDS) intravenous tPA trials demonstrated that vessel recanalization improves stroke outcome, yet few patients receive IV tPA, mainly due to the narrow three hour time window available for initiation of this therapy (50). There is clearly a need to extend the time window for treatment. However, beyond three hours from symptom onset, clinical exam alone cannot identify patients with salvageable penumbral tissue. It is in this setting that MRI offers the potential to identify patients who may benefit most from late recanalization therapies. However, it is important to

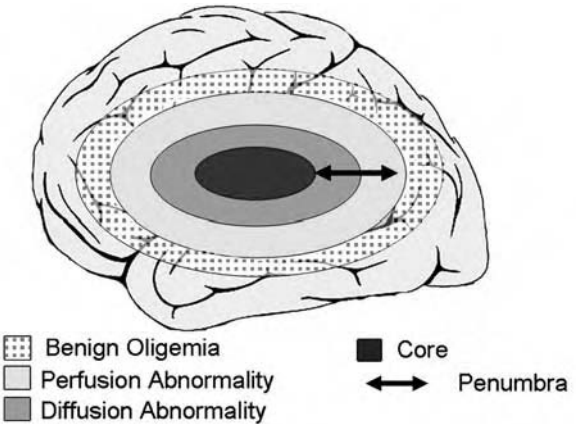

FIGURE 6 Operational definition of MRI defined ischemic penumbra where the penumbra equals not only regions of diffusion–perfusion mismatch but also a portion of the diffusion abnormality itself. Of note, the outer rim of the perfusion deficit may indicate benign oligemia and therefore is not included in the penumbra.

recognize that the number of patients who will benefit from treatment (those with an existing penumbra) progressively decreases over time.

Multimodal MRI may permit therapeutic decisions to be based on individual patient pathophysiological information, allowing the time window to be extended in appropriate patients. Results from the phase II desmoteplase in acute ischemic stroke trial support this approach (51) These studies demonstrated a positive dose response relationship for good clinical outcome and reperfusion, employing MRI selection of patients with diffusion–perfusion mismatch for treatment with intravenous desmoteplase three to nine hours from onset. Other clinical trials to definitively prove the clinical utility of this approach are currently ongoing. These include, trials designed to confirm the clinical utility of the MRI mismatch hypothesis, trials designed to demonstrate the utility of selecting for acute therapies patients with a penumbral pattern, and trials actually selecting only patients with penumbral patterns for late therapies to optimize both the efficacy and safety of these treatments.

FUTURE GOALS

There are a number of important future directions for MRI of the penumbra. Further work is needed to validate quantitative perfusion imaging and demonstrate its ability to differentiate penumbra from benign oligemia. Of particular importance is the need for employment of standardized methodologies for postprocessing and analysis to allow comparison of data across studies and institutions. Further, refinement of the MRI defined model for the ischemic penumbra is needed. Rapidly advancing technology will allow validation and incorporation of new MR techniques, including MR spectroscopy, flow heterogeneity measures, and MRI oxygen extraction fraction techniques into acute stroke protocols. These techniques have the potential to further augment existing multivariate models in delineating infarct core, penumbra, and benign oligemia. Ironically, rapid advances in MRI technology have the potential to impede progress as these advances make previous work performed on less advanced systems obsolete.

CONCLUSIONS

Enormous advances in imaging of acute stroke have emerged with the advent of diffusion–perfusion MRI in the acute stroke setting. The diffusion–perfusion mismatch model provides a simple estimation of the extent of the ischemic penumbra. More refined models of the MRI defined penumbra are in development. Therapeutic salvage of the MRI penumbra has now been demonstrated in humans and ongoing clinical trials are exploring the utility of employing MRI to select patients for late reperfusion therapies. A multimodal MRI approach to acute stroke evaluation provides critical information on individual patient pathophysiology and may assist in individualizing and optimizing therapeutic decisions.

REFERENCES

1. Warach S, Chien D, Li W, Ronthal M, Edelman RR. Fast magnetic resonance diffusion-weighted imaging of acute human stroke [published erratum appears in Neurology 1992; 42(11):2192]. Neurology 1992; 42(9):1717–1723.
2. Sorensen AG, Buonanno FS, Gonzalez RG, et al. Hyperacute stroke: evaluation with combined multisection diffusion-weighted and hemodynamically weighted echo-planar MR imaging. Radiology 1996; 199(2):391–401.
3. Baird AE, Benfield A, Schlaug G, et al. Enlargement of human cerebral ischemic lesion volumes measured by diffusion-weighted magnetic resonance imaging. Ann Neurol 1997; 41(5):581–589.
4. Le Bihan D. Molecular diffusion nuclear magnetic resonance imaging. Magn Reson Q 1991; 7(1):1–30.
5. Moseley ME, Kucharczyk J, Mintorovitch J, et al. Diffusion-weighted MR imaging of acute stroke: correlation with T2-weighted and magnetic susceptibility-enhanced MR imaging in cats. Am J Neuroradiol 1990; 11(3):423–429.
6. Schlaug G, Siewert B, Benfield A, Edelman RR, Warach S. Time course of the apparent diffusion coefficient (ADC) abnormality in human stroke. Neurology 1997; 49(1):113–119.
7. Nagesh V, Welch KM, Windham JP, et al. Time course of ADCw changes in ischemic stroke: beyond the human eye! Stroke 1998; 29(9):1778–1782.

8. Rosen BR, Belliveau JW, Buchbinder BR, et al. Contrast agents and cerebral hemodynamics. Magn Reson Med 1991; 19(2):285–292.
9. Ostergaard L, Weisskoff RM, Chesler DA, Gyldensted C, Rosen BR. High resolution measurement of cerebral blood flow using intravascular tracer bolus passages. Part I: mathematical approach and statistical analysis. Magn Res Med 1996; 36(5):715–725.
10. Rempp KA, Brix G, Wenz F, Becker CR, Guckel F, Lorenz WJ. Quantification of regional cerebral blood flow and volume with dynamic susceptibility contrast-enhanced MR imaging. Radiology 1994; 193(3):637–641.
11. Smith AM, Grandin CB, Duprez T, Mataigne F, Cosnard G. Whole brain quantitative CBF, CBV, and MTT measurements using MRI bolus tracking: implementation and application to data acquired from hyperacute stroke patients [In Process Citation]. J Magn Reson Imaging 2000; 12(3):400–410.
12. Buxton RB, Frank LR, Wong EC, Siewert B, Warach S, Edelman RR. A general kinetic model for quantitative perfusion imaging with arterial spin labeling. Magn Reson Med 1998; 40(3):383–396.
13. Siewert B, Schlaug G, Edelman RR, Warach S. Comparison of EPISTAR and T2*-weighted gadolinium-enhanced perfusion imaging in patients with acute cerebral ischemia. Neurology 1997; 48(3):673–679.
14. Detre JA, Leigh JS, Williams DS, Koretsky AP. Perfusion imaging. Magn Reson Med 1992; 23(1):37–45.
15. Lövblad KO, Laubach HJ, Baird AE, et al. Clinical experience with diffusion-weighted MR in patients with acute stroke. AJNR Am J Neuroradiol 1998; 19(6):1061–1066.
16. Ay H, Buonanno FS, Rordorf G, et al. Normal diffusion-weighted MRI during stroke-like deficits. Neurology 1999; 52(9):1784–1792.
17. Kidwell CS, Chalela JA, Saver JL, et al. Comparison of MRI and CT for detection of acute intracerebral hemorrhage. JAMA 2004; 292(15):1823–1830.
18. Barber PA, Darby DG, Desmond PM, et al. Identification of major ischemic change. Diffusion-weighted imaging versus computed tomography. Stroke 1999; 30(10):2059–2065.
19. Warach S, Pettigrew LC, Dashe JF, et al. Effect of citicoline on ischemic lesions as measured by diffusion-weighted magnetic resonance imaging. Citicoline 010 Investigators. Ann Neurol 2000; 48(5):713–722.
20. Lansberg MG, O'Brien MW, Tong DC, Moseley ME, Albers GW. Evolution of cerebral infarct volume assessed by diffusion-weighted magnetic resonance imaging. Arch Neurol 2001; 58(4):613–617.
21. Beaulieu C, de Crespigny A, Tong DC, Moseley ME, Albers GW, Marks MP. Longitudinal magnetic resonance imaging study of perfusion and diffusion in stroke: Evolution of lesion volume and correlation with clinical outcome. Ann Neurol 1999; 46:568–578.
22. Warach S, Dashe JF, Edelman RR. Clinical outcome in ischemic stroke predicted by early diffusion-weighted and perfusion magnetic resonance imaging: a preliminary analysis. J Cereb Blood Flow Metab 1996; 16(1):53–59.
23. Lovblad KO, Baird AE, Schlaug G, et al. Ischemic lesion volumes in acute stroke by diffusion-weighted magnetic resonance imaging correlate with clinical outcome. Ann Neurol 1997; 42(2):164–170.
24. Barber PA, Darby DG, Desmond PM, et al. Prediction of stroke outcome with echoplanar perfusion- and diffusion-weighted MRI. Neurology 1998; 51(2):418–426.
25. Ostrem JL, Kidwell CS, Saver JL, et al. Basilar artery occlusion: diffusion-perfusion MRI characterization of tissue salvage in patients receiving intra-arterial thrombolysis. Stroke 2002; 33:360.
26. Linfante I, Llinas RH, Schlaug G, Chaves C, Warach S, Caplan LR. Diffusion-weighted imaging and National Institutes of Health Stroke Scale in the acute phase of posterior-circulation stroke. Arch Neurol 2001; 58(4):621–628.
27. Darby DG, Barber PA, Gerraty RP, et al. Pathophysiological topography of acute ischemia by combined diffusion- weighted and perfusion MRI. Stroke 1999; 30(10):2043–2052.
28. Marchal G, Beaudouin V, Rioux P, et al. Prolonged persistence of substantial volumes of potentially viable brain tissue after stroke: a correlative PET-CT study with voxel-based data analysis [see comments]. Stroke 1996; 27(4):599–606.
29. Heiss WD, Huber M, Fink GR, et al. Progressive derangement of periinfarct viable tissue in ischemic stroke. J Cereb Blood Flow Metab 1992; 12:193–203.
30. Jansen O, Schellinger P, Fiebach J, Hacke W, Sartor K. Early recanalisation in acute ischaemic stroke saves tissue at risk defined by MRI [letter]. Lancet 1999; 353(9169):2036–2037.
31. Schellinger PD, Fiebach JB, Jansen O, et al. Stroke magnetic resonance imaging within 6 hours after onset of hyperacute cerebral ischemia. Ann Neurol 2001; 49(4):460–469.
32. Marks MP, Tong DC, Beaulieu C, Albers GW, de Crespigny A, Moseley ME. Evaluation of early reperfusion and i.v. tPA therapy using diffusion- and perfusion-weighted MRI [see comments]. Neurology 1999; 52(9):1792–1798.
33. Taleb M, Lovblad KO, El-Koussy M, et al. Reperfusion demonstrated by apparent diffusion coefficient mapping after local intra-arterial thrombolysis for ischaemic stroke. Neuroradiology 2001; 43(7):591–594.
34. Parsons MW, Barber PA, Chalk J, et al. Diffusion- and perfusion-weighted MRI response to thrombolysis in stroke. Ann Neurol 2002; 51(1):28–37.

35. Dijkhuizen RM, Berkelbach van der Sprenkel JW, Tulleken KA, Nicolay K. Regional assessment of tissue oxygenation and the temporal evolution of hemodynamic parameters and water diffusion during acute focal ischemia in rat brain. Brain Res 1997; 750(1–2):161–170.
36. Kidwell CS, Saver JL, Mattiello J, et al. Thrombolytic reversal of acute human cerebral ischemic injury shown by diffusion/perfusion magnetic resonance imaging. Ann Neurol 2000; 47(4):462–469.
37. Hasegawa Y, Fisher M, Latour LL, Dardzinski BJ, Sotak CH. MRI diffusion mapping of reversible and irreversible ischemic injury in focal brain ischemia. Neurology 1994; 44(8):1484–1490.
38. Chalela JA, Kang DW, Luby M, et al. Early magnetic resonance imaging findings in patients receiving tissue plasminogen activator predict outcome: Insights into the pathophysiology of acute stroke in the thrombolysis era. Ann Neurol 2004; 55(1):105–112.
39. Rose SE, Janke AL, Griffin M, Finnigan S, Chalk JB. Improved prediction of final infarct volume using bolus delay-corrected perfusion-weighted MRI: implications for the ischemic penumbra. Stroke 2004; 35(11):2466–2471.
40. Sobesky J, Zaro Weber O, Lehnhardt FG, et al. Does the mismatch match the penumbra? Magnetic resonance imaging and positron emission tomography in early ischemic stroke. Stroke 2005; 36(5):980–985.
41. Sitburana O, Koroshetz WJ. Magnetic resonance imaging: implication in acute ischemic stroke management. Curr Atheroscler Rep 2005; 7(4):305–312.
42. Grandin CB, Duprez TP, Smith AM, et al. Which MR-derived perfusion parameters are the best predictors of infarct growth in hyperacute stroke? Comparative study between relative and quantitative measurements. Radiology 2002; 223(2):361–370.
43. Neumann-Haefelin T, Wittsack HJ, Wenserski F, et al. Diffusion- and perfusion-weighted MRI. The DWI/PWI mismatch region in acute stroke. Stroke 1999; 30(8):1591–1597.
44. Thijs VN, Adami A, Neumann-Haefelin T, Moseley ME, Marks MP, Albers GW. Relationship between severity of MR perfusion deficit and DWI lesion evolution. Neurology 2001; 57(7):1205–1211.
45. Schlaug G, Benfield A, Baird AE, et al. The ischemic penumbra: operationally defined by diffusion and perfusion MRI. Neurology 1999; 53(7):1528–1537.
46. Rose SE, Chalk JB, Griffin MP, et al. MRI based diffusion and perfusion predictive model to estimate stroke evolution. Magn Reson Imaging 2001; 19(8):1043–1053.
47. Wu O, Koroshetz WJ, Ostergaard L, et al. Predicting tissue outcome in acute human cerebral ischemia using combined diffusion- and perfusion-weighted MR imaging. Stroke 2001; 32(4):933–942.
48. Jacobs MA, Mitsias P, Soltanian-Zadeh H, et al. Multiparametric MRI tissue characterization in clinical stroke with correlation to clinical outcome: part 2. Stroke 2001; 32(4):950–957.
49. Kidwell CS, Alger JR, Saver JL. Beyond mismatch: evolving paradigms in imaging the ischemic penumbra with multimodal magnetic resonance imaging. Stroke 2003; 34(11):2729–2735.
50. NINDS rt-PA Stroke Group. Tissue plasminogen activator for acute ischemic stroke. N Engl J Med 1995; 333:1581–1587.
51. Hacke W, Albers G, Al-Rawi Y, et al. The Desmoteplase in Acute Ischemic Stroke Trial (DIAS): a phase II MRI-based 9-hour window acute stroke thrombolysis trial with intravenous desmoteplase. Stroke 2005; 36(1):66–73.

15 Perfusion Computed Tomography and Xenon-Computed Tomography: Current Status and Implications for Therapy

15a. Perfusion Computed Tomography

Patrik Michel
Neurology Service, Centre Hospitalier Universitaire Vaudois, Lausanne, Switzerland

Max Wintermark
Department of Radiology, Neuroradiology Section, University of California at San Francisco, San Francisco, California, U.S.A.

Julien Bogousslavsky
Clinique Valmont–Genolier, Montreux, Switzerland

THE NEED FOR RAPID AND RELIABLE PENUMBRA IMAGING

Stroke mechanisms, size, location, and relative proportion of penumbra and infarct are quite variable between patients. According to positron emission tomography (PET) and magnetic resonance imaging (MRI)-based studies, survival (1) of the penumbra is highly individual and may last from less than three hours to beyond 48 hours (2,3). By six hours, about 75% of patients still have a meaningful, but highly variable penumbra. These data suggest that there is a need for a reliable and rapid imaging technique for the assessment of individual penumbra in acute stroke patients. This imaging technique should identify patients who may benefit from late recanalization. It should also identify patients with no penumbra, for whom thrombolysis-induced recanalization may not be associated with benefit, but who have a significant risk of intracranial hemorrhage, even in the early phase.

Whether infarction occurs depends mainly on the local blood flow lowering below critical thresholds and on the duration of ischemia (4,5), but multiple other factors, such as temperature, hypoxemia, glucose concentration, blood pressure, or genetic factors, are suspected (6) or have been shown (7) to influence penumbral survival. In the absence of effective measures to restore perfusion or to protect it, most of the penumbra eventually evolve towards infarction (8).

It is now well established that early recanalization by thrombolysis (9,10) and avoidance of additional tissue by control of physiological and metabolic parameters (11) improve neurological outcome. Only a few (MRI-based) studies, however, have attempted to show that this improvement is due to salvage of the penumbra (12,13).

The time-dependence of all these acute stroke treatments has been known for a long time in laboratory animals and has also clearly been shown for thrombolysis in humans (14). Given the fact that penumbra decreases progressively with time (2,15), it is probably the loss of penumbra rather than the time itself that leads to a loss of effectiveness of acute stroke treatments. Considering the high interinvididual variability of penumbra, it therefore seems logical to replace the time clock by a penumbra clock, that is, to consider "penumbra is brain" (16). Appropriately designed studies might show in the future that the current time window for intravenous (IV) and intra-arterial thrombolysis is too long for patients with little penumbra and too short for patients with a persistent penumbra. Also, patients with unknown onset of stroke (aphasia, agnosia), waking up with a stroke, or having an epileptic seizure at stroke onset may become candidates for treatment, based on the demonstration of a significant penumbra on perfusion imaging.

Therefore, the identification of ischemic but salvageable tissue should be one of the main goals of cerebral imaging in acute stroke.

PERFUSION COMPUTED TOMOGRAPHY DATA ACQUISITION

Perfusion computed tomography (PCT) with iodinated contrast may be used in two ways: (*i*) as a slow-infusion/whole-brain technique and (*ii*) as dynamic PCT with first-pass bolus-tracking methodology. The latter is preferable as it is quantitative and allows accurate identification of the ischemic penumbra (17,18).

Patients with suspected acute stroke are being taken to the helical computed tomography (CT) scan within 10 to 20 minutes after being admitted to the emergency room. In patients without contraindications for iodinated contrast, a noncontrast baseline cerebral CT is immediately followed by PCT. Finally, a computed tomography angiography (CTA) of the head and neck and a contrast-enhanced CT of the brain are performed. The entire procedure takes approximately 10 minutes and image processing and analysis another 5 to 10 minutes. Image acquisition and processing usually overlap.

The PCT examination consists of two 40-second series separated by five minutes, each series consisting of one image per second in cine mode during iv administration of iodinated contrast material. The acquisition parameters for both series are 80 kVp and 100 mA. For each series, CT scanning is initiated seven seconds after injection of 50 mL of iso-osmolar iodinated contrast material at a rate of 5 mL/s into an antecubital vein using a power injector. The delay before the arrival of the contrast material allows baseline images without contrast enhancement to be acquired. Multidetector-array technology currently allows the acquisition of data from two adjacent 10 mm sections for each series. The two successive PCT series thus allow the acquisition of data for four adjacent 10 mm cerebral CT sections.

PERFUSION COMPUTED TOMOGRAPHY DATA PROCESSING AND ANALYSIS

Analysis of the acquired data is performed according to the central volume principle, which is reported to give the most accurate results for low injection rates of iodinated contrast material (19). The PCT data are transferred to a workstation and analyzed using a dedicated perfusion analysis software to create parametric maps of regional cerebral blood volume (rCBV), mean transit time (MTT), and regional cerebral blood flow (rCBF). The rCBV map is calculated from a quantitative estimation of the partial size averaging effect, which is completely absent in a reference pixel at the center of the large superior sagittal venous sinus. The impulse function and the related MTT maps result from a deconvolution of the parenchymal time–concentration curves by a reference arterial curve. Finally, the rCBF values can be calculated from the rCBV and MTT values for each pixel using the following equation rCBF = rCBV/MTT. The maps can then be displayed graphically (Fig. 1A–C) and interpreted by comparing the different parameters according to Table 1.

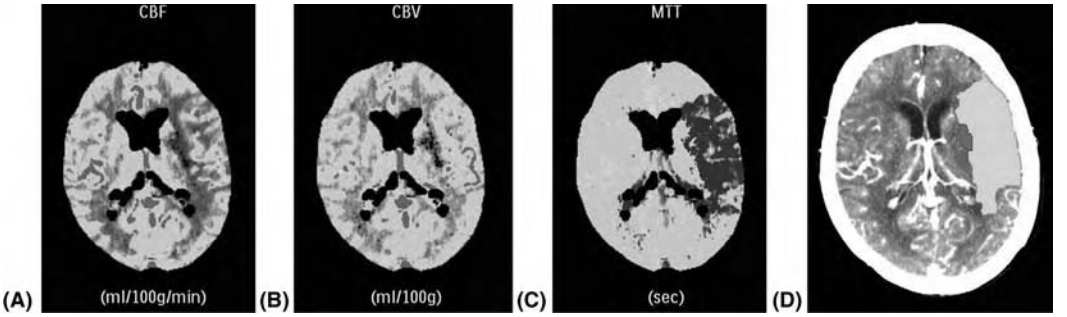

FIGURE 1 (*See color insert.*) A 77-year-old patient found on awakening with aphasia and right hemiparesis, National Institute of Health Stroke Scale = 20. Perfusion computed tomography maps depicting (**A**) regional cerebral blood flow, (**B**) regional cerebral blood volume, (**C**) mean transit time MTT, and (**D**) core-infarct maps according to a threshold model. In (**D**), grey indicates reversible ischemia (penumbra) and red low likelihood of survival (infarct). *Abbreviations*: CBF cerebral blood flow; CBV cerebral blood volume; MTT, mean transit time. *Source*: From Ref. 20.

TABLE 1 Alterations of Regional Mean Transit Time, Regional Cerebral Blood Volume, and Regional Cerebral Blood Flow in Case of Ischemia (Comparison with Contralateral Homologous Region)

	MTT	rCBF	rCBV
Healthy parenchyma	=	=	=
Transient ischemic attack	↑	=	↑
Penumbra	↑↑	↓	↑
Infarct	↑↑↑	↓↓	↓

Abbreviations: MTT, mean transit time; rCBF, regional cerebral blood flow; rCBV, regional cerebral blood volume.

Straightforward maps of the penumbra and infarct core are calculated according to the method developed by Wintermark et al. (20). According to their recently refined thresholds (21), the total ischemic area (penumbra and infarct) is defined as including cerebral pixels with greater than 145% prolongation of rMTT compared with the corresponding region in the contralateral cerebral hemisphere, defined as healthy on the basis of clinical symptomatology. Within this selected area, 2.0 mL/100 g represents the rCBV threshold: pixels belong to the infarct core if the RCBV value is inferior to the threshold and to the penumbra id if the rCBV value is superior to the threshold. Salvageable penumbra is displayed in green, and tissue with low likelihood of survival (infarct core) is displayed in red (Figs. 1D and 2C). Lesion surface on the final PCT maps is measured automatically on each of the four slices, and the volume of the penumbra and infarct (core) can then be calculated by multiplication with the slice thickness (10 mm).

INTERPRETATION OF PERFUSION COMPUTED TOMOGRAPHY IMAGES

The extent of regional abnormalities is usually largest with rMTT, followed by rCBF and rCBV (22). MTT is the most sensitive for decreased blood flow, but may also be prolonged without significant ischemia, such as in transient ischemic attacks. rCBF is more specific in identifying

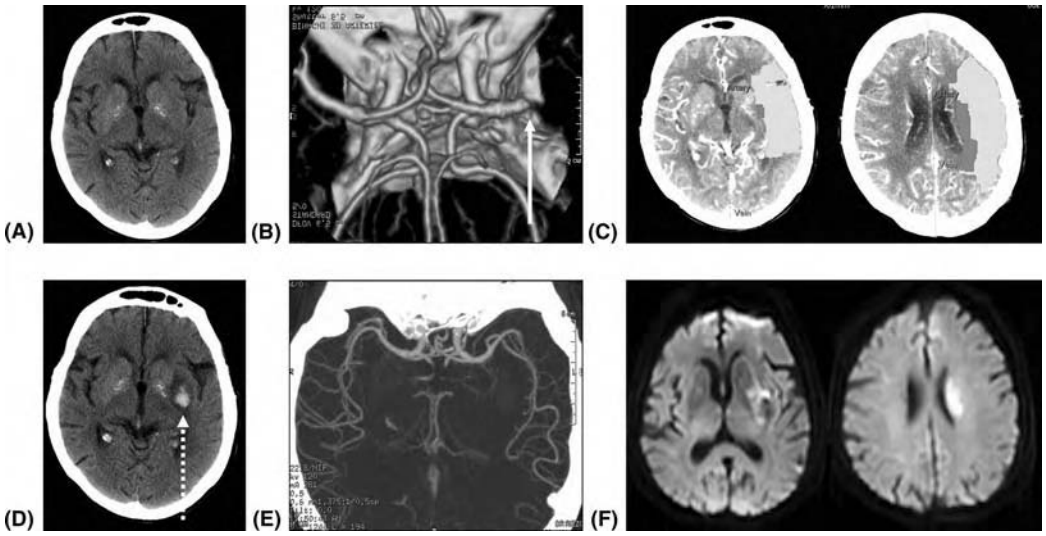

FIGURE 2 (*See color insert*.) Same patient as in Figure 1. (*Upper row*): Imaging at 12 hours after going to bed: (**A**) plain computed tomography (CT), (**B**) CT angiography with occlusion of the middle cerebral artery (white arrow), and (**C**) perfusion-CT with threshold maps. Then given intravenous thrombolysis with rt-PA at 13 hours after going to bed and 2.5 hours after waking (approved study protocol, informed consent from family). (*Lower row*): (**D**) plain CT at 24 hours with a small left basal ganglion bleed (*dotted arrow*). (**E**) CT angiography with repermeabilization and (**F**) diffusion-weighted magnetic resonance imaging at five days, showing a small, partially hemorrhagic lesion.

salvageable tissue, and rCBV is the most specific parameter for irreversibly damaged tissue (22–26). Thus, it may be best to evaluate the CBF and MTT maps for abnormalities and then to use the CBV maps to try to estimate the severity of the infarct core compared with the penumbra (17,27).

Using the threshold maps developed by Wintermark et al. (20,28), distinguishing reversible from irreversible ischemia becomes quite easy and has high interobserver agreement (29).

PERFORMANCE OF PERFUSION COMPUTED TOMOGRAPHY

In a recently presented analysis by Reichhart et al. (30) of 81 consecutive patients with middle cerebral artery (MCA)-stroke undergoing PCT and CTA before IV thrombolysis in the three-hour window, good quality images were obtained in 93% (movement artifacts in 5%, contrast injection failure in 2%) (30). Median acquisition time was 10 minutes, and in no patient, the three-hour threshold was trespassed because of the additional imaging represented by PCT and CTA. No case of renal failure or significant contrast allergy was seen.

Although noncontrast CT scanning has a poor sensitivity for detecting acute ischemia, PCT has an overall sensitivity above 75% for ischemic stroke, above 90% for territorial infarcts in the supratentorial regions, and a high specificity for ischemia (23,25,28,31–33). It should be noted that PCT abnormalities are present even in the earliest phase of stroke.

PCT shows brain perfusion alterations in about 25% patients with transient ischemic attacks, sometimes still being present after the resolution of patients' symptoms (34). Focal hypo- and hyperperfusion in relation to epileptic seizures and correlating with foci on EEG have been described (35). In patients with aura-accompanied migraines, occasional nonterritorial hyoperfusion contralateral to the aura symptoms are found (36). In the absence of an abnormality on PCT in a patient with stroke symptoms, one might suspect a posterior fossa stroke, a lacunar stroke, or a stroke-imitating condition (migraine, Todd's paralysis, venous thrombosis, encephalitis, conversion syndrome). Acute stroke treatments might be inappropriate. In contrast, focal hypoperfusion may rarely be present in a patient with a focal status epilepticus or migraine. Acute stroke treatment would also be inappropriate in such settings (Fig. 3).

Besides the study of acute ischemic stroke and acute aphasia (37), PCT has also been used to estimate cerebrovascular reserve, tolerance of temporary balloon occlusions (27), ischemia after subarachnoid haemorrhage (38,39), diffuse anoxic brain injury, head trauma (40), and brain tumors (27).

COMPUTED TOMOGRAPHY ANGIOGRAPHY DATA ACQUISITION AND PROCESSING

The cerebral and cervical CTA is performed using the following parameters: 120 kVp, 240 mA, slice thickness 2 to 2.5 mm, slice acquisition interval 1 to 2 mm, pitch 1.5:1, IV administration of 50 mL of iodinated contrast material at a rate of 3 mL/s, and an acquisition delay of 15 seconds.

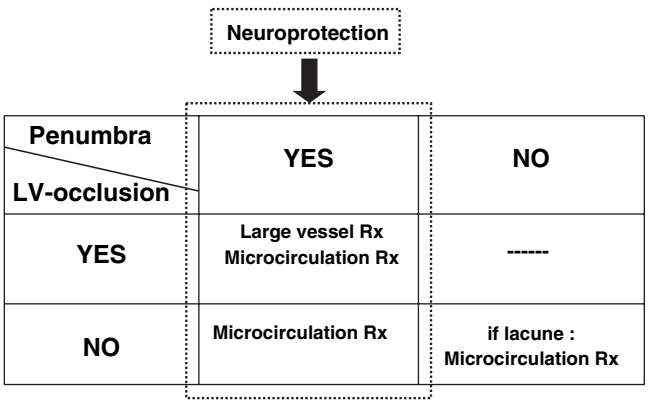

FIGURE 3 Acute ischemic stroke treatment strategies based on noninvasive assessment of penumbra and vessels. Independent of imaging results, all patients should be treated with general measures (control of O2, temperature, blood pressure, glucose, etc.). *Abbreviations*: LV, large vessel; Rx, treatment.

Data acquisition is performed from the origin of the aortic arch branch vessels to the circle of Willis. Maximum-intensity projections in axial, sagittal, and coronal planes (Fig. 2E) and three-dimensional reconstructions (Fig. 2B) are typically obtained.

PERFORMANCE OF COMPUTED TOMOGRAPHY ANGIOGRAPHY

The pathogenesis, location, degree, and recanalization of arterial occlusion in ischemic stroke is highly variable, even within one vascular territory (41–43). Multiple interventions and techniques have been (44–46) or are currently being studied (47) in order to obtain recanalization of the cerebral macro- and microcirculation.

CTA is a readily available and promising method that can be added to the admission CT survey of acute stroke patients, unless there are contraindications to iodinated contrast. CTA has been shown to identify the site of arterial occlusion in acute ischemic stroke patients, with similar accuracy compared with DSA and MRA (41,48). In this situation, CTA has been used alone (26) or in conjunction with perfusion imaging (22,23,25,49). Only a few pilot studies have considered its predictive value (20,50). These studies demonstrated CTA to be a moderate predictor for clinical outcome by itself but a very useful predictor when used together with PCT. Although it was suggested that patients with occlusion of the internal carotid artery bifurcation and poor leptomeningeal collaterals on CTA may have little potential for benefit from thrombolytic therapy (51), its value for predicting the response to treatment is insufficiently known (52).

COMPARISON OF MAGNETIC RESONANCE AND COMPUTED TOMOGRAPHY-BASED ACUTE STROKE IMAGING

For clinical use, CT and MR-based perfusion imaging are clearly superior to other imaging techniques of penumbra. Both are quite fast, feasible in the emergency setting, and can be performed using facilities that are readily available. Both methods afford functional imaging of brain hemodynamics as well as anatomical correlations (53).

In regard to information about brain perfusion, PCT appears at least equivalent to MRI (26,54,55). Significant correlation have been demonstrated between PCT-CBV and diffusion-weighted imaging (DWI), between PCT-MTT and perfusion-weighted imaging (PWI)-TTP and between CTA source images with DWI (26,55). If threshold models are used, PCT core correlates well with DWI and PCT total ischemia with PWI-MTT (20).

The linear relationship between contrast concentration and signal intensity is an important advantage of CT perfusion imaging over gadolinium-based MR perfusion imaging, allowing a more quantitative estimation of CBF (17,56).

Both CTA and MRA detect significant stenosis and vascular malformations quite reliably (41,48,57,58), but comparative studies have not been reported. Whereas CTA may better identify arterial calcifications, MRA is probably more specific in diagnosing cervical artery dissections (59).

Valid criticisms of MRI include its cost, limited availability, more difficult patient monitoring, pace-maker incompatibility, and the longer time required for scanning (60). Some drawbacks of PCT and CTA, such as the impossibility of serial examinations (amount of contrast, radiation) or failure to show lacunar or posterior fossa lesions, are counterbalanced by the availability of CTs in most emergency rooms, its easy accessibility, and the easy monitoring of patients. As most hospitals have spiral CTs, PCT and CTA imaging in the emergency room does not require installation of any new equipment, but only of new software. Further validation of this method would therefore allow penumbra imaging to be performed in smaller hospitals with limited MRI access where most stroke patients arrive.

Are Perfusion Computed Tomography and Computed Tomography Angiography Independent Predictors of Prognosis After Stroke?

Acute penumbral and arterial imaging should provide prognostic information beyond the known predictors of clinical outcome and should do so within the first hours following stroke

onset (16). Known predictors of death after ischemic stroke are higher age, higher initial National Institute of Health Stroke Scale (NIHSS) score, decreased consciousness on presentation, early ischemic changes on noncontrast CT (61,62), large infarct size on acute MRI (63), large hemispheral stroke syndrome (64), ischemic stroke subtype, fever, hypertension, atrial fibrillation, congestive heart failure, hyperglycemia, and elevated C-reactive protein (65).

Dynamic PCT using thresholds reliably identifies penumbra and core tissue and closely predicts final stroke volume (20,24,25,31,66). Similarly, arterial pathology on CTA has partially been shown to predict outcome (20,67). When compared with standard imaging (61,68,69), acute advanced functional imaging also performs better in predicting the clinical status and outcome. Thijs et al. (70) found a Spearman's correlation coefficient of 0.68 between lesion volume on DWI and Barthel index at one month, and Nabavi et al. (50) a coefficient of 0.7 between a combination of PCT and CTA and three months' outcome. Using PCT thresholds, Wintermark et al. (20) report a good correlation between the amount of penumbra and early NIHSS improvement if the vessel is recanalized; also, there is low clinical improvement to expect if the penumbra accounts for less than 30% of the ischemic volume. Low CBF values in lenticulostriate lacunar strokes predict poorer radiological and clinical outcome (71).

In the 75 patients of a recent series of PCT with good quality images before IV thrombolysis by Reichhart et al. (30), multivariate stepwise logistic regression showed that the best predictors for dependency (mRS >2) at three months were patient age and the total ischemia volume on PCT (core plus penumbra). At 24 hours, best multivariate predictors were the 24-hour NIHSS, non-recanalization at 24 hours on CTA, and the initial penumbra volume on PCT. Differential analysis of the value of ischemia volumes in recanalizers and nonrecanalizers has not yet been performed in this group.

With further validation and greater availability of acute penumbral and arterial imaging, it will likely become a major determinant in the selection of potentially dangerous and costly stroke treatments.

Do Perfusion Computed Tomography and Computed Tomography Angiography Predict Treatment Response?

Acute stroke imaging should predict the response to treatment and the associated risks. It should indicate in advance in which patients a particular treatment is likely to improve, worsen, or leave unchanged the natural history of the disease. Concerning thrombolysis, the following factors are known to predict higher efficacy: shorter time to treatment, lower NIHSS score, and early recanalization (6). Lower age is another, although less well established, favorable predictor. On the contrary, early ischemic changes on plain CT (62) and stroke subtype (72) have no predictive value. It is also known that there is a higher risk of thrombolysis-related hemorrhage with increasing age, higher stroke severity, higher rt-PA dose, hyperglycemia, diabetes, acute use of aspirine, and a history of cardiac disease.

The risk is not increased by longer time to lysis, hyperdense MCA sign, or previous aspirine use (73).

In the 75 patients of a recent series of PCT with good quality images before IV thrombolysis (30), there was no control group without thrombolysis; therefore, predictors of treatment response could not be established. Interestingly, the presence or absence of a large vessel occlusion before thrombolysis was not a significant predictor of outcome in this group, contrary to what was observed in a series of nonthrombolyzed patients (50,74). This suggests that IV thrombolysis may be particularly effective if an initial large vessel occlusion is present. In the same population, however, large volume of ischemia (large penumbra plus core volumes) was an independent predictor of intracranial haemorrhage after IV thrombolysis (75).

How Can Perfusion Computed Tomography and Computed Tomography Angiography Influence Acute Stroke Management?

Given the limited amount of information available, it is premature to know whether and in what situation patient outcome can and will be influenced by acute perfusion and vascular imaging. However, it is easily conceivable that this will be the case. Examples for such perfusion and vascular imaging based treatment decisions could be

1. replacement of the time criterion by the demonstration of the absence or presence of a significant amount of salvageable tissue (13),
2. elimination of traditional exclusion criteria for thrombolysis and recanalization (epileptic seizure (35) and wake-up and unknown onset stroke (76) (Figs. 1 and 2),
3. better patient selection for intra-arterial versus IV recanalization (presence or absence of accessible large artery pathology on CTA), and
4. identification of patients with significant penumbra for neuroprotective treatments.

Combining these hypotheses, PCT and CTA (or perfusion–diffusion MRI and MRA) could help select patients for appropriate treatment or for specific study protocols.

Areas of Uncertainty

Comparison of PCT with PET in healthy controls show that quantitative measures of blood flow are accurate (77). This comparison should also be done in acute stroke patients. Accuracy of infarct prediction by PCT should also be validated in patients with and without severe cervical artery (carotid) disease and at different ages of ischemia (3, 6, and 12 hours). Although PCT thresholds have been established for irreversible ischemia (20), it has to be kept in mind that duration of ischemia is a similarly important factor as are flow thresholds (4,5). Furthermore, PCT does not directly assess oxygen extraction nor biochemical and electrical features of ischemic tissue. These variables might also be useful in evaluating the potential of tissue to survive despite acute ischemia (78,79).

The placement and size of regions-of-interest (ROIs) may influence results of PCT significantly (80,81). Semi-automated or other standardized methods to do this need to be developed. Similarly, the choice of the input artery is important. The availability of clinical information (indicating the side of stroke) and concurrent interpretation of CTA results may be helpful to do so correctly. The reproducibility of the creation and interpretation of PCT maps has not been well investigated, even if the use of threshold maps with semi-automated selection of ROIs (20) should overcome this problem.

Other limitations of PCT are its current limited spatial coverage. However, this limitation will be overcome with the introduction of the 64-slice CT scanners. In our experience, thalamic, mesencephalic, and cerebellar lesions can be visualized if the positioning of the slices is guided by clinical information. Exposure to radiation prohibits repeated use of PCT and CTA. Iodinated contrast can occasionally be associated with allergy, hyperthyroidism, or renal failure, although this seems to occur rarely (30).

CONCLUSIONS

Dynamic PCT shows significant diagnostic and pronostic value in acute ischemic stroke patients and allows us to differentiate reversible from irreversible ischemia. This technique is rapid and available on most currently used spiral CT scanners. Together with CT-angiography, it adds valuable information that may potentially influence management. It can also be used to assess a wide range of patients with various cerebrovascular conditions. Its limitations are the insufficient assessment of brainstem and small lesions. Whether and how it may improve patient outcome still needs to be evaluated in large prospective studies.

REFERENCES

1. Heiss WD. Imaging the ischemic penumbra and treatment effects by PET. Keio J Med 2001; 50(4):249–256.
2. Read SJ, Hirano T, Abbott DF, et al. The fate of hypoxic tissue on 18F-fluoromisonidazole positron emission tomography after ischemic stroke. Ann Neurol 2000; 48(2):228–235.
3. Darby DG, Barber PA, Gerraty RP, et al. Pathophysiological topography of acute ischemia by combined diffusion-weighted and perfusion MRI [comment]. Stroke 1999; 30(10):2043–2052.
4. Jones TH, Morawetz RB, Crowell RM, et al. Thresholds of focal cerebral ischemia in awake monkeys. J Neurosurg 1981; 54(6):773–782.
5. Astrup J, Siesjo BK, Symon L. Thresholds in cerebral ischemia—the ischemic penumbra. Stroke 1981; 12(6):723–725.

6. Adams HP Jr, Adams RJ, Brott T, et al. Guidelines for the early management of patients with ischemic stroke: a scientific statement from the Stroke Council of the American Stroke Association. Stroke 2003; 34(4):1056–1083.
7. Parsons MW, Barber PA, Chalk J, et al. Diffusion- and perfusion-weighted MRI response to thrombolysis in stroke. Ann Neurol 2002; 51(1):28–37.
8. Furlan M, Marchal G, Viader F, Derlon JM, Baron JC. Spontaneous neurological recovery after stroke and the fate of the ischemic penumbra [comment]. Ann Neurol 1996; 40(2):216–226.
9. Anonymous. Generalized efficacy of t-PA for acute stroke. Subgroup analysis of the NINDS t-PA Stroke Trial. Stroke 1997; 28(11):2119–2125.
10. Hacke W, Kaste M, Fieschi C, et al. Randomised double-blind placebo-controlled trial of thrombolytic therapy with intravenous alteplase in acute ischaemic stroke (ECASS II). Second European-Australasian Acute Stroke Study Investigators [see comments]. Lancet 1998; 352(9136):1245–1251.
11. Boysen G, Christensen H. Early stroke: a dynamic process. Stroke 2001; 32(10):2423–2425.
12. Parsons MW, Barber PA, Desmond PM, et al. Acute hyperglycemia adversely affects stroke outcome: a magnetic resonance imaging and spectroscopy study. Ann Neurol 2002; 52(1):20–28.
13. Hacke W, Albers G, Al-Rawi Y, et al. The Desmoteplase in Acute Ischemic Stroke Trial (DIAS): a phase II MRI-based 9-hour window acute stroke thrombolysis trial with intravenous desmoteplase. Stroke 2005; 36(1):66–73.
14. Hacke W, Donnan G, Fieschi C, et al. Association of outcome with early stroke treatment: pooled analysis of ATLANTIS, ECASS, and NINDS rt-PA stroke trials. Lancet 2004; 363(9411):768–774.
15. Darby DG, Barber PA, Gerraty RP, et al. Pathophysiological topography of acute ischemia by combined diffusion-weighted and perfusion MRI. Stroke 1999; 30(10):2043–2052.
16. Michel P, Reichhart M, Wintermark M, Meuli R., Bogousslavsky J. Prise en charge des attaques cérébrales à l'aide du CT de perfusion [Stroke management using perfusion-CT]. Schweiz Arch Neurol Psychiatr 2004; 155:148–151.
17. Wintermark M, Maeder P, Thiran JP, Schnyder P, Meuli R. Quantitative assessment of regional cerebral blood flows by perfusion CT studies at low injection rates: a critical review of the underlying theoretical models [review] [81 refs]. Eur Radiol 2001; 11(7):1220–1230.
18. Latchaw RE, Yonas H, Hunter GJ, et al. Guidelines and recommendations for perfusion imaging in cerebral ischemia: a scientific statement for healthcare professionals by the writing group on perfusion imaging, from the Council on Cardiovascular Radiology of the American Heart Association. Stroke 2003; 34(4):1084–1104.
19. Axel L. Cerebral blood flow determination by rapid-sequence computed tomography: theoretical analysis. Radiology 1980; 137(3):679–686.
20. Wintermark M, Reichhart M, Thiran JP, et al. Prognostic accuracy of cerebral blood flow measurement by perfusion computed tomography, at the time of emergency room admission, in acute stroke patients. Ann Neurol 2002; 51(4):417–432.
21. Wintermark M, Flanders AE, Velthuis B, et al. Perfusion-CT assessment of infarct core and penumbra: receiver operating characteristic curve analysis in 130 patients suspected of acute hemispheric stroke. Stroke 2006; 37(4):979–985.
22. Eastwood JD, Lev MH, Azhari T, et al. CT perfusion scanning with deconvolution analysis: pilot study in patients with acute middle cerebral artery stroke. Radiology 2002; 222(1):227–236.
23. Koenig M, Kraus M, Theek C, Klotz E, Gehlen W, Heuser L. Quantitative assessment of the ischemic brain by means of perfusion-related parameters derived from perfusion CT. Stroke 2001; 32(2): 431–437.
24. Klotz E, Konig M. Perfusion measurements of the brain: using dynamic CT for the quantitative assessment of cerebral ischemia in acute stroke. Eur J Radiol 1999; 30(3):170–184.
25. Mayer TE, Hamann GF, Baranczyk J, et al. Dynamic CT perfusion imaging of acute stroke. AJNR Am J Neuroradiol 2000; 21(8):1441–1449.
26. Schramm P, Schellinger PD, Fiebach JB, et al. Comparison of CT and CT angiography source images with diffusion-weighted imaging in patients with acute stroke within 6 hours after onset. Stroke 2002; 33(10):2426–2432.
27. Hoeffner EG, Case I, Jain R, et al. Cerebral perfusion CT: technique and clinical applications. Radiology 2004; 231(3):632–644.
28. Wintermark M, Fischbein NJ, Smith WS, Ko NU, Quist M, Dillon WP. Accuracy of dynamic perfusion CT with deconvolution in detecting acute hemispheric stroke. AJNR Am J Neuroradiol 2005; 26(1):104–112.
29. Wintermark M, Fischbein NJ, Smith WS, Ko NU, Quist M, Dillon WP. Accuracy of dynamic perfusion CT with deconvolution in detecting acute hemispheric stroke. AJNR Am J Neuroradiol 2005; 26(1):104–112.
30. Reichhart MD, Bezerrra DC, Wintermark M, et al. Predictive value of penumbra and vascular occlusion state in stroke patients treated with iv rt-PA within 3 hours [abstr]. Neurology 2005; 64: A263.
31. Koenig M, Klotz E, Luka B, Venderink DJ, Spittler JF, Heuser L. Perfusion CT of the brain: diagnostic approach for early detection of ischemic stroke. Radiology 1998; 209(1):85–93.

32. Hunter GJ, Hamberg LM, Ponzo JA, et al. Assessment of cerebral perfusion and arterial anatomy in hyperacute stroke with three-dimensional functional CT: early clinical results [comment]. AJNR Am J Neuroradiol 1998; 19(1):29–37.
33. Wintermark M, Fischbein NJ, Smith WS, Ko NU, Quist M, Dillon WP. Accuracy of dynamic perfusion CT with deconvolution in detecting acute hemispheric stroke. AJNR Am J Neuroradiol 2005; 26(1):104–112.
34. Michel P, Reichhart M, Wintermark M, Maeder PH, Bogousslavsky R. Perfusion-CT in transient ischemic attacks [abstr]. Stroke 2005; 36:484.
35. Bezerra DC, Michel P, Reichhart M, Wintermark M, Meuli R, Bogousslavsky J. Perfusion-CT guided acute thrombolysis in patients with seizures at stroke onset [abstr]. Stroke 2005; 36:484.
36. Gonzalez-Delgado M, Michel P, Reichhart M, Wintermark M, Maeder Ph, Bogousslavsky J. The significance of focal hypoperfusion during migraine with aura [abstr]. Stroke 2005; 36:444.
37. Croquelois A, Wintermark M, Reichhart M, Meuli R, Bogousslavsky J. Aphasia in hyperacute stroke: language follows brain penumbra dynamics. Ann Neurol 2003; 54(3):321–329.
38. Wintermark M, Ko NU, Smith WS, Liu S, Higashida RT, Dillon WP. Vasospasm after subarachnoid hemorrhage: utility of perfusion CT and CT angiography on diagnosis and management. AJNR Am J Neuroradiol 2006; 27(1):26–34.
39. van dS, I, Wermer MJ, van der GY, Velthuis BK, van de Kraats CI, Rinkel GJ. Prognostic value of cerebral perfusion-computed tomography in the acute stage after subarachnoid hemorrhage for the development of delayed cerebral ischemia. Stroke 2006; 37(2):409–413.
40. Wintermark M, van Melle G, Schnyder P, et al. Admission perfusion CT: prognostic value in patients with severe head trauma. Radiology 2004; 232(1):211–220.
41. Shrier DA, Tanaka H, Numaguchi Y, Konno S, Patel U, Shibata D. CT angiography in the evaluation of acute stroke. AJNR Am J Neuroradiol 1997; 18(6):1011–1020.
42. Arnold M, Schroth G, Nedeltchev K, et al. Intra-arterial thrombolysis in 100 patients with acute stroke due to middle cerebral artery occlusion. Stroke 2002; 33(7):1828–1833.
43. Kassem-Moussa H, Graffagnino C. Nonocclusion and spontaneous recanalization rates in acute ischemic stroke: a review of cerebral angiography studies. Arch Neurol 2002; 59(12):1870–1873.
44. Furlan A, Higashida R, Wechsler L, et al. Intra-arterial prourokinase for acute ischemic stroke. The PROACT II study: a randomized controlled trial. Prolyse in acute cerebral thromboembolism. JAMA 1999; 282(21):2003–2011.
45. The IMS Study Group. Combined intravenous and intra-arterial recanalization for acute ischemic stroke: The Interventional Management of Stroke Study. Stroke 2004; 35(4):904–911.
46. Alexandrov AV, Molina CA, Grotta JC, et al. Ultrasound-enhanced systemic thrombolysis for acute ischemic stroke. N Engl J Med 2004; 351(21):2170–2178.
47. Smith WS, Sung G, Starkman S, et al. Safety and efficacy of mechanical embolectomy in acute ischemic stroke: results of the MERCI trial. Stroke 2005; 36(7):1432–1438.
48. Knauth M, von KR, Jansen O, Hahnel S, Dorfler A, Sartor K. Potential of CT angiography in acute ischemic stroke. AJNR Am J Neuroradiol 1997; 18(6):1001–1010.
49. Lev MH, Segal AZ, Farkas J, et al. Utility of perfusion-weighted CT imaging in acute middle cerebral artery stroke treated with intra-arterial thrombolysis: prediction of final infarct volume and clinical outcome. Stroke 2001; 32(9):2021–2028.
50. Nabavi DG, Kloska SP, Nam EM, et al. MOSAIC: multimodal stroke assessment using computed tomography: novel diagnostic approach for the prediction of infarction size and clinical outcome. Stroke 2002; 33(12):2819–2826.
51. Wildermuth S, Knauth M, Brandt T, Winter R, Sartor K, Hacke W. Role of CT angiography in patient selection for thrombolytic therapy in acute hemispheric stroke. Stroke 1998; 29(5):935–938.
52. Jovin TG, Yonas H, Gebel JM, et al. The cortical ischemic core and not the consistently present penumbra is a determinant of clinical outcome in acute middle cerebral artery occlusion. Stroke 2003; 34(10):2426–2433.
53. Michel P, Bogousslavsky J. Penumbra is brain: no excuse not to perfuse. Ann Neurol 2005; 58(5):661–663.
54. Wintermark M, Reichhart M, Cuisenaire O, et al. Comparison of admission perfusion computed tomography and qualitative diffusion- and perfusion-weighted magnetic resonance imaging in acute stroke patients. Stroke 2002; 33(8):2025–2031.
55. Eastwood JD, Lev MH, Wintermark M, et al. Correlation of early dynamic CT perfusion imaging with whole-brain MR diffusion and perfusion imaging in acute hemispheric stroke. AJNR Am J Neuroradiol 2003; 24(9):1869–1875.
56. Zimmerman RD. Stroke wars: episode IV CT strikes back. AJNR Am J Neuroradiol 2004; 25(8):1304–1309.
57. Liu Y, Karonen JO, Vanninen RL, et al. Acute ischemic stroke: predictive value of 2D phase-contrast MR angiography—serial study with combined diffusion and perfusion MR imaging. Radiology 2004; 231(2):517–527.
58. Josephson SA, Bryant SO, Mak HK, Johnston SC, Dillon WP, Smith WS. Evaluation of carotid stenosis using CT angiography in the initial evaluation of stroke and TIA. Neurology 2004; 63(3):457–460.

59. Schievink WI. Spontaneous dissection of the carotid and vertebral arteries. N Engl J Med 2001; 344(12):898–906.
60. Lev MH, Koroshetz WJ, Schwamm LH, Gonzalez RG. CT or MRI for imaging patients with acute stroke: visualization of "tissue at risk"? Stroke 2002; 33(12):2736–2737.
61. Hill MD, Rowley HA, Adler F, et al. Selection of acute ischemic stroke patients for intra-arterial thrombolysis with pro-urokinase by using ASPECTS. Stroke 2003; 34(8):1925–1931.
62. Hill MD, von Kummer R, Levine S, et al. ASPECT overview of NINDS, ECASS, and ATLANTIS [abstr]. TAST Symposium, Whistler, Canada, 2004.
63. Fisher M, Albers GW. Applications of diffusion-perfusion magnetic resonance imaging in acute ischemic stroke. Neurology 1999; 52(9):1750–1756.
64. Neumann-Haefelin T, du Mesnil de RR, Fiebach JB, et al. Effect of incomplete (spontaneous and post-thrombolytic) recanalization after middle cerebral artery occlusion: a magnetic resonance imaging study. Stroke 2004; 35(1):109–114.
65. Rundek T, Sacco RL. Outcome following stroke. In: Mohr JP, Choi DW, Grotta JC, Weir B, Wolf PA. Stroke. Pathophysiology, Diagnosis and Management [Generic]. 4th ed. Philadelphia: Churchill Livingstone, 2004.
66. Parsons MW, Pepper EM, Chan V, et al. Perfusion computed tomography: prediction of final infarct extent and stroke outcome. Ann Neurol 2005; 58(5):672–679.
67. Nabavi DG, Cenic A, Henderson S, Gelb AW, Lee TY. Perfusion mapping using computed tomography allows accurate prediction of cerebral infarction in experimental brain ischemia. Stroke 2001; 32(1):175–183.
68. Johnston KC, Connors AF Jr, Wagner DP, Knaus WA, Wang X, Haley EC Jr. A predictive risk model for outcomes of ischemic stroke. Stroke 2000; 31(2):448–455.
69. Warach S, Pettigrew LC, Dashe JF, et al. Effect of citicoline on ischemic lesions as measured by diffusion-weighted magnetic resonance imaging. Citicoline 010 Investigators. Ann Neurol 2000; 48(5):713–722.
70. Thijs VN, Lansberg MG, Beaulieu C, Marks MP, Moseley ME, Albers GW. Is early ischemic lesion volume on diffusion-weighted imaging an independent predictor of stroke outcome? A multivariable analysis. Stroke 2000; 31(11):2597–2602.
71. Yamada M, Yoshimura S, Kaku Y, et al. Prediction of neurologic deterioration in patients with lacunar infarction in the territory of the lenticulostriate artery using perfusion CT. AJNR Am J Neuroradiol 2004; 25(3):402–408.
72. Marler JR, Tilley BC, Lu M, et al. Early stroke treatment associated with better outcome: the NINDS rt-PA stroke study. Neurology 2000; 55(11):1649–1655.
73. Hacke W, Donnan G, Fieschi C, et al. Association of outcome with early stroke treatment: pooled analysis of ATLANTIS, ECASS, and NINDS rt-PA stroke trials. Lancet 2004; 363(9411):768–774.
74. Arnold M, Nedeltchev K, Brekenfeld C, et al. Outcome of acute stroke patients without visible occlusion on early arteriography. Stroke 2004; 35(5):1135–1138.
75. Bezerra DC, Reichhart MD, Wintermark M, et al. The volume of perfusion defect within 3 hours of stroke onset is a predictor of intracranial hemorrhage after iv rt-PA therapy. Neurology 2005; 64(suppl 1):A264.
76. Gonzalez-Delgado M, Michel P, Reichhart M, Meuli R, Bogousslavsky J. Perfusion- and angio-CT in stroke of unknown onset [abstr]. Cerebrovasc Dis 2004; 18(suppl 5):99.
77. Kudo K, Terae S, Katoh C, et al. Quantitative cerebral blood flow measurement with dynamic perfusion CT using the vascular-pixel elimination method: comparison with H2(15)O positron emission tomography. AJNR Am J Neuroradiol 2003; 24(3):419–426.
78. Nicoli F, Lefur Y, Denis B, Ranjeva JP, Confort-Gouny S, Cozzone PJ. Metabolic counterpart of decreased apparent diffusion coefficient during hyperacute ischemic stroke: a brain proton magnetic resonance spectroscopic imaging study. Stroke 2003; 34(7):e82–e87.
79. Heiss WD, Sobesky J, Smekal U, et al. Probability of cortical infarction predicted by flumazenil binding and diffusion-weighted imaging signal intensity: a comparative positron emission tomography/magnetic resonance imaging study in early ischemic stroke. Stroke 2004; 35(8):1892–1898.
80. Wintermark M, Thiran JP, Maeder P, Schnyder P, Meuli R. Simultaneous measurement of regional cerebral blood flow by perfusion CT and stable xenon CT: a validation study. AJNR Am J Neuroradiol 2001; 22(5):905–914.
81. Sanelli PC, Lev MH, Eastwood JD, Gonzalez RG, Lee TY. The effect of varying user-selected input parameters on quantitative values in CT perfusion maps. Acad Radiol 2004; 11(10):1085–1092.

15b. Xenon-Computed Tomography-Cerebral Blood Flow Assessment of Ischemic Penumbra in Acute Stroke

Tudor G. Jovin
Department of Neurology, Stroke Institute, University of Pittsburgh Medical Center, VA Pittsburgh Health Care System, Pittsburgh, Pennsylvania, U.S.A.

Lawrence R. Wechsler
Department of Neurology, Stroke Institute, University of Pittsburgh Medical Center, Pittsburgh, Pennsylvania, U.S.A.

Rishi Gupta
Department of Neurology, Michigan State University, Lansing, Michigan, U.S.A.

Howard Yonas
Department of Neurosurgery, University of New Mexico Health Sciences Center, Albuquerque, New Mexico, U.S.A.

INTRODUCTION

A major approach to acute ischemic stroke therapy consists of reversing the process through which threatened brain tissue supplied by the occluded vessel ultimately undergoes infarction. The two main treatment modalities aiming to achieve this goal are vessel recanalization and neuroprotection. Significant advances made in recent years in the area of intravenous and intra-arterial recanalization strategies have translated into improved clinical outcomes. Nevertheless, it is hoped that, mainly through improved patient selection, acute stroke therapy will lead to even better outcomes, less side effects, and expansion of the therapeutic window resulting in significantly larger numbers of patients who will benefit from this treatment (1–3). Several neuroprotectant compounds have shown efficacy in animal models of stroke but no such drug has shown clinical efficacy in humans (4). It is widely believed, however, that demonstrating clinical benefit from neuroprotectants in humans is only a matter of time. It is likely that benefit will be shown in the future, especially if neuroprotection is applied to acute stroke patients selected based on physiology rather than on time and when combined with recanalization strategies.

Since the publication of the The National Institute of Neurological Disorders and Stroke (NINDS) trial (5) showing benefit of intravenous tissue plasminogen activator (t-PA) administered within three hours of symptoms onset, several clinical trials have unsuccessfully attempted to show benefit from intravenous thrombolysis beyond this time window (6–10). Similar to current clinical practice, these trials based selection of patients for thrombolytic therapy on time from symptom onset and a noncontrasted head computed tomography (CT) showing the absence of hemorrhage. This approach may not be ideal, as a wide spectrum of clinical outcomes is observed when thrombolytics are administered according to chronological criteria (11), suggesting that the amount of salvageable brain tissue within the same time window varies from individual to individual. A fixed therapeutic time window in acute stroke has been questioned by several authors (2,12), and increasingly, selection of patients undergoing acute stroke therapy based on physiological criteria and on knowledge of the vascular occlusion site has been deemed more appropriate (2,13). Neuroimaging is the main tool available for assessing both cerebral pathophysiology and the site of vascular occlusion. The main aim of assessing cerebral pathophysiology is to distinguish the reversible areas of injury from irreversible damage, which constitutes the fundamental principle in selecting patients for acute stroke interventions.

The information obtained by imaging must be sufficiently valuable to offset the possibility of increasing the area of irreversible damage during the time needed to perform the study. CT and magnetic resonance imaging (MRI) technologies used individually or in combination are the imaging modalities that are currently best suited for these purposes.

Recently published clinical trials have shown that utilization of MR-based imaging modalities such as mismatch between perfusion-weighted (PW) and diffusion-weighted (DW) MRI can help select patients for acute stroke therapies (14,15). Since the diffusion abnormality is presumed to represent an approximation of the irreversible ischemic lesion, the area of mismatch between DWI and PWI is considered the territory still viable but at risk of undergoing infarction and corresponds theoretically to the concept of ischemic penumbra. The major shortcoming of this concept derives from the lack of quantitative data provided by MRI. It has been shown that the DWI lesion is not precise in distinguishing between irreversible and reversible ischemia (16,17). It incorporates both types of ischemia and therefore cannot be considered equivalent to the ischemic core. Additionally, the PWI lesion has been shown to incorporate both imminently threatened brain and brain that will not undergo infarction as a consequence of persistent vessel occlusion (18,19). Since, by definition, penumbra represents the tissue that will undergo infarction with continuous vessel occlusion, assessment of penumbral extent based on perfusion MR is not precise.

MRI is feasible in acute stroke, but in addition to the shortcomings outlined earlier, it may be limited by longer times needed to obtain the scan (20) and by motion artifact. MRI also requires a sophisticated infrastructure for its performance, which greatly limits the number of centers with the capability of providing around the clock services.

CT-based perfusion studies and CT angiography are believed to be at least equivalent in providing the type of physiological data needed to select patients for acute stroke therapy (21). Given that CT is more widespread and easier to obtain at most hospitals, finding parameters to select acute stroke patients with CT-based technology may lead to an increase in the number of patients eligible for acute stroke therapy.

Stable xenon gas can be used in conjunction with CT imaging to define the pathophysiological constellation favorable for acute stroke intervention. Its major advantage over other imaging modalities is that, by virtue of the quantitative cerebral blood flow (CBF) data provided by this technology, it allows an accurate assessment of brain tissue at risk (penumbra) in relationship to infarcted tissue (core) in a relatively fast and cost-efficient manner. In this review, we will discuss the potential of the xenon-CT-CBF technology to assess ischemic penumbra and ischemic core in acute stroke and its value as a pathophysiology-based selection tool for acute stroke therapy.

ACUTE STROKE PATHOPHYSIOLOGY: THE ISCHEMIC PENUMBRA

As reviewed elsewhere in this book, of critical importance for appropriate physiology-based patient selection for acute stroke therapies is the accurate assessment of the relationship between core, penumbra, and oligemia distal to the occluded large vessel (22).

The difference in tissue outcome following arterial occlusion is based on the concept of CBF thresholds below which neuronal integrity and function is differentially affected (23,24), in a time dependent process. Several investigators (25,26) have studied the relationship between electroencephalography (EEG) changes and regional CBF during carotid clamping in patients undergoing carotid endarterectomy. It was found that EEG would slow down if mean CBF fell below 23 mL/100 g/min, whereas at values below 15 mL/100 g/min, the EEG would become flat. In baboons, Symon et al. (27) demonstrated that brain tissue perfused between certain CBF values (22–28 mL/100 g/min), even with prolonged hypoperfusion, stops functioning but maintains its structural integrity and, most importantly, can be salvaged with reperfusion. The time dependence of ischemic thresholds was subsequently demonstrated (28) in primate studies, documenting that the CBF values below which brain tissue becomes infarcted are dependent upon the duration of vessel occlusion. However, it is believed that gray matter is more susceptible to infarction than white matter and within the gray matter the basal ganglia have a lower ischemic tolerance than the cortex (29).

PENUMBRA AND CORE

Astrup et al. (30) proposed that the ischemic core represents the tissue that is irreversibly damaged. Positron emission tomography (PET) studies in humans suggest that beyond a certain time limit (probably no longer than an hour) it corresponds to CBF values of less than 7 mL/100 mg/min (31–33) to 12 mL/100 mg/min (34,35). The ischemic penumbra represents the tissue that is functionally impaired but structurally intact and corresponds to a high CBF limit of 17 to 22 mL/100 mg/min and a low CBF limit of 7 to12 mL/100 mg/min. Evidence in the literature suggests that there is temporal evolution of the core, which grows at the expense of penumbra (35–37) (Fig. 1). However, the speed with which this process is completed varies from individual to individual. This may explain the great variability in outcomes observed with recanalization therapy for the same vascular occlusion site. Christou et al. (38) reported that in middle cerebral artery (MCA) occlusion treated with intravenous t-PA, even when recanalization occurs within two hours post symptoms onset, only 50% of patients achieve excellent outcomes (38). In contrast, excellent outcomes have been achieved in selected patients with acute stroke due to MCA occlusion revascularized with extracranial-intracranial (EC-IC) bypass as far out as 48 hours post symptoms onset (39). One of the proposed mechanisms for growth of the ischemic core is progressive recruitment of penumbral areas into the core (36). It is known that the ischemic penumbra represents a dynamic phenomenon. If vessel occlusion persists, the penumbra may shrink due to progressive recruitment into the core. Alternatively, it may return to a normal state following vessel recanalization or possibly neuroprotectant interventions. It, thus, appears that the ischemic penumbra represents a buffer between core and oligemia, a transitional state between evolution into permanent ischemia as one possibility, and transformation into normal tissue as the other possibility. On the basis of a rat model of middle cerebral artery occlusion studied in a multimodal fashion assessing CBF, metabolism, and gene expression, Ginsberg et al. (37) concluded that the penumbra lies within a narrow range of perfusion and thus is precariously dependent on small perfusion pressure changes. The penumbra, being the site of severe metabolism/flow dissociation, is electrophysiologically dynamic, undergoes recurrent depolarizations, and is metabolically unstable.

Contrary to long-held belief, recent evidence suggests that penumbral brain tissue of significant extent is present beyond six hours of stroke onset in a large proportion of patients (31). PET studies using the tissue hypoxia marker ^{18}F-fluoroimidosonidazole included patients studied within 6 to, as late as, 51 hours after stroke onset and reported the existence of penumbra comprising 30% to 45% of the total ischemic tissue at risk (40).

OLIGEMIA

Another compartment, termed "oligemia," represents the mildly hypoperfused tissue from the normal range down to around 20 to 22 mL/100 g/min (27). It is believed that under normal circumstances this tissue is not at risk of infarction in humans (22). Although this compartment is known to survive in the hyperacute stage of arterial occlusion (first 6–12 hours), little is known about its fate if vessel occlusion persists. It is likely that this compartment is further compartmentalized into a more benign range (from normal CBF to 30 mL/100 g/min), which is unlikely to undergo infarction even with continuous vessel occlusion. This contention is supported by the work showing that in patients with a mean ipsilateral hemispheric CBF of 30 mL/100 g/min or above during balloon test occlusion (BTO) of the internal carotid artery (ICA), subsequent vessel sacrifice carried a very small risk of subsequent stroke (41,42). In contrast, the 20 to 30 mL/100 g/min range may not portend a good prognosis. Marshall et al. (43) showed that the only variable that accurately predicted the risk of stroke after ICA sacrifice was the presence of hemispheric CBF under 30 mL/100 g/min on prior BTO (43). Although this compartment may not be imminently threatened to undergo infarction (27), it is conceivable that ongoing vessel occlusion possibly in conjunction with aggravating factors, such as fever, hyperglycemia, hypotension, acidosis, hypercarbia, may lead to a slow progression toward infarction. Analyzing different CBF thresholds as predictors of infarction, Jovin et al. (44) found that regions of interest (ROIs) with CBF values of 20 mL/100 g/min on xenon-CT-CBF scans in patients with acute MCA occlusion were 70% sensitive and 70% specific for predicting final infarction, whereas the sensitivity/specificity

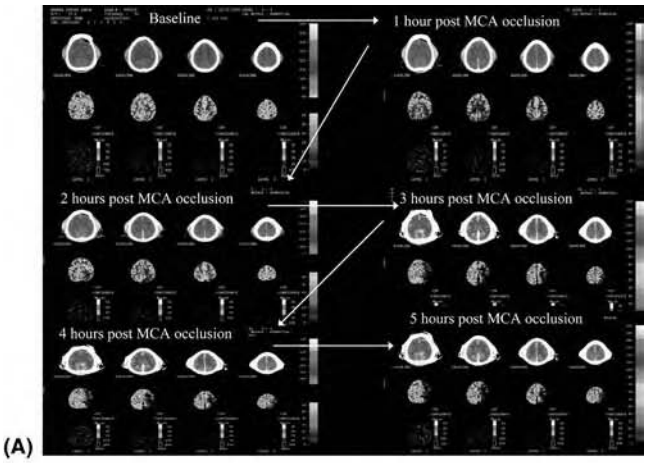

(A)

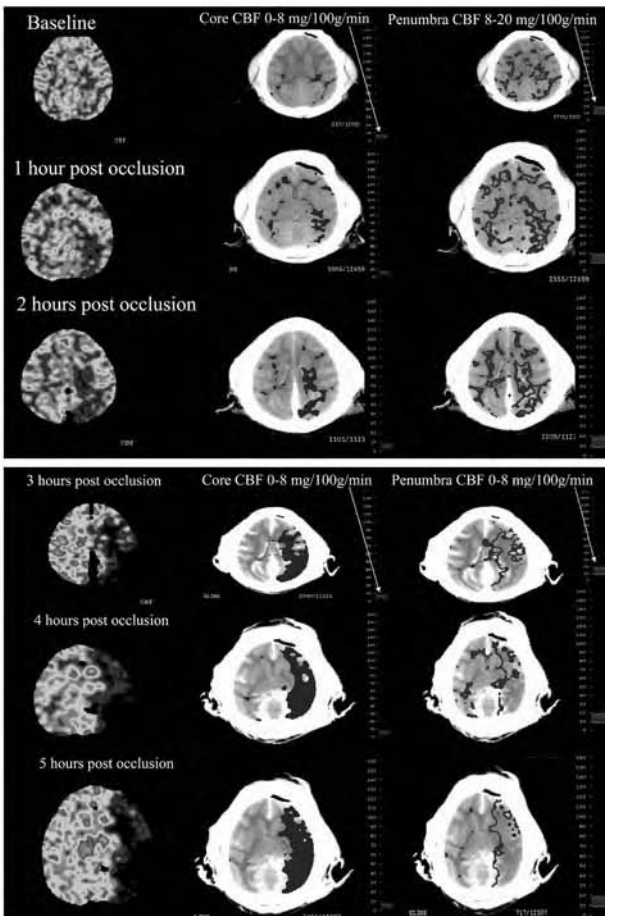

(B)

FIGURE 1 (*See color insert*.) Progressive growth of core at the expense of penumbra in a primate model of acute middle cerebral artery (MCA) occlusion (**A**) Serial xenon-computed tomography (CT)-cerebral blood flow (CBF) studies at four levels in the brain of a rhesus monkey. Studies were performed at baseline and at one hour interval for five consecutive hours following acute MCA occlusion. Cerebral blood flow values expressed in mL/100 g brain/min are displayed on a color scale, with darkest colors representing the lowest CBF values and lightest colors representing the highest CBF values. There is a progressive decline of regional CBF in the left hemisphere. (**B**) Voxels corresponding to CBF values of 0 to 8 mL/100 g brain/min (ischemic core purple) and voxels corresponding to CBF values of 8 to 20 mL/100 g brain/min (ischemic penumbra, blue) were separated out of the CBF map at one level in the brain and superimposed on the native CT scan. There is a progressive growth of core paralleled by a progressive penumbral shrinkage. *Abbreviations*: MCA, middle cerebral artery; CBF, cerebral blood flow.

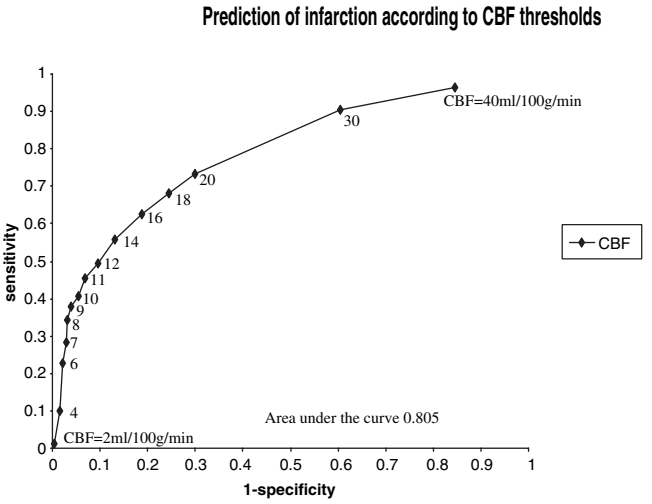

FIGURE 2 Prediction of infarction according to cerebral blood flow thresholds. *Abbreviation:* CBF, cerebral blood flow.

of CBF values of 30 mL/100 g/min changed to 95% and 35%, respectively (Fig. 2). This data set included both patients who recanalized early and those who did not. Therefore, it is clear that some brain with perfusion in this CBF range will eventually undergo infarction. Establishing the natural history of this flow compartment in the presence of continuous vessel occlusion is an important task for the future that will clarify the indication and timing of revascularization therapy in patients with large vessel occlusive disease who present with hemispheric CBF values in this range.

POTENTIAL LIMITATIONS OF PERFUSION-BASED TECHNIQUES IN ESTIMATING ISCHEMIC CORE AND PENUMBRA

A word of caution must be exercised when assessing core, penumbra, and oligemia with perfusion-based technologies. As mentioned earlier, the fate of the hypoperfused brain distal to an occluded artery is dependent on two main parameters: extent of CBF impairment and duration of occlusion. Depending on their quantitative versus qualitative nature, various brain perfusion assessment technologies represent a snapshot in time that measure tissue perfusion with different degrees of accuracy. In determining brain viability, however, the assumption is made that vessel occlusion is continuous, starting from the onset of patient's symptoms and continuing up to the point of the perfusion study. Although this assumption may be correct in the majority of acute stroke patients, the dynamic phenomenon of vessel recanalization and re-occlusion has been described and can occur in the absence of detectable clinical change. In those (probably rare) circumstances, of only intermittent vessel occlusion, tissue viability based on only one measurement in time will be inaccurate. Figure 3 demonstrates an example of a patient at our institution who presented with severe clinical deficit with minor clinical fluctuations and had severe hemispheric hypoperfusion in the ischemic core range by xenon-CT-CBF at five hours postsymptoms onset. A cerebral angiogram performed immediately after the xenon-CT scan showed near occlusive thrombus in ipsilateral MCA. The patient was not treated with recanalization therapy. A follow-up brain MRI demonstrated that large areas perfused in the core range on the xenon-CT scan had actually escaped infarction. We postulate that, in this patient, the thrombus was only intermittently occlusive and that the CBF study was performed when the vessel was occluded. However, the patient recanalized spontaneously, and the hypoperfusion in the core range had not been of sufficient duration to result in infarction.

XENON-COMPUTED TOMOGRAPHY-CEREBRAL BLOOD FLOW TECHNIQUE

Xenon-133 has been utilized since the 1960s to calculate CBF. The initial administration was via intracarotid injection (45) that has since been replaced with noninvasive methods through either

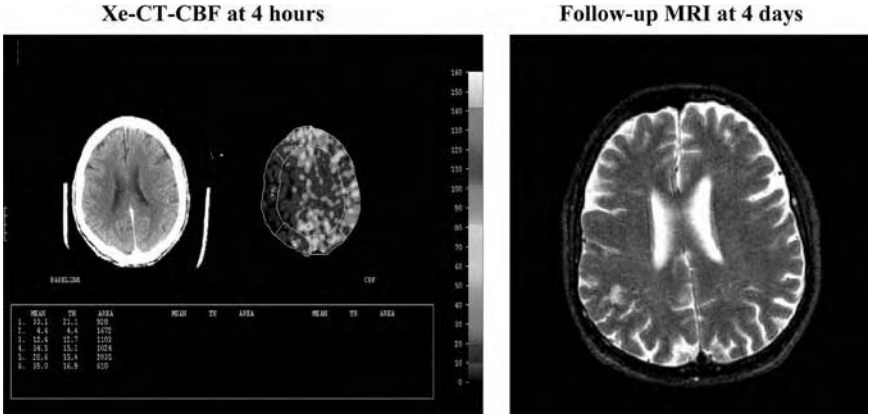

FIGURE 3 An example of area with core range cerebral blood flow values that escape infarction due to intermittently occlusive thrombus. A 70-year-old man with left hemiparesis and neglect at four hours after onset of symptoms; NIHSS 12; cerebral angiogram: R middle cerebral artery thrombus. *Abbreviations*: MRI, magnetic resonance imaging; Xe-CT-CBF, xenon-computed tomography-cerebral blood flow.

intravenous administration (46) or stable gas inhalation (47). The latter method of administration can be used in conjunction with CT imaging, which greatly increases the resolution of this technique. This method requires simple calculations to account for the distribution of the inert gas within the brain. Several variables must be accounted for in order to obtain reliable CBF values. These variables are related mathematically and can be expressed via the Kety–Schmidt equation:

$$C_{\text{xebr}}(T) = \lambda\kappa\int C_{\text{xeart}}(t)\mathrm{e}^{-\kappa(T-\mathrm{t})}\mathrm{d}t \tag{1}$$

$C_{\text{Xebr}}(T)$ is the concentration of xenon in the brain, λ is the blood–brain partition coefficient, k is the flow rate constant, and $C_{\text{Xeart}}(t)$ is the arterial concentration of xenon and can be expressed by the following equation (37):

$$C_{\text{Xeart}}(t) = C_{\text{Xemax}}(1 - \mathrm{e}^{-bt}). \tag{2}$$

C_{Xemax} is the maximum arterial xenon concentration in mg/mL and b is the arterial uptake rate constant. C_{Xemax} is related to the solubility of xenon gas (S_{Xe}) in blood and the percent uptake of the gas $C(\%)_{\text{max}}$ as follows:

$$C_{\text{Xemax}} = C(\%)_{\text{max}}\,(5.15)\,(S_{\text{Xe}})(0.01). \tag{3}$$

The solubility of xenon is related to the hematocrit (Hct) as follows:

$$S_{\text{Xe}} = 0.1 + 0.0011\ (\%\ \text{Hct}). \tag{4}$$

Once these equations are solved, the Hounsfield enhancement (HE) on CT can be obtained in relation to the mass attenuation coefficients of water (U_{p}^{w}) and xenon (U_{p}^{Xe}).

$$\text{HE} = C_{\text{Xebr}}/(U_{\text{p}}\text{w}/U_{\text{p}}\text{Xe}). \tag{5}$$

Two unenhanced CT images of the brain are obtained prior to administration of xenon. The gas is then inhaled and six xenon-enhanced images are obtained at predetermined levels. The unenhanced images are averaged and then subtracted from the enhanced images yielding a C_{Xebr} for several thousand voxels at each level studied.

This quantification method has been validated previously and has been shown to be an accurate technique for obtaining CBF values (48). Normal values for CBF are 80 ± 20 mL/100 g/min in the cortical gray matter and 20 ± 2 mL/100 g/min for white matter (49). These values decline with advancing age, especially in patients with cerebrovascular disease (50).

Administration of xenon has few side effects and was found to be safe in a large cohort of patients studied at The University of Pittsburgh. The most common side effects noted were headaches (0.4%), nausea/vomiting (0.2%), and seizures (0.2%) based on a cohort of 1830 patients (51).

XENON-COMPUTED TOMOGRAPHY FOR ACUTE ISCHEMIC STROKE

Due to its ability to quantify ischemia, xenon-CT-CBF has several clinical applications in acute ischemic stroke making it a powerful tool for guiding acute stroke treatment. Although a plain, noncontrasted head CT when interpreted by highly trained physicians is capable of delineating the extent of critical ischemia with high specificity, it lacks sensitivity. Studies have shown that the extent of early CT changes noted on initial CT images in the hyperacute stage correlates to poor outcome and increased likelihood of hemorrhage after administration of thrombolytics (52–54). Although plain CT imaging is rapid and timely for acute stroke, it does not accurately delineate the severity of tissue irreversibly compromised in relationship to the tissue at risk. This information is vital to deciding on patients who may benefit from acute stroke interventions. The average time to obtain a CT, CT angiogram (CTA), and xenon-CT in the emergency room in one study was 44 minutes (55). This study was conducted prior to the advent of ultrafast helical CT scanners. In our experience with ultrafast helical CT technology, images can be obtained and processed in under 30 minutes. Adding a xenon-CT-CBF study to a standard head CT protocol requires roughly 15 minutes (4.5 minutes for inhalation of xenon and 10 minutes for computer calculations) (56). Though this appears to be lengthy, it is likely shorter than MRI sequences that include transportation out of the ER, clearance of patients for metal objects, acquisition and interpretation of images, and transportation back to the ER for therapeutic intervention.

XENON-COMPUTED TOMOGRAPHY-CEREBRAL BLOOD FLOW–BASED ASSESSMENT OF CORE, PENUMBRA, AND OLIGEMIA AND SELECTION OF PATIENTS FOR ACUTE STROKE THERAPY

Clinical trials studying thrombolytic therapy for ischemic stroke have focused on chronology-based therapy usually in heterogeneous groups of stroke patients with respect to vascular occlusion site (5,6,57). More recently, it has been noted that a significant proportion of patients with unknown time of onset (wake up strokes) do not have pathophysiological characteristics much different from those who present within a six-hour time window (58). When patients are selected for acute stroke therapy based on these pathophysiological characteristics (MRI-based PWI–DWI mismatch), benefit from thrombolysis has been shown within a greatly extended therapeutic window (14). Time-based selection of patients has been proven to be beneficial very early after onset of symptoms, when the majority of patients have a favorable pathophysiological constellation and more sophisticated imaging tests may not be justified. The next step is to identify patients beyond this ultra-early window that may benefit from revascularization or neuroprotective therapies.

In a retrospective case series from our institution, Iacob et al. reported that out of 184 consecutive patients with acute ischemic stroke, 45 patients (24%) had evidence of persistent large vessel occlusion (ICA, MCA, or tandem lesions). Of these 45 patients, 14 (31%) experienced significant clinical progression evidenced by an increase in their National Institutes of Health Stroke Scale (NIHSS) by four points, in a delayed fashion beyond 24 hours from symptoms onset. The other 31 patients had a more rapid course of neurological deterioration without clinical fluctuation. On presentation, all patients with a delayed deterioration had evidence of large areas of hypoperfusion on perfusion imaging studies, far exceeding the areas of infarction. Clinical deterioration was paralleled by imaging evidence of stroke progression (347.2% increase in infarct volume at 48–96 hours compared with infarct volume 24 hours postadmission). This study indicates that a significant proportion of patients with large vessel occlusion have large penumbral areas upon presentation. Moreover, as high as one-third of these patients experience growth of core slowly over days rather than rapidly over hours (59).

These patients may be the prime targets for revascularization therapy within time frames that greatly exceed currently used time windows.

The value of xenon-CT-CBF in identifying these patients was demonstrated by Kilpatrick et al. (55) who studied 51 patients with acute ischemic stroke who underwent a CT/CTA and xenon-CT-CBF study on admission. This study showed that patients with occluded vessels and CBFs in the penumbral range were highly likely to have a new infarct on a subsequent CT scan. Conversely, if a patient had a patent vessel and/or normal CBF values, the likelihood of a new infarct on subsequent head CTs was low.

Jovin et al. (13) performed assessment of core and penumbra within time frames currently used for thrombolytic therapy in a retrospective case series of 36 patients with proven MCA occlusion who were studied with xenon-CT-CBF within six hours of symptoms onset. Twenty-three of these patients underwent intra-arterial thrombolysis, making possible an accurate determination of recanalization status at two hours. The cortical core and penumbra were assessed based on previously established perfusion thresholds using a voxel-based method. The methodology used for assessment of core and penumbra was as follows: CT images of 1 cm slice thickness were obtained along the orbito-meatal line at four levels with 5 mm separation, the lowest level being at the level of the basal ganglia. The CBF data obtained were analyzed with the commercially provided software (Diversified Diagnostic Products Inc., Houston, Texas, U.S.A.). The analysis included all four levels and was limited to the cortical MCA territory ipsilateral to the occlusion site. Contralateral cortical MCA territories were used as controls. Anatomical templates that are part of the xenon-CT computer software determined the outer 2 cm of the cortical MCA territory consisting of an average mix of 1:1 gray and white matter. The mean cortical MCA territory flow for each level was calculated and displayed by the standard computer software. The overall mean MCA CBF (ipsilateral and contralateral) was calculated by averaging the MCA CBF from all four levels. The xenon-CT computer software divided the outer 2 cm of the entire cortex on each of the four brain slices into 20 ROIs and computed the average CBF values for each of these ROIs. Six adjacent ROIs comprise the cortical MCA territory on one side and on one brain slice, such that the entire MCA territory on one side is composed of 24 ROIs.

Voxels of size 1 × 1 × 10 mm corresponding to a CBF range of 0 to 8 mL/100 g/min were separated out of each level and counted by the computer software in both the ipsilateral and the contralateral MCA territory. Areas of lack of flow due to prominent cortical sulci were not excluded from analysis. For each side, the voxels corresponding to this flow range in all four levels were summated to yield a value representing the total number of voxels in the 0 to 8 mL/100 g/min range. This number was then divided by the sum of voxels corresponding to the entire (i.e., not separated by flow thresholds) MCA territory in the same four levels and expressed as percentage of ischemic core to the MCA territory. In a similar fashion, the number of voxels in the MCA territory corresponding to a CBF range of 8 to 20 mL/100 g/min were summated and divided by the total number of voxels for the MCA territory, to yield percentage penumbra. Voxels corresponding to CBF range greater than 20 mL/100 g/min were expressed as noncore/nonpenumbra (NC/NP).

To validate the voxel-based approach, percentage core, penumbra, and NC/NP for ipsilateral and contralateral MCA territory were obtained by dividing the number of ROIs with a mean CBF of <8 mL/100 g/min, 8 to 20 mL/100 g/min, and >20 mL/100 g/min, respectively, by 24 (the total number of ROI corresponding to the MCA territory on each side). These values were correlated to the percentages of core, penumbra, and NC/NP obtained through voxel-based analysis, and an excellent correlation was found, which validated the voxel-based analysis.

This study found that penumbra was present in all patients studied and was relatively constant in size, comprising approximately 30% of the cortical MCA territory. In contrast, the core was highly variable ranging from 7% to 70 % cortical MCA territory. Despite similar penumbral volumes, patients with small core were more likely to have a favorable outcome than patients with large core. Interestingly, this applied both to patients who recanalized at two hours and to those who did not recanalize. It, thus, appears that whereas significant penumbral volumes are present in the majority of patients presenting with MCA occlusion within six hours from symptoms onset, patients who are unlikely to benefit from revascularization therapy are those with large core volumes. In those patients, the theoretical benefit derived from preventing

penumbral volumes from undergoing infarction through revascularization is offset by the detrimental effect of reperfusing large areas of "dead" brain. Based on their findings, the authors of this study concluded that in patients with proven proximal MCA occlusion and seen within six hours of onset, the extent of core and not that of penumbra should primarily guide revascularization therapy in patients with acute stroke. These findings are validated by several other studies. Hill et al. (60) reported that the ASPECT score on plain CT is correlated to response to intra-arterial thrombolysis in the PROACT II trial. The ASPECT score quantifies the degree of early ischemic changes on head CT, based on a 10-point scale (54). Since early ischemic changes were found to be highly correlated with regional CBF and thus the extent of core (13), the findings of Hill et al. provide indirect support to the concept that the extent of ischemic core drives outcomes in acute stroke. Similarly, Lev et al. (61) found that in patients with acute stroke, the extent of diminished cerebral blood volume on perfusion studies (thought to represent irreversible ischemia) determines outcome in stroke.

In agreement with studies using different imaging methods to assess contralateral CBF (62–64), the findings of Jovin et al. suggest that in acute MCA occlusion, CBF is frequently diminished in the contralateral MCA territory with significant contralateral cortical areas perfused at penumbra thresholds (mean MCA CBF ipsilateral vs. contralateral 17.3 mg/100 mL/min vs. 37.4 mg/100 mL/min, $P < 0.00001$ and mean ipsilateral vs. contralateral % penumbra l flow range: 32.1% vs. 21.3%, $P = 0.0002$; areas with dilated cortical sulci not excluded). The reasons for the observed depression in contralateral CBF (diaschisis) are poorly understood. They may be related to depressed metabolic demands in the contralateral hemisphere resulting in secondarily reduced blood flow values. Nevertheless, the implications for these findings are that the assessment of regional perfusion in the ipsilateral hemisphere based on the false assumption that contralateral CBF is normal, as is the case with most qualitative cerebral perfusion assessment techniques, may be subject to inherent methodological bias and may lead to inaccurate assessment of cerebral perfusion.

Patients undergoing stroke intervention with large areas of ischemic core tissue are at a higher risk of hemorrhage and cerebral edema. Patients with mean CBFs in the ipsilateral MCA territory in the 9 to 13 mL/100 g/min range are at a significantly higher risk of developing symptomatic hemorrhage and malignant edema (65,66). In a small series of 23 patients with MCA occlusion who were studied with xenon-CT-CBF prior to undergoing intra-arterial thrombolysis, hemorrhage was significantly more common in those with a higher percentage of the core, whereas the extent of penumbra was not associated with the risk of intracerebral hemorrhage or malignant edema (13). In this series, among the 13 patients who recanalized, those with hemorrhage had twice the volume of ischemic core in comparison to patients without hemorrhage ($40 \pm 20\%$ vs. $20 \pm 11\%$, $P = 0.0023$). Determining the extent of core beyond which reperfusion becomes detrimental or futile has not been accomplished and constitutes a major challenge for the future of acute stroke therapy.

Appropriate selection of patients for reperfusion therapy not only implies excluding from treatment patients who will not benefit from recanalization due to large areas of irreversible ischemia. The other important feature is exclusion from aggressive and potentially high-risk therapies of those patients who will have a favorable clinical outcome without interventions. Defining the CBF values that will have a benign natural history aids in this endeavor. Firlik et al. (67) showed that xenon-CT may help to predict a subgroup of patients who will show neurological improvement when studied within eight hours of stroke onset. Of the 53 patients studied, eight (15%) improved to normal within 24 hours. The mean CBFs of these eight patients was 35 mL/100 g/min versus 17 mL/100 g/min in patients who continued to decline. Thus, patients with CBFs greater than 30 mL/100 g/min may not require interventions. This has been corroborated with BTO studies performed prior to sacrifice of the ICA as discussed earlier.

On the basis of these data, one may hypothesize that patients with large vessel occlusion in the anterior circulation (MCA/ICA) should be revascularized regardless of the time from symptoms onset if no or little hypodensity is present on CT (ASPECTS >7) and if CBF values are higher than 15 mL/100 g/min (to minimize the risk of hemorrhage and edema) and lower than 30 mL/100 g/min (CBF values higher than this portend an excellent prognosis without any aggressive therapies).

CONCLUSIONS

Acute stroke therapy is rapidly evolving with emphasis placed on optimal patient selection based on pathophysiology rather than on time, resulting in extended time windows that allow treatment of an increasing number of acute stroke patients. As physiology-based imaging modalities are more commonly utilized for patient selection, it has become evident that rigid time windows are not applicable to individual patients. Xenon-CT has an important role in acute stroke therapeutic interventions, as it is quantitative, reproducible, and can safely be obtained within a relevant time window. Given its ability to accurately assess penumbra, core, and oligemia in patients with acute stroke due to large vessel occlusion, it can provide valuable physiological data that can optimize patient selection and aid in acute stroke management.

REFERENCES

1. Albers GW. Expanding the window for thrombolytic therapy in acute stroke. The potential role of acute MRI for patient selection. Stroke 1999; 30:2230–2237.
2. Baron JC, von Kummer R, del Zoppo GJ. Treatment of acute ischemic stroke. Challenging the concept of a rigid and universal time window. Stroke 1995; 26:2219–2221.
3. Donnan GA, Howells DW, Markus R, Toni D, Davis SM. Can the time window for administration of thrombolytics in stroke be increased? CNS Drugs 2003; 17:995–1011.
4. DeGraba TJ, Pettigrew LC. Why do neuroprotective drugs work in animals but not humans? Neurol Clin 2000; 18:475–493.
5. The National Institute of Neurological Disorders and Stroke rt-PA Stroke Study Group. Tissue plasminogen activator for acute ischemic stroke. N Engl J Med 1995; 333:1581–1587.
6. Multicentre Acute Stroke Trial--Italy (MAST-I) Group. Randomised controlled trial of streptokinase, aspirin, and combination of both in treatment of acute ischaemic stroke. Lancet 1995; 346:1509–1514.
7. The Multicenter Acute Stroke Trial--Europe Study Group. Thrombolytic therapy with streptokinase in acute ischemic stroke. N Engl J Med 1996; 335:145–150.
8. Clark WM, Wissman S, Albers GW, Jhamandas JH, Madden KP, Hamilton S. Recombinant tissue-type plasminogen activator (Alteplase) for ischemic stroke 3 to 5 hours after symptom onset. The ATLANTIS Study: a randomized controlled trial. Alteplase Thrombolysis for Acute Noninterventional Therapy in Ischemic Stroke. JAMA 1999; 282:2019–2026.
9. Clark WM, Albers GW, Madden KP, Hamilton S. The rtPA (alteplase) 0- to 6-hour acute stroke trial, part A (A0276g): results of a double-blind, placebo-controlled, multicenter study. Thromblytic therapy in acute ischemic stroke study investigators. Stroke 2000; 31:811–816.
10. Donnan GA, Davis SM, Chambers BR, et al. Streptokinase for acute ischemic stroke with relationship to time of administration: Australian Streptokinase (ASK) Trial Study Group. JAMA 1996; 276:961–966.
11. Hacke W, Donnan G, Fieschi C, et al. Association of outcome with early stroke treatment: pooled analysis of ATLANTIS, ECASS, and NINDS rt-PA stroke trials. Lancet 2004; 363:768–774.
12. von Kummer R. The time concept in ischemic stroke: misleading. Stroke 2000; 31:2523–2525.
13. Jovin TG, Yonas H, Gebel JM, et al. The cortical ischemic core and not the consistently present penumbra is a determinant of clinical outcome in acute middle cerebral artery occlusion. Stroke 2003; 34:2426–2433.
14. Hacke W, Albers G, Al-Rawi Y, et al. The Desmoteplase in Acute Ischemic Stroke Trial (DIAS): a phase II MRI-based 9-hour window acute stroke thrombolysis trial with intravenous desmoteplase. Stroke 2005; 36:66–73.
15. Hjort N, Butcher K, Davis SM, et al. Magnetic resonance imaging criteria for thrombolysis in acute cerebral infarct. Stroke 2005; 36:388–397.
16. Marx JJ, Thoemke F, Mika-Gruettner A, et al. Diffusion-weighted MRT in vertebrobasilar ischemia. Application, sensitivity, and prognostic value. Nervenarzt 2004; 75:341–346.
17. Guadagno JV, Warburton EA, Jones PS, et al. The diffusion-weighted lesion in acute stroke: heterogeneous patterns of flow/metabolism uncoupling as assessed by quantitative positron emission tomography. Cerebrovasc Dis 2005; 19:239–246.
18. Kajimoto K, Moriwaki H, Yamada N, et al. Cerebral hemodynamic evaluation using perfusion-weighted magnetic resonance imaging: comparison with positron emission tomography values in chronic occlusive carotid disease. Stroke 2003; 34:1662–1666.
19. Sobesky J, Zaro Weber O, Lehnhardt FG, et al. Does the mismatch match the penumbra? Magnetic resonance imaging and positron emission tomography in early ischemic stroke. Stroke 2005; 36:980–985.
20. Kang DW, Chalela JA, Dunn W, Warach S. MRI screening before standard tissue plasminogen activator therapy is feasible and safe. Stroke 2005; 36:1939–1943.
21. Eastwood JD, Lev MH, Wintermark M, et al. Correlation of early dynamic CT perfusion imaging with whole-brain MR diffusion and perfusion imaging in acute hemispheric stroke. AJNR Am J Neuroradiol 2003; 24:1869–1875.

22. Baron JC. Perfusion thresholds in human cerebral ischemia: historical perspective and therapeutic implications. Cerebrovasc Dis 2001; 11(suppl 1):2–8.
23. Jennett WB, Harper AM, Gillespie FC. Measurement of regional cerebral blood-flow during carotid ligation. Lancet 1966; 2:1162–1163.
24. Boysen G. Cerebral blood flow measurement as a safeguard during carotid endarterectomy. Stroke 1971; 2:1–10.
25. Trojaborg W, Boysen G. Relation between EEG, regional cerebral blood flow and internal carotid artery pressure during carotid endarterectomy. Electroencephalogr Clin Neurophysiol 1973; 34:61–69.
26. Sundt TM Jr, Sharbrough FW, Anderson RE, Michenfelder JD. Cerebral blood flow measurements and electroencephalograms during carotid endarterectomy. J Neurosurg 1974; 41:310–320.
27. Symon L, Branston NM, Strong AJ, Hope TD. The concepts of thresholds of ischaemia in relation to brain structure and function. J Clin Pathol Suppl (R Coll Pathol) 1977; 11:149–154.
28. Jones TH, Morawetz RB, Crowell RM, et al. Thresholds of focal cerebral ischemia in awake monkeys. J Neurosurg 1981; 54:773–782.
29. Marcoux FW, Morawetz RB, Crowell RM, DeGirolami U, Halsey JH Jr. Differential regional vulnerability in transient focal cerebral ischemia. Stroke 1982; 13:339–346.
30. Astrup J, Siesjo BK, Symon L. Thresholds in cerebral ischemia - the ischemic penumbra. Stroke 1981; 12:723–725.
31. Marchal G, Beaudouin V, Rioux P, et al. Prolonged persistence of substantial volumes of potentially viable brain tissue after stroke: a correlative PET-CT study with voxel-based data analysis. Stroke 1996; 27:599–606.
32. Marchal G, Benali K, Iglesias S, Viader F, Derlon JM, Baron JC. Voxel-based mapping of irreversible ischaemic damage with PET in acute stroke. Brain 1999; 122(Pt 12):2387–2400.
33. Furlan M, Marchal G, Viader F, Derlon JM, Baron JC. Spontaneous neurological recovery after stroke and the fate of the ischemic penumbra. Ann Neurol 1996; 40:216–226.
34. Heiss WD, Kracht LW, Thiel A, Grond M, Pawlik G. Penumbral probability thresholds of cortical flumazenil binding and blood flow predicting tissue outcome in patients with cerebral ischaemia. Brain 2001; 124:20–29.
35. Heiss WD. Ischemic penumbra: evidence from functional imaging in man. J Cereb Blood Flow Metab 2000; 20:1276–1293.
36. Raichle ME. The pathophysiology of brain ischemia and infarction. Clin Neurosurg 1982; 29:379–389.
37. Ginsberg MD. Adventures in the pathophysiology of brain ischemia: penumbra, gene expression, neuroprotection: the 2002 Thomas Willis Lecture. Stroke 2003; 34:214–223.
38. Christou I, Alexandrov AV, Burgin WS, et al. Timing of recanalization after tissue plasminogen activator therapy determined by transcranial doppler correlates with clinical recovery from ischemic stroke. Stroke 2000; 31:1812–1816.
39. Jovin TG, Yonas H, Hammer MD, Wechsler L, Shchelshkov E, Gebel JM. Extracranial-intracranial bypass for evolving cerebral ischemia in patients selected by neuroimaging: a novel indication for an old operation. J Neurosurg 2004; 100:A192.
40. Read SJ, Hirano T, Abbott DF, et al. The fate of hypoxic tissue on 18F–fluoromisonidazole positron emission tomography after ischemic stroke. Ann Neurol 2000; 48:228–235.
41. Linskey ME, Jungreis CA, Yonas H, et al. Stroke risk after abrupt internal carotid artery sacrifice: accuracy of preoperative assessment with balloon test occlusion and stable xenon-enhanced CT. AJNR Am J Neuroradiol 1994; 15:829–843.
42. Mathis JM, Barr JD, Jungreis CA, et al. Temporary balloon test occlusion of the internal carotid artery: experience in 500 cases. AJNR Am J Neuroradiol 1995; 16:749–754.
43. Marshall RS, Lazar RM, Young WL, et al. Clinical utility of quantitative cerebral blood flow measurements during internal carotid artery test occlusions. Neurosurgery 2002; 50:996–1004; discussion 1004–1005.
44. Jovin TG, Grahovac SZ, Kanal E, Yonas H, Gebel JM, Wechsler L. Early ischemic changes on head CT in acute stroke: predictive value for infarction and correlation with regional cerebral blood flow. Stroke 2003; 34:254.
45. Lassen NA, Ingvar DH. Radioisotopic assessment of regional cerebral blood flow. Prog Nucl Med 1972; 1:376–409.
46. Austin G, Horn N, Rouhe S, Hayward W. Description and early results of an intravenous radioisotope technique for measuring regional cerebral blood flow in man. Eur Neurol 1972; 8:43–51.
47. Gur D, Good WF, Wolfson SK Jr, Yonas H, Shabason L. In vivo mapping of local cerebral blood flow by xenon-enhanced computed tomography. Science 1982; 215:1267–1268.
48. Latchaw RE, Yonas H, Hunter GJ, et al. Guidelines and recommendations for perfusion imaging in cerebral ischemia: a scientific statement for healthcare professionals by the writing group on perfusion imaging, from the Council on Cardiovascular Radiology of the American Heart Association. Stroke 2003; 34:1084–1104.
49. Yonas H, Darby JM, Marks EC, Durham SR, Maxwell C. CBF measured by Xe-CT: approach to analysis and normal values. J Cereb Blood Flow Metab 1991; 11:716–725.
50. Shaw TG, Mortel KF, Meyer JS, Rogers RL, Hardenberg J, Cutaia MM. Cerebral blood flow changes in benign aging and cerebrovascular disease. Neurology 1984; 34:855–862.

51. Latchaw RE, Yonas H, Pentheny SL, Gur D. Adverse reactions to xenon-enhanced CT cerebral blood flow determination. Radiology 1987; 163:251–254.
52. von Kummer R, Allen KL, Holle R, et al. Acute stroke: usefulness of early CT findings before thrombolytic therapy. Radiology 1997; 205:327–333.
53. Larrue V, von Kummer R, del Zoppo G, Bluhmki E. Hemorrhagic transformation in acute ischemic stroke. Potential contributing factors in the European Cooperative Acute Stroke Study. Stroke 1997; 28:957–960.
54. Barber PA, Demchuk AM, Zhang J, Buchan AM. Validity and reliability of a quantitative computed tomography score in predicting outcome of hyperacute stroke before thrombolytic therapy. ASPECTS Study Group. Alberta Stroke Programme Early CT Score. Lancet 2000; 355:1670–1674.
55. Kilpatrick MM, Yonas H, Goldstein S, et al. CT-based assessment of acute stroke: CT, CT angiography, and xenon-enhanced CT cerebral blood flow. Stroke 2001; 32:2543–2549.
56. Firlik AD, Kaufmann AM, Wechsler LR, Firlik KS, Fukui MB, Yonas H. Quantitative cerebral blood flow determinations in acute ischemic stroke. Relationship to computed tomography and angiography. Stroke 1997; 28:2208–2213.
57. Hacke W, Kaste M, Fieschi C, et al. Randomised double-blind placebo-controlled trial of thrombolytic therapy with intravenous alteplase in acute ischaemic stroke (ECASS II). Second European-Australasian Acute Stroke Study Investigators. Lancet 1998; 352:1245–1251.
58. Fink JN, Kumar S, Horkan C, et al. The stroke patient who woke up: clinical and radiological features, including diffusion and perfusion MRI. Stroke 2002; 33:988–993.
59. Iacob T, Jovin TG, Mendez OE, et al. Gradual neurological deterioration due to slow progression of cerebral ischemia is prevalent in stroke due to large vessel occlusion. Stroke 2004; (35):339.
60. Hill MD, Rowley HA, Adler F, et al. Selection of acute ischemic stroke patients for intra-arterial thrombolysis with pro-urokinase by using ASPECTS. Stroke 2003; 34:1925–1931.
61. Lev MH, Segal AZ, Farkas J, et al. Utility of perfusion-weighted CT imaging in acute middle cerebral artery stroke treated with intra-arterial thrombolysis: prediction of final infarct volume and clinical outcome. Stroke 2001; 32:2021–2028.
62. Lagreze HL, Levine RL, Pedula KL, Nickles RJ, Sunderland JS, Rowe BR. Contralateral flow reduction in unilateral stroke: evidence for transhemispheric diaschisis. Stroke 1987; 18:882–886.
63. Slater R, Reivich M, Goldberg H, Banka R, Greenberg J. Diaschisis with cerebral infarction. Stroke 1977; 8:684–690.
64. Lavy S, Melamed E, Portnoy Z. The effect of cerebral infarction on the regional cerebral blood flow of the contralateral hemisphere. Stroke 1975; 6:160–163.
65. Firlik AD, Yonas H, Kaufmann AM, et al. Relationship between cerebral blood flow and the development of swelling and life-threatening herniation in acute ischemic stroke. J Neurosurg 1998; 89:243–249.
66. Goldstein S, Yonas H, Gebel JM. Acute cerebral blood flow as a predictive physiologic marker for symptomatic hemorrhagic conversion and clinical herniation after thrombolytic therapy. Stroke 2000; 31(1):275.
67. Firlik AD, Rubin G, Yonas H, Wechsler LR. Relation between cerebral blood flow and neurologic deficit resolution in acute ischemic stroke. Neurology 1998; 51:177–182.

16 Magnetic Resonance Imaging of Ischemic Penumbra: New Techniques

16a. Gradient Echo

Jun Hatazawa
Department of Nuclear Medicine and Tracer Kinetics, Osaka University Graduate School of Medicine, Suita, Osaka, Japan

Eku Shimosegawa
Department of Radiology and Nuclear Medicine, Akita Research Institute of Brain and Blood Vessels, Akita, Japan

INTRODUCTION

Misery perfusion is a pathological condition that exists in ischemic brain with reduced cerebral blood flow (CBF) but a relatively preserved cerebral metabolic rate of oxygen ($CMRO_2$) (1). It is found in patients with chronic steno-occlusive carotid or cerebral arteries (1) and in patients with acute ischemic stroke (2) and has been defined as an elevated cerebral oxygen extraction fraction (OEF) observed by positron emission tomography (PET). Ischemic penumbra was originally defined as an area of ischemic brain that was functionally inactive but viable (3) and that overlapped an area of misery perfusion. An increased OEF leads to an increased blood deoxyhemoglobin concentration in cerebral capillaries and veins. Deoxyhemoglobin is a paramagnetic substance that can be detected by T2* signal changes during gradient echo magnetic resonance (MR) imaging (4).

MAGNETIC RESONANCE IMAGING WITH GRADIENT ECHO PULSE SEQUENCES

In classic spin-echo pulse sequences (5), a 90° radiofrequency (RF) pulse is first given to produce transverse magnetization and then a 180° pulse is given to reverses the direction of all transverse magnetization and form a signal echo. Although the directions of the magnetic dipoles have changed, the directions of the local magnetic inhomogeneities have not. Therefore, the transverse relaxation measured in spin-echo sequences is due entirely to true T2 relaxation effects.

Gradient-echo (or field-echo) MR imaging was introduced by Frahm and coworkers in 1985 (6). This imaging technique utilizes a reversal of the frequency-encoding gradient to rephase the relaxation of the transverse magnetization. The formation of a signal echo by gradient reversal does not eliminate the dephasing effects of magnetic field inhomogeneities. Therefore, the signal decay in gradient-echo MR imaging depends on true T2 relaxation plus the relaxation caused by the magnetic field inhomogeneities. The transverse magnetization decay is represented by T2*, which is defined as follows:

$$1/T2^* = 1/T2 + \gamma\pi\Delta B_0,$$

where γ is the gyromagnetic ratio and ΔB_0 is the magnetic field inhomogeneity across a voxel. Gradient-echo MR produces larger signal changes than spin-echo MR because this technique is highly sensitive to both intravascular and extravascular susceptibility effects. However, changes in T2* are difficult to quantify because of the complexity of the ΔB_0 component (7,8).

T2* AND DEOXYHEMOGLOBIN

Because deoxyhemoglobin is paramagnetic and oxyhemoglobin is diamagnetic, changes in hemoglobin oxygenation levels affect local magnetic field homogeneity. This is called the blood

oxygenation level-dependent (BOLD) phenomenon (3). In ischemic brain tissues, the deoxyhemoglobin concentration is increased because of the large OEF of the arterial blood supply. The T2 and T2* relaxation times decrease as the deoxyhemoglobin concentration increases because of the increased presence of magnetic field inhomogeneities. Spin-echo MR is most sensitive to objects with a size of 5 to 10 μm. This scale is on the order of capillary and red blood cells. The spin-echo-based BOLD effect is related to the fraction of deoxyhemoglobin inside erythrocytes, resulting in a quantitative relationship between blood oxygenation and T2. However, the T2 signal changes are small. In contrast, gradient-echo MR is sensitive to structures larger than 20 μm, such as venules and veins. By comparing T2 and T2*, we can characterize the source of the vascular response: when T2* < T2, the signal originates predominantly from the veins; but when T2* = T2, the signal originates from the capillary level (8).

T2* SIGNAL REDUCTION IN AN EXPERIMENTAL MODEL FOR BRAIN ISCHEMIA

In several experimental studies, T2*-sensitive MR imaging showed a rapid reduction in signal intensity in ischemic brain. De Crespigny et al. (9) used a 2 T MR scanner and demonstrated a rapid loss of the T2* signal from ischemic brain after inflating a balloon to occlude the middle cerebral artery in cats. On reperfusion after 2.5 minutes of occlusion, an immediate T2* signal intensity overshoot was observed, possibly representing an increase in the delivery of oxygenated blood. These observations indicate that gradient-echo MR can detect luxury perfusion after reperfusion in ischemic brain tissues. Roussel et al. (10) studied the T2* signal intensity in relation to water diffusion abnormalities in ischemic rat brains using a 2.35 T scanner. Upon occlusion, the intensity of the T2* signal decreased beyond that of the diffusion abnormality. In the core area of the abnormal diffusion, the intensity of the T2* signal returned toward its baseline level after one to two hours of occlusion; however, it remained depressed in the surrounding area. Dijkhuizen et al. (11) performed gradient-echo MR using a 4.5 T scanner in rats subjected to a 60-second period of anoxia. Anoxia reduced the intensity of the T2* signal because of the inflow of deoxygenated blood. Their study demonstrated that the balance between deoxyhemoglobin and oxyhemoglobin can be sensitively detected using gradient-echo MR.

T2* SIGNAL REDUCTION IN ISCHEMIC STROKE PATIENTS

Experimental studies using gradient-echo MR at a magnetic field strength of 2 T or more have indicated that the T2* signal change is a potential alternative marker for detecting misery perfusion. Although PET techniques using $^{15}O_2$, $H_2{}^{15}O$, or $C^{15}O$ have been used to detect misery perfusion in ischemic stroke patients, these methods are not feasible in clinical settings. The detection of misery perfusion using gradient-echo MR combined with perfusion and diffusion MR is very promising for the diagnosis and treatment of stroke patients.

Tamura et al. (12) studied T2* signal changes during gradient-echo echo-planar MR in patients with acute ischemic stroke. They performed dynamic susceptibility contrast-enhanced MR (DSC-MR) within four hours of onset in six patients with unilateral cerebral artery occlusions. T2*-weighted images taken before the arrival of the contrast medium showed hypointense areas in the territory of the occluded cerebral arteries. Brain lesions with these hypointense T2* signals became infarcted in five of the six patients. One patient showed a hypointense T2* signal in the territory of an occluded region of the left middle cerebral artery at 1.7 hours of onset. An MR examination performed on day 3 of hospitalization showed the recanalization of the occluded artery and a normal T2* signal. No signs of infarction were found in this patient. Therefore, T2* hypointensities may be reversible if perfusion is restored within a certain time period. DSC-MR signals observed before the arrival of the contrast medium in the brain may be valuable for identifying areas of misery perfusion that could be previously detected using only PET. Figure 1A shows a precontrast DSC-MR image taken in a patient with an acute embolic occlusion of the left middle cerebral artery (1.7 hours after onset). Compared with the right hemisphere, the reduction in the intensity of the T2* signal is evident (indicated by the arrow). This lesion progressed to a complete infarction (Fig. 1B).

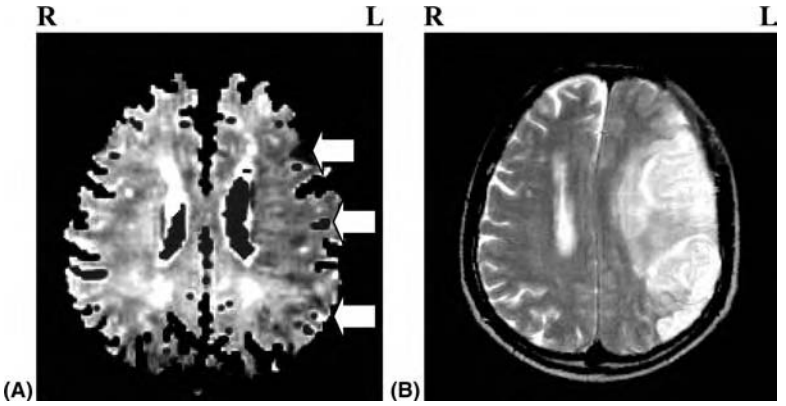

FIGURE 1 T2*MR image (**A**) 1.5 hours after onset and follow-up T2 weighted image (**B**) 3 days after onset in patient with an acute embolic occlusion of the left middle cerebral artery.

Hypointensities appearing on gradient-echo MR images should be further analyzed with regard to the mismatch between perfusion and diffusion in combined MR studies. The magnitude of the T2* signal change is relative and is not yet usable as a quantifiable index of oxygen extraction. The relevance of T2* signal changes should be further examined and compared with the results of PET studies.

REFERENCES

1. Baron JC, Bousser MG, Rey A, Guillard A, Comar A, Castaigne P. Reversal of focal "misery perfusion syndrome" by extra-intracranial arterial bypass in hemodynamic cerebral ischemia: a case study with ^{15}O positron emission tomography. Stroke 1981; 12:454–459.
2. Shimosegawa E, Hatazawa J, Ibaraki M, Toyoshima H, Suzuki A. Metabolic penumbra of acute brain infarction: a correlation with infarct growth. Ann Neurol 2005; 57:495–504.
3. Astrup J, Siesjo BK, Symon L. Thresholds in cerebral ischemia-the ischemic penumbra. Stroke 1981; 12:723–725.
4. Ogawa S, Lee TM, Nayak AS, Glynn P. Oxygenation-sensitive contrast in magnetic resonance imaging of rodent brain at high magnetic fields. Magn Reson Med 1990; 14:68–78.
5. Hahn EL. Spin echoes. Phys Rev 1950; 80:580–594.
6. Hasse A, Frahm J, Matthaei D, et al. FLASH imaging: rapid NMR imaging using low flip angle pulses. J Magn Reson 1986; 67:217.
7. Hendrick RE, Raff U. Image contrast and noise. In: Stark DD, Bradley WG, eds. Magnetic Resonance Imaging. 2nd Ed. St. Louis: Mosby-Year Book, 1992:109–144.
8. Kennan RP. Gradient echo and spin echo methods for functional MRI. In: Moonen CT, Bandettini PA, eds. Functional MRI. Berlin: Springer 1999:127–1368.
9. De Crespigny AJ, Wendland MF, Derugin N, Kozniewska E, Moseley ME. Real time observation of transient focal ischemia and hyperemia in cat brain. Magn Reson Med 1992; 27:391–397.
10. Roussel SA, van Bruggen N, King MD, Gardian DG. Identification of collaterally perfused areas following focal cerebral ischemia in the rat by comparison of gradient echo and diffusion-weighted MRI. J Cereb Blood Flow Metab 1995; 15:578–586.
11. Dijkhuizen RM, van der Sprenkel JWB, Tulleken KAF, Nicolay K. Regional assessment of tissue oxygenation and the temporal evalution of hemodynamic parameters and water diffusion during acute focal ischemia in rat brain. Brain Res 1997; 750:161–170.
12. Tamura H, Hatazawa J, Toyoshima H, Shimosegawa E, Okudera T. Detection of deoxygenation-related signal chonage in acute ischemic stroke by T2*-weighted magnetic resonance imaging. Stroke 2002; 33:967–971.

16b. "Penumbra" Defined by Magnetic Resonance Imaging: Oxygen Extraction Fraction and Cerebral Metabolic Rate of Oxygen Utilization

Weili Lin and Hongyu An
Department of Radiology, University of North Carolina at Chapel Hill, Chapel Hill, North Carolina, U.S.A.

Yang Wu
Department of Biomedical Engineering, University of North Carolina at Chapel Hill, Chapel Hill, North Carolina, U.S.A.

Quan Zhu
Department of Electrical and Computer Engineering, Duke University, Durham, North Carolina, U.S.A.

Katie Vo
Mallinckrodt Institute of Radiology, Washington University School of Medicine, St. Louis, Missouri, U.S.A.

Jin-Moo Lee
Department of Neurology, Washington University School of Medicine, St. Louis, Missouri, U.S.A.

Chung Y. Hsu
Department of Neurology, Washington University School of Medicine, St. Louis, Missouri, U.S.A., and Dr. Chi-Chin Huang Stroke Research Center, Taipei Medical University, Taipei, Taiwan

INTRODUCTION

Extensive efforts have been devoted to develop means to better identify those stroke patients with a salvageable "ischemic penumbra" beyond the three-hour window that may benefit from tissue plasminogen activator (tPA) therapy. This chapter focuses on advances in magnetic resonance imaging (MRI) that may assist in delineating the penumbra that is amenable to therapeutic interventions including thrombolytic therapy with tPA, particularly some of the recently proposed MR approaches for delineating tissue viability based on measurement of cerebral blood flow (CBF), oxygen extraction fraction (OEF), and cerebral metabolic rate of oxygen utilization ($CMRO_2$).

BACKGROUND

One of the major advantages associated with positron emission tomography (PET) is its ability to obtain quantitative measures of physiological parameters that are highly relevant to ischemia-induced alterations of cerebral hemodynamics. Therefore, PET could potentially be one of the most powerful means to determine tissue viability; it is capable of measuring CBF, OEF, and more importantly cerebral metabolic rate of oxygen utilization ($CMRO_2$). For instance, in sequential PET measurements performed during middle cerebral artery occlusion (MCAO) (two hours) and 12 to 24 hours of reperfusion in a primate model, Frykholm et al. (1) reported an elevation in OEF accompanied by a reduction in CBF during the acute phase, followed by a return of OEF to baseline values if blood flow was not restored. In contrast, $CMRO_2$ exhibited a more stable pattern and demonstrated a time-course consistent with a shrinking penumbra. Similar results were also observed by Giffard et al. (2) who demonstrated that a prolonged MCA occlusion (20 hours) in primates resulted in the previously shown biphasic reponse of OEF. Giffard et al. (2) further demonstrated that $CMRO_2$ remained stable in regions that did not progress to infarction, whereas a reduction in $CMRO_2$ was observed in regions evolving to infarction. Their findings underscore the potential utility of $CMRO_2$ as a biomarker for delineating infarct from viable tissues (i.e., penumbra).

Given the evidence mentioned earlier demonstrating that a severe decline in $CMRO_2$ may be indicative of irreversible injury, several groups have since attempted to determine a $CMRO_2$ threshold that accurately delineates infarction from viable tissues (1,3–7). With the exception of our study (7), all of the studies to date have employed PET to determine $CMRO_2$ threshold for irreversible ischemic injury. Frykholm et al. (1) reported that ischemic penumbra exhibited OEF > 125% and $CMRO_2$ > 45%, whereas ischemic core demonstrated $CMRO_2$ < 45% of that in the contralateral hemisphere. Similarly, using a model of transient MCA occlusion in anesthetized baboons, Touzani et al. (4) concluded that when $CMRO_2$ fell below 40% of that of the contralateral hemisphere in the acute setting, the tissue eventually became infarcted. In a human study, Powers et al. (3) employed PET for regional measurements of CBF and $CMRO_2$ in 50 patients with varying degrees of cerebral ischemia and established a minimum $CMRO_2$ of 1.3 mL/100 g/min for maintaining brain viability, corresponding to 37% to 39% of the normal values (3.29–3.45 mL/100 g/min) (8).

Although PET is perhaps one of the most appropriate imaging approaches for delineating tissue viability under ischemic conditions, three major shortcomings associated with PET have substantially reduced its potential clinical utility, particularly in the acute setting. First, it is invasive—the required arterial line to obtain quantitative measures may make it difficult for patients who are candidates for tPA treatment. Second, the required onsite cyclotron further imposes limitations on the availability of PET to only a few major medical centers. Finally, an extensive effort will be needed to ensure the continued operation of a cyclotron 24 hours a day and seven days a week. Therefore, imaging approaches capable of providing physiological measures similar to PET, particularly $CMRO_2$, are greatly needed. We will specifically address the potential possibility of using a novel MRI approach for obtaining measures of $CMRO_2$ in vivo in the following section.

MAGNETIC RESONANCE-MEASURED CEREBRAL BLOOD FLOW, OXYGEN EXTRACTION FRACTION, AND CEREBRAL METABOLIC RATE OF OXYGEN UTILIZATION

In light of the limitations associated with PET and the potential confounds associated with MR diffusion-weighted imaging (DWI)/perfusion-weighted imaging (PWI) mismatch in delineating irreversibly injured from viable tissue (see elsewhere in this volume), alternative approaches are highly needed. Towards this end, we have recently developed an MRI approach capable of deriving a parameter that can potentially reveal similar physiological information as that of PET $CMRO_2$. We will refer to this MR measured physiological parameter as MR cerebral oxygen metabolism index (MR–COMI) hereafter (9–13). The MRI approach to obtain in vivo measures of MR–COMI, the validation studies of this newly developed method, and its potential clinical applications are detailed in the next section.

Magnetic Resonance–Measured Cerebral Blood Flow

In order to obtain measures of MR–COMI, two physiological parameters are needed, namely CBF and MR-derived cerebral OEF (MR–OEF). We will first discuss how CBF can be obtained, followed by the estimates of MR–OEF.

Several methods are readily available for measuring CBF using MR perfusion techniques (14–17), including the dynamic susceptibility contrast (DSC)(14) and arterial spin labeling (ASL) (15–17) methods. The former requires the injection of a contrast agent, whereas the latter is noninvasive. Since errors in the measures of CBF will propagate to the final calculation of MR–COMI, it is imperative to ensure that the estimates of CBF are as accurate as possible. In our studies, we have used the DSC approach since this method is more widely used clinically, for studies of acute stroke patients.

In order to minimize the effects of recirculation, fitting the concentration time curves to a gamma-variate function (18) has been widely employed. Although this approach has been shown to be effective, it, however, has major limitations, namely the success of this approach hinges largely on the extent to which MR signal is altered in the presence of a contrast agent and on a temporal separation between the first and subsequent passages of the contrast agent.

When normal and young volunteers are studied, these two requirements are easily fulfilled, making it straightforward to separate the first passage from the recirculation. In contrast, substantially broadened concentration curves with a reduced signal change may be present in patients with cardiovascular and/or cerebrovascular diseases. Under such condition, it can be challenging to effectively minimize recirculation. The temporal separation between the first passage and the recirculation is no longer valid where hypoperfusion occurs. We have developed an approach based on the independent component analysis (ICA) to minimize the effects of recirculation (19). ICA has been widely used to determine the underlying independent signal sources from observed data with minimal knowledge of the sources (20–25). A comparison of CBF obtained using the gamma-variate fitting (Fig. 1A) and the ICA approach (Fig. 1B) in an acute stroke patient is show in Figure 1. While similar CBF is obtained in the putative normal hemisphere between the two approaches, CBF is higher using ICA when compared with that obtained using gamma-variate fitting, underscoring the importance of minimizing the effects of recirculation in the calculation of CBF.

Measurement of Cerebral Oxygen Extraction Fraction Using Magnetic Resonance Imaging

With the advent of fast imaging techniques and the improved understanding of the biophysical basis of blood-oxygen level dependent (BOLD) contrast mechanisms (26–29), MRI now has the potential for use in studying the pathophysiology of disordered brain-oxygen metabolism. Specifically, it has been demonstrated that when the concentration of deoxyhemoglobin is increased, a decrease in T2 and T2* is anticipated, resulting in a decrease in MR signal intensity in both T2- and T2*-weighted images, and vice versa. With animal models, many investigators demonstrated that BOLD effects can be utilized to monitor the changes of oxygen saturation in vivo under pathophysiological conditions such as hypoxia (14,30–35), hyper- and hypocapnia (31,36,37), hemodilution (38), and ischemia (39,40). Figure 2 demonstrates how MR signal behaves under both experimental hypercapnia and hypoxia, respectively. The images shown in Figure 2 were acquired from a rat using a T2*-weighted sequence, which is highly sensitive to changes in deoxyhemoglobin concentration. Figure 2A shows the T2*-weighted image acquired under the baseline condition. With hypercapnia (Fig. 2B), an increase in CBF with concurrent vasodilation is anticipated, resulting in a reduction in OEF, which in turn leads to a decrease in deoxyhemoglobin concentration and an increase in MR signal (Fig. 2B). Note that the visibility of the venous vessels is markedly diminished. In contrast, under the hypoxic condition, the increased OEF leads to an increase in deoxyhemoglobin concentration. As a result, a reduction in MR signal is observed (Fig. 2C). Together, these results demonstrate that the MR BOLD contrast approach could be used to provide insights into alterations of blood oxygenation in vivo.

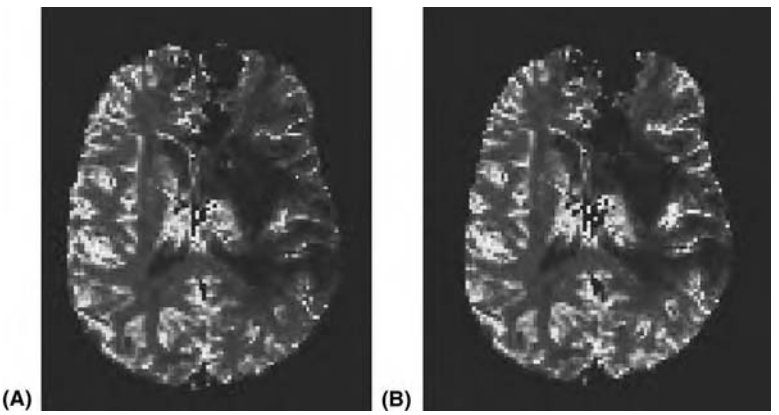

FIGURE 1 A comparison of cerebral blood flow maps obtained using the gamma-variate fitting (**A**) and the independent component analysis (**B**) approaches for minimizing the effects of recirculation is shown.

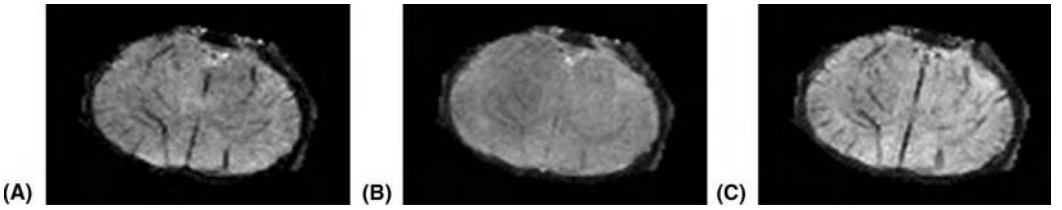

FIGURE 2 Magnetic resonance signal behaviors under baseline condition (**A**), hypercapnia (**B**), and hypoxia (**C**).

However, all of these studies only focused on relative measurements of cerebral blood oxygen saturation and little attention was given to quantitative aspects of BOLD effects. Recently, extensive efforts have been devoted to developing approaches for obtaining quantitative measures of BOLD effects, including experimental (41–43) and theoretical (44–48) methods. Among these approaches, the signal model proposed by Yablonskiy and Haacke (46) focused on deoxyhemoglobin-induced signal loss outside of the intravascular space, which could potentially be detected with a gradient-echo imaging approach. In this chapter, we will focus our discussion on the signal model proposed by Yablonskiy and Haacke (46).

Assuming blood vessels form an interconnecting network of long cylinders with random orientations, Yablonskiy and Haacke (46) indicated that a relation between R2′ and cerebral blood oxygenation can be derived as

$$R2' = \lambda \cdot \gamma \cdot \frac{4}{3} \cdot \pi \cdot \Delta\chi_0 \cdot cHct \cdot (Ya - Yv) \cdot B_0$$

where λ is the fractional blood volume containing deoxyhemoglobin or venous cerebral blood volume (vCBV) in our case. Therefore, λ and vCBV are interchangeable hereafter. γ is the gyromagnetic ratio, cHct is the fractional cerebral hematocrit, B_0 is the main magnetic field strength, Y_a and Y_v are the arterial and venous oxygen saturation, respectively, and $\Delta\chi_0$ is the susceptibility difference between the fully oxygenated and the fully deoxygenated blood which has been measured to be 0.18 ppm/Hct in cgs units (47). If one can experimentally determine R2′ and vCBV, a measure of MR-based cerebral oxygen extraction (MR–OEF) defined as MR–OEF = Y_a–Y_v (or 1–Y_v when the arterial blood is fully oxygenated) can be obtained.

Magnetic Resonance-Based Venous Cerebral Blood Volume and Magnetic Resonance-Based Cerebral Oxygen Extraction

With the understanding of the putative underlying biophysical mechanisms associated with BOLD effects, we have developed imaging methods to acquire images that can be subsequently processed using the theoretical model proposed by Yablonskiy and Haacke (46) for obtaining MR-based vCBV and MR–OEF. More detailed descriptions of the imaging approaches can be found in Refs. (10–13), and here we will provide results on our ability of obtaining in vivo measures of vCBV and MR–OEF, respectively.

Measures of Venous Cerebral Blood Volume

In order to determine whether or not the experimentally measured vCBV using the newly developed approach behaves in accordance with known physiological responses, hypercapnia was induced in rats. Since the effects of hypercapnia on vCBV are largely unknown due to the lack of approaches for obtaining measures of vCBV, we have modified the experimental protocol by acquiring images after injecting an iron-based contrast agent, AMI227. In so doing, the susceptibility caused by the presence of AMI227 will be much larger than that induced by deoxyhemoglobin and will uniformly affect both arterial and venous blood pools. In other words, the measured blood volume will no longer be vCBV but the conventional CBV, allowing for a direct comparison of the results obtained using the newly developed approach to that obtained using established approaches such as the steady state and DSC. In this study, the steady-state approach was employed to serve this purpose.

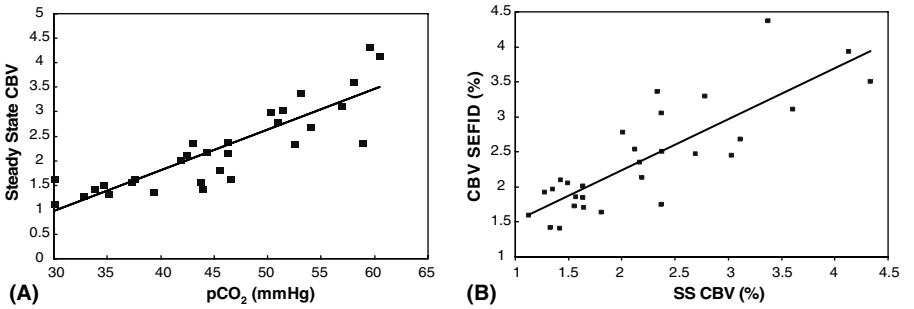

FIGURE 3 A linear relationship between magnetic resonance-measured cerebral blood volume (CBV) and $PaCO_2$ is shown (**A**) consistent with the expected physiological behavior. In addition, a highly linear relationship is also obtained between the new approach of obtaining CBV and a commonly used steady-state approach (**B**). *Abbreviations*: CBV, cerebral blood volume; SS, steady state.

Each rat was placed under three different $PaCO_2$ levels, including normal condition ($PaCO_2 = 36.4 \pm 4.96$ mmHg), mild (45.6 ± 6.32 mmHg), and moderate hypercapnia (54.0 ± 4.88 mmHg). CO_2-induced increase in CBV was observed in all rats using both the proposed and the steady-state approaches. A highly linear relation ($r = 0.87$) was observed between CBV and $PaCO_2$ (Fig. 3A) using the steady-state approach, consistent with our previous findings. In addition, a linear relation ($r = 0.83$) is also observed between the CBV obtained using the newly developed approach and that from the steady state (Fig. 3B). Together, these findings suggest that the proposed method is capable of providing measures of CBV that are consistent with the anticipated physiological alteration during hypercapnia, in agreement with the well-established steady-state approach.

Similar studies were also conducted in normal subjects with the exception that no contrast agent was given. Under these circumstances, vCBV in normal subjects under experimental hypercapnia can be determined. Human subjects underwent experimental hypercapnia and images were acquired during normo- (room air) and hypercapnia (97% O_2 and 3% CO_2). A representative result from a human subject is shown in Figure 4 during normocapnia (Fig. 4A) and hypercapnia (Fig. 4B), demonstrating an increase in vCBV during hypercapnia. Quantitative measures of vCBV in gray and white matter revealed that the mean vCBV in white matter increased from $3.34 \pm 0.46\%$ to $3.82 \pm 0.83\%$, whereas in gray matter, it increased from $4.16 \pm 0.47\%$ to $4.80 \pm 0.56\%$ during transition from normocapnia to hypercapnia. These results suggest two important findings. First, cerebral veins also dilate in response to hypercapnia, similar to the total CBV. Second, the newly developed approach is capable of obtaining vCBV in human subjects, which may offer a new tool to assess alteration of vCBV in patients with cerebrovascular diseases.

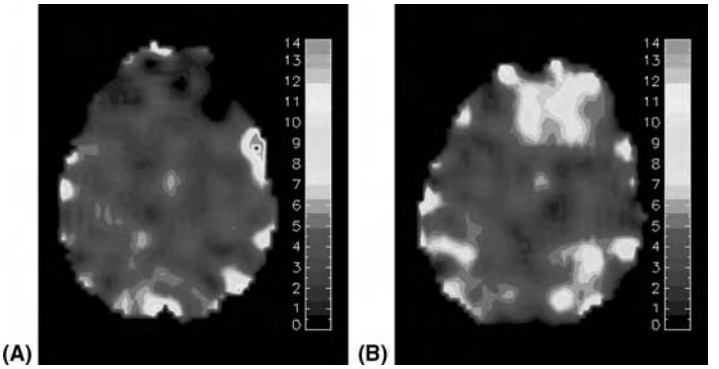

FIGURE 4 Venous cerebral blood volume (vCBV) maps obtained from a normal volunteer under normo- (**A**) and hypercapnic (**B**) conditions are shown, demonstrating an increased vCBV during hypercapnia when compared with that during normocapnia.

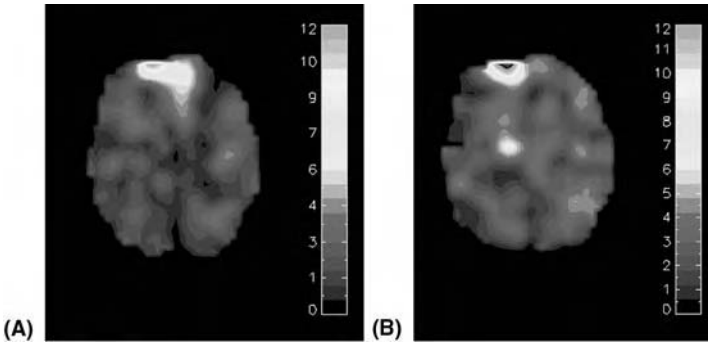

FIGURE 5 Magnetic resonance measured venous cerebral blood volume (vCBV) (**A**) and total CBV (**B**) from a normal volunteer.

Finally, with the ability of measuring vCBV in vivo, we have further investigated the ratio of vCBV to total CBV (tCBV) in human subjects (49). This was done by acquiring two sets of CBV images using the newly developed approach. The two sets of images were identical with the exception that one was acquired prior to and the other was acquired after the injection of an MR contrast agent. Therefore, the images acquired prior to the injection of a contrast agent provide estimates of vCBV, whereas the images obtained after the injection of contrast allow estimates of tCBV. Representative vCBV and tCBV maps from a normal volunteer is shown in Figure 5A and B, respectively. The quantitative analysis revealed vCBV and tCBV to be $2.46 \pm 0.28\%$ and $3.20 \pm 0.41\%$, respectively, which in turn provided a vCBV/tCBV ratio of 0.77 ± 0.04, in excellent agreement with results reported in the literature.

Measures of Magnetic Resonance–Based Cerebral Oxygen Extraction

Representative cerebral venous blood oxygenation (Y_v) maps (MR–OEF = Y_a–Y_v, where Y_a is the arterial blood oxygenation) from one rat undergoing control, mild hypoxia and control, severe hypoxia and another rat undergoing hypercapnia are shown in Figure 6, demonstrating the high-quality MR Y_v maps as well as its ability to discern changes of Y_v in response to experimental conditions. Consistent with the anticipated cerebral hemodynamic responses to hypoxia and hypercapnia, a mild reduction and severe reduction in Y_v were observed under the two hypoxic conditions, respectively, whereas an increase in Y_v was observed during hypercapnia. In addition, the Y_v is similar between the two control states, demonstrating the stability of the proposed approaches.

Similar studies were also carried out on normal volunteers. MR images were acquired during both normocapnia (medical air) and hypercapnia (97% O_2 and 3% CO_2). A representative example from a subject is shown in Figure 7 during normocapnia (Fig. 7A) and hypercapnia (Fig. 7B), respectively. The image acquired during hypercapnia showed a substantial reduction in OEF, consistent with the expected physiological response. Quantitative measures of OEF for both gray matter and white matter during normocapnia and hypercapnia are shown in Figure 7C, demonstrating a consistent and significant reduction ($P < 0.01$) in OEF during hypercapnia for both gray and white matter. These results again demonstrate that the newly developed approach is capable of providing measures of OEF under experimental conditions and the results are consistent with that reported in the literature using other modalities.

Finally, the effects of magnetic field strengths are also investigated. This is of critical importance since the sensitivity to susceptibility effects depends on the field strength with a

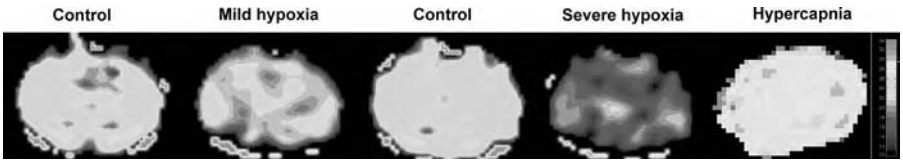

FIGURE 6 Magnetic resonance venous cerebral blood oxygenation under different experimental conditions, including hypoxia and hypercapnia. The grayscale bar represents the blood oxygenation.

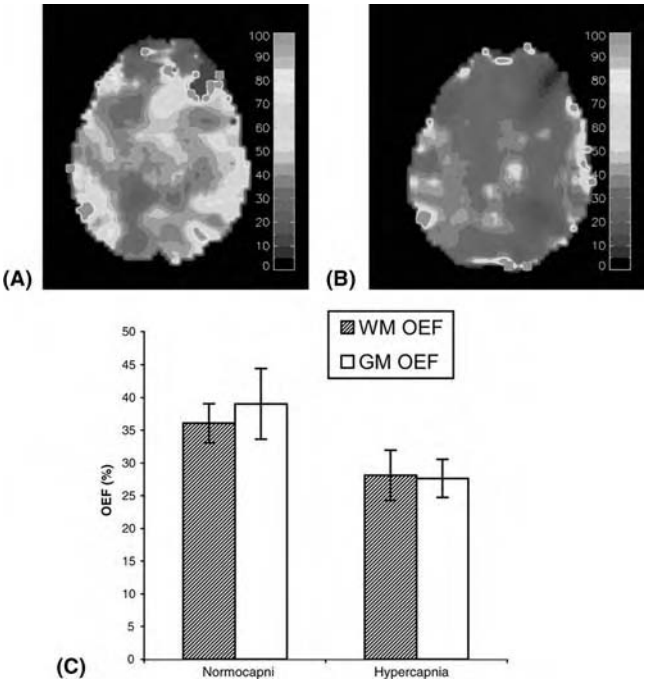

FIGURE 7 Oxygen extraction fraction (OEF) maps during normo- (**A**) and hypercapnia (**B**) are shown. Quantitative measures of OEF in gray and white matter under normo- and hypercapnia are shown in (**C**). *Abbreviations*: OEF, oxygen extraction fraction; GM, gray matter; WM, white matter.

higher magnetic field having a greater sensitivity to susceptibility effects. We have imaged subjects at 1.5 T ($n = 12$) and 3 T ($n = 5$), respectively. Both OEF and vCBV were obtained from all subjects and a region-of-interest (ROI) analysis was employed to obtain measures of OEF and vCBV. Both the OEF and vCBV are essentially identical between the two field strengths. Two conclusions can be drawn based on these findings. First, although the sensitivity to susceptibility effects depends on the static magnetic field, similar results for OEF and vCBV are obtained across the two field strengths (1.5 and 3 T). Second and most importantly, a normal OEF on the order of 45% is obtained using the newly developed approach, in excellent agreement with that reported by many investigators using PET. These results suggest that the newly developed approach can provide an accurate measure of OEF in vivo.

Magnetic Resonance Measured Cerebral Oxygen Metabolism

With the ability of obtaining CBF and MR-OEF using MRI, it is now possible to obtain in vivo MR-COMI, which is defined as the product of CBF and MR-OEF. Although we have defined MR-COMI based on the notion of PET $CMRO_2$, it must be noted that there are several fundamental differences between the derivation of MR-COMI and PET $CMRO_2$. First, the implications of the values between the two may be different. MR-COMI gives a value, which is the theoretical volume of blood from which 100% of oxygen can be extracted (i.e., oxygen clearance), whereas PET $CMRO_2$ gives an absolute value of oxygen extracted from a given volume of blood. Therefore, the values between the two may be related but could be different. Second, the definition of MR-COMI is slightly different from that of PET $CMRO_2$. The PET $CMRO_2$ is defined as the product of CBF, OEF, and arterial oxygen content (CaO_2), whereas CaO_2 is not included for MR-COMI. Nevertheless, this is a minor difference and can be easily incorporated into MR-COMI, although we anticipate that CaO_2 should remain rather stable. Finally, PET $CMRO_2$ is typically obtained using a brief inhalation of ^{15}O (50), whereas MR-COMI, as mentioned previously, is the product of CBF and the extent of cerebral blood desaturation on each pass through the brain. Despite these differences, the physiological information derived from the two modalities should be similar.

MR-COMI was measured from five healthy volunteers. Both quantitative estimates of OEF and CBF were obtained, allowing for the calculation of MR-COMI. A representative

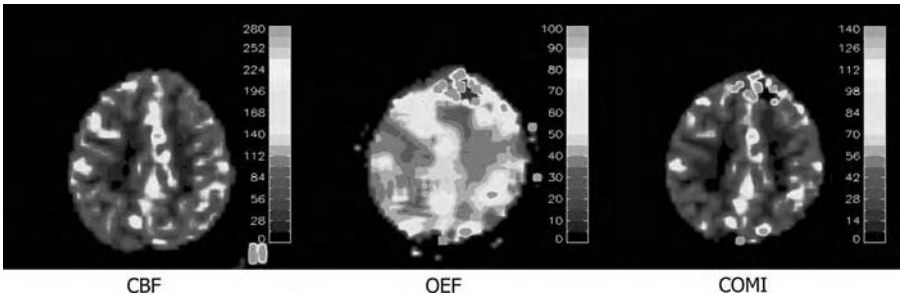

FIGURE 8 Magnetic resonance-measured cerebral blood flow, oxygen extraction fraction, and cerebral oxygen metabolism index from a normal volunteer are shown. *Abbreviations*: CBF, cerebral blood flow; COMI, cerebral oxygen metabolism index; OEF, oxygen extraction fraction.

example for CBF, OEF, and MR-COMI maps is shown in Figure 8A to C, respectively. As anticipated, a clear demarcation between gray and white matter MR-COMI is seen, in good agreement with the results reported in the literature. More importantly, an MR-COMI of 28.94 ± 3.26 mL/min/100 g and 12.57 ± 3.11 mL/min/100 g was obtained for both the gray and white matter, respectively, suggesting that the gray matter utilizes more oxygen than white matter under normal physiological conditions. These results yield a gray matter to white matter MR-COMI ratioof 2.37 ± 0.37, which is comparable to the reported values in the literature.

Applications of Magnetic Resonance Measured Cerebral Metabolic Oxygen Index

In this section, we will provide preliminary evidence on how MR-COMI can potentially be used to depict temporal alteration of cerebral oxygen metabolism during cerebral ischemia in both rats and acute stroke patients.

Rats underwent 90 minutes MCAO. MR-OEF and DWI were obtained every 15 minutes throughout the entire MCAO episode. CBF was obtained at 90 minutes post-MCAO using the DSC approach. Since an intraluminal suture MCAO was used in this study, CBF should remain stable for the entire 90 minutes imaging session. Immediately after the imaging session, the suture was withdrawn from the MCA to restore CBF for reperfusion. A T2-weighted sequence was used to acquire images 24 hours after MCAO. Representative examples from three rats [rows (A)–(C)]with different degrees of ischemic injuries are shown in Figure 9. Temporal evolution of MR-COMI, CBF at 90 minute, and T2-weighted images at 24 hours are shown for each rat. Using the size of the T2 lesion as an index for ischemic severity, the severity progressively decreases from rows (A) to (C). In row (A), MR-COMI is markedly reduced immediately after MCAO and throughout the entire ischemic duration, suggesting that the brain tissue is severely

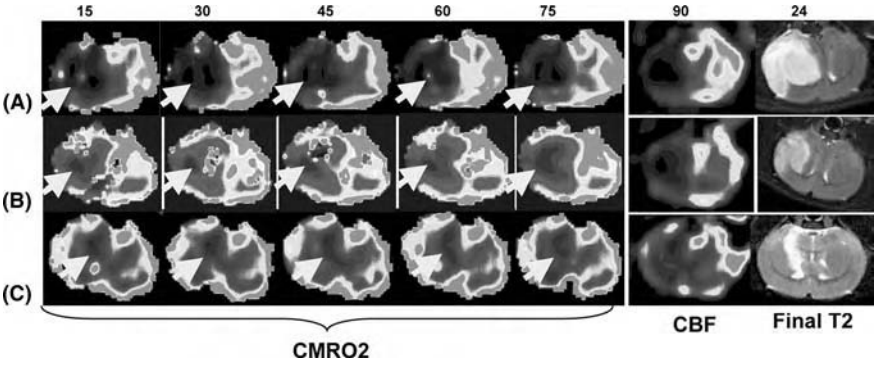

FIGURE 9 (*See color insert.*) Temporal and spatial evolution of cerebral metabolic ratio of oxygen maps from three rats (rows **A**–**C**) with different degrees of ischemic injury are shown. In addition, the cerebral blood flow and T2-weighted images obtained at 90 minutes and 24 hours after middle cerebral artery occlusion are also provided, respectively. *Abbreviations*: CBF, cerebral blood flow; $CMRO_2$, cerebral metabolic ratio of oxygen.

injured immediately after MCAO onset. The region with a substantial reduction of MR-COMI observed at 75 minutes after MCAO is similar to the final T2 lesion (24 hours). In contrast, although a large region of mild MR-COMI reduction is observed in row (B), only a small region with a severe reduction of MR-COMI is observed immediately after MCAO (arrow) and this region continues to evolve as a function time (arrow). The temporal characteristics of MR-COMI in row (C) are similar to that in row (B); the region with severely diminished MR-COMI is initially small and continues to evolve as a function of time. Nevertheless, the final T2 lesion is much smaller when compared with that in rows (A) and (B), demonstrating the spatial sensitivity of the proposed method.

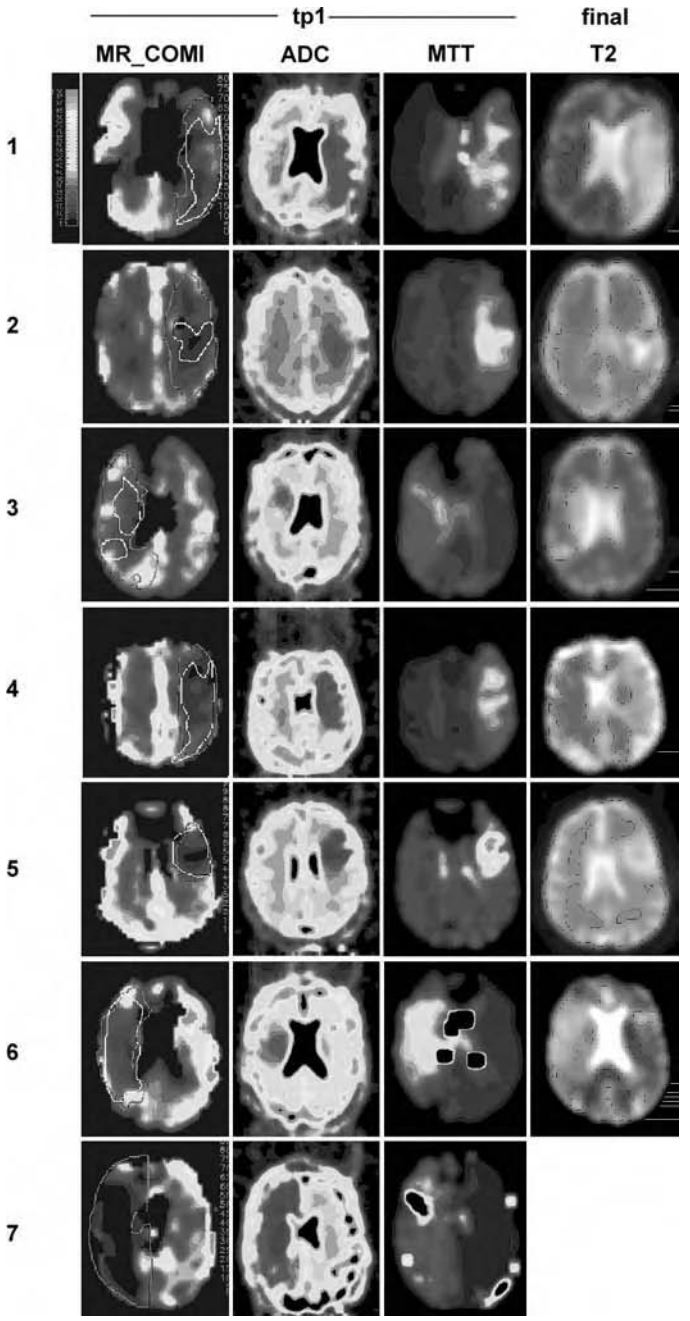

FIGURE 10 Magnetic resonance cerebral oxygen metabolism index, apparent diffusion coefficient, mean transit time, and final T2 are shown for seven acute stroke patients. *Abbreviations*: ADC, apparent diffusion coefficient; MR-COMI, magnetic resonance cerebral oxygen metabolism index; MTT, mean transit time.

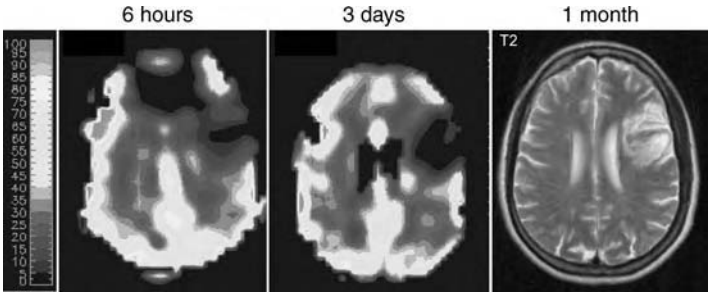

FIGURE 11 Magnetic resonance cerebral oxygen metabolic index maps obtained at six hours (**A**) and three days (**B**) and final lesion (**C**) from patient 5 shown in Figure 10 are shown.

The potential clinical utility of MR-COMI was also evaluated in seven stroke patients at 4.5 ± 0.9 hours (tp1), three to five days (tp2), and one to three months (tp3) after symptom onset (7). DWI, CBF, OEF, and $CMRO_2$ were obtained from each patient at both tp1 and tp2, whereas only T2-weighted images were obtained at tp3. Figure 10 shows the $CMRO_2$, apparent diffusion coefficient (ADC), and mean transit time (MTT) maps of all seven patients, obtained at tp1 (within six hours of stroke onset). Also shown is the coregistered T2-weighted image obtained at the final tp3 (patient 7 expired prior to tp2). Superimposed on the tp1 MR-$CMRO_2$ map are the tp3 T2 lesion area (white, outlining the final infarct) and the tp1 MTT-defined lesion area (red, outlining the "area at risk"). Five of the seven patients exhibited substantial DWI/PWI mismatched defects at tp1, whereas the remaining two patients (patients 5 and 7) had matched DWI/PWI regions (mismatch within 5 cc). Brain regions with very low $CMRO_2$ (indicated by the dark contours) fell within the areas of final infarct, suggesting that a threshold for irreversible injury may be measurable and predictive of final infarct using this technique. An example of the temporal evolution of the $CMRO_2$ map obtained from one patient (patient 5) is shown in Figure 11. The ADC and MTT-defined lesion volumes for this patient were 11.35 and 14.76 cc, respectively, and represented matched defects suggesting the absence of viable brain tissue in the ischemic region. However, the $CMRO_2$ image (Fig. 11A) revealed a much smaller region with substantial reduction in $CMRO_2$ and a larger surrounding area of progressively increasing $CMRO_2$. The low $CMRO_2$ at the frontal region in Figure 11A (arrow) is caused by the susceptibility effects in the CBF maps derived from dynamic contrast studies. Matched DWI/PWI lesions persisted at tp2, whereas the lesion volume defined by MR-$CMRO_2$ (Fig. 11B) was substantially larger than that seen at tp1. Finally, the MR-$CMRO_2$-defined lesion volume at tp2 matched the final lesion volume defined by the T2-weighted image (Fig. 11C) obtained at week 4.

An aggregate analysis of all patients at tp1 revealed that $CMRO_2$ measured in final infarct regions (defined by tp3 T2 lesions) was 0.40 ± 0.24 of the contralateral region. The brain region "at risk for infarction," defined by the mismatched tp1 MTT-defined lesion subtracting the final infarct area revealed an MR-$CMRO_2$ value 0.55 ± 0.11 of the respective regions in the contralateral hemisphere. The progressive increase in $CMRO_2$ values from infarct core to salvaged brain tissue suggests that a threshold value may distinguish reversibly injured tissue from tissue in an advanced state of injury destined to evolve to infarction if reperfusion does not occur. The value of 40% of $CMRO_2$ defining acutely irreversibly damaged tissue is in good agreement with the results reported in previous PET studies (1,3,4).

CONCLUSION

Noninvasive approaches to provide direct insights into tissue viability have been extensively pursued by a number of investigators using different imaging modalities. Although new approaches are emerging, definitive solutions remain to be established. In this chapter, we demonstrated the potential to detect tissue viability based on an MR-derived physiological parameters that provide physiological parameters that are comparable to those obtained using PET $CMRO_2$. While results are encouraging, systematic validation in animals and stroke patients with adequate sample sizes are needed to establish the validity of the MRI approaches.

Acknowledgments
We would like to thank Dr. Hamid Krim at North Carolina State University for conceptual and technical input in the development of the ICA approach for minimizing the effects of recirculation. This work is supported in parts by a grant from NIH (WL), R01 NS054079.

REFERENCES

1. Frykholm P, Andersson JL, Valtysson J, et al. A metabolic threshold of irreversible ischemia demonstrated by PET in a middle cerebral artery occlusion-reperfusion primate model. Acta Neurol Scand 2000; 102(1):18–26.
2. Giffard C, Young AR, Kerrouche N, Derlon JM, Baron JC. Outcome of acutely ischemic brain tissue in prolonged middle cerebral artery occlusion: a serial positron emission tomography investigation in the baboon. J Cereb Blood Flow Metab 2004; 24(5):495–508.
3. Powers WJ, Grubb RL, Darriet D, Raichle ME. Cerebral blood flow and cerebral metabolic rate of oxygen requirements for cerebral function and viability in humans. J Cereb Blood Flow Metab 1985; 5(4):600–608.
4. Touzani O, Young AR, Derlon JM, Baron JC, MacKenzie ET. Progressive impairment of brain oxidative metabolism reversed by reperfusion following middle cerebral artery occlusion in anaesthetized baboons. Brain Res 1997; 767(1):17–25.
5. Heiss WD, Podreka I. Role of PET and SPECT in the assessment of ischemic cerebrovascular disease. Cerebrovasc Brain Metab Rev 1993; 5(4):235–263.
6. Heiss WD, Graf R, Grond M, Rudolf J. Quantitative neuroimaging for the evaluation of the effect of stroke treatment. Cerebrovasc Dis 1998; 8(suppl 2):23–29.
7. Lee JM, Vo KD, An H, et al. Magnetic resonance cerebral metabolic rate of oxygen utilization in hyperacute stroke patients. Ann Neurol 2003; 53(2):227–232.
8. Leblanc R. Physiologic studies of cerebral ischemia. Clin Neurosurg 1991; 37:289–311.
9. An H, Lin W, Celik A, Lee YZ. Quantitative measurements of cerebral metabolic rate of oxygen utilization using MRI: a volunteer study. NMR in Biomedicine 2001; 14(7–8):441–447.
10. An H, Lin W. Quantitative measurements of cerebral blood oxygen saturation using magnetic resonance imaging. J Cereb Blood Flow Metab 2000; 20(8):1225–1236.
11. An H, Lin W. Cerebral oxygen extraction fraction and cerebral venous blood volume measurements using magnetic resonance imaging: effects of magentic field variation. Magn Reson Med 2002; 47:958–966.
12. An H, Lin W. Quantitative measurements of cerebral oxygen extraction fraction and cerebral venous blood volume during normocapnia and hypercapnia using an asymmetric spin echo sequence. Magn Reson Med 2003; 50:708–716.
13. An H, Lin W. Impact of intravascular signal on quantitative measures of cerebral oxygen extraction and blood volume under normo- and hypercapnic conditions using an asymmetric spin echo approach. Magn Reson Med 2003; 50(4):708–716.
14. Rosen BR, Turner R, Hunter GJ, Fordham JA. MR depicts perfusion of brain and heart. Diagn Imaging (San Franc) 1991; 13(11):105–110.
15. Alsop DC, Detre JA. Reduced transit-time sensitivity in noninvasive magnetic resonance imaging of human cerebral blood flow. J Cereb Blood Flow Metab 1996; 16(6):1236–1249.
16. Wong EC, Buxton RB, Frank LR. Quantitative perfusion imaging using arterial spin labeling. Neuroimaging Clin N Am 1999; 9(2):333–342.
17. Detre JA, Samuels OB, Alsop DC, Gonzalez-At JB, Kasner SE, Raps EC. Noninvasive magnetic resonance imaging evaluation of cerebral blood flow with acetazolamide challenge in patients with cerebrovascular stenosis. J Magn Reson Imaging 1999; 10(5):870–875.
18. Davenport R. The derivation of the gamma-variate relationship for tracer dilution curves. J Nucl Med 1983; 24(10):945–948.
19. Wu Y, An H, Krim H, Lin W. An independent component analysis approach for minimizing effects of recirculation in dynamic susceptibility contrast magnetic resonance imaging. J Cereb Blood Flow Metab 2006. Online, July 16, 2006.
20. Bell AJ, Sejnowski TJ. An information-maximization approach to blind separation and blind deconvolution. Neural Comput 1995; 7(6):1129–1159.
21. Cardoso J. Blind signal separation: statistical principles. Proc IEEE Special Issue Blind Identification Estimation 1998; 90:2009–2026.
22. Comon P. Independent component analysis: a new concept? Signal Process 1994; 36:287–314.
23. Havvannen A. Fas and robust fixed-point algorithms for independent component analysis. IEEE Trans Neural Netw 1999; 10:626–634.
24. Havvannen A, Karhunen J, Oja E. Independent component analysis. New York: John Wiley & Sons, 2001.
25. Havvannen A, Oja E. A Fas fixed-point algorithm for independent component analysis. Neural Comput 1997; 91:1483–1492.

26. Ogawa S, Lee TM. Magnetic resonance imaging of blood vessels at high fields: in vivo and in vitro measurements and image simulation. Magn Reson Med 1990; 16(1):9–18.
27. Ogawa S, Lee TM, Barrere B. The sensitivity of magnetic resonance image signals of a rat brain to changes in the cerebral venous blood oxygenation. Magn Reson Med 1993; 29(2):205–210.
28. Ogawa S, Lee TM, Kay AR, Tank DW. Brain magnetic resonance imaging with contrast dependent on blood oxygenation. Proc Natl Acad Sci USA 1990; 87(24):9868–9872.
29. Ogawa S, Lee TM, Nayak AS, Glynn P. Oxygenation-sensitive contrast in magnetic resonance image of rodent brain at high magnetic fields. Magn Reson Med 1990; 14(1):68–78.
30. Prielmeier F, Nagatomo Y, Frahm J. Cerebral blood oxygenation in rat brain during hypoxic hypoxia. Quantitative MRI of effective transverse relaxation rates. Magn Reson Med 1994; 31(6):678–681.
31. Jezzard P, Heineman F, Taylor J, et al. Comparison of EPI gradient-echo contrast changes in cat brain caused by respiratory challenges with direct simultaneous evaluation of cerebral oxygenation via a cranial window. NMR Biomed 1994; 7(1–2):35–44.
32. Hoppel BE, Weisskoff RM, Thulborn KR, Moore JB, Kwong KK, Rosen BR. Measurement of regional blood oxygenation and cerebral hemodynamics. Magn Reson Med 1993; 30(6):715–723.
33. Rostrup E, Larsson HB, Toft PB, Garde K, Henriksen O. Signal changes in gradient echo images of human brain induced by hypo- and hyperoxia. NMR Biomed 1995; 8(1):41–47.
34. Kennan RP, Scanley BE, Gore JC. Physiologic basis for BOLD MR signal changes due to hypoxia/hyperoxia: separation of blood volume and magnetic susceptibility effects. Magn Reson Med 1997; 37(6):953–956.
35. Lin W, Paczynski RP, Celik A, Kuppusamy K, Hsu CY, Powers WJ. Experimental hypoxemic hypoxia: changes in R2* of brain parenchyma accurately reflect the combined effects of changes in arterial and cerebral venous oxygen saturation. Magn Reson Med 1998; 39(3):474–481.
36. Davis TL, Kwong KK, Weisskoff RM, Rosen BR. Calibrated functional MRI: mapping the dynamics of oxidative metabolism. Proc Natl Acad Sci USA 1998; 95(4):1834–1839.
37. Lin W, Celik A, Paczynski RP, Hsu CY, Powers WJ. Quantitative magnetic resonance imaging in experimental hypercapnia: improvement in the relation between changes in brain R2 and the oxygen saturation of venous blood after correction for changes in cerebral blood volume. J Cereb Blood Flow Metab 1999; 19(8):853–862.
38. Lin W, Paczynski RP, Celik A, Hsu CY, Powers WJ. Effects of acute normovolemic hemodilution on T2*-weighted images of rat brain. Magn Reson Med 1998; 40(6):857–864.
39. De Crespigny AJ, Wendland MF, Derugin N, Kozniewska E, Moseley ME. Real-time observation of transient focal ischemia and hyperemia in cat brain. Magn Reson Med 1992; 27(2):391–397.
40. Ono Y, Morikawa S, Inubushi T, Shimizu H, Yoshimoto T. T2*-weighted Magnetic Resonance Imaging of cerebrovascular reactivity in rat reversible focal cerebral ischemia. Brain Res 1997; 744(2):207–215.
41. Foltz WD, Merchant N, Downar E, Stainsby JA, Wright GA. Coronary venous oximetry using MRI. Magn Reson Med 1999; 42(5):837–848.
42. Thulborn KR, Waterton JC, Matthews PM, Radda GK. Oxygenation dependence of the transverse relaxation time of water protons in whole blood at high field. Biochim Biophys Acta 1982; 714(2):265–270.
43. Wright GA, Hu BS, Macovski A. 1991 I.I. Rabi Award. Estimating oxygen saturation of blood in vivo with MR imaging at 1.5 T. J Magn Reson Imaging 1991; 1(3):275–283.
44. Stables LA, Kennan RP, Gore JC. Asymmetric spin-echo imaging of magnetically inhomogeneous systems: theory, experiment, and numerical studies. Magn Reson Med 1998; 40(3):432–442.
45. Kennan RP, Zhong J, Gore JC. Intravascular susceptibility contrast mechanisms in tissues. Magn Reson Med 1994; 31(1):9–21.
46. Yablonskiy DA, Haacke EM. Theory of NMR signal behavior in magnetically inhomogeneous tissues: the static dephasing regime. Magn Reson Med 1994; 32(6):749–763.
47. van Zijl PC, Eleff SM, Ulatowski JA, et al. Quantitative assessment of blood flow, blood volume and blood oxygenation effects in functional magnetic resonance imaging [see comments]. Nat Med 1998; 4(2):159–167.
48. Weisskoff RM, Kiihne S. MRI susceptometry: image-based measurement of absolute susceptibility of MR contrast agents and human blood. Magn Reson Med 1992; 24(2):375–383.
49. An H, Lin W. Cerebral venous and arterial blood volumes can be estimated separately in humans using magnetic resonance imaging. Magn Reson Med 2002; 48(4):583–588.
50. Mintun MA, Vlassenko AG, Shulman GL, Snyder AZ. Time-related increase of oxygen utilization in continuously activated human visual cortex. Neuroimage 2002; 16(2):531–537.

16c. Arterial Spin Labeling

John A. Detre
Departments of Neurology and Radiology, University of Pennsylvania, Philadelphia, Pennsylvania, U.S.A.

Timothy Q. Duong
Yerkes Imaging Center, Division of Neuroscience and Department of Neurology, Emory University, Atlanta, Georgia, U.S.A.

INTRODUCTION

Although ischemic penumbra can be operationally defined in many ways, the earliest definitions considered thresholds in the reduction of cerebral blood flow (CBF) in the ischemic core and surrounding regions (1). While the ischemic penumbra can now be defined by cellular and molecular events, hypoperfusion remains the proximate cause of cerebral ischemia and a critical physiological parameter in its mechanism. The concept of ischemic thresholds is also universally recognized to have a temporal component—shorter the durations of reversibility occurring in regions, greater the reductions in CBF (2). Accordingly, serial measurements of CBF are ideally required to fully characterize the relationships between CBF and ischemic outcomes, both clinically and in experimental models.

Arterial spin-labeled (ASL) perfusion MRI provides a completely noninvasive method for quantification of CBF, using magnetically labeled arterial blood water as an endogenous and nominally diffusible flow tracer (3). It is conceptually analogous to the CBF measurements made with ^{15}O-H_2O and positron emission tomography (PET) scanning, except that no exogenous or radioactive tracer is required. Instead, radiofrequency (RF) excitation is used to alter the magnetization of arterial blood water proximal to the tissue of interest; for CBF, arterial blood water is typically labeled at the base of the brain or in the neck. Another major difference is that ^{15}O decays with a half-life of two minutes, whereas ASL blood water decays with T1, which is on the order of one to two seconds, depending on the field strength and tissue type. ASL perfusion MRI measurements can, therefore, be made quickly, and rapid changes in CBF can be followed. Although ASL only produces an approximately 1% change in magnetization of the brain, this effect can be reliably measured using modern imaging equipment.

Because ASL is completely noninvasive and the ASL "tracer" is extremely short-lived, it can also be repeated indefinitely. This is a unique difference from other methods for CBF imaging, where repeatability is limited by either radiation dose limits in radionuclide methods or accumulation of the tracer for vascular contrast methods such as dynamic susceptibility contrast (DSC) based perfusion MRI. ASL perfusion MRI is also directly quantifiable in classical units of tissue perfusion (mL/g/min) with measurements, knowledge, or assumptions about the labeling efficiency, arterial transit time from the labeling location to the tissue of interest, and T1 relaxation rates in blood and tissue. Modifications of ASL imaging sequences also allow an arterial transit time to be calculated (4). This measure may have physiological significance independent of CBF, potentially indicating the recruitment of collateral flow pathways.

The earliest models for quantifying CBF, based on ASL data, used a modification of the Block equations for longitudinal magnetization with added terms for the delivery of labeled spins by CBF and their removal by venous outflow (3). A well-mixed compartment was also assumed, allowing the venous concentration of label to be replaced with the brain concentration adjusted by the blood:brain partition coefficient for water following the Kety–Schmitt model. Subsequent models for quantifying CBF have also considered an arterial blood water compartment (5) and finite permeability of water (6).

ARTERIAL SPIN LABELING METHODOLOGY

Several approaches exist for carrying out ASL. They fall into two main categories: pulsed ASL (PASL), which uses a spatially localized RF excitation to saturate or invert the arterial magnetization with respect to the tissue magnetization (7–9,10), and continuous ASL (CASL) (11), which uses a velocity-driven adiabatic excitation (12) to invert spins flowing through a designated labeling plane (Fig. 1). In the theoretical limit, CASL methods provide over two-fold greater labeling than PASL methods, though in practice the relative improvement tends to be somewhat less (9,10). Several methods for selective labeling of individual arteries have also been developed. Some are based on the use of separate small RF coils (13,14), whereas others rely on gradient-based localization (15–17). The ability to selectively label individual arteries is unique to ASL among noninvasive CBF imaging techniques.

ASL was initially reported in the early 1990s for single slices, and CBF measurements were validated against other approaches including flowmeter (18), microspheres (19), hydrogen clearance (20), autoradiographic methods (21), and ^{15}O-PET CBF (22,23,24). However, several key methodological advances have greatly improved the utility of ASL perfusion MRI. The introduction of a postlabeling delay (5) to allow labeled blood–water to move from the arterial circulation into the microcirculation and tissue greatly reduced the dependency of calculated CBF on variations in arterial transit time and produced CBF images that were far less contaminated by artifacts due to residual label in large arteries that were present in early studies (25). Improved spatial localization for PASL and strategies to control for the spatially dependent off-resonance effects of CASL (26) have permitted multislice ASL, which is necessary for clinical applications and beneficial for research applications. The increased signal strength and prolongation of T1 relaxation rates with increased magnetic field strength act in tandem to greatly improve the sensitivity of high-field ASL (27). The use of surface coils and parallel imaging also increased the sensitivity of ASL methods (28). Finally, under certain circumstances, it is possible to suppress the magnetization from static brain–water, which amplifies the ASL effect from approximately 1% to up to 100% of the measured signal (22,23). Taken together, these methodological advances have resulted in a 10-fold improvement in the sensitivity of ASL over the past decade. An example of a current ASL perfusion MRI study from human brain is shown in Figure 2. Continued methodological development is focusing on improving labeling efficiency and optimizing strategies for measuring the ASL effect in brain and other organs.

ARTERIAL SPIN LABELING IN ISCHEMIA

Over the past decade, several studies in animal models and human patients have also established the utility of ASL perfusion MRI for measuring CBF in cerebrovascular disease and stroke. ASL has been used for serial imaging of CBF in animal models (29–31). Brain tissue with perfusion deficits below a critical threshold (2) experiences metabolic energy failure, membrane depolarization, and subsequent cytotoxic edema. These changes precipitate a reduction in the

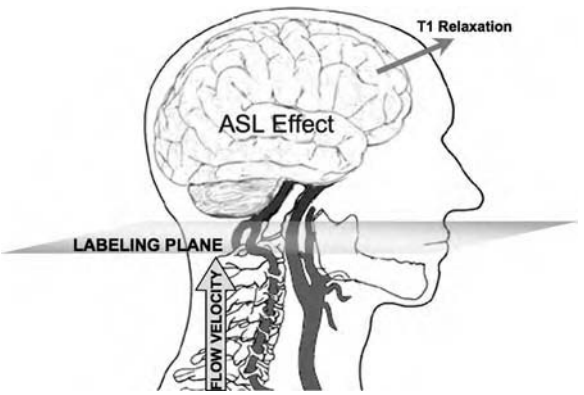

FIGURE 1 A schematic diagram illustrating continuous arterial spin labeling. Velocity-driven adiabatic fast passage inverts arterial blood water flowing towards the brain as it passes through the labeling plane. The resulting arterial blood water has opposite magnetization to the static brain water and produces a small decrease in magnetic resonance imaging signal that is measured by comparison with a control condition without arterial spin labeling. The regional magnitude of these signal changes is dependent on cerebral blood flow, which delivers labeled spins to the region, and T1 relaxation, which causes the label to decay. *Abbreviation*: ASL, arterial spin labeling. *Source*: From Refs. 11 and 12.

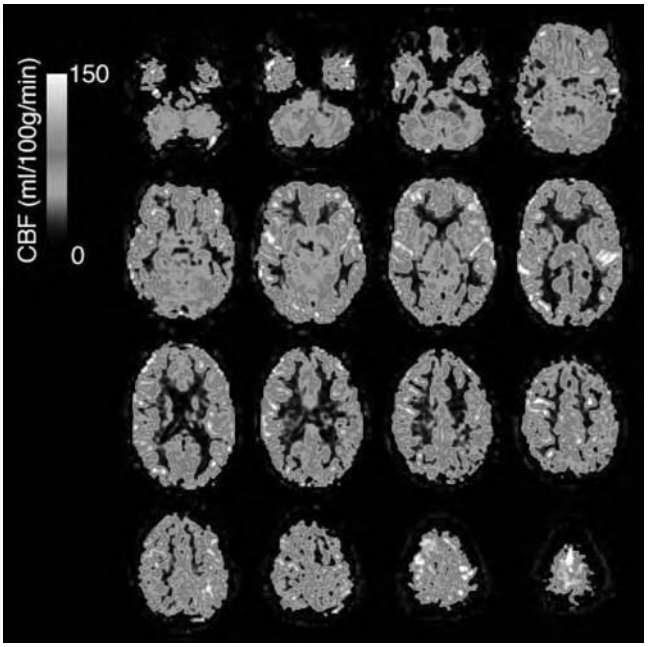

FIGURE 2 (*See color insert*.) Multislice continuous arterial spin labeling perfusion magnetic resonance imaging obtained at 3 T from a normal volunteer in approximately 10 minutes with spin echo echoplanar imaging. *Abbreviation*: CBF, cerebral blood flow.

apparent diffusion coefficient (ADC) of brain–water (32), which has been well characterized in animal models of stroke. During the acute phase, the area of ADC abnormality is typically smaller relative to the area of perfusion deficit. As ischemia evolves, most of this ADC abnormality expands and, eventually, coincides with the area of perfusion deficit. The difference in the abnormal region defined by the abnormal perfusion and diffusion contrast in acute stroke is referred to as the "perfusion–diffusion" mismatch, and represents potentially salvageable tissue corresponding to the "ischemic penumbra." An example of the application of ASL perfusion MRI in a rat stroke model is shown in Figure 3.

Critical CBF and ADC thresholds below which infarctions are destined to develop can be defined by correlation with endpoint histology (31). Although there are limitations of this approach, it provides a simple and practical means to define the ischemic penumbra and infarcted tissues at different time points after stroke. This approach has also been used to study the effects of reperfusion (33,34) and other therapeutic interventions (35). For example, the data shown in Figure 3 suggest that about half of the penumbral tissue was salvaged when reperfusion was performed 60 minutes after occlusion, compared with no reperfusion. One limitation of extending this approach to the clinic is that CBF and ADC critical thresholds are defined at one single time point after stroke onset, while it is well known that the duration of CBF reduction should also be taken into account (2). Objective classification of ischemic penumbra, normal, and infarcted tissues (such as using automated clustering algorithm based on multispectral CBF, ADC, and other MRI data) is clearly important and has been demonstrated in stroke models (33,34) and to some extent in humans (36).

In human patients with acute stroke and chronic cerebrovascular disease, ASL perfusion MRI has been used to demonstrate the presence of chronic asymptomatic and symptomatic hypoperfusion (37–39). Although these studies have demonstrated the feasibility of using ASL to characterize the ischemic penumbra, accurate measurement of low CBF values has remained challenging because signal changes are particularly small and arterial transit times can be significantly longer than T1 of arterial blood water. However, most of the existing data on ASL in experimental and clinical stroke were acquired at 1.5 T using early methodology, with several-fold lower sensitivity than that is now available. Figure 4 shows multislice ASL data along with diffusion weighted imaging (DWI) acquired at 1.5 Tesla in a patient at six hours after symptom onset. A region of hypoperfusion in clearly evident, and is considerably larger than

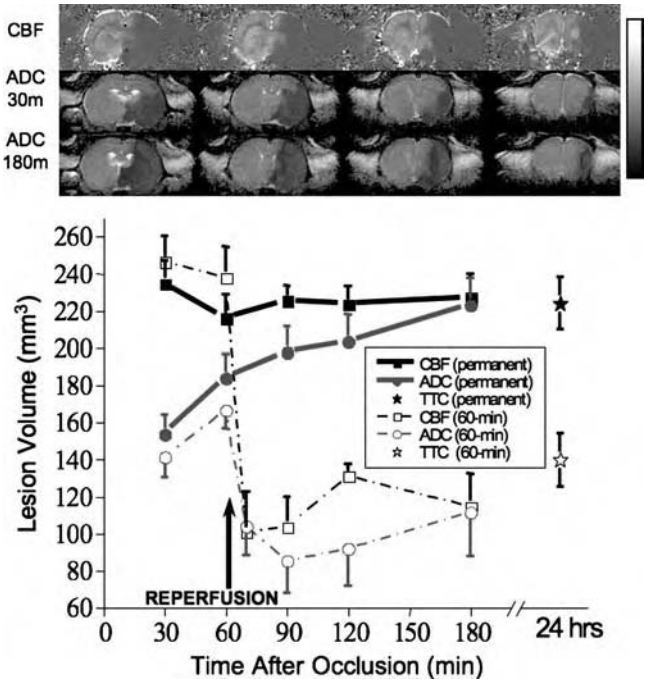

FIGURE 3 (*Top*) Cerebral blood flow (CBF) maps at 30 minutes, apparent diffusion coefficient maps at 30 and 180 minutes after permanent middle cerebral artery occlusion. CBF was measured using continuous arterial spin labeling (ASL) with a separate neck coil for ASL. Gray scale indicates CBF ranging from 0 to 1 mL/g/min and apparent diffusion coefficient (ADC) ranging from 0 to 1 x 10^{-3} mm^2/sec. (*Bottom*) Evolution of ADC- and CBF-defined lesion volumes for permanent ($n = 6$) and 60-minute ($n = 6$) stroke. CBF-defined lesion volume of the permanent stroke was constant, whereas ADC-defined lesion volume of the permanent stroke grew bigger with time. Reperfusion salvaged substantial tissues, and some of these tissues showed delayed cell death, as indicated by gradual increase in ADC lesion volume over time after reperfusion. Final infarct volumes were obtained by triphenyl tetrazolium chloride histology at 24 hours after ischemia. *Abbreviations*: ADC, apparent diffusion coefficient; CBF, cerebral blood flow; TTC, triphenyl tetrazolium chloride.

the ischemic [3]core[2] as demonstrated by DWI hyperintensity. However, gradations in ischemia are not well demonstrated. The recent improvements in ASL methodology described earlier should facilitate the transition of ASL perfusion MRI from feasibility to practical utility in basic and clinical research on the ischemic penumbra.

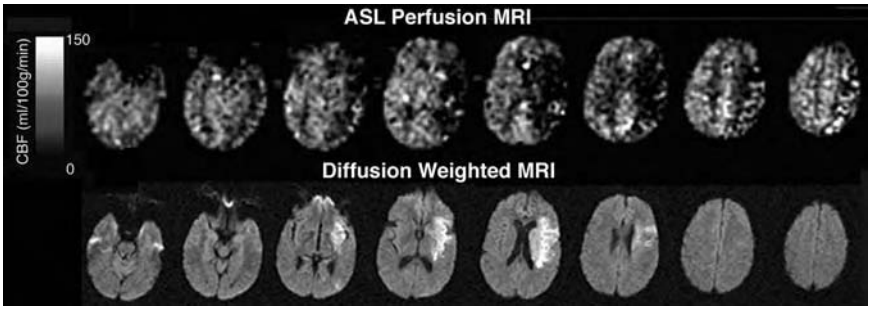

FIGURE 4 Continuous arterial spin-labeled (ASL) perfusion magnetic resonance imaging (MRI) and diffusion-weighted MRI (DWI) obtained at 1.5 T from a 56-year-old man with hemiparesis due to carotid dissection six hours after symptom onset. DWI shows cytotoxic injury primarily around insular cortex, whereas perfusion MRI shows hypoperfusion in affecting most of the middle cerebral artery distribution, suggesting a large penumbral zone. However, owing to the weak ASL effect in the hypoperfused region, cerebral blood flow (CBF) values are difficult to distinguish from zero. High-field ASL should dramatically increase ASL sensitivity for low CBF values. *Abbreviations*: ASL, arterial spin labeling; CBF, cerebral blood flow; MRI, magnetic resonance imaging.

REFERENCES

1. Astrup J, Siesjo BK, Symon L. Thresholds in cerebral ischemia—the ischemic penumbra. Stroke 1981; 12:723–725.
2. Hossmann KA. Viability thresholds and the penumbra of focal ischemia. Ann Neurol 1994; 36(4):557–565.

3. Detre JA, Leigh JS, Williams DS, Koretsky AP. Perfusion imaging. Magn Reson Med 1992; 23:37–45.
4. Wang J, Alsop DC, Song HK, et al. Arterial transit time imaging with flow encoding arterial spin tagging (FEAST). Magn Reson Med 2003; 50(3):599–607.
5. Alsop DC, Detre JA. Reduced transit-time sensitivity in noninvasive magnetic resonance imaging of human cerebral blood flow. J Cereb Blood Flow Metab 1996; 16:1236–1249.
6. Parkes LM, Tofts PS. Improved accuracy of human cerebral blood perfusion measurements using arterial spin labeling: accounting for capillary water permeability. Magn Reson Med 2002; 48(1):27–41.
7. Edelman RR, Siewert B, Darby DG, et al. Qualitative mapping of cerebral blood flow and functional localization with echo-planar MR imaging and signal targeting with alternating radio frequency. Radiology 1994; 192:513–520.
8. Kim SG, Tsekos NV. Perfusion imaging by a flow-sensitive alternating inversion recovery (FAIR) technique: application to functional brain imaging. Magn Reson Med 1997; 37(3):425–435.
9. Wong EC, Buxton RB, Frank LR. A theoretical and experimental comparison of continuous and pulsed arterial spin labeling techniques for quantitative perfusion imaging. Magn Rason Med 1998; 40:348–355.
10. Wong EC, Buxton RB, Frank LR. Quantitative imaging of perfusion using a single subtraction (QUIPSS and QUIPSS II). Magn Reson Med 1998; 39:702–708.
11. Williams DS, Detre JA, Leigh JS, Koretsky AP. Magnetic resonance imaging of perfusion using spin inversion of arterial water. Proc Natl Acad Sci USA 1992; 89:212–216.
12. Sardashti M, Schwartzberg DG, Stomp GP, Dixon WT. Spin labeling angiography of the carotids by presaturation and simplified adiabatic inversion. Magn Reson Med 1990; 15:192–200.
13. Detre JA, Zhang W, Roberts DA, et al. Tissue specific perfusion imaging using arterial spin labeling. NMR Biomed 1994; 7:75–82.
14. Zaharchuk G, Ledden PJ, Kwong KK, Reese TG, Rosen BR, Wald LL. Multislice perfusion and perfusion territory imaging in humans with separate label and image coils. Magn Reson Med 1999; 41:1093–1098.
15. Hendrikse J, van der Grond J, Lu H, van Zijl PC, Golay X. Flow territory mapping of the cerebral arteries with regional perfusion MRI. Stroke 2004; 35(4):882–887.
16. Werner R, Norris DG, Alfke K, Mehdorn HM, Jansen O. Continuous artery-selective spin labeling (CASSL). Magn Reson Med 2005; 53(5):1006–1012.
17. Jones CE, Wolf RL, Detre JA, et al. Structural MRI of carotid artery atherosclerotic lesion burden and characterization of hemispheric cerebral blood flow before and after carotid endarterectomy. NMR Biomed 2006; 19(2):198–208.
18. Williams DS, Grandis DJ, Zhang W, Koretsky AP. Magnetic resonance imaging of perfusion in the isolated rat heart using spin inversion of arterial water. Magn Reson Med 1993; 30(3):361–365.
19. Walsh EG, Minematsu K, Leppo J, Moore SC. Radioactive microsphere validation of a volume localized continuous saturation perfusion measurement. Magn Reson Med 1993; 31:147–153.
20. Pell GS, King MD, Proctor E, et al. Comparative study of the FAIR technique of perfusion quantification with the hydrogen clearance method. J Cereb Blood Flow Metab 2003; 23(6):689–699.
21. Ewing JR, Cao Y, Knight RA, Fenstermacher JD. Arterial spin labeling: validity testing and comparison studies. J Magn Reson Imaging 2005; 22(6):737–740.
22. Ye FQ, Berman KF, Ellmore T, et al. H(2)(15)O PET validation of steady-state arterial spin tagging cerebral blood flow measurements in humans. Magn Reson Med 2000; 44(3):450–456.
23. Feng C M, Narayana S, Lancaster JL, et al. CBF changes during brain activation: fMRI vs. PET. Neuroimage 2004; 22(1):443–446.
24. Ye FQ, Frank JA, Weinberger DR, McLaughlin AC. Noise reduction in 3D perfusion imaging by attenuating the static signal in arterial spin tagging (ASSIST). Magn Reson Med 2000; 44(1):92–100.
25. Roberts DA, Detre JA, Bolinger L, Insko EK, Leigh JS Jr. Quantitative magnetic resonance imaging of human brain perfusion at 1.5 T using steady-state inversion of arterial water. Proc Natl Acad Sci USA 1994; 91:33–37.
26. Alsop DC, Detre JA. Multisection cerebral blood flow MR imaging with continuous arterial spin labeling. Radiology 1998; 208:410–416.
27. Wang J, Alsop DC, Li L, et al. Comparison of quantitative perfusion imaging using arterial spin labeling at 1.5 and 4.0 Tesla. Magn Reson Med 2002; 48(2):242–254.
28. Wang Z, Wang J, Connick TJ, Wetmore GS, Detre JA. Continuous ASL perfusion MRI with an array coil and parallel imaging at 3T. Magn Reson Med 2005; 54(3):732–737.
29. Hoehn-Berlage M, Norris DG, Kohno K, Mies G, Leibfritz D, Hossmann KA. Evolution of regional changes in apparent diffusion coefficient during focal ischemia of rat brain: the relationship of quantitative diffusion NMR imaging to reduction in cerebral blood flow and metabolic disturbances. J Cereb Blood Flow Metab 1995; 15(6):1002–1011.
30. Lythgoe MF, Thomas DL, Calamante F, et al. Acute changes in MRI diffusion, perfusion, T(1), and T(2) in a rat model of oligemia produced by partial occlusion of the middle cerebral artery. Magn Reson Med 2000; 44(5):706–712.

31. Shen Q, Meng X, Fisher M, Sotak CH, Duong TQ. Pixel-by-pixel spatiotemporal progression of focal ischemia derived using quantitative perfusion and diffusion imaging. J Cereb Blood Flow Metab 2003; 23(12):1479–1488.
32. Moseley ME, Cohen Y, Mintotovitch J, et al. Early detection of regional cerebral ischemia in cats: comparison of diffusion—and T2-weighted MRI and spectroscopy. Magn Reson Med 1990; 14:330–346.
33. Shen Q, Fisher M, Sotak CH, Duong TQ. Effects of reperfusion on ADC and CBF pixel-by-pixel dynamics in stroke: characterizing tissue fates using quantitative diffusion and perfusion imaging. J Cereb Blood Flow Metab 2004; 24(3):280–290.
34. Shen Q, Ren H, Fisher M, Bouley J, Duong TQ. Dynamic tracking of acute ischemic tissue fates using improved unsupervised ISODATA analysis of high-resolution quantitative perfusion and diffusion data. J Cereb Blood Flow Metab 2004; 24(8):887–897.
35. Bardutzky J, Meng X, Bouley J, Duong TQ, Ratan R, Fisher M. Effects of intravenous dimethyl sulfoxide on ischemia evolution in a rat permanent occlusion model. J Cereb Blood Flow Metab 2005; 25(8):968–977.
36. Wu O, Koroshetz WJ, Ostergaard L, et al. Predicting tissue outcome in acute human cerebral ischemia using combined diffusion- and perfusion-weighted MR imaging. Stroke 2001; 32(4):933–942.
37. Detre JA, Alsop DC, Vives LR, Maccotta L, Teener JW, Raps EC. Noninvasive MRI evaluation of cerebral blood flow in cerebrovascular disease. Neurology 1998; 50:633–641.
38. Chalela JA, Alsop DC, Gonzalez-Atavalez JB, Maldjian JA, Kasner SE, Detre JA. Magnetic resonance perfusion imaging in acute ischemic stroke using continuous arterial spin labeling. Stroke 2000; 31:680–687.
39. Jefferson AL, Glosser G, Detre JA, Sinson G, Liebeskind DS. Neuropsychological and perfusion MR imaging correlates of revascularization in a case of moyamoya syndrome. AJNR Am J Neuroradiol 2006; 27(1):98–100.

17 Clinical/Imaging Mismatch as an Index of the Penumbra

Jane F. Prosser
Department of Neurology, Royal Melbourne Hospital, Melbourne, Victoria, Australia

Antoni Davalos
Department of Neurosciences, Hospital Germans Trias i Pujol, Universitat Autonoma de Barcelona, Badalona, Spain

Stephen M. Davis
Department of Neurology, Royal Melbourne Hospital and University of Melbourne, Melbourne, Victoria, Australia

INTRODUCTION

Thrombolytic therapy in acute stroke patients is presently limited to the three-hour time window developed in clinical trials (1). If the time window is to be extended, and treatment targeted towards those most likely to benefit, more refined selection strategies are required. The ischemic penumbra is a variable region of critically hypoperfused but potentially salvageable tissue (2). The volume of penumbral tissue typically decreases with time as the infarct expands, but the duration of the potential therapeutic window is variable (3). Rapid, accurate detection of the presence and extent of penumbral tissue may permit thrombolysis to be delivered on the basis of each patient's unique stroke pathophysiology.

Diffusion-weighted imaging (DWI) identifies bioenergetically compromised tissue, and perfusion-weighted imaging (PWI) allows visualization of hypoperfused tissue (4,5). Mismatch between a larger PWI lesion and a smaller DWI lesion has been proposed to approximate the ischemic penumbra (6). It is now appreciated that the diffusion lesion may include potentially salvageable tissue, and the perfusion lesion may include regions of benign oligemia, but magnetic resonance imaging (MRI) is noninvasive and widely available (7,8).

Widespread use of the PWI–DWI mismatch paradigm to identify tissue-at-risk has been complicated by the technical complexities surrounding magnetic resonance perfusion imaging. As yet, there is neither consensus regarding the perfusion parameter and threshold that most accurately represents hypoperfused at-risk but salvageable tissue, nor is there an agreement on how "mismatch" itself is defined. In addition, many centers do not have rapid access to the technology required to generate and interpret perfusion maps. These difficulties have prompted consideration of potential alternative techniques to identify patients with substantial penumbral tissue without the use of MR perfusion imaging.

SEVERE STROKE, SMALL DIFFUSION-WEIGHTED IMAGE LESION: THE "CLINICAL-DIFFUSION MISMATCH"

It has been recognized that patients with clinically severe strokes may have very small DWI lesions on acute MRI, especially if imaging is performed early. The term "clinical-diffusion mismatch" (CDM) has been coined by Davalos et al. (9) to describe this paradox. The clinical deficit in these patients is presumably caused by widespread dysfunction of neural networks secondary to hypoperfusion (and/or diaschisis), which is insufficient to impair cellular homeostasis and water diffusion except in the ischemic "core." This assumption has been borne out by a number of studies that have found greater correlation between acute PWI lesion volumes and clinical stroke severity scores than between acute DWI lesion volumes and clinical scores (10–12). Davalos proposed that the National Institutes of Health Stroke Scale (NIHSS) might be useful as a surrogate measure of the volume of hypoperfused tissue, potentially bypassing some of the difficulties associated with MR perfusion imaging.

The original CDM paper was designed to test this new mismatch paradigm: that the presence of CDM would predict early stroke outcome and final infarct volume, regardless of the presence or absence of PWI–DWI mismatch (13). For the purposes of the analysis, CDM was defined arbitrarily as an NIHSS ≥8 and a DWI volume ≤25 mL. An NIHSS ≥8 has been associated with a high rate of neurological deterioration, a low frequency of spontaneous recovery, and cortical perfusion deficits in previous reports, and an exploratory post hoc analysis of the data demonstrated that almost all patients in this cohort with an NIHSS <8 had DWI volumes of <25 mL.

One hundred and sixty-six patients with hemispheric ischemic stroke were imaged with DWI within 12 hours of symptom onset and in survivors at 72±12 hours and 30±7 days. NIHSS score was evaluated just prior to the first MRI and at 24 and 72 hours. Emergent stroke therapies, including thrombolysis with recombinant tissue plasminogen activator (rtPA), were administered according to published guidelines. The MRIs were analyzed by neuroradiologists blinded to the clinical data using a manual segmentation method that took approximately 30 minutes of workstation time per sequence per patient.

CDM was found in 87 patients (52%, Group A). Patients without CDM were divided into those with large "matched" deficits (Group B, NIHSS ≥8, DWI ≥25mL) and those with small "matched" deficits (Group C, NIHSS <8, DWI ≤25mL).

Clinical and neuroimaging outcomes were different in patients with and without CDM. DWI lesion growth at day 3 was significantly greater in patients with CDM, as was the final infarct volume measured on fluid-attenuated inversion recovery sequence at day 30, after adjustment for baseline imbalances in known prognostic variables. This effect was seen in all patients but was more pronounced in those who did not receive reperfusion therapies. Among patients who did not receive reperfusion therapies, those with CDM were more likely to suffer early neurological deterioration (an increase in NIHSS >4 points) than those with small "matched" deficits [adjusted OR 22 (2.6, 183) $P = 0.004$] and large "matched" deficits [adjusted OR 2.9(1.1, 7.3) $P = 0.028$].

These findings are consistent with the assumption that the NIHSS score crudely reflects the total volume of ischemic brain and that CDM defines a group of patients with, on average, large volumes of tissue-at-risk as indicated by a greater likelihood of neurological deterioration and infarct expansion.

DOES CLINICAL-DIFFUSION MISMATCH CORRESPOND TO PERFUSION–DIFFUSION MISMATCH?

The critical issue for clinical practice is the reliability of CDM in predicting the presence of tissue-at-risk in individual patients. In the absence of a readily available gold standard for detection of penumbral tissue, our group evaluated the test performance characteristics of CDM against PWI–DWI mismatch as a surrogate for the "true" penumbra (14).

Patients presenting with sudden onset of a neurological deficit consistent with a cortical ischemic stroke who underwent emergent DWI and PWI imaging within 24 hours of stroke onset were eligible. Patients with cerebral hemorrhage or clinical syndromes consistent with lacunar and brainstem stroke were excluded.

Stroke onset was defined as the last time the patient was known to be without a neurological deficit. Clinical assessment including NIHSS was performed immediately prior to MRI. Subacute MRI was performed in surviving patients three to five days after symptom onset. Patients treated with rtPA or enrolled in a thrombolysis trial, those with evidence of hemorrhagic transformation causing mass effect, and those without a subacute scan were excluded from outcome analyses ($n = 30$).

CDM was initially defined as NIHSS ≥8, DWI ≤25 mL, in accordance with Davalos' paper (13). Acute PWI–DWI mismatch was examined as a continuous variable defined as: mismatch volume = $\mathrm{PWI}_{\mathrm{vol}} - \mathrm{DWI}_{\mathrm{vol}}$. PWI–DWI mismatch was also assessed as a categorical variable defined as: mismatch = $\mathrm{PWI}_{\mathrm{vol}} - \mathrm{DWI}_{\mathrm{vol}} / \mathrm{DWI}_{\mathrm{vol}} \times 100 > 20\%$ (15,16). Subacute DWI expansion was calculated as $\mathrm{DWI}_{\text{subacute vol}} / \mathrm{DWI}_{\text{acute vol}}$.

MRI scans were obtained with a 1.5 T echo-planar imaging (EPI)-equipped whole-body scanner. Postprocessing of raw DWI and PWI data was performed using the commercial software package Stroketool (Digital Imaging Systems, Dusseldorf, Germany). Isotropic DWI

TABLE 1 Baseline Clinical and Imaging Data

Time window (hr)	0–6	>6–24
n	54	25
Left hemisphere	32/54 (59%)	14/25 (56%)
Male	31/54 (57%)	13/25 (52%)
Median acute NIHSS (range)	14 (3–23)	9 (4–28)
Mean acute DWI volume (mL) (SEM)	38.6 (6.44)	33.4 (11.0)
Mean acute PWI volume (mL) (SEM)	110.2 (13.3)	52.4 (11.69)
PWI–DWI mismatch	40/54 (71%)	11/25 (44%)
Clinical–diffusion mismatch	22/54 (41%)	12/25 (48%)

Abbreviations: DWI, diffusion-weighted imaging; NIHSS, National Institutes of Health Stroke Scale; PWI, perfusion–weighted imaging; SEM, Standard error of the mean.

images were obtained by averaging the signal from all orthogonal directions with the highest diffusion weighting ($b = 1000$). Perfusion maps using T_{max} were calculated using the single-value decomposition method. The arterial input function was selected from a branch of the middle cerebral artery contralateral to the infarct. A semi-automated thresholding technique was used to calculate the volume of tissue with $T_{max} > 4$ seconds relative to a comparable region in the unaffected hemisphere.

DWI lesion volumes were measured manually using planimetric techniques. A standard window level was applied to the isotropic images. Volume measurements were determined by investigators blinded to NIHSS scores. Inter- and intra-observer variability of DWI volume measurements in our group has been previously published and is less than 5% (10).

A total of 79 patients were included in the study. Mean patient age was 72 ± 10 years. Median time to MRI scan from stroke onset was 5.3 hours (range 1.5–23); 54 patients (64%) were imaged within six hours. Median NIHSS and mean DWI and PWI lesion volumes were all larger in the zero to six hours group (Table 1).

Prevalence of Clinical-Diffusion Mismatch Relative to Perfusion-Weighted Imaging–Diffusion-Weighted Imaging Mismatch

A total of 34/79 (43%) patients fulfilled the proposed definition of CDM, and 51 (65%) had PWI–DWI mismatch. In the 54 patients imaged within six hours, CDM was present in 22 (41%) and PWI–DWI mismatch in 40 (75%). In the patients studied between 6 and 24 hours, CDM was present in 12/25 (48%) and PWI–DWI mismatch in 11 (44%, Table 1).

Correlation of Acute Stroke Volumes and NIHSS

Acute DWI volume and NIHSS score were not significantly correlated in patients imaged within six hours ($r = 0.21$, $P = 0.13$). Between 6 and 24 hours, there was a highly significant positive correlation between DWI volume and NIHSS score ($r = 0.82$, $P < 0.001$). Acute PWI volume was positively correlated with NIHSS score both in the sub-six-hour cohort ($r = 0.49$, $P < 0.001$) and in the 6-to-24-hour cohort ($r = 0.59$, $P = 0.002$). For any given NIHSS score, patients with left-sided lesions had similar PWI volumes compared with those with right-sided lesions [coefficient −0.81 (−1.64, 0.02) (cube root of PWI volume), $P = 0.055$].

In the sub-six-hour cohort, the NIHSS was trichotomized as mild (0–7), moderate (8–14), and severe (15–23) to ascertain if quantitative information about stroke volume could be inferred from clinical stroke severity as measured by the NIHSS (Fig. 1). In the mild category, DWI and PWI volumes were not significantly different ($P = 0.5$). However, in the moderate and severe categories, the PWI volume was significantly larger than the DWI volume ($P < 0.001$ in both cases). The median DWI and PWI lesion volumes tended to increase with increasing stroke severity, though this was much more prominently seen in the PWI volumes.

Sensitivity and Specificity Analysis

The sensitivity of CDM (NIHSS ≥8, DWI ≤25 mL) in predicting PWI–DWI mismatch was 55% (95% CI 40–69%) and the specificity was 79% (95% CI 59–92%) (Table 2). In sub-six-hour patients,

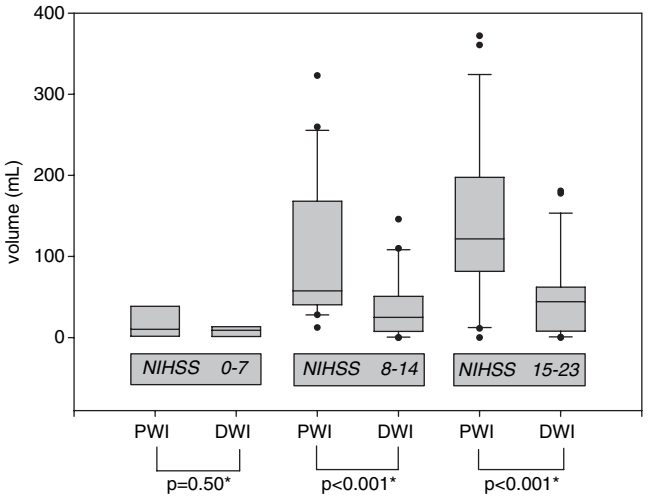

FIGURE 1 Box plot describing perfusion-weighted imaging (PWI) (T_{max} + 4 seconds) and diffusion-weighted imaging (DWI) volumes for strokes of increasing severity as categorized by the NIHSS, in patients imaged within six hours of symptom onset. For moderate and severe strokes (NIHSS ≥8), median PWI lesion volume is significantly higher than the corresponding DWI volume. Both median DWI and PWI lesion volumes tend to increase with increasing stroke severity, but PWI volume is better correlated with NIHSS. *Mann–Whitney rank sum test.

the sensitivity of CDM in detecting PWI–DWI mismatch was 53%, (95% CI 36–68%), with a specificity of 93% (95% CI 64–100%) and a correct classification rate of 59% (Fig. 2). Altering the definition of CDM changed its test performance characteristics (Fig. 3). Decreasing the DWI cutpoint or increasing the NIHSS threshold resulted in greater specificity at the price of reduced sensitivity. Below a DWI volume of 25 mL, no increase in specificity was achieved with either NIHSS threshold or DWI volume. No combination of a single DWI volume cutpoint and a single NIHSS threshold was both highly sensitive and highly specific. The kappa statistic for agreement between CDM and PWI–DWI mismatch was 0.29 (0.11–0.48) for all patients and 0.32 (0.13–0.51) for the zero to six-hour time window, indicating modest but statistically significant agreement beyond that which would be expected by chance alone.

Predicting Subacute Tissue Fate

Subacute MRI scans were used to assess the ability of CDM to predict DWI expansion. The median DWI expansion ratio in CDM-positive patients (2.3, inter-quartile range 1.5–5.4) was significantly greater than in CDM-negative patients (1.4, inter-quartile range 1.1–2.4, $P = 0.012$). A similar degree of DWI expansion was seen in patients with PWI–DWI mismatch (median expansion ratio 2.3, inter-quartile range 1.4–5.6; Fig. 4). Significant DWI expansion (>20%) was observed in 22/22 patients with CDM and 27/28 with PWI–DWI mismatch. Univariate linear regression indicated that CDM was a better predictor of DWI expansion in patients imaged within six hours ($r^2 = 0.29$, $P = 0.013$) relative to those imaged 6 to 24 hours ($r^2 = 0.10$, $P = 0.031$).

TABLE 2 Sensitivity and Specificity Analysis for Clinical–Diffusion Mismatch as a Test for Perfusion-Weighted Imaging–Diffusion-Weighted Imaging Mismatch

Time window	All patients ($n = 79$)	0–6 h ($n = 54$)
Sensitivity (95% CI)	55% (40–69%)	53% (36–68%)
Specificity (95% CI)	79% (59–92%)	93% (66–100%)
PPV (95% CI)	82% (65–93%)	95% (77–100%)
NPV (95% CI)	49% (34–64%)	41% (24–59%)
Correctly classified	63%	63%
Area under ROC curve (95% CI)	0.67 (0.56–0.77)	0.73 (0.62–0.83)

Abbreviations: NPV, negative predictive value; PPV, positive predictive value; ROC, receiver-operating characteristic.

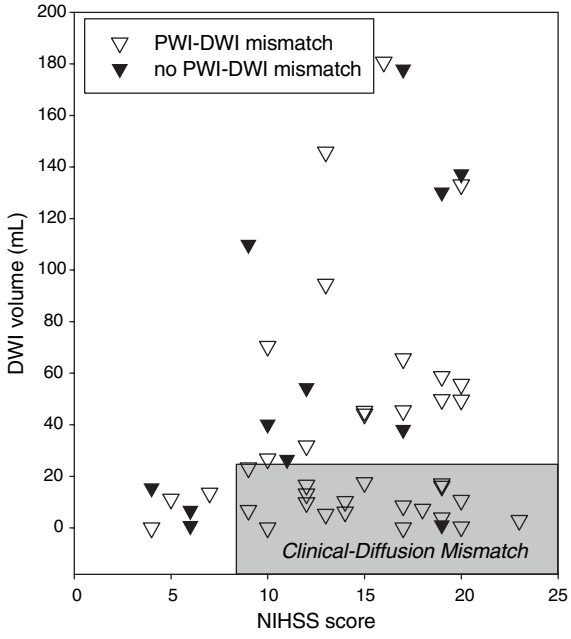

FIGURE 2 Scatter plot of diffusion-weighted imaging (DWI) lesion volumes versus NIHSS scores for patients imaged within six hours of symptom onset. In this cohort, the proposed definition of clinical-diffusion mismatch (CDM) has a high positive predictive value for perfusion–diffusion mismatch (PDM) (all but one CDM patient also have PDM). *Abbreviation*: PWI, perfusion-weighted imaging.

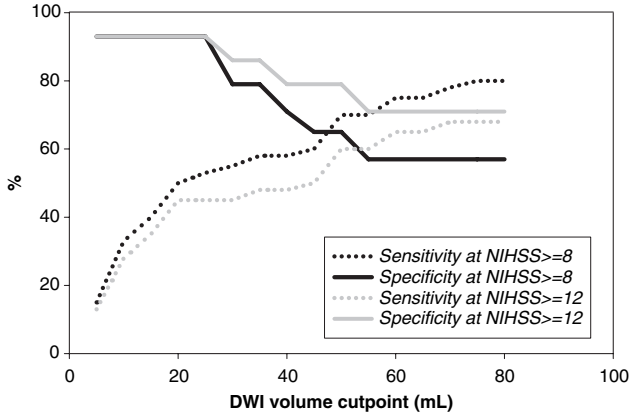

FIGURE 3 Plot demonstrating sensitivity and specificity (%) of clinical-diffusion mismatch (CDM) for perfusion–diffusion mismatch (PDM) at increasing diffusion-weighted imaging (DWI) volume cutpoints and two NIHSS thresholds. Specificity declines above a DWI volume of 25 mL. An NIHSS threshold of ≥8 is more sensitive than a threshold of ≥12. A high degree of sensitivity and specificity cannot be achieved with any one definition of CDM. *Abbreviation*: DWI, diffusion-weighted imaging.

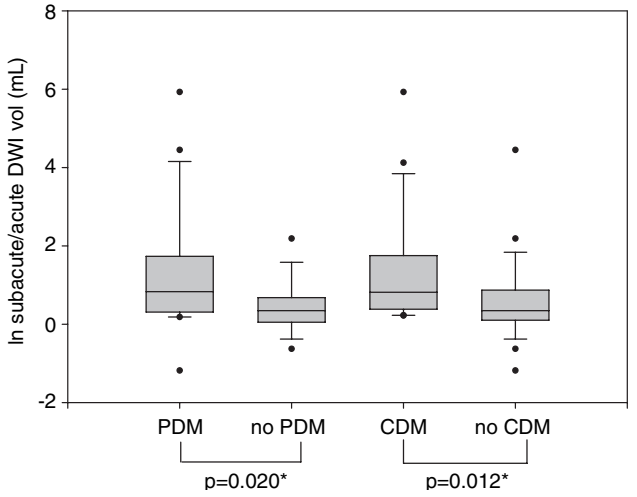

FIGURE 4 Box plot demonstrating subacute diffusion-weighted imaging (DWI) expansion ratios for clinical-diffusion mismatch (CDM) and perfusion–diffusion mismatch (PDM) patients. Both CDM and PDM patients show a similar, significant degree of subacute DWI expansion. *Mann–Whitney rank sum test.

Predicting Change in NIHSS

There was no statistically significant difference in the proportion of patients suffering early neurological deterioration (defined as an increase of ≥4 points on NIHSS at 72 hours) between CDM-positive and negative patients (2/22 vs. 5/27, $P = 0.44$) and between those with and without PWI–DWI mismatch (2/28 vs. 5/17, $P = 0.09$).

CLINICAL-DIFFUSION MISMATCH IS LESS COMMON THAN PERFUSION-WEIGHTED IMAGING–DIFFUSION-WEIGHTED IMAGING MISMATCH

We found that CDM was present in 41% of our cohort imaged within six hours of symptom onset. This is similar to that reported by Davalos, who found that 74% had CDM sub-three hours and 48% from three to six hours (13) This was significantly lower than the corresponding proportion with perfusion–diffusion mismatch (76%) studied within the same time interval.

CLINICAL SCORES AS SURROGATES FOR ACUTE LESION VOLUMES

The concept of CDM is based on the assumption that the acute NIHSS score is a useful surrogate marker of the total volume of functionally impaired brain tissue, which could potentially replace PWI in the assessment of acute stroke patients. If this assumption is correct, the NIHSS should be more strongly correlated with the acute PWI volume than the DWI volume in patients with PWI–DWI mismatch. Indeed, PWI deficits have been previously reported to be more strongly correlated than DWI lesion volume with acute clinical scores (10–12). The present study adds to the existing evidence that within six hours, where a high proportion of patients have PWI–DWI mismatch, acute NIHSS scores are correlated more strongly with PWI than DWI lesion volumes. Thus, the rationale for using acute NIHSS as a surrogate for PWI is supported by the available data. There are, however, some important caveats—the quantitative relationship between NIHSS score and actual perfusion lesion volume is loose, even in this selected patient group. The NIHSS may systematically overestimate the hypoperfused volume because of diaschisis, or underestimate it if some hypoperfused at-risk tissue retains function. In addition, we excluded patients with brainstem and lacunar syndromes as correlation of NIHSS score with stroke volume is likely to be poor in the posterior circulation and in lacunar stroke (17). The NIHSS may also be biased against right hemisphere strokes (systematically underestimating stroke volumes relative to left hemisphere lesions with the same NIHSS score, especially at low NIHSS scores), though we did not observe this in our patient cohort, where there were relatively few subjects with NIHSS <8 (18,19).

Bearing in mind limitations of the NIHSS, Reineck et al. (20) have proposed using a battery of language tests in left hemisphere stroke patients as a surrogate for the acute PWI volume. The same group has previously demonstrated superior correlations between PWI volumes and tests of hemispatial neglect than with NIHSS (21).They found reasonable correlations between test scores and stroke volumes. Intriguingly, they demonstrated that CDM defined in this way predicted potential for short-term language improvement, rather than deterioration, and hypothesized that this was due to spontaneous reperfusion. Whether this mismatch paradigm is superior (or adds incremental value) to the NIHSS-based CDM was not addressed in the study.

CLINICAL-DIFFUSION MISMATCH AS A DIAGNOSTIC TOOL

Specificity (93%) and positive predictive value (95%) within the six-hour time window appear to be the major strengths of CDM using the proposed criteria. The sensitivity of CDM is at best only modest. It is apparent that no single combination of NIHSS threshold and DWI volume cut point could be both sensitive and specific (Fig. 2). Reducing the DWI cutpoint to less than 25 mL or increasing the NIHSS threshold above eight does not lead to a useful increase in specificity. It is possible that reducing the NIHSS threshold below eight may lead to improved sensitivity without sacrificing specificity but there were too few subjects in our cohort with NIHSS scores below eight to attempt a meaningful analysis.

Davalos' group (22) has subsequently presented data comparing PWI–DWI mismatch with CDM. They studied 79 patients under 12 hours and found PDM in 75% and CDM in 47%. They found that the two definitions agreed in 31 patients, with no agreement in 34, and a kappa statistic of 0.16. Based on their data, the calculated sensitivity of CDM as a test for PWI–DWI mismatch is 53%, with 70% specificity (in patients studied within 12 hours of stroke onset). Data on sub-six-hour patients were not presented separately.

A further small study of 39 patients examining exactly the same question generated a kappa of 0.04, indicating no correspondence between the groups other than that would be expected by chance alone (23). This result is surprising, given the known positive correlations between the NIHSS and stroke volumes, especially PWI.

An alternative strategy to a threshold method for defining a clinical-imaging mismatch is suggested in a recent paper by Kent et al. (24), exploring the utility of clinical-CT mismatch. They first attempted to define a matched deficit by analyzing a group of patients in whom an NIHSS score and CT brain were performed at 24 hours after stroke onset. They used a linear regression of NIHSS on ASPECTS score [a validated measure of early infarct extent on CT (25)] to define a matched deficit, presuming no mismatch at 24 hours. They then used this regression in a larger group of patients to generate an "expected" acute ASPECTS score based on the acute NIHSS and quantified mismatch as the difference between the observed and expected ASPECTS score. This concept could potentially be applied to CDM to generate a continuous scale of DWI volumes and corresponding NIHSS scores to enable those patients with potential penumbral tissue but an NIHSS <8 or a DWI >25 mL to be evaluated.

The accuracy of CDM as a diagnostic test to predict the presence of perfusion–diffusion mismatch is critically dependent on the definition of PWI–DWI mismatch. Presently, there is no gold standard MRI definition of PWI–DWI mismatch. We selected a definition based on the perfusion parameter T_{max}, which is the time to peak MR signal intensity change after deconvolution. It has been shown previously that $T_{max} + 2$ and $T_{max} + 4$ seconds correlate best with acute NIHSS (12). In a recent systematic comparison of PWI–DWI mismatch definitions, we have found that one based on $T_{max} + 4$ seconds is a very conservative estimate of the volume of actual tissue-at-risk (26). Given the remaining uncertainty of the significance of moderate oligemia ($T_{max} < 4$ seconds), we did not include this tissue in our PWI–DWI definition. In fact, doing so would have only resulted in a decrease in the specificity of CDM with no effect on the sensitivity.

It is also apparent that the time of assessment affects CDM performance. In our study, the proportion of patients with CDM is higher in the 6-to-24-hour window than in the zero to six-hour window. This is not biologically plausible, as CDM should become less frequent with increasing duration of symptoms, in concordance with PWI–DWI mismatch (3) The poor performance of CDM in predicting PWI–DWI mismatch beyond a six-hour time window may partially reflect the patient sample. In our study, patients assessed beyond six hours had smaller DWI lesion volumes and NIHSS scores compared to those assessed more acutely (though many still fulfilled criteria for CDM). This is consistent with the previously reported observation that milder strokes tend to present later (27). As the time from onset increases, these smaller lesions are increasingly likely to represent completed strokes rather than small DWI lesions within a larger perfusion abnormality. It may be that a more specific definition may be required if CDM is to be usefully applied beyond a six-hour time window.

CONCLUSION

Our study and others confirm that although CDM appears to have a relatively low sensitivity for detecting PWI–DWI mismatch, the presence of CDM is highly predictive of subsequent expansion of the acute DWI lesion three to five days after symptom onset. This supports the hypothesis that patients with CDM have tissue that is at risk for infarction, but also potentially amenable to salvage, though we note that the subacute MRI scans may overestimate the final infarct volume because of the presence of edema. Overall, our results appear supportive of the original definition of CDM, and are consistent with its rationale, as an NIHSS score ≥8 was originally chosen due to its association with higher rates of early neurological deterioration and lower frequency of spontaneous recovery (13,28,29).

CDM may be a useful approach for selection of patients for acute stroke therapy as CDM has now been shown to predict infarct expansion. In addition, our data demonstrates statistically significant agreement between CDM and PWI–DWI mismatch, with very high specificity and positive predictive value in patients studied within six hours of onset. However, CDM is not particularly sensitive for PWI–DWI mismatch, and a recent abstract with a similar study design demonstrated poor agreement between CDM and PWI–DWI mismatch (no better than could be expected by chance) (23). We suggest that CDM should be independently, prospectively tested as a predictor of response to thrombolysis. Although the PWI–DWI mismatch hypothesis remains unproven at this point, selection for thrombolysis based on CDM (as opposed to PWI–DWI mismatch) would avoid the extra scan time and problems of interpretation associated with PWI.

The studies that form the basis of this analysis were performed in a highly selected patient population from tertiary referral hospitals. The results cannot be generalized to all acute stroke patients. Nonetheless, the concept of CDM warrants testing in a multicenter randomized controlled trial of thrombolysis in acute stroke.

REFERENCES

1. The National Institute of Neurological Disorders and Stroke rt-PA Stroke Study Group. Tissue plasminogen activator for acute ischemic stroke. N Engl J Med 1995; 333:1581–1588.
2. Astrup J, Siesjo BK, Symon L. Thresholds in cerebral ischemia—the ischemic penumbra. Stroke 1981; 12:723–725.
3. Darby DG, Barber PA, Gerraty RP, et al. Pathophysiological topography of acute ischemia by combined diffusion-weighted and perfusion MRI. Stroke 1999; 30:2043–2052.
4. Kidwell CS, Saver JL, Mattiello J, et al. Diffusion-perfusion mr evaluation of perihematomal injury in hyperacute intracerebral hemorrhage. Neurology 2001; 57:1611–1617.
5. Baird AE, Warach S. Magnetic resonance imaging of acute stroke [erratum appears in J Cereb Blood Flow Metab 1998; 18(10):preceding 1047]. 1998; 583–609.
6. Schlaug G, Benfield A, Baird AE, et al. The ischemic penumbra: Operationally defined by diffusion and perfusion MRI. Neurology 1999; 53:1528–1537.
7. Kidwell CS, Saver JL, Mattiello J, et al. Thrombolytic reversal of acute human cerebral ischemic injury shown by diffusion/perfusion magnetic resonance imaging. Ann Neurol 2000; 47:462–469.
8. Parsons MW, Yang Q, Barber PA, et al. Perfusion magnetic resonance imaging maps in hyperacute stroke: Relative cerebral blood flow most accurately identifies tissue destined to infarct. Stroke 2001; 32:1581–1587.
9. Davalos ALR, Pedraz S, Castillo J. The clinical-DWI mismatch: a new diagnostic clue in the treatment of acute ischemic stroke. Stroke 2003; 34:254.
10. Barber PA, Darby DG, Desmond PM, et al. Prediction of stroke outcome with echoplanar perfusion- and diffusion-weighted MRI. Neurology 1998; 51:418–426.
11. Mitsias PD, Jacobs MA, Hammoud R, et al. Multiparametric mri isodata ischemic lesion analysis: Correlation with the clinical neurological deficit and single-parameter MRI techniques. Stroke 2002; 33:2839–2844.
12. Shih LC, Saver JL, Alger JR, et al. Perfusion-weighted magnetic resonance imaging thresholds identifying core, irreversibly infarcted tissue. Stroke 2003; 34:1425–1430.
13. Davalos A, Blanco M, Pedraza S, et al. The clinical-DWI mismatch: a new diagnostic approach to the brain tissue at risk of infarction. Neurology 2004; 62:2187–2192.
14. Prosser J, Butcher K, Allport L, et al. Clinical-diffusion mismatch predicts the putative penumbra with high specificity. Stroke 2005; 36:1700–1704.
15. Parsons MW, Barber PA, Chalk J, et al. Diffusion- and perfusion-weighted MRI response to thrombolysis in stroke. Ann Neurol 2002; 51:28–37.
16. Coutts SB, Simon JE, Tomanek AI, et al. Reliability of assessing percentage of diffusion-perfusion mismatch. Stroke 2003; 34:1681–1683.
17. Linfante I, Llinas RH, Schlaug G, Chaves C, Warach S, Caplan LR. Diffusion-weighted imaging and national institutes of health stroke scale in the acute phase of posterior-circulation stroke. Arch Neurol 2001; 58:621–628.
18. Fink JN, Selim MH, Kumar S, et al. Is the association of national institutes of health stroke scale scores and acute magnetic resonance imaging stroke volume equal for patients with right- and left-hemisphere ischemic stroke? Stroke 2002; 33:954–958.
19. Nighoghossian N, Hermier M, Adeleine P, et al. Baseline magnetic resonance imaging parameters and stroke outcome in patients treated by intravenous tissue plasminogen activator. Stroke 2003; 34:458–463.

20. Reineck LA, Agarwal S, Hillis AE. "Diffusion-clinical mismatch" is associated with potential for early recovery of aphasia. Neurology 2005; 64:828–833.
21. Hillis AE, Wityk RJ, Barker PB, Ulatowski JA, Jacobs MA. Change in perfusion in acute nondominant hemisphere stroke may be better estimated by tests of hemispatial neglect than by the national institutes of health stroke scale. Stroke 2003; 34:2392–2396.
22. Davalos A, Blanco M, Pedraza S, et al. Clinical-diffusion mismatch predicts penumbra in patients with salvageable ischemic brain: P265. Stroke 2005; 36:489.
23. Lansberg M, Thijs V, Bammer R, et al. Who is most likely to benefit from TPA? The perfusion-diffusion and clinical-diffusion mismatch models disagree. Stroke 2005; 36:437.
24. Kent DM, Hill MD, Ruthazer R, et al. "Clinical-CT mismatch" and the response to systemic thrombolytic therapy in acute ischemic stroke. Stroke 2005; 36:1695–1699.
25. Barber PA, Demchuk AM, Zhang J, Buchan AM. Validity and reliability of a quantitative computed tomography score in predicting outcome of hyperacute stroke before thrombolytic therapy. Aspects study group. Alberta stroke programme early CT score. Lancet 2000; 355:1670–1674.
26. Butcher K, Parsons M, MacGregor L, et al. Refining the perfusion-diffusion mismatch hypothesis. Stroke. 2005; 36(6):1153–1159.
27. Menon SC, Pandey DK, Morgenstern LB. Critical factors determining access to acute stroke care. Neurology 1998; 51:427–432.
28. DeGraba TJ, Hallenbeck JM, Pettigrew KD, Dutka AJ, Kelly BJ. Progression in acute stroke: Value of the initial NIH stroke scale score on patient stratification in future trials. Stroke 1999; 30:1208–1212.
29. Tong DC, Yenari MA, Albers GW, O'Brien M, Marks MP, Moseley ME. Correlation of perfusion- and diffusion-weighted MRI with NIHSS score in acute (<6.5 hour) ischemic stroke [see comment]. Neurology 1998; 50:864–870.

18 The Topography of the Ischemic Penumbra

Romesh Markus
Department of Neurology, St. Vincent's Hospital, and Department of Medicine, University of New South Wales, Sydney, Australia

David Reutens
Department of Medicine, Monash Medical Center, Melbourne, Victoria, Australia

Geoffrey A. Donnan
National Stroke Research Institute, Austin Health, University of Melbourne, Melbourne, Victoria, Australia

INTRODUCTION

Focal cerebral ischemia initiates a complex series of pathophysiological changes in the vascular territory of the occluded artery. Hypoperfused, hypoxic but initially viable tissue (the ischemic penumbra) is progressively transformed to infarction as a result of a time dependent cascade of functional and metabolic changes induced by ischemia (1). The ischemic penumbra is, therefore, a dynamic region that undergoes change in both time and space.

Acute stroke therapy is aimed at salvaging the ischemic penumbra on the assumption that limiting infarct size will result in improved neurological outcome (2). The time and space components of the ischemic penumbra have important therapeutic implications. The time component or duration of survival of the ischemic penumbra is tightly linked to the time window in which therapeutic interventions are likely to be beneficial (3). The functional benefit resulting from successful therapeutic intervention is linked to the volume and location or the space component of the ischemic penumbra that is saved from undergoing infarction.

The dynamic nature of the ischemic penumbra mandates that study of its topography must be correlated with the duration of ischemia. In experimental stroke in animal models, it is possible to analyze the dynamic changes that occur in location of the ischemic penumbra by performing serial imaging studies. In contrast, in humans, we are limited to usually one or at most two to three imaging studies that give a single "snapshot" in time of the penumbra. In this chapter, we review the data regarding penumbral topography from experimental stroke models and then discuss the methodology, validation, and results of a model that enables quantitative analysis of penumbral topography in humans with ischemic stroke.

TOPOGRAPHY OF PENUMBRA IN EXPERIMENTAL ANIMAL MODELS

Repeated multitracer positron emission tomography (PET) studies have been used to document serial pathophysiological changes in the brain following experimental ischemia induced by middle cerebral artery (MCA) occlusion in baboons (4–6), cats (7), and dogs (8).

PET Studies in Primates

Following permanent MCA occlusion in monkeys, raised oxygen extraction fraction (OEF) was observed by Tenjin et al. (9) in regions with cerebral blood flow (CBF) reduction between 18 and 31 mL/100 g/min. OEF was significantly raised in the core of ischemia where the CBF was most severely reduced (<18 mL/100 g/min) when the study was performed one hour after occlusion. Nine hours after occlusion, the OEF values were lower compared with those one and three hours after occlusion.

Pappata et al. (4) observed a similar increase in OEF in the area of hypoperfusion one hour after permanent MCA occlusion in baboons. Impaired oxidative metabolism indicated by reduced cerebral metabolic rate of oxygen ($CMRO_2$) and declining OEF was observed in the

deep MCA region when the study was repeated three to four hours after MCA occlusion. Prolonged tissue viability in the cortical MCA territory was suggested by the observation of relatively preserved $CMRO_2$ and increased OEF at three to four hours.

Kuge et al. (10) determined serial CBF and cerebral metabolic rate of glucose (CMR_{glc}) using PET in a thromboembolic stroke model in the baboon. In the ischemic core that underwent infarction, CBF was severely reduced at one hour, and decreased further with time. In contrast, the cortical region that survived without infarction was less severely hypoperfused at one hour, showing uncoupling of the CBF and CMR_{glc}, which resolved with gradual recovery of the CBF.

These observations that earlier and more severe metabolic changes occurred in the deep MCA territory than in the cortical MCA territory after focal ischemia were replicated in experiments conducted by Touzani et al. (11). These investigators performed sequential multitracer PET studies before, and 1, 4, 7, and 24 hours and 14 to 29 days after permanent MCA occlusion in baboons. They observed that the volume of severely hypometabolic tissue, as defined by decreased $CMRO_2$, increased and evolved from the deep MCA territory to the cortical territory over 24 hours until it was maximal in the chronic stage study. Infarcts were confirmed by histology 19 to 41 days after occlusion, and the pattern of evolution of the hypometabolic tissue was taken to indicate transition of penumbral tissue to infarction, which in this model occurred over days.

The effect of reperfusion on the spatial and temporal evolution of infarction was subsequently examined by performing temporary MCA occlusion in the same baboon model (5,6,12). Reperfusion at six hours after MCA occlusion was associated with an approximately 85% decrease in volume of the final infarct, defined histologically at four weeks, in comparison with that following permanent MCA occlusion (12). Reperfusion at six hours was associated with reversal and limitation of the temporal and spatial evolution of the hypometabolic volume on serial PET studies suggesting salvage of penumbral tissue (5,6).

PET Studies in Cats

In cats, studied sequentially with multitracer PET following permanent MCA occlusion, Heiss et al. (7) reported an immediate decrease of CBF to <30% of control levels on arterial occlusion. Initially, there was relative preservation of $CMRO_2$ and increase in OEF in this region. With time, there was spread of the ischemic penumbra from the center to the borders of the MCA territory. This sequence of metabolic changes, indicating transition of the penumbra to necrosis evolved until infarction was complete, 18 to 24 hours after MCA occlusion (Fig. 1).

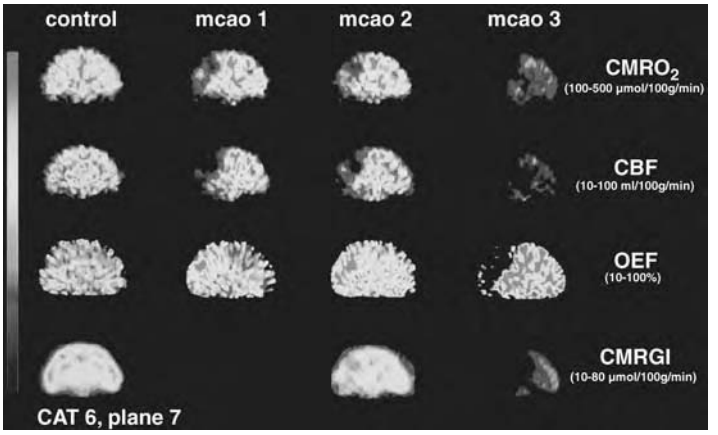

FIGURE 1 Sequential qualitative positron emission tomography images of a coronal section of a cat at three time points after permanent MCAO. Control image was obtained 30 minutes prior to occlusion MCAO. MCAO 1, 2, and 3 correspond to 1, 2 to 3, and 18 to 24 hours after occlusion. The progressive deterioration of oxygen consumption in the MCA territory corresponds to the spreading of the area with increased oxygen extraction fraction. *Abbreviations*: CBF, cerebral blood flow; CMRGI, cerebral metabolic rate of glucose; $CMRO_2$, cerebral metabolic rate of oxygen; MCAO, middle cerebral artery occlusion; OEF, oxygen extraction fraction. *Source*: From Ref. 7.

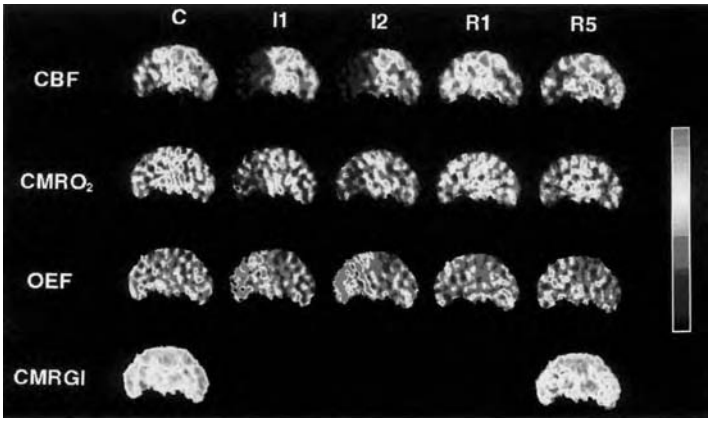

FIGURE 2 Sequential positron emission tomography images from a cat that survived transient MCAO. Images show cerebral blood flow, $CMRO_2$, OEF, and cerebral metabolic rate of glucose before (C), immediately (I1), and 30 minutes after the start of 60 minutes of MCAO (I2), as well as immediately (R1) and 4.5 hours after reperfusion (R5). In this animal, during the ischemic period, $CMRO_2$ did not deteriorate further and the OEF increase persisted. Hyperperfusion was not pronounced in this animal. *Abbreviations*: CBF, cerebral blood flow; $CMRO_2$, cerebral metabolic rate of oxygen; CMRGl, cerebral metabolic rate of glucose; MCAO, middle cerebral artery occlusion OEF, oxygen extraction fraction. *Source*: From Ref. 13.

The effect of the duration of ischemia on these sequential metabolic changes observed with multitracer PET was studied in a reversible MCA occlusion model in cats (13). Transient MCA occlusion in this model for 30, 60, and 120 minutes was followed by reperfusion for 24 hours (Fig. 2).

An immediate decrease of CBF to <30% of control levels with preserved $CMRO_2$ and increased OEF was observed in the MCA territory in all cats on arterial occlusion—an observation similar to that following permanent MCA occlusion. Reperfusion within 30 minutes of MCA occlusion was associated with rapid normalization of CBF and $CMRO_2$, and all cats survived without infarction. The initial OEF elevation persisted throughout the ischemic period in cats that survived 24 hours of reperfusion following MCA occlusion for 60 and 120 minutes, and their infarcts were restricted to the center of the MCA territory. In contrast, in animals that died, the initial OEF increase was short-lived, indicating that irreversible damage of brain tissue had occurred during the period of ischemia (Fig. 3).

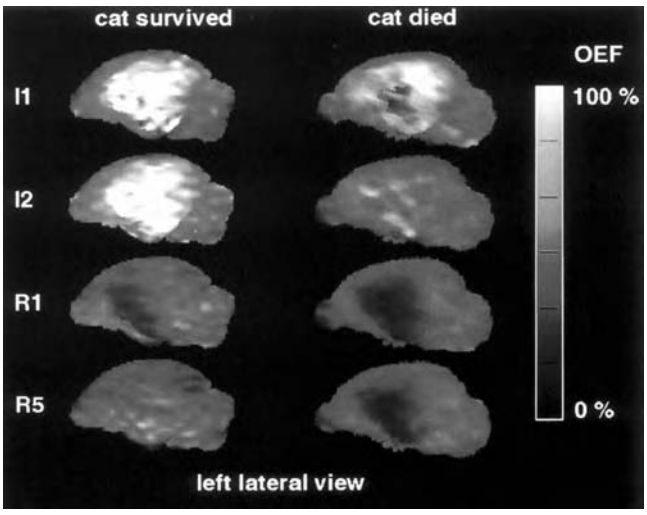

FIGURE 3 OEF and functional outcome in cats following transient middle cerebral artery occlusion. Two examples of variable development of OEF during ischemia (I1, I2) and reperfusion (R1, R5). Reconstructed surface views of OEF show dynamic deterioration in OEF in the cat that finally died, as compared to an almost complete recovery in the surviving cat. *Abbreviation*: OEF, oxygen extraction fraction. *Source*: From Ref. 13.

The applicability of the central benzodiazepine ligand, ^{11}C-Flumazenil (^{11}C-FMZ), that binds to glutamate and γ-amino-butyric acid (GABA) receptors on neurons (14) was tested for its ability to detect irreversibly injured cortical regions after transient MCA occlusion in cats (15). The defect in FMZ binding two to three hours after MCA occlusion was related to the region with severely depressed oxygen consumption and the size of the infarct.

Experimental Studies in Rats

Ginsberg et al. (16) developed a technique of spatial alignment of autoradiographic and histological datasets from rats subjected to MCA occlusion into a common spatial template. This method permitted three-dimensional analysis of the topography of the ischemic penumbra and pixel-by-pixel correlation with histological changes. In rats subjected to MCA occlusion local cerebral blood flow (LCBF) or glucose utilization (LCMRglc) were measured autoradiographically at 1.5 hours postocclusion. The ischemic penumbra (defined as LCBF 20–40% of control) surrounded the ischemic core (defined as LCBF 0–20% of control), particularly, at the anterior and posterior poles of the core zone. The averaged LCMRglc/LCBF ratio dataset revealed marked metabolism-flow uncoupling in penumbral pixels, averaging nearly five-fold above control ratio values. Histopathological infarction after a three-day survival was highly correlated with the severity of LCBF reduction at two hours post-MCA occlusion with 70% of infarcted pixels having LCBF values in the core range (17).

In rats studied by magnetic resonance imaging (MRI), restricted diffusion was observed one hour after MCA occlusion only at the center of the perfusion deficit, but at 24 hours encompassed the entire region, which at one week showed changes of infarction on histology (18). These qualitative descriptions are compatible with the concept of dynamic infarct expansion occurring at the expense of the ischemic penumbra (19).

In summary, these findings from sequential studies in several different experimental animal stroke models show that the transition of viable penumbral tissue to irreversible infarction is a dynamic process that evolves spatially and temporally, and have given important insights into the duration and factors influencing its survival (20). These studies have also shown that the progress of penumbra to infarction can be stopped by timely reperfusion limiting the infarct to the ischemic core. This indicates that the topographical relationship between penumbra and infarct core has crucial implications for the likely functional benefit from reperfusion.

TOPOGRAPHY OF PENUMBRA IN HUMAN ISCHEMIC STROKE

The spatial and temporal evolution of the ischemic penumbra has been assumed to be similar in humans and animals, although this assumption has not been previously tested (19). In humans using multitracer PET, investigators have identified hypoperfused tissue with preserved energy metabolism, compatible with penumbra in the acute stages after stroke (21,22). This tissue was observed predominantly over the cortical mantle and was present on early, but not follow-up, PET scans. Late CT showed a corresponding area of infarction. Survival of this tissue was associated with a better neurological outcome (23). Investigators using MRI have described several different patterns of mismatch between perfusion and diffusion abnormalities reflecting the heterogeneous topography of human stroke (24). However, this technique has yet to be used to obtain a quantitative evaluation of the temporal evolution of the penumbra.

A method of mapping the distribution of the penumbra in humans, applicable to different imaging modalities, including both PET and MRI, would be useful to characterize factors that influence its spatial extent. A reliable method of identifying the spatial location of the penumbra is of importance because the location as well as the volume of penumbra may have a bearing on the potential outcome of interventions aimed at tissue salvage. Although persistence of penumbral tissue has been demonstrated in many patients studied within 24 hours of stroke onset (19), to be beneficial, thrombolysis must be instituted within three to six hours (25,26). A variety of neuroprotective strategies administered within 24 hours have not shown benefit in humans despite their effectiveness in animal models (27). Although there are many other potential explanations that may account for these findings, it has been suggested that within the

ischemic zone there are regions, where different pathophysiological mechanisms account for conversion of penumbral tissue to infarction (28). These subcompartments will have different times of survival and, therefore, different time windows of therapeutic opportunity, and may have differing impacts on clinical outcome. Further exploration of these intriguing findings requires a method of systematically characterizing the spatial extent of the penumbra.

Quantitative Analysis of Penumbral Topography in Humans

In humans following ischemic stroke, repeated studies to evaluate the topography of the penumbra is often not practical, given the short time duration of its existence. The heterogeneity of infarct topography in human stroke precludes simple anatomical comparison of the spatial location of the ischemic penumbra between patients. To be useful, the method used to map the spatial extent of the ischemic penumbra in patients must take into account variations in infarct topography, and allow tissues presumed to be in a similar pathophysiological state to be grouped together. Such a grouping would also allow characterization of the temporal evolution of the penumbra identified by repeated study in the same patient and useful quantitative statistical comparisons between groups of patients.

A method of mapping the distribution of the penumbra in humans, applicable to different imaging modalities including both PET and MRI, would be useful to characterize factors that influence its spatial extent. The authors have described and validated a method of characterizing the three-dimensional spatial extent of the penumbra relative to the patient's final infarct in an easily comprehended map, which we have termed the "Penumbragram" (29).

Penumbragram: Description of Method

This method requires datasets of the penumbra volume (PV) and final infarct volume (IV) for individual patients. These are coregistered into the same coordinate space to yield three-dimensional datasets with each voxel representing corresponding anatomical locations in the brain of each patient. The three-dimensional distribution of the penumbra is then mapped relative to a fixed, objectively chosen reference point within the corresponding final IV of the patient.

The center of the final infarct was chosen as the reference point based on the observation of infarct expansion from the center to the periphery of the ischemic regions in animal stroke models. The coordinates of the center of gravity (COG) of the IV in each of the p dimensions (x, y, and z) are given by:

$$\mathrm{COG}_p = \frac{\sum C_{p_i} nC_{pi}}{\sum nC_{pi}}$$

where C_{pi} refers to the ith coordinate of dimension p and nC_{pi} refers to the number of voxels within the infarct with that coordinate. The Euclidean distance between each voxel in the IV and the COG is then calculated. Voxels forming the central and peripheral zones of the infarct were operationally defined as those with distances less than and greater than the median distance, respectively. Figure 4 shows a schematic diagram of the steps involved in the construction of the map of penumbral distribution, termed the "Penumbragram." Figure 5 shows the three-dimensional topography of the ischemic penumbra in an individual patient.

Penumbragram: Validation of the Model

The model was validated in patients with ischemic stroke, who had significant volumes of hypoxic penumbral tissue identified by ^{18}F-fluoromisonidazole (FMISO) PET scanning within 48 hours of stroke onset.

In this group of patients, as expected physiologically with time from stroke onset, there was a significant negative correlation of penumbra distribution in the central zone of the infarct and a positive correlation in the external zone (Fig. 6).

Principal components analysis was used to assess the validity of infarct segmentation by treating each region independently without a priori assumptions made about the regions comprising the central, peripheral, or external zones of the infarct. Groups of regions showing

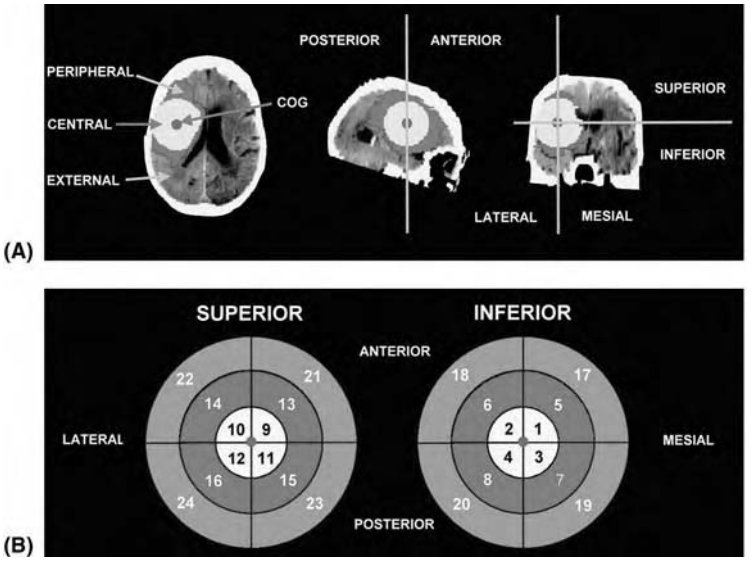

FIGURE 4 A schematic representation of the construction of a penumbragram. (**A**) Voxels comprising the central and peripheral zones of the infarct volume (IV) are shown in white and dark gray, respectively, and those external to the IV in the ipsilateral hemisphere are light gray. The horizontal plane divides the IV into superior and inferior halves, which are represented in the lower panel. Anterior/posterior and mesial/lateral planes passing through the center of gravity further subdivide each half. These subdivisions yield 4 regions in each central, peripheral, and external zone of the superior and inferior halves of the IV. (**B**) The penumbragram summarizes and anatomically represents the three-dimensional IV data set, with the central, peripheral, and external zones of the IV corresponding to the inner, middle, and external circles for the superior and inferior halves. The regions are numbered 1 to 24 with regions 1 to 4 and 9 to 12 comprising the central zone, 5 to 8 and 13 to 16 comprising the peripheral zone and 17 to 24 the external zones. The penumbragram displays the percentage of penumbral voxels that anatomically correspond to each of these 24 regions. It is thus a map of the three-dimensional distribution of the penumbra relative to a fixed, objectively chosen and physiologically meaningful reference point within the final infarct. *Abbreviation*: COG, center of gravity. *Source*: From Ref. 29.

similar patterns of change in penumbral volume over time were identified by factor analysis. There was good correspondence between regions with decline in PV with time and the predefined central zone of the infarct, and between regions with increase in PV and the external zone defined by the model (Fig. 7).

The reliability of the method was assessed by the internal consistency statistic, Cronbach's alpha. For the regions that correlated negatively with time from stroke onset, Cronbach's alpha was 0.84, suggesting that these regions are a reliable measure of the infarct core that is penumbral early after stroke onset. Cronbach's alpha for the four regions which correlated positively with time was 0.9, suggesting that these regions reliably measure peri-infarct tissue.

Penumbragram: Quantifying Three-Dimensional Temporal Evolution of the Penumbra

As discussed earlier, spatial evolution of the ischemic penumbra in humans is limited by the inability to perform serial imaging studies at defined time points after stroke onset. The Penumbragram model that enables collation of penumbral images from different patients scanned at different intervals after stroke onset was used to provide insight into spatial and temporal evolution of the ischemic penumbra in humans.

The Penumbragram model was applied to analyze the evolution of the ischemic penumbra identified by ^{18}F-FMISO PET in patients with acute MCA territory stroke ($n = 19$; <6 hours, 4; 6–16 hours, 4; 16–24 hours, 5; 24–48 hours, 6) (30). A composite Penumbragram was generated for each time epoch (<6, 6–16, 16–24, and >24 hours). This reflected the average distribution of the penumbra in each of the 24 regions for the group of patients studied within each time interval (Fig. 8). The temporal evolution of the ischemic penumbra within the central, peripheral, and regions external to the final infarct was examined by multivariate analysis of

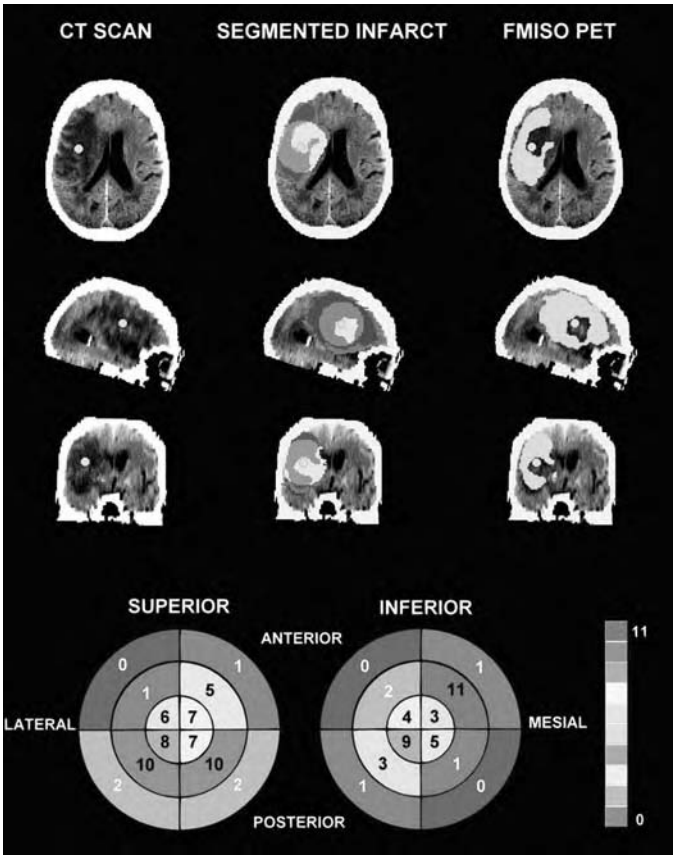

FIGURE 5 The three-dimensional spatial topography of the ischemic penumbra identified by ^{18}F-fluoromisonidazole positron emission tomography six hours after stroke onset mapped in a penumbragram. *Abbreviations*: FMISO, fluoromisonidazole; PET, positron emission tomography. *Source*: From Ref. 29.

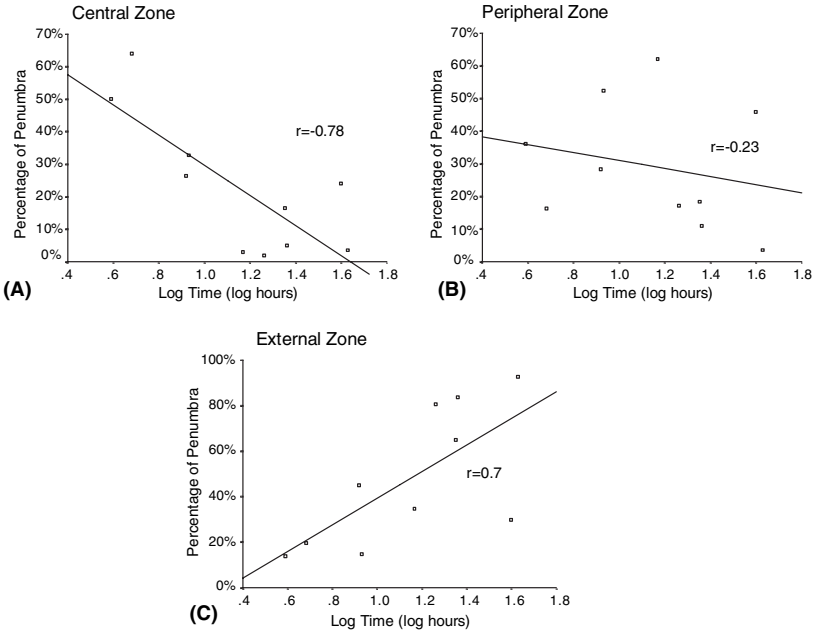

FIGURE 6 The percentage of penumbra observed in the central (**A**), peripheral (**B**), and external zones (**C**) of the infarct plotted against the logarithmic transformation of time. *Source*: From Ref. 29.

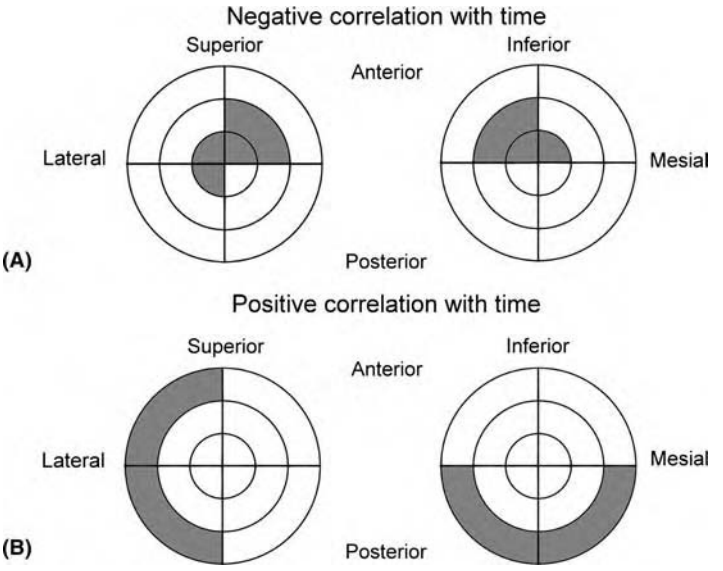

FIGURE 7 Correspondence of the regions identified by factor analysis as having significant negative (**A**) and positive (**B**) correlations of penumbral volume with time from stroke onset with those defined a priori in the penumbragram. *Source*: From Ref. 30.

covariance (ANCOVA) using regional volume as the dependent variable, region and time interval as main effects, and the penumbral volume for each patient as a covariate.

Significantly, higher volumes of penumbral tissue was observed in the region corresponding to the center of the infarct in patients studied within six hours of stroke onset, whereas in those studied at later times the penumbra was mostly present in the periphery or external to the infarct (Fig. 8). The interaction between the interval from stroke onset to PET scanning and distribution of the ischemic penumbra within the central, peripheral, and regions external to

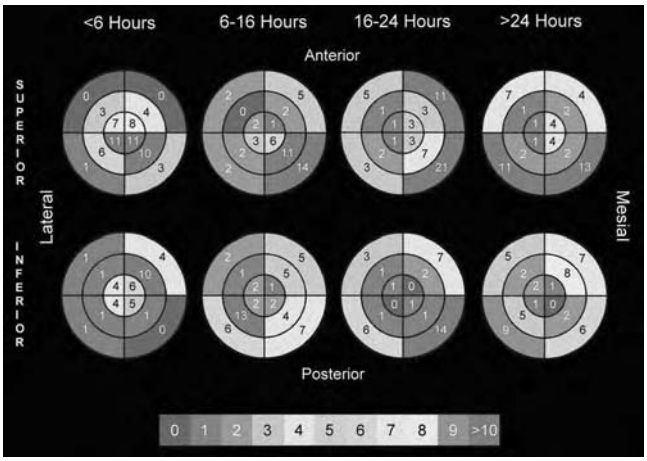

FIGURE 8 (*See color insert.*) Temporal evolution of the ischemic penumbra. Penumbragrams characterizing the temporal evolution of the ischemic penumbra identified by ^{18}F-fluoromisonidazole positron emission tomography scanning in patients following acute middle cerebral artery territory ischemic stroke. The composite penumbragrams with the proportion of penumbral volume in each infarct and peri-infarct region for each time epoch (<6, 6–16, 16–24, and 24–48 hours) after stroke onset are shown. The number in each region refers to the percentage of total hypoxic volume. A higher volume of penumbral tissue is observed in the central region in patients studied within six hours of onset ($P < 0.05$; ANCOVA) compared with those studied at later time points, where it occurs mainly in the periphery or external to the infarct. A superior, mesial and posterior predominance of penumbral tissue distribution is seen at all time points. *Source*: From Ref. 30.

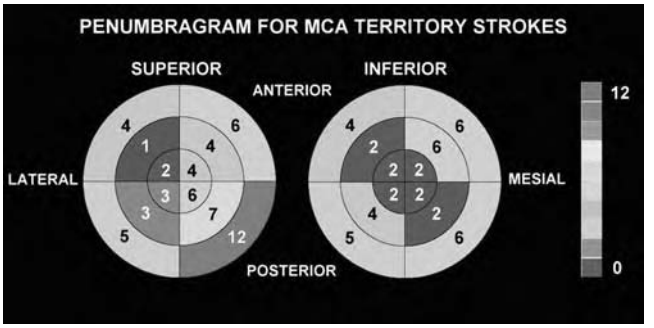

FIGURE 9 Three-dimensional topography of the ischemic penumbra in patients with MCA territory stroke. Composite penumbragram displaying the spatial distribution of the ischemic penumbra identified by ^{18}F-fluoromisonidazole positron emission tomography scanning in patients ($n = 19$) with MCA territory ischemic stroke. The percentage of penumbral voxels in each region is color-coded according to the spectral color bar shown on the right. A superior, medial and posterior predominance ($P < 0.05$; ANCOVA) of hypoxic tissue is seen, perhaps reflecting the pattern of collateral circulation. *Abbreviation*: MCA, middle cerebral artery. *Source*: From Ref. 30.

the final infarct was significant (ANCOVA; $P < 0.05$). The temporal change of the location of the ischemic penumbra is consistent with infarct expansion at the expense of the penumbra beginning at the center of the ischemic region and extending to its periphery.

Penumbragram: Quantifying Three-Dimensional Spatial Topography of the Penumbra

A composite Penumbragram summarizing the distribution of the ischemic penumbra identified by ^{18}F-FMISO PET in the group of 19 patients with acute MCA territory stroke was used to map the topography of the penumbra. The spatial topography of the ischemic penumbra in the superior/inferior, mesial/lateral, and anterior/posterior regions relative to the center of the infarct was analyzed by ANCOVA, with Bonferroni correction applied to correct for repeated measurements. The volume of penumbra in region was used as the dependent variable with region as the main effect and penumbral volume for each patient as a covariate. A Bonferroni correction was applied to correct repeated measurements.

In patients with MCA territory strokes the penumbra was distributed mainly superiorly, medially, and posterior in the cortex (ANCOVA; $P < 0.05$), as shown in Figure 9. This distribution is presumed to reflect the source of collateral flow from leptomeningeal, anterior cerebral, and posterior cerebral tributaries.

Penumbragram: Limitations of the Method

Although this model would be accurate in most cases of MCA infarcts, it may be erroneous in some instances. The geographic center would best correspond to the true center in infarcts with convex surfaces—a situation that predominates in reality in most MCA territory infarcts. For infarcts with concave surfaces or irregular shape as in striatocapsular infarcts, algorithms based on skeletonizing may give a better approximation of the true center of the infarct. The algorithm can be applied to each infarcted region in patients with multiple infarcts.

CONCLUSION

In human ischemic stroke, the evolution of the penumbra occurs from central to peripheral regions of the infarct as observed in animal models. In MCA territory strokes, the penumbra is located mainly in the superior, medial, and posterior regions, most likely reflecting the pattern of collateral circulation.

The spatial and temporal evolution of the ischemic penumbra has important clinical and pathophysiological implications. A number of neurobiological factors are likely to explain the spatial and temporal evolution of the penumbra. Susceptibility to ischemia may differ in different

parts of the vascular territory according to predominant cell type, vascular architecture, and collateral circulation. In addition, different survival time profiles within compartments in the penumbra may reflect disparate pathophysiological mechanisms leading to infarction as postulated by Heiss et al. (28). For example, critically hypoperfused tissue within the central ischemic region may have a more rapid evolution to irreversible damage and a shorter therapeutic time window for tissue salvage than tissue bordering this zone, in which additional secondary and delayed cellular mechanisms may underlie progression to cell death.

This model of penumbral evolution supports early reperfusion but indicates that the location of the penumbra and its distribution in gray and white matter compartments, may influence the choice of adjunct therapeutic strategies such as neuroprotection and the time window for their effectiveness.

REFERENCES

1. Dirnagl U, Iadecola C, Moskowitz MA. Pathobiology of ischaemic stroke: an integrated view. Trends Neurosci 1999; 22:391–397.
2. Fisher M. Characterizing the target of acute stroke therapy. Stroke 1997; 28:866–872.
3. Baron JC, von Kummer R, del Zoppo GJ. Treatment of acute ischemic stroke. Challenging the concept of a rigid and universal time window. Stroke 1995; 26:2219–2221.
4. Pappata S, Fiorelli M, Rommel T, et al. PET study of changes in local brain hemodynamics and oxygen metabolism after unilateral middle cerebral artery occlusion in baboons. J Cereb Blood Flow Metab 1993; 13:416–424.
5. Touzani O, Young AR, Derlon JM, et al. Progressive impairment of brain oxidative metabolism reversed by reperfusion following middle cerebral artery occlusion in anaesthetized baboons. Brain Res 1997; 767:17–25.
6. Young AR, Sette G, Touzani O, et al. Relationships between high oxygen extraction fraction in the acute stage and final infarction in reversible middle cerebral artery occlusion: an investigation in anesthetized baboons with positron emission tomography. J Cereb Blood Flow Metab 1996; 16: 1176–1188.
7. Heiss WD, Graf R, Wienhard K, et al. Dynamic penumbra demonstrated by sequential multitracer PET after middle cerebral artery occlusion in cats. J Cereb Blood Flow Metab 1994; 14:892–902.
8. De Ley G, Weyne J, Demeester G, et al. Experimental thromboembolic stroke studied by positron emission tomography: immediate versus delayed reperfusion by fibrinolysis. J Cereb Blood Flow Metab 1988; 8:539–545.
9. Tenjin H, Ueda S, Mizukawa N, et al. Positron emission tomographic measurement of acute hemodynamic changes in primate middle cerebral artery occlusion. Neurol Med Chir (Tokyo) 1992; 32:805–810.
10. Kuge Y, Yokota C, Tagaya M, et al. Serial changes in cerebral blood flow and flow-metabolism uncoupling in primates with acute thromboembolic stroke. J Cereb Blood Flow Metab 2001; 21: 202–210.
11. Touzani O, Young AR, Derlon JM, et al. Sequential studies of severely hypometabolic tissue volumes after permanent middle cerebral artery occlusion. A positron emission tomographic investigation in anesthetized baboons. Stroke 1995; 26:2112–2119.
12. Young AR, Touzani O, Derlon JM, et al. Early reperfusion in the anesthetized baboon reduces brain damage following middle cerebral artery occlusion. Stroke 1997; 28:632–638.
13. Heiss WD, Graf R, Lottgen J, et al. Repeat positron emission tomographic studies in transient middle cerebral artery occlusion in cats: residual perfusion and efficacy of postischemic reperfusion. J Cereb Blood Flow Metab 1997; 17:388–400.
14. Sette G, Baron JC, Young AR, et al. In vivo mapping of brain benzodiazepine receptor changes by positron emission tomography after focal ischemia in the anesthetized baboon. Stroke 1993; 24:2046–2057; discussion 2057–2048.
15. Heiss WD, Graf R, Fujita T, et al. Early detection of irreversibly damaged ischemic tissue by flumazenil positron emission tomography in cats. Stroke 1997; 28:2045–2051; discussion 2051–2042.
16. Ginsberg MD, Back T, Zhao W. Three-dimensional metabolic and hemodynamic imaging of the normal and ischemic rat brain. Acta Neurochir Suppl 1996; 66:44–49.
17. Ginsberg MD, Belayev L, Zhao W, et al. The acute ischemic penumbra: topography, life span, and therapeutic response. Acta Neurochir Suppl 1999; 73:45–50.
18. Quast MJ, Huang NC, Hillman GR, Kent TA. The evolution of acute stroke recorded by multimodal magnetic resonance imaging. Magn Reson Imaging 1993; 11:465–471.
19. Baron JC. Mapping the ischaemic penumbra with PET: implications for acute stroke treatment. Cerebrovasc Dis 1999; 9:193–201.
20. Touzani O, Roussel S, MacKenzie ET. The ischaemic penumbra. Curr Opin Neurol 2001; 14:83–88.

21. Heiss WD, Huber M, Fink GR, et al. Progressive derangement of periinfarct viable tissue in ischemic stroke. J Cereb Blood Flow Metab 1992; 12:193–203.
22. Marchal G, Beaudouin V, Rioux P, et al. Prolonged persistence of substantial volumes of potentially viable brain tissue after stroke: a correlative PET-CT study with voxel-based data analysis. Stroke 1996; 27:599–606.
23. Furlan M, Marchal G, Viader F, et al. Spontaneous neurological recovery after stroke and the fate of the ischemic penumbra. Ann Neurol 1996; 40:216–226.
24. Darby DG, Barber PA, Gerraty RP, et al. Pathophysiological topography of acute ischemia by combined diffusion- weighted and perfusion MRI. Stroke 1999; 30:2043–2052.
25. The NINDS rt-PA Stroke Study Group. Tissue plasminogen activator for acute ischaemic stroke. N Engl J Med 1995; 333:1581–1587.
26. Furlan A, Higashida R, Wechsler L, et al. Intra-arterial prourokinase for acute ischemic stroke. The PROACT II study: a randomized controlled trial. Prolyse in Acute Cerebral Thromboembolism. JAMA 1999; 282:2003–2011.
27. Morgenstern LB. What have we learned from clinical neuroprotective trials? Neurology 2001; 57:45S–47S.
28. Heiss WD, Thiel A, Grond M, Graf R. Which targets are relevant for therapy of acute ischemic stroke? Stroke 1999; 30:1486–1489.
29. Markus R, Donnan G, Kazui S, et al. Penumbral topography in human stroke: methodology and validation of the "Penumbragram". Neuroimage 2004; 21:1252–1259.
30. Markus R, Reutens DC, Kazui S, et al. Topography and temporal evolution of hypoxic viable tissue identified by 18F-fluoromisonidazole positron emission tomography in humans after ischemic stroke. Stroke 2003; 34:2646–2652.

19 The Penumbra and Intracerebral Hemorrhage

Ken Butcher
Division of Neurology, University of Alberta, Edmonton, Alberta, Canada

Romesh Markus
Department of Neurology, St. Vincent's Hospital, and Department of Medicine, University of New South Wales, Sydney, Australia

INTRODUCTION

Primary intracerebral hemorrhage (ICH) refers to spontaneous, nontraumatic bleeding from intraparenchymal blood vessels, resulting from pathological alteration of vessels by the effects of long-standing hypertension or cerebral amyloid angiopathy (1). ICH accounts for 10% to 20% of all strokes worldwide (2). Of these, approximately 30% to 50% will die within 30 days of onset and the majority of survivors will be left with significant long-term disability (3,4). Despite the huge burden ICH represents, no acute intervention has been proven to be effective in improving mortality or functional outcome after this type of stroke. Current evidence indicates that surgical hematoma resection does not significantly alter outcome (5). Similarly, a number of medical treatments have been shown to be unhelpful or even harmful in the management of acute ICH. These include steroids, osmotic diuretics, and hemodilution (6–9). More recently, acute hemostatic therapy has been shown in a single randomized controlled trial to attenuate hematoma expansion and improve clinical outcome (10).

The question of the existence of penumbral tissue in primary ICH is best addressed in two parts. The first is the more specific question of an ischemic penumbra, as defined in previous chapters. The second is to consider the penumbra in a more general sense; cerebral tissue that is not immediately injured by the effects of the acute event, but also at risk for secondary progressive damage subacutely or over even longer periods. We shall make the case that there is little to support the existence of an ischemic penumbra, but substantial evidence for the more general definition.

The existence and nature of the penumbra in ICH is arguably the most pressing outstanding information required by clinicians to make rational management decisions in ICH patients. The recognition that hematoma volume is not static in a significant proportion of patients, has revolutionized the approach to ICH management (11). In addition to the promising treatment effects of hemostatic therapy, there is increasing evidence that clot expansion is correlated with acute systolic blood pressure (12,13). Furthermore, there is some limited evidence from retrospective studies, that higher systolic blood pressure is associated with poor clinical outcome (14,15). The hypothesis that blood pressure reduction may attenuate hematoma expansion is therefore an intriguing possibility. It has also been postulated, however, that compression of the microvasculature surrounding the hematoma may result in decreased cerebral blood flow (CBF) (16). Therefore, some clinicians remain concerned that acute blood pressure reduction may aggravate, or even precipitate, cerebral ischemia within the perihematomal region and/or more globally. These two theories therefore lend themselves to opposing blood pressure management strategies, and the clinical dilemma will only be resolved with randomized controlled trials, which are currently underway (17,18). Of course, proponents of the ischemic hypothesis consider such a trial potentially dangerous. Fortunately, a number of experimental and clinical studies of CBF in ICH have already been performed, which support the safety of such a trial.

PART I: BLOOD FLOW CHANGES IN INTRACEREBRAL HEMORRHAGE
Experimental Evidence

Several animal models of ICH have been developed to assess for any changes in CBF, metabolic rate, and/or ischemia following ICH (Table 1). Studies have been done mainly in rats, but also cats, dogs, and monkeys. Changes in CBF have been documented using a variety of techniques, including ^{14}C-iodoantipyrine autoradiography, hydrogen clearance, radiolabelled microspheres, and carbon-black dilution (19–28). The effect of a rapidly developing mass on local blood flow has been examined using an inflatable balloon placed within the parenchyma of rat brains (24,26,29). In most cases, this resulted in acute CBF reductions and even ischemic changes, which appear to be proportional to the duration of balloon inflation. Similarly, measurement of regional CBF following autologous blood injection into rat brains has revealed perihematomal oligemia acutely (22,30,31). Unlike the pattern seen with balloon inflation, however, this reduction in blood flow was transient, normalizing in most cases within hours, and most severe during the first minutes following injection.

Qureshi et al. (32) used arterial pressure to inject autologous blood into the deep white matter of dogs, in an effort to more accurately simulate acute ICH. Measurement of CBF using radiolabeled microspheres did not reveal any hypoperfusion in the periclot white matter. The authors concluded that the slower injection time of 15 to 20 minutes under arterial pressure, rather than a more rapid introduction of blood in the previous rodent experiments, accounted

TABLE 1 Summary of Studies of Cerebral Blood Flow and/or Ischemic Changes Following Experimental Intracerebral Hemorrhage

Investigator/study	Animal	Hematoma model	Primary findings
Kingman et al. (81)	Rat	50 μL balloon inflated over 25 sec, for 2.5 min−2.5 h, ± deflation	CBF reduced in ipsilateral basal ganglia and cortex, which was proportional to the duration of inflation; deflation did not restore CBF
Sinar et al. (24)	Rat	50 μL balloon inflated over 20 sec, for 10 min then deflated	CBF reduced in frontal cortex with inflation, reduced in ipsilateral caudate at 4 h, ischemic histopathology in caudate at 4 h
Nehls et al. (25)	Rat	50 μL balloon inflation over 20 sec, for 5 min or 4 h	CBF reduced in ipsilateral caudate, more prominent after 4 h inflation
Nehls et al. (26)	Rat	50 μL balloon inflation over 20 sec, for 10 min or 24 h	CBF reduced in ipsilateral caudate and cortex after 24 h, but not at 10 min inflation, ischemic histopathology in all animals
Ropper et al. (82)	Rat	Autologous blood injection; 0.24–0.28 mL over 1 sec into caudate	Coma and global decrease in CBF 30% below baseline associated with hematoma induction
Mendelow et al. (21)	Rat	Autologous blood injection; arterial pressure ± IVH	CBF reduced in ipsilateral hemisphere with contained hemorrhage and bilaterally in cases of uncontained hemorrhage
Nath et al. (22)	Rat	Autologous blood injection; 25/50/100 μL blood over 2.5 min at 100 mmHg	CBF reduction around hematoma and ipsilateral hemisphere proportional to volume; no change in cerebral perfusion pressure
Nath et al. (30)	Rat	Autologous blood injection; 25 μL over 10 sec at 100 mm Hg	CBF reduced in caudate and overlying cortex at 1 min, but not at 10 min or 3 h; structural cortical damage, but not in the caudate, consistent with ischemia see on histopathology
Patel et al. (83)	Rat	Autologous blood injection; 100/200 μL at a rate of 10 μL/min into caudate	Perihematomal ischemic histopathology, which was proportional to clot volume
Yang et al. (28)	Rat	Autologous blood injection; 100 μL over 5 min	CBF reduced globally at 1 h, normalized at 4 h, reduced at 24–48 h; edema related to increased blood–brain barrier permeability
Bullock et al. (27)	Monkey	Autologous blood injection; arterial pressure	CBF reduced in all regions at 15 and 50 min; most prominent ipsilateral caudate and white matter
Kobari et al. (84)	Cat	Autologous blood injection; arterial pressure	Hemispheric CBF reduced bilaterally, CBV reduced <2% bilaterally
Qureshi et al. (19)	Dog	Autologous blood injection; 7.5 mL over 20–30 min	No change in global measures of oxygen extraction or metabolism

Abbreviations: CBF, cerebral blood flow; CBV, cerebral blood volume.

for the observed lack of CBF reduction. As CBF measurements did not begin until 45 minutes after injection, it remains possible, however, that transient oligemia may simply have been missed. Thus, the general pattern of blood flow changes in animal models is one of hyperacute reduction, followed by spontaneous resolution. These changes are moderate in both severity and volume of tissue affected. Although histopathological studies done as part of a number of these studies did reveal changes consistent with ischemia, it is also possible that cellular injury occurred secondary to alternative mechanisms (see Part II) (24,26,30,33).

Nuclear Medicine Investigations

Studies of acute and subacute ICH using nuclear medicine scans have produced conflicting results, with respect to the etiology of perihematomal edema. Several single photon emission computerized tomography (SPECT) studies of ICH have demonstrated acute but transient focally decreased blood flow in the region of the hematoma (Table 2). Sills et al. (34) used ^{99m}Tc-hexamethylpropylenamine oxime (Tc-HMPAO) SPECT to demonstrate circumferential hypoperfusion in the perihematomal region of seven patients, imaged at an average of 51 hours after symptom onset. Mayer et al. (35) used the same technique and reported perihematomal hypoperfusion more acutely (mean 18 hours) (36). In addition, repeat imaging at a mean of 72 hours after symptom onset indicated that CBF normalized in all patients. The hypoperfused region corresponded topographically to the visibly enlarged edema seen on CT scans and, in one case, to areas of hematoma expansion (36). The hypoperfused volumes were also positively correlated to the volume of edema expansion. Siddique et al. (36) showed a similar pattern of

TABLE 2 Single-Photon Emission Computerized Tomography Investigations of Blood Flow in Intracerebral Hemorrhage

Investigator /study (ligand)	Number of patients	Location of ICH	Time of study/studies from symptom onset	Primary findings
Tanizaki (85) (inhaled 133Xe)	13 (all treated surgically)	Putamen	Scan 1: preoperative Scan 2: within seven days of surgery performed 13–82 days after onset	Scan 1: Ipsilateral hemispheric hypoperfusion in all 13 patients Scan 2: Postoperative CBF improved in two thirds of the patients
Rousseaux et al. (86) (Tc-HMPAO)	20	Thalamus (7) Lenticulostriate (5) Subcortical (8)	1–95 d	Remote hypoperfusion in ipsilateral frontal cortex in 19 patients and contralateral cerebellum in 16 cases
Sills et al. (87) (Tc-HMPAO)	7	Lobar (3) Putamen (3) Thalamic (1)	28–63 h	Decreased perihematomal rCBF in all patients
Mayer et al. (35) (Tc-HMPAO)	23	Putamen (12) Thalamic (6) Gangliothalamic (2)	Scan 1: <36 h Scan 2: 24–120 h later	Scan 1: Perihematomal decreased rCBF Scan 2: Flow deficit volume (region of decreased rCBF) decreased by 55% from scan 1; cortical hyperemia (not perihematomal) in four patients
Siddique et al. (88) (Tc-HMPAO)	13 (4 treated surgically)		Scan 1: <48 h Scan 2: 4–7 d later	Scan 1: Perfusion of the ipsilateral hemisphere improved between scan 1 and scan 2 (mean 3.9% increase in flow), in all surgically treated patients; perfusion decreased (6), did not change (1) or improved (2) in conservatively managed patients (mean 3.6 % decrease in flow)
Siddique et al. (36) (Tc-HMPAO)	11	Basal ganglia(3) Lobar (8)	Scan 1: Within "days" (number not specified) Scan 2: 6–9 months later	Perfusion measures for scan 1 were not given, but perfusion improved by at least 15% on scan 2 in the perihematomal region (7.2–71.3 mL) in all patients

Abbreviations: HMPAO, hexamethylpropylenamine oxime; ICH, intracerebral hemorrhage; rCBF, regional cerebral blood flow.

acute hypoperfusion, which was no longer present when patients were reimaged six to nine months postictus (36). These reports, therefore, appeared to support the hypothesis that there is the potential for secondary ischemic changes in the acute stages of ICH. Nonetheless, the SPECT studies indicated the presence only of reduced CBF, as measurements of oxygen extraction fraction (OEF) or cerebral metabolic rate are not possible with this technique, and, therefore, the changes cannot be concluded to represent ischemia.

Focal hyperperfusion has been identified with SPECT studies as well. Mayer did observe cortical hyperemia distal to the ICH in four patients (35). This was seen more commonly in patients with lobar hemorrhages, on their second (subacute scan). In addition, a number of investigators have reported increases in CBF observed with N-isopropyl-p-[^{123}I]iodoamphetamine (^{123}I-IMP) SPECT. These reports are found, largely in abstract form, in the Japanese language literature and have been summarized by Miyazawa et al. (37).

Several investigators have used positron emission tomography (PET) tracers that measure tissue metabolism as well as blood flow, in an effort to more definitively address the question of ischemia in the perihematomal zone (Table 3). The first published report included patients studied over a wide time period; one week to more than a month after symptom onset. They reported that CBF was most often decreased diffusely in the hemisphere ipsilateral to the hemorrhage, but also in a restricted perihematomal region (38). They also found two cases of distinct increases in CBF, consistent with luxury perfusion around the hematoma. Finally, they observed four cases of perihematomal hypoperfusion and increased OEF suggestive of ischemia in their series of 21 patients. This occurred only in patients with very large hematomas (>4.5 cm diameter).

Another group reported perihematomal reductions in CBF in two patients, after correcting for partial volume effects caused by the hematoma itself (39). The same investigators later reported that cerebral oxygen metabolism (cerebral metabolic rate of oxygen; $CMRO_2$) and OEF

TABLE 3 Positron Emission Tomography Investigations of Blood Flow in Intracerebral Hemorrhage

Investigator/study (ligand)	Number of patients	Location of ICH	Time of study/studies from symptom onset	Primary findings
Uemura et al. (38) (^{15}O)	21	Thalamus (14) Putamen (3) Subcortical (4)	<10 d (n = 13 scans) 11–30 d (n = 12 scans) >30 d (n = 8 scans)	CBF, OEF, and $CMRO_2$ decreased in the perihematomal region and diffusely in the ipsilateral hemisphere Perihematomal CBF increased (luxury perfusion) in two patients OEF moderately increased (misery perfusion) diffusely over both hemispheres only in four patients with large hematomas (diameter >4.5 cm)
Videen et al. (39) (^{15}O)	2	Putamen (2)	9 and 22 h	Perihematomal CBF decreased; preserved cortical CBF
Zazulia et al. (40) (^{15}O)	19	Basal ganglia (7) Thalamus (5) Lobar (3)	5–22 h	rCBF and $CMRO_2$ reduced in the perihematomal region, but no increase in OEF
Powers et al. (41) (^{15}O)	14	Putamen (6) Thalamus (6) Lobar (2)	Scan 1: 6–22 h Scan 2: 10 min after pharmacological reduction of MAP by 15 mmHg	Perihematomal rCBF decreased in most patients on scan 1, but no significant change in either global CBF or perihematomal rCBF after BP reduction
Hirano et al. (42) (FMISO)	6	Putamen (2) Thalamus (2) Lobar (2)	24–43 h	No evidence of hypoxia in any patient
Markus et al. (44) (FMISO)	9	Putamen (5) Thalamus (2) Lobar (1)	<48 h	Small volume of hypoxic voxels identified in two patients with large hematoma volumes (>60 mL)

Abbreviations: $CMRO_2$, cerebral metabolic rate of oxygen; ICH, intracerebral hemorrhage; rCBF, regional cerebral blood flow; OEF, oxygen extraction fraction.

values were both decreased in a 1-cm wide hypoperfused region surrounding the hematoma, relative to the contralateral side, in 19 patients studied with multitracer $H_2{}^{15}O/{}^{15}O$ PET 5 to 22 hours after onset of ICH (40). The decreased OEF indicated that metabolic demand was reduced to a greater extent than CBF in this perihematomal region. These changes are the opposite of what is observed in penumbral tissue following ischemic stroke when CBF is reduced to a greater extent than $CMRO_2$ with elevation of OEF. Only a single patient had scattered areas of high OEF, consistent with misery perfusion, in the perihematomal region. This patient had a hematoma volume of 41 mL, which was greater than the mean of 26 mL, although four patients with larger clots had low OEF. The authors, therefore, concluded that in the majority of patients, CBF changes were secondary to decreased metabolic demands and not ischemia. Finally, this group also evaluated the safety of acute blood pressure reduction in ICH. These investigators performed PET scans before and after blood pressure reduction (41). Fourteen patients with moderate sized supratentorial ICH were randomized to treatment with either intravenous nicardipine or labetalol between 6 and 22 hours after symptom onset. CBF was moderately reduced in the perihematomal regions of most patients prior to treatment. Mean arterial pressures were reduced by an average of 16.7 ± 5.4% (119 mmHg, range 90–133 mmHg). No significant changes in CBF in the perihematomal region or elsewhere were detected following treatment with either drug.

Studies with the PET ligand ^{18}F-fluoromisonidazole (FMISO) in patients with ICH have revealed findings that are concordant with that of multitracer PET studies (42). This tracer, which binds to severely hypoxic tissue and has been used to identify penumbral tissue in ischemic stroke, can therefore be used to differentiate tissue with decreased blood flow secondary to lower metabolic demands from that which is truly deprived of oxygen (43). Additional FMISO investigations by one of the authors revealed small volumes (0.6 mL and 1.4 mL) of hypoxic tissue using voxel based statistical parametric mapping in the perihematomal region in two of nine patients imaged within 48 hours of ICH onset (Fig. 1) (44). These patients both had large hematoma volumes of 52.3 and 83.8 mL, respectively. These small regions of hypoxic tissue, relative to the total perihematomal volume, were considered unlikely to be clinically significant.

Thus, nuclear medicine studies indicate that ischemia is unlikely to be a major cause of neuronal injury in the perihematomal region in most patients. Although CBF does decrease hyperacutely, this is not associated with the features of either hypoxia or ischemia in the majority of patients. The decreases in CBF appear more likely to be secondary to decreased metabolic demands in the tissue surrounding the hematoma and this appears to be a transient phenomenon.

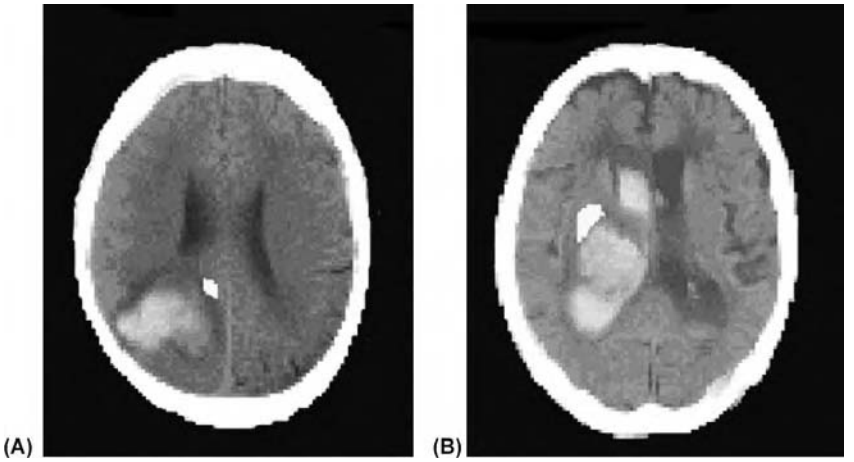

FIGURE 1 Coregistered ^{18}F-fluoromisonidazole positron emission tomography and computerized tomography images from patients imaged 31 (**A**) and 24 hours (**B**) after onset of lobar and thalamic intracerebral hemorrhage (ICH), respectively. Hypoxic tissue was identified by voxel-based statistical parametric mapping within the hematoma and surrounding 2 cm margin. Patient in (**A**) had an ICH volume of 52 mL with a hypoxic volume of 1 mL. Patient in (**B**) had an ICH volume of 84 mL and a hypoxic volume of 1.5 mL.

Magnetic Resonance Imaging Investigations

Stroke clinicians have been somewhat reluctant to consider magnetic resonance imaging (MRI) a reliable tool for the clinical assessment of intracranial hemorrhage. This is based on the ease of identification of blood on CT scans and the perceived difficulty associated with visualization of acute hemorrhage on MRI. In fact, blood is readily identifiable on MRI and the use of multiple sequences provides additional information regarding the age of blood products. Two recent trials have confirmed that acute ICH can be reliably identified and differentiated from ischemic stroke, using MRI alone (45,46). This does require a basic understanding of the basic patterns and mechanisms of MRI changes in ICH.

Blood products become apparent on MRI due to disruptions in local magnetic fields, sometimes called the susceptibility effect. Substances that have this effect are referred to as paramagnetic. Blood products that are paramagnetic include deoxyhemoglobin, methemoglobin, and hemosiderin. In contrast, oxyhemoglobin is not paramagnetic and, therefore, not visible with MRI. In addition to oxyhemoglobin and deoxyhemoglobin, acute blood also contains significant amounts of water, which is heavily T2-weighted. Thus, acute blood has a mixed signal on traditional T2-weighted images (47,48). Studies of hyperacute ICH indicate that the susceptibility effects are first observed where deoxyhemoglobin initially forms, at the periphery of the hematoma (49). This is useful in delineating the boundary of the hematoma, from the rim of perihematomal edema, as the latter is always hyperintense on T2-weighted images (Fig. 2). The hypointensity associated with increasing amounts of deoxyhemoglobin progressively spreads into the hematoma core over time. In addition, sequences including gradient echo and T2*, which are more susceptible to the paramagnetic effects of deoxyhemoglobin, make acute blood even more obvious on MRI (33,50).

Perfusion-Weighted Imaging

The most commonly used MRI perfusion imaging technique is the dynamic susceptibility contrast method. This perfusion-weighed MRI (PWI) sequence allows the visualization of areas of decreased CBF via bolus tracking of intravascular gadolinium contrast media as it transits through the cerebral circulation (see Chapter 15). PWI sequences have been utilized in an effort to assess for blood flow changes in ICH. A total of 59 acute ICH patients in three separate studies have been studied with PWI (Table 4). The first study of six patients with acute ICH

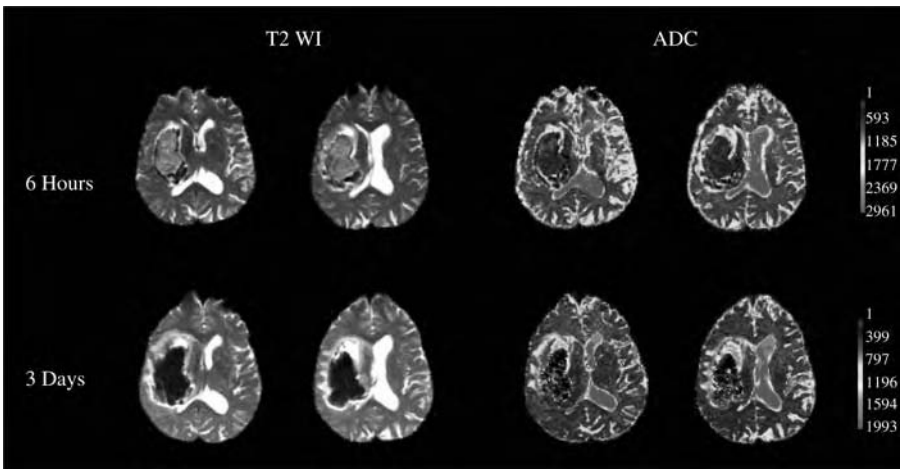

FIGURE 2 T2-weighted magnetic resonance imaging (T2WI, *left*) demonstrating a large acute putamenal hematoma imaged six hours after onset and perihematomal edema, which expands over 72 hours. Acute hematoma volume was 51 mL, as measured on CT. Blood appears black due to the paramagnetic effects of the deoxyhemoglobin, and edema bright on the T2-weighted images. The apparent diffusion coefficient (ADC; *right*) maps indicate elevated rates of water movement in the perihematomal region (units are 10^{-6} mm^2/sec), which are strongly correlated to edema volume both acutely and subacutely. This is most consistent with edema of plasma origin and not ischemia.

TABLE 4 Magnetic Resonance Imaging Investigations of Blood Flow/Perihematomal Edema Etiology in Intracerebral Hemorrhage

Investigator/study	Number of patients	Location of ICH	Time of study/studies from symptom onset	Primary findings
Carhuapoma et al. (54) (DWI and MRS)	9	Basal ganglia (5) Thalamus (1) Lobar (3)	1–9 d	Increased perihemtomal ADC in 8/9 Voxels with decreased ADC in 1/9 (80 mL hematoma) MRS: Lactate in 2/5 patients, but not associated with ADC decrease
Kidwell et al. (51) (PWI and DWI)	12 (DWI) 6 (PWI)	Putamen (5) Thalamus (4) Lobar (3)	<5 h	Perihematomal Tmax delay (hypoperfusion) in 2/6 patients Rim of perihematomal decreased ADC values in three patients with large hematoma volumes and mass effect
Schellinger et al. (52) (PWI and DWI)	32	Subcortical (27) Lobar (5)	1.3–5.75 h	Perihematomal (4/32) and diffuse ipsilateral hemispheric (14/32) MTT delay (hypoperfusion) MTT was inversely correlated with time to imaging Perihematomal ADC was decreased (7/32), increased or normal (25/32) and unrelated to perfusion or outcome
Butcher et al. (53) (PWI and DWI)	21 acute 12 subacute	Putamen (14) Thalamus (3) Caudate (1) Lobar (2)	Scan 1: 4.5–110 h (50% <21 h) Scan 2: 3–5 d (median 4.5 d)	Transient perihematomal (11/21) and diffuse ipsilateral hemispheric (9/21) MTT delay (hypoperfusion) in patients with larger hematoma volumes, all of which resolved by scan 2 Elevated ADC values positively correlated with perihematomal edema volumes acutely and subacutely

Abbreviations: ADC, apparent diffusion coefficient; DWI, diffusion-weighted imaging; ICH, intracerebral hemorrhage; MRS, magnetic resonance spectroscopy; MTT, mean transit time; PWI, perfusion-weighted imaging; T_{max}, time to peak of the impulse residue.

demonstrated no evidence of focally decreased blood flow in the perihematomal region (51). More consistently, these authors observed a relative hypoperfusion of the cerebral hemisphere ipsilateral to the hematoma. The two largest PWI studies in ICH reported mild hypoperfusion in the perihematomal region and/or more diffusely throughout the ipsilateral hemisphere in approximately half (29/53) of the patients studied (Fig. 3) (52,53). The severity of these changes appears to be inversely correlated to the time of imaging (52). One of the authors has also observed that both perihematomal and diffuse hemispheric perfusion changes occur only in larger hematomas, generally larger than 15 mL. Furthermore, repeat imaging demonstrated that hypoperfusion is transient, resolving completely within three to five days (53). Finally, this study also included an analysis of relative CBF and CBV (rCBF and rCBV) in the perihematomal region. Although, rCBF was decreased moderately, commensurate with a prolongation of MTT, no changes in rCBV were observed (Fig. 3). This is inconsistent with the traditional hypothesis that perihematomal oligemia results from compression of the local microvasculature by the hematoma mass effect. Furthermore, maintenance of rCBV is incompatible with cerebral ischemia.

The inability to demonstrate significant hypoperfusion in patients with small hematomas may be a limitation of studying blood flow with MRI. The paramagnetic effects of deoxyhemoglobin extend beyond the hematoma itself, making determination of blood flow immediately adjacent to the clot impossible. It is, therefore, possible that smaller hematomas are associated with a more restricted zone of perihematomal hypoperfusion—below the resolution of PWI. This problem may be overcome by studying blood flow with CT (discussed subsequently).

Diffusion-Weighted Imaging

MRI also provides another tool useful in identification of ischemic tissue. Diffusion-weighted imaging (DWI) is based on the principle of detection of spontaneous water molecule movement

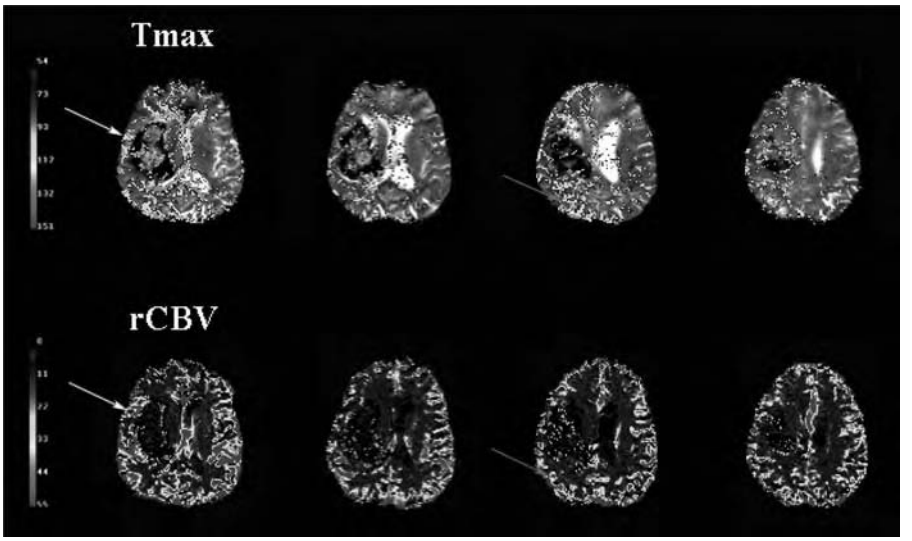

FIGURE 3 (*See color insert*.) Example of perihematomal blood flow changes in a patient with a putamenal intracerebral hemorrhage (six hours after onset; same patient as Fig. 2). Blood again appears black due to the paramagnetic effects of deoxyhemoglobin. Time to peak of the impulse response curve (Tmax) is delayed >2 seconds (colored voxels) in regions of decreased blood flow (units are 1/10 sec). This patient had perihematomal (*white arrows*) and diffuse ipsilateral hemispheric T_{max} delay (*red arrows*). Relative cerebral blood volume (rCBV; arbitrary units) in the perihematomal region and ipsilateral hemisphere is maintained, however, which is inconsistent with ischemia.

within the brain (see Chapter 15). Areas of diffusion restriction are thought to represent cytotoxic edema. The degree of bioenergetic compromise can be quantified by the apparent diffusion coefficient (ADC), which is decreased in regions where sodium–potassium ATPase function has failed. Four DWI studies in a total of 71 acute ICH patients have been reported (Table 4) (51–53,54). Perihematomal diffusion restriction was reported in 11 patients from two studies (51,52). The degree and volume of the diffusion restriction and volume of the affected regions were moderate in all cases. Most patients have been observed to have elevated ADC values in the perihematomal region and this has been interpreted as evidence that edema is plasma derived or vasogenic (5). In a larger subsequent serial study of diffusion changes in ICH, one of the authors reported that rADC is consistently elevated in the perihematomal region (53). Furthermore, the ADC was directly correlated to the volume of edema, independent of hematoma size, at both the acute and subacute time points. In essence, higher rates of water movement in the periclot region were associated with larger edema volumes. This was highly consistent with edema of plasma origin and not ischemia (Fig. 2) (53).

In the three studies of concurrent DWI and PWI in acute ICH, none have reported ischemic signatures, that is, a reduction of ADC, in association with perfusion changes. In one study, a limited number of voxels with ADC decreases were observed in a single patient, but this was not associated with any focal change in CBF in the same region (51). This suggests that any periclot diffusion restriction changes resulted from failure of energy metabolism that is not related to ischemia. Similarly, prolongation of contrast transit time, consistent with relative hypoperfusion, is not associated with any reduction in ADC (Fig. 2) (52). Consistent with nuclear medicine investigations, the results of MRI studies therefore indicate that ischemia is not a major factor in secondary injury, following ICH.

Magnetic Resonance Spectroscopy

Magnetic resonance spectroscopy (MRS) has also been used to study the mechanisms of secondary injury in ICH. Hydrogen MRS has been shown to be highly sensitive for the detection of acute ischemic metabolites, specifically lactate (55). MRS is also capable of demonstrating decreases in *N*-acetylaspartate (NAA) levels that occur following neuronal loss. One serial MRS study in 20 ICH patients has been published (56). This study examined the frontal

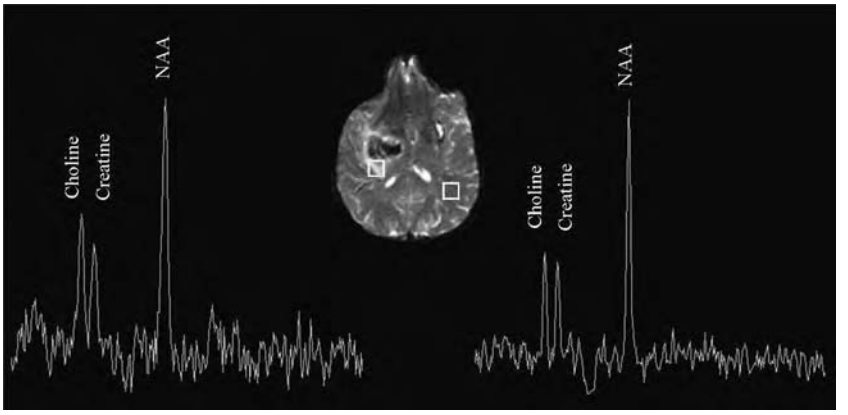

FIGURE 4 Example of hydrogen magnetic resonance spectroscopy in a patient with a putamenal intracerebral hemorrhage (ICH), imaged 16 hours after symptom onset. The spectra on the left correspond to the perihematomal region of interest (white square) and that on the right corresponds to the region in the contralateral hemisphere. At this stage, neuronal integrity and energy metabolism is intact, indicated by the normal *N*-acetylaspartate (NAA), choline and creatine levels. There is no lactate present, which would appear as a peak to the right of the NAA, under ischemic conditions. The hemosiderin deposit and gliotic cavity in the contralateral putamen is evidence of a previous ICH, which was asymptomatic.

cortical regions, following ICH located in the basal ganglia. The authors reported sequentially decreasing NAA levels when patients were studied within 48 hours of symptom onset and then again at two and four weeks, but no elevations in lactate. This was consistent with neuronal loss in the absence of ischemia. Although the study did not address the perihematomal region, it confirms that much of the secondary injury that occurs in ICH is not due to ischemia. One other study of five ICH patients studied subacutely has been reported (54). Small amounts of perihematomal lactate were found in two patients, one of whom had had a surgical resection performed. The investigators found no ischemic signatures using DWI in either of these patients, however, and concluded that the lactate resulted from nonischemic mechanism(s), which has been reported previously (57,58). One of the authors (KB) has performed single voxel hydrogen MRS in a small number of acute ICH patients. The technique is somewhat unreliable as the magnetic field required for MRS is disrupted by the paramagnetic effects of the hematoma. Nonetheless, spectra can be obtained within the edematous region, as seen on T2-weighted images. We have been able to demonstrate the absence of lactate, suggesting once again that ischemia is not a major factor in edema formation (Fig. 4).

Computerized Tomography (Xenon and Perfusion) Investigations

Absolute CBF can be determined using CT combined with the inhalation of the inert gas xenon. Several xenon CT studies in acute ICH patients have been reported (Table 5). Unfortunately, many of these studies are inconsistent with each other, with no obvious explanation in terms of methodology, timing of imaging, or hematoma volume. A number of studies report focally increased rCBF, which has been interpreted as luxury perfusion, around the hematoma of some patients. The largest of these studies reported elevated rCBF in 23 of 102 patients studied between one and six days after symptom onset (mean 2.7 days). Serial studies indicate that this is a transient phenomenon, resolving one to two weeks after symptom onset. It does appear that hyperperfusion has been reported only in patients imaged more than 12 hours after symptom onset. The reason(s) for this increase in perihematomal blood flow are not entirely clear, but may represent a recovery of neuronal function after the initial insult of the expanding hematoma.

Gebel et al. (59) studied the effect of acute blood pressure reduction on CBF by imaging five ICH patients within 24 hours of symptom onset immediately prior to and after administration of intravenous hypotensive agents. None of the patients had evidence of hypoperfusion when imaged initially. Reduction of systolic blood pressure to 130 to 140 mmHg resulted in an increase in regional cortical CBF in three of the five patients. In two patients, significant

TABLE 5 Computerized Tomography Investigations of Blood Flow in Intracerebral Hemorrhage

Investigator/study	Number of patients	Location of ICH	Time of study/studies from symptom onset	Primary findings
Suzuki et al. (89) (Xenon CT)	7	Putamen (7)	Scan 1: <4 d Scan 2: 4–14 d Scan 3: 14–25 d	Decreased ipsilateral hemispheric rCBF, but increased perihematomal rCBF (luxury perfusion) on scan 1, that decreased on scan 2 and scan 3
Kitahara et al. (90) (Xenon CT)	11	Putamen (11); all treated with aspiration through burr hole craniotomy	Preoperative: 4 Immediately postoperative: 4 1 wk: 5 2–3 wk: 4 >4 wk: 11	Reduced rCBF in ipsilateral hemisphere relative to control patients (no comparison to contralateral hemisphere); CBF increased transiently after surgical evacuation of hematoma and then decreased to below preoperative levels
Miyazawa et al. (37) (Xenon CT)	165	Putamen (87) Thalamus (37) Subcortical (27) Cerebellum (9) Brain stem (4)	1–6 day (mean 2.7): 102 1 wk-1 month: 19 >1 month: 44 NB: not a longitudinal study	Increased perihematomal rCBF (luxury perfusion) in 24/102 (23.5%) patients acutely, but in 0 patients imaged >1 wk after symptom onset.
Gebel et al. (59) (Xenon CT)	5		Scan 1: <24 h Scan 2: Post BP reduction to 160–170 mmHg systolic Scan 3: Post BP reduction to 130–140 mmHg systolic	No rCBF changes on scan 1 Scan 2/3: cortical rCBF increased (3/5); no change (2/5). Significant decreases in perihematomal rCBF and/or global CBF occurred post BP reduction (2/5).
Rosand et al. (61) (CT Perfusion)	5	Putamen (1) Thalamus (2) Lobar (2)	3–23 h	Perihematomal rCBF decreased in all patients, immediately adjacent (<2 mm) to the hematoma

Abbreviations: ICH, intracerebral hemorrhage; rCBF, regional cerebral blood flow.

decreases in perihematomal rCBF and/or global CBF were observed, but this was not associated with any neurological deterioration.

More recently, CT has been used to measure CBF changes, by tracking intravascular iodinated (nonionic) contrast media (60). Although currently limited to imaging only a portion of the brain, this technique is not susceptible to the artifacts caused by blood constituents in the way that MRI is. CT perfusion imaging also has other practical advantages in ICH. It can be performed immediately after noncontrast CT, which is performed on all acute ICH patients. The examination time is very short (<1 minute) and it actually has higher spatial resolution than both PET and MRI. Finally, no special equipment, apart from a power injector, is required, making the technology readily available in most hospitals treating acute ICH patients.

One CT perfusion study in ICH patients has been published (61). This study included five patients imaged between 9 and 23 hours after symptom onset. The authors reported a gradient of decreased rCBF, extending from the perimeter of the hematoma. The reductions in rCBF were only borderline significant, relative to the contralateral hemisphere, within 2 mm of the hematoma itself. The authors also found some evidence, that reduced rCBF was reduced to a greater extent in patients imaged earliest after symptom onset and in those with larger hematoma volumes. One of the authors (KB) has completed pilot CT perfusion studies in acute ICH patients that demonstrate very restricted regions of decreased rCBF in the perihematomal region (Fig. 5). Regional reduction in CBF tends to occur in a non-uniform distribution, identical to that observed with the MRI studies.

Summary of Evidence for Blood Flow Changes in Intracerebral Hemorrhage

Assessed together, the experimental and clinical studies indicate that acute ICH is associated with a transient zone of hypoperfusion in most cases. Perihematomal hypoperfusion is seen most commonly in the hyperacute stages and in association with larger clot volumes.

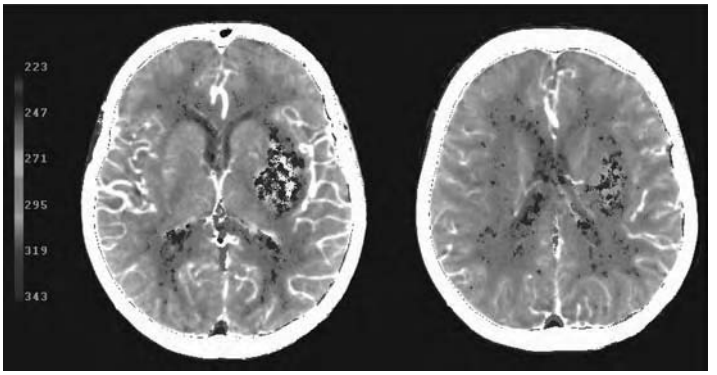

FIGURE 5 Computerized tomography perfusion (CTP) study in a patient with a moderate sized putamenal hematoma 5.5 hours after symptom onset. Perihematomal delay of CT contrast media is indicated by dark voxels (Tmax delay >2 seconds, relative to the contralateral hemisphere; units = 1/10 sec). The CTP study demonstrates perihematomal hypoperfusion immediately adjacent to the clot, which is not visible with PWI magnetic resonance imaging scans (compare with Fig. 3)

All investigations reveal a pattern of spontaneous resolution of the blood flow deficits subacutely. In addition, there is some evidence that a period of hyperperfusion can follow the acute reduction in CBF at least in some patients. This seems to have been recognized most frequently on xenon CT and to a lesser extent on SPECT and PET studies. This likely reflects timing of the imaging studies relative to symptom onset. Hyperperfusion has not been detected with MRI, but this may reflect the use of time domain perfusion measures (mean transit time; MTT and time–to-peak of the impulse residue; Tmax), which are likely to be less sensitive to increases in CBF (51–53). Although one of the authors' own MRI investigation did include rCBF measurements acutely, subacute assessments were limited to MTT (53).

Although hypoperfusion occurs in the same physical space as perihematomal edema, the two do not appear to be causally related. Instead, it seems more likely that hypoperfusion results from a decrease in metabolic rate. The edema itself is most certainly plasma derived, rather than cytotoxic. There is little evidence for cellular ischemia in most patients, the exceptions occurring in those with extremely large hematomas.

PART II: SECONDARY INJURY IN INTRACEREBRAL HEMORRHAGE

Experimental Evidence

As described in Part I, experimental ICH has been used to study transient CBF changes. Animal models have also been used to study the etiology and natural history of perihematomal edema as well as nonischemic mechanisms of secondary injury. A representative, but by no means exhaustive list of some of these studies is provided in Table 6.

Wagner et al. (62) developed an autologous blood model of ICH in the pig in order to study perihematomal edema formation. These authors used intravenous Evans blue dye to demonstrate that the blood–brain barrier remains intact in this model of ICH. Despite this, perihematomal edema developed in a similar manner to that seen in patients with ICH. It was concluded that edema resulted from the oncotic pressure exerted by the plasma proteins within the injected blood clot. Clotting proteins have been implicated in other aspects of perihematomal injury as well. Thrombin, plasmin, and plasminogen, which are all involved in clot formation and retraction, injected directly into the brains of rats has been shown to result in an active inflammatory response and cell death (63). Furthermore, it has also been shown that neutrophils, cytotoxic (CD8) lymphocytes, and microglia appear in the edematous tissue surrounding experimental hematomas within four hours, and become maximal at two to three days (7). Inflammatory cells have also been associated with increased matrix metalloproteinase activity (67). Inflammatory activity has been associated with ongoing neuronal death, which persists for at least four weeks—a time period that is certainly consistent with the concept of extended penumbral tissue (65).

TABLE 6 Summary of Studies of Secondary Injury Following Experimental Intracerebral Hemorrhage

Investigator/study	Animal	Hematoma model	Primary findings
Xue et al. (64)	Rat	Autologous blood injection	Apoptosis and inflammatory cells
Gong et al. (69)	Rat	Autologous blood injection	Apoptotic cells in the perihematomal region
Wagner (62)	Pig	Autologous blood injection	Edematous perihematomal injection in presence of intact blood brain barrier
Wagner and coworkers (91)	Pig	Autologous blood injection	No perihematomal edema when heparin injected with blood
Qureshi et al. (92)	Rabbit	Autologous blood injection; arterial pressure	Apoptotic cells and necrosis within the hematoma; swollen, edematous, but intact cells in the perihematomal region
Qureshi et al. (93)	Rabbit	Autologous blood injection; arterial pressure	Microdialysis demonstrated transient elevations in glutamate and other excitatory amino acids in the hemisphere ipsilateral to the ICH at 30 min
Xue (63)	Rat	Thrombin, plasmin, plasminogen injections	Apoptosis and inflammatory cells in the perihematomal region at 48 hr after injection of thrombin and plasmin
Ardizzone et al. (94)	Rat	Autologous blood (lysed) injection	Glucose hypermetabolism in the perihematomal region, which was blocked by glutamate antagonists
Del Bigio et al. (65)	Rat	Bacterial collagenase injection	Neutrophil and macrophage invasion of the perihematomal region from surrounding tissue was associated with neuronal loss
Power et al. (67)	Rat	Bacterial collagenase injection	Macrophage and matrix metalloproteinase activation
Nagatsuna et al. (66)	Rat	Bacterial collagenase injection	Neutrophil and macrophage infiltration of the perihematomal region, which was suppressed by the thrombin inhibitor argatroban

Abbreviation: ICH, intracerebral hemorrhage.

Glutamate release and excitotoxicity in the perihematomal region have also been implicated in secondary injury (68). Dying neurons are the most likely source of the excess excitatory amino acids, which in turn are toxic to nearby cells. Other clinical and experimental evidence suggests that a significant number of perihematomal region cells undergo programmed cell death. Histochemical analysis in ICH animal models have revealed DNA fragmentation consistent with apoptosis (69,70).

Assessed together, animal models of ICH indicate that perihematomal edema initially results from the oncotic forces of proteins involved in the coagulation cascade. These proteins in turn appear to elicit an inflammatory response, involving neutrophils, macrophages, and matrix metalloproteinase activation. This immune response likely also initiates apoptosis in some cells. Neuronal injury results in the release of glutamate and other excitatory amino acids, beginning the excitotoxic cascade. Ultimately, all of these events result in necrosis.

Hematoma Expansion

The perihematomal region may also be considered penumbral, in the sense that it is at risk of further injury, as it is now recognized that hematoma expansion occurs for several hours in many patients. Although bleeding in ICH was long thought to be brief and selflimited due to the tamponade effect of a mass within the intracranial compartment, a number of CT-based studies have shown this to be false. Two retrospective studies have shown that hematomas do, in fact continue to expand for several hours after symptom onset in a significant proportion of patients (71,72). Kazui et al. found a 40% or greater expansion in volume in 20% of patients imaged within 48 hours. In patients imaged within three hours, however, expansion was seen in 36%, suggesting that the majority of hematoma growth occurs early (72). Similarly, Fujii et al. (71) found 26% of patients imaged within two hours of symptom onset experienced expansion of at least 50% of baseline volume. In the only prospective study, baseline CT scan within three hours of symptom onset was followed by repeat imaging one hour later (11). The authors observed significant hematoma expansion (>33% volume) in 26% of patients. Repeat imaging at 20 hours after the baseline scan revealed expansion in an additional 12% of patients (11).

Hematoma expansion appears to be clinically significant, as it has been shown to be associated with neurological deterioration and impaired functional recovery (11,12,72,73). Growth of the hematoma has been associated with elevated systolic blood pressure, poorly controlled diabetes mellitus, low fibrinogen levels, and heavy alcohol consumption (12,73). These may allow the development of potential therapeutic strategies, aimed at prevention of hematoma expansion. As with ischemic stroke, however, treatment of this type of "penumbra" will most likely be successful only in the hyperacute stages. Acute hemostatic therapy, with recombinant Factor VIIa, has been shown in a randomized controlled trial to attenuate hematoma expansion and improve clinical outcome, if administered within four hours of symptom onset (10). A confirmatory phase III trial is currently underway. The other intriguing possibility is that rapid blood pressure reduction may also decrease the frequency of hematoma expansion. In one center, where aggressive blood pressure reduction to 140 to 160 mmHg systolic is part of routine care, expansion was seen in only 17% of patients admitted within two hours of symptom onset (13). This is considerably lower than the expansion rate observed in the observational studies. Similarly, another center reported that targeting maximum systolic blood pressure to ≤150 mmHg was associated with expansion in 9% of cases (74). This was significantly lower than the expansion rate of 30%, seen in those where maximum systolic blood pressure targets were 160 mmHg or higher. Although no cases of cerebral ischemia were reported, the safety and efficacy of this intervention can only be confirmed through ongoing randomized controlled trials (17,18).

Perihematomal Edema

Visible perihematomal edema on CT has been shown to be present in most patients imaged within three hours of symptom onset (75). Edema volumes increase by approximately 75% over the subsequent 20 hours (75). Paradoxically, lower relative edema, an index of absolute hematoma relative to hematoma volume, at 24 hours is associated with worse clinical outcomes (76). This has led to the hypothesis that early perihematomal edema may represent successful blood clotting. Excess clotting proteins, in particular, thrombin may contribute to larger edema volumes through an oncotic effect. This is supported by the observation that patients in whom clotting is inhibited through the use of antithrombotic therapies, as occurs secondary to thrombolysis for acute coronary syndromes, very little perihematomal edema forms (77).

As described in Part I, one of the authors' examination of perihematomal changes indicated that edema volume is highly correlated to the velocity of water movement, calculated as the ADC (53). Furthermore, this link between water mobility and edema volume was seen at the acute and subacute (3–5 days) time points. Thus, edema volumes tend to increase as a function of increased water diffusion, which extends peripherally from the hematoma. The total duration of edema expansion is not known. Retrospective serial CT study analysis is made difficult by the fact that both the proximal and distal borders of the edema volume become less distinct with time, and as the hematoma contracts. One group assessed the significance of continued edema growth by assessing only its mass effects, as revealed by the development and/or progression of midline shift (78). Edema, was associated with midline shift in 7/76 patients and in all cases, this occurred relatively late (9–21 days) after symptom onset. In contrast, earlier increases in mass effect, seen in 10/76 patients 4.8 to 41 hours after onset, were all associated with hematoma enlargement.

Etiology of Secondary Injury in Intracerebral Hemorrhage Patients

What evidence is there that the perihematomal edematous region of ICH patients is subjected to the same processes seen in animal models and can therefore be considered penumbral? The studies are limited in number, but most of the pathophysiological mechanisms observed in experimental studies do appear to be relevant clinically. The most direct evidence comes from histopathological examination of tissue from ICH patients. Qureshi et al. (79) studied tissue from 12 patients who underwent hematoma evacuation one to five days after symptom onset (79). It was found that apoptotic cells represented an average of 38% of the sample. Necrotic cells accounted for 25% of the sample, although this was much higher in the single patient who had surgical evacuation performed relatively late, on day five. Presumably, these pathological samples represented the hematoma core itself to a greater extent than the perihematomal region.

There is some indirect evidence that inflammation and excitotoxicity are both involved in secondary neuronal injury in humans as well. Castillo et al. (80) measured serum inflammatory and excitatory amino acid levels in patients with acute ICH. Tumor necrosis factor-α and interleukin-6 levels were increased and these correlated with the volume of perihematomal hypodensity seen on subacute CT scans. These findings are not definitive, but consistent with an active inflammatory response in the perihematomal region. The same study revealed systemic evidence of excess glutmatgeric activity, which was also found to be predictive of poor clinical outcome (80). Furthermore, the glutamate levels were significantly correlated to the volume of the residual cavity left by the hematoma at three months.

SUMMARY AND CONCLUSIONS

Although the pathophysiological responses to ICH are complex and incompletely understood, experimental and clinical evidence is coalescing to form a coherent sequence. There certainly is an acute but transient decrease in CBF in some patients, particularly those with large hematomas, but this does not appear to be related etiologically to edema formation or secondary cerebral injury. Instead, proteins involved in clot formation have direct oncotic and indirect toxic effects on the surrounding tissue. The subsequent inflammatory, excitotoxic, and apoptotic cascade ultimately results in the necrotic cavity that is found in survivors of ICH.

The perihematomal region may be considered penumbral from the point of view that it is at risk for catastrophic injury secondary to hematoma expansion in the first hours after symptom onset. Furthermore, the natural history of this tissue is to become edematous and subject to inflammatory responses, which ultimately lead to necrosis. This secondary injury occurs over several weeks, thus there is potential for many therapeutic interventions over a wide time period. Hyperacute therapy should be aimed at prevention of hematoma extension. Longer-term strategies may be aimed at inhibiting thrombin itself, ameliorating the inflammatory response, or the apoptotic signaling mechanisms.

We have made the case that there is little to support the more specific hypothesis of an ischemic penumbra in ICH. Nonetheless, we must concede that it remains unknown whether or not cerebral ischemia could result from hemodynamic alterations, such as a rapid decline in arterial pressure, in the acute period. It remains possible that the acutely elevated arterial pressures seen in the first hours after ICH are in fact a homeostatic response, which ensures that the cerebral perfusion pressure is maintained despite the mass effect of an intracerebral hematoma. The clinician's dilemma is that it seems if acute blood pressure reduction is to be effective from the point of view of preventing hematoma growth, it will have to be accomplished within the first few hours after symptom onset. While this seems like a rational therapeutic decision, the possibility of cerebral ischemia resulting from blood pressure reduction cannot be ruled out, particularly in those patients with very large hematomas and associated increases in intracranial pressure. Clearly, clinical equipoise exists and a rational approach will only be developed after the completion of randomized controlled trials (17,18). In addition, the evidence that inflammatory, excitotoxic, and apoptotic mechanisms are important in secondary injury is strong enough that potential penumbral treatments aimed at these targets should be developed.

REFERENCES

1. Butcher K, Laidlaw J. Current intracerebral haemorrhage management. J Clin Neurosci 2003; 10:158–167.
2. Thrift AG, Donnan GA, McNeil JJ. Epidemiology of intracerebral hemorrhage. Epidemiol Rev 1995; 17:361–381.
3. Broderick JP. Handbook of Neuroepidemiology. New York: Marcel Decker Inc, 1994.
4. Counsell C, Boonyakarnkul S, Dennis M. Primary intracerebral haemorrhage in the Oxfordshire community stroke project, 2: prognosis. Cerebrovasc Dis 1995; 5:26–34.
5. Mendelow AD, Gregson BA, Fernandes HM, et al., for the STICH Investigators. Early surgery versus initial conservative treatment in patients with spontaneous supratentorial intracerebral haematomas in the International Surgical Trial in Intracerebral Haemorrhage (STICH): a randomised trial. Lancet 2005; 365:387–397.
6. Bauer RB, Tellez H. Dexamethasone as treatment in cerebrovascular disease. 2. A controlled study in acute cerebral infarction. Stroke 1973; 4:547–555.

7. Poungvarin N, Bhoopat W, Viriyavejakul A, et al. Effects of dexamethasone in primary supratentorial intracerebral hemorrhage. N Engl J Med 1987; 316:1229–1233.
8. Bae HG, Lee KS, Yun IG, et al. Rapid expansion of hypertensive intracerebral hemorrhage. Neurosurgery 1992; 31:35–41.
9. Italian Acute Stroke Study Group. Haemodilution in acute stroke: results of the Italian haemodilution trial. Lancet 1988; 1:318–321.
10. Mayer SA, Brun NC, Begtrup K, et al., for the Recombinant Activated Factor VII Intracerebral Hemorrhage Trial Investigators. Recombinant activated factor VII for acute intracerebral hemorrhage. N Engl J Med 2005; 352:777–785.
11. Brott T, Broderick J, Kothari R, et al. Early Hemorrhage Growth in Patients With Intracerebral Hemorrhage. Stroke 1997; 28:1–5.
12. Kazui S, Minematsu K, Yamamoto H, Sawada T, Yamaguchi T. Predisposing Factors to Enlargement of Spontaneous Intracerebral Hematoma. Stroke 1997; 28:2370–2375.
13. Takizawa K, Suzuki A, Nagate K, et al. Blood pressure control in acute stages of hypertensive intracerebral hemorrhage to prevent growth of hematoma. Tokyo: NEURON publishing, 2002.
14. Willmot M, Leonardi-Bee J, Bath PM. High blood pressure in acute stroke and subsequent outcome: a systematic review. Hypertension 2004; 43:18–24.
15. Fogelholm R, Avikainen S, Murros K. Prognostic value and determinants of first-day mean arterial pressure in spontaneous supratentorial intracerebral hemorrhage. Stroke 1997; 28:1396–1400.
16. Mendelow AD. Mechanisms of ischemic brain damage with intracerebral hemorrhage. Stroke 1993; 24:I115–117.
17. Anderson C, Butcher K, Huang Y, et al. INTERACT (Intensive Blood Pressure Reduction in Acute Cerebral Haemorrhage Trial): rationale, design and early results. J Neurol Sciences 2005; 238(suppl 1):S381
18. Qureshi AI, Mohammad YM, Yahia AM, et al. A prospective multicenter study to evaluate the feasibility and safety of aggressive antihypertensive treatment in patients with acute intracerebral hemorrhage. J Intensive Care Med 2005; 20:34–42.
19. Qureshi AI, Wilson DA, Hanley DF, Traystman RJ. No evidence for an ischemic penumbra in massive experimental intracerebral hemorrhage. Neurology 1999; 52:266–272.
20. Kobari M, Gotoh F, Tomita M, et al. Bilateral hemispheric reduction of cerebral blood volume and blood flow immediately after experimental cerebral hemorrhage in cats. Stroke 1988; 19: 991–996.
21. Mendelow AD, Bullock R, Teasdale GM, Graham DI, McCulloch J. Intracranial haemorrhage induced at arterial pressure in the rat. Part 2: short term changes in local cerebral blood flow measured by autoradiography. Neurol Res 1984; 6:189–193.
22. Nath FP, Jenkins A, Mendelow AD, Graham DI, Teasdale GM. Early hemodynamic changes in experimental intracerebral hemorrhage. J Neurosurg 1986; 65:697–703.
23. Nath FP, Kelly PT, Jenkins A, Mendelow AD, Graham DI, Teasdale GM. Effects of experimental intracerebral hemorrhage on blood flow, capillary permeability, and histochemistry. J Neurosurg 1987; 66:555–562.
24. Sinar EJ, Mendelow AD, Graham DI, Teasdale GM. Experimental intracerebral hemorrhage: effects of a temporary mass lesion. J Neurosurg 1987; 66:568–576.
25. Nehls DG, Mendelow AD, Graham DI, Sinar EJ, Teasdale GM. Experimental intracerebral hemorrhage: progression of hemodynamic changes after production of a spontaneous mass lesion. Neurosurgery 1988; 23:439–444.
26. Nehls DG, Mendelow DA, Graham DI, Teasdale GM. Experimental intracerebral hemorrhage: early removal of a spontaneous mass lesion improves late outcome. Neurosurgery 1990; 27:674–682; discussion 682.
27. Bullock R, Brock-Utne J, van Dellen J, Blake G. Intracerebral hemorrhage in a primate model: effect on regional cerebral blood flow. Surg Neurol 1988; 29:101–107.
28. Yang GY, Betz AL, Chenevert TL, Brunberg JA, Hoff JT. Experimental intracerebral hemorrhage: relationship between brain edema, blood flow, and blood-brain barrier permeability in rats. J Neurosurg 1994; 81:93–102.
29. Kingman TA, Mendelow AD, Graham DI, Teasdale GM. Experimental intracerebral mass: description of model, intracranial pressure changes and neuropathology. J Neuropathol Exp Neurol 1988; 47:128–137.
30. Nath FP. Effects of experimental intracerebral hemorrhage on blood flow, capillary permeability, and histochemistry. J Neurosurg 1987; 66:555–562.
31. Bullock R, Mendelow AD, Teasdale GM, Graham DI. Intracranial haemorrhage induced at arterial pressure in the rat. Part 1: description of technique, ICP changes and neuropathological findings. Neurol Res 1984; 6:184–188.
32. Qureshi AI, Wilson DA, Hanley DF, Traystman RJ. Pharmacologic reduction of mean arterial pressure does not adversely affect regional cerebral blood flow and intracranial pressure in experimental intracerebral hemorrhage. Crit Care Med 1999; 27:965–971.

33. Patel MR, Edelman RR, Warach S. Detection of hyperacute primary intraparenchymal hemorrhage by magnetic resonance imaging. Stroke 1996; 27:2321–2324.
34. Sills C, Villar-Cordova C, Pasteur W, et al. Demonstration of hypoperfusion surrounding intracerebral hematoma in humans. J Stroke Cerebrovasc Dis 1996; 6:17–24.
35. Mayer SA, Lignelli A, Fink ME, et al. Perilesional blood flow and edema formation in acute intracerebral hemorrhage: a SPECT study. Stroke 1998; 29:1791–1798.
36. Siddique MS, Fernandes HM, Wooldridge TD, Fenwick JD, Slomka P, Mendelow AD. Reversible ischemia around intracerebral hemorrhage: a single-photon emission computerized tomography study. J Neurosurg 2002; 96:736–741.
37. Miyazawa N, Mitsuka S, Asahara T, et al. Clinical features of relative focal hyperfusion in patients with intracerebral hemorrhage detected by contrast-enhanced xenon CT. AJNR Am J Neuroradiol 1998; 19:1741–1746.
38. Uemura K, Shishido F, Higano S, et al. Positron emission tomography in patients with a primary intracerebral hematoma. Acta Radiol Suppl 1986; 369:426–428.
39. Videen TO, Dunford-Shore JE, Diringer MN, Powers WJ. Correction for partial volume effects in regional blood flow measurements adjacent to hematomas in humans with intracerebral hemorrhage: implementation and validation. J Comput Assist Tomogr 1999; 23:248–256.
40. Zazulia AR, Diringer MN, Videen TO, et al. Hypoperfusion without ischemia surrounding acute intracerebral hemorrhage. J Cereb Blood Flow Metab 2001; 21:804–810.
41. Powers WJ, Zazulia AR, Videen TO, et al. Autoregulation of cerebral blood flow surrounding acute (6 to 22 hours) intracerebral hemorrhage. Neurology 2001; 57:18–24.
42. Hirano T, Read SJ, Abbott DF, et al. No evidence of hypoxic tissue on 18F-fluoromisonidazole PET after intracerebral hemorrhage. Neurology 1999; 53:2179–2182.
43. Markus R, Reutens DC, Kazui S, et al. Hypoxic tissue in ischaemic stroke: persistence and clinical consequences of spontaneous survival. Brain 2004; 127:1427–1436.
44. Markus R, Reutens D, Kazui S, Read S, Hirano T, Donnan G. Hypoxic potentially viable tissue surrounding intracerebral hemorrhage in humans identified by [18F]-Fluoromisonidazole and Positron Emission Tomography (PET). Intern Med J 33(suppl):A50.
45. Schellinger PD, Jansen O, Fiebach JB, Hacke W, Sartor K. A standardized MRI stroke protocol: comparison with CT in hyperacute intracerebral hemorrhage. Stroke 1999; 30:765–768.
46. Kidwell CS, Chalela JA, Saver JL, et al. Comparison of MRI and CT for detection of acute intracerebral hemorrhage. JAMA 2004; 292:1823–1830.
47. Zamani AA. Imaging of intracranial hemorrhage. In: Rumbaugh CL, Wang A, Tsai FY, eds. Cerebrovascular Disease Imaging and Interventional Treatment Options. New York: Igaku-Shoin, 1995:232–247.
48. Hayman L, Taber K, Ford J, Bryan R. Mechanisms of MR signal alteration by acute intracerebral blood: old concepts and new theories. AJNR Am J Neuroradiol 1991; 12:899–907.
49. Linfante I, Llinas RH, Caplan LR, Warach S. MRI features of intracerebral hemorrhage within 2 hours from symptom onset. Stroke 1999; 30:2263–2267.
50. Lin DD, Filippi CG, Steever AB, Zimmerman RD. Detection of intracranial hemorrhage: comparison between gradient-echo images and b(0) images obtained from diffusion-weighted echo-planar sequences. AJNR Am J Neuroradiol 2001; 22:1275–1281.
51. Kidwell CS, Saver JL, Mattiello J, et al. Diffusion-perfusion MR evaluation of perihematomal injury in hyperacute intracerebral hemorrhage. Neurology 2001; 57:1611–1617.
52. Schellinger PD, Fiebach JB, Hoffmann K, et al. Stroke MRI in intracerebral hemorrhage: is there a perihemorrhagic penumbra? Stroke 2003; 34:1674–1679.
53. Butcher K, Baird T, MacGregor L, Desmond P, Tress B, Davis S. Perihematomal edema in primary intracerebral hemorrhage is plasma derived. Stroke 2004; 35:1879–1885.
54. Carhuapoma JR, Wang PY, Beauchamp NJ, Keyl PM, Hanley DF, Barker PB. Diffusion-weighted MRI and proton MR spectroscopic imaging in the study of secondary neuronal injury after intracerebral hemorrhage. Stroke 2000; 31:726–732.
55. Parsons MW, Li T, Barber PA, et al. Combined (1)H MR spectroscopy and diffusion-weighted MRI improves the prediction of stroke outcome. Neurology 2000; 55:498–505.
56. Kobayashi M, Takayama H, Suga S, Mihara B. Longitudinal changes of metabolites in frontal lobes after hemorrhagic stroke of basal ganglia: a proton magnetic resonance spectroscopy study. Stroke 2001; 32:2237–2245.
57. Okada Y, Kloiber O, Hossmann KA. Regional metabolism in experimental brain tumors in cats: relationship with acid/base, water, and electrolyte homeostasis. J Neurosurg 1992; 77:917–926.
58. Mun-Bryce S, Kroh FO, White J, Rosenberg GA. Brain lactate and pH dissociation in edema: 1H- and 31P-NMR in collagenase-induced hemorrhage in rats. Am J Physiol 1993; 265:R697–R702.
59. Gebel JM, Kassam A, Snyder J, et al. Effects of aggressive blood pressure reduction on cerebral blood flow in patients with acute intracerebral hemorrahge [abstr, International Stroke Conference]. Stroke 2000; 31:275–346.
60. Wintermark M, Maeder P, Thiran JP, Schnyder P, Meuli R. Quantitative assessment of regional cerebral blood flows by perfusion CT studies at low injection rates: a critical review of the underlying theoretical models. Eur Radiol 2001; 11:1220–1230.

61. Rosand J, Eskey C, Chang Y, Gonzalez RG, Greenberg SM, Koroshetz WJ. Dynamic single-section CT demonstrates reduced cerebral blood flow in acute intracerebral hemorrhage. Cerebrovasc Dis 2002; 14:214–220.
62. Wagner KR. Lobar intracerebral hemorrhage model in pigs: rapid edema development in perihematomal white matter. Stroke 1996; 27:490–497.
63. Xue M. Acute tissue damage after injections of thrombin and plasmin into rat striatum. Stroke 2001; 32:2164–2169.
64. Xue M, Del Bigio MR. Intracerebral injection of autologous whole blood in rats: time course of inflammation and cell death. Neurosci Lett 2000; 283:230–232.
65. Del Bigio MR, Yan H-J, Buist R, Peeling J, del Zoppo GJ. Experimental intracerebral hemorrhage in rats: magnetic resonance imaging and histopathological correlates. Stroke 1996; 27:2312–2320.
66. Nagatsuna T, Nomura S, Suehiro E, Fujisawa H, Koizumi H, Suzuki M. Systemic administration of argatroban reduces secondary brain damage in a rat model of intracerebral hemorrhage: histopathological assessment. Cerebrovasc Dis 2005; 19:192–200.
67. Power C, Henry S, Del Bigio MR, et al. Intracerebral hemorrhage induces macrophage activation and matrix metalloproteinases. Ann Neurol 2003; 53:731–742.
68. Qureshi AI, Ali Z, Suri MF, et al. Extracellular glutamate and other amino acids in experimental intracerebral hemorrhage: an in vivo microdialysis study. Crit Care Med 2003; 31(5):1482–1489.
69. Gong C, Boulis N, Qian J, Turner DE, Hoff JT, Keep RF. Intracerebral hemorrhage-induced neuronal death. Neurosurgery 2001; 48:875–882; discussion 882–883.
70. Qureshi AI, Suri MF, Ostrow PT, et al. Apoptosis as a form of cell death in intracerebral hemorrhage. Neurosurgery 2003; 52(5):1041–1047. discussion 1047–1048.
71. Fujii Y, Tanaka R, Takeuchi S, Koike T, Minakawa T, Sasaki O. Hematoma enlargement in spontaneous intracerebral hemorrhage. J Neurosurg 1994; 80:51–57.
72. Kazui S, Naritomi H, Yamamoto H, Sawada T, Yamaguchi T. Enlargement of spontaneous intracerebral hemorrhage: incidence and time course. Stroke 1996; 27:1783–1787.
73. Fujii Y, Takeuchi S, Sasaki O, Minakawa T, Tanaka R. Multivariate analysis of predictors of hematoma enlargement in spontaneous intracerebral hemorrhage. Stroke 1998; 29:1160–1166.
74. Ohwaki K, Yono E, Nagashima H, Hirata M, Nakagomi T, Tamura A. Blood pressure management in acute intracerebral hemorrhage: relationship between elavated blood pressure and hematoma enlargement. Stroke 2004; 35:1353–1367.
75. Gebel JM, Jr., Jauch EC, Brott TG, et al. Natural history of perihematomal edema in patients with hyperacute spontaneous intracerebral hemorrhage. Stroke 2002; 33:2631–2635.
76. Gebel JM Jr, Jauch EC, Brott TG, et al. Relative edema volume is a predictor of outcome in patients with hyperacute spontaneous intracerebral hemorrhage. Stroke 2002; 33:2636–2641.
77. Gebel JM, Brott TG, Sila CA, et al. Decreased perihematomal edema in thrombolysis-related intracerebral hemorrhage compared with spontaneous intracerebral hemorrhage. Stroke 2000; 31:596–600.
78. Zazulia AR, Diringer MN, Derdeyn CP, Powers WJ. Progression of mass effect after intracerebral hemorrhage. Stroke 1999; 30:1167–1173.
79. Qureshi AI, Suri MF, Ostrow PT, et al. Apoptosis as a form of cell death in intracerebral hemorrhage. Neurosurgery 2003; 52:1041–1047; discussion 1047–1048.
80. Castillo J, Davalos A, Alvarez-Sabin J, et al. Molecular signatures of brain injury after intracerebral hemorrhage. Neurology 2002; 58:624–629.
81. Kingman TA, Mendelow AD, Graham DI, Teasdale GM. Experimental intracerebral mass: time-related effects on local cerebral blood flow. J Neurosurg 1987; 67:732–738.
82. Ropper AH, Zervas NT. Cerebral blood flow after experimental basal ganglia hemorrhage. Ann Neurol 1982; 11:266–271.
83. Patel TR, Schielke GP, Hoff JT, Keep RF, Lorris Betz A. Comparison of cerebral blood flow and injury following intracerebral and subdural hematoma in the rat. Brain Res 1999; 829:125–133.
84. Kobari M, Gotoh F, Tomita M, et al. Bilateral hemispheric reduction of cerebral blood volume and blood flow immediately after experimental cerebral hemorrhage in cats. Stroke 1988; 19:991–996.
85. Tanizaki Y. Improvement of cerebral blood flow following stereotactic surgery in patients with putaminal haemorrhage. Acta Neurochir (Wien) 1988; 90:103–110.
86. Rousseaux M, Steinling M, Huglo D, Mazingue A, Barbaste P. Perfusion mapping with Tc-HMPAO in cerebral haematomas. J Neurol Neurosurg Psychiatry 1991; 54:1040–1043.
87. Sills C, Villar-Cordova C, Pasteus W, et al. Demonstration of hypoperfusion surrounding intracerebral haemorrhage in humans. J Stroke Cerebrovasc Dis 1996; 6(1):17–24.
88. Siddique MS, Fernandes HM, Arene NU, Wooldridge TD, Fenwick JD, Mendelow AD. Changes in cerebral blood flow as measured by HMPAO SPECT in patients following spontaneous intracerebral haemorrhage. Acta Neurochir Suppl 2000; 76:517–520.
89. Suzuki R, Ohno K, Matsushima Y, Inaba Y. Serial changes in focal hyperemia associated with hypertensive putaminal hemorrhage. Stroke 1988; 19:322–325.
90. Kitahara T, Yamashita T, Kashiwagi S, Kawakami N, Ishihara H, Ito H. Hemodynamics of hypertensive putaminal hemorrhage evaluated by xenon-enhanced computed tomography and acetazolamide test. Acta Neurol Scand Suppl 1996; 166:139–143.

91. Xi G, Wagner KR, Keep RF, et al. Role of blood clot formation on early edema development after experimental intracerebral hemorrhage. Stroke 1998; 29:2580–2586.
92. Qureshi AI, Ling GS, Khan J, et al. Quantitative analysis of injured, necrotic, and apoptotic cells in a new experimental model of intracerebral hemorrhage. Crit Care Med 2001; 29:152–157.
93. Qureshi AI, Ali Z, Suri MF, et al. Extracellular glutamate and other amino acids in experimental intracerebral hemorrhage: an in vivo microdialysis study. Crit Care Med 2003; 31:1482–1489.
94. Ardizzone TD, Lu A, Wagner KR, Tang Y, Ran R, Sharp FR. Glutamate receptor blockade attenuates glucose hypermetabolism in perihematomal brain after experimental intracerebral hemorrhage in rat. Stroke 2004; 35:2587–2591.

20 Extending the Time Window for Therapy

Numthip Chitravas
National Stroke Research Institute, Austin Health, Victoria, Australia

Geoffrey A. Donnan
National Stroke Research Institute, Austin Health, University of Melbourne, Melbourne, Victoria, Australia

INTRODUCTION

Acute stroke interventions for all forms of stroke that have been proven to be of benefit based on level 1 evidence include the management of patients in stroke units (ischemic and hemorrhagic stroke), use of oral aspirin within 48 hours (ischemic stroke only), and intravenous (IV) tissue-type plasminogen activator (tPA) within three hours of stroke onset (ischemic stroke only) (1–4). The number needed to treat (NNT) to benefit one person for stroke unit management is 18 (morbidity and mortality), for tPA is 10 (morbidity) and for aspirin is 83 (mortality). For aspirin, there is a strong possibility that the benefit is an early secondary preventive effect, so will not be discussed further.

The most biologically effective treatment for acute ischemic stroke is IV tPA administered within three hours of symptom onset (1,5). However, despite the strong evidence supporting its effectiveness, only 2% to 4% of all stroke patients currently receive tPA (6). The main reasons for this seem to be the narrow window of opportunity for treatment (three hours) and the increased risk of hemorrhage. Hence, extending this brief therapeutic time window for thrombolysis as well as other forms of therapy is an important means by which patients' outcomes may be improved. In this chapter, we will address the various ways in which this may be achieved.

IS EXTENDING THE TIME WINDOW FOR THERAPY POSSIBLE?

The possibility of extending the therapeutic time window is entirely dependent on the duration and extent of the surviving ischemic penumbra. As shown in earlier chapters, the evidence for duration of the ischemic penumbra seems to vary between species. In humans, the existing data has shown that the duration of the ischemic penumbra is up to 48 hours (Table 1) (7–9).

Using magnetic resonance (MR) parameters, Darby et al. (10) showed that perfusion weighted image (PWI)/diffusion weighted image (DWI) mismatch as an index of the penumbra existed for at least 24 hours poststroke. As shown in Figure 1, even though the PWI > DWI pattern is more common at an earlier stage, 44% of the patients had penumbra tissue at 24 hour after stroke. An even longer duration of the penumbra has been demonstrated by other investigators. Heiss et al. (9) showed that the maximum amount of tissue that could be salvaged decrements steadily to about 48 hours when at least some penumbral tissue remained. Similarly, using ^{18}F-fluoromisonidazole (FMISO) as a positron emission tomography (PET) marker of hypoxic tissue to identify the penumbra, Read et al. (8) were able to document the presence of significant areas of potentially viable tissue up to 42 hours postischemic stroke. This was confirmed by Markus et al. (7) using the same technique. They also showed that spontaneous survival of penumbra tissue leads to a favorable neurological outcome even 12 to 48 hours after stroke onset. Figure 2 shows the relationship between the prevalence of hypoxic tissue as a penumbral marker (measured by FMISO PET) and time after stroke onset.

Based on our current understanding of the extent and duration of the ischemic penumbra in humans and the observed therapeutic time window for thrombolysis of three hours and perhaps indirect evidence of some benefit up to about 4.5 hours based on a recent meta-analysis, a theoretical model of the potential to expand this therapeutic window can be constructed (11).

TABLE 1 Maximum Duration of the Ischemic Penumbra in Humans

Author	Technique	Penumbral measure	Maximum duration
Heiss et al. (9)	PET	OEF	48 h
Read et al. (8)	PET	18 FMISO	42 h
Darby et al. (10)	MR	PWI/DWI mismatch	24 h

Abbreviations: DWI, diffusion weighted imaging; FMISO, fluoromisonidazole; MR, magnetic resonance; OEF, oxygen extraction fraction; PET, positron emission tomography; PWI, perfusion weighted imaging.

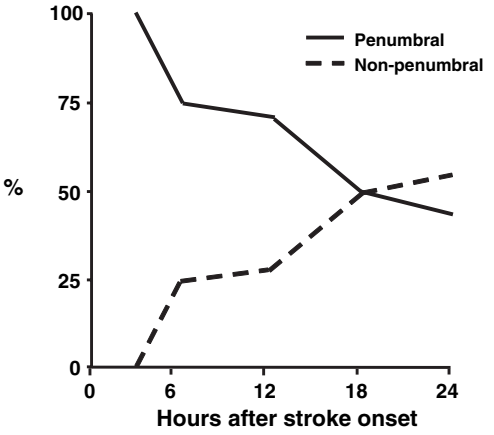

FIGURE 1 Plot of penumbral or nonpenumbral patterns as a percentage of total number of patients magnetic resonance imaging-scanned within each period. *Source*: Adapted from Ref. 10.

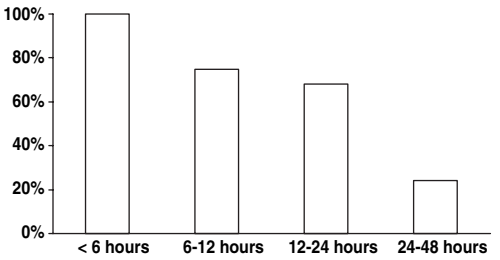

FIGURE 2 Proportion of patients with penumbra using fluoromisonidazole positron emission tomography. *Source*: Adapted from Ref. 7.

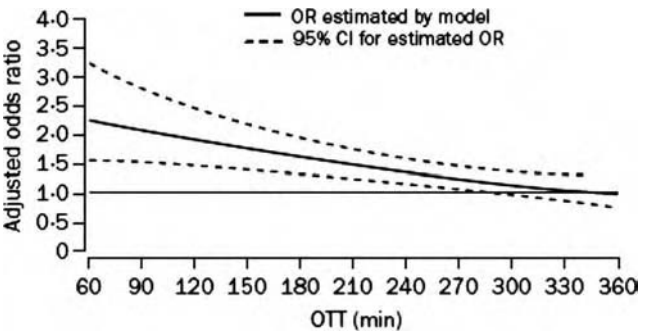

FIGURE 3 Model estimating odds ratio for favorable outcome at three months in recombinant tissue plasminogen activator treated patients compared with controls by onset to treatment. *Abbreviations*: OR, odds ratio; OTT, onset to treatment. *Source*: Adapted from Ref. 11.

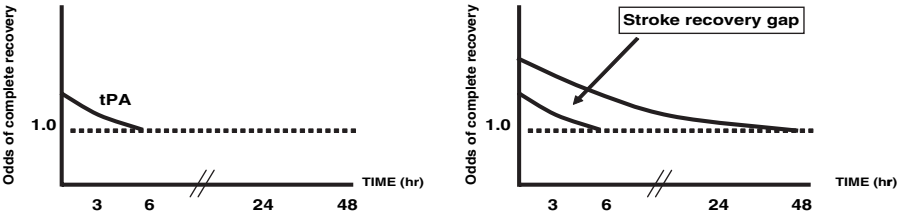

Recovery curves with time for tPA plotted with potential for recovery based on our current understanding of the extent and duration of the penumbra.

FIGURE 4 The relationship between the odds of recovery to near normal functional status (compared to controls) and time after stroke onset. While tissue plasminogen activator has improved the odds of recovery, there is still a considerable "stroke recovery gap" based on our understanding of the duration of the ischemic penumbra. *Abbreviation*: tPA, tissue plasminogen activator. *Source*: Adapted from Ref. 103.

Although the actual tissue salvaged can be increased by using thrombolytic therapy, as can be seen in Figure 3, there is obvious potential for additional tissue salvage at longer time windows based on our understanding of the presence of at least some penumbra up to 48 hours (Fig. 2). Hence, a "tissue salvage gap" or "stroke recovery gap" exists between current practice and theoretical limits of tissue salvage and therefore clinical recovery (Fig. 4). In other words, narrowing the gap will improve the amount of tissue that can be salvaged as well as extending the time window for treatment. Clearly this will expand the treatment to larger numbers of patients in clinical practice.

POTENTIAL METHODS OF EXTENDING THE THERAPEUTIC WINDOW

There are a number of possible approaches to extending the therapeutic window and hence reducing the stroke recovery gap. These include the use of neuroprotection, enhancing the spontaneous recanalization rate, and improving patient selection for therapy based on imaging techniques or vascular territory involved in the ischemic stroke process.

Prolonging Penumbral Duration with Neuroprotectants

As discussed earlier and shown in Figures 1 and 2, there is a progressive disappearance of the ischemic penumbra with time. A logical approach to extending the time window while waiting for the spontaneous recanalization and tissue salvage would be to arrest the transition of the ischemic penumbra to infarction. This could be done by using neuroprotectants: in other words, "freezing" the penumbra by this means would increase the amount of salvageable tissue while waiting for the spontaneous reperfusion to occur.

In animal models of focal cerebral ischemia, various neuroprotective strategies have been under investigation (12). In spite of the obvious benefit achieved in terms of reduction of infarct volumes and improved neurological outcome in these models, translation into the human paradigm has been difficult (13). Numerous trials of neuoprotection in humans have been unsuccessful or prematurely stopped because of safety concerns or lack of efficacy. One reason why neuroprotectants have not been successful in clinical trials in humans may be the relatively small sample sizes or lack of appropriate use of surrogate outcome measures in phase II trials (14). A useful surrogate may be the ability of the given neuroprotectant to freeze penumbra, as outlined earlier. A recent experimental study using normobaric oxygen (NBO) supports this concept. The use of this neuroprotectant was shown to widen reperfusion time window in rats by as much as two hours (15). The general concept of arresting the progression (or "freezing") of the penumbra to infarction is shown in Figure 5. As can be seen, the rate of infarct expansion is slower because the neuroprotective agents and the penumbra persist for longer, although the final infarct size may not necessarily be smaller.

Interestingly, this concept has also been expanded to the human sphere. In a pilot study by Singhal et al. (16) MR imaging (MRI)-measured infarct volume at different time points was used as a surrogate outcome. The DWI lesion volume at four hours was significantly reduced in NBO-treated patients with ischemic stroke compared with the placebo group (room

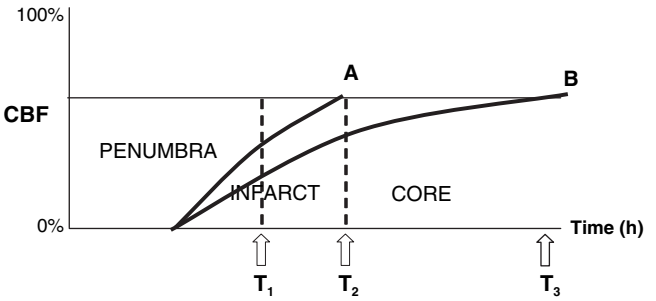

FIGURE 5 A schematic diagram illustrating "freezing" of the ischemic penumbra using neuroprotectants. The evolution of the penumbra to infraction in controls occurs as per curve A with approximate therapeutic window T1. After neuroprotection, evolution of the penumbra is slower or "frozen" as in curve B and with a longer therapeutic time window for reperfusion or other intervention at T2. However, the ultimate volume of infraction at T2 and T3 may be the same unless reperfusion occurs. *Abbreviation*: CBF, cerebral blood flow.

air). In addition, a significantly improved NIHSS was found at 24 hours in the NBO-treated group. Clearly, the same principle could be applied to other neuroprotective agents using a similar experimental paradigm.

Freezing the Penumbra and Enhancing Spontaneous Recanalization: Combination Therapy

A logical extension of the concepts raised in the previous section is to combine the penumbral freezing approach with an enhancement of the spontaneous recanalization rate with thrombolytic agents. In the Prolyse in Acute Cerebral Thromboembolism (PROACT) trial in which thrombolysis was achieved intra arterially using prourokinase (pro-UK), the rate of spontaneous partial/complete recanalization in heparin-treated patients was 18% within the six-hour therapeutic window. This rate was enhanced up to 66% in the pro-UK arm. To increase the proportion of salvageable tissue available by freezing the penumbra by using a neuroprotective agent during this time frame is an attractive proposition. Indeed, the use of a combination of neuroprotection and thrombolysis has been addressed on numerous occasions in animal models showing at least an additive effect (17–25). These are summarized in Table 2. Important points to note are that the experimental models have all involved elements of reperfusion, including the rat thromboembolic model, which is perhaps closest to the human paradigm. However, because of the variable extent of infarction in this model, somewhat larger sample sizes are required. This may, in part, be an explanation for the negative findings of Overgaard and coworkers (18), who used a combination of 2,3-dihydroxy-6-nitro-7-sulfamoyl-benzo[f]-quinoxaline-2-3-dione (NBQX) with tPA and showed that although both drugs individually reduced infarct size, there was no significant additive effect combined. This issue needs to be explored further in larger animal models, using differing time windows to therapy to get a better understanding of the conditions under which additive effects may occur.

However, in humans there is less data available (Table 3) (26,27,28). In most of the studies, the sample sizes are too small to assess clinical outcomes but, importantly, combination therapies have raised no safety issues. In the ASTIN trial, approximately 27% of patients with acute ischemic stroke treated with neutrophil inhibitory factor (NIF) within six hours of ischemic stroke onset received tPA (28). There was no improvement in stroke recovery, but the safety of NIF was established.

Although neither magnesium sulfate infusion nor induced hypothermia have been studied in a trial designed for testing the combination with thrombolytic agents, their proven safety and feasibility were established. Using a three-hour therapeutic time window, concomitant IV tPA and magnesium sulfate is being studied in the ongoing trial, FAST-MAG, phase III. The trial aims to evaluate the efficacy of hyperacute, paramedic-initiated magnesium sulfate administration in improving the longterm functional outcome of patients with acute stroke, as measured by the modified Rankin scale (MRS). Twenty percent of patients (from total *n* of 1298) will receive reperfusion therapy [tPA or Mechanical Embolus Removal in

TABLE 2 Experimental Studies Using Animal Models of Interaction Between Thrombolytic and Neuroprotective Agents

Author	Neuroprotectant	Action	Thrombolytic agent	Experimental model	Outcome
Lekieffre et al. (17)	Elipiodil	NMDA antag (poly?) VSCC	tPA	Rat thromboembolic	Additive
Sereghy et al. (18)	Dizocilpine	Excitatory antag	tPA	Rat thromboembolic	Additive
Overgaard and coworkers (18)	NBQX		tPA	Rat thromboembolic	No additive effect
Yang et al. (19)	Topiramate	Enhances GABA inibits Glu release	UK	Rat	Additive
Andersen et al. (20)	Citicholine	Membrane repair, reduces FFa release	tPA	Rat thromboembolic	Additive
Shuaib and coworkers (19)	Citicholine	Membrane repair, reduces FFa release	UK	Rat thromboembolic	Additive
Bowes et al. (21)	Monoclonal Abs against leukocyte adhesion molecules	Anti-inflammatory	tPA	Rabbit	Additive
Zhang et al. (22)	Monoclonal Abs against leukocyte adhesion molecules	Anti-inflammatory	tPA	Rat	Additive
Zhang et al. (23)	Proteasome inhibitor PS-519	Anti-inflammatory	tPA	Rat thromboembolic	Additive
Sanchez et al. (23)	U-74389-G	Free radical scavenger	tPA	Rat thromboembolic	No additive effect
Orozco et al. (25)	21 amino steroid U7+006F	Free radical scavenger	tPA	Rabbit	No additive effect

Abbreviations: GABA, γ-aminobutyric acid; NBQX, 2,3-dihydroxy-6-nitro-7-sulfamoyl-benzo[f]quinoxaline-2-3-dione; NMDA, *N*-methyl-D-aspartate; tPA, tissue plasminogen activator; UK, urokinase; VSCC, voltage-sensitive calcium channels.

Cerebral Ischemia (MERCI) Retriever] with either IV magnesium sulfate or placebo. The study does not aim to test the hypothesis of extending the time window, but nevertheless the hope of extending the therapeutic time window will be implied if IV magnesium sulfate potentiates the benefit of tPA.

TABLE 3 Human Studies of Patients with Acute Ischemic Stroke Using Combination Therapy

Author	Neuroprotectant	Action	Thrombolytic agent	Study design	Sample size	OTT	Outcome
Grotta (26)	IV lubelazole 5 d		IV tPA 0.9 mg/kg	RCT	90	≤3 h	No safety issues
Lyden et al. (27)	IV clomethiazole 68 mg/kg		IV tPA 0.9 mg/kg, max 90 mg	RCT	101	≤3 h	No safety issues
ASTIN (28)	IV/NIF	Neutrophil inhibition	tPA 0.9 mg/kg	Adaptive RCT	966	<6 h	No difference in clinical improvement safe; not increased incidence of infection

Abbreviations: ASTIN, acute stroke therapy by inhibition of neutrophils; IV, intravenous; NIF, neutrophil inhibitory factor; OTT, onset time to treatment; RCT, randomized controlled trial; tPA, tissue plasminogen activator.

Mild hypothermia is a powerful neuroprotective strategy in preclinical models. Pilot studies in stroke and the recent positive trials after cardiac arrest have generated significant interest in this strategy (29–32). In the cooling for acute ischemic brain damage (COOL-AID) study, a phase-2 study with a 12-hour window and using an endovascular cooling device to 33°C, the feasibility and safety of moderate hypothermia in acute ischemic stroke is being tested (33). The 22 patients who received thrombolytic therapy were also included (10 in the treatment group and 12 in controls). There was no statistical improvement in neurological outcome at 30 days in the hypothermia group, but there was a trend toward lower growth of infarct volume based on day 3 to 5 MRI examination in the hypothermia group (90.0% vs. 108.4%, P = NS). Larger trials are needed to determine whether hypothermia can freeze the penumbra and extend the time window for treatment with thrombolytic agents.

Further Enhancing Recanalization and Reperfusion Within the Life of the Penumbra

Intravenous Thrombolytic Agents

The time window established for efficacy using IV tPA for acute ischemic stroke is three hours based on the NINDS trial (1,34). However, in a further analysis of the NINDS trial, the risk-to-benefit ratio of IV tPA becomes rapidly unfavorable as time elapses, because less brain tissue can be saved and the risk of cerebral hemorrhage might outweigh the benefit (35).

Many studies have explored the value of IV tPA given beyond the three-hour window, with the general aim to improve the short time window of benefit. This hypothesis has been tested in European Cooperative Acute Stroke Study I (ECASS I) and European-Australian Cooperative Acute Stroke Study II (ECASSII) with a three to six-hour time window for patient enrollment (5,36). Despite the nonsignificant results, it revealed a trend toward efficacy for therapy between three and six hours and the hemorrhagic complication rate was comparable to the NINDS trial.

For the three to five hours window after stroke symptom onset, investigators for the Acute Noninterventional Therapy in Ischemic Stroke (ATLANTIS) trial demonstrated that therapy was unlikely to be beneficial. Further, it showed that the patients who received IV thrombolytic treatment (alteplase 0.9 mg/kg) had a significantly increased 10-day hemorrhage rate and showed a trend toward higher 90-day mortality rate versus controls (37).

There are many possible explanations for these inconclusive findings. These include the time to treatment (i.e., 80% of patients in ATLANTIS were enrolled four to five hours after symptom onset) and insufficient study numbers to detect a difference beyond three hours.

Recently, to improve the statistical power, a pooled analysis of ATLANTIS, ECASS, and NINDS recombinant tPA (rtPA) stroke trials was conducted (11). As mentioned earlier, a potential benefit beyond three hours was suggested, perhaps up to about 4.5 hours, since this is the point at which the lower 95% confidence limit (CI) for the adjusted odds ratio for a favorable outcome crossed unity. The asymptotic effect of time on a steadily reducing benefit can be seen in Figure 6. In addition, in the subgroup analysis, the odds ratio for favorable outcome was 1.40 (1.05–1.85) for those treated within 181 to 270 minutes. These findings support the possibility that some patients may benefit from treatment beyond the current three-hour window.

There are a number of ongoing studies to test the hypothesis that there may be a benefit of thrombolysis beyond the three-hour time window. In the ongoing double-blind, placebo-controlled ECASS III study, the investigators are assessing the potential benefit of thrombolysis in the three to four-hour time window after acute stroke onset. Meanwhile the large (n = 6000) International Stroke Trial III (IST-III) will provide important data for tPA administration within six hours of ischemic stroke.

Intra-arterial Thrombolytic Agents

The concept of this approach is that intra-arterial (IA) administration of thrombolytic agents may offer higher concentrations of the drug at the site of vessel occlusion with lower systemic concentrations. This may result in higher recanalization rates and the mechanical disruption of the clot may also contribute to clot dissolution.

The studies in which the IA approach was tested most vigorously were the PROACT trials I and II. These were large scale, multicenter randomized controlled trials in which IA

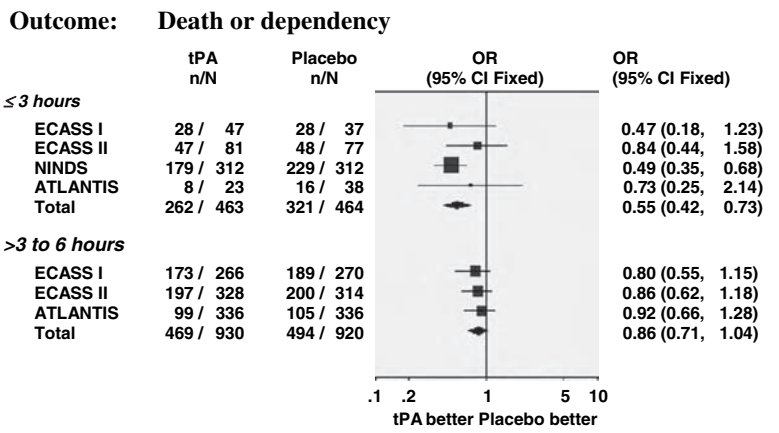

FIGURE 6 Meta-analysis of trials of intravenous tissue plasminogen activator in acute ischemic stroke stratified for time windows to therapy zero to three hours and more than three to six hours. *Abbreviations*: OR, odds ratio; tPA, tissue plasminogen activator. *Source*: Adapted from Ref. 103.

thrombolysis (IAT) alone was administered in patients who otherwise received heparin within the time window up to six hours after stroke onset (38,39). The outcome as defined by good-to-excellent score on the MRS (MRS ≤2) was achieved by 40% of pro-UK patient as opposed to 25% in the control group ($P = 0.043$). However, when compared with pre-existing reports in the IV tPA study (NINDS, ECASSII, ATLANTIS), a higher rate of symptomatic intracerebral hemorrhage was reported in the pro-UK group (10%). While this single trial was not thought to be sufficient evidence to obtain FDA approval, nevertheless, the data have led to the adoption of protocols for the administration of IA tPA at some centers.

Similarly, an increased risk of symptomatic intracerebral hemorrhage (ICH) was found in a meta-analysis of IAT therapy (40). Twenty-seven studies were reviewed with 852 patients who received IAT and 100 control subjects, and it was shown that the IAT group had an odds ratio of 2.4 (95% CI: 1.45–3.85) for favorable outcome and a lower mortality rate compared to controls (IAT, 27.2%; control group, 40%, $P = 0.004$).

Despite level-1 evidence strongly supporting the superiority of IAT over heparinization, a head-to-head comparison of IA versus IV thrombolysis has never been done. Given that there are inevitable delays in many centers to initiate IAT compared to the simpler IV approach, this delay is of some concern. The inexorable progression of ischemic penumbra to infarction as well as impairment of vascular integrity and blood–brain barrier over time might worsen the benefit/risk ratio (36).

Combined Routes of Administration for Thrombolytics

Details of published studies in which there is a combination of IA and IV thrombolytic (IA/IVT) treatment a re summarized in Table 4. This approach has emerged based on the concept that the strategy could allow early treatment of stroke (with IV medication), while the resources to deliver IA therapy are being organized. In other words, this combines the rapid (IV) and definitive endovascular (IA) approaches. Increasing the efficacy of thrombolytic treatment via combination routes of treatment should narrow the stroke recovery gap and, therefore, extend the currently limited time window.

This approach was first used by Freitag et al. who used combined IV tPA and IA plasmin (41). Later on, the Emergency Management of Stroke (EMS) bridging trial compared recanalization rates between combined IA/IVT with IAT alone, with a three-hour time window after stroke onset to treatment (42). A higher recanalization rate as well as the feasibility of coadministration of IA/IVT was found without increasing the risk of sICH. Even though the 90-day mortality rate seemed to be higher in IV/IAT group, the small number of subjects in IA/IVT

TABLE 4 Combined Intravenous/Intra-arterial Thrombolysis

Study	Study design	Sample size (*n*)	OTT	RCN	90 days mortality	MRS 0–1 90 d	MRS 0–2 90 d	sICH	Comment
EMS (42)	RCT	35	3 h	54% (TIMI 3)	29%	35%	47%	0% at 24 h 12% at 72 h	No difference in clinical outcome between combination group and IA. The mortality was non significantly higher in treatment group
IMS (47)	NR open	80	3 h	11% (TIMI 3)	16%	30%	43%	6.3%	Average tPA dose 59 mg (NINDS 69 mg)
Ernst et al. (43)	RT open	20	3 h	69% (TIMI 2–3)	10%	—	65%	5%	
Zaidat et al. (44)	RT open	18	6 h	80%	20%	40%	60%	20%	Studied in patients with carotid occlusion
Suarez et al. (44)	NR open	45	3 h	75%	17%	—	—	0%	Patients selected for IA based on DWI/PWI mismatch and MRA
Hill et al. (45)	NR open	8	3 h	86% (TIMI 1–3)	0%		37%	0%	PWI/DWI mismatch for selection IA given before IV
Keris et al. (46)	NR open	45	6 h	41% (TIMI 3)	17% at 30 d	—	—	17%	Reverse approach IA/IV
Freitag et al. (41)	NR open	—	—	—	—	—	—	—	Lys-plasminogen as adjunct
Lisboa (40)	Meta-analysis	28	—	—	21.4%	—	—	10.7%	
Flaherty et al. (48)	NR open	62	3 h	23%	18%	35%	50%	8%	
NINDs rtPA (104)	RCT	211	3 h	—	21%	32%	39%	6.6%	
NINDS placebo (104)	RCT	182	3 h	—	24%	18%	28%	1.0%	

Abbreviations: DWI, diffusion weighted imaging; EMS, emergency management of stroke; IA, intra-arterial; IMS, interventional management of stroke; IV, intravenous; MRA, magnetic resonance angiography; MRS, modified Rankin scale; NINDS, National Institutes of Neurological Disorders and Stroke; NR, nonrandomized; OTT, onset time to treatment; PWI, perfusion weighted imaging; RCN, recanalization; RCT, randomized controlled trial; RT, retrospective; sICH, symptomatic intracerebral hemorrhage; TIMI, thrombolysis in myocardial infarction; tPA, tissue plasminogen activator.

group ($n = 17$) confounds the interpretation. Observational studies also confirm the feasibility of combination IA/IVT (43,44).

In two studies, the combined IA/IV approach was used, together with a selection of patients based on MR PWI/DWI criteria (44,45). Recanalization rates were also greater (80% or more) in the combined group than the IV therapy alone. Moreover, a reverse approach with IA therapy preceding the IV contribution has also been studied with an open design, the rational being that the early IA approach would maximize the probability of recanalization, while continuous IV infusion would increase the efficacy of therapy (46). Again, the hemorrhagic complication rate was not significantly increased.

The single arm, pilot study, NIH Interventional Management of Stroke (IMS) trial, comparing combined IA/IV and IVT with historical controls of standard dose tPA in NINDS, confirms the high rate of recanalization in IA/IVT group and the comparable safety profile (odds ratio of mortality = 1.35; CI: 0.78–2.37) of this technique (47). Although not significant, a trend of better outcome at three months than conventional IV tPA (from NINDS data) was found.

Although the focus of these combination therapy trials has been on the efficacy and safety profiles, most of the studies have set the onset-to-treatment window at less than three hours and have, therefore, not extended the time window for therapy usefully. There are, however, a few observational studies in which a time window up to six hours has been used (47,48). Further, in comparing combined IA/IVT with IVT, historical controls only were used, so there is a need to test this comparison within a formal randomized controlled trial.

Newer Thrombolytic Agents

Novel fibrinolytic agents have been developed in response to the failure of tPA to achieve rapid reperfusion and, in addition, hoping to minimize hemorrhagic complications with greater fibrin specificity (49,50). Increasing of recanalization rate as well as reducing the hemorrhagic transformation is an attractive way to extend the time window of reperfusion therapy. A summary of studies of these agents in humans using various therapeutic time windows after stroke onset is seen in Table 5. Agents have their own unique properties, which are outlined as follows:

1. *Tenecteplase (TNK)*. This agent is genetically modified from tPA. It has 14-fold greater fibrin specificity than alteplase, and therefore allows TNK to be active at the site of high fibrin concentrations such as within recent clot rather than systemically (51). The longer half-life of TNK and slower plasma clearance also makes it possible to be given in bolus form. In addition, TNK has an 80-fold greater resistance to PAI-1 (52).

   Unlike tPA, TNK administration is associated with a lesser procoagulant effect. Indeed, both systemic plasminogen activation and plasmin generation are commonly seen after tPA therapy. In a pilot dose escalation safety study of TNK in acute ischemic stroke, patients were treated less than three hours after symptom onset with IV TNK (53). No symptomatic ICH within 36 hours of treatment was observed among any of the patients within a dose of 0.4 mg/kg. The neurological improvement was comparable but not superior to historical rtPA-treated of NINDS trial (to provide comparable time epochs, the NINDS subgroup of onset to treatment time 91 to 180 minutes was used). A phase 2b study of TNK in treatment of acute ischemic stroke is being conducted to test the hypothesis that TNK might have a higher efficacy and safety profile than tPA. Hence, TNK may provide a welcome treatment option, should this hypothesis be substantiated, and increase the possibility that thrombolytic treatment may be later introduced beyond a fixed three-hour window.
2. *Desmetoplase*. Similarly, desmetoplase is being used as a more effective and safer thrombolytic agent than tPA to extend the time window for therapy. In the Desmoteplase in acute ischemic stroke trial (DIAS), this hypothesis was also tested (54). Desmetoplase is an effective plasminogen activator derived from vampire bat (Desmodus rotendus) saliva [D rotundus salivary plasminogen activator (DSPA)]. In contrast to tPA, it acts by direct activation of plasminogen to plasmin and is selective for fibrin-bound plasminogen. Further, desmetoplase does not appear to have the neurotoxic effects seen with tPA caused by n-methyl–D-aspartate-induced neurodegeneration (55). In DIAS, acute ischemic stroke

TABLE 5 Human Studies of Newer Thrombolytic and Fibrinolytic Agents in Various Time Windows

Study	Study design	N (mode of treatment)	Maximal time window	Drug/route	Partial or completed RCN n (%)	sICH	Overall mortality	Favorable outcome	Comment
Qureshi et al. (56)	NR open	16	9 h	Reteplase, IA	14 (88%)	6.2%	56%	—	
Hacke et al. (54)	RCT, phase II	104	9 h	Desmoteplase IV	—	26.7 (part I) 2.2 (part II)		49% reperfusion	Used PWI/DWI mismatch to select the patient
Furlan et al. (39)	RCT	121	6 h	Pro-urokinase	108 (66%)	10%	25%		
Haley et al. (53)	NR, open	88	3 h	Tenecteplase IV	—	0% in dose ≤ 0.4 mg/kg	12–24 %	MRS 0–1 = 32–36%	The results are comparable to NINDS tPA group
ASS (1994)	RCT	64	6 h	Ancrod	—	0%	12.5%	Better neurological outcome in ancrod	
STAT (63)	RCT	248	3 h	Ancrod	—	5.2%	8.9%		
Liu et al.(105)	Review	1456	24 h	Defibrase	—	—	—	Fibrinogen depleting agents moderately reduced the proportion of patients who were dead or disabled at the end of follow-up ($P = 0.002$)	

Abbreviations: DWI, diffusion weighted imaging; IA, intra-arterial; IV, intravenous; MRS, modified Rankin scale; NINDS, National Institutes of Neurological Disorders and Stroke; NR, nonrandomized; OTT, onset time to treatment; PWI, perfusion weighted imaging; RCN, recanalization; RCT, randomized controlled trial; sICH, symptomatic intracerebral hemorrhage; STAT, The Stroke Treatment with Ancrod Trial; tPA, tissue plasminogen activator.

patients with PWI/DWI mismatch within the window of three to nine hours after onset were enrolled. Substantially improved early reperfusion rates and clinical efficacy were found in the treatment group, and the rate of symptomatic ICH was low. Moreover, a subgroup analysis demonstrated clinical benefit for the six- to nine-hour time window. The DIAS Phase III trial is ongoing in an endevor to confirm this finding.

3. *Reteplase*. Reteplase is a third generation tPA, a nonglycosylated deletion mutant of wild-type tPA. This agent is also expected to increase the efficacy of thrombolysis by improving the rate of recanalization. A small prospective human clinical trial evaluated the safety and efficacy of IA reteplase in 16 patients with ischemic stroke who were poor candidates for IV alteplase therapy. Thirteen of the 16 patients (80%) received thrombolytic drug beyond three hours from stroke onset and five (30%) received therapy beyond six hours. Near complete or complete recanalization was observed after treatment in 88% of the patients (56). Again, this result suggests that the time window may be extended beyond three hours using newer thrombolytic agents. However, larger numbers of patients in a randomized controlled trial are obviously required to confirm this preliminary finding. A study of reteplase combined with abxicimab intravenously in the ROSIE trial will be discussed later.
4. *Pro-UK*. This is a glycosolated 411 aminoacid single chain proenzyme precursor of UK. At the thrombus surface, single chain r-pro-UK is activated to two chain urolinase by fibrin-associated plasmin (57). As mentioned earlier, there are several published randomized studies of IA pro-UK in acute cerebral thromboembolism (PROACT I and II) (39). Despite an increased frequency of early symptomatic intracranial hemorrhage, there was no difference in overall mortality, and treatment with r-pro UK within six hours after the onset of acute middle cerebral artery (MCA) occlusive stroke significantly improves modified Rankin score at 90 days.
5. *Plasmin and microplasmin*. These are new emerging fibrinolytic agents. Both plasmin and microplasmin act directly on fibrin. However, plasmin is inactivated by circulation antiplasmin. Therefore, it should be applied locally or intra-arterially. Unlike plasmin, microplasmin is resistant to circulating antiplasmin and can be used intravenously. In an animal model of embolic stroke, IV microplasmin demonstrated a significant reduction in PWI lesion growth compared with controls at 24 hours after MCA occlusion (58). Moreover, there is data to suggest that microplasmin has an additional lytic-independent neuroprotective effect (59).
6. *Ancrod*. Ancrod is a purified fraction of venom from the Malaysian pit viper (Calloselasma rhodostoma). It produces rapid defibrinogenation by splitting fibrinopeptide A from fibrinogen (60,61). Hence, this causes anticoagulation by depleting the substrate needed for thrombus formation. Although it is not a fibrinolytic agent per se, it will be discussed here for convenience. This fibrinogen-depleting agent reduces fibrinogen in blood plasma, reduces blood viscosity, and therefore increases cerebral blood flow. A randomized trial of ancrod suggested that it was both safe and beneficial in stroke patients treated up to six hours (62). The stroke treatment with ANCROD trial (STAT) was conducted with 500 patients who were randomized within three hours of ischemic stroke onset and a significant outcome benefit was seen for ancrod (42.2% favorable outcome of Barthel index ≥95 vs. 34.4% in placebo group, $P = 0.04$). Symptomatic bleeding occurred in 5.2% of cases. Better outcome was achieved with lower fibrinogen levels, and symptomatic intracerebral hemorrhage was more likely to occur under these circumstances (63). A parallel European trial with ANCROD using a six-hour time window was also commenced, but the study was prematurely terminated because of a failed futility assessment at a preplanned interim analysis. Further, the 90-day mortality was higher in the ANCROD group compared to placebo (64). Recently, there was a Cochrane review in which three trials were included (including one ongoing trial) of acute stroke treated with ancrod within five days of stroke onset. The review demonstrated that fibrinogen-depleting agents moderately reduced the proportion of patients who were dead or disabled at the end of follow-up (RR 0.90; 95% CI: 0.82–0.98). However, there was no statistically significant difference in deaths from all causes during the scheduled treatment period. Although the fibrinogen-depleting agents seemed to provide benefit in extending the treatment window, there is still insufficient evidence to be certain that they are safe and efficacious.

Newer Antiplatelet Agents

The discovery that the final common step in platelet aggregation is through the binding of fibrinogen to the activated platelet integrin, glycoprotein (GP) IIb/IIIa, has opened the door for the development of novel and potentially more effective antithrombotic therapies (64). Since then, the use of GPIIb/IIIa antagonists in stroke has been the subject of a wide range of investigations. GPIIb/IIIa receptor antagonists include:

1. Abciximab, the first GPIIb/IIa inhibitor available, which is made from the Fab fragments of an immunoglobulin that targets the GPIIb/IIIa receptor on the platelet membrane. Its mechanism of action is inhibition of GP IIb/IIIa at its receptor on the platelets; it may occupy some receptors for weeks.
2. Tirofiban, which is a nonpeptide inhibitor of GP IIb/IIIa receptors.
3. Eptifibatide, which is a nonpeptide tyrosine derivative.

GPIIb/IIIa receptor antagonists promote or enhance thrombolysis by downregulating platelet aggregation and thrombin generation (impeding rethrombosis) (65). It also attenuates the inflammation, improves microcirculation and collateral circulation, hence preventing further lesion expansion. By the properties mentioned earlier, the GPIIb/IIIa receptor antagonists might slow the progression of penumbral tissue to infarction.

Abciximab is a platelet aggregation inhibitor mainly used during and after coronary artery procedures such as angioplasty to prevent platelets from aggregating and causing thrombus formation within the coronary artery. Abciximab has been studied alone in acute ischemic stroke. Its safety has been proved with the same dose as used in the treatment of coronary artery disease (0.25 mg/kg followed by 12 hours infusion at the rate of 0.125 μg/kg/min), when administered up to 24 hours after stroke onset (66). The AbESTT phase II trial also confirmed its reasonable safety profile (67). The trial enrolled 400 patients within six hours of onset of ischemic stroke, and a trend of favorably functional outcome (MRS $\leq$2) at three months was observed (68). In addition, early neurological improvement and attenuation of ischemic lesion growth in DWI were found in an exploratory, MRI-guided open-label trial of IV abxicimab administration 3 to 24 hours after acute ischemic stroke (69). The ongoing randomized, double-blind placebo-controlled trial of AbESTT phase III, which planned to enroll as many as 1800 patients, has been recently temporary suspended because of safety concerns, while the entire benefit–risk profile of abxicimab is assessed for acute ischemic stroke before coming to a final recommendation of whether or not enrollment in the trial should resume.

The combination of tPA and GPIIb/IIIa antagonists in acute ischemic stroke has also been explored. The powerful antiplatelet properties of GPIIb/IIIa inhibitors make them potentially useful adjuvant agents combined with thrombolysis and may extend the time window for therapy. In an animal model of MCA occlusion, the combination of IV Abxicimab with tPA significantly reduced infarct volume and maintained vascular integrity (70). Even more importantly, it was safe without increasing incidence of hemorrhagic transformation and supported the potential to increase the time window for thrombolytic therapy. However, in a primate model of stroke, efficacy was not proven, probably due to small subject numbers (71). In humans, one small prospective study showed combined half dose systemic IV tPA (0.45 mg/kg) and that abciximab is safe and effective. It appeared to achieve higher recanalization rates than IV tPA alone with time windows up to 12 hours (72). Clearly, there is a need to determine the safety and efficacy of combination reteplase and abciximab in randomized controlled trials. The reopro retavase reperfusion of stroke safety study-imaging evaluation trial (ROSIE) was commenced in 2002 and it is ongoing. The study extends the time window of reteplase infusion from three hours up to 24 hours with coadministration of IV abciximab. An outcome measure is MRI-reperfusion at 24 hours posttreatment. The ROSIE-CT trial is identical to ROSIE, but image evaluation is done with CT for patients who are not eligible for MRI. The combination of abciximab, IAT together with mechanical devices to remove clot will be discussed later in this chapter. Table 6 demonstrates the study of abciximab in various time windows after stroke onset.

Tirofiban is a highly effective antiplatelet agent with proven efficacy in the treatment of acute coronary syndromes and experimental cerebral ischemia. In a small study of patients

TABLE 6 Study of Abciximab in Various Time Windows

Study	Study design	Sample size	OTT	Dose	Outcome
Abciximab in acute ischemic stroke (66)	RCT	74	≤24 h	0.25 mg/kg infusion in 30 min follow by 0.125 μg/kg/min infusion over 12 h	No difference in clinical outcome No sICH
Mitsias et al. (69)	NR open	29	3–24 h	Same as above	No difference in MRI growth at 24 h NIHSS 4 points decreased at 48 to 72 h (P <0.001)
AbESTT phase II (67)	RCT	400	≤6 h (92% of patients were treated in 3–6 h)	Same as above	No difference in clinical outcome No sICH
AbESTT phase III (106)	RCT	Aiming for 1800	≤5 h (n = 1200) 5–6 h or ≤2.5 h after awake (n = 600)	Same as above	Temporary suspended because of safety concern
Gahn et al. (72)	NR open	27	Median = 5 h	tpa IV 0.45 mg/kg, Abciximab dose is same as above	Higher recanalization
ROSIE, ROSIE CT (107)	RT open	72	3–24 h	Reteplase in 5 escalating doses (0, 2.5, 5, 7.5, 10 U), Abciximab dose is same as above	Ongoing

Abbreviations: AbESTT, Abciximab Emergent Stroke Treatment Trial; IA, intra-arterial; IV, intravenous; MRI, magnetic resonance imaging; NR, nonrandomized; OTT, onset time to treatment; RCN, recanalization; RCT, randomized controlled trial; ROSIE, Reopro Retavase Reperfusion of Stroke Safety Study; sICH, symptomatic intracerebral hemorrhage; tPA, tissue plasminogen activator.

with acute ischemic stroke with time for administration ranging from 2 to 51 (median 5) hours, the safety and feasibility of tirofiban alone was examined (73). Patients with progressively deteriorating acute ischemic stroke were treated with body-weight adjusted IV tirofiban for a mean period of 46 hours and compared with a matched group of acute, but stable ischemic stroke patients. There was no significant increase in the cerebral bleeding rate. Later, the efficacy of tirofiban was found in an open pilot study (74). Administration of weight-adjusted tirofiban beginning within nine hours after symptom onset of stroke resulted in smaller infarct volume by T2 weighted-MRI at one week compared with controls receiving IV unfractionated heparin only (P = 0.029). Again, no patient in this pilot developed sICH. The safety of tirofiban in acute ischemic stroke (SaTIS), a larger phase II study (n = 240), will assess the safety of tirofiban in an extended time window from 6 to 22 hours after stroke onset.

Tirofiban may be suitable as a single therapeutic or as an adjunct therapeutic to thrombolysis with alteplase for the treatment of stroke. It may enhance the efficacy of thrombolytics and reduce potentially fatal adverse effects, such as ICH, by lowering tPA dosage as required. Results from a small case series indicated that tirofiban, administered within three hours after stroke onset followed by 48-hour infusion, combined with low dose tPA was associated with improvement in MCA recanalization without symptomatic hemorrhage (75). It should be noted that a body weight-adjusted dose of tirofiban with infusion period of 24 hours was also used in this study. It appears that combination therapy (lowdose tPA plus body weight adjusted tirofiban) improves neurological deficits and reduces infarct growth on DWI/T2 MR74. The maximum time window used in the study was 4.5 hours after stroke onset. Table 7 demonstrates the study of tirofiban in various time windows after stroke onset.

Eptifibatide (Integritin), like other antagonists of platelet receptor GPIIb/IIIa, functions by blocking the binding of the adhesive proteins fibrinogen and von Willebrand factor to GPIIb/IIIa on the surface of activated platelets. It is a potent antithrombotic, because the binding

TABLE 7 Study of Tirofiban in Various Time Windows

Study	Study design	Sample size	OTT	Dose	Outcome
Junghans et al. (73)	NR open	35	2–51 h (median 5 h)	Tirofiban 0.4 µg/kg infusion in 30 min follow by 0.1 µg//kg/min in 24 hours	No difference in clinical outcome No sICH
Junghans (73)	Case series	20	Median 9 h	Same as above	Significant improvement in 1 wk-T2weighted MRI infarct volume
Siebler (SaTIS)	RCT	240	6–22 h	Same as above	Measure safety (ongoing)
Stefan (75)	Case series	19	≤3 h	Tirofiban dose is same as above and intravenous — tPA 20 mg bolus in 15 cases, 10 mg bolus plus 40 mg infusion in the other 4 cases.	68% recanalisation (TIMI 2,3) significant smaller in DWI lesion growth no sICH
Sietz et al. (75)	NR open	47	Mean 2 h (max 4.5 h)	Tirofiban dose is same as above but infusion in 24 hr.-tPA 20 mg bolus	Significant improvement in 1 wk-T2weighted MRI infarct volume No sICH

Abbreviations: DWI, diffusion weighted imaging; NR, nonrandomized; OTT, onset time to treatment; PWI, perfusion weighted imaging; sICH, symptomatic intracerebral hemorrhage; TIMI, thrombolysis in myocardial infarction.

of these proteins to GP IIb/IIIa is the event that precipitates platelet aggregation and subsequent arterial thrombus formation. Eptifibatide has been tested previously combined with IA tPA and showed a trend to achieving better recanalization with good clinical outcome at three months (76). Currently, the randomized multicenter trial (CLEAR) is evaluating the safety of eptifibatide in combination with IV tPA within three hours after ischemic stroke onset. In the ROSIE-2 trial, the acceptable dose of eptifibatide is now being determined. This is a randomized open-label trial designed to enroll 150 patients within three hours after stroke. All patients will receive IV alteplase plus aspirin (81 mg) and tinzaprin (low molecular weight-heparin), then assigned to one of the five dosing groups of eptifibatide. In this latter trial, the reperfusion by MRI at both 2 and 24 hours as well as clinical recovery at 24 hours will be evaluated. If safety and efficacy can be established using this combination approach, a longer time window may be explored. Table 8 demonstrates the study of eptifibatide in stroke.

Use of Devices to Enhance Revascularization

Revascularization or recanalization of major vessels is the key to reperfusion at a microvascular level. Given the earlier discussion in which it was established that the ischemic penumbra may exists up to 48 hours in some individuals postvessel occlusion, revascularization during this time window would seem to be feasible. Obviously, the initial forays into this area need to be focused on shorter time windows to establish efficacy and safety. The majority of techniques discussed here will, therefore, be conducted within this relatively short time windows. The exception is the endovascular photo acoustic recanalization (EPAR) laser system that is being tested in patients up to 24 hours with posterior circulation ischemia, which may be more forgiving in terms of therapeutic time window. There are many parallels with advances made in the management of acute coronary syndromes, where we have seen a movement from thrombolysis as the main mode of revascularization to angioplasty alone.

As in percutaneous transluminal coronary angioplasty, the percutaneous intracranial angioplasty intervention was also classified into four categories: (*i*) immediate angioplasty, to be performed as soon as possible after thrombolysis; (*ii*) delayed angioplasty, to be performed within several hours or a few days after thrombolysis; (*iii*) rescue angioplasty, to be performed after failed thrombolysis; and (*iv*) primary (direct) angioplasty, to be performed instead of thrombolysis. In interest of brevity, we will restrict our discussion to direct angioplasty.

TABLE 8 Study of Combined Thrombolytic Agents and Eptifibatide in Various Time Windows

Study	Study design	Sample size	OTT	Dose	Outcome
Mcdonald et al. (76)	NR open	37	Mean 4 h 21 min	Eptifibatide 90 microgram bolus follow by 0.5–2.0 μg/kg/min infusion tPA dose is unknown	Recanalization (TIMI 2,3) 58% No difference in clinical outcome No sICH
CLEAR (108)	RCT, dose escalation	100	≤3 h	Eptifibatide 75 microgram bolus follow by 0.75 μg/kg/min infusion tPA 0.3 mg/kg intravenous administration	Safety (ongoing)
ROSIE2 (109)	RT, open label, dose escalation	150	≤3 h	Five escalating dosing groups for eptifibatide: 0, 45, or 90 μg/kg bolus only, 90 μg/kg bolus plus 0.25 μg/kg/min infusion for 24 h, or 90 μg/kg bolus plus 0.5 μg/kg/min infusion for 24 h eptifibatide in 5 doses Standard IV tPA, plus aspirin 81 mg orally (or 120 mg rectally) and tinzaparin 80 anti-Xa IU/kg subcutaneously	Aim to fine the acceptable dose of eptifibatide (ongoing)

Abbreviations: CLEAR, Combined Approach to Lysis Utilizing Eptifibatide and rt-PA in Acute Ischemic Stroke; IV, intravenous; NR, nonrandomized; OTT, onset time to treatment; ROSIE 2, Reperfusion of stroke Safety study Imaging Evaluation—2; RT, retrospective; TIMI, thrombolysis in myocardial infarction; tPA, tissue plasminogen activator.

Primary or Direct Percutaneous Transluminal Angioplasty

The general principle of this approach is similar to that in the coronary circulation where immediate angiography was performed postischemic stroke onset and a site of vessel occlusion identified. Balloon angioplasty is then performed by advancing the catheter into the site of occlusion (clot, atheroma, or both) and then the balloon inflated to achieve recanalization. There have been two small published case series to date using this approach with maximum time for reperfusion of five and six hours (77,78). It can be concluded that the technique is feasible and safe, but larger studies are required to prove its efficacy in improving clinical outcomes (Table 9).

Endovascular Devices

Investigators have been constantly searching for more rapid ways to disrupt clots and enhance revascularization. The obvious advantage of this is to prolong the time window for stroke treatment.

The endovascular devices are best classified as (*i*) mechanical clot disruption/removal devices (*ii*) suction thrombectomy devices and (*iii*) laser- or Doppler-assisted thrombolysis devices.

1. Mechanical clot disruption or removal devices: These clot retriever devices rely on the delivery of a device distal to the thrombus while the device remains constrained in a microcatheter. The unconstrained component of the device is then expanded to capture the thrombus or atheromatous emboli as the device is withdrawn.

   Three examples are microsnare, Neuronet Endovascular Snare, and clot-retrieval devices. Microsnares have long been used to retrieve foreign bodies from cerebral vessels. Recently, case reports have described successful retrieval of IA clots lodged in intracranial arteries via gooseneck microsnare in the setting of acute ischemic stroke (79–81). The substantial improvement occurred without hemorrhagic complications, and the maximal time window to treatment was 12 hours.

TABLE 9 Overview of Mechanical Interventions in Acute Stroke Therapy

Study	Study design	N (mode of treatment)	Max OTT	Interventions	RCN	90 days mortiality	MRS 0–190 d	MRS 0–290 d	sICH	Comment
Nakano et al. (78)	Case series	10	—	Direct PTA	80%	—	—	—	0%	Max. time from stroke onset to reperfusion = 6 h
Nakano et al. (77)	NR open	34	—	Direct PTA	91.2%	—	18%	25%	2.9%	Max. time from stroke onset to reperfusion = 5 h
Wikholm et al. (79)	Case reports	5	10 h	Gooseneck microsnare	—	—	—	—	0%	Substantial neurological improvement
Chopko (80)	Case report	1	4.5 h	Gooseneck microsnare	—	—	—	—	—	Substantial neurological improvement
Favrole (81)	Case report	3	12 h	Gooseneck microsnare	2 (66%)	—	—	—	0%	Substantial neurological improvement
Mayer (82)	Case report	5	10 h	Neuronet Endovascular snare	3 (60%)	100%	3 (60%)	—	0%	Only include basilar artery occlusion cases
Neuronet Endovascular Evaluation in Embolic stroke Disease [NEED (82)]	RCT	—	—	Neuronet Endovascular snare	—	—	—	—	—	Ongoing
MERCI I/II (83)	Single arm, open	151	8 h	MERCI retrieval device	46% (TIMI 2 or 3)	43.5%	—	22.6%	5%	Use historical controls in the analysis. Recanalization rate is significantly greater than sponataneous recanalization rate of placebo arm in PROACT trial

MR RESCUE (110)	RCT	60 (total *n*=120	8 h	Concentric clot retriever	—	—	—	—	—	Ongoing, primary outcome is MRS at 90 d
Qureshi et al. (84)	NR open	19	9 h	Balloon angioplasty or Gooseneck microsnare	78% (TIMI 3 or 4)	—	—	—	0%	Use low dose of reteplase as an adjunctive treatment Select the patients who were considered poor candidates for IV alteplase therapy
Lutsep (85)	Case report	3	5 h	Suction thrombectomy	3 (100%; TIMI 3)	—	1/3	—	—	—
Bellon (86)	Case report	3	6 h	Angiojet	—	—	—	—	—	The potential of rapid, large-burden thrombus removal from ICA occlusion was shown
Berlis (87)	NR open	34	6 and 24 h	EPAR laser system	41%	38.2% at d 30	—	5% at D 30	5.9%	Thirteen patients in this trial received intra-arterial tPA as an adjunctive therapy
Alexandrov (88)	RCT	63	3 h	Transcranial doppler ultrasonography	49% (TIMI 3)	15%	42%	—	4.8%	2 MHz ultrasound device was used. No significant clinical improvement found
Daffertshofer (90)	RCT	14	6 h	Transcranial low-frequency ultrasonography	29%	21%	—	—	36%	Thirteen patients in treatment group showed sign of intracranial bleeding on MRI vs. 5 in 12 in controls

Abbreviations: IV, intravenous; MERCI, mechanical embolus removal in cerebral ischemia; MR RESCUE, MR and Recanalization of Stroke Clots Using Embolectomy; MRS, modified Rankin scale; NR, nonrandomized; OTT, onset time to treatment; PROACT, Prolyse in Acute Cerebral Thromboembolism; RCN, recanalization; sICH, symptomatic intracerebral hemorrhage; TIMI, thrombolysis in myocardial infarction.

Neuronet endovascular snare (self-expanding nitinol basket; Guidant) is a new-generation snare device with a basket shape also devised specifically for acute stroke treatment. Preliminary experience has been reported as part of the ongoing large, multicentered, Neuronet Evaluation in Embolic stroke Disease trial in Europe. The device was shown to be practical and safe in recanalizing the basilar artery with a maximal time window of 10 hours (82).

The MERCI retrieval device has attracted considerable public attention and is the only FDA approved clot retriever. The name is derived from the MERCI trial and is a corkscrew-like apparatus, which resides in the catheter tip until it is ready to be burrowed into the clot (83). Results of phase I/II trials of a mechanical thrombectomy device suggest that mechanical retrieval of clots is a safe and effective treatment for ischemic stroke, which may prolong the treatment time window up to eight hours. In their intention to treat analysis, 69 of 151 (46%) patients achieved recanalization as measured by thrombolysis in myocardial infarction grade II or III. Importantly, the rate of symptomatic intracerebral hemorrhage was not higher than the pre-existing data of IV thrombolysis (tPA group of NINDS) or stroke intervention trials (PROACT I/II), in spite of higher recanalization rates. In the ongoing MR RESCUE trial, neurological outcome is being measured to determine if patients will benefit substantially from a mechanical embolectomy with the concentric clot retriever device, when eligible patients are identified based on MR diffusion–perfusion criteria.

In another approach, the combination of mechanical clot disruption in concert with IAT has shown promising results (84). This may be another viable treatment option for acute ischemic stroke patients who are not eligible for IVT because of severe neurologic deficits and/or presentation more than three hours after stroke onset. In a trial in which 19 patients were enrolled, adjunctive treatment of reteplase IAT (maximum dose of 4 U) administered through seperselective catheterization was followed by snare manipulation for distal occlusions and angioplasty for proximal occlusions of the MCA ($n = 9$), cervical ICA ($n = 7$), and other sites ($n = 3$). Overall, a high recanalization rate (78%) was observed without vascular complications with the maximal time window of nine hours.

2. Suction thrombectomy device: After initial reports of simple catheter-based suction thrombectomy, more sophisticated devices have been developed (85). For example, the AngioJet takes advantage of the venturi principle and uses saline jets that are directed back into the catheter to create a low-pressure zone around the catheter tip, inducing aspiration of the surrounding thrombus. The device has been approved by the FDA for use in arteriovenous dialysis grafts and fistulae and for treatment of coronary arteries, saphenous vein grafts, and peripheral vessels. In spite of difficulties, because of the lack of catheter flexibility, a report of three cases with a six-hour time window showed the potential for rapid clot removal (86). Later, the smaller NeuroJet was developed, but the initial feasibility and safety study was stopped after arterial dissections proved to be a problem. A redesigned device is now being investigated in the phase 1 Thrombectomy In Middle cerebral artery Embolism (TIME) trial in patients presenting within six hours of stroke onset.

3. Laser- or doppler-assisted thrombolysis: Laser-assisted thrombolysis offers the potential for rapid clot disruption resulting in clot emulsification. The laser power source is delivered by fiber optics to the tip of the 1 mm catheter at the treatment site where it is converted into acoustic energy, which then causes the clot to emulsify inside the catheter tip.

   The safety and feasibility of laser-assisted thrombolysis device in acute stroke patients has been reported in the phase II multicenter trial assessing the EPAR laser system (87). Patients in this study received IA laser thrombolytic treatment within six hours of stroke onset for anterior circulation and within 24 hours for posterior circulation occlusion. The recanalization rate was approximately 41%, and a comparable rate of sICH in NINDS tPA group was found. Of note, 13 patients in this study had additional treatment with IA rtPA. This new technique appears to be safe and obviously may provide a means of extending the window for treatment of acute ischemic stroke.

   A longer time window of treatment by a laser-assisted device was also reported when using the LaTIS laser device, which has the same principle of action as EPAR laser system. The window was extended up to eight hours in anterior circulation and 24 hours in posterior circulation stroke. Both devices have the potential to extend the time window for therapy.

The combination of ultrasound with thrombolytic therapy is the other recently developed mechanically assisted thrombolytic intervention. In humans, both internally and externally applied, low frequency, pulse-wave ultrasonography with IV tPA have been used (88–90). The most practical is the externally applied technique where acceleration of arterial recanalization was found using a diagnostic 2 MHz transcranial ultrasound device (88). In the first RCT reported, a time window of three hours was used and higher recanalization rates and acceptable sICH were demonstrated. Although, there was no significant clinical improvement at three months compared with IV tPA alone, the results were encouraging enough to generate the hypothesis that shortening of recanalization times could contribute to optimizing the effect of acute thrombolytic stroke therapy, and perhaps extend the time window for treatment. In another study in which the ultrasound device used had a wider beam and lower frequency of 300 kHz and a time window of six hours, an unexpected increased in sICH occurred that resulted in a premature cessation of the trial (90). However, neither morbidity nor treatment-related mortality or recanalization rates differed between the combined treatment group and tPA alone.

PATIENT SELECTION FOR THROMBOLYTIC TREATMENT BASED ON VASCULAR TERRITORY OF ISCHEMIA

Although, definitive evidence is lacking, there is a general belief that the more extensive collateral circulation in the posterior arterial territory allows longer time windows of therapy. To date, there have been no comparative studies of the duration of the ischemic penumbra between anterior and posterior circulations, although this is clearly needed. The other main driver for long time window therapies in the posterior circulation is the high morbidity and mortality of basilar artery occlusion (91–93). Hence, investigators have used an almost random empirical approach for IAT for acute vertebrobasilar occlusion with the time windows up to 72 hours after acute stroke onset (Table 10).

The strongest evidence for efficacy is from a nonrandomized cohort study using historical controls, in which 65 consecutive patients with clinical signs of severe brainstem ischemia and angio-demonstrated vertebro-basilar occlusion were retrospectively analyzed (93). Forty-three patients received local IAT therapy (UK or streptokinase), two-thirds within 24 hours after stroke onset (six of them within six hours). Higher recanalization rates were demonstrated angiographically among treated patients, and the patients who displayed recanalization had a significantly higher survival rate and a favorable clinical outcome. Later, many small nonrandomized open-label trials and case series as well as a meta-analysis including 164 patients with posterior circulation stroke showed a similar trend toward favorable outcomes (although there were no controls), and roughly half of the patients survived (94–99). The maximal time window of any of these open studies was 82 hours.

Evidence supporting efficacy of IVT treatment in posterior circulation stroke in the time beyond 3 hours after onset symptoms has also been reported (100–102). Recently, Lindsberg et al. (101) enrolled 50 consecutive patients with angiographically proven basilar artery occlusion in whom IV alteplase (0.9 mg/kg) was given. The time window for therapy was 12 hours if the onset of symptoms was sudden and 48 hours if the symptoms were gradually progressing. The study showed that the rate of recanalization, survival, and independent functional outcome are comparable with those reported with endovascular approaches and recommended the conduct of a larger randomized controlled trial. Hence, it can be seen that there is an accumulating amount of nonrandomized data to suggest that it is safe and feasible to extend the time window in the posterior circulation, perhaps up to 24 hours or more. There is a clear need for a large, randomized, controlled trial to provide evidence to guide clinical practice more precisely.

SELECTION OF PATIENTS BASED ON IMAGING TECHNIQUES

Because acute ischemic stroke is a highly heterogeneous disease, not every patient's time window for treatment is the same. Experimental studies in different animal models have found wide variations in the potential time window for treatment efficacy, ranging from just a few minutes to as long as 48 hours. In humans, imaging and biochemical studies in acute stroke patients similarly suggest that the window for potential efficacy may be prolonged in selected

TABLE 10 Study Thrombolytic Therapy in Posterior Circulation Ischemic Stroke

Study	Study design	N (mode of treatment)	Maximal time window	Drug/route	Lesion of occlusion	Partial or completed rcnn (%)	sICH	Overall mortality	Favorable outcome	Comment
Hacke et al. (93)	Case series	43	76 h	UK or SK, IA	VB	19 (44%)	6%	69%	—	
Zeumer et al. (97)	NR, open	28	8 h (mean)	UK, IA	—	21 (75%)	7%	46%	—	
Becker et al. (95)	Case series	12	48 h	UK, IA	VB	9 (75%)	15%	75%	—	
Macleod et al. (96)	RCT	8	≤24 h	UK, IA	VB	—	—	—	—	Inconclusive data due to small number
Levy et al. (98)	Meta-analysis	164	48 h	UK, IA	VB, BA	91 (55%)	—	—	—	
Arnold et al. (94)	NR, open	40	12 h	UK, IA	BA	32 (80%)	5%	42%	—	
Cross et al. (99)	NR, open	24	82 h	UK, IA	BA	Not indicate	12.5%	63%	—	
Huemer et al. (100)		16	7 h	IV		10 (62%)	—	—	—	
Lindsberg et al. (101)	NR, open	50	48 h	tPA IV	BA	26 (52%)	14%	40%	—	
Montavont et al. (102)	NR, open	18	9 h	tPA IV	VB,BA	—	0%	—	MRS 0–2 = 27%	
Ground (111)	Case series	12	3 h	tPA IV	VB, BA	—	—	—	MRS 02 = 75%	
Brandt (112)	Case series	51	48 h	tPA IV, UK IA	VB, BA	26 (51%)	18%	68%		

Abbreviations: BA, basilar artery; IA, intra-arterial; IV, intravenous; MRS, modified Rankin scale; NR, nonrandomized; RCT, randomized controlled trial; TIMI, thrombolysis in myocardial infarction; tPA, tissue plasminogen activator; UK, urokinase; VB, vertebral artery; VB, vertebrobasilar artery.

individuals (7–9). The most promising imaging tools to identify these patients are multimodal MRI and CT. They both can delineate the extent of ischemic core, still salvageable penumbra, presence of large-vessel occlusion, and unthreatened regions of benign oligemia. By identifying individuals in whom substantial salvageable tissue still persists beyond 3 hours, this may obviate the classical limitations of the stroke therapeutic time window (103). As shown in previous chapters and the next, many investigators are now validating these new imaging techniques.

REFERENCES

1. The National Institute of Neurological Disorders and Stroke rt-PA Stroke Study Group. Tissue plasminogen activator for acute ischemic stroke. N Engl J Med 1995; 333(24):1581–1587.
2. CAST (Chinese Acute Stroke Trial) Collaborative Group. CAST: randomised placebo-controlled trial of early aspirin use in 20,000 patients with acute ischaemic stroke. Lancet 1997; 349(9066):1641–1649.
3. International Stroke Trial Collaborative Group. The International Stroke Trial (IST): a randomised trial of aspirin, subcutaneous heparin, both, or neither among 19435 patients with acute ischaemic stroke. Lancet 1997; 349(9065):1569–1581.
4. Langhorne P, Williams BO, Gilchrist W, Howie K. Do stroke units save lives? Lancet 1993; 342(8868):395–398.
5. Hacke W, Kaste M, Fieschi C, et al. Intravenous thrombolysis with recombinant tissue plasminogen activator for acute hemispheric stroke. The European Cooperative Acute Stroke Study (ECASS). JAMA 1995; 274(13):1017–1025.
6. O'Connor RE, McGraw P, Edelsohn L. Thrombolytic therapy for acute ischemic stroke: why the majority of patients remain ineligible for treatment. Ann Emerg Med 1999; 33(1):9–14.
7. Markus R, Reutens DC, Kazui S, et al. Hypoxic tissue in ischaemic stroke: persistence and clinical consequences of spontaneous survival. Brain 2004; 127(Pt 6):1427–1436.
8. Read SJ, Hirano T, Abbott DF, et al. The fate of hypoxic tissue on 18F-fluoromisonidazole positron emission tomography after ischemic stroke. Ann Neurol 2000; 48(2):228–235.
9. Heiss WD, Huber M, Fink GR, et al. Progressive derangement of periinfarct viable tissue in ischemic stroke. J Cereb Blood Flow Metab 1992; 12(2):193–203.
10. Darby DG, Barber PA, Gerraty RP, et al. Pathophysiological topography of acute ischemia by combined diffusion-weighted and perfusion MRI. Stroke 1999; 30(10):2043–2052.
11. Hacke W, Donnan G, Fieschi C, et al. Association of outcome with early stroke treatment: pooled analysis of ATLANTIS, ECASS, and NINDS rt-PA stroke trials. Lancet 2004; 363(9411):768–774.
12. O'Collins Tori MM, Donnan G, Laura H, van der Worp B, David H. 1026 experimental treatments in acute stroke. Ann Neurol 2006; 59(3):467–477.
13. Stroke Therapy Academic Industry Roundable (STAIR) Group. Recommendations for standards regarding preclinical neuroprotective and restorative drug development. Stroke 1999; 30(12): 2752–2758.
14. Fisher M, Albers GW, Donnan GA, et al. Enhancing the development and approval of acute stroke therapies: stroke therapy academic industry roundtable. Stroke 2005; 36(8):1808–1813.
15. Kim HY, Singhal AB, Lo EH. Normobaric hyperoxia extends the reperfusion window in focal cerebral ischemia. Ann Neurol 2005; 57(4):571–575.
16. Singhal AB, Benner T, Roccatagliata L, et al. A pilot study of normobaric oxygen therapy in acute ischemic stroke. Stroke 2005; 36(4):797–802.
17. Lekieffre D, Benavides J, Scatton B, Nowicki JP. Neuroprotection afforded by a combination of eliprodil and a thrombolytic agent, rt-PA, in a rat thromboembolic stroke model. Brain Res 1997; 776(1–2):88–95.
18. Sereghy T, Overgaard K, Boysen G. Neuroprotection by excitatory amino acid antagonist augments the benefit of thrombolysis in embolic stroke in rats. Stroke 1993; 24(11):1702–1708.
19. Yang Y, Li Q, Shuaib A. Enhanced neuroprotection and reduced hemorrhagic incidence in focal cerebral ischemia of rat by low dose combination therapy of urokinase and topiramate. Neuropharmacology 2000; 39(5):881–888.
20. Andersen M, Overgaard K, Meden P, Boysen G, Choi SC. Effects of citicoline combined with thrombolytic therapy in a rat embolic stroke model. Stroke 1999; 30(7):1464–1471.
21. Bowes MP, Rothlein R, Fagan SC, Zivin JA. Monoclonal antibodies preventing leukocyte activation reduce experimental neurologic injury and enhance efficacy of thrombolytic therapy. Neurology 1995; 45(4):815–819.
22. Zhang RL, Zhang ZG, Chopp M, Zivin JA. Thrombolysis with tissue plasminogen activator alters adhesion molecule expression in the ischemic rat brain. Stroke 1999; 30(3):624–629.
23. Zhang L, Zhang ZG, Zhang RL, et al. Postischemic (6-hour) treatment with recombinant human tissue plasminogen activator and proteasome inhibitor PS-519 reduces infarction in a rat model of embolic focal cerebral ischemia. Stroke 2001; 32(12):2926–2931.

24. Sanchez C, Alonso de Lecinana M, Diez-Tejedor E, Carceller F, Vega A, Roda JM. Treatment of embolic cerebral infarct via thrombolysis and cytoprotection with U-74389-G in rats. Rev Neurol 1998; 27(158):653–658.
25. Orozco J, Mendel RC, Hahn MR, Guthkelch AN, Carter LP. Influence of a 'brain protector' drug 21-amino steroid on the effects of experimental embolic stroke treated by thrombolysis. Neurol Res 1995; 17(6):423–425.
26. Grotta J. Combination Therapy Stroke Trial: recombinant tissue-type plasminogen activator with/without lubeluzole. Cerebrovasc Dis 2001; 12(3):258–263.
27. Lyden P, Jacoby M, Schim J, et al. The clomethiazole acute stroke study in tissue-type plasminogen activator-treated stroke (CLASS-T): final results. Neurology 2001; 57(7):1199–1205.
28. Krams M, Lees KR, Hacke W, Grieve AP, Orgogozo JM, Ford GA. Acute stroke therapy by inhibition of neutrophils (ASTIN): an adaptive dose-response study of UK-279,276 in acute ischemic stroke. Stroke 2003; 34(11):2543–2548.
29. Kammersgaard LP, Rasmussen BH, Jorgensen HS, Reith J, Weber U, Olsen TS. Feasibility and safety of inducing modest hypothermia in awake patients with acute stroke through surface cooling: a case-control study: the Copenhagen stroke study. Stroke 2000; 31(9):2251–2256.
30. Kollmar R, Schabitz WR, Heiland S, et al. Neuroprotective effect of delayed moderate hypothermia after focal cerebral ischemia: an MRI study. Stroke 2002; 33(7):1899–1904.
31. Bernard SA, Gray TW, Buist MD, et al. Treatment of comatose survivors of out-of-hospital cardiac arrest with induced hypothermia. N Engl J Med 2002; 346(8):557–563.
32. The Hypothermia After Cardiac Arrest Study Group. Mild therapeutic hypothermia to improve the neurologic outcome after cardiac arrest. N Engl J Med 2002; 346(8):549–556.
33. De Georgia MA, Krieger DW, Abou-Chebl A, et al. Cooling for acute ischemic brain damage (COOL AID): a feasibility trial of endovascular cooling. Neurology 2004; 63(2):312–317.
34. Kwiatkowski TG, Libman RB, Frankel M, et al. Effects of tissue plasminogen activator for acute ischemic stroke at one year. National Institute of Neurological Disorders and Stroke Recombinant Tissue Plasminogen Activator Stroke Study Group. N Engl J Med 1999; 340(23):1781–1787.
35. Marler JR, Tilley BC, Lu M, et al. Early stroke treatment associated with better outcome: the NINDS rt-PA stroke study. Neurology 2000; 55(11):1649–1655.
36. Hacke W, Kaste M, Fieschi C, et al. Randomised double-blind placebo-controlled trial of thrombolytic therapy with intravenous alteplase in acute ischaemic stroke (ECASS II). Second European-Australasian Acute Stroke Study Investigators. Lancet 1998; 352(9136):1245–1251.
37. Clark WM, Wissman S, Albers GW, Jhamandas JH, Madden KP, Hamilton S. Recombinant tissue-type plasminogen activator (Alteplase) for ischemic stroke 3 to 5 hours after symptom onset. The ATLANTIS Study: a randomized controlled trial. Alteplase thrombolysis for acute noninterventional therapy in ischemic stroke. JAMA 1999; 282(21):2019–2026.
38. del Zoppo GJ, Higashida RT, Furlan AJ, Pessin MS, Rowley HA, Gent M. PROACT: a phase II randomized trial of recombinant pro-urokinase by direct arterial delivery in acute middle cerebral artery stroke. PROACT Investigators. Prolyse in acute cerebral thromboembolism. Stroke 1998; 29(1):4–11.
39. Furlan A, Higashida R, Wechsler L, et al. Intra-arterial prourokinase for acute ischemic stroke. The PROACT II study: a randomized controlled trial. Prolyse in acute cerebral thromboembolism. JAMA 1999; 282(21):2003–2011.
40. Lisboa RC, Jovanovic BD, Alberts MJ. Analysis of the safety and efficacy of intra-arterial thrombolytic therapy in ischemic stroke. Stroke 2002; 33(12):2866–2871.
41. Freitag HJ, Becker VU, Thie A, et al. Lys-plasminogen as an adjunct to local intra-arterial fibrinolysis for carotid territory stroke: laboratory and clinical findings. Neuroradiology 1996; 38(2):181–185.
42. Lewandowski CA, Frankel M, Tomsick TA, et al. Combined intravenous and intra-arterial r-TPA versus intra-arterial therapy of acute ischemic stroke: Emergency management of stroke (EMS) bridging trial. Stroke 1999; 30(12):2598–2605.
43. Ernst R, Pancioli A, Tomsick T, et al. Combined intravenous and intra-arterial recombinant tissue plasminogen activator in acute ischemic stroke. Stroke 2000; 31(11):2552–2557.
44. Zaidat OO, Suarez JI, Santillan C, et al. Response to intra-arterial and combined intravenous and intra-arterial thrombolytic therapy in patients with distal internal carotid artery occlusion. Stroke 2002; 33(7):1821–1826.
45. Hill MD, Barber PA, Demchuk AM, et al. Acute intravenous—intra-arterial revascularization therapy for severe ischemic stroke. Stroke 2002; 33(1):279–282.
46. Keris V, Rudnicka S, Vorona V, Enina G, Tilgale B, Fricbergs J. Combined intraarterial/intravenous thrombolysis for acute ischemic stroke. AJNR Am J Neuroradiol 2001; 22(2):352–358.
47. The IMS Study Investigators. Combined intravenous and intra-arterial recanalization for acute ischemic stroke: the interventional management of stroke study. Stroke 2004; 35(4):904–911.
48. Flaherty ML, Woo D, Kissela B, et al. Combined IV and intra-arterial thrombolysis for acute ischemic stroke. Neurology 2005; 64(2):386–388.
49. Wolpert SM, Bruckmann H, Greenlee R, Wechsler L, Pessin MS, del Zoppo GJ. Neuroradiologic evaluation of patients with acute stroke treated with recombinant tissue plasminogen activator. The rt-PA Acute Stroke Study Group. AJNR Am J Neuroradiol 1993; 14(1):3–13.

50. Mori E, Yoneda Y, Tabuchi M, et al. Intravenous recombinant tissue plasminogen activator in acute carotid artery territory stroke. Neurology 1992; 42(5):976–982.
51. Cannon CP, McCabe CH, Gibson CM, et al. TNK-tissue plasminogen activator in acute myocardial infarction. Results of the thrombolysis in myocardial infarction (TIMI) 10A dose-ranging trial. Circulation 1997; 95(2):351–356.
52. Keyt BA, Paoni NF, Refino CJ, et al. A faster-acting and more potent form of tissue plasminogen activator. Proc Natl Acad Sci USA 1994; 91(9):3670–3674.
53. Haley EC Jr, Lyden PD, Johnston KC, Hemmen TM. A pilot dose-escalation safety study of tenecteplase in acute ischemic stroke. Stroke 2005; 36(3):607–612.
54. Hacke W, Albers G, Al-Rawi Y, et al. The Desmoteplase in acute ischemic stroke trial (DIAS): a phase II MRI-based 9-hour window acute stroke thrombolysis trial with intravenous desmoteplase. Stroke 2005; 36(1):66–73.
55. Liberatore GT, Samson A, Bladin C, Schleuning WD, Medcalf RL. Vampire bat salivary plasminogen activator (desmoteplase): a unique fibrinolytic enzyme that does not promote neurodegeneration. Stroke 2003; 34(2):537–543.
56. Qureshi AI, Ali Z, Suri MF, et al. Intra-arterial third-generation recombinant tissue plasminogen activator (reteplase) for acute ischemic stroke. Neurosurgery 2001; 49(1):41–48; discussion 48–50.
57. Pannell R, Gurewich V. Pro-urokinase: a study of its stability in plasma and of a mechanism for its selective fibrinolytic effect. Blood 1986; 67(5):1215–1223.
58. Suzuki Y, Chen F, Ni Y, Marchal G, Collen D, Nagai N. Microplasmin reduces ischemic brain damage and improves neurological function in a rat stroke model monitored with MRI. Stroke 2004; 35(10):2402–2406.
59. Lapchak PA, Araujo DM, Pakola S, Song D, Wei J, Zivin JA. Microplasmin: a novel thrombolytic that improves behavioral outcome after embolic strokes in rabbits. Stroke 2002; 33(9):2279–2284.
60. Bell WR, Pitney WR, Goodwin JF. Therapeutic defibrination in the treatment of thrombotic disease. Lancet 1968; 1(7541):490–493.
61. Reid HA, Chan KE, Thean PC. Prolonged coagulation defect (defibrination syndrome) in Malayan viper bite. Lancet 1963; 1:621–626.
62. The Ancrod Stroke Study Investigators. Ancrod for the treatment of acute ischemic brain infarction. Stroke 1994; 25(9):1755–1759.
63. Sherman DG, Atkinson RP, Chippendale T, et al. Intravenous ancrod for treatment of acute ischemic stroke: the STAT study: a randomized controlled trial. Stroke treatment with ancrod trial. JAMA 2000; 283(18):2395–2403.
64. Leclerc JR. Platelet glycoprotein IIb/IIIa antagonists: lessons learned from clinical trials and future directions. Crit Care Med 2002; 30(5 suppl):S332–S340.
65. Choudhri TF, Hoh BL, Zerwes HG, et al. Reduced microvascular thrombosis and improved outcome in acute murine stroke by inhibiting GP IIb/IIIa receptor-mediated platelet aggregation. J Clin Invest 1998; 102(7):1301–1310.
66. The Abciximab in Ischemic Stroke Investigators. Abciximab in acute ischemic stroke: a randomized, double-blind, placebo-controlled, dose-escalation study. Stroke 2000; 31(3):601–609.
67. Abciximab Emergent Stroke Treatment Trial (AbESTT) Investigators. Emergency administration of abciximab for treatment of patients with acute ischemic stroke: results of a randomized phase 2 trial. Stroke 2005; 36(4):880–890.
68. Adams HP Jr, Leclerc JR, Bluhmki E, Clarke W, Hansen MD, Hacke W. Measuring outcomes as a function of baseline severity of ischemic stroke. Cerebrovasc Dis 2004; 18(2):124–129.
69. Mitsias PD, Lu M, Silver B, et al. MRI-guided, open trial of abciximab for ischemic stroke within a 3- to 24-hour window. Neurology 2005; 65(4):612–615.
70. Zhang L, Zhang ZG, Zhang R, et al. Adjuvant treatment with a glycoprotein IIb/IIIa receptor inhibitor increases the therapeutic window for low-dose tissue plasminogen activator administration in a rat model of embolic stroke. Circulation 2003; 107(22):2837–2843.
71. Qureshi AI, Suri MF, Ali Z, et al. Intraarterial reteplase and intravenous abciximab for treatment of acute ischemic stroke A preliminary feasibility and safety study in a non-human primate model. Neuroradiology 2005; 47(11):845–854.
72. Gahn G KA, Putz V, Becker U. Recanlisation of middle cerebral artery occlusion after either t-PA of t-PA combined with abciximab. Stroke 2004; 35(1):291.
73. Junghans U, Seitz RJ, Aulich A, Freund HJ, Siebler M. Bleeding risk of tirofiban, a nonpeptide GPIIb/IIIa platelet receptor antagonist in progressive stroke: an open pilot study. Cerebrovasc Dis 2001; 12(4):308–312.
74. Junghans U, Seitz RJ, Ritzl A, et al. Ischemic brain tissue salvaged from infarction by the GP IIb/IIIa platelet antagonist tirofiban. Neurology 2002; 58(3):474–476.
75. Straub S, Junghans U, Jovanovic V, Wittsack HJ, Seitz RJ, Siebler M. Systemic thrombolysis with recombinant tissue plasminogen activator and tirofiban in acute middle cerebral artery occlusion. Stroke 2004; 35(3):705–709.
76. McDonald CT ODJ, Bemporad J. The clinical utility of intravenous integrilin combined with intra-arterial tissue plasminogen activator in acute ischemic stroke: The MGH experience. Stroke 2002; 33(1):359.

77. Nakano S, Iseda T, Yoneyama T, Kawano H, Wakisaka S. Direct percutaneous transluminal angioplasty for acute middle cerebral artery trunk occlusion: an alternative option to intra-arterial thrombolysis. Stroke 2002; 33(12):2872–2876.
78. Nakano S, Yokogami K, Ohta H, Yano T, Ohnishi T. Direct percutaneous transluminal angioplasty for acute middle cerebral artery occlusion. AJNR Am J Neuroradiol 1998; 19(4):767–772.
79. Wikholm G. Transarterial embolectomy in acute stroke. AJNR Am J Neuroradiol 2003; 24(5):892–894.
80. Chopko BW, Kerber C, Wong W, Georgy B. Transcatheter snare removal of acute middle cerebral artery thromboembolism: technical case report. Neurosurgery 2000; 46(6):1529–1531.
81. Favrole P, Saint-Maurice JP, Bousser MG, Houdart E. Use of mechanical extraction devices in basilar artery occlusion. J Neurol Neurosurg Psychiatry 2005; 76(10):1462–1464.
82. Mayer TE, Hamann GF, Brueckmann HJ. Treatment of basilar artery embolism with a mechanical extraction device: necessity of flow reversal. Stroke 2002; 33(9):2232–2235.
83. Smith WS, Sung G, Starkman S, et al. Safety and efficacy of mechanical embolectomy in acute ischemic stroke: results of the MERCI trial. Stroke 2005; 36(7):1432–1438.
84. Qureshi AI, Siddiqui AM, Suri MF, et al. Aggressive mechanical clot disruption and low-dose intra-arterial third-generation thrombolytic agent for ischemic stroke: a prospective study. Neurosurgery 2002; 51(5):1319–1327; discussion 1327–1329.
85. Lutsep HL, Clark WM, Nesbit GM, Kuether TA, Barnwell SL. Intraarterial suction thrombectomy in acute stroke. AJNR Am J Neuroradiol 2002; 23(5):783–786.
86. Bellon RJ, Putman CM, Budzik RF, Pergolizzi RS, Reinking GF, Norbash AM. Rheolytic thrombectomy of the occluded internal carotid artery in the setting of acute ischemic stroke. AJNR Am J Neuroradiol 2001; 22(3):526–530.
87. Berlis A, Lutsep H, Barnwell S, et al. Mechanical thrombolysis in acute ischemic stroke with endovascular photoacoustic recanalization. Stroke 2004; 35(5):1112–1116.
88. Alexandrov AV, Molina CA, Grotta JC, et al. Ultrasound-enhanced systemic thrombolysis for acute ischemic stroke. N Engl J Med 2004; 351(21):2170–2178.
89. Mahon BR, Nesbit GM, Barnwell SL, et al. North American clinical experience with the EKOS MicroLysus infusion catheter for the treatment of embolic stroke. AJNR Am J Neuroradiol 2003; 24(3):534–538.
90. Daffertshofer M, Gass A, Ringleb P, et al. Transcranial low-frequency ultrasound-mediated thrombolysis in brain ischemia: increased risk of hemorrhage with combined ultrasound and tissue plasminogen activator: results of a phase II clinical trial. Stroke 2005; 36(7):1441–1446.
91. Archer CR, Horenstein S. Basilar artery occlusion: clinical and radiological correlation. Stroke 1977; 8(3):383–390.
92. Ferbert A, Bruckmann H, Drummen R. Clinical features of proven basilar artery occlusion. Stroke 1990; 21(8):1135–1142.
93. Hacke W, Zeumer H, Ferbert A, Bruckmann H, del Zoppo GJ. Intra-arterial thrombolytic therapy improves outcome in patients with acute vertebrobasilar occlusive disease. Stroke 1988; 19(10):1216–1222.
94. Arnold M, Nedeltchev K, Schroth G, et al. Clinical and radiological predictors of recanalisation and outcome of 40 patients with acute basilar artery occlusion treated with intra-arterial thrombolysis. J Neurol Neurosurg Psychiatry 2004; 75(6):857–862.
95. Becker KJ, Monsein LH, Ulatowski J, Mirski M, Williams M, Hanley DF. Intraarterial thrombolysis in vertebrobasilar occlusion. AJNR Am J Neuroradiol 1996; 17(2):255–262.
96. Macleod MR, Davis SM, Mitchell PJ, et al. Results of a multicentre, randomised controlled trial of intra-arterial urokinase in the treatment of acute posterior circulation ischaemic stroke. Cerebrovasc Dis 2005; 20(1):12–17.
97. Zeumer H, Freitag HJ, Zanella F, Thie A, Arning C. Local intra-arterial fibrinolytic therapy in patients with stroke: urokinase versus recombinant tissue plasminogen activator (r-TPA). Neuroradiology 1993; 35(2):159–162.
98. Levy EI, Firlik AD, Wisniewski S, et al. Factors affecting survival rates for acute vertebrobasilar artery occlusions treated with intra-arterial thrombolytic therapy: a meta-analytical approach. Neurosurgery 1999; 45(3):539–545; discussion 545–548.
99. Cross DT III, Moran CJ, Akins PT, Angtuaco EE, Derdeyn CP, Diringer MN. Collateral circulation and outcome after basilar artery thrombolysis. AJNR Am J Neuroradiol 1998; 19(8):1557–1563.
100. Huemer M, Niederwieser V, Ladurner G. Thrombolytic treatment for acute occlusion of the basilar artery. J Neurol Neurosurg Psychiatry 1995; 58(2):227–228.
101. Lindsberg PJ, Soinne L, Tatlisumak T, et al. Long-term outcome after intravenous thrombolysis of basilar artery occlusion. JAMA 2004; 292(15):1862–1866.
102. Montavont A, Nighoghossian N, Derex L, et al. Intravenous r-TPA in vertebrobasilar acute infarcts. Neurology 2004; 62(10):1854–1856.
103. Donnan GA, Howells DW, Markus R, Toni D, Davis SM. Can the time window for administration of thrombolytics in stroke be increased? CNS Drugs 2003; 17:995–1011.
104. Tissue plasminogen activator for acute ischemic stroke. The National Institute of Neurological Disorders and Stroke rt-PA Stroke Study Group. N Engl J Med 1995; 333(24):1581–1587.

105. Liu M, Counsell C, Zhao XL, Wardlaw J. Fibrinogen depleting agents for acute ischaemic stroke. Cochrane Database Syst Rev 2003; (3):CD000091.
106. Abciximab Emergent Stroke Treatment Trial (AbESTT) Investigators. Trial suspended because of safety concern. This was not published but is listed on a website http://clinicaltrials.gov/ct/gui/show/NCT00073372
107. ReoPro Retavase Reperfusion of Stroke Safety Study—imaging evaluation and ReoPro retarase reperfusion of stroke saftely study-imaging evalution with computed tomography. Not published as yet. http://www.strokecenter.org/trials/TrialDetail.aspx?tid=438, http://www.strokecenterorg/trails/TrailDetail.aspx?tid=462.
108 Combined approach to lysis utilizing eptifibatide and rt-PA in acute ischemic stroke. Not published yet. http:www.strokecenter/org/trials/Trial Detail.aspx?tid=478.
109. Reperfusion of Stroke Safety Study Imaging Evaluation-2. Not published as yet. http://www.strokecenter.org/trails/TrailDetail.aspx?trd=538.
110. MR and recanalization of stroke clots using embolectomy. Not published as yet. http://www.strokecenter.org/trials/TrialDetail.aspx?tid=559.
111. Grond M, Rudolf J, Schmulling S, Stenzel C, Neveling M, Heiss WD. Early intravenous thrombolysis with recombinant tissue-type plasminogen activator in vertebrobasilar ischemic stroke. Arch Neurol 1998; 55(4):466–469.
112. Brandt T, von Kummer R, Muller-Kuppers M, Hacke W. Thrombolytic therapy of acute basilar artery occlusion. Variables affecting recanalization and outcome. Stroke 1996; 27(5):875–881.

21 Magnetic Resonance in the Selection of Stroke Therapies

Stephen M. Davis
Department of Neurology, Royal Melbourne Hospital and University of Melbourne, Melbourne, Victoria, Australia

Joachim Röther
Department of Neurology, Klinikum Minden, Hannover Medical School, Minden, Germany

Geoffrey A. Donnan
National Stroke Research Institute, Austin Health, University of Melbourne, Melbourne, Victoria, Australia

INTRODUCTION

The definition of tissue at risk of infarction is an important goal in the selection of acute stroke patients likely to benefit from thrombolytic therapy and to extend the therapeutic time window. The concept of the ischemic penumbra, defined as an area of severely hypoperfused but potentially restorable tissue around the irreversibly infarcted core, was introduced by Astrup et al. (1). Over two decades ago, they predicted that cerebral imaging could potentially be used to rapidly diagnose this partially ischemic region, that might be amenable to therapy (2).

Over 25 years later a range of imaging modalities are available to measure an approximation of the penumbra. Of these technologies, MRI has become the optimal imaging technique for acute stroke patients. Diffusion-weighted MRI (DWI) identifies acute ischemic tissue with cytotoxic edema, perfusion-weighted MRI (PWI) delineates hypoperfused brain areas, and MR angiography (MRA) depicts the intracranial vasculature. A mismatch between a larger PWI lesion and smaller DWI lesion is considered to represent the ischemic penumbra (3).

The majority of acute stroke patients have this MRI-penumbral signature within six hours of stroke onset (4,5). The penumbra is commonly, but not invariably, associated with proximal arterial occlusion and is time dependent. It widely held that the presence of a significant amount of penumbral tissue, beyond the clinically confirmed three-hour time window, would identify responders to thrombolytic therapy. Preliminary studies have shown benefit from thrombolytic therapy beyond the established three-hour window. In the past, there was concern about the reliability of MRI in the diagnosis of intracerebral hemorrhage (ICH). However, MR sequences such as T2*-weighted gradient-echo MRI are highly sensitive in the detection of blood products and shown to be even more sensitive than computed tomography (CT) in the detection of ICH (6,7).

Despite the advantages of MRI, a number of specific problems have to be considered when stroke MRI is applied to define penumbral tissue. Different methods of definition of penumbral tissue are extensively discussed in this book. This chapter will focus on the progress made using MRI techniques in providing a "tissue clock" in acute brain ischemia and their application in selection of therapy in acute stroke.

PENUMBRAL IMAGING USING MAGNETIC RESONANCE IMAGING

Using echoplanar MRI, the combination of DWI, PWI, and MRA provides a rapid assessment of the ischemic infarct core (DWI), the underlying arterial pathology (MRA), and the tissue-at-risk (PWI>DWI mismatch). The concept that mismatch, defined by perfusion exceeding diffusion lesion volumes, was postulated as an operational definition of the penumbra by Warach and coworkers in the late 1990s (8–10). It was shown that the high-intensity signal on

DWI identified tissue that was usually destined to infarct. The typically larger, hypoperfused region included both the severely ischemic core and the at-risk tissue in the mismatch region. In Melbourne, we demonstrated that PWI>DWI mismatch in the middle cerebral artery (MCA) territory usually correlated with occlusion of the trunk or major branches of the MCA on MRA, but a minority of patients had mismatch with normal MRA (11) (Fig. 1).

Kidwell et al. (12) suggested two important modifications to the MRI-based (PWI>DWI mismatch) penumbral concept. It was shown that hyperintense DWI lesions do not invariably progress to frank infarction and that the variable degrees of DWI lesion reversibility could be demonstrated with intra-arterial thrombolysis (13). In a small patient group, reversal of DWI lesions was seen in some subjects, although late secondary injury and completed infarction sometimes followed. The pretreatment tissue apparent diffusion coefficient (ADC) values were lowest in the patients not showing reversal, intermediate in those with reversal and secondary decline, and highest in those with sustained reversal (13). The Hamburg MRI group showed, that areas of ADC normalization can be found in as many as 20% of acute stroke patients studied by MRI within the first six hours of stroke onset (14).

ADC normalization in human stroke correlated with earlier studies in animal models that had demonstrated DWI reversibility (15). Furthermore, even more severe ADC decreases could normalize in case of rapid reperfusion. Thus, ADC normalization depends more on the duration and severity of ischemia, rather than the absolute value (16,17).

The second modification to the PWI>DWI mismatch concept was that the hypoperfused area on PWI in acute ischemia includes regions of only mildly reduced perfusion, which typically survive, in contrast with more severely ischemic regions, which were true penumbral tissue with a variable fate. These less severely hypoperfused regions are considered to represent benign oligemia. Perfusion thresholds have been applied to the various PWI parameters, to test these hypotheses: regions of very severe hypoperfusion, with mean contrast transit times (MTT) ≥6 seconds compared with the normal hemisphere, nearly always went on to infarct, whereas those with lesser degrees of hypoperfusion (MTT delay of 4–6 seconds) had a variable likelihood of progression to infarction (18). Conversely, regions with MTT delays of two to three seconds

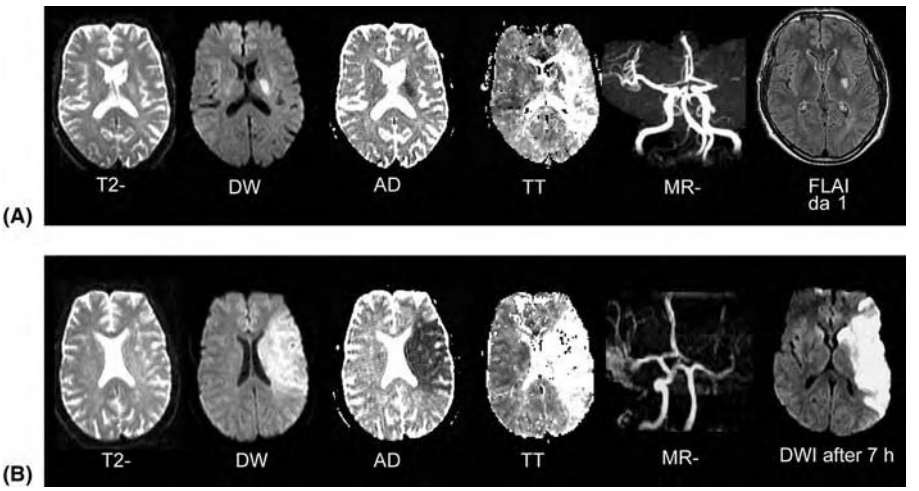

FIGURE 1 (**A**) MRI study one and five hours after symptom onset with aphasia and hemiparesis (NIHSS 14). Magnetic resonance angiography (MRA) depicts middle cerebral artery (MCA) occlusion with large diffusion-weighted MRI/perfusion-weighted MRI mismatch in the MCA territory. Thrombolysis results in recanalization and tissue salvage. Only a small striatocapsular infarction is present at follow-up MRI the next day. MRA and PWI are completely normal (data not shown). (**B**) In contrast, stroke magnetic resonance imaging in a patient with a severe deficit (NIHSS 21) two hours after symptom onset shows a large diffusion lesion in more than two-thirds of the MCA territory due to ICA and MCA occlusion. There is only a small area of DWI/PWI mismatch in the posterior part of the MCA territory. The patients were not treated with regional tissue plasminogen activator because of the large DWI lesion. Follow-up MRI after seven hours shows recruitment of penumbra into the infarction. The patient developed malignant MCA infarction and was treated by hemicraniectomy. *Abbreviations*: AD, apparent diffusion; DW, diffusion-weighted; MR, magnetic resonance; TT, transit time. *Source*: From Ref. 58.

typically survived, and therefore these were likely to represent regions of benign oligemia. Other groups similarly found that using Tmax, rather than MTT, a value of six to eight seconds optimally predicted core infarcted tissue at seven days (19,20).

These observations led to a modified definition of the penumbra. It is now thought to be more accurately represented by the PWI>DWI mismatch area, minus the oligemic rim, but including some of the DWI core with less severely decreased ADC values (as seen in Fig. 6, Chapter 14, Kidwell et al.). The precise definition is still evolving, with further research into the optimal measures of perfusion and tissue viability thresholds. Ischemic stroke is a dynamic process and one would anticipate that perfusion thresholds should be time dependent and would be altered by reperfusion, spontaneous, or induced. In Melbourne, we found in support of this hypothesis, that the MTT delay was compatible with tissue salvage and was inversely correlated with the duration of ischemic symptoms, in patients in whom blood flow was restored (21). Thrombolysis altered the thresholds, so that more severely ischemic tissue can be rescued. Thus, perfusion thresholds for recovery or infarction were dependent on the time of reperfusion.

Considerable debate surrounds the choice of which PWI parameter should be used in defining a mismatch. Most centers have used time-domain parameters, including MTT (estimated either with a deconvolution operation or first moment of the signal intensity curve), Time to Peak (TTP) or Tmax (TTP after deconvolution) (19–22). In Hamburg, we have suggested that regional cerebral blood flow (rCBF) may be the best PWI measure to demonstrate truly oligemic regions (23). Currently, there is no gold standard, because PWI does not provide absolute values of CBF. In addition, different strategies are used for standardizing the semi-quantitative values. These include normalization to the contralateral hemisphere, the arterial input function, or published positron emission tomography rCBF values for normal tissue (24).

Use of differing perfusion parameters and thresholds considerably alter the identification and frequency of the penumbra. For example, Tmax and MTT volumes on PWI are significantly lower than those calculated with TTP and FMT (first moment transit time). Thresholds are used to exclude tissue with benign oligemia, but different groups have decided not to use thresholds, or chosen thresholds of +2 or +4 seconds, relative to the contralateral hemisphere. Most groups use ≥20% to define mismatch. We suggested that use of Tmax +2 seconds was an attractive perfusion marker and that this identified a penumbral frequency of 73% in the pilot Echoplanar Imaging Thrombolytic Evaluation Trial (EPITHET) study (25). Regardless of the precise MRI definition, the penumbra is regarded as the target of potentially salvageable tissue in acute ischemic stroke.

The presence of the penumbra is strictly time linked. We and others showed that the penumbra as defined by PWI–DWI mismatch, was present in around 80% of patients in the first six hours after symptom onset (4,26). Intriguingly, however, the penumbra is still present in up to 40% of patients at 24 hours using MRI. The finding of potentially salvageable tissue many hours after stroke onset correlates with evidence obtained from ^{15}O and $^{18}FMISO$ PET imaging and raises the possibility that some tissue might be rescued at much later time intervals than are currently considered (27,28).

Evolution of Brain Ischemia and Expansion of the Ischemic Core

Serial MR imaging show that ischemia-related brain damage is a dynamic process. The DWI core typically expands to a variable extent into the PWI boundary due to a number of influences, including perfusion failure, neurotoxic cascade, physiological parameters (including temperature, hyperglycemia, and oxygenation), and apoptosis, defined as programed cell death (9,29). Besides the duration of the ischemia, the dynamics of the growth of the infarct core depends on the site of the vessel occlusion: proximal vascular occlusions lead to large infarctions and have a high potential for infarct growth (30).

In 49 patients with MCA infarcts who underwent imaging within six hours of stroke onset, we demonstrated serial evolution of PWI and DWI changes over time (31). These patients had not received thrombolytic therapy. When imaged in the subacute period three to five days after stroke onset, patients with acute PWI>DWI mismatch showed substantial reperfusion, and expansion of the DWI core. PWI lesions contracted by a median of 85% between acute and subacute time points, consistent with reperfusion, and DWI lesions grew by 136%. Patients with major reperfusion were more likely to be functionally independent, while those with

infarct growth were more likely to be dependent at outcome (31). We had previously shown that patients without mismatch typically did not show DWI growth and predicted that they were less likely to respond to thrombolysis (29).

However, given that ADC normalization occurs in some patients treated with acute reperfusion strategies, those patients without mismatch may also be potential responders in some cases (32). Hence, testing the mismatch hypothesis in treatment trials requires that nonmismatch patients are also studied.

Pilot Magnetic Resonance Imaging Studies Evaluating Thrombolytic Therapy in Ischemic Stroke

These observations led to studies to select potential treatment responders for thrombolysis, based on their cerebral pathophysiology, rather than solely by trial-based time windows and clinical factors. In the pilot EPITHET study, we studied 19 sub six-hour stroke patients with DWI, PWI, and MRA before intravenous thrombolysis, repeated at three to five days at the subacute stage after treatment and then at the 90-day outcome stage (33) (Fig. 2). Ischemic lesion evolution and clinical outcomes of this cohort were compared with those of 21 matched, historical controls. In patients with PWI>DWI mismatch on MRI, recanalization, reperfusion and penumbral salvage, attenuation of infarct expansion, and reduction of outcome infarct volume were all significantly smaller in the tissue plasminogen activator (tPA) group compared with the controls. Furthermore, these MRI surrogate outcomes correlated with measures of clinical improvement, such as an improvement of ≥7 points on the NIHSS, or functional independence on the modified Rankin scale. We showed that more severely hypoperfused tissue, which is usually destined for infarction, could be rescued by successful reperfusion within this time window (21).

Schellinger et al. (34) also showed that recanalization, using open label tPA, attenuated lesion growth, correlating with better outcomes. Within the German Stroke Competence Network, we found a good correlation between tPA therapy and recanalization with higher

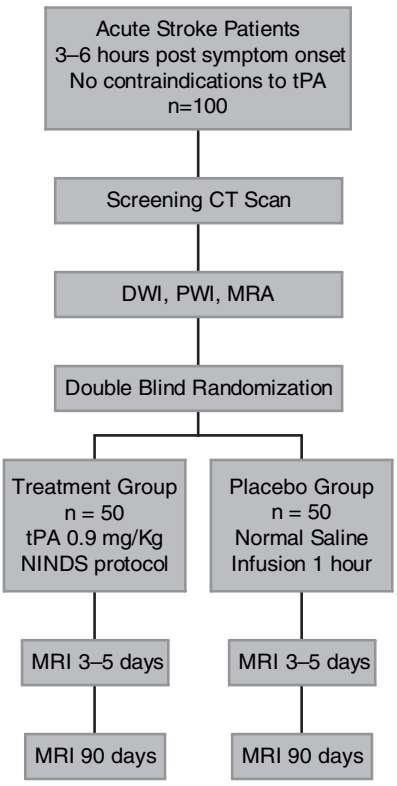

FIGURE 2 Echoplanar Imaging Thrombolytic Evaluation trial design. Flow diagram of the EPITHET protocol. *Abbreviations*: tPA, tissue plasminogen activator; MRA, magnetic resonance angiography; NINDS, The National Institute of Neurological Disorders and Stroke; MRI, magnetic resonance imaging.

recanalization rates in the early time window (<3 hours) as compared to three to six hours (4). The largest series of MRI-selected acute stroke patients (<6 hours) treated by tPA compared the German data bank with the pooled data of the large stroke tPA trials (35) in an open, nonrandomized study (36). From 174 MRI-selected tPA patients, 62% (n = 108) were treated in ≤3 hours and 38% (n = 66) after three to six hours. Favorable outcome was more frequent in MRI-selected tPA patients compared with pooled tPA patients, and symptomatic intracerebral hemorrhage rates were lower. This study supports that it is safe and effective to expand the time window for intravenous (IV)-tPA up to six hours in patients with tissue-at-risk as defined by MRI. The case for MRI-based selection beyond three hours is further supported by the finding that there was no significant difference in the degree and volume of PWI and DWI impairment in the sub-three and three-to-six-hour groups (37).

As noted previously, the finding of DWI reversal in a proportion of cases treated by thrombolysis raises the question as to whether the MRI mismatch signature is necessary to indicate a likely response to therapy and whether nonmismatch patients might also benefit. Chalela et al. (38) showed shrinkage of DWI lesion volume in a proportion of cases after thrombolytic treatment; however, functional improvements were associated with reperfusion on MRI, rather than DWI reversal. Reperfusion of more than 30% in MTT volume, two hours after tPA administration, was a useful predictor of clinical outcome.

More recently, we showed that DWI reversal to some degree occurred in 67% tPA treated patients and in only 36% of those managed conservatively, although not achieving statistical significance (39). DWI expansion was attenuated by tPA in a time-dependent manner, however, tissue fate in regions of depressed ADC is variable and cannot be predicted solely by ADC values (39).

This has been supported by recent work from Fiehler et al. (14), indicating that ADC normalization (defined as normalization of ADC values in >5 mL tissue with acutely reduced ADC values) occurred in 20% of patients after thrombolysis and was associated with earlier time-to-treatment, and reperfusion in those with more distal vessel occlusions, particularly involving white matter and the basal ganglia. This question will only be resolved with the results of the current prospective randomized MRI-based thrombolytic trials.

Acute Stroke Trials Utilizing Magnetic Resonance Imaging to Evaluate Thrombolysis

A number of prospective acute stroke trials currently evaluate the application of stroke MRI to predict the response to thrombolysis (Table 1). The promising results of the EPITHET pilot study (33) led us to the design of a prospective, randomized, placebo-controlled trial in

TABLE 1 Current Trials Evaluating Thrombolysis Based on Penumbral Selection

Trial	Thrombolytic modality	Time window (hr)	Study design	Initial findings
EPITHET	tPA	3–6	Randomized controlled trial 100 patients. Patients treated without reference to MRI findings	Various definitions of mismatch predict DWI expansion. Reperfusion limits expansion
DEFUSE	tPA	3–6	Open-label study 80 patients. All patients receive tPA regardless of MRI results	Intermediate PWI lesions, mismatch and reperfusion predict good outcome
DIAS	Desmoteplase	3–9	Dose escalating trial. Initial study 102 patients completed. Only patients with mismatch treated	Identification of a safe, effective dose that enhances reperfusion and improves outcomes
MR RESCUE	Mechanical embolectomy	0–8	Prospective randomized controlled trial. Treatment stratified for mismatch	Pilot results indicate benefits in those with a penumbra and reperfusion
ROSIE	Abciximab + reteplase	3–24	Open label, dose escalation, safety, and proof-of-principle study	Proceeding

Abbreviations: DEFUSE, DWI Evolution for Understanding Stke Etiology; DIAS, desmoteplase in acute ischemic; DWI, diffusion-weighted MRI; EPITECH, Echoplanar Imaging Thrombolytic Evaluation trial; PWI, perfusion-weighted MRI; ROSIE, Reperfusion of Stroke Safety Study-Imaging Evaluation.

100 patients, randomizing patients to either tPA or placebo, between three to six hours after stroke onset. Patients are studied with PWI and DWI before and after thrombolysis, but MRI criteria are not utilized in patient selection. A pretreatment CT scan is used to exclude patients with hemorrhage or major early ischemic change. The EPITHET trial is being conducted to test the hypothesis that stroke patients with PWI>DWI mismatch will benefit from tPA beyond the clinically defined three-hour time window. The primary endpoint is growth of the DWI-defined ischemic core. We hypothesize that this will be attenuated by tPA therapy in patients with mismatch (21,33). We also hypothesize that reperfusion will be enhanced by tPA in those with an ischemic penumbra. The trial is being conducted in 13 centers in Australia, New Zealand, and an additional site in Belgium. The study is close to completion. In the first 40 patients enrolled, a significant mismatch volume (defined as PWI > DWI mismatch of more than 20%) was found in 50% to 83% of patients, depending on the PWI definition used (40). All definitions of mismatch predicted DWI expansion, but imperfectly. These relative perfusion measures often tend to either under- or overestimate the true volume of tissue-at-risk. The definition that best predicts the response to thrombolysis will not be known until the data are unblinded. Irrespective of mismatch, however, reperfusion appears to limit DWI expansion in the three to six hour time window.

Other studies use stroke MRI as a surrogate marker for tissue response to thrombolysis. The DEFUSE study (DWI Evolution for Understanding Stroke Etiology) was an open-label trial of 80 patients in the United States, aimed at delineation of PWI and DWI measures that predict response to tPA in the three to six hour time window. The DEFUSE trial showed that favorable clinical outcome with tPA is predicted by mismatch and early reperfusion. However, a small subset of patients with 'malignant reperfusion,' with very large (>100 mL) baseline DWI and/or PWI lesions did not benefit and had a substantial risk of hemorrhage (41). However, in contrast to EPITHET, the DEFUSE trial is not randomized. The Desmotyplase in Acute Stroke Trial (DIAS) evaluated the safety and efficacy of different intravenous doses of the thrombolytic agent desmoteplase, using MRI surrogate markers such as reperfusion to select the optimal dose for pivotal trials (42). The initial trial involved 102 patients, enrolled three to nine hours after stroke onset, selected on the criterion of at least 20% PWI>DWI mismatch. Reperfusion was assessed four to eight hours after stroke onset and clinical outcome at 90 days. This trial showed that a specific dose was associated with a low rate of ICH, with significantly enhanced reperfusion and improved functional outcome (42). A larger trial is underway.

The MR RESCUE trial is evaluating mechanical thrombolysis up to eight hours in patients with mismatch. A pilot study showed that significant clinical benefits were confined to those with a penumbra and successful recanalization (43). The ROSIE trial (Reopro Retavase Reperfusion of Stroke Safety Study-Imaging Evaluation) is evaluating the safety and efficacy of abciximab and reteplase in acute ischemic stroke with MR evidence of a perfusion deficit, 3 to 24 hours after onset, by measurement of reperfusion (44).

Trials in Neuroprotection

The inclusion of acute stroke patients with heterogeneous etiologies is considered one reason for the failure of acute stroke trials, especially with neuroprotective drugs (45). Recent phase II trials in acute stroke patients have utilized stroke MRI to "enrich" the population being studied by selecting more homogeneous patients with a vessel occlusion on MRA, a DWI/PWI mismatch, or at least a cortical PWI lesion. These MRI criteria help to exclude lacunar stroke and patients without mismatch in a time window later than three hours (in the range up to 24 hours). These techniques may potentially improve the results of neuroprotective trials and thrombolytic trials in an extended time window.

Identification of Patients with Increased Risk for Hemorrhage

In the National Institute of Neurological Disorders and Stroke (NINDS) trial, symptomatic hemorrhagic transformation (SICH) occurred in 6.4% of patients treated with thrombolysis, on CT (46). We showed, that secondary hemorrhagic transformation of ischemic infarction is predominantly associated with local reperfusion in the region with the most severe hypoperfusion (47) but is not necessarily associated with clinical worsening or a poor prognosis (48).

Markers of severe perfusion impairment, such as the extent of hypoattenuation in CT, are a risk factor for SICH (49).

Whereas in the past, MRI was thought to be less reliable than CT to rule out ICH, recent studies have shown that MRI detects hemorrhage with high accuracy (7). Indeed, MRI is even more accurate than CT for the detection of chronic ICH (6).

Because of the high sensitivity of MRI for the detection of ICH and its advantages in evaluation of acute ischemia, MRI is being used as a primary imaging tool in an increasing number of stroke centers. In acute stroke, MRI reveals hypointense lesions in T2*-weighted images (HLE or cerebral microbleeds) occurring in approximately 12% to 20% of ischemic stroke patients (50,51). The main concern has been whether they might be a marker of increased risk of sICH after thrombolytic therapy or not (52,53). HLE are thought most likely to represent old microbleeds (54) and may explain why 20% of all SICH occur outside the arterial territory of the presenting stroke (46). Furthermore, these HLE may also indicate an increased risk both of primary and secondary brain hemorrhages (55). A large worldwide database with more than 800 tPA-treated patients was recently collected by Fiehler et al. (56) and observed HLE in 20% and SICH in 4.2% of the patients. There was no difference in the rate of SICH between the patients with or without HLE and the data from this large study does not support the hypothesis that patients with HLE are at higher risk for SICH after thrombolysis therapy. However, an increased risk for rare patients with multiple CMBs (>5) cannot completely be ruled out.

CONCLUSIONS

Imaging plays a major role in the selection of stroke patients for thrombolytic therapy. Whether this role remains limited to CT scanning (for exclusion of hemorrhage and major early ischemic signs), or whether more advanced tools such as MRI, CT angiography, and CT perfusion will become the procedures of choice is still being defined. The MRI penumbral index provides a noninvasive measure of threatened brain tissue and has enabled a better understanding of the pathophysiology of acute stroke evolution. Rapid detection of the penumbra provides a potential substrate for patient selection for treatment. There is increasing support from various studies for this hypothesis, and indeed, some debate as to whether there is sufficient evidence to safely select patients for thrombolysis, or other reperfusion approaches, beyond the clinical three-hour time window.

A number of issues remain to be resolved. These include the optimal perfusion parameter using MRI and whether thresholding should be applied. This, together with further information about the response to thrombolysis of ischemic tissue with varying degrees of bioenergetic compromise, will allow a more precise measure of the penumbral region in acute ischemic stroke. Other information required from current trials will include the risk of hemorrhagic transformation after thrombolysis in relation to baseline perfusion and diffusion deficits, and the relationship between recanalization on MRA and reperfusion on PWI. We consider that evidence from randomized, prospective trials is required to more precisely define algorithms for therapy beyond three hours, but that there are good prospects for individualized selection of thrombolysis, based on neuroimaging of the ischemic penumbra. Furthermore, such evidence is likely to be translated to other imaging modalities for penumbral diagnosis, such as CT perfusion techniques (57). Application of penumbral imaging modalities beyond three hours should allow a substantially greater number of patients to be treated.

REFERENCES

1. Astrup J, Symon L, Branston NM, Lassen NA. Cortical evoked potential and extracellular K+ and H+ at critical levels of brain ischemia. Stroke 1977; 88:51–57.
2. Astrup J, Siesjo BK, Symon L. Thresholds in cerebral ischemia—the ischemic penumbra. Stroke 1981; 12:723–725.
3. Warach S, Dashe JF, Edelman RR. Clinical outcome in ischemic stroke predicted by early diffusion-weighted and perfusion magnetic resonance imaging: a preliminary analysis. J Cereb Blood Flow Metab 1996; 16(1):53–59.

4. Röther J, Schellinger PD, Gass A, et al. Effect of intravenous thrombolysis on MRI parameters and functional outcome in acute stroke <6 hours. Stroke 2002; 33(10):2438–2445.
5. Barber PA, Darby DG, Desmond PM, et al. Prediction of stroke outcome with echoplanar perfusion- and diffusion-weighted MRI. Neurology 1998; 51(2):418–426.
6. Kidwell CS, Chalela JA, Saver JL, et al. Comparison of MRI and CT for detection of acute intracerebral hemorrhage. JAMA 2004; 292(15):1823–1830.
7. Fiebach JB, Schellinger PD, Gass A, et al. Stroke magnetic resonance imaging is accurate in hyperacute intracerebral hemorrhage: a multicenter study on the validity of stroke imaging. Stroke 2004; 35(2):502–506.
8. Baird AE, Benfield A, Schlaug G, et al. Enlargement of human cerebral ischemic lesion volumes measured by diffusion-weighted magnetic resonance imaging. Ann Neurol 1997; 41(5):581–589.
9. Baird AE, Warach S. Magnetic resonance imaging of acute stroke. J Cereb Blood Flow Metab 1998; 18(6):583–609.
10. Davis S, Tress B, Barber PA, et al. Echoplanar magnetic resonance imaging in acute stroke. J Clin Neurosci 2000; 7(1):3–8.
11. Barber PA, Davis SM, Darby DG, et al. Absent middle cerebral artery flow predicts the presence and evolution of the ischemic penumbra. Neurology 1999; 52(6):1125–1132.
12. Kidwell CS, Alger JR, Saver JL. Beyond mismatch: evolving paradigms in imaging the ischemic penumbra with multimodal magnetic resonance imaging. Stroke 2003; 34(11):2729–2735.
13. Kidwell CS, Saver JL, Starkman S, et al. Late secondary ischemic injury in patients receiving intraarterial thrombolysis. Ann Neurol 2002; 52(6):698–703.
14. Fiehler J, Knudsen K, Kucinski T, et al. Predictors of apparent diffusion coefficient normalization in stroke patients. Stroke 2004; 35(2):514–519.
15. Minematsu K, Li L, Sotak C, Davis M, Fisher M. Reversible focal ischemic injury demonstrated by diffusion-weighted magnetic resonance imaging in rats. Stroke 1992; 23:1304–1311.
16. Fiehler J, Foth M, Kucinski T, et al. Severe ADC decreases do not predict irreversible tissue damage in humans. Stroke 2002; 33(1):79–86.
17. Fiehler J, Knab R, Reichenbach JR, Fitzek C, Weiller C, Rother J. Apparent diffusion coefficient decreases and magnetic resonance imaging perfusion parameters are associated in ischemic tissue of acute stroke patients. J Cereb Blood Flow Metab 2001; 21(5):577–584.
18. Parsons MW, Yang Q, Barber PA, et al. Perfusion magnetic resonance imaging maps in hyperacute stroke: relative cerebral blood flow most accurately identifies tissue destined to infarct. Stroke 2001; 32(7):1581–1587.
19. Shih LC, Saver JL, Alger JR, et al. Perfusion-weighted magnetic resonance imaging thresholds identifying core, irreversibly infarcted tissue. Stroke 2003.
20. Neumann-Haefelin T, Wittsack HJ, Wenserski F, et al. Diffusion- and perfusion-weighted MRI. The DWI/PWI mismatch region in acute stroke. Stroke 1999; 30(8):1591–1597.
21. Butcher K, Parsons M, Baird T, et al. Perfusion thresholds in acute stroke thrombolysis. Stroke 2003; 34(9):2159–2164.
22. Warach S, Pettigrew LC, Dashe JF, et al. Effect of citicoline on ischemic lesions as measured by diffusion-weighted magnetic resonance imaging. Citicoline 010 investigators. Ann Neurol 2000; 48(5):713–722.
23. Fiehler J, von Bezold M, Kucinski T, et al. Cerebral blood flow predicts lesion growth in acute stroke patients. Stroke 2002; 33:2421–2425.
24. Ostergaard L, Smith DF, Vestergaard-Poulsen P, et al. Absolute cerebral blood flow and blood volume measured by magnetic resonance imaging bolus tracking: comparison with positron emission tomography values. J Cereb Blood Flow Metab 1998; 18(4):425–432.
25. Butcher KS, Parsons M, MacGregor L, et al. Refining the perfusion–diffusion mismatch hypothesis. Stroke 2005; 36(6):1153–1159.
26. Darby DG, Barber PA, Gerraty RP, et al. Pathophysiological topography of acute ischemia by combined diffusion- weighted and perfusion MRI. Stroke 1999; 30(10):2043–2052.
27. Marchal G, Beaudouin V, Rioux P, et al. Prolonged persistence of substantial volumes of potentially viable brain tissue after stroke: a correlative PET–CT study with voxel-based data analysis. Stroke 1996; 27(4):599–606.
28. Read SJ, Hirano T, Abbott DF, et al. The fate of hypoxic tissue on 18F-fluoromisonidazole positron emission tomography after ischemic stroke. Ann Neurol 2000; 48(2):228–235.
29. Barber P, Darby D, Desmond P, et al. Prediction of stroke outcome with echoplanar perfusion- and diffusion- weighted MRI. Neurology 1998; 51(2):418–426.
30. Fiehler J, Knudsen K, Thomalla G, et al. Vascular occlusion sites determine differences in lesion growth from early apparent diffusion coefficient lesion to final infarct. AJNR Am J Neuroradiol 2005; 26(5):1056–1061.
31. Barber PA, Parsons MW, Desmond PM, et al. The use of PWI and DWI measures in the design of "proof-of-concept" stroke trials. J Neuroimaging 2004; 14(2):123–132.
32. Hjort N, Butcher K, Davis SM, et al. Magnetic resonance imaging criteria for thrombolysis in acute cerebral infarct. Stroke 2005; 36(2):388–397.

33. Parsons MW, Barber PA, Chalk J, et al. Diffusion- and perfusion-weighted MRI response to thrombolysis in stroke. Ann Neurol 2002; 51(1):28–37.
34. Schellinger P, Jansen O, Fiebach J, et al. Monitoring intravenous recombinant tissue plasminogen activator thrombolysis for acute ischemic stroke with diffusion and perfusion MRI. Stroke 2000; 31(6):1318–1328.
35. Hacke W, Donnan G, Fieschi C, et al. Association of outcome with early stroke treatment: pooled analysis of ATLANTIS, ECASS, and NINDS rt-PA stroke trials. Lancet 2004; 363(9411):768–774.
36. Thomalla G, Schwark C, Sobesky J, et al. Outcome and symptomatic bleeding complications of intravenous thrombolysis within 6 hours in MRI-selected stroke patients: comparison of a German multicenter study with the pooled data of ATLANTIS, ECASS and NINDS tPA trials. Stroke 2006; 37(3):852–858.
37. Fiehler J, Kucinski T, Knudsen K, et al. Are there time-dependent differences in diffusion and perfusion within the first 6 hours after stroke onset? Stroke 2004; 35(9):2099–2104.
38. Chalela JA, Kang DW, Luby M, et al. Early magnetic resonance imaging findings in patients receiving tissue plasminogen activator predict outcome: Insights into the pathophysiology of acute stroke in the thrombolysis era. Ann Neurol 2004; 55(1):105–112.
39. Loh PS, Butcher KS, Parsons MW, et al. Apparent diffusion coefficient thresholds do not predict the response to acute stroke thrombolysis. Stroke 2005; 36(12):2626–2631.
40. Butcher K, Macgregor L, Parsons M, et al. Multiple definitions of PWI-DWI mismatch reliably predict infarct growth (World Stroke Congress abstract)J. Stroke 2004; 35:e174.
41. Albers GW, Thijs VN, Wechsler L, et al. Magnetic resonance imaging profiles predict clinical response to early reperfusion: the diffusion and perfusion imaging evaluation for understanding stroke evoluation (DEFUSE) study. Ann Neurol 2006; 60:508–517.
42. Hacke W, Albers G, Al-Rawi Y, et al. The Desmoteplase in Acute Ischemic Stroke Trial (DIAS): a phase II MRI-based 9-hour window acute stroke thrombolysis trial with intravenous desmoteplase. Stroke 2005; 36(1):66–73.
43. Smith WS, Sung G, Starkman S, et al. Safety and efficacy of mechanical embolectomy in acute ischemic stroke: results of the MERCI trial. Stroke 2005; 36(7):1432–1438.
44. Chalela JA, Ezzeddine M, Latour L, Warach S. Reversal of perfusion and diffusion abnormalities after intravenous thrombolysis for a lacunar infarction. J Neuroimaging 2003; 13(2):152–154.
45. Fisher M. Recommendations for advancing development of acute stroke therapies: Stroke Therapy Academic Industry Roundtable 3. Stroke 2003; 34(6):1539–1546.
46. NINDS: The National Institute of Neurological Disorders and Stroke rt-PA Stroke Study Group. Tissue plasminogen activator for acute ischemic stroke. N Engl J Med 1995; 333:1581–1587.
47. Fiehler J, Remmele C, Kucinski T, et al. Reperfusion after severe local perfusion deficit precedes hemorrhagic transformation: an MRI study in acute stroke patients. Cerebrovasc Dis 2005; 19(2):117–124.
48. von Kummer R. Brain hemorrhage after thrombolysis: good or bad? Stroke 2002; 33(6):1446–1447.
49. Larrue V, von Kummer R, Muller A, Bluhmki E. Risk factors for severe hemorrhagic transformation in ischemic stroke patients treated with recombinant tissue plasminogen activator: a secondary analysis of the European–Australasian Acute Stroke Study (ECASS II). Stroke 2001; 32(2):438–441.
50. Kidwell CS, Saver JL, Villablanca JP, et al. Magnetic resonance imaging detection of microbleeds before thrombolysis: an emerging application. Stroke 2002; 33(1):95–98.
51. Nighoghossian N, Hermier M, Adeleine P, et al. Old microbleeds are a potential risk factor for cerebral bleeding after ischemic stroke: a gradient-echo T2*-weighted brain MRI study. Stroke 2002; 33(3):735–742.
52. Senior K. Microbleeds may predict cerebral bleeding after stroke. Lancet 2002; 359(9308):769.
53. Zimmerman RD. Stroke wars: episode IV CT strikes back. AJNR Am J Neuroradiol 2004; 25(8): 1304–1309.
54. Fazekas F, Kleinert R, Roob G. Histopathologic analysis of foci of signal loss on gradient-echo T2*-weighted MR images in patients with spontaneous intracerebral hemorrhage: evidence of microangiopathy-related microbleeds. AJNR Am J Neuroradiol 1999; 20:637–642.
55. Kato H, Izumiyama M, Izumiyama K, Takahashi A, Itoyama Y. Silent cerebral microbleeds on T2*-weighted MRI: correlation with stroke subtype, stroke recurrence, and leukoaraiosis. Stroke 2002; 33(6):1536–1540.
56. Fiehler J, Boulanger J, Kakuda W, et al. Bleeding risk analysis in stroke by T2*-weighted imaging before thrombolysis (BRASIL): a multicenter study of 600 patients of the MR Stroke Collaborative Group. Stroke 2006; 37(2):636.
57. Wintermark M, Reichhart M, Cuisenaire O, et al. Comparison of admission perfusion computed tomography and qualitative diffusion- and perfusion-weighted magnetic resonance imaging in acute stroke patients. Stroke 2002; 33(8):2025–2031.
58. Thomala GJ, Kucinski T, Schoder V, et al. Prediction of malignant middle cerebral artery infarction by early perfusion- and diffusion-weighted magnetic resonance imaging. Stroke 2003; 34(8):1892–1899.

Index

about the book...

This source presents the current status of concepts and research on the ischemic penumbra and identifies the latest methods for clinicians to quickly and efficiently recognize viable cerebral tissue for enhanced stroke management. Focusing on state-of-the-science technologies and cutting-edge trends, this volume examines imaging strategies utilizing PET, SPECT, MR, and CT for improved identification of key areas for intervention and therapy in the management of stroke patients.

With lucid chapters by international authorities on the topic, including the originator of the ischemic penumbra concept, Professor Lindsay Symon, this volume provides a comprehensive view of the ischemic penumbra ranging from neurochemical processes to clinical implications, imaging, and therapy...contains the first authoritative discussion of the thresholds and duration of the ischemic penumbra documented in various species, with sections that outline cerebral blood flow levels and their effects on important biochemical parameters...supplies an authoritative series of chapters individually focused on current imaging techniques to target the location and extent of the penumbra...outlines the relevance of the ischemic penumbra to specific therapies, such as extending time windows for therapy...and studies the determination of the presence of penumbra using a novel imaging/clinical mismatch concept, with clinical evidence and validation to date.

about the editors...

GEOFFREY A. DONNAN is Professor of Neurology, University of Melbourne, Australia, and Director of the National Stroke Research Institute, Australia. Dr. Donnan was cofounder of the Australian Stroke Trials Network and is a Past President of the Stroke Society of Australasia and the Australian Association of Neurologists. The author of more than 300 peer reviewed journal publications, 51 book chapters, and numerous professional publications and presentations, he is Editor-In-Chief of the *International Journal of Stroke*. Dr. Donnan is the recipient of the William Feinberg Award for excellence in stroke research from the American Stroke Association (2007).

JEAN-CLAUDE BARON is Professor of Stroke Medicine, Department of Clinical Neurosciences, University of Cambridge, United Kingdom. A Fellow of the Royal College of Physicians and the Academy of Medical Sciences, Dr. Baron is recognized as one of the most prominent European stroke experts, and is the recipient of the Johann Jacob Wepfer Award (2005) for continuous outstanding work in the field of cerebrovascular diseases and the role of penumbra in ischemic stroke.

STEPHEN M. DAVIS is Professor of Neurology, University of Melbourne, Victoria, Australia, and Director of Neurosciences, Royal Melbourne Hospital, Victoria, Australia. He is a past President of the Stroke Society of Australasia, the co-founder of the Australasian Stroke Trials Network, and President-Elect of the Australian and New Zealand Association of Neurologists. He has published over 240 refereed journal papers, co-authored 2 other texts on stroke, and numerous book chapters. He serves on 7 editorial boards including *Stroke, Cerebrovascular Diseases,* and the *International Journal of Stroke*.

FRANK R. SHARP is Professor of Neurology at the M.I.N.D. Institute at the University of California at Davis. His work has included participating in the development of the 2-deoxyglucose method to map active regions of brain, and the development of the c-fos method to map single activated neurons in the brain. His group was the first to demonstrate that different types of acute injury in brain and genetic diseases of brain have specific genomic profiles that are manifested in the brain, as well as in the blood.

Printed in the United States of America

DK901X

ISBN 978-084933990-5

90000

9 780849 339905

informa
healthcare
www.informahealthcare.com

52 Vanderbilt Avenue
New York, NY 10017

Telephone House
69-77 Paul Street
London EC2A 4LQ, UK